5101 250
Flat-Plate
Solar Array Project

DOE/JPL-1012-99
Distribution Category UC-63b

Progress Report 23

for the Period September 1983 to March 1984

and Proceedings of the 23rd Project Integration Meeting

Prepared for
U.S. Department of Energy
Through an Agreement with
National Aeronautics and Space Administration
by
Jet Propulsion Laboratory
California Institute of Technology
Pasadena, California

JPL Publication 84-47

5101-250
Flat-Plate
Solar Array Project

DOE/JPL-1012-99
Distribution Category UC-63b

Progress Report 23

for the Period September 1983 to March 1984

and Proceedings of the 23rd Project Integration Meeting

Prepared for
U.S. Department of Energy
Through an Agreement with
National Aeronautics and Space Administration
by
Jet Propulsion Laboratory
California Institute of Technology
Pasadena, California

JPL Publication 84-47

Prepared by the Jet Propulsion Laboratory, California Institute of Technology, for the U.S. Department of Energy through an agreement with the National Aeronautics and Space Administration.

The JPL Flat-Plate Solar Array Project is sponsored by the U.S. Department of Energy and is part of the Photovoltaic Energy Systems Program to initiate a major effort toward the development of cost-competitive solar arrays.

This publication reports on work done under NASA Task RE-152, Amendment 66, DOE NASA IAA No. DE-AI01-76ET20356.

ABSTRACT

This report describes progress made by the Flat-Plate Solar Array Project during the period September 1983 to March 1984. It includes reports on silicon sheet growth and characterization, module technology, silicon material, cell processing and high-efficiency cells, environmental isolation, engineering sciences, module reliability and project analysis and integration. It includes a report on, and copies of visual presentations made at, the 23rd Project Integration Meeting held at Pasadena, California, on March 14 and 15, 1984.

NOMENCLATURE

A	Ampere(s)
Å	Angstrom(s)
ac	Alternating current
AM	Air mass (e.g., AM1 = unit air mass)
AR	Antireflective
ASEC	Applied Solar Energy Corp.
a-Si	Amorphous silicon
ASME	American Society of Mechanical Engineers
ASTM	American Society for Testing and Materials
BA	Butyl acrylate
BOS	Balance of System (non-array elements of a PV system)
BSF	Back-surface field
BSR	Back-surface reflection
C	Celsius (temperature scale)
CER	Controlled-environment reactor
CPVC	Chlorinated polyvinyl chloride
c-Si	Single-crystal silicon
CVD	Chemical vapor deposition
CVT	Chemical vapor transport
Cz	Czochralski (classical silicon crystal growth method)
dc	Direct current
DCS	Dichlorosilane
DI	De-ionized
DOE	U.S. Department of Energy
EBIC	Electron-beam-induced current
EFG	Edge-defined film-fed growth (silicon ribbon growth method)

EMA	Ethylene methyl acrylate
EPDM	Ethylene-propylene-diene monomer
EPRI	Electric Power Research Institute
EPSDU	Experimental process system development unit
ESP	Edge-supported pulling (silicon-sheet production process)
EVA	Ethylene vinyl acetate
FBR	Fluidized-bed reactor
FF	Fill factor
FSA	Flat-Plate Solar Array Project
FSR	Free-space reactor
GE	General Electric Co.
GFCI	Ground-fault circuit interruptor
h	heat transfer coefficient; hour(s)
HEM	Heat-exchange method (silicon-crystal ingot-growth method)
I_{sc}	Short-circuit current
I-V	Current-voltage
ID	Inside diameter
IEEE	Institute of Electrical and Electronics Engineers
IIT	Illinois Institute of Technology
IITRI	IIT Research Institute
IPEG	Improved Price Estimation Guidelines
IPEG2	IPEG, non-computerized
IPEG4	IPEG, computerized
IR	Infrared
ITO	Indium-tin oxide
J_{sc}	Short-circuit current density
JPL	Jet Propulsion Laboratory

K	degree(s) Kelvin
k	Equilibrium constart
LAPSS	Large-area pulsed solar simulator
LASS	Low-angle silicon sheet growth method
LBIC	light-beam-induced current
LPE	Liquid-phase epitaxy
MBE	Molecular-beam epitaxy
MEPSDU	Module experimental process system development unit
mgSi	Metallurgical-grade silicon
MIS	Metal-insulator-semiconductor (cell configura*ion)
MSEC	Mobil Solar Energy Corp.
m-Si	Microcrystalline silicon
MT	Metric ton(s)
MW	Megawatt(s)
NASA	National Aeronautics and Space Administration
NEC	National Electrical Code
NMA	Non-mass-analyzed
NOC	Nominal operating conditions
NOCT	Nominal operating cell temperature
OFHC	Oxygen-free hard copper
O&M	Operating and maintenance
P	Power
P_{max}	Maximum power
PA&I	Project Analysis and Integration Area (of FSA)
P/FR	Problem-failure report
PC	Power conditioner
PCS	Power-conditioning system
PC/TS	Performance Criteria/Test Standards (SERI)

PDU	Process development unit
PE	Polyethylene
PEBA	Pulsed electron beam annealing
PIM	Project Integration Meeting
PMMA	Polymethyl methacrylate
PnBA	Poly-n-butyl acrylate
ppba	Parts per billion, atomic
ppma	Parts per million, atomic
ppmw	Parts per million, weight
PU	Polyurethane
PV	Photovoltaic(s)
PVB	Polyvinyl butyral
PVC	Polyvinyl chloride
PVD	Physical vapor deposition
R&D	Research and development
RCA	RCA Corp.
RES	Residential Experiment Station
RH	Relative humidity
RTV	Room-temperature vulcanized
S	Incident solar energy density
s	second(s)
SAMIS	Standard Assembly-Line Manufacturing Industry Simulation
SCE	Southern California Edison Co.
SEM	Scanning electron microscope
SERI	Solar Energy Research Institute
SIMRAND	SIMulation of Research ANd Development Projects
SIMS	Secondary ion mass spectroscopy
SMUD	Sacramento Municipal Utility District

SOA	State of the art
SOC	Standard operating conditions (module performance)
SOLMET	Solar radiation surface meteorological observations
STC	Silicon tetrachloride
STC	Standard test conditions
T	Temperature
TCM	Transparent conducting material
TCS	Trichlorosilane
TEM	Transmission electron microscope
TMY	Typical meteorological year
TREI	Texas Research and Engineering Institute
TTU	Texas Tech University
U	Superficial velocity
U_{mf}	Minimum fluidization velocity
UCC	Union Carbide Corp.
UCP	Ubiquitous crystallization process
UL	Underwriters Laboratories
UV	Ultraviolet
V_{oc}	Open-circuit voltage
W_p	Peak watt(s)
y	mol % silane
η	Greek letter eta: efficiency
σ_{xx}	Greek letter sigma: lateral stress
Ω	Greek letter omega: resistance in ohms

METRIC CONVERSION FACTORS

Approximate Conversions to Metric Measures

Symbol	When You Know	Multiply by	To Find	Symbol
		LENGTH		
in	inches	*2.5	centimeters	cm
ft	feet	30	centimeters	cm
yd	yards	0.9	meters	m
mi	miles	1.6	kilometers	km
		AREA		
in^2	square inches	6.5	square centimeters	cm^2
ft^2	square feet	0.09	square meters	m^2
yd^2	square yards	0.8	square meters	m^2
mi^2	square miles	2.6	square kilometers	km^2
	acres	0.4	hectares	ha
		MASS (weight)		
oz	ounces	28	grams	g
lb	pounds	0.45	kilograms	kg
	short tons (2000 lb)	0.9	tonnes	t
		VOLUME		
tsp	teaspoons	5	milliliters	ml
Tbsp	tablespoons	15	milliliters	ml
fl oz	fluid ounces	30	milliliters	ml
c	cups	0.24	liters	l
pt	pints	0.47	liters	l
qt	quarts	0.95	liters	l
gal	gallons	3.8	liters	l
ft^3	cubic feet	0.03	cubic meters	m^3
yd^3	cubic yards	0.76	cubic meters	m^3
		TEMPERATURE (exact)		
°F	Fahrenheit temperature	5/9 (after subtracting 32)	Celsius temperature	°C

*1 in = 2.54 (exactly). For other exact conversions and more detailed tables, see NBS Misc. Publ. 286, Units of Weights and Measures, Price $2.25, SD Catalog No. C13.10:286.

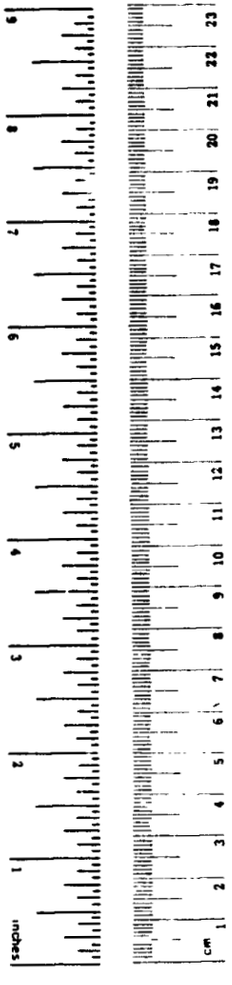

Approximate Conversions from Metric Measures

Symbol	When You Know	Multiply by	To Find	Symbol
		LENGTH		
mm	millimeters	0.04	inches	in
cm	centimeters	0.4	inches	in
m	meters	3.3	feet	ft
m	meters	1.1	yards	yd
km	kilometers	0.6	miles	mi
		AREA		
cm^2	square centimeters	0.16	square inches	in^2
m^2	square meters	1.2	square yards	yd^2
km^2	square kilometers	0.4	square miles	mi^2
ha	hectares (10,000 m^2)	2.5	acres	
		MASS (weight)		
g	grams	0.036	ounces	oz
kg	kilograms	2.2	pounds	lb
t	tonnes (1000 kg)	1.1	short tons	
		VOLUME		
ml	milliliters	0.03	fluid ounces	fl oz
l	liters	2.1	pints	pt
l	liters	1.06	quarts	qt
l	liters	0.26	gallons	gal
m^3	cubic meters	35	cubic feet	ft^3
m^3	cubic meters	1.3	cubic yards	yd^3
		TEMPERATURE (exact)		
°C	Celsius temperature	9/5 (then add 32)	Fahrenheit temperature	°F

CONTENTS

PROGRESS REPORT

PROJECT INTEGRATION MEETING

PROCEEDINGS

PROGRESS REPORT

Project Summary

INTRODUCTION

This report describes the activities of the Flat Plate Solar Array Project (FSA) from October 1983 through March 1984, including the 23rd FSA Project Integration Meeting (PIM), held on March 14 and 15, 1984.

FSA, sponsored by the U.S. Department of Energy (DOE), has the responsibility for advancing solar array technology while encouraging industry to reduce the price of arrays to a level at which photovoltaic (PV) electric power systems will be competitive with more conventional power sources. This responsibility has included developing the technology for producing low cost, long life photovoltaic modules and arrays. More than 100 organizations have participated in FSA sponsored research and development of low cost solar module manufacturing and mass production technology, the transfer of this technology to industry for commercialization, and the development and testing of advanced prototype modules and arrays. Economic analyses were used to select, for sponsorship, those research and development efforts most likely to result in significant cost reductions. Set forth here is an account of the progress that has been made during the reporting period.

SUMMARY OF PROGRESS

Long duration tests in the conversion of silane to silicon continue at the Union Carbide Corp. (UCC) experimental process system development unit (EPSDU) at Washougal, Washington. Continuous operation of the six-inch diameter fluidized bed reactor (FBR) for up to 45 hours has produced silicon (Si) particles up to 500 micrometers in diameter. The maximum silane feed concentration was 24 mole % in hydrogen, at an average silane feed rate of 2 kg/h. The FBR is now being fitted with a silicon liner to reduce contamination of the Si from the reactor walls. Silane continues to be produced in the EPSDU by the conversion of metallurgical grade Si (mgSi) to silane.

In the six-inch diameter research FBR at the Jet Propulsion Laboratory (JPL), the conversion of up to 100% silane to Si has been demonstrated without the formation of excessive fines. The amounts of silicon fines have been reduced by use of a secondary injection of silane. A quartz liner is being inserted in the FBR to reduce contamination of the Si.

Successful experiments on the formation Si seed particles for use in FBRs continue at the California Institute of Technology.

Hemlock Semiconductor Corp., Hemlock, Michigan, has continued experiments, at their own expense, on the conversion of trichlorosilane (TCS)

PROJECT SUMMARY

Metallo-organic decomposition (MOD) inks and liquids have been formulated by Purdue University. Silver neodecanoate is the most promising material.

Laser-assisted electroplating of copper was successfully demonstrated by Westinghouse. Grid lines as thin as 25 micrometers were applied at the local plating rate of 12 micrometers per second.

Initial experiments have been performed in a large-area amorphous-silicon (a-Si) deposition research chamber at JPL. Determination of key parameters in large-area deposition chambers are to be researched with the goal of achieving low-cost, stable, uniform, high-quality films.

Amorphous silicon solar cells supplied by Chronar Corp., Princeton, New Jersey, and ARCO Solar, Inc., Woodland Hills, California, are being used by Clemson University, Clemson, South Carolina, and JPL to set up performance measurements baseline data for future cell and module measurements.

An RFP for the purchase of a-Si and other thin-film modules has been issued. Those modules that can be purchased will be subjected to performance measurements and environmental testing like those of the crystalline-Si Block I procurement in 1975-76.

Laboratory techniques to interrogate directly the chemistry of the interfacial chemical bond between EVA and glass and EVA and aluminum have been separately devised by J. Koenig, Case Western Reserve University, Cleveland, OH, and J. Boerio, University of Cincinnati, Cincinnati, OH, respectively.

JPL developed a computer program to determine power loss from PV arrays due to shorted solar cells for specified module-array electrical configurations. Using the program, JPL determined optimum series-parallel configurations for minimizing power loss for short cells, and the cost-effective failure level for shorted cells.

Hot-spot testing of ARCO Solar, Inc. modules for the Sacramento Municipal Utility District (SMUD) central-station project provided data on operational conditions. Guidelines are being developed for future central station application tests.

Experimental modules that passed the Underwriters Laboratories Class B burning-brand test were developed and tested in collaboration with ARCO Solar, Inc. Modules using Kapton and fiberglass cloth as rear films passed the test.

A research forum was conducted on Array Design for Central Stations in Sacramento, California. Proceedings of the forum are in press.

A computer program has been developed to analyze optical and electrical losses in a transparent coating polymer (TCP)-coated solar cell. Various TCP characteristics that would permit a TCP to be used as a solar cell top side conductor have been determined.

Studies continue on a PV power system sensitivity analysis that shows the effects on module cost and efficiency of the many system parameters involved in meeting the cost-to-generate goal.

to dichlorosilane (DCS) in the process development unit (PDU). Hemlock has tripled the output of DCS from the PDU and fed it to Siemens-type reactors for conversion to silicon.

Analysis and experiments continue on the electrochemical refining of mgSi at Energy Materials Corp., South Lancaster, Massachusetts, and at Solar Energy Research Institute (SERI), Golden, Colorado.

A dendritic-web Si ribbon 6 meters in length was grown during 6 1/2 hours of continuous melt replenishment by Westinghouse Electric Corp., Pittsburgh, Pennsylvania.

A method of measuring residual stress in Si ribbons by bonding electrical resistance-type foil gauges to the ribbon was demonstrated by JPL. After the gauges are bonded to the ribbon, the ribbon outside the gauges is removed, the strain in the remaining ribbon is measured and the stress is calculated.

The residual stress distribution across the width of EFG ribbon was determined by the University of Illinois at Chicago by use of a shadow Moire technique that is suitable for use on rough surfaces.

A miniworkshop on the effects of stress and strain in high-speed-grown Si ribbons was attended by 30 participants in the comprehensive ribbon stress-strain effort, with open and enthusiastic exchanges of information and ideas on the overall study approach, results, progress and problems.

A floating emitter solar cell structure for high efficiency cells has been proposed by C.T. Sah and Associates.

Electrically active defects in Si sheet have been detected by use of an EBIC technique using cryogenic cooling at JPL.

Films of SiN_x for passivating Si surfaces were deposited at temperatures of only 150°C by plasma-enhanced chemical vapor deposition at the University of Washington.

A new method of measuring minority carrier lifetime and surface recombination velocity in the base region of a solar cell has been developed at the University of Florida.

The calibrated LBIC method has been perfected at the University of Pennsylvania, and microcomputer solar-cell modeling has been extended to include multilayered regions, the p-n junction space-charge region and the base region in addition to the front region.

Simultaneous front-junction and back-junction formation has been achieved using liquid dopants and a belt furnace by Westinghouse.

An investigation of ion implantation and annealing of non-Cz Si sheet materials has been completed by Spire Corp., Bedford, Massachusetts. The correct annealing cycle can enhance the performance of solar cells made from a number of these materials.

PROJECT SUMMARY

Manufacturing cost analyses of a Si modules by a Japanese program and by a JPL program led to significantly different results, due to different methods of treating capital costs. This emphasizes the need to understand the methodologies used in performing costing analyses.

Area Reports

MATERIALS AND DEVICES RESEARCH AREA

Silicon Materials Research Task and Advanced Silicon Sheet Task

INTRODUCTION

The objectives of the Silicon Materials Research Task and the Advanced Silicon Sheet Task are to identify the critical technical barriers to low-cost silicon (Si) purification and sheet growth that must be overcome to produce a photovoltaic (PV) cell substrate material at a price consistent with Flat-Plate Solar Array Project (FSA) objectives, and then to perform and support research and development to overcome those barriers.

Present solar-cell technology is based mainly on the use of Si wafers obtained by ID slicing of Czochralski (Cz)-grown ingots from Siemens-reactor-produced seminconductor-grade Si. This method of obtaining single-crystal Si wafers is tailored to the needs of semiconductor-device production (e.g., integrated circuits and discrete power and control devices other than solar cells). The small market offered by present solar-cell users does not justify industry's development of the high-volume Si production techniques that would result in low-cost PV electrical energy.

It is important to develop alternative low-cost processes for producing refined Si and sheet material suitable for long-life, high-efficiency solar PV energy conversion. To meet FSA objectives, research must be performed to overcome the barriers to the success of the most promising processes for producing large quantities of pure Si and large areas of crystallized Si at a low, competitive cost. The form of the refined Si must be suitable for use in the sheet-growth processes, and these must in turn be suitable for direct incorporation into automated solar-array industry schemes.

Silicon purification processes involving deposition of the material from silane and dichlorosilane are being pursued because these two substances can be purified relatively easily and, because of their high reactivity, they can be more readily decomposed or reduced to form Si than can trichlorosilane (TCS), which is used today in the conventional process. Research on two other processes that offer promise for making less-pure, solar-cell-grade Si by refinement of metallurgical-grade Si (mgSi) was recently undertaken because of the potential for further reduction of product cost.

FSA-funded improvements of the standard Cz ingot-growth process by reduction of expendable-material costs and improvement of ingot growth rate, together with improved slicing techniques, have developed the technology so that large areas of Si can be produced. Growth of large ingots by casting techniques, such as the semicrystalline casting process, may reduce sheet costs further.

Growth of crystalline Si material in a geometry that does not require cutting to achieve proper thickness is an obvious way to eliminate costly processing and material waste. Growth techniques such as edge-supported pulling (ESP), edge-defined film-fed growth (EFG), low-angle Si sheet (LASS), and dendritic-web growth are candidates for such solar-cell material.

In addition to research on processes for Si refinement and sheet formation, various supporting studied are under way to investigate key problems in both these categories.

SUMMARY OF PROGRESS

Silicon Material Research Task

Semiconductor-Grade Silicon Refinement Process

Silicon Refinement Using Silane (Union Carbide Corp.)

The objective of this R&D program is to solve the critical problems of silane decomposition in fluidized-bed reactors (FBRs) for producing semiconductor-grade silicon (Si) for PV applications. Three long-duration tests were conducted on the 6-in.-diameter FBR in the process development unit (PDU), for a total time of more than 80 hours. The longest single continuous test duration was nearly 45 hours. In the long-duration tests, seed particles of 300-micrometer mean diameter were grown to approximately 500-micrometer diameter. The maximum silane feed concentration was 24 mole % in hydrogen, and the average silane feed rate was approximately 2 kg/hour. A four-in.-diameter Czochralski ingot was pulled from the product of the 45-hour test. The first 14 in. of a 16-in.-long ingot was determined to be single-crystal.

Product from the FBR was analyzed for impurities using emission spectroscopy and neutron activation analysis; results indicated that the wall material (Incoloy 800H) is contaminating the Si. The PDU is undergoing modifications to introduce a suitable impurity barrier to minimize contamination from the wall. A study of various coatings and liner materials resulted in the selection of a high-purity polysilicon liner as the first choice. A technical review was conducted at JPL with critiques from Task consultants J. Routbort (Argonne National Laboratory) in abrasion phenomena and T. Fitzgerald in fluidized-bed technology. The review confirmed the findings and endorsed the approaches being taken by Union Carbide Corp. (UCC) (silicon liner) and JPL (quartz liner; see section titled "Research on Silane Pyrolysis in Fluidized-Bed Reactors") to the problem of reducing wall contamination. Procurement of the liner system is under way.

Silicon Refinement Using Dichlorosilane (Hemlock Semiconductor Corp.)

Hemlock is investigating the critical portions of a process for making semiconductor-grade Si, in which DCS is made from TCS by a redistribution reaction using an organic amino functional catalyst, and the DCS is then reduced by hydrogen to produce Si in a chemical-vapor-deposition step using Siemens-type reactors.

MATERIALS AND DEVICES RESEARCH AREA

The final report on the Phase I and Phase II effort was distributed. Highlights of the work were presented in Progress Report 21. The draft final report on the research progam on the cold-metal-wall Si deposition reactor was delivered to JPL and was reviewed by cognizant JPL personnel. The comments given to Hemlock are being incorporated into the document. Highlights of the effort were presented in Progress Report 22.

The program in which Hemlock, at its expense, tripled the output of the DCS PDU to about 200 lb/hour and fed the DCS to various combinations of mid-sized and large-sized Siemens-type Si deposition reactors, was completed at the end of December 1983. The purpose of the effort was to characterize further the performance of the PDU and the reactors and to supply DCS for the cold-wall-reactor program. The PDU contained to operate satisfactorily. A report on the program was submitted to JPL by Hemlock, and is being reviewed.

Solar-Cell Grade Silicon Refinement Processes

Electrochemical Refining of Metallurgical--rade Silicon

(Energy Materials Corp.)

The objective of this contract is to demonstrate the technical feasibility of producing high-purity Si from metallurgical-grade Si in a process using a Cu_3Si:Si anode in a fused-salt electrochemical cell.

The transport of Si in the Cu_3Si:Si anode was considered in a diffusion model by the Harvard University consultant to the contract. The first question was whether the model is consistent with the experimentally observed current density and whether this density value is close to the diffusion-limited value. The conclusion is that a deposition rate commensurate with three to four times the experimental maximum current density can be obtained without a diffusion limitation. At the higher densities the rate may be limited by electrochemical factors. The analysis is being extended to consider the diffusion of impurities through the Cu_3Si:Si to the anode surface.

In the experimental program, the first checkout test of the electrolysis cell resulted in a Si product containing a salt dispersion. Since this is evidence of the presence of H_2O, additional care will be used in the next test to eliminate all of the H_2O.

The fragility of the anodes is another problem; it is being dealt with by using extra precautions in placing the anodes in the cell. The question of the effect of the extent of reaction on the electrode structure thus becomes additionally important.

MATERIALS AND DEVICES RESEARCH AREA

Chemical Vapor Transport Process for Purifying Metallurgical-Grade Silicon

(Solar Energy Research Institute)

The objective of this research is to investigate a process in which a Cu_3Si:Si anode reacts with HCl to produce chlorosilanes, which are then decomposed on hot Si filaments to produce Si. Early results had shown the capability of preparing a product containing <2 ppma total impurities. The transport rate was shown to vary as $(\text{time})^{-1/2}$, which is consistent with a model in which the rate is limited by diffusion of Si in the anode.

A larger reactor with a deposition rate capability of about 11 g/hour has been constructed and is being tested. The transport rate, product purity, and energy use will be determined.

Silicon Refinement Process Supporting Studies

Silicon Particle Growth Research

(California Institute of Technology)

In the program at Caltech to study the formation and growth of Si particles by pyrolyzing silane, a larger, modified apparatus for the control of gas-phase nucleation and the growth of aerosol particles was constructed. The heated zone is 50 mm in diameter and 600 mm long. The apparatus was put into operation with the intent of increasing the particle size from 0.1 micrometer to a range of 25 to 50 micrometers (mass mean diameter). Separation and collection of particles also is receiving increased emphasis. Previously, particles up to 3.5-micrometer mass mean diameter have been grown in an apparatus 9 mm in diameter and 388 mm long. In preliminary experiments with the large apparatus, particles up to 100 micrometers in diameter (mass mean diameter of 9 micrometers) using 2 mole % silane were produced; however, the large particles were not dense.

The program was extended for one year (through September 1984). This will enable a more thorough theoretical treatment of the final stage of particle growth as well as an effort to grow larger particles.

Microwave Heating of Fluidized-Bed-Reactor Bed (Superwave Technology Inc.)

A new contract to Superwave Technology Inc., Santa Clara, California, for a feasibility study of microwave heating of a silicon fluidized-bed-reactor bed in the steady-state mode was started on February 22. The first meeting on this effort, which is scheduled to be completed on April 30, 1984, was held at the contractor's facility to discuss the design of the test system and the requirements for demonstrating feasibility of the concept.

MATERIALS AND DEVICES RESEARCH AREA

Research on Silane Pyrolysis in Fluidized-Bed Reactors (JPL)

JPL is conducting FBR research with the objective of characterizing the deposition of Si from silane and providing information upon which significant improvements in this process can be based. Work was continued to establish the process and basic mechanism for deposition of Si from the decomposition of silane onto FBR particles and to characterize the purity of the product. Neutron activation analysis showed heavy contamination of Si particles by the stainless-steel wall material. The primary mechanism was identified as erosion of the wall. Various wall materials, including nonmetallic liners or coatings, were considered to achieve high abrasion resistance and wall-contamination-free products. The best choice was considered to be a quartz liner. A design for the support and seal of a clear fused-quartz liner for the existing Type 316 stainless-steel reactor was established and its fabrication is under way.

Experiments with secondary injection of small amounts of silane at a point 13 in. above the distributor were conducted to increase the scavenging of the Si fines produced by homogeneous decomposition of silane, thereby increasing the efficiency of Si deposition. Reduction of fines in the exit filter from 10% to 6% of the total amount of Si present in the silane was realized, with a corresponding increase of Si product formation in the bed. An analysis confirmed the merits of the location of the secondary silane injection port.

Effort continued to investigate the feasibility of fluid jet milling to prepare clean FBR seed. The jet mill is lined with a nonmetallic material to eliminate metal contaminants from the product seed. For feed material in a 500- to 700-micrometer diameter range, one pass produced 15% in the desired range of 75 to 355 micrometers; after two passes, 28% was in the desired range. The results appear promising for the production of uncontaminated FBR seed. Fabrication of a polyethylene-lined device is under way.

A report titled "Silicon Production in a Fluidized-Bed Reactor: A Parameter Study" was published. It summarizes the JPL effort in which a six-in.-diameter engineering-scale FBR for investigating the pyrolysis of silane to produce semiconductor-grade silicon was designed, constructed, and tested to establish reactor design parameters for the distributor, cooling system, heaters, silicon withdrawal system, etc. Experiments were conducted to establish the mass balance, silicon production rate, and particle growth rate. The data indicate that more than 90% of the silicon fed is deposited on the seed particles as product, the remainder ending as fines that are swept from the FBR. It was demonstrated that up to 100% silane can be fed into the reactor without excessive fines formation. A paper titled "Fines in Fluidized Bed Silane Pyrolysis" was published in the March 1984 issue of the Journal of the Electrochemical Society.

Modeling of Silane Pyrolysis in Fluidized-Bed Reactors

(Washington University at St. Louis)

The objective of this effort, which started in December 1983, is to develop a comprehensive model for making Si by silane pyrolysis in

fluidized-bed reactors. This model should be useful in interpreting laboratory and pilot plant data and in designing large FBRs. To relate the production rate of Si and the particle size to the operating conditions of bed temperature, gas feed rate and composition, and solids seeding rate that will guarantee the minimizing of submicrometer particle formation, it is necessary to model the reactions of silane pyrolysis as well as fluidized-bed hydrodynamics.

The available information on homogeneous and heterogeneous pathways for silane pyrolysis was reviewed, and rate forms for modeling purposes were selected. The current understanding of fluidized-bed phenomena were reviewed, and an appropriate model structure was suggested.

SUMMARY OF PROGRESS

Advanced Silicon Sheet Task

Shaped-Sheet Technology

Edge-Defined Film-Fed Growth

(Mobil Solar Energy Corp.)

The primary goal of this program is to develop a model for obtaining temperature field--residual stress relationships applicable to Si ribbon growth at high speeds and to apply this model subsequently to a growth system that has been modified and improved to produce low-stress ribbon at high speeds.

In one subtask, a computer code developed at Harvard University to calculate stress with plastic deformation in steady-state sheet growth is being applied to study temperature-field stress relationships. The stress state is parameterized by a two-dimensional temperature field and growth speed. Incorporation of time-dependent stress relaxation effects is through a creep law to model the impact of plastic flow on the sheet residual stress state. A second aspect of the program deals with the development of a model to predict the temperature field in a moving sheet from given system component temperatures (i.e., the sheet environment) and experimental means to verify the model. This work is attempting to integrate temperature-field modeling in the solid, taking into account real system geometries with a more detailed heat-transfer model developed at the Massachusetts Institute of Technology for the die top and meniscus regions below the growth interface.

During this period, both modeling and experimental work were in progress to attempt to apply the stress analysis at a more quantitative level. The modeling is examining stress and temperature field relationships in a search for low-stress growth configurations. The experimental efforts are in studying the high-temperature creep response of Si to provide information on the constitutive relationship, develop a technique to measure the temperature field in the sheet during growth, and develop means to measure residual stress distributions. A temperature sensor based on fiber optics has been constructed for the temperature field measurements. A laser interferometry technique is being evaluated at the University of Illinois at Chicago for residual stress measurements.

Stress analysis at Harvard University examined the implication of non-zero stresses at the growth interface on model predictions. Stress distributions at distances greater than about 1 mm from the interface are shown to be independent of the interface stress at high creep intensities, and the predictions based on zero initial stress can be used with confidence. This subtask at Harvard University was terminated, and the process of transferring the computer codes to Mobil Solar Energy Corp. (MSEC) was completed. Using this computer code, studies of temperature and stress field relationships in sheet growth are under way at MSEC.

The development of finite-element models for sheet growth at MIT was also completed. The analysis will continue to be refined and applied to model growth of 10-cm-wide ribbon to test certain aspects of the model with available experimental data on impurity segregation and on interface shape. These programs for temperature and stress calculations will be applied to analyze the simplified ribbon growth configuration that is being constructed to test the stress model. During this reporting period, attempts to verify aspects of the stress and temperature field modeling with the 10-cm cartridge system have had limited success. Due to the complexity of growth environment at the interface, it has not been possible to use the fiber optic sensor. The cartridge system has lacked flexibility to allow imposition of changes in growth conditions and system temperature fields in a known and controllable manner to study stress and temperature field relationships at a quantitative level.

Construction of a simplified ribbon-growth system for purposes of testing the stress-analysis model is nearly complete. This growth system will be installed in Furnace 17 after completion of creep environments. The main departures from the 10-cm cartridge system design involve simplification of the post-growth cooling environment by use of simple graphite insulation geometries. It will be possible to determine more accurately the temperatures of these components and of the ribbon surface to give more confidence to temperature field specifications for the stress calculations.

In the primary creep response studies of displacement versus time for float-zone silicon deformed by four-point bending at 1360°C, a range of loads from 8.0 to 15.5 MPa maximum surface stress was used. All samples were (111) surface oriented, and the bending axis was <110>. Low and high magnification photomicrographs of the defect configurations produced at the low and high loads were obtained. Comparison of the dislocation configurations at the lower stresses shows that the final dislocation configurations achieved after 10 seconds at the two temperatures are qualitatively similar, and the dislocation densities are also comparable for a given stress level. A one-to-one comparison is not possible for the high stress because the transient loading times are significantly shorter (approximately 4 seconds at 1215°C and approximately 1 second at 1360°C) than for the lower stress (10-second) experiments. More detailed analysis of these responses is being continued.

Displacement-time curves for Cz silicon wafers stressed at 1215°C were also obtained. Creep response for all Cz samples is significantly reduced as compared with that for EFG material at a given stress and temperature. The Cz material used in the experiments had a relatively high substitutional carbon level of approximately 4×10^{17} atoms/cc and higher. It appears that oxygen exerts a greater effect on the creep response than does carbon in this range of concentrations. These studies are continuing.

The current design of the fiber-optic probe appears to have reasonable stability and reproducibility sufficient to make it useful for measurements of ribbon temperatures. It has been calibrated in crystal-growth Furnace 17 under conditions that expose the fiber-optics circuit to conditions encountered in an actual system. The results of several calibration runs that involved

thermal cycling through the range from 1100°C to 1400°C are encouraging. No further work on fiber optics thermometry is being done pending testing of the crystal-growth system mentioned above.

The first residual stress distributions were obtained on EFG material using a shadow-Moire technique of interferometry. The experimental results are encouraging in that stress variations across the sample width are observed, which was not possible with earlier techniques. Additional testing must be carried out to measure the responsiveness of the technique to stress changes produced by variations in growth conditions.

Dendritic Web Ribbon Growth

(Westinghouse Electric Corp.)

Westinghouse is conducting research on the key problems associated with a process for making a thin, wide-ribbon form of single-crystal Si directly from melt. "Dendritic" refers to the wire-like supporting dendrites on each side of the ribbon, and "web" refers to the Si sheet that results from the freezing of the liquid film between the bounding dendrites as the latter are raised from molten Si.

As part of the investigation of management of the silicon-ribbon temperature profile, initial calculations were performed to include the effect of heat loss by thermal conduction through the gas. It was found that even in the lid region, where gas conduction should be most pronounced, the conduction contribution was negligible. In view of these results, actual modification of the computer model to include gas conduction effects does not appear to be warranted for present purposes. An approach to using computer models for calculating the maximum possible width of low-stress ribbon for a given thickness is being developed. Formulation of the concept is under way.

Two new growth configurations using dynamic control of thermal elements were tested. The first was based on the J460 static configuration, which has exhibited excellent ribbon growth characteristics, and the dynamic configuration shows promise in being able to combine the enhanced growth velocity resulting from dynamic control and the wide-growth, low-stress characteristics of the J460 design. The other new dynamic configuration incorporated a low-stress top shield, and results were encouraging in that growth with enhanced velocity could be achieved at different lid positions. Further work is needed to optimize growth for both of the new configurations.

Westinghouse wrote the operating procedure for the sheet-growth machine that is used to produce dendritic-web silicon ribbon and sent copies to JPL with complete sets of engineering drawings for the equipment (including control system), as a contract deliverable.

The present contract ended on March 8. A one-year extension was negotiated.

MATERIALS AND DEVICES RESEARCH AREA

Low-Angle Silicon Sheet

(Energy Materials Corp.)

A new contract was started on March 12. The aim of the program is to overcome the critical barriers to the low-angle silicon sheet (LASS) ribbon growth of high-quality material at high linear growth velocities. Specific tasks of the contract involve the investigation of the parameters that affect the growth of single-crystal ribbon. Here the design of various silicon melt pump designs, cold shoe/jet configurations, and crucible and thermal modifier configurations will be tested in the existing furnace to optimize the growth parameters. Another task will emphasize the growth of high-quality ribbon. This effort involves assembling a separate growth chamber and positive-pressure facility to grow the ribbons in a clean environment. Throughout the period of the contract, the ribbon grown under the program will be evaluated to test the effects of any modification made to the system.

Ingot Technology

Semicrystalline Casting

(Semix Inc.)

This report period marks the conclusion of the contracted effort with Semix that was a continuation of the cooperative agreement established in 1980 with the Department of Energy. The later efforts under the agreement had been focused on specific research elements concerned with casting of Si blocks using the ubiquitous crystallization process (UCP). This focus had been designated in an effort to produce a program consistent with the DOE goals of high-risk, high-payoff research.

Within this last reporting period several investigations were under way:

(1) Minority carrier diffusion length in blocks.

(2) Thermal model for UCP.

(3) Sources of structure in cast blocks.

The first of these efforts involves the use of laser beams to generate and measure the density and decay time of minority carriers in a solid brick. This approach provides a method of evaluating cast blocks before their wafering, and thus saves considerable wafering expense. In this method, one laser beam is transmitted through a region of the brick under investigation. A second beam is transmitted through a region of the brick under investigation. A second beam is pulsed perpendicular to the first beam at a frequency capable of producing significant numbers of minority carriers and with energy intense enough to penetrate significantly into the bulk material. Up to the present, lasers with a wavelength of 1.32 micrometers and approximately 1.10 micrometers have been used, respectively, for the two lasers. The variations in intensity of the transmitted beam are measured using a detector. The decay time of the absorption peak can be translated into diffusion length.

The investigations at the time of the conclusion of the program has shown that the process is feasible. Measurements several centimeters into the bulk had been made, and results showed correlation with other minority carrier lifetime measurements. At the conclusion of the development, however, the amount of data generated had been limited. Especially missing were results from material with large variations in physical properties.

The second investigation still under way at the conclusion of this program involved the development of a computer model for describing the heat flows in the solidifying ingot as functions of heat inputs and outputs. The model was based on finite difference methods and included consideration of heat generation and volume expansion on solidification. Present state of the model involves description of two two-dimensional sections of the ingot, one in the center of each side and one through each corner. Simple but realistic flows were considered, and the calculated contours appear to be reasonable. Extensive additional development of the model is needed, including a three-dimensional form, and a much wider variety of heat input and output distributions will be required before the model can be considered to be fully useful.

The final effort within the program included ongoing studies of the development of structure, particularly intragrain structure, in the cast ingots during solidification. The details of this study are quite varied and complex. A number of reasonable conclusions can be drawn. The first conclusion relates to the development of deformation structure within grains of the casting as a result of thermal stresses during ingot casting. Both differential thermal expansion and trapped liquid volumes are potential sources of such deformation. The deformation structure takes the form of dislocations that eventually configure themselves into low-angle grain boundaries resembling polygonization.

Another conclusion from these microstructure studies is the deleterious effect of steps and ridges on grain boundaries that appear to act as locking points between neighboring grains. These points then result in deformation structure emanating from these points.

More detailed studies of these and other structure studies are available in the literature. Because this program has now concluded, release of additional results from these studies is at the discretion of Semix. Requests for access to these and other results should be taken directly to Semix.

Silicon Sheet Supporting Studies

Modification of Silicon Surface Properties by Fluid Adsorption

(University of Illinois at Chicago)

The program on the abrasive wear of Si in the presence of various fluids was completed, and the draft final report was written, submitted to JPL, and reviewed by cognizant JPL personnel. The requested changes were incorporated, and the report is being published. A follow-on effort is planned. The highlights of the program were presented in Progress Report 22.

An effort on measuring residual stress in Si sheet using laser interferometry was started. The apparatus was set up and was used to produce interference fringes on the surface of a concentrically loaded round Cz Si wafer. The density and distribution of the fringes were analyzed and the residual stresses determined. These stresses ranged from 0 to 40 MPa and were axisymmetric. Also, a shadow Moire technique that is suitable for use with rough surfaces was used to determine the residual stress distribution across the width of EFG ribbon. The results indicated that each method is feasible.

Analysis of Stress/Strain Relationships

(University of Kentucky)

A report titled "An Improved Analysis of the Thermal Buckling of Silicon Sheet," written by Professor O. Dillon and Professor R. DeAngelis of the University of Kentucky, was received. The report presents a buckling analysis for an elastic cantilever plate subjected to a temperature profile. The analysis predicts a torsional buckling mode and also predicts sheet thicknesses that will result in buckling.

The elastic and plastic analyses on buckling of silicon ribbon were begun.

Solid-Liquid Interface Studies

(Solar Energy Research Institute)

The aim of this effort is to investigate the shape and stability of the Si solid-liquid interface in high-speed growth techniques as functions of the impurity content, the thermal environment, and most important, the rapid solidification rate. Toward this end, SERI modified a float-zone furnace in a way that allows horizontal ribbon growth. This involved designing and building a ribbon pulling mechanism, opening a side port in the furnace through which to pull the ribbon, and working out a silicon melt confinement system. Two silicon confinement methods were tried: a cold-crucible technique and novel method that has been submitted to JPL as a new technology disclosure for evaluation for possible patent action. The modified furnace was tested and several ribbon-growing experiments were attempted by did not succeed because the thermal environment of the new melt confinement system had not been optimized. The program was terminated because development of the method was shown to require a greater level of effort and manpower than this program has available. The effort was restructured for a study of the optimization of highly doped silicon crystals for high-efficiency solar cells.

Materials Properties Modification (JPL)

The testing on the effects of light on the strength of Si wafers was completed. The results confirm earlier results, which indicated that the strength increases with increasing light intensity. The data still show large scatter but are statistically meaningful. The data are being analyzed, and a report is being prepared.

Tests were conducted by JPL on Westinghouse dendritic-web silicon ribbon that demonstrated the feasibility of a destructive method for measuring residual stress in sheet silicon. In this method, electrical resistance-type foil gages are bonded to Si sheet, the gages and attached Si are cut from the sheet, and the strain in three directions is read, allowing calculation of the principal stress. Measurements on a piece of dendritic web ribbon that had slightly rippled deformations gave relatively low values of residual stress, ranging from compressive stress of 200 $lb/in.^2$ to tension stress of 1000 $lb/in.^2$.

Research Forum

One major FSA goal is to understand and overcome the limitations that stress/strain and deformation effects are placing on the rate at which ribbon suitable for solar cells can be grown. A miniworkshop on the effects of stress and strain in high-speed-grown silicon ribbons was held January 10 and 11 at the Westinghouse R&D Center, Pittsburgh, Pennsylvania. It was attended by about 30 persons, including representatives of subcontractors, DOE, SERI, and JPL. Its objectives were to bring together the key persons directly involved in the ribbon stress/strain program, familiarize them with the latest research and results on this subject, exchange ideas, and assist in formulating future research activities.

The miniworkshop was successful in that there was a great deal of enthusiastic interchange of information and opinion, and all of its objectives were achieved. In particular, areas of research were identified that must be addressed to improve understanding of the stress/strain/deformation problem. These include measurement of actual temperature distributions in the growing ribbons and in the growth environment, understanding of the dynamics of the lattice near the solidification zone, observation of deformation during growth, determination of accurate high-temperature creep data for silicon, integration of elastic and inelastic modeling, and systematic experimental evaluation of the various ribbon growth models.

Device Research Task

INTRODUCTION

The objective of the Device Research Task is to identify and implement research and development activities in the Materials and Devices Area to meet the near-term and long-term objectives of FSA. Task activities encompass research in device physics, device structure, material-device property interaction, and measurement techniques for physical, chemical and electrical evaluation of devices and materials.

Technical Approach, Organiztion and Coordination

To meet FSA objectives, efforts are now directed toward characterization of various silicon-sheet materials, material-device property interaction investigation, and measurement techniques. The program of the Task is structured accordingly.

The program of the Task also includes JPL in-house activities to conduct basic research in materials and devices characterization to support contractor needs and other Tasks of the Materials and Devices Area.

SUMMARY OF PROGRESS

Cornell University

The objective of this contract is to characterize the structural, chemical, and electrical properties of silicon sheet material in as-grown and processed forms.

Research has been concentrated on understanding the disappearance of EBIC contrasting of grain boundaries and dislocations when EFG material is preannealed at high temperatures before the formation of the p-n junction. It is believed that the disappearance of electrical activity at these structural defects is caused by the formation of competing gettering centers. The most likely process leading to the formation of these competing gettering centers is the precipitation of carbon, which has not been studied as a means of gettering electrically active impurities. In solar materials, precipitation of carbon offers an alternative to gettering by oxygen precipitation. Carbon-based gettering should be particularly effective for those transition metals that are strong carbide formers.

Applied Solar Energy Corp.

Work has continued on refining the calibrated light-spot scan system and applying it to silicon solar cells made from the HEM, Silso, and UCP cast silicon materials. The quality of the material and the influence of grain boundaries in various parts of these materials is being studied by this system.

MATERIALS AND DEVICES RESEARCH AREA

Cell fabrication and analysis on cells made using silicon ribbons obtained from different sources is continuing.

C. T. Sah Associates

The barriers to achieving high-efficiency silicon solar cells have been considered and analyzed. They include: (1) recombination in the bulk emitter, base and back surface field layers at the point impurity and defect centers, their enhancement due to heavy doping, and interband recombination; (2) recombination at the interface states on the front and back, and at the metal (Si and SiO_2) Si interfaces; and (3) recombination at gross imperfections on the damaged cell perimeter or edge and in the bulk.

Research Triangle Institute

Development of phenomena submodels have been completed and incorporated into the transport equations for computer simulation.

The major point of departure of the modelling program is the analytical method used to analyze physical systems. To obtain an accurate representation of a physical system, the geometry is discretized into mesh points. In a one-dimensional geometry, the segments are defined by a series of parallel planes. The segments may be taken as then as required to obtain the accuracy desired. The differential equations, governing the behavior of the physical system, are applied to each segment, and a closed-form solution is obtained in each of the segments. If the boundary conditions at each of the planes defining the segments are known, then there exists a recursion relationship between the constants of integration of the solutions obtained in each segment.

This method has been applied to semiconductor devices and has been shown to give excellent agreement between computer simulation and experimental data.

University of California at Los Angeles

The technique of molecular-beam epitaxy (MBE) in silicon is still in the developmental stages. A procedure has recently been developed at UCLA for growing expitaxial layers with the high doping density necessary to form a tunnel junction between two solar cells. The mobility in these films is close to the bulk value. Mesa diodes fabricated from these films show poor reverse characteristics. Typically, the breakdown voltage is 70% of the predicted value but the leakage current is high ($>0.5\ \mu A$ for 20-mil-diameter diodes at -0.5 volts). It is suspected that the poor electrical properties are caused by the presence of carbon at the interface.

Two solar cells fabricated from the MBE-grown samples have efficiencies of 4.7% at AM1.5. This is significantly better than previous samples.

The sharpness of profiles grown using MBE means that simple models using the abrupt junction approximation are applicable. Computations indicate that the cascade cell may be significantly more efficient than a single cell as long as there is no large recombination of carriers at the tunnel junction. Calculations show that the open-circuit voltage for the cascade cell could be >1 V.

University of Florida

A mathematical method that systematically and compactly describes response to transient excitation of various types has been partially developed. This method enables comparison among all existing transient measurements for a wide variety of different solar cell designs, and it clarifies the inaccuracies resulting from many experimental techniques in wide use. Led by the mathematical treatment and related physical theory. the results obtained have been examined by a method apparently not used much before, using short-circuit current response after removal of applied forward voltage.

University of Pennsylvania

The calibrated light-beam-induced current (LBIC) method has been perfected and microcomputer solar cell modelling has been extended to include multilayered regions as well as the p-n junction space charge region and the base region in addition to the front region. The multilayer feature has been successfully applied to structures with varying doping profiles, using impurity concentration data obtained from spreading resistance profiles, and corresponding mobility values. Good fits between the measured LBIC data and the modelled spectral collection efficiencies could be obtained by using the impurity profile data, where such fits had not been obtained previously by single layer modelling. Devices with front-layer thicknesses of 100 μm, 40 μm, 2 μm, and 0.3 μm were evaluated for surface recombination velocity and minority carrier lifetime.

Ion-implanted solar cells with oxide-passivated surfaces were obtained and performance by the spectral LBIC method before and after removal of the oxide layer showed a substantial increase of the surface recombination velocity upon removal of the passivation.

The method has recently been applied to the analysis of base regions, and the minority lifetime in the layer between the high-low junction and back contact has been determined, as well as the lifetime in the principal, less heavily doped base layer.

University of Southern California

The cryogenic calorimeter has been constructed, and initial performance tests are in process. Theoretical studies have been carried out in parallel with experimental work, in preparation for planned measurements of deep-level

impurity absorption at near-IR wavelengths. Room-temperature calorimetric measurements have been made on pure silicon in the near-IR as part of an effort to determine background absorption present.

University of Washington

A plasma-enhanced chemical vapor deposition (PECVD) system has been assembled and is being used to grow silicon nitride films on silicon substrates. The system is based on a plasma etcher, which has been modified for plasma-assisted chemical vapor deposition. In this capacitively-coupled parallel plate system, substrates are supported on the grounded electrode, which can be heated to 350°C. Process gases enter the reaction chamber below the grounded electrode, flow radially inward between electrodes, and exit through an exhaust at the center. To induce the deposition reaction, a 30-kHz RF glow discharge is established between the electrodes at power densities up to 8000 W/m^2. For SiN deposition the reactant gases are silane and ammonia. Initial efforts have concentrated on relating film deposition rate and index of refraction to growth parameters.

Optical constants are being determined for silicon nitride films and are being related to film growth parameters. Films grown on silicon substrates are characterized by measuring the reflectance for wavelengths between 300 nm and 1200 nm. These data are used to calculate index of refraction (N) versus wavelength, and film thickness. To date, films grown on silicon exhibit indices of refraction in the range of 1.9 to 2.25. Work is in progress to determine both N and K versus wavelength. These results will eventually be used to calculate photon transmittance into silicon.

The Si-N/Si interface will be characterized for films grown on both p-type and n-type silicon substrates, as well as on silicon n-p solar cells. Interface properties of interest are the fast-state density, fixed charge and surface recombination velocity. Capacitance-based measurements will be used to determine fast-state density and fixed charge. Approaches to measuring surface recombination velocity are under consideration.

PROCESS DEVELOPMENT AREA

INTRODUCTION

The objective of the Process Development Area is to conduct research in critical technology areas of conventional photovoltaic device and module formation. Process research is grouped into three areas for reporting convenience: surface preparation, junction formation and metallization.

SUMMARY OF PROGRESS

Process research efforts have continued with an increased emphasis in investigation of new energy technologies. Three new contracts were awarded: two for new energy technologies, one for junction formation. Two new technology reports and one patent application were submitted.

Two major items of research equipment were installed during the reporting period, prompted by the emphasis on higher cell efficiency and increased module reliability.

Surface Preparation

A no-cost contract was awarded to Solec International to investigate application of antireflective (AR) coatings by roller coating. JPL laboratory facilities will be used by Solec. Results will be published.

Junction Formation

Westinghouse Electric Corp., Advanced Energy Systems Division, has demonstrated simultaneous front and back dopant profiling using liquid dopants in both belt and diffusion furnaces. However, cross-contamination continues to be a problem. Different oxide diffusion masks are being evaluated to solve this problem.

Solarex Corp. has completed its polycrystalline silicon material contract. Cell surfaces were characterized by fabricating 400 minicells on each wafer. When wafers from different manufacturers were compared, some similarities were found: polycrystalline cells always have lower open-circuit voltage than Cz control cells: excess data scatter correlates with shunting inclusions; there is a strong correlation between quasineutral recombination and electrically active grain and subgrain boundaries.

Metallization

Metallo-organic decomposition (MOD) inks and liquids have been formulated by Purdue University. Silver neodecanoate is the most promising material, but other metals, solvents and rheology adjusters are being examined. Material purity has surfaced as a major limitation.

PROCESS DEVELOPMENT AREA

The importance of viscosity measurement for characterization and process control of thick-film inks was brought out by Electrink, Inc. A need for proper measurement technique and data interpretation was reported.

Diffusion-barrier research by Caltech is moving into exploration of interfacial reactions between the barriers and underlying substrate material or overlying metals. Ten technical papers were published as a result of this research.

A new research tool, real-time scanning electron microscopy, was used to examine the controlled-atmosphere firing of the molybdenum-tin thick-film system. This novel approach shows great promise in interpretation of sintering phenomena. Spectrolab, Inc. used this tool to determine that the tin does not act as a liquid-phase sintering medium.

PROJECT ANALYSIS AND INTEGRATION AREA

INTRODUCTION

The objective of the Project Analysis and Integration Area (PA&I) is to support the planning, analysis, integration, and decision-making activities of FSA. Accordingly, PA&I supports the Project by developing and documenting Project plans based, in part, on the technical and economic assessments of the various technical options performed by PA&I. Goals for module technical performance and costs, derived from National Photovoltaics Program goals, are established by PA&I for each of the major technical activities in the Project. Assessments of progress toward achievement of goals are performed to guide decision-making within the Project.

SUMMARY OF PROGRESS

Analysis of Losses in a TCP-Coated Solar Cell

PA&I, in cooperation with the Reliability and Engineering Sciences Area, has developed a computer program to aid in the analysis of the power losses found in a transparent conducting polymer (TCP)-coated solar cell due to the optical and electrical properties of the TCP. The program is used to calculate the short-circuit current density (J_{SC}) when a silicon cell is coated by a TCP. The TCP film properties affecting light transmission, and consequentially J_{SC}, are thickness, index of refraction, and absorptivity. The effect of the conductivity of the TCP will be investigated by calculating its sheet resistivity at varying thicknesses and the combined sheet resistivity of the TCP on a standard silicon cell.

Expected power losses will be calculated using J_{SC} and combined sheet resistivities while varying the TCP properties. A parametric study of the power losses versus TCP properties will assist in the search for a TCP that will have the least possible losses.

Silicon Cost Analysis

A report titled "A Probabilistic Analysis of Silicon Cost" (JPL Document No. 5101-246, JPL Publication 83-94), summarizing the results of a silicon cost study, has been published.

Silicon material costs represent both a cost driver and an area where improvement can be made in the cost of manufacture of photovoltaic modules. This study analyzes the cost of three processes for the production of low-cost silicon that are being developed within the National Photovoltaics Program. The costing approach is based on probabilistic inputs and makes use of two models developed at the Jet Propulsion Laboratory: SIMRAND (SIMulation of Research ANd Development) and IPEG (Improved Price Estimation Guidelines).

PROJECT ANALYSIS AND INTEGRATION AREA

The costing approach, assumptions, and limitations are detailed in the study along with a verification of the methodology. The results are presented in the form of cumulative probability distributions for silicon cost. These results indicate that there is a 55% chance of reaching the DOE target of $16/kg for silicon material. This is a technologically achievable cost based on expert forecasts of the results of ongoing research and development and do not imply any market prices for a given year.

Photovoltaics System Sensitivity Analysis

Work is in progress on a PV system sensitivity analysis. This work focuses on the impacts of system parameters on allowable flat-plate module cost and efficiency. Flat-plate tracking, BOS efficiency, area-related BOS cost, capital cost, module efficiency, O&M costs, indirect costs, and insolation parameters are varied to determine allowable module cost. Early results of this work were presented at DOE in January, and changes in several values that are used to derive FSA goals were recommended.

A presentation in the Plenary Session (see Proceedings) describes the status of these deliberations on flat-plate module goals.

Comparisons of Costing Techniques

Since the last PIM, an opportunity arose to compare a Japanese costing methodology for amorphous silicon manufacturing with the IPEG2 model of SAMICS. Capital costs were treated differently in the two models, leading to significant differences in cost estimates for strongly capital-intensive processes. Using the Japanese methodology, typical manufacturing cost estimates will be lower than SAMICS results, due to the omission of return on equity investment and income taxes in those estimates. Because the overhead in the Japanese method was proportional to operating cost, these estimates were lower than SAMICS by 80% (1-megawatt case) to 60% (100-megawatt case). This illustrates why a costing standard is important, and why it is necessary to understand the underlying costing methods when estimates are compared using different methods.

ADVANCED PROCESSES AREA

Amorphous Silicon Task

INTRODUCTION

The objective of the Amorphous Silicon Deposition Task is to determine the key parameters to be used in large-area deposition-chamber designs. The approach is to explore the multidimensional "parameter space" of a-Si deposition using a highly flexible learning apparatus to approximate optimal combinations. Generic data generated by this procedure will be applicable to deposition chambers being designed in the PV industry.

SUMMARY OF PROGRESS

A large (30-in. diameter x 54 in. long) vacuum chamber has been furnished with a fixture (box) containing large (15 x 15 in.) electrodes for depositing silicon by plasma-assisted chemical vapor deposition. The chamber has been fitted with an oxidizing exhaust treatment device that conditions the effluent before exhausting it into the atmosphere.

Several experiments have been performed to determine the parameters influencing electrode stability and uniformity of deposition. With the aid of SERI, the apparatus has produced a-Si depositions from pure silane that have good uniformity and resistance to peeling (passes the standard Scotch tape test). With the apparatus now functioning, parametric experiments will begin.

Advanced Processes Task

INTRODUCTION

The objective of the Advanced Processes Area is to investigate processes that are advanced beyond the state of the art and can be viewed as next-generation technologies.

Advanced Processes include those high-risk areas associated with the formation of next-generation photovoltaic devices and modules or the use of new, high-risk process technologies.

SUMMARY OF PROGRESS

Process research efforts have continued with an increased emphasis in investigation of new energy technologies. Two new contracts were awarded: one each for laser-assisted metallization and thin-film deposition.

ADVANCED PROCESS AREA

Junction Formation

Spire Corp. completed its investigation of ion implantation and annealing of non-Cz silicon sheet materials. There were significant differences in the response of different materials to identical processes. Selection of the appropriate annealing cycle can enhance performance of many materials.

Metallization

Laser-assisted electroplating of copper was successfully demonstrated by Westinghouse Electric Corp., R&D Division. Lines as thin as 25 micrometers were applied at a local plating rate of 12 micrometers per second. This system is not optimized, so narrower lines and higher rates are probably possible. Laser pyrolysis was used to define some lines on silicon with spun-on silver neodecanoate as the metal source. Laser photolysis research has been delayed due to environmental considerations and may be deferred due to process cost consideration.

Thin Films

A new contract has been signed with Superwave, Inc. Santa Clara, Calif., for microwave-enhanced deposition of thin films. Better control and lower process energy costs are possible benefits.

RELIABILITY AND ENGINEERING SCIENCES AREA

INTRODUCTION

The objectives of the Reliability and Engineering Sciences Area are to develop the reliability-durability technology base required to achieve 30-year-life flat-plate photovoltaic modules and to develop the engineering sciences base required to integrate low-cost cell and module technologies into cost-effective and safe arrays that meet the operational requirements of future large-scale applications. Elements of the first objective include failure mechanism identification and understanding; module reliability prediction tools; test, measurement and failure analysis technologies, and 30-year-life materials and designs. Elements of the second objective include operational and safety requirements, electrical and fire safety technologies, structural design technologies, temperature control technologies, and electrical circuit technologies.

These items are addressed in the context of the DOE Five-Year-Plan and are reported herein in a structure corresponding to the organization of the Plan.

SUMMARY OF PROGRESS

Materials Research: Testing of Thin-Film Cells and Modules

Researchers at Clemson University and at JPL are working with samples of amorphous-silicon cells supplied by Chronar Corp. and ARCO Solar, Inc., to set up a performance measurements baseline for use with amorphous-silicon cells and modules.

An RFP has been prepared for the purchase of thin-film modules, and is being issued to five potential suppliers of amorphous-silicon and other thin-film modules for the procurement of a sampling of modules to be subjected to performance measurement and environmental testing. The objective is much the same as that for the Block I procurement in 1976: to determine the problems posed by thin-film module fabrication, to establish a basis for performing measurements, and to assess the status of the industry.

Collector Research: Advanced Module Development

As a first step toward a high-efficiency module, a contract has been signed with Spire Corp. to develop a module with an efficiency of 12% to 13% at NOCT. The module design has been completed and cell processing experiments are nearly completed.

A design team has been assembled to initiate activities on the 12%-efficient $\$100/m^2$ module development. The effort is proceeding toward specifying a strawman design as a basis for developing a procurement plan. A study of the tradeoff between efficiency and $\$/m^2$ is in progress to support selection of module design characteristics.

Systems Research: Module Reliability

Reliability and Physics Studies

1. Reliability and Durability of Electrical Insulation

The aging deterioration of organic insulation materials subjected to long-term electrical stresses is extremely complex, and in an outdoor environment, thermal, mechanical and chemical actions may be simultaneously ongoing in an electrically stressed material; this may further contribute to insulation breakdown. Other mechanisms that can lead to electrical breakdown of organic insulators can originate in manufacturing defects (voids, cracks, etc.) and/or ionic impurities (electrochemical effects), and from aging such as delamination, mechanical generation of cracks, and chemical generation of ionic components.

With a view toward electrical insulation stability, advanced elastomeric encapsulation materials are being developed to be intrinsically free of in-situ ionic impurities, have ultralow water absorption, be weather-stable (UV, oxygen), and have high mechanical flexibility. Despite these positive efforts toward improving insulation durability and reliability, a capability of predicting the service life of organic insulation materials is not yet a realized technology.

Recently, however, Spectrolab, Inc., developed a computer program to model the level of electrical field intensities and stresses associated with the geometries of encapsulated solar cells. This was part of the FSA technical program related to accelerated aging of encapsulation pottant materials, and it was desired to have knowledge of typical electrical stress levels to which pottants would be subjected in service.

An analysis of the Spectrolab computer data led serendipiditously to an unexpected finding related to the dielectric strength of electrical insulation materials. In essence, it appears that a fundamental definition of an intrinsic dielectric strength of insulation materials has been identified, which could be stated as a basic material property independent of any test technique or service environment. This is similar to other pure material properties such as Young's modulus, index of refraction, and coefficient of thermal expansion.

Future work will endeavor to validate experimentally this new dielectric strength concept, as part of experimental programs related to electrical stress aging.

2. Electrochemical Corrosion Research

Electrochemical corrosion characterization research continues with investigation of the degradation mechanisms of different metallization systems and system interactions with different

encapsulant polymeric materials. A series of in-house tests subjected two-cell minimodules to 85°C/3% RH, 85°C/70% RH and 85°/C98% RH continuous exposures for 2000 h (83 days). Test samples included EVA, PVB and RTV encapsulation of various solar cells with Ti-Pd-Ag, printed Ag and Ni-solder contacts. All minimodule samples were aged under forward-voltage bias during the constant environmental tests. Data obtained from the tests, including I-V histories, cell capacitance, leakage current, series resistance and corona-inception voltage, are being reduced to formulate a life-prediction methodology. Another series of tests was initiated in January for 60°C/70% RH, 60°C/40% RH, 60°C/3% RH and 85°C/40°C constant environments to provide lower-bound data for the life-prediction methodology using the encapsulant and metallization varieties noted above. A study of the data from these tests is providing a clear understanding of the physics of corrosion mechanisms.

3. Reliability and Durability of Bonding Materials

J. Koenig has developed the laboratory techniques necessary to interrogate the chemistry of the interfacial[5] chemical bond between EVA and glass directly. This recent accomplishment was reported at the 23rd PIM, at which he also showed first-ever infrared spectra of the interfacial chemistry. Some minor laboratory details remain to be completed, after which it is planned to monitor chemically the interface of an EVA-glass specimen that will undergo exposure to accelerated aging.

Separately, J. Boerio has also achieved laboratory capability to interrogate directly the chemistry of the interfacial chemical bond between EVA and aluminum. Once a good EVA-aluminum bond is achieved, accelerated aging studies will begin. Boerio also intends to examine combinations of EVA-solder and EVA-nickel.

4. Photothermal Degradation Research

In-house photothermal degradation research has been divided into understanding the mechanism of degradation by monitoring and characterizing key intermediates, and generating a data base by carrying out accelerated photothermal aging of material specimens to validate the proposed mechanism.

Two key chemical intermediates of polymer photothermal degradation outdoors have been identified as peroxy radicals and tertiary carbon radicals. Because of the short-lived nature of these radicals, all previous studies were carried out at low temperature, 77K. A laser-flash electron spin resonance (ESR) experimental apparatus, capable of detecting photothermally generated, short-lived radicals in situ, has been set up at JPL. Peroxy and tertiary carbon radicals have been detected at room temperature, in a polymeric

medium, for the first time. Studies of temperature dependence of the kinetics of these radicals are being conducted. Preliminary data indicate that extremely short-lived radicals can also be monitored at 100°C. Their decay rates will provide data on the analytical relationship between degradation rate and magnitude of key stress variables, such as UV, O_2, and temperature.

Accumulation of data on photothermal aging of material specimens is being continued. Material properties are monitored as functions of photon flux, temperature and time. Exposure at a 6-sun UV level has been completed and exposure at a 3-sun UV level is being done.

Efforts are continuing at the Polytechnic Institute of Brooklyn to synthesize various derivatives of 2 (2-hydroxyphenyl) 2H-benzotriazole by condensation of the diazonium salt of 4-methoxy=2=nitroaniline, to prepare a new and more permanent ultraviolet stabilizer.

Recent modeling studies by the University of Toronto suggest that the best way to stabilize a polymer against outdoor degradation is to dissolve an additive (in very low concentration) that can trap peroxy radicals and also decompose hydroperoxide. The model can now take into account one time-temperature variation. The useful lifetime (5% oxidation) of an unstabilized polyethylene, for example, is predicted to vary from a few months in hot weather (100°F) to almost two years in cool weather (45°F). Preliminary attempts have been made to monitor the model predictions regarding stabilization and the possible failure mechanisms: wrinkling embrittlement due to scission and/or crosslinking, discoloration and other effects due to buildup of unsaturated groups in the polymer.

Exposure of encapsulation materials on outdoor heated weathering racks is continuing at Springborn Laboratories, with emphasis on monitoring the kinetics of stabilizer loss.

5. Reliability Prediction and Management

Two presentations summarizing the overall status of module reliability from both mechanisms and circuit-redundancy perspectives were presented at the 23rd PIM. A paper including these data is to be presented in a plenary session at the IEEE Photovoltaic Specialists Conference in May. The present work updates the reliability goals for 13 principal failure mechanisms and defines the research status of each. Detailed life-prediction modeling efforts are nearing completion on electrochemical corrosion, and are being initiated on photothermal degradation.

RELIABILITY AND ENGINEERING SCIENCES AREA

Module and Array Engineering Sciences

1. Circuit Analysis and Degradation Quantification

A computer program was developed to determine the power loss due to shorted cells for a given source-circuit series-parallel configuration after N years with a constant yearly failure rate. The completion of this program satisfied the February milestone requirement to have circuit analysis tools for shorted cells operational. In addition to completing the program, the following tasks were completed and reported upon at the PIM: (1) the optimum series-parallel configurations for minimizing power loss for shorted cells were determined; (2) the cost-effective failure level for shorted cells was determined.

The conclusions reported at the PIM were: (1) the power loss due to shorted cells increases with increased use of paralleling and cross ties; (2) yearly failure rates greater than 1/10,000 lead to power losses in excess of the allocation for cell failures.

2. Operating Temperature Characterization of Roof-Mounted Arrays

The ongoing activity has concentrated on evaluating the influence of environment on module thermal performance. The emphasis was placed on reducing uncertainties involved in NOCT testing and analytical predictions. Preliminary results were presented at the 23rd PIM. A refined methodology to take into account changes in ground reflection, ground IR emission and sky radiation was established. It was demonstrated that the uncertainty band can now be reduced to around $1^{o}C$.

Work is also under way to simplify the procedure for determining the NOCT of a solar-cell module. This work, which is supported by the environmental test activity, indicates that adequate accuracy of measurement of NOCT can be obtained using techniques in which comparative measurements are made on a module and a reference plate.

3. Hot-Spot Heating with Complex Series-Parallel Source Circuits

Hot-spot testing was completed on a panel consisting of SMUD ARCO Solar, Inc., modules installed at the JPL test site. The tests provided data relating the degree of hot-spot heating to the following parameters: types of shadow conditions; back-bias power dissipated; module series-parallel configuration, and level of current imbalance. The data are being used to develop guidelines for future testing of modules to determine hot-spot susceptibility in central-station applications where multiparallel cell strings are prevalent, leading to a risk of current imbalance and severe

hot-spot heating. This information, along with guidelines for circuit design strategies to reduce the risk of hot-spot problems, will be presented in a paper at the IEEE Photovoltaic Specialists Conference in May.

4. Bypass Diode Integration Studies

The draft of the General Electric Co. final report on the integration of bypass diodes in photovoltaic modules and arrays is being reviewed. A major issue is an order-of-magnitude price difference for field-installed diode packages as determined by different organizations. Discussions with GE, Hughes Aircraft Co., and ARCO are progressing to resolve the issue.

5. Module Flammability Research

In collaboration with ARCO, a series of burning-brand tests was performed on experimental modules using high-temperature, back-surface materials and improved module construction techniques. The purpose was to learn how different back-surface materials were affected and whether module construction techniques might effect greater resistance to flammability for hydrocarbon resin-potted PV modules.

Five types of materials were evaluated: Kapton aromatic polyamide film, two kinds of woven fiberglass cloth, Neoprene rubber (as both a molded sheet and a latex coating), stainless-steel foil and aluminum foil. The aluminum was tested as part of a four-layer composite. Where the flame-resistant layer was either an electrical insulator or was electrically isolated from the PV circuit, the material was configured as a substitute back cover as well as an add-on layer over ARCO's present back-surface material. Two different adhesives, a thermosetting type (TS) and a pressure-sensitive type (PS), were tested for bonding the additional flame-proof materials to the standard back cover.

Results of the tests indicate that the more promising configurations include softly bonded Kapton; non-wettable (by EVA), densely-woven fiberglass; highly crosslinked Neoprene sheet or latex compounded for maximum flame retardance; stainless-steel foil (2-mil); and thick (1.0 mil) aluminum foil. These configurations will be subjected to Class B and Class A spread-of-flame tests and Class A burning-brand tests in the third quarter.

RELIABILITY AND ENGINEERING SCIENCES AREA

Module Performance and Failure Analysis

1. Solar-Cell Parametric Reliability Testing

During the second quarter of fiscal year 1984, FSA conducted four different types of cell parametric reliability testing with a contractor, Clemson University. At Clemson, the following four testing activities are under way on encapsulated and unencapsulated cells.

a. Real-Time Rooftop Testing

Individual cells were placed in specially designed cell holders and exposed to a real-time, outdoor rooftop environment. Results indicate differences between cell types relative to whether or not they are encapsulated and to various metallization types.

b. Water-Exposure Test

Individual cells were placed in the pressure-immersion-temperature test chamber at the U.S. Coast Guard R&D Center Center in Groton, Connecticut. Test results are still being analyzed, but initial review seems to indicate that water exposure of cells is less degrading than humidity exposure. Analysis of data is expected during the next reporting period.

c. Arrhenius-Type Temperature-Humidity Testing

Cells are being exposed in two separate series of temperature-humidity accelerated-stress tests. The two series of temperature-humidity tests are at 80°C/85% RH and 93°C/85% RH. Early indications are that the degradation rate of cells exposed to the higher temperature-humidity combination (93°C/85% RH) will be higher. A somewhat similar test with higher humidity, at constant temperature, is still under way; it includes several different cell designs and materials.

d. Schottky Barrier Formation Failure Analysis

In addition to cell testing, Clemson is involved in failure analysis of cells. One potential cell failure mechanism found in accelerated stress testing of p-on-n cells is Schottky barrier formation on the back-side contact. Papers on this work have been presented at a JPL seminar and at the 23rd PIM, and will be presented at the IEEE Photovoltaic Specialists Conference in May.

2. Module Parametric Reliability Testing

The development of humidity degradation rates continues for generic module designs, based on comparisons of humidity testing cycles and humidity-temperature data from SOLMET weather tapes. Blocks III and IV minimodules subjected to endurance testing at Wyle Laboratories in environments of 85°C, 100°C, 85°C/85% RH, 85°C/70% RH and 40°C/93% RH test levels are undergoing analysis at JPL; test data will be used in determining module degradation-rate curves for various failure mechanisms. Minimodules tested in the 85°C/85% RH environment were returned to JPL in January for failure analysis and data reduction. Procurement of Block V minimodules was completed, providing recent EVA designs for parametric testing.

3. Module Environmental Testing

The environmental test activity has continued with the testing of Block V modules, both Group 1 and Group 2, and commercial modules of the same period as Block V. Testing of the Block V Group 1 modules, which included ARCO, GE, MSEC, Solarex Corp. (two types) and Spire Corp., is complete except for the large-cell Solarex modules and the Spire modules. Solarex has yet to complete the 200-cycle temperature test and Spire modules for hot-spot and 200-cycle tests have not been delivered. Tests of the Group 1 commercial modules "like Block V" obtained from ASEC, Photowatt International, Inc., Solavolt International and Solenergy Corp. have been completed. Group 2 modules from ARCO and ASEC are nearing the end of the Block V testing sequence.

Results of environmental testing performed during this period:

Vendor Code	Quantity	Test	Results
US4Q	4	Twist	Satisfactory
US5P	4 4 4 1	T-50 HF-10 M-10K HS-100	Discoloration (corrosion) of grids, interconnects, buses; also metals in J-box. Slight warping of J-box covers. One of three cells got hot, had a slight yellow stain, and changed electrical properties. Module power was essentially unchanged.
BM2H	4	M-10K	Satisfactory
BM2H	4	Twist	Satisfactory
BD24	10	Hi-pot/ Cont'y	Improved modules submitted for retest of interconnects. Four of the 10 failed the continuity test.

RELIABILITY AND ENGINEERING SCIENCES AREA

Vendor Code	Quantity	Test	Results
	2	T-50	Satisfactory.
LS5H	4	HF-10	Some delamination 4 modules:
	4	M-10K	1, 1, 5, and 6 cell cracks respectively. 5 x 10 cm delamination 1 module.
	4	HL-1.0	Satisfactory except another module of the 4 has marginal electrical degradation.
LBMH	1	HS-100	One cell suffered 11% power loss, 2 others satisfactory. Cell with loss cracked, probably by handling in test.
LBOH	4	Twist	Satisfactory.
		HL-1.0	Electrically OK.
B2OH	4	M-10K	Satisfactory.
	4	Twist	Satisfactory.
YS4Q	4	Twist	Satisfactory.
YS5H	1	T-200	Electrical degradation 8%, visual OK.
	4	Twist	Satisfactory.
	4	HL-1.0	Electrically satisfactory.
YL5H	6	T-50	Bus bars at one end twisted, intermittently shorting out the diode. Cells sagged and touching. Electrical failure after mechanical cycling.
	1	HY-100	Satisfactory.
BR2H	6	T-50	Backside wrinkled, all modules.
BQ4H	6	T-50	Serious delamination at frame seals near terminals at one end.
	4	HF-10	Tedlar shrinkage, loose terminal housings.
	1	HS-100	Satisfactory.
BFOJ	4	M-10K	Small glass crack in a corner, splits
	4	twist	in white Mylar.

RELIABILITY AND ENGINEERING SCIENCES AREA

Vendor Code	Quantity	Test	Results
SP5H	4	T-50	Back-surface delamination of areas near terminals extending as long as 20 cm and generally involving several cells.
	4	HF-10	
	4	M-10K	
BW0H	2	T-200	Interconnect fatigue, weld separation (see failure analysis).
	4	M-10K	Satisfactory.
	4	Twist	Satisfactory.
	1	HS-100	Satisfactory.
BX2H	6	T-50	Backside wrinkling and delam at sides, J-box and covers warped, all modules.
	10	Hi-pot/	Hipot satisfactory. Frame continuity: failed.
	2	T-200	Satisfactory.
BX3H	3	Cont'y	One module of 3 failed despite new-style grounding bracket.
BX3J	10	Cont'y	New modules submitted with additional frame bonding strap. Modules passed.
BE0H	6	T-50	Discoloration of grid lines. Electrically satisfactory.
	2	T-200	Grids, interconnects and buses discolored, back surface wrinkles.
	4	HF-10	Extensive delamination at module edges, sometimes extending from frame seal to cells.

Notes:
- T-50 = 50 thermal cycles, -40°C to = 90°C
- T-200 = 150 additional thermal cycles
- HF-10 = 85°C/85% RH, 20 h, then -40°C 0.5 h, 10 cycles
- M-10K = 10,000 cycles at ±2.4 kPa mechanical loading
- HS-100 = 100 cycles of 3 cells, hot day, reverse bias, worst condition
- HL-1.0 = 25-mm hailstones at 52 mi/h
- Twist = Mounting surface non-planarity of 20 mm/m
- Hi-pot = 3000 V for 1 min
- Cont'y = Current of 2 x I_{sc} through metal frame elements.

4. Module Field Testing

Daily data collection at the JPL field test site was discontinued in January. Final I-V data could not be acquired due to in trumentation and array circuit control failures. All of the current weather and irradiance data that was stored on the hard disk was archived to magnetic tape. The control files that are used to schedule tasks were also stored on magnetic tapes for use should the system be reactivated in the future.

Under these conditions it is estimated that if the system were to be reactivated it would take 40 to 60 hours to get the system back on line and to affect the repairs required in the instrumentation and array control circuits. The latter should be modified if reactivation is considered.

The SMUD-type array-level hot-spot testing was completed. Data were obtained for seven modules that were internally wired in up to five different configurations and shadowed in several ways. The data obtained were given to the Module and Array Engineering Task for analysis. These data consisted of computer printouts of the voltage and currents of each string of cells under test, the array voltage and current, selected cell temperatures, irradiance data and air temperature, all as functions, of time, and detailed temperature data using the infrared camera system.

During this period field-test workers carried the data logger to Florida Solar Energy Center to take I-V curves of the modules installed there for JPL.

5. Electrical Measurement Technology Development

A formal "Procedure for the Calibration of Type II (Secondary Terrestrial Photovoltaic Devices Using a Solar Simulator Filtered to Closely Match Air Mass 1.5 Direct Normal Irradiance" was completed. This will be the governing document at JPL for the calibration of reference cells in a solar simulator until the emergence of an ASTM or other consensus standard. The procedure relies upon direct sunlight calibration of six reference cells of varied spectral response which were calibrated simultaneously in June 1983.

Special measurements on modules or secondary calibrations of reference cells were made for ARCO, Hughes, Solar Energy Research Institute (SERI), Solar Power Corp., Solec International, Inc., and Spire, and a special group of six reference cells was sent to SERI for their calibration exercise in Florida in April. Special modules measured included a Sanyo amorphous-silicon-cell module, a Chronar Corp. amorphous module and a unique module provided by TriSolar Corporation of Bedford, Mass. A calibrated reference cell was lent to Yale University, which is working on high-efficiency inversion-layer cell.

6. Failure Analysis and Reporting

An interesting failure analysis involved a module in which an aluminum bus bar extending across the width of the module grew in length during the thermal cycling and ruptured interconnects welded to the bar. Analysis of the phenomenon ascribes the behavior to interactions involving (1) the superior adhesion between PVB and both glass and aluminum, (2) the glass transition temperature, T_g, of the PVB, (3) the thermal coefficient of expansion of aluminum, (4) the elastic limit of the aluminum, (5) the thermal coefficient of expansion of glass, and (6) the range of the temperature cycle. There is also evidence that relatively pure aluminum may "grow" even during relatively moderate temperature excursions (e.g., $-40^{\circ}F$ to $+120^{\circ}F$) in the absence of externally applied stresses. The analysis points up the need to understand thoroughly the interactions between materials.

RECENT TECHNICAL PUBLICATIONS

1. Fourth Annual Report, Clemson University, October, 1983.

2. "Source Circuit Design Overview," R.G. Ross, Jr., Central-Station Research Forum Proceedings, Sacramento, California, December 5, 1983 (in press).

3. "Hot-Spot Heating in Central-Station Arrays," C.C. Gonzalez, Central-Station Research Forum Proceedings, Sacramento, California, December 5, 1983 (in press).

4. "Electrical Insulation Design Requirements and Reliability Goals," R.G. Ross, Jr., Central-Station Research Forum Proceedings, Sacramento, California, December 5, 1983 (in press).

5. "Lab Experience with Voltage Breakdown," G.R. Mon, Central-Station Research Forum Proceedings, Sacramento, California, December 5, 1983 (in press).

6. "Qualification Testing and Electrical Measurements: Practice and Problems," M.I. Smokler, Central-Station Research Forum Proceedings, Sacramento, California December 5, 1984 (in press).

7. "Hi-Pot Qualification Test Experience," J.S. Griffith, Central-Station Research Forum Proceedings, Sacramento, California December 5, 1984 (in press).

8. "Breakdown of Organic Insulators," E.F. Cuddihy, Central-Station Research Forum Proceedings, Sacramento, California December 5, 1984 (in press).

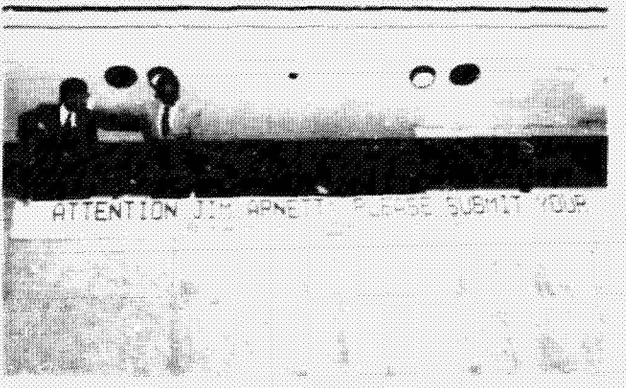

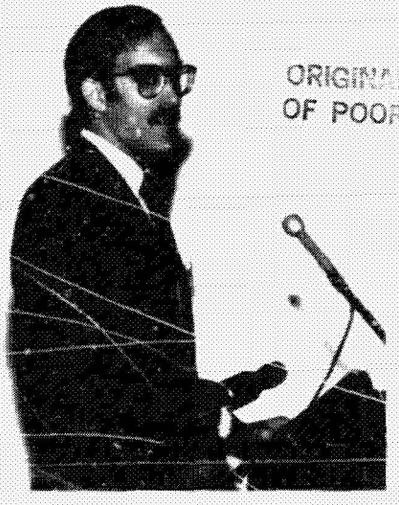

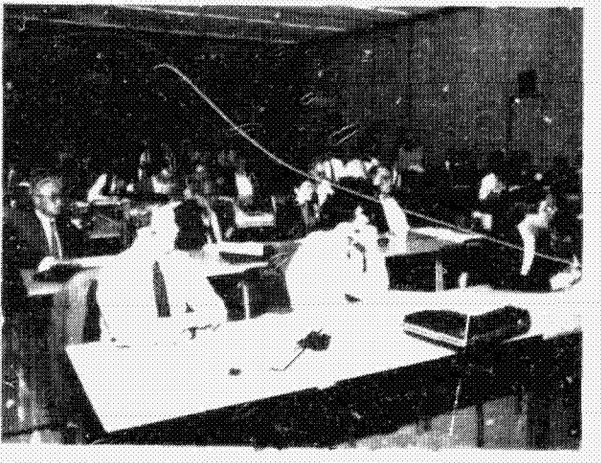

PROCEEDINGS

INTRODUCTION

The 23rd Project Integration Meeting (PIM) of the Flat-Plate Solar Array Project (FSA) of the Jet Propulsion Laboratory (JPL) was held at the Pasadena Center, Pasadena, California, March 14-15, 1984. The PIM theme was "Large Photovoltaic Array Technology and Cost Sensitivities."

In the plenary session on March 14, presentations were made on array cost sensitivities and goals, large-array experience, systems considerations for large arrays, array technology status and research, and technical issues of high-efficiency solar cells. On March 15 a panel discussion of "Needs and Issues: Large PV Arrays" was held.

During the past two years much effort has been devoted to four large PV array designs for central-station power plants and for a large rooftop design. Operational experience has been obtained from two of the plants. Two more plants will go into operation in mid-1984, and a fifth will become operational in 1985. In December 1983 FSA held a research forum on the Design of Flat-Plate Photovoltaic Arrays for Central Stations. As a consequence of these activities, this PIM focused on large-array technology and related cost sensitivites. The advent of large panels integrated into even larger arrays makes it imperative that future modules be designed from an array viewpoint, the future module cost and effeciency goals should be evaluated in a tradeoff of all the factors involved in present and potential PV system cost and performance.

The PIM continues to enable two-way communication between the government and the private photovoltaics community regarding present and future photovoltaic activities. This exchange is required to assess recent progress; to identify, implement, and evaluate the integration of activities; to gain perspective of trends and new developments, and to guide the near-term and long-term planning and adjustment of priorities within the Project.

A summary of plenary-session presentations follows.

Plenary Sessions

SUMMARY

W. T. Callaghan, Manager of the Flat-Plate Solar Array Project (FSA), opened the meeting by welcoming the participants in the Project Integration Meeting (PIM), especially those representing the utilities and utility-related organizations. The encouraging progress and experience gained recently in the use of the flat-plate modules in central-station applications are vital achievements as photovoltaics matures.

Mort Prince, Chief, Collector and Research Branch, U.S. Department of Energy (DOE), presented a short discussion of the Administration's optimistic view of photovoltaics and of continuing strong support in Congress. He noted that DOE considers crystalline silicon technology as a strong contender for photovoltaic (PV) use through this decade, and that he believes that the present shortage of polysilicon is temporary.

A presentation on flat-plate module requirements for meeting National Photovoltaics Program goals was given by R.W. Aster of the FSA Project Analysis and Integration (PA&I) Area. The five-year goal of flat-plate collector research is to establish by 1988 technologies that industry can apply to scaled-up production of modules. The modules should be compatible with a PV system capable of generating power at $0.15/kWh. Module costs are parametric with module efficiencies and with balance-of-system (BOS) costs and efficiencies. Since the 22nd PIM, when a presentation was given on this topic, a subject for work and discussion has been the values to be assumed in performing trade-off analyses: comparisons of module efficiency vs cost requirements for different insolation values and area BOS costs were presented.

A report on progress by ARCO Solar, Inc. in developing module, array, sun tracker, and associated hardware for central-station PV power plants was presented by J.C. Arnett of ARCO. The Lugo (1 MW) plant at Hesperia, California, and the Carrisa Plain (4 3/4 MW) plant in California Valley, California, pioneered the use of two-axis sun trackers for flat-plate modules. Operational experience at the Lugo plant (15 months) and at Carrisa Plain (three months) has shown that they operate well and are reliable. ARCO is also providing the modules and arrays for the first and second phases of the Sacramento Municipal Utility District (SMUD) central-station plant. The modules are integrated into subpanels in a way that reduces manufacturing, assembly, and installation costs.

Progress on the first and second phases of the SMUD central-station PV power plants, which is scheduled to total 100 MW of generating capacity in 1993, was presented by M.R. Wool of Acurex. The first phase (1 MW) of this plant, with single axis tracking arrays, is scheduled to be in operation in mid-year 1984. It is estimated that the installed cost of the first phases will be less than the targeted cost of $12/watt. The lower projected costs for future phases of the plant are encouraging.

A comprehensive presentation on the design and the status of the Georgetown University Photovoltaic Higher Education National Exemplar Facility was presented by G.J. Naff of Hughes Aircraft Co. The 300 kW rooftop

installation on a Georgetown University building in Washington, DC, is expected to be in operation in mid-1984. The complexity of mounting large arrays on a number of roofs of a multistory building and integration of the power system into the building was described. The 2 x 4-ft modules with semicrystalline solar cells are being supplied by Solarex Corp. The modules passed qualification testing at Jet Propulsion Laboratory (JPL).

A summary of the Sandia National Laboratories PV Systems and Applications PIM, held February 14 through 16, 1984, was presented by M.G. Thomas of Sandia. The systems are providing data on long-term performance, reliability, degradation and operation and maintenance. It is essential that there be a comparison of predicted and actual performance to make assessments. Progress has been made in devising advanced-performance power-conditioning systems for both small and large installations. The performance of large utility-connected installations has been acceptable to the utilities.

An overview of electrical circuit design for large PV installations and its influence on array reliability was presented by C.C. Gonzales of the FSA Reliability and Engineering Sciences Area. The objective of these studies has been to determine cost-optimum circuit-design practices that will minimize the effect of component problems on system energy cost. The presentation covered the methodology for developing circuit-design options to control the effects of component failure and mismatch, identification of component failure mechanisms and potential solutions, some examples of design options, and the status of circuit-design efforts. Power losses for various types and frequencies of failures and strategies to reduce losses were presented.

PV array durability for central station applications was discussed by G.R. Mon of the FSA Reliability and Engineering Sciences Area. To achieve 30-year array life, the the array must be designed and fabricated with acceptable power degradation rates, component failure rates and little maintenance. Results of FSA activities in the establishment of durability goals, the identification of key degradation mechanisms, the status of degradation mechanism physics and parametric dependencies, the development of accelerated tests and degradation prediction models, and the identification of cost-effective solutions were presented. Key remaining issues were summarized.

A summary of operation and maintenance (O&M) issues from the Design of Photovoltaic Arrays for Central Stations Research Forum was presented by P.K. Henry of the FSA Project Analysis and Integration Area. Past studies of O&M costs have ranged from $\$2.00/m^2$ per yr to $\$2.50/m^2$ per yr. Based upon present knowledge of failure mechanisms and rates, it is recommended that $\$1.10/m^2$ per yr for fixed arrays and $\$1.40/m^2$ per yr for tracking arrays be used as O&M cost estimates. Better understanding of, and data on, failure mechanisms and failure rates are required to establish better cost estimates. Recently installed large arrays will provide more relevant O&M data than have previous small experimental arrays. Data collection and analysis is a vital requirement.

An overview of the technical issues of high-efficiency crystalline silicon solar cells was presented by K.M. Koliwad, FSA Project Technologist. Establishment of the technologies that industry can apply to the production of 15% efficient crystalline silicon modules is the DOE goal. The production of

sufficiently efficient large-area solar cells using low-cost silicon sheet is beyond the state of the art. The primary barriers that must be overcome are the inadequate quality of low-cost silicon sheet and inherent limitations of state-of-the-art cell structures. Extensive research is required on silicon sheet, understanding device physics and the design and processing of solar cells.

John Day of Strategies Unlimited was chairman of a panel discussion on Needs and Issues: Large PV Arrays. S.T. Carlisle of Southern California Edison (SCE) explained that utility's commitment to renewable energy, including PV. The results of purchases of PV-generated electric power from ARCO Solar Electric Power, Inc. (the Lugo plant) have been good, with no major problems. SCE believes that more and larger PV plants are needed to gain long-range experience. Efficiencies must be increased because of area-related costs. K.M. Matsuda of Pacific Gas & Electric Co. said that array efficiencies must be increased. The utilities want Federal and state tax credits so that they can install large systems now and not wait until PV is totally cost competitive. E.J. Simburger of Aerospace Corp. discussed the needs in five categories: capital-investment criteria, performance characteristics as matched with utility requirements, maturity of technology, the "buildability" of the system, and an accepted standard for gathering and analyzing performance data. M.G. Thomas of Sandia expressed a need for obtaining operation and maintenance experience and costs. Martin Recchuite of ARCO Solar, Inc. stressed the need to continue funding SMUD and continuing the tax credits until the price of PV systems comes down so that large PV systems can be erected during the next few years. R.G. Ross, Jr., FSA Project Analysis and Integration Area Manager, emphasized the need for higher efficiency and higher reliability.

Three presentations were made during the late news period. J.F. Hoelscher of Solarex Corp. briefly described the plans of his company to design, build and operate a central station PV plant at Adelanto, California, near Victorville. J.L. Young of Union Carbide Corp. described briefly the beginning of design work on a 3000 MT/yr polysilicon plant that would become operational in this decade. R. Shoen of RSA Architects described a proposed solar village in the Middle East. There is considerable interest, in a number of countries, in villages using PV.

ARRAY COST SENSITIVITIES AND GOALS

JET PROPULSION LABORATORY

R.W. Aster

Recommended Revision of Parameter Values in the Five-Year Research Plan

	ORIGINAL VALUE	RECOMMENDED VALUE
Research Goal (1982 $/kWh)	0.15	No Change
Fixed Charge Rate	0.18	0.153
Other Financial Parameters		No Change
Indirect Cost Multiplier	1.5	1.5 (includes M&D)
BOS Efficiency	0.81	0.865
Module Efficiency Adjustment (NOC)	–	0.88
Area Related BOS: Fixed	50	50
1-Axis	–	70
2-Axis	–	90
Annual O&M Cost: Fixed	2.28	1.1
Tracking	–	1.4
Insolation (kWh/m^2-yr): Fixed	2365	2250
1-Axis	–	2700
2-Axis	–	3000

The Insolation Issue

It has been recommended elsewhere that the insolation parameter be reduced from 2250 to 1623 kWh/m^2-yr.

This figure is an appropriate average for part of the Pacific Northwest, the Great Plains, along with the Mississippi River, and in the Southeast.

However, the first major utility markets are expected to be in the Southwest. Southern California Edison Co. (SCE) recently announced its intention of purchasing 2150 MW of renewable energy, including 350 MW of solar, by 1992 (Dr. L. T. Papay, V.P., Advanced Engineering, SCE).

The likelihood of meeting PV module goals based on the parameters shown earlier is significant.

The likelihood of meeting goals based on the lower insolation value is negligible, within the schedule given in the Five-Year Research Plan.

PV Module Cost and Efficiency Goals Consistent With 15c/kWh

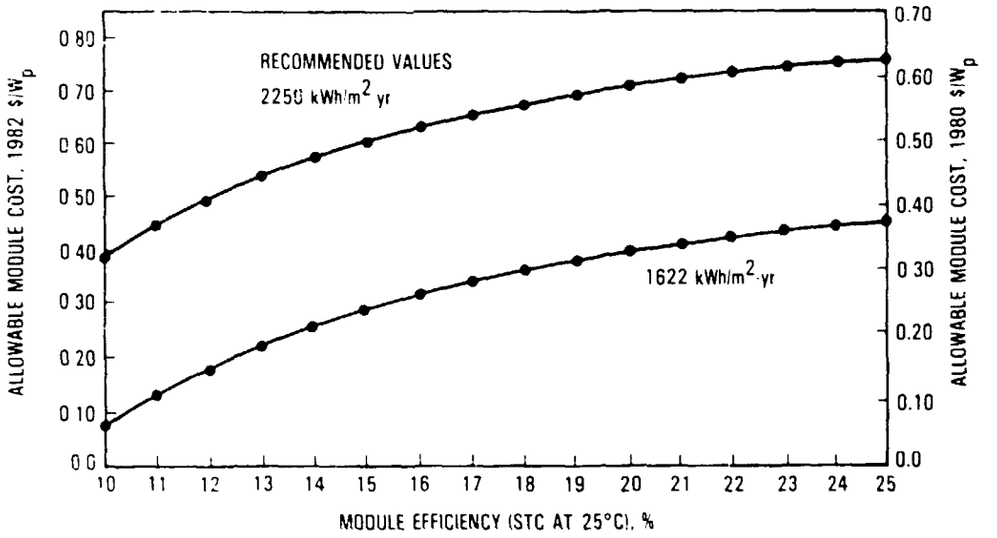

Sensitivity Analysis

A report is being prepared that gives allowable module cost/efficiency curves, given changes in these parameters:

- Annual insolation
- BOS efficiency
- Energy goal
- Area-related BOS cost
- Fixed charge rate
- Indirect costs
- O&M cost
- Fixed, 1-axis and 2-axis tracking

It also describes the change in PV energy cost if the following parameters are changed simultaneously:

- Module cost and efficiency
- Area-related BOS and power-related BOS costs
- Module cost, efficiency, and degradation rate
- Module cost, efficiency, and replacement rate
- Module cost, efficiency, and indirect costs

Sensitivity Analysis Products

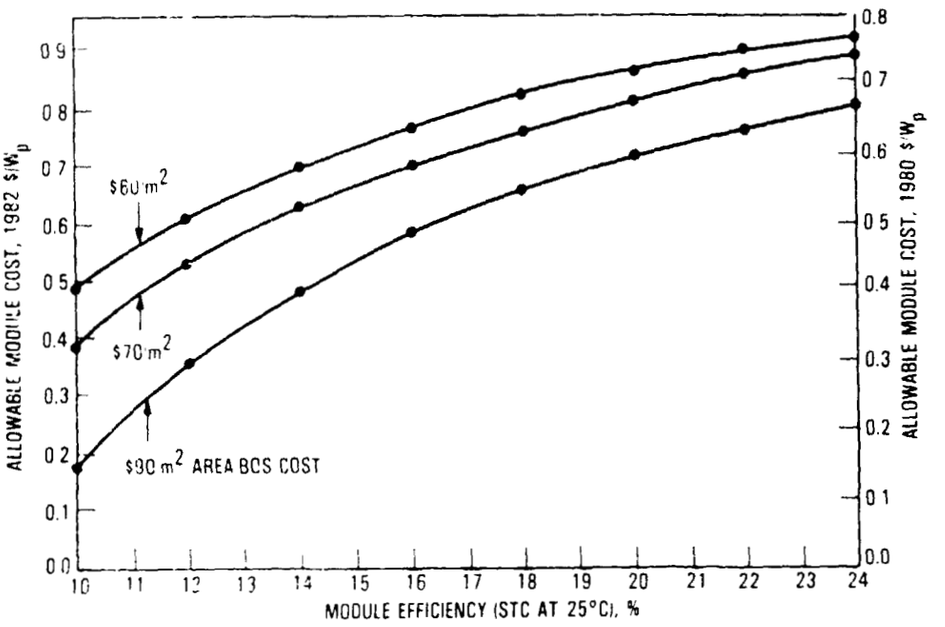

FLAT-PLATE SINGLE-AXIS TRACKING

ACUREX CORP.

M.R. Wool

SMUD Photovoltaic Powerplant Project

Phase	Objective	Year	Size (MW)	Costs (1983 $) ($/Watt)	($M)
I	Technology benchmark and demonstration	1984	1	12	12
II	Develop system design and PV sources	1985	1	10	10
III	Scale up and support PV industry	1987	5	7	35
IV	Quantity purchase to reduce PV cost	1990	20	4	80
V	Complete 100-MW system installation	1993	73	2.5	183
			100		320

System Design Selection

FIRST MEGAWATT

	Energy (GWH)	Power (MW)	Cost ($M)	Relative Cost ÷ Benefit
Flat Panel				
— Fixed structure	2.2	0.63	10.9	1.14
— One-axis tracking	2.7	0.76	11.5	1.00
— Two-axis tracking	3.0	0.78	18.2	1.42
Two-axis Concentrator	2.7	0.74	17.0	1.46

Verification Array Data: Typical Insolation Profile

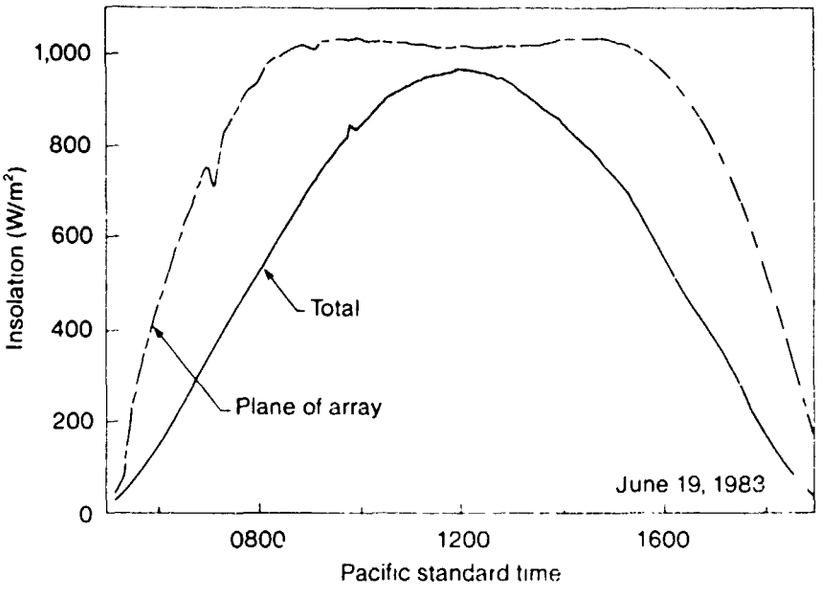

Verification Array Data: Typical Power and Efficiency Profile

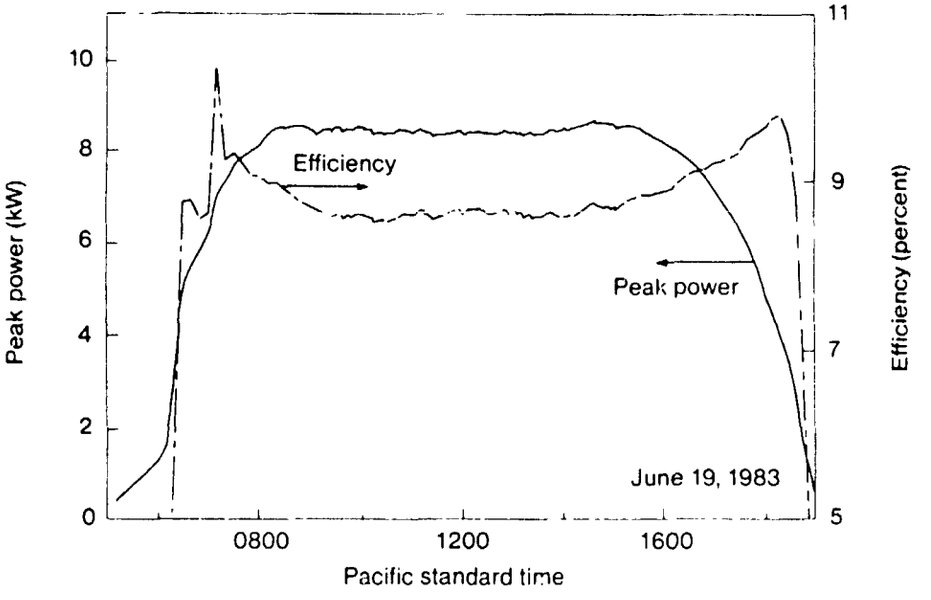

System Cost Reductions

	Costs ($/Watt$_{DC}$) Phase I	Target	Design Approach
Site preparation	0.34	0.15	Allow terrain variations
Foundations and installation	0.45	0.25	Longer span, fewer posts
Panel structure and electrical	0.61	0.22	Unitize panel assembly
Field wiring and power conditioning	0.58	0.34	Standardize PCU, reduce grounding
Startup contingencies	0.15	0.04	Reduce with experience
BOS subtotal	2.14	1.00	
PV panels	5.45	1.55	At 10 percent aperture efficiency
Engineering	2.41	0.15	
Total	10.00	2.70	

SMUD PV Balance-of-System Cost Progress

	SMUDPV1 Actuals	SMUDPV2 Estimate	Target
Site preparation	.34	.15	.15
Foundations and installation	.45	.30	.25
Structure	.37	.28	.18
Array electrical	.24	.04	.04
Field wiring	.16	.15	.15
PCU & control building	.42	.41	.19
Startup	.15	.10	.04
Total $/Watt$_{DC}$	2.14	1.46	1.00

GEORGETOWN UNIVERSITY PHOTOVOLTAIC HIGHER EDUCATION NATIONAL EXEMPLAR FACILITY (PHENEF)

HUGHES AIRCRAFT CO.

G.J. Naff

System Requirements and Parameters Overview

o SYSTEM POWER AT S. O. C.	-	300 kWp
o SYSTEM VOLTAGE	-	480 Y/277V 3 PHASE 60 HZ
o POWER FACTOR	-	90 PERCENT MINIMUM
o SYSTEM HARMONIC DISTORTION	-	5 PERCENT MAXIMUM EMI: 3400 PERCENT VOLT - μ SEC
o ARRAY POWER DEGRADATION		15 PERCENT MAXIMUM/20 YEARS
o ARRAY DESIGN LIFETIME	-	20 YEARS MINIMUM
o AVAILABLE ARRAY AREA	-	ABOUT 36,000 SQ. FT.
o ARRAY ROOFTOP	-	WATERTIGHT
o INSTRUMENTATION NETWORK	-	ODAS; WEATHER STATION; MODULES/ROOF TEMP.
o MAINTENANCE & REPAIR		MODULE REMOVAL, TEST EQUIP.; REMOTE MONITOR: SAFETY ALARMS

SYSTEM DESIGN AND WIRING TOPOLOGY

PHENEF System Parameters

PARAMETER	HUGHES/GU PHENEF
PEAK POWER @ SOC	300 kW PK MIN
CONFIGURATION	BIPOLAR NEUTRAL RESISTIVELY GROUNDED
OCV (OPTIMAL CENTER VOLTAGE)	± 228 VDC
MAIN BUS CURRENT AT PEAK POWER	660 ADC
OPEN CIRCUIT VOLTAGE (MAX. VOC)	<800 VDC

36 PV Module Bipolar Source Circuit

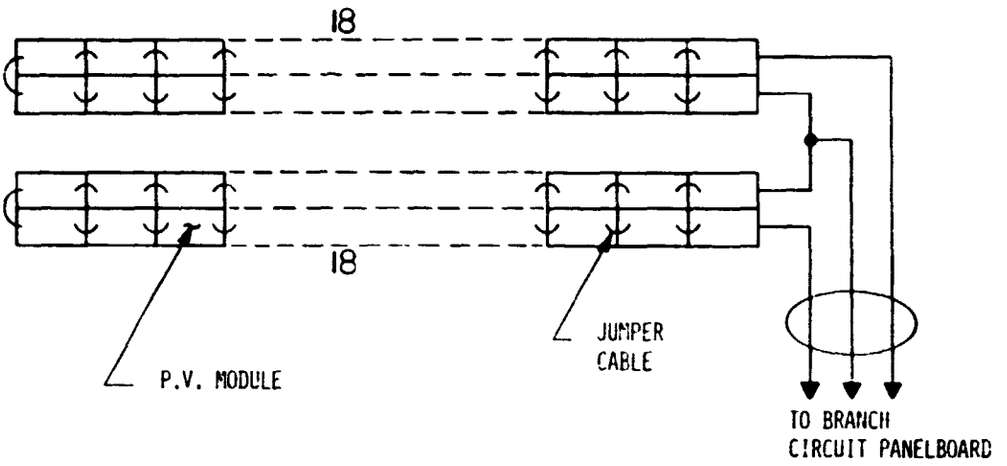

Simplified Block Diagram

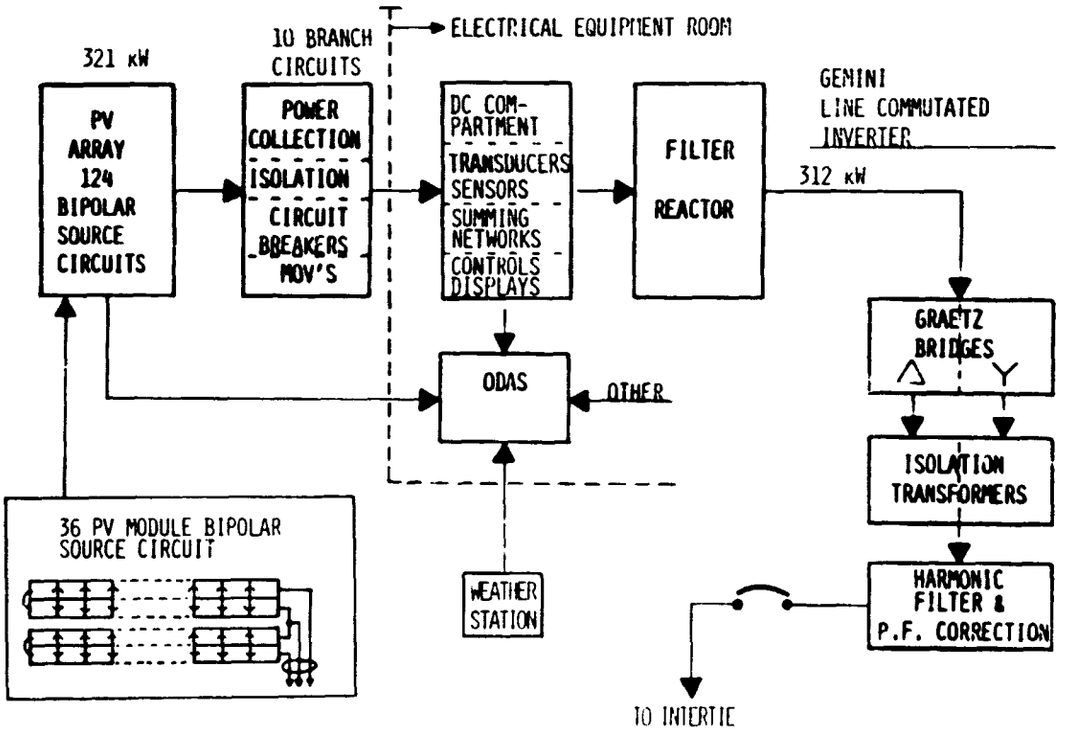

Shadow Analyses

- HOURLY PHOTOGRAPHS - DAWN TO DUSK
- SAME DAY EACH MONTH FOR SIX CONSECUTIVE MONTHS

QUALIFICATION AND TESTING OF PV MODULES

PV Module

- o FULLY TESTED BY JPL PER BLOCK V 5101 - 162
- o PRODUCTION ADHERES TO PREDETERMINED MANUFACTURING PROCESSES
- o MODULES SUBJECTED TO UL790 FIRE RESISTANCE TEST
- o FULL MECHANICAL/VISUAL INSPECTION
- o PREDETERMINED ACCEPTANCE TEST PROCEDURES
  - o HUGHES-FURNISHED REFERENCE CELL STANDARDS (DSET/ASTM #178)
  - o CALIBRATED MODULES
  - o SOURCE INSPECTION/LOT SAMPLES
- c SOLAREX CURRENTLY DELIVERY 4% ABOVE REQUIREMENT

Interface Control Drawing (ICD)

- o o SPECIFICATION DEFINES BASIC PARAMETERS
- o o INTERFACE CONTROL DRAWING IDENTIFIES:
  - o CONFIGURATION
  - o DIMENSIONS
  - o PARTS
  - o MATERIALS
  - o PROCESS SPECIFICATIONS
  - o QUALITY ASSURANCE PROVISIONS
- o o THE ICD AND SUBTIER DOCUMENTS MUST BE APPROVED BY HUGHES
- o o SIGNIFICANT REVISIONS TO ICD & SUBTIER DOCUMENTS MUST ALSO BE APPROVED BY HUGHES

Module Electrical Characteristics

- 72 WATTS MINIMUM LOT AVERAGE AT 16.2 VOLTS
- 67 WATTS MODULE MINIMUM AT 16.2 VOLTS
- MEASURED AT 1000 W/M2, AM 1.5, 28oC
- 3000 VOLT ELECTRICAL VOLTAGE INSULATION
- 3 ENCAPSULATED BYPASS DIODES (12 CELLS/DIODE)
- SOLARLOK CONNECTORS (UL RECOGNIZED)
- SIZE: TWO FT. BY FOUR FT. LAMINATE

Reference Cells

- FIVE 2 X 2 cm CELLS PROVIDED BY SOLAREX
  - 2 EA. - SOLAREX FOR ACCEPTANCE TESTING
  - 2 EA. - HUGHES SOURCE INSPECTION FOR SAMPLE VERIFICATION
  - 1 EA. - MOUNTED ON PHENEF ROOF
- IDENTICAL IN TYPE TO MODULE'S CELLS
- FABRICATED AND CALIBRATED BY DSET LABORATORIES, ARIZONA
- TO ASTM DRAFT DOCUMENT #178 "STANDARD METHOD FOR THE CALIBRATION AND CHARACTERIZATION OF NON-CONCENTRATOR TERRESTRIAL PHOTOVOLTAIC REFERENCE CELLS UNDER GLOBAL IRRADIANCE"

Calibrated Modules

- TWO MODULES
- I-V CURVES GENERATED USING EACH OF 5 REFERENCE CELLS
  EACH OF 5 REFERENCE CELLS
  VENDOR SIMULATOR
- AVERAGE I-V CURVE DETERMINED FOR EACH MODULE
  (I.E. CALIBRATED I-V CURVE)
- CHECKED USING JPL SIMULATOR

Simulator Verification

- CALIBRATED MODULE TESTED UNDER VENDOR SIMULATOR
  BEFORE AND AFTER ACCEPTANCE TESTING DAILY
- BOTH I-V CURVES MUST AGREE WITHIN $\pm$ 2% OF CALIBRATED I-V CURVE
  - ACCEPTANCE TESTING OF MODULES O. K.
  - VERIFIES SIMULATOR/DATA ACQUISITION SYSTEM
- NON-AGREEMENT - ACCEPTANCE TESTING NOT VALID

Acceptance Testing

- EACH MODULE SUBJECT TO:
  - MECHANICAL/PHYSICAL INSPECTION
  - VOLTAGE INSULATION TEST
    - <50 u AMPS @ 3000 VDC
    - USES SAMPLE OF ACTUAL SUPPORT STRUCTURE
  - DIODE VERIFICATION TEST - OPENS & SHORTS
    - ACCEPTABLE (I-V) CURVE SHOWS NO SHORTS
    - DARK REVERSE VOLTAGE SHOWS NO OPENS
  - ELECTRICAL PERFORMANCE TEST
    - I-V CURVE @ 1000 W/M^2, AM 1.5, 28^{o}C
    - I @ 16.2 - CURRENT GROUPS
    - HUGHES SUPPLIED REFERENCE CELLS

Conclusions

STRINGENT SPECIFICATION GUARANTEES

ENVIRONMENTAL PERFORMANCE

STRUCTURAL/PHYSICAL INTERFACES

ELECTRICAL PERFORMANCE

- SOLAREX CURRENTLY DELIVERING MODULES
- 4% ABOVE REQUIREMENT

COST EFFECTIVE

- CHEAPER TO ASSURE FACTORY MODULE PERFORMANCE THAN TO ADJUST IN FIELD

ARRAY ROOFTOP DESIGN SUPPORT STRUCTURES

- o WATERTIGHT ROOF
- o AESTHETIC
- o WEIGHT - LESS THAN 10 PSF
- o SAFETY - FALLING ICE & SNOW
- o WALKABLE
- o GROUNDING

Rafter-Purlin Support Structure

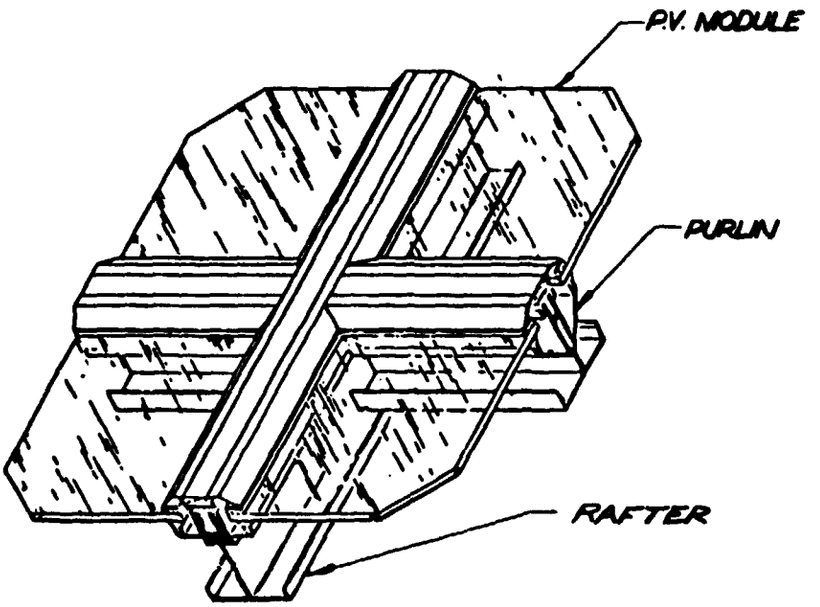

ORI
OF PO

Typical Grid Anchor Detail

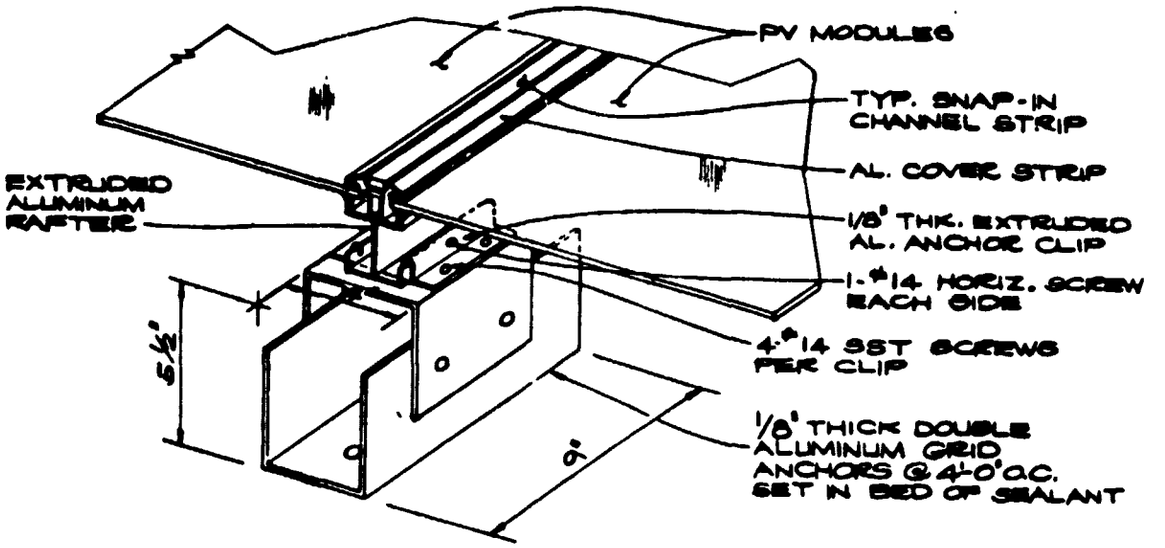

Power Conversion and Control System

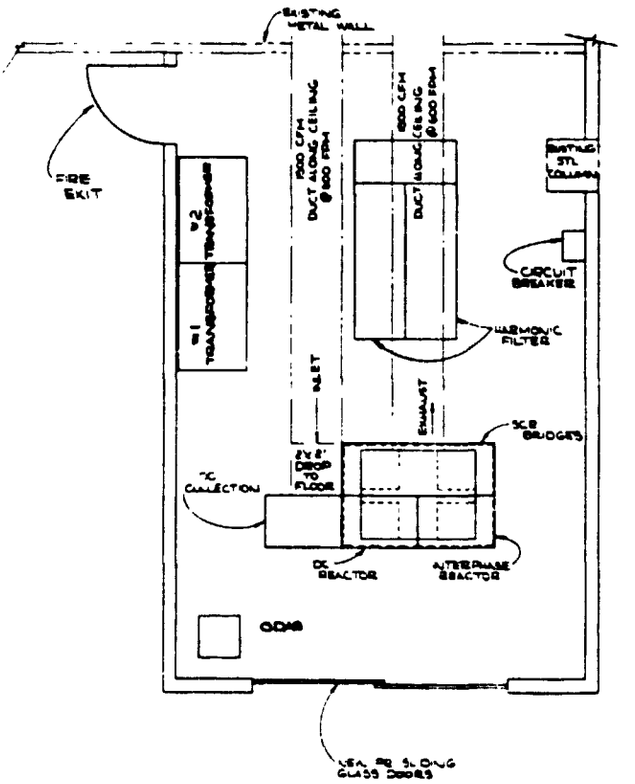

Electrical Protection

- LINE FAULT & OVERCURRENT PROTECTION
  - ARCING DC CURRENTS (TO GROUND) - CURRENT LIMITED
  - MAGNETIC BLOW-OUT DC RELAYS & CONTACTORS
  - THERMAL MAGNETIC TRIP CIRCUIT BREAKERS (250VDC)
  - AIR MAGNETIC CONTACTORS - 1000V; 1000 AMPS
- BIDIRECTIONAL FAULT TRIP COORDINATION
- AUTOMATIC ALARM RELAYS U. SECURITY TIE-IN
- SYSTEM SAFETY SHUTDOWN - CROWBARS
- BRANCH CIRCUIT PANELBOARD ENCLOSURES (10)
  - BLOCKING DIODES
  - SURGE ARRESTORS (MOVs)
  - EMI FILTERS
- REMOTE POWER MONITORING - U. CENTRAL ENERGY CENTER

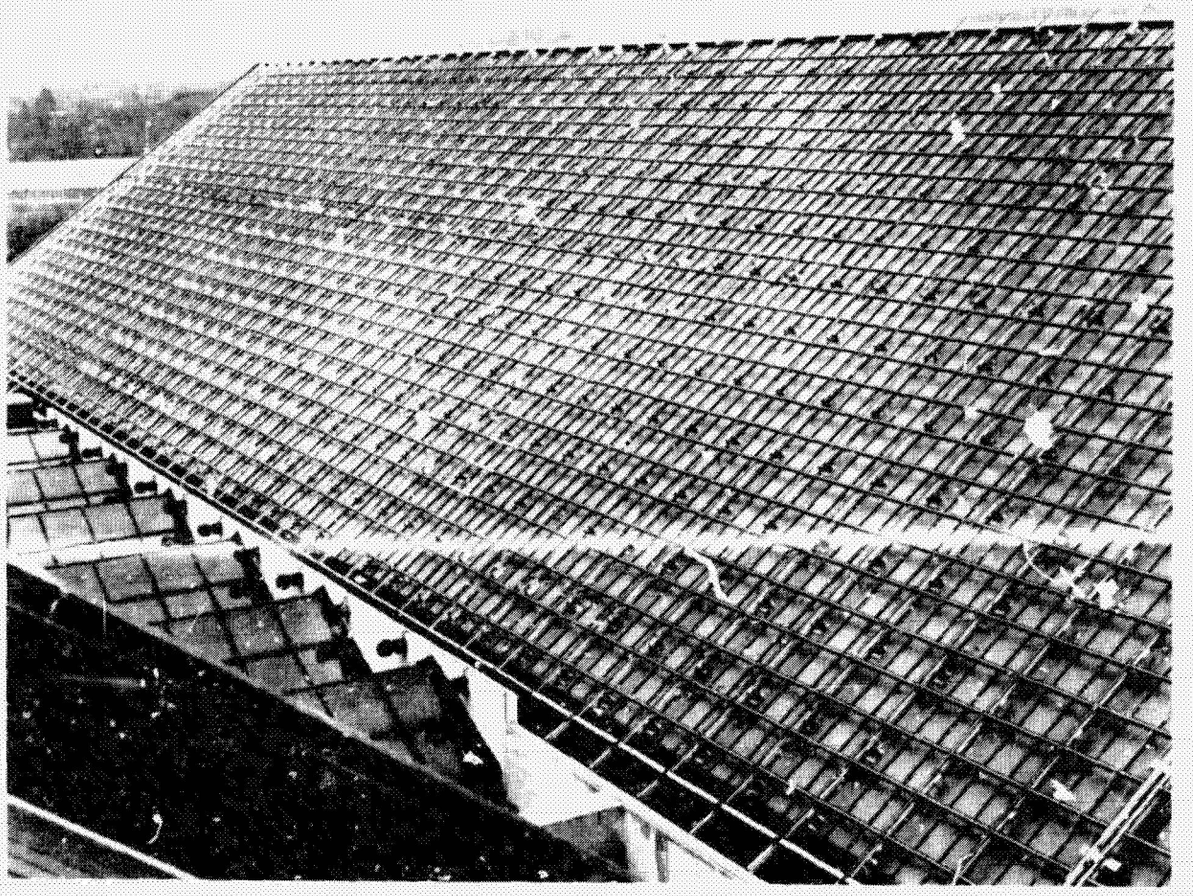

PHOTOVOLTAIC SYSTEMS DEVELOPMENT AND EVALUATION

SANDIA NATIONAL LABORATORIES

M.G. Thomas

Systems Research and Evaluation

SYSTEMS EXPERIMENTS ARE PROVIDING DATA ON

- o LONG TERM PERFORMANCE
- o RELIABILITY
- o DEGRADATION
- o OPERATION AND MAINTENANCE

COMMUNICATION IS IMPORTANT - ESPECIALLY IN SYSTEM DESIGN

- o WE NEED GOOD SUMMARIES
- o WE NEED MAJOR EFFORTS TO SIMPLY EXPLAIN OUR RESULTS

COMPARISON OF PREDICTED AND ACTUAL PERFORMANCE IS ESSENTIAL TO SYSTEMS DEVELOPMENT ASSESSMENTS

- o SIMPLE MODELS PROVIDE ACCURATE PREDICTIONS
- o INPUT DATA -- ESPECIALLY INSOLATION DOMINATE MODELS

DATA MONITORING AT 15 MINUTE INTERVALS IS ADEQUATE

- o FOR ENERGY INPUT
- o LOADS (LAST YEAR)

THERE MAY BE MORE VALUE FOR THE DSG THAN JUST THE ENERGY IT PRODUCES

O&M COSTS HAVE BEEN $\$7/M^2/YR$.
THESE HAVE BEEN MAINLY UNSCHEDULED
INCREASED PCS RELIABILITY, IN PARTICULAR, WILL GREATLY REDUCE THIS FIGURE

Utility Session Summary

OPERATIONS

- PV SYSTEM OUTPUT SWINGS DUE TO CHANGING CLOUD COVER HAVE HIGH RAMP RATES
- UNDER WORST CASE CONDITIONS POTENTIAL EXISTS FOR EXCEEDING ACE CRITERIA, DEPENDENT ON:
  - CAPACITY OF PV SYSTEM RELATIVE TO UTILITY SYSTEM
  - TYPE OF GENERATION UTILIZED FOR REGULATION (RAMP RATE)
- SIMPLE SOLUTIONS AVAILABLE:
  - WEATHER FORECASTING
  - LESS DENSE ARRAY FIELD
  - GEOGRAPHIC DISPERSION
  - ALTER REGULATING GENERATION
- PROGRAM BEING DOCUMENTED FOR GENERAL UTILITY USE

T&D IMPACTS

- ARENA OF [illegible] CONCERN, PRIME POINTS OF INTEREST:
  - SAFETY - NO RUN-ON OR ISLANDING
  - FAULTS PROTECTION - NO RUN-ON, NO EFFECT ON COORDINATION
  - MAGNITUDE AND EFFECT OF REVERSE POWER FLOW
- HARMONICS
  - VERY THOROUGH DATA GATHERED AT ONE LOCATION INDICATES THAT HARMONIC INJECTION FROM ADVANCED PCU'S IS "IN THE NOISE"
    - MAGNITUDES SIMILAR TO COMMON HOUSEHOLD DEVICES
    - MAGNITUDES SIGNIFICANTLY LESS THAN WINDOW AIR CONDITIONER
  - WORK BY SE RES URG TO CONTINUE AT VARYING LOCATIONS:
    - AMBIENT LEVELS
    - HARMONIC IMPEDANCES
    - PROPAGATION MECHANISMS
  - GENERALIZE WORK AND APPLY COMPUTER ANALYSIS
- UTILITY CONTRACTS
  - CONFIRM UTILITY ACCEPTANCE OF ADVANCED PCU'S
  - UTILITY INTERFACE ASPECTS
  - ISLANDING POTENTIAL
  - PROVIDE DIRECTION FOR FUTURE U-I WORK

PCS Session Summary

SMALL PCS DEVELOPMENT STATUS

- SEVERAL ADVANCED PERFORMANCE UNITS ARE COMMERCIALLY AVAILABLE
- EXCELLENT PERFORMANCE UNDER DETAILED EXAMINATIONS AND FIELD TESTS
- PRESENT COSTS ARE ~$1.00/W WITH QUANTITY PROJECTIONS AT $.35/W

PCS ENGINEERING EVALUATION PROGRAM

- EVALUATIONS HAVE ACCELERATED THE DESIGN EVOLUTION PROCESS
- OUR UNDERSTANDING OF UTILITY INTERFACE REQUIREMENTS HAS MATURED
- NEARLY ALL PERFORMANCE PROBLEMS HAVE BEEN SOLVED BY MINOR CIRCUIT CHANGES (BASIC DESIGN APPROACHES ARE SOUND)

REMAINING/NEEDS

- A SIMPLIFIED PCS TEST PROCEDURE IS NEEDED FOR THE USER
- "UTILITY COMPATIBILITY IN GENERAL" SHOULD BE STAMPED ON THE UNIT NOT NEGOTIATED AT THE SITE

LARGE PCS DEVELOPMENT STATUS

- o LOOKING AT DESIGN APPROACHES FROM 1-10 MW AND 20-200 kW
- o LOOKING FOR VOLUME EFFECTS AT LOW POWER
- o BENEFITTING FROM OTHER TECHNOLOGY EXPERIENCE FOR HIGH POWER (MHD, FUEL CELL, BATTERY)
- o POOLING OF RESOURCES OVERCOMES HIGH FRONT-END ENGINEERING AND DEVELOPMENT COSTS
- o FIELDING OF AN ADVANCED 5 MW UNIT BY 1986 IS POSSIBLE (SMUD?)
- o FUTURE POTENTIAL OF 3-4 TIMES COST REDUCTION FROM CURRENT COSTS

Array BOS Session

INSTALLATION EXPERIENCE

- o SIGNIFICANT COST REDUCTION IN RESIDENTIAL BOS HAS NOT OCCURRED -- BUILDING BLOCK APPROACH WILL BE PURSUED
- o BASED ON "LESSONS LEARNED" WITH SMUD PV1 ($160/M^2 BOS), BOS COST FOR SMUD PV2 IS EXPECTED TO BE $90/M^2
- o LUGO FACILITY EXPERIENCED PROBLEMS WITH AVAILABILITY OF DC SWITCHGEAR, BYPASS DIODE FAILURES, AND LARGE NEUTRAL CURRENTS
- o BUILDING BLOCK DESIGN RESULTED IN BOS COST REDUCTION FOR CONCENTRATOR ARRAY FIELD
  - BASED ON BUILDING BLOCK APPROACH, 1 MW SIZE TURNKEY SYSTEM IS OFFERED AT PRICE OF $7.00/$W_p$
- o ROOF-MOUNTED ARRAYS OFFER SEVERAL DIFFERENT AND POSSIBLY COSTLY BOS REQUIREMENTS

FIELD DESIGN

- o INCORPORATION OF BYPASS DIODES MAY BE A SIGNIFICANT COST DRIVER -- STUDIES ARE NEEDED TO ESTABLISH COST EFFECTIVENESS
- o HIGH VOLTAGE CIRCUITS DO NOT OFFER ANY NEAR TERM COST ADVANTAGES -- LOW VOLTAGE DESIGN ($\pm$400 V_{DC}) WILL BE PURSUED FOR LARGE FIELDS
- o FACTORY PROCURED PANEL ASSEMBLIES MAY OFFER AN EFFECTIVE APPROACH TO REDUCING INTERMODULE CONNECTION AND DIODE PROTECTION COSTS
- o PROJECTED BOS COST FOR 100 MW MODULAR FLAT PLATE FIELD IS \$52/M^2
- o INTERIM GROUNDING PRACTICES MANUAL FOR LARGE SIZE PV FIELDS HAS BEEN PUBLISHED

Remaining Issues for Large-System Development

KEY SANDIA PROJECTS

ARRAY FIELD DEVELOPMENT - HAL POST

PCS DEVELOPMENT - TOM KEY

What Is the Best Strategy for Electrical Protection?

LAST YEAR'S ISSUES	ANSWERS
A. GROUNDING - WHICH METHOD IS MOST	FOR REASONABLE FAILURE RATES, NO REAL ECONOMIC DRIVERS. SOLID GROUND SLIGHTLY FAVORED OVER RESISTANCE GROUND
B. FAULT PROTECTION - WHAT STRATEGY	SOURCE CIRCUIT LEVEL
C. MAINTENANCE	DEPENDENT ON FAILURE TYPE, BUT AT LOW FAILURE RATES, SCHEDULE FIX UPON NEED (NO REGULAR SCHEDULE REQUIRED)

PRESENT ISSUE

DIODING - COST vs BENEFIT - CURRENT ESTIMATES ARE GREATER THAN \$10/M^2 WITH 1 BYPASS DIODE/SERIES BLOCK (ANOMALY EXISTS BETWEEN ESTIMATE AND CURRENT FIELD COST TO MANUFACTURER FOR INSTALLATION)

What Is the Best System Design?

DO NOT HAVE OPTIMIZED DESIGNS FOR ONE-AXIS AND 2-AXIS TRACKING FLAT PLATE

RFQ ISSUED FOR OPTIMIZED DESIGNS

What Should We Pursue in PCS Development?

LAST YEAR'S ISSUES	ANSWERS	
A. SIZE	5 MW	20-100 kW
B. VOLTAGE	400-500 V_{DC} (DIPOLAR)	400-500 V_{DC} (MONOPOLAR)

4 EXISTING CONTRACTS FOR INNOVATIVE DESIGNS

PRESENT ISSUE

VOLUME ADVANTAGE VS SIZE ADVANTAGE

COMPLEMENTARY TECHNOLOGY DEVELOPMENT

Residential Status

BECAUSE A LARGE AMOUNT OF DATA HAS BEEN COLLECTED FOR RESIDENTIAL PV SYSTEMS, SUPPORT NEEDED FOR THE RESIDENTIAL PROGRAM HAS DECREASED. HOWEVER, THERE ARE MANY UNRESOLVED ISSUES WHICH ARE THE BASIS FOR THE CONTINUED RESIDENTIAL PROGRAM.

Issues Remaining for Residential PV Systems

1. INSTALLATION COSTS - MODULAR APPROACH MAY SOLVE
2. RELIABILITY AND SAFETY
3. COST EFFECTIVENESS
4. EDUCATION

The Residential Program

SMALL PCS TESTING AT SNLA

UTILITY TESTING OF SMALL PCS AT RES's

MODULAR BUILDING BLOCK RFQ

FLAMMABILITY/SAFETY TESTING AT JPL

RES TESTING OF NEW TECHNOLOGY MODULES + PCS

SOURCE-CIRCUIT DESIGN CONSIDERATIONS

JET PROPULSION LABORATORY

C.C. Gonzalez

Agenda Items

- **Definition of a source circuit**
- **Objective of source-circuit design effort**
- **Methodology for developing source-circuit design options to control impact of component failure and mismatch**
- **Identification of component failure mechanisms and solution alternatives**
- **Example of the use of source-circuit design options**
- **Current status of source-circuit design effort**

Objective

To determine cost-optimum circuit design practices that will minimize the impact of component problems on the system energy cost

Source-Circuit Definition

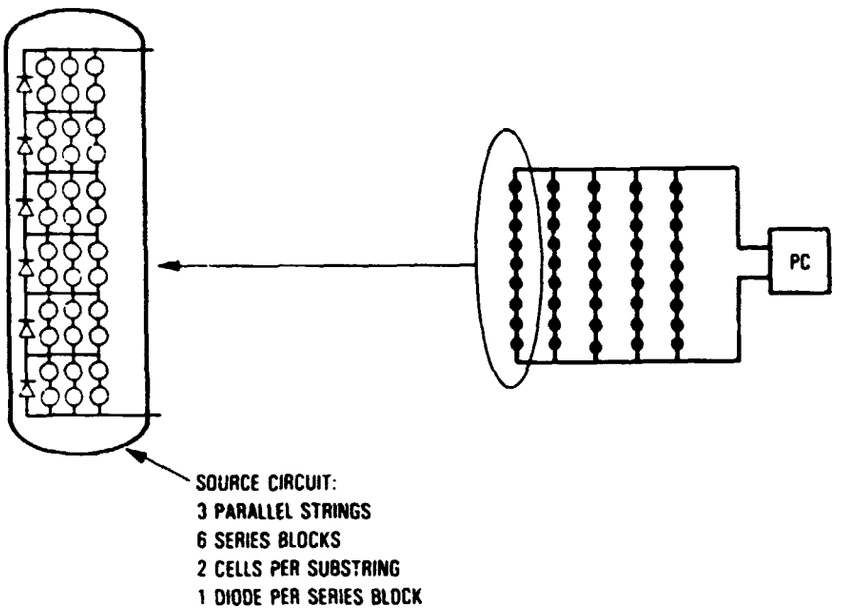

Component Problems Influenced by Source-Circuit Design

- **Open circuits**
  - **Interconnect fatigue**
  - **Cracked cells**
- **Short-circuited cells**
- **Mismatched cells**
- **Arcs**
  - **Ground fault**
  - **In-circuit**
- **Hot-spot cell heating**
- **Shadowed cells**

Component Problems and Related Issues

Component Problem	Phenomena Understood	Problem Level Understood	System Impact Quantified	Circuit Solutions Derived	Cost-Effective Circuit Defined	Cost-Effective Failure Level Defined
Open circuits; interconnect fatigue & cracked cells						
Short-circuited cells						
Mismatched cells						
Ground-fault arcs						
In-circuit arcs						
Hot-spot cell heating						
Shadowed modules						

Solution Alternatives

- Cell paralleling (parallel cell strings in modules or crossties between modules)
- Cell contact redundancy
- Multiple interconnects between cells
- Bypass diodes
- Cell circuit layout
- Frequent cross-strapping
- Ground-fault interrupters
- Resistance ground

Solution Alternatives Matrix

Problems	Cell Paralleling	Contact Redundancy	Multiple Interconnects	Bypass Diodes	Cell Circuit Layout	Frequent Cross-Strapping	Ground-Fault Interrupt	Resistance Ground
Shadowed Cells	+			+	+	+		
Interconnect Fatigue	+		+	+		+		
Cracked Cells	+	+		+		+		
Shorted Cells	−					−		
Mismatched Cells	+			+		+		
Ground-Fault Arc							+	+
In-Circuit Arcs	+	+	+	+				
Hot-Spot Heating	−			+		−		

Cell-Paralleling and Cross-Strapping Issues

- Quantify system impact of circuit options
- Quantify system impact of failure levels
- Define cost-effective circuit
- Define allowable failure levels

Array Power Loss

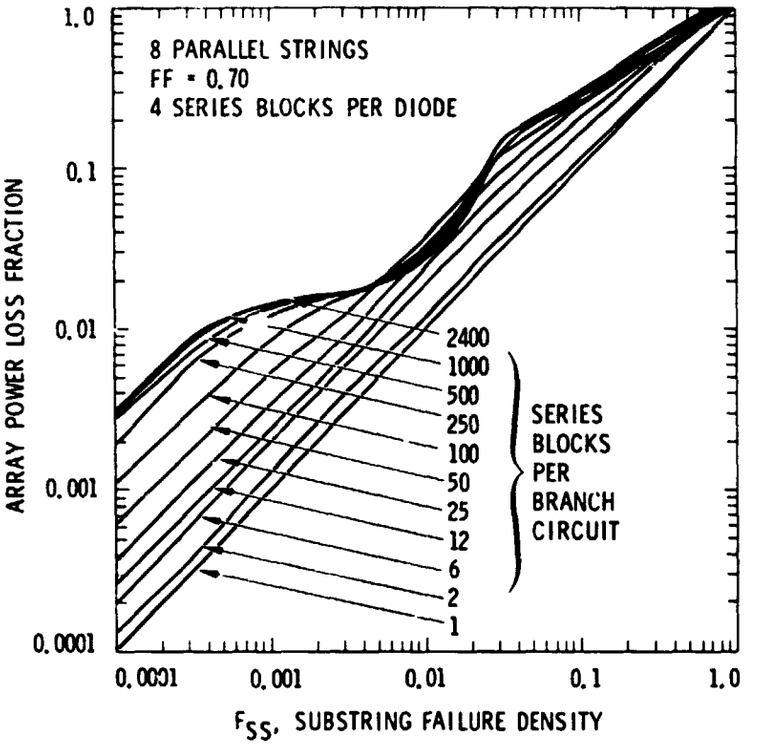

Fraction of Power Loss After 5 Years vs Circuit Redundancy

- 1000 Series Cells
- 450-Volt Source Circuit
- One Diode Per Series Block
- Cell Failure Rate = 0.0001 (Open-Circuit)
- Cell Failure Rate = 0.0001 (Short-Circuit)

Cells Per Substring	Series Blocks	CELLS IN PARALLEL				
		1	4	8	16	
← Unacceptable Hot-Spot Heating →						
20	50	<0.001 0.011 <0.012	0.001 0.050 0.051	0.001 0.025 0.026	0.001 0.015 0.016	
10	100	<0.001 0.005 <0.006	0.001 0.022 0.023	0.002 0.013 0.015	0.002 0.008 0.010	← Optimum Design Region
5	200	<0.001 0.003 <0.004	0.002 0.010 0.012	0.002 0.007 0.009	0.002 0.004 0.006	
2	500	<0.001 0.001 <0.002	0.002 0.004 0.006	0.004 0.003 0.007	0.006 0.002 0.008	} Sensitive To Shorted Cells

Top Line: Short-Circuit Failure
Mid Line: Open-Circuit Failure
Bottom Line: Total

- 1000 Series Cells
- 450-Volt Source Circuit
- One Diode Per Series Block
- Cell Failure Rate = 0.0001 (Open-Circuit)
- Cell Failure Rate = 0.001 (Short-Circuit)

Cells Per Substring	Series Blocks	CELLS IN PARALLEL				
		1	4	8	16	
← Unacceptable Hot-Spot Heating →						
20	50	<0.005 0.011 <0.016	0.007 0.050 0.057	0.007 0.025 0.032	0.008 0.015 0.023	
10	100	<0.005 0.005 <0.010	0.008 0.022 0.030	0.009 0.013 0.022	0.010 0.008 0.018	
5	200	<0.005 0.003 <0.008	0.011 0.010 0.021	0.014 0.007 0.021	0.016 0.004 0.020	
2	500	<0.005 0.001 <0.006	0.017 0.004 0.021	0.030 0.003 0.033	0.050 0.002 0.052	} Sensitive To Shorted Cells

Optimum Design Region

Top Line: Short-Circuit Failure
Mid Line: Open-Circuit Failure
Bottom Line: Total

Analysis Results

- **Optimum circuit design strategy for central stations:**
  - **8-16 (or more) parallel strings; cross ties no more frequently than every 6 cells, and a bypass diode every 15-18 cells**
- **Allowable failure levels:**
  - **Open circuits -- 1/10,000 per year**
  - **Short circuits -- 1/10,000 per year**

Comparison of Strategies

Strategy	Advantages	Disadvantages
A. Increased use of parallel strings	1. Redundant current paths in case of open circuits 2. Reduces mismatch losses when cell mismatch occurs	1. Increased loss of power in case of diode turn-on 2. Increased risk of current imbalance during back-biasing 3. Increased loss of power due to cell short-circuiting
B. Increased use of cross ties	1. Redundant current paths in case of open circuits 2. Reduces mismatch losses when cell mismatch occurs	1. Increased risk of current imbalance and hot-spot heating 2. Increased loss of power due to cell short-circuiting
C. Use of bypass diodes	1. Reduces power loss due to open circuits 2. Reduces hot-spot heating problems 3. Reduces risk of in-circuit arcing	

Status Summary: Component Problems and Related Issues

Component Problem	Phenomena Understood	Problem Level Understood	System Impact Quantified	Circuit Solutions Derived	Cost-Effective Circuit Defined	Cost-Effective Failure Level Defined
Open circuits/interconnect fatigue & cracked cells	●	●	●	●	●	●
Short circuit cells	●	○	◔	●	○	◕
Mismatched cells	●	●	◐	●	◔	◔
Ground-fault arcs	●	◐	◔	●	◐	◐
In-circuit arcs	●	●	●	●	●	●
Hot-spot cell heating	●	◐	●	●	◐	●
Shadowed modules	●	◐	●	●	●	●

Key Remaining Issues

- **Shorted cells**
  - **Quantify field failure level**
- **Mismatched cells**
  - **Improve model of failure impact on system**
- **Ground-fault arcs**
  - **Quantify field failure level using prototype detector circuits**
- **Hot-spot cell heating**
  - **Quantify current imbalance problem**
  - **Improve qualification test**

CENTRAL-STATION ARRAY DURABILITY CONSIDERATIONS

JET PROPULSION LABORATORY

G.R. Mon
R.G. Ross, Jr.

Objective

To achieve the technology base

for 30-year array life

- **Acceptable power degradation rates**
- **Acceptable component failure rates**
- **Acceptable maintenance costs**

Durability and Reliability Research Elements

- **Establishment of durability goals**
- **Identification of key degradation mechanisms**
- **Qualitative understanding of mechanism physics**
  - **Governing materials parameters**
  - **Governing environmental-stress parameters**
- **Quantification of parameter dependencies**
- **Development of accelerated tests**
- **Degradation prediction models**
  - **Mechanism degradation prediction**
  - **System cost-energy impact analysis**
- **Identification of cost-effective solutions**
  - **Materials of construction**
  - **Component design features**
  - **Circuit redundancy and reliability features**

Strawman Degradation Allocations: 30-Year-Life Advanced Technology

Type of Degradation	Specific Mechanism	Mechanism Allocation
Fixed Drop in Power	Soiling	3%
	Mismatch	1%
Constant Degradation Rate	Cell open circuit	0.00001 per year
	Cell corrosion	0.2% per year
	Yellowing	0.2% per year
Constant O&M	Voltage breakdown	0.1/mile/year†
	Glass breakage	0.002 per year†
	Mod. open circuits	0.002 per year†

†At $140 per replacement of 1.5 m^2 module

Key Failure Modes and Mechanisms

- Electrical interconnect breakage
  - Thermal cycling, wind loading
- Solar cell cracking
  - Thermal cycling, hail impact
- Encapsulant delamination
  - Thermal cycling, humidity, UV
- Encapsulant physical degradation
  - Temperature, humidity, UV
- Cell metallization deterioration
  - Temperature, humidity, voltage
- Electrical insulation breakdown
- Optical surface soiling

Key Durability Issues

MECHANISM	PARAMETER DEPENDENCIES QUANTIFIED	QUALIFICATION TEST AVAILABLE	LIFE PREDICTION CAPABILITY	COST-EFFECTIVE SOLUTIONS DEFINED
INTERCONNECT FATIGUE				
HAIL-IMPACT DAMAGE				
CELL CRACKING				
ENCAPSULANT DELAMINATION				
ENCAPSULANT PHYSICAL DEGRADATION				
CELL GALVANIC CORROSION				
ELECTROCHEMICAL CORROSION				
ELECTRICAL INSULATION BREAKDOWN				
SOILING				

Fatigue Information: OFHC Copper

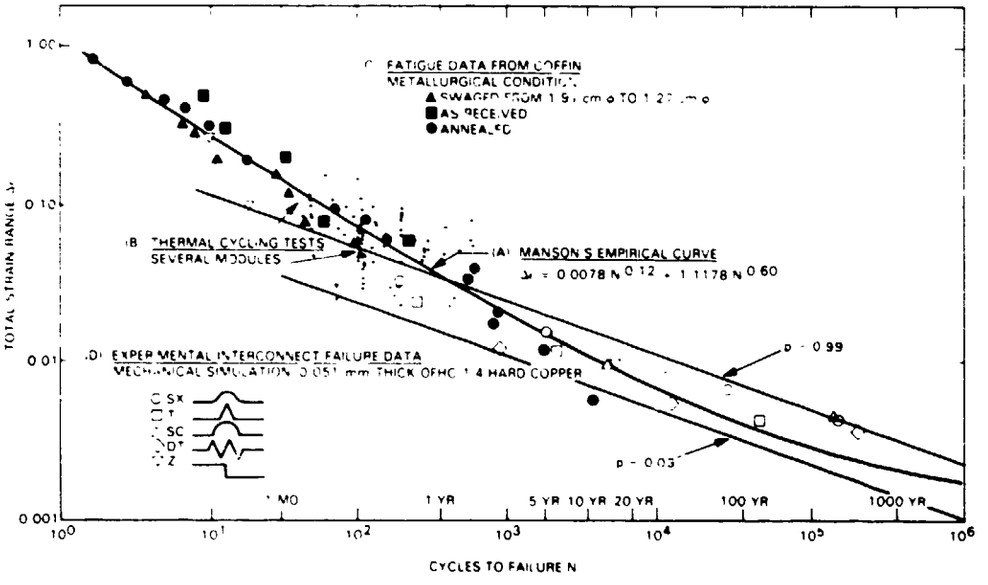

Statistical Fatigue Curves for OFHC 1/4-Hard Copper

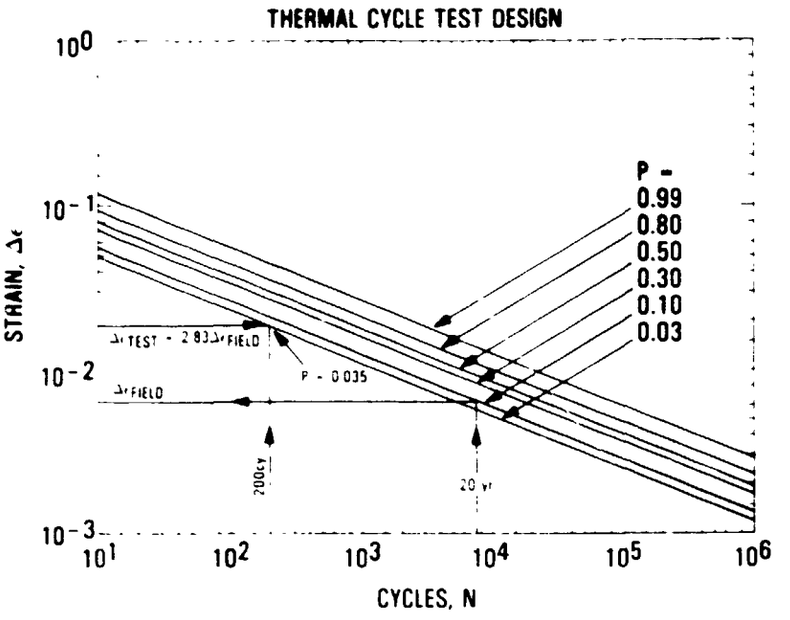

Module Interconnect Design Procedures

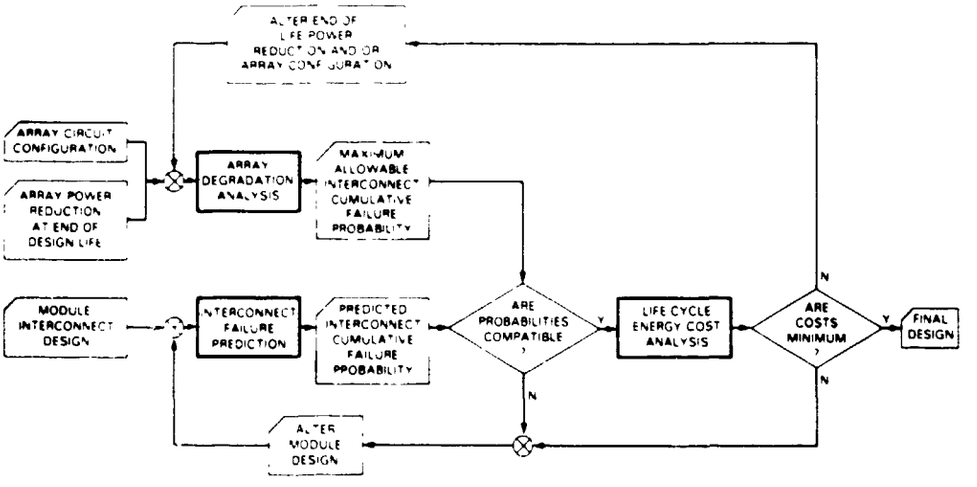

Percentage of Life-Cycle Energy Cost Increment
Due to Doubly Redundant Interconnects

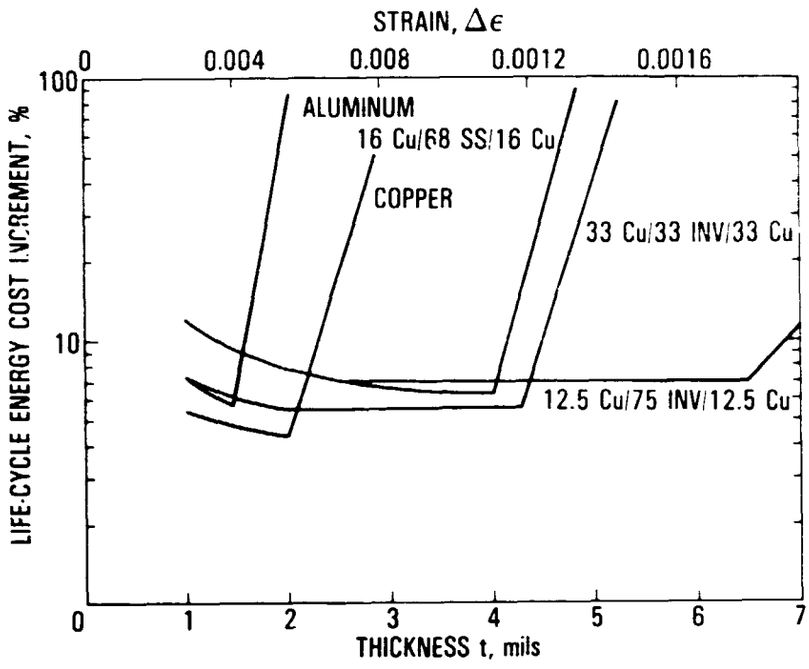

Durability Research Status

Mechanism	Parameter Dependencies Quantified	Qualification Test Available	Life Prediction Capability	Cost Effective Solutions Defined
Interconnect Fatigue	●	●	●	●
Hail Impact Damage	●	●	●	●
Cell Cracking	●	●	●	●
Encapsulant Delamination	◐	◕	○	◐
Encapsulant Physical Degradation	◕	○	◐	●
Cell Galvanic Corrosion	●	●	●	●
Electrochemical Corrosion	●	◐	◕	◕
Electrical Insulation Breakdown	○	○	○	◔
Soiling	●	○	◕	◕

Key Remaining Issues

- Electrical insulation breakdown
  - Understand degradation process under bias-temperature-humidity stressing
  - Develop cost-effective design criteria
- Electrochemical corrosion
  - Develop qualification test
  - Develop cost-effective design criteria
- Encapsulant delamination
  - Understand mechanism involved in breakdown of chemical bonding
  - Develop experimental method to monitor interfacial debonding
- Encapsulant physical degradation
  - Develop model of physical degradation
  - Develop accelerated tests, qualification tests
- Soiling
  - Understand longevity of surface coatings
  - Development of optimal performance coatings

Major Reliability Problems

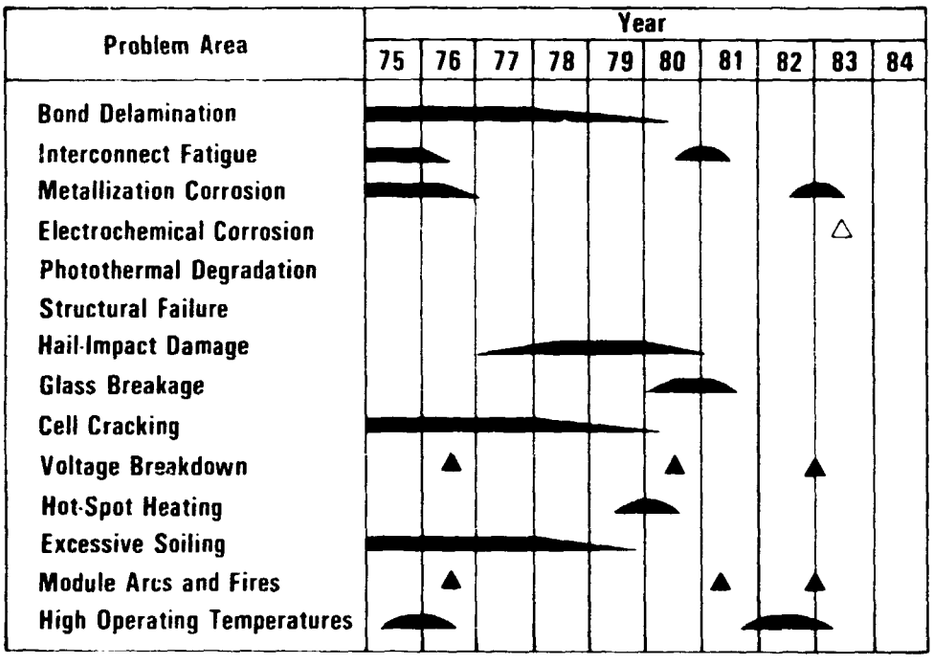

Reliability & Durability Developments: 1975 to 1984

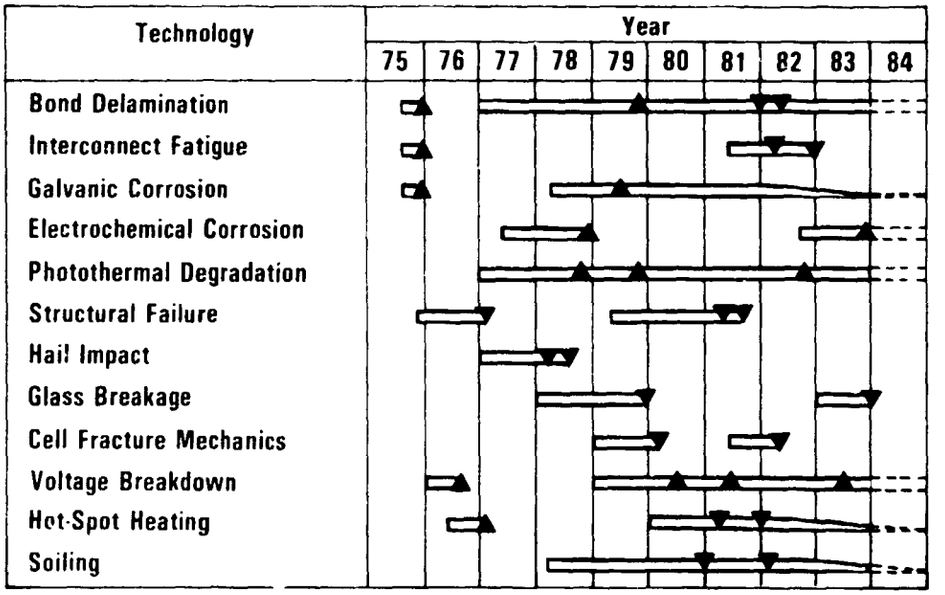

OPERATIONS AND MAINTENANCE

JET PROPULSION LABORATORY

P.K. Henry

Summary of O&M Issues From Central-Station Research Forum

- **Allowable O&M cost**
  - **Various studies estimate O&M costs at $2.00/m^2-yr to $2.50/m^2-yr**
  - **DOE Five-Year Research Plan assumes $2.28/m^2-yr O&M costs**
  - **Recommendation to change Research Plan O&M costs to $1.10/m^2-yr (fixed-array) and $1.40/m^2-yr (tracking array)**
- **Array O&M strategy**
  - **Design array to be fault-tolerant**
  - **Array design should include some fault locating equipment**
  - **Array design should provide for easy component replacement**
  - **Replace modules only if necessary for safety, equipment protection or overall array performance adversely affected**
- **Determination of failure modes, rates and O&M costs**
  - **Failure mechanisms and failure rates of array components not yet well understood**
  - **Recently installed large arrays will yield much more relevant O&M data than small experimental arrays**
  - **O&M costs are not likely to be a large contributor to bus-bar energy costs**

PRECEDING PAGE BLANK-NOT FILMED

Program Goals and Economic Assumptions (Value Recommended for 1-Axis Tracking)

Levelized Electricity Cost Equation From Program Plan:

$$\overline{EC} = \left[\frac{FCR}{8760 \cdot CF}\right] [INDC] [A(\$MSQMD + \$MSQBS) + \$KWBS] + A \cdot G \cdot CRF \left[\frac{\$MSQOM}{8760 \cdot CF}\right]$$

$\overline{EC}$	levelized electricity cost in current dollars	$0.15/kWh
FCR	fixed charge rate	0.153
	general inflation rate	0.085
	discount rate	0.125
CF	annual system capacity factor (1-axis tracking)	0.308
INDC	indirect cost multiplier	1.50
G	present worth factor based on a 12.5% discount rate and 30-year lifetime	18
CRF	capital recovery factor for a 12.5% discount rate and 30-year lifetime	0.129
	average peak isolation	1.0kW/m^2
	balance-of-system efficiency	0.865
	module efficiency	10% to 25%
$MSQBS	BOS area-related cost	60-90 $/m^2
$KWBS	BOS power-related costs	$150/kW
$MSQOM	annual O&M costs	$1.40/m^2-year (tracking array)

TECHNICAL ISSUES OF HIGH-EFFICIENCY SILICON SOLAR CELLS

JET PROPULSION LABORATORY

K.M. Koliwad

Department of Energy Goal

"THE FIVE YEAR GOAL OF FLAT PLATE COLLECTOR RESEARCH IS TO ESTABLISH THE TECHNOLOIGIES BY 1988 WHICH INDUSTRY CAN APPLY TO THE PRODUCTION OF 15% EFFICIENT CRYSTALLINE SILICON MODULES..."

NATIONAL PHOTOVOLTAIC PROGRAM, 5 YEAR RESEARCH PLAN 1984 - 1988
PHOTOVOLTAICS: ELECTRICITY FROM SUNLIGHT MAY 1983 U.S. DOE PAGE 16

Introduction

- MODULE EFFICIENCY OF 15% (NOCT) REQUIRES SOLAR CELLS OF EFFICIENCIES IN THE RANGE OF 18% TO 20% (AM1.5)

- ATTAINMENT OF SUCH LEVELS OF SOLAR CELL EFFICIENCIES USING LARGE AREA AND LOW-COST SILICON SHEET IS BEYOND THE STATE-OF-THE-ART

- INADEQUATE QUALITY OF THE LOW-COST SILICON SHEETS AND THE INHERENT LIMITATIONS OF THE STATE-OF-THE-ART CELL STRUCTURES ARE THE PRIMARY BARRIERS

- EXTENSIVE RESEARCH IS REQUIRED TOWARDS IMPROVING THE QUALITY OF THE LOW-COST SILICON SHEET AND EXTENDING THE UNDERSTANDING OF DEVICE PHYSICS, DESIGN AND PROCESSING

Efficiency Limits

- BASED ON FUNDAMENTAL PHYSICAL MECHANISMS THE ABSOLUTE EFFICIENCY LIMIT FOR SILICON SOLAR CELLS IS ABOVE 30%

- THE BEST EFFICIENCY REPORTED TO-DATE IS 19% (AM1)
  - FLOAT-ZONE SILICON SHEET
  - 2 cm x 2 cm CELL AREA
  - MINP CELL STRUCTURE USING TUNNELING CONTACTS

- THE BEST EFFICIENCY ACHIEVED TO-DATE ON LOW-COST SILICON SHEET IS 16% (AM1)
  - DENDRITIC WEB RIBBON
  - 2 cm x 2 cm CELL AREA
  - N^+PP^+ CELL STRUCTURE

- CARRIER RECOMBINATION LOSSES WITHIN THE BULK AND AT SURFACES OF THE CELL LARGELY ACCOUNT FOR THE DIFFERENCE

Primary Causes of Losses

1. LIGHT GENERATED CURRENT:
   - A. OPTICAL SURFACE PROPERTIES (REFLECTION)
   - B. CONTACT COVERAGE
   - C. INCOMPLETE ABSORPTION (THICKNESS)
   - D. RECOMBINATION OUTSIDE DEPLETION REGION (BULK AND SURFACE, INCLUDING CONTACTS)
   - E. ("DEAD LAYERS")

2. OPEN CIRCUIT VOLTAGE:
   - A. RECOMBINATION OUTSIDE DEPLETION REGION (BULK AND SURFACE, INCLUDING CONTACTS)
   - B. BANDGAP NARROWING
   - C. "CURRENT LEAKAGE"

3. FILL FACTOR:
   - A. } SAME AS OPEN CIRCUIT VOLTAGE
   - B. }
   - C. }
   - D. RECOMBINATION IN DEPLETION REGION
   - E. SERIES RESISTANCE

CONVERSION EFFICIENCY	20%	17%
1. LIGHT GENERATED CURRENT		
FUNDAMENTAL LIMIT (AM1)	44 mA cm-2	
A. OPTICAL SURFACE PROPERTIES (REFLECTION)	0.97	0.95 (±0.02)
B. CONTACT COVERAGE	0.966	0.97
C. INCOMPLETE ABSORPTION (THICKNESS)		
D. RECOMBINATION OUTSIDE DEPLETION REGION (BULK AND SURFACE INCLUDING CONTACTS)	0.92	0.88 (DISTRIBUTION ASSUMED)
E. ("DEAD LAYERS")	1.0	1.0 (DISTRIBUTION ASSUMED)
OVERALL COLLECTION EFFICIENCY	0.86	0.81
LIGHT GENERATED CURRENT (AM1)	37.9 mA cm^{-2}	35.5 mA cm^{-2}
2. OPEN CIRCUIT VOLTAGE		
FUNDAMENTAL LIMIT	0.836 V	
A. RECOMBINATION OUTSIDE DEPLETION REGION (BULK AND SURFACE, INCLUDING CONTACTS)	0.60	0.54
B. BANDGAP NARROWING		
C. "CURRENT LEAKAGE"	1.0	1.0
OPEN CIRCUIT VOLTAGE	0.661 V	0.594 V
3. FILL FACTOR		
FUNDAMENTAL LIMIT	0.96	
A. } SAME AS OPEN CIRCUIT VOLTAGE	0.84	0.84
B. }		
C. }	1.0	1.0
D. RECOMBINATION IN DEPLETION REGION	0.97	0.975
E. SERIES RESISTANCE	0.98	0.975
FILL FACTOR	0.80	0.80

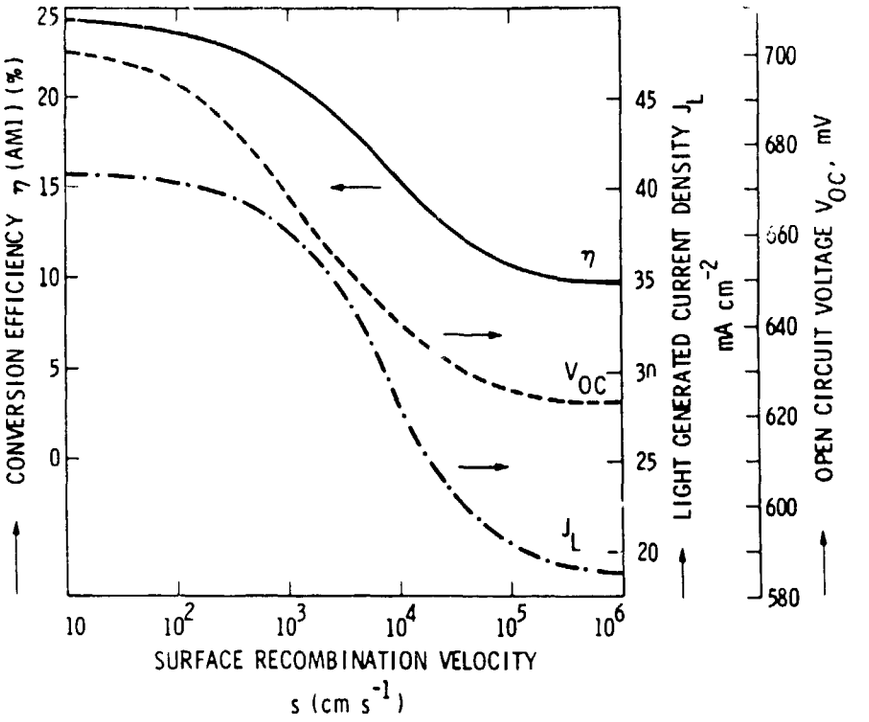
CONVERSION EFFICIENCY η (AM1) (%)
LIGHT GENERATED CURRENT DENSITY J_L mA cm^{-2}
OPEN CIRCUIT VOLTAGE V_{OC}, mV
η
V_{OC}
J_L
SURFACE RECOMBINATION VELOCITY
s (cm s^{-1})

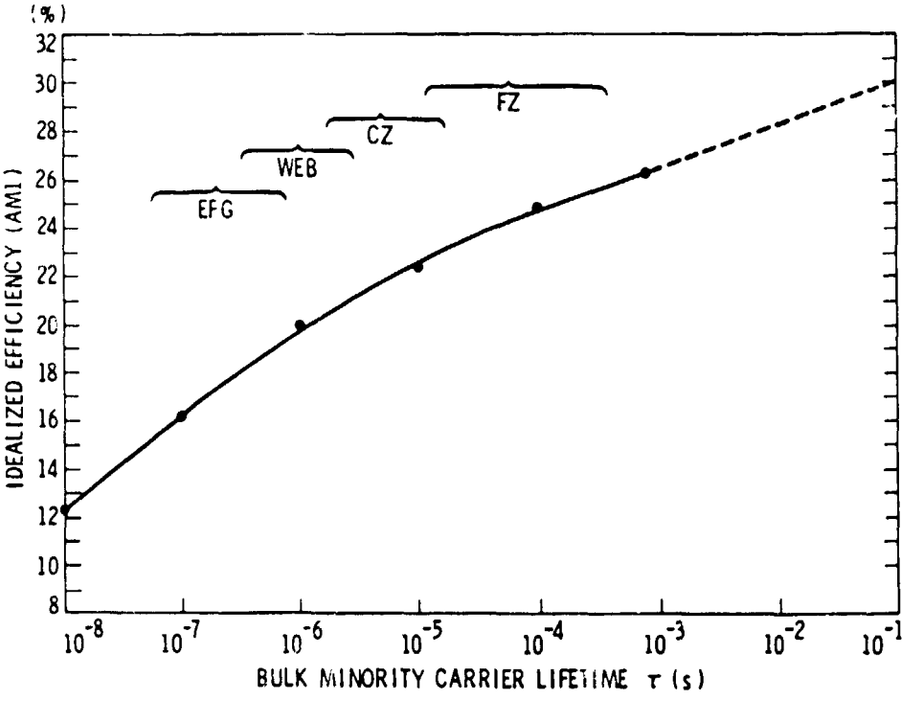
(%)
IDEALIZED EFFICIENCY (AM1)
EFG
WEB
CZ
FZ
BULK MINORITY CARRIER LIFETIME τ (s)

Research Approaches

- BULK LOSS CONTROL
  - HIGH QUALITY SHEET GROWTH (HIGH τ)
  - BULK DEFECT PASSIVATION
  - CARRIER LIFETIME MEASUREMENT TECHNIQUES IN HEAVILY DOPED THIN LAYERS
- SURFACE LOSS CONTROL
  - FUNDAMENTAL UNDERSTANDING OF THE ORIGIN AND NATURE OF SURFACE/INTERFACE STATES AND SURFACE RECOMBINATION MECHANISMS
  - SURFACE RECOMBINATION VELOCITY MEASUREMENT TECHNIQUES
  - SURFACE PASSIVATION
- PROCESS
  - HEAVY DOPING EFFECTS
  - INNOVATIVE CURRENT COLLECTION DESIGNS. (e.g. TUNNELING CONTACTS, CHARGEABLE TRANSPARENT CONDUCTING POLYMERS)
- MODELING
  - BETTER PHENOMENA SIMULATION
  - PROCESS SENSITIVITY ANALYSIS
  - DESIGNS FOR EFFECTIVE LOSS REDUCTION

Summary

- ACHIEVEMENT OF 20% EFFICIENT LARGE AREA SOLAR CELLS USING LOW-COST SILICON SHEET IS A DIFFICULT TASK AND IT REQUIRES:
  - UNDERSTANDING OF ALL ASPECTS OF CARRIER RECOMBINATION LOSSES
  - INNOVATIVE DESIGNS AND PROCESSES BASED ON SOUND MODELING
- RESEARCH IS SHOWING PROMISING RESULTS

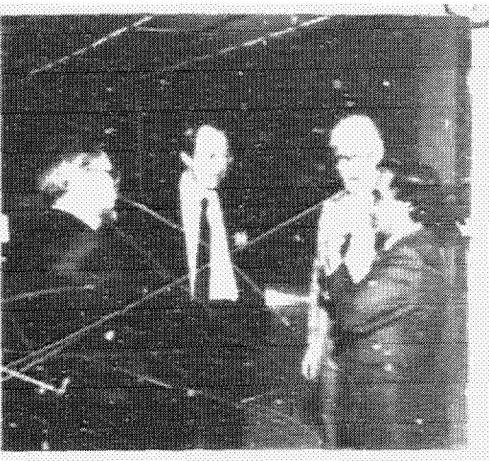

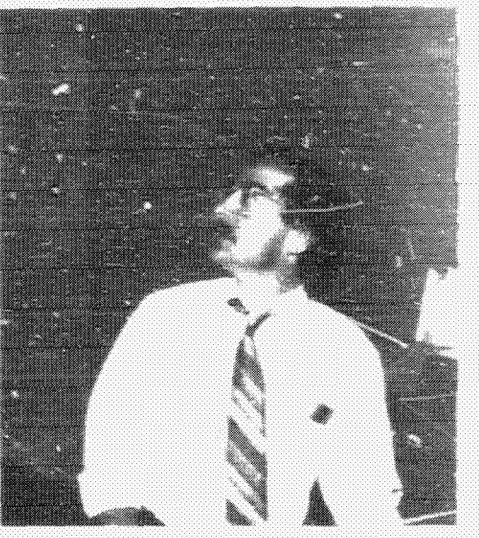

N85 15261

Technical Sessions

HIGH-EFFICIENCY SILICON SOLAR CELL RESEARCH

T. Daud, Chairman

Reports of research progress in high-efficiency solar cells and characterization and measurements were presented by eight contractors, SERI, and JPL.

Research Triangle Institute reported on its comprehensive silicon solar-cell computer modeling. Various single-junction and multijunction structures with phenomena submodels have been incorporated and recursion relationships for numerical analysis have been set up. Both low-level and high-level injection, with and without ambipolar transport, are incorporated. A list of future activities including fabrication of solar cells for correlation was presented.

A. Mokashi of JPL reported on efficiency estimation and sensitivity modeling. The one-dimensional code developed at Purdue University has been made operational at JPL for sensitivity analysis of cell design parameters, to compare innovative and conceptual designs for high efficiency, and identify barriers to high efficiency. In addition, a device-processing code (SUPREM) developed at Stanford University has also been made operational at JPL. The capabilities and operation of these programs were described.

A report on barriers to achieving high efficiency was presented by C.T. Sah Associates. Various loss mechanisms and their limiting values were discussed to show that to achieve greater than 20% efficiency, bulk recombination should be lower than 60 cm/second and the saturation current must be reduced below 10^{-13} A/cm^2.

New designs of matter insulator n-p (MINP) were discussed and a new structure called a floating emitter cell was proposed for 20% and higher efficiencies.

A molecular beam epitaxy (MBE) technique for making high-efficiency silicon solar cells was described by the University of California at Los Angeles. Growth apparatus and procedure were explained. Numerical analysis of a two-junction, cascade all-silicon cell was described. This cell has structures that can be obtained using MBE. Efficiency higher than that of single-junction cells is possible if the minority carrier recombination can be lowered at the tunnel junction to below 10^4 cm/second. Further work to solve cell leakage is to continue.

The Joint Center for Graduate Study (JCGS) presented progress in its investigation of silicon surface passivation by silicon nitride deposition. The plasma-enhanced CVD system has been made operational, deposition variables have been studied, and optical properties of nitride films (SiN) are being evaluated toward a good antireflective coating. In addition, a C-V technique with the Rosier method is being used for characterization of the SiN-Si interface.

HIGH-EFFICIENCY SILICON SOLAR CELL RESEARCH

R.H. Kachare of JPL discussed the research forum to be held July 9 through 11 at Phoenix, Arizona, titled "High-Efficiency Crystalline Silicon Solar Cells." Sessions and subjects to be covered were highlighted.

J.B. Milstein of SEkI described the high-efficiency silicon cell program at SERI. Details of solar cells with 17% and higher efficiencies were given. He reported that M. Green in Australia has sent a cell to SERI for measurement that showed 19.07% efficiency. ASEC, Spire and Westinghouse have also demonstrated : igher than 17% efficiency.

The University of Pennsylvania described a measurement technique for minority carrier lifetime and surface recombination velocity s, using calibrated spectral light-beam induced current (LBIC). The current obtained by a light beam of frequency low enough to penetrate the front region only is used with a curve-fitting model to extract the information. Results on Spire fabricated cells with and without oxide passivation were presented. BSF structure-doping profiles with modeling calculations and results were given. Minority-carrier lifetime values in regions of the cell during its fabrication and data on its degradation during fabrication were obtainable by this technique.

The University of Florida described the new technique of short-circuit current decay (SCCD) for and s measurement in the base region of the cell. This technique is based on a two-part analysis of a solar cell using Laplace transforms. After the higher-mode transients die out, the first-mode transient in the current of a cell gives the necessary information. Sensitivity analysis was presented to show data acquisition with better accuracy.

L.J. Cheng of JPL presented work on low-temperature electron-beam induced current (EBIC) using a scanning electron microscope. Polycrystalline wafers show more electrical activity at lower tempeatures; this gives a more sensitive technique for the study of defects in silicon. Temperature effects on recombination with respect to Fermi level were explained. In addition, a stress-related model of web ribbon was presented to relate defects to growth parameters and thermal profiles.

Cornell University described its characterization work on silicon ribbon. Thermal annealing and electrical activity of defects were analyzed. The role of carbon in EFG ribbon along with temperature cycling was evaluated. Various X-ray diffraction patterns were analyzed to obtain strain-field-related information. Dislocation twin interaction and coalescing of boundaries that may form large-angle grain boundaries after thermal treatment was discussed.

Work on impurity analysis using cryogenic laser calorimetry was described by the University of Southern California. Spectroscopy apparatus and method were described. Relative advantages and disadvantages were discussed.

HIGH-EFFICIENCY SOLAR-CELL DESIGN MODELING

RESEARCH TRIANGLE INSTITUTE

M.F. Lamorte

Program Goals

1. Develop comprehensive computer models to simulate single-junction and multiple-junction silicon solar cell structures shown in the matrix:

Top \ Base	P	P+	PP+
n	•	•	•
n+	•	•	•
n+n	•	•	•

2. Incorporate into the computer models the following phenomena submodels:
   - Effects due to—temperature
     Impurity concentration
     Defect energy levels
     High injection
     Surface states
   - Front surface field
   - Back surface field
   - Oxide charged insulator
   - Carrier confinement
   - Bandgap narrowing
   - Depletion region recombination
   - Surface recombination
   - Series resistance
   - Metal contact shadowing
   - Anti-reflection coatings

3. Fabricate 2 cm × 2 cm n^+p and n^+pp^+ near-optimized silicon solar cells
4. Fully characterize the cells with respect to V_{oc}, I_{sc}, P_{mp} V_{mp}, I_{mp}, η, Q over the temperature range 25° C to 150° C.
5. Assess the accuracy of the computer modeling program and correct phenomena submodels and/or analysis to obtain better than 5% agreement with experimental data.
6. Determine and quantify phenomena that gives rise to solar cell losses, through analysis and simulation studies.
7. Obtain new cell structures and designs that minimize these losses.

Accomplishments

1. Formulation of computer simulation using the Recursion Relationship Method.
2. An option may be exercised from the keyboard to use the nonambipolar or ambipolar solution.

3. In addition to the phenomena submodels listed in Figure 2, the following are also incorporated into the simulation program:
   - Bandgap narrowing using Fermi-Dirac statistics
   - Nonequilibrium np product using Fermi-Dirac statistics
   - Built-in and induced electric field components in quasi-neutral regions, applicable under low and high injection levels
   - Photovoltage effect on depletion width
   - Trap level concentration dependency on impurity concentration
   - Composite electron and hole lifetime relationships that include SRH, TAA, and BBA
   - Front and back surface recombination velocities that include SRH, TAA, and BBA
   - Electron and hole mobilities and diffusivities that are valid under low and high injection levels, and in nondegenerate and degenerate materials

Recursion Relationship Method Formulation

- Incorporates a comprehensive set of phenomena submodels and capability
- Combines low CPU costs of closed-form methods with high simulation accuracy of numerical integration methods
- Discretized into f-mesh points
- Transport equations constructed to contain a comprehensive set of phenomena submodels
- Appropriate transport equations applied to each mesh point
- Mesh point separations are reduced so that some coefficients in the continuity equation(s) may be considered constant at its mesh point
- Closed-form analytical solutions are obtained at positions midway between mesh points
- Value of the dependent variable at adjacent mesh points is governed by the analytical solution obtained in the region between the mesh points

Recursion Relationship Method Execution

- f-analytical solutions are obtained which contain 2f-constants of integration
- Apply the 2f-boundary conditions that are appropriate to the field of f-mesh points
- 2f-simultaneous equations result
- 2f-constants of integration are solved for explicitly, and recursion relationships are shown to exist
- Behavior of dependent variable and derived parameters may be determined because the numerical value of the 2f-constants of integration are known
- Method is applicable to the temporal analysis in 3-dimensions (x, y, z, t)

Comparison of Numerical Integration and Recursion Relationship Methods

Characteristic	Computer Simulation Method	
	Numerical Integration	RTI Recursion Relationship
Use in general application	Yes	Yes
Discretization	Required	Required
Criteria imposed on discretization	The use of insufficient mesh points does not allow for the solution to converge	None required for convergence
Simulation accuracy	Accuracy depends on the number of mesh points	Accuracy depends on the number of mesh points
Discretization limits	Excessively high CPU cost and running time results when large number of mesh points are used	Large number of mesh points may be used without excessively high penalty in CPU cost and running time
Guess solution	Required	Not required*
CPU running time	Low 150 sec (rare), typically 2-3 hours, high is greater than 15 hours	Typically 10 sec
Use as a laboratory or manufacturing tool	No; not cost effective; not practiced	Yes, high benefit/cost ratio

*In the Recursion Relationship Method, the closed form analytical solution is equivalent to the "guess solution" which is required in the numerical integration method. Because the closed form analytical solution in each segment (i.e., surrounding each mesh point) is unique, the use of the CPU is never required

Future Activities

1. Complete the application of the Recursion Relationship Method to silicon solar cell structures and obtain the recursion relationship.
2. Complete computer code for all phenomena submodels and recursion relationships.
3. Incorporate erfc and Gaussian impurity concentration profiles, as well as provisions for arbitrary profiles.
4. Debug computer program.
5. Fabricate and characterize n^+p and n^+pp^+ solar cells.
6. Simulate fabricated cell structures and assess simulation accuracy and, if necessary, verify accuracy of phenomena submodels with experimental data.
7. Commence simulation studies.

N85 15263

EFFICIENCY ESTIMATION AND SENSITIVITY MODELING

JET PROPULSION LABORATORY

A.R. Mokashi

Presentation

- OBJECTIVE
- APPROACH
- AVAILABLE MODELS
- SCAP1D
- SUPREM
- SEEMA

Objective

DEVELOP AN EXHAUSTIVE AND COMPREHENSIVE ANALYTICAL TOOL FOR EVALUATING THE PERFORMANCE OF A CRYSTALLINE SILICON SOLAR CELL OF A GIVEN DESIGN

- CONSIDER CELL PROCESS PARAMETERS AS INPUT DATA
- PERFORM SENSITIVITY ANALYSIS OF CELL DESIGN PARAMETERS
- COMPARE INNOVATIVE AND CONCEPTUAL DESIGNS FOR ACHIEVING HIGH EFFICIENCY (NEAR 20%)
- USE AS AN AID IN IDENTIFYING PARAMETERS LIMITING CELL EFFICIENCY BELOW 20%

Approach

- SEARCH LITERATURE AND EXPLORE AVAILABILITY OF STATE-OF-THE-ART MODELS WHICH ARE APPLICABLE AND USEFUL
- ACQUIRE COPIES OF USEFUL MODELS
- DEVELOP A SCHEME INCORPORATING THESE MODELS
  - IMPROVEMENTS
  - MODIFICATIONS
  - ADDITIONS

- **SOLAR CELL EFFICIENCY ESTIMATION METHODOLOGY AND ANALYSIS (SEEMA) MODELING EFFORT IS DIVIDED INTO TWO PARTS**
  - **A. SILICON SOLAR CELL PERFORMANCE SIMULATION**
  - **B. CELL FABRICATION PROCESS SIMULATION**
- **THE TWO SIMULATION MODELS CAN BE USED INDEPENDENTLY AND/OR IN COMBINATION**

Available Models

SOLAR CELL SIMULATION MODELS SCAP1D AND SCAP2D

- DR. RICHARD SCHWARTZ AND HIS TEAM (PURDUE UNIVERSITY)
  - ONE DIMENSIONAL AND TWO DIMENSIONAL COMPUTER CODES TO SIMULATE CONVENTIONAL AND CONCENTRATOR CELLS
  - SCAP1D IS CONSIDERED SUITABLE FOR SEEMA FOR ANALYSING CELLS USED IN FLATPLATE COLLECTORS
  - A COPY OF SCAP1D IS OBTAINED FROM PURDUE UNIVERSITY
  - SCAP1D IS FUNCTIONAL AT JPL

CELL FABRICATION PROCESS SIMULATION MODELS

- STANFORD HAS DEVELOPED A NUMBER OF SOFTWARE PACKAGES IN ELECTRONICS/CAD-CAM AREA
- AMONG THEM SUPREM II AND SUPREM III ARE CONSIDERED TO BE VERY USEFUL FOR SEEMA
- A COPY OF SUPREM II HAS BEEN ACQUIRED AND IS BEING INSTALLED AT JPL
- A COPY OF SUPREM III IS BEING PROCURED

SCAP1D

(SOLAR CELL ANALYSIS PROGRAM IN ONE DIMENSION)

BRIEF DESCRIPTION

A SEMICONDUCTOR DEVICE IS MODELED BY SOLVING

- POISSON'S EQUATION ,
- HOLE CONTINUITY EQUATION AND
- ELECTRON CONTINUITY EQUATION

IN CONJUNCTION WITH

- TRANSPORT EQUATIONS

NUMERICALLY IN ONE DIMENSION.

TRANSPORT EQUATIONS ARE DERIVED FOR HEAVILY DOPED SEMICONDUCTOR DEVICES

- EFFECTS OF HEAVY DOPING :
  - MODIFIED BAND STRUCTURE AND
  - INFLUENCE OF FERMI-DIRAC STATISTICS

ARE COMPLETELY DESCRIBED BY TWO PARAMETERS

- EFFECTIVE BAND SHRINKAGE, ΔG, AND
- EFFECTIVE ASSYMETRY FACTOR, γ

- NET RECOMBINATION RATE IS CONSIDERED TO BE SUM OF SCHOCKLEY- READ-HALL AND AUGER PROCESSES

- SOLUTION OF THESE EQUATIONS GIVES :
  - ELECTROSTATIC POTENTIAL, V,
  - HOLE CARRIER DENSITY, p,
  - ELECTRON CARRIER DENSITY, n,

FROM WHICH

- CURRENT THROUGH THE DEVICE MAY BE EVALUATED

Flow Diagram for Equilibrium Solution

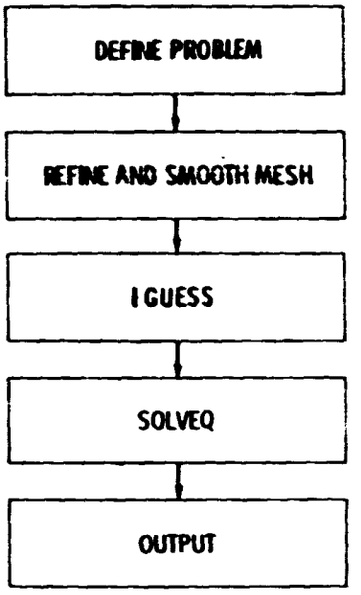

Flow Diagram for Non-Equilibrium Solution

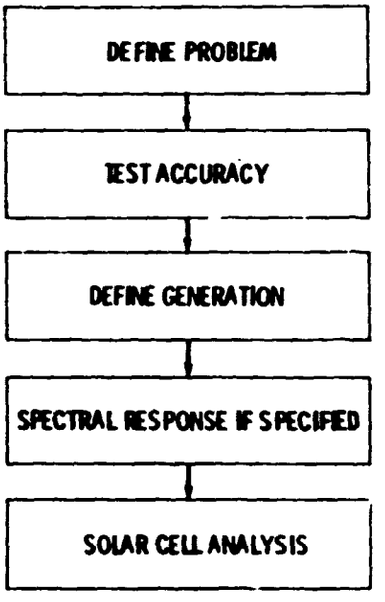

Computer Time

The one dimensional computer program requires about one minute (on a CDC 6600) to compute an I-V curve for six applied biases using 500 nodes. A complete solar cell analysis can be performed in about one and one-half minutes at an intensity of one sun.

Problem Summary: Sample Run Made During the Visit

```
DOPING PROFILE : ERFC (Complementary Error Function)

DOPING DENSITY (ND-NA) PER CM3 =  4.000E+20 AT  X =   0  MICRONS
                               = -1.000E+18 AT  X = 300  MICRONS
JUNCTION DEPTH:

FRONT      = 0.30 MICRON                    BACK = 2.00  MICRONS

BULK DOPING = -1.500E+16/CM3     BULK RESISTIVITY = 0.950  OHM-CM

TEMPERATURE = 27.00 C            DEVICE THICKNESS = 300.0 MICRONS

LAYER : 1    SHEET RESISTANCE = 28.201

LAYER : 2    SHEET RESISTANCE = 29.872

NUMBER OF MESH POINTS        = 250        SHADOW = 0

SLOTBOOM BANDGAP NARROWING MODEL

OPTICAL  GENERATION  RATE :          AM 1.5

SOLAR CONCENTRATION                = 1.00 TIMES

INCIDENT POWER                     = 0.08318 WATTS/CM2

GENERATED CARRIERS/INCIDENT PHOTON  = 0.59334

BACK CONTACT OHMIC,              SF = 1.000E+04 CM/SEC

MINORITY CARRIER LIFETIMES :   TAUP = 1.000E-05 SEC

                               TAUN = 1.000E-05 SEC

SHR TRAP LEVEL :            (ET-EV) = 0.5600 EV

SOLAR CELL PARAMETERS :          JSC = 1.06636E-02   VOC = 0.58576
                                 VMP = 0.50693       VBI = 1.0021
                            CELL AREA = 1.0E+00 CM2   RS = 0
                  COLLECTION EFFICIENCY = 0.8916
                          FILL FACTOR = 0.8228
                           EFFICIENCY = 0.1777
```

Current Variation Across Cell Thickness During Maximum Power Point Conditions

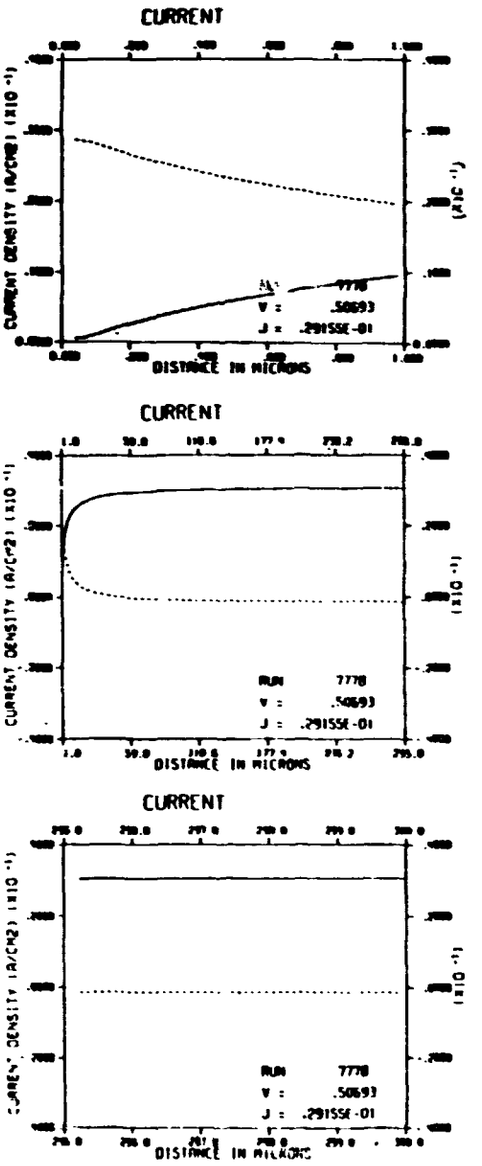

Recombination Variation Across Cell Thickness During Maximum Power Point Conditions

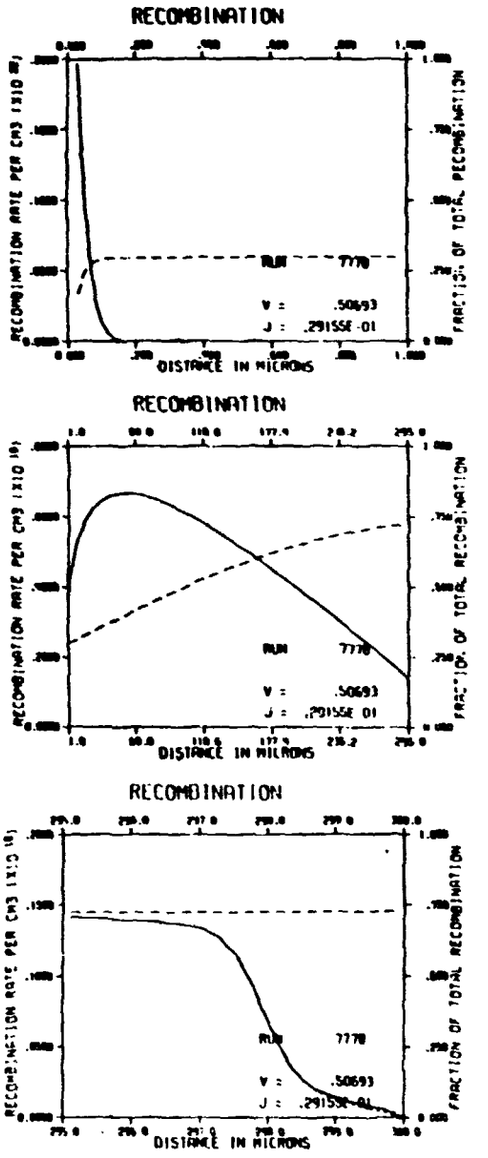

SUPREM II (Version 0.05)

- SIMULATES THE PROCESSING OF SILICON SEMICONDUCTOR DEVICES
- MOST COMMONLY USED PROCESSING STEPS ARE HANDLED BY THE PROGRAM
  - HIGH TEMPERATURE - DIFFUSION UNDER BOTH INERT AND OXIDIZING AMBIENTS
  - GAS SOURCE PREDEPOSITION
  - ION IMPLANTATION
  - EPITAXIAL GROWTH
  - ETCHING AND
  - DEPOSITION OF DOPED AND UNDOPED SILICON DIOXIDE
- NUMERICAL SOLUTION OF THE DIFFUSION UP TO FOUR IMPURITIES IS IMPLEMENTED WHICH INCLUDES HIGH CONCENTRATION AND QED EFFECTS
- OXIDATION OF SILICON IS MODELED ACCORDING TO DEAL-GROVE EQUATION, MODIFIED TO ACCOUNT FOR
  - HIGH PRESSURE CONDITIONS AND
  - HIGH IMPURITY CONCENTRATIONS AT THE OXIDIZING INTERFACE
- OUTPUT OF RESULTING IMPURITY DISTRIBUTIONS IS
  - PRINTED OR PLOTTED
- INFORMATION OBTAINED INCLUDE
  - JUNCTION DEPTHS, SHEET RESITIVITIES AND
  - THRESHOLD VOLTAGES

SUPREM III

- ONE DIMENSIONAL SIMULATION PROGRAM WHICH MODELS MANY INTEGRATED CIRCUIT FABRICATION PROCESSES
- CALCULATES SELECTED ELECTRICAL CHARACTERISTICS FROM SIMULATED DEVICE STRUCTURE AND IMPURITY DISTRIBUTIONS
- VARIETY OF DEVICE STRUCTURES MAY BE MODELED UP TO FIVE SEPARATE LAYERS ALLOWED
  - DEFAULT MATERIALS
    - SILICON
    - POLYSILICON
    - SILICON DIOXIDE
    - SILICON NITRIDE AND
    - ALUMINUM
- THE IMPURITIES WHICH MAY BE
  - IMPLANTED
  - DIFFUSED OR
  - DEPOSITED ARE
  - ARSENIC
  - ANTIMONY
  - PHOSPHORUS AND
  - BORON

SEEMA

- USE SCAP1D FOR SOLAR CELL SIMULATION
- USE SUPREM II OR III FOR CELL PROCESS SIMULATION
- USE SCAP1D AND SUPREM IN ISOLATION OR IN COMBINATION
- PROVIDE IMPROVEMENTS, ADDITIONS, AND MODIFICATIONS TO THESE PROGRAMS

N85 15264

BARRIERS TO ACHIEVING HIGH EFFICIENCY

C.T. SAH ASSOCIATES

C.T. Sah

TECHNOLOGY
MATERIAL AND FUNDAMENTAL LIMITATIONS ON HIGH EFFICIENCY SOLAR CELL PERFORMANCE.

REPORT DATE
03/14/1984 23ND PIM (21 months)

APPROACH
- ACCURATE MINOIRTY CARRIER RECOMBINATION RATE MEASUREMENTS BY NEW CAPACITANCE TRANSIENT METHOD AT TI, ZN AND AU; AND
- NEW CELL STRUCTURES OF LOW RECOMBINATION.

CONTRACTOR
C. T. SAH ASSOCIATES

GOALS
- ACCURATE DETERMINATION OF MINORITY CARRIER RECOMBINATION RATES AT DOMINANT IMPURITY CENTERS.
- COMPUTER-AIDED PREDICTION OF MAXIMUM ALLOWABLE RECOMBINATION CENTER DENSITY FROM ACCURATE RATE DATA ABOVE.
- DELINEATION OF FUNDAMENTAL LIMITATIONS ON EFFICIENCY ABOVE 20% (AM1).
- DEVELOPMENT OF NEW CELL STRUCTURES FOR VERY HIGH EFFICIENCY.

STATUS
- THERMAL CAPTURE RATE DETERMINATION
  - NEW CAPACITANCE TRANSIENT METHOD FOR BOTH MAJORITY AND MINORITY CARRIER THERMAL EQUILIBRIUM CAPTURE RATES HAS BEEN APPLIED TO MANY IMPURITIES.
  - CAPTURE RATES AT DOUBLE DONOR TITANIUM CENTERS AND DOUBLE ACCEPTOR ZINC CENTERS OVER WIDE TEMPERATURE RANGES COMPLETED. TITANIUM RESULTS IN PRESS AT JOURNAL OF APPLIED PHYSICS; ZINC IS WRITTEN UP.
  - CAPUTRE RATES AT THE TWO GOLD LEVELS ARE IN PROGRESS.
- HIGH EFFICIENCY LIMITATIONS
  - LIMITING PARAMETERS AND GEOMETRIES ARE DELINEATED AND PRESENTED AT WORKSHOP.
  - NEW HIGH EFFICIENCY AND NEW VERY HIGH EFFICIENCY CELL STRUCTURES ARE INVENTED;
  - PRELIMINARY DESIGN CALCULATIONS SHOW GREATER THAN 20% WITH FEW CONSTRAINTS.

Parameters Characterizing a p/n Junction Solar Cell

EQUATION

$$J = J_L - J_1(e^{qV_J/kT} - 1) - J_m(e^{qV_J/mkT} - 1)$$

m = 1 → 2 Space Charge Layer
m = 2 High Level QNR's
m = 4 Surface Channel
m > 2 → 4 Resistive Shunts

HIGH EFFICIENCY CELL

- Avoid nonideal recombination components (THEY GIVE LOW FF.)
- Maintain low injection level.

••• $J_m = 0$

$$J = J_L - J_1(e^{qV_J/kT} - 1)$$

Parameters Affecting the Performance of High-Efficiency Silicon Solar Cells

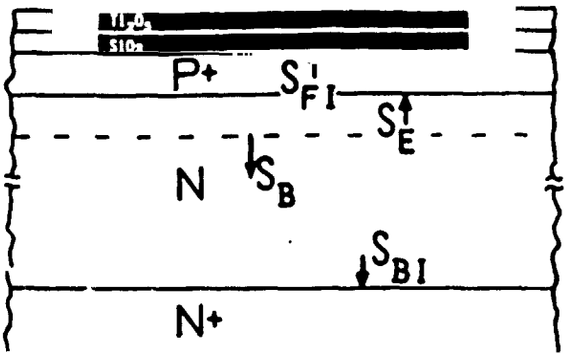

HIGH EFFICIENCY SILICON p/n JUNCTION
SOLAR CELL CHARACTERIZATION PARAMETER

- $J = J_L - J_1 e^{qV/kT} - 1$
- $J_L = 32$ mA/cm^2 at AM1 (89 mW/cm^2)
- $J_1 = qP_B S_B + qN_E S_E$ where:
  - BASE (Thin: $T_B \ll L_B$) $S_B = (T_B/\tau_B) + S_{BI}$
  - EMITTER (Thin: $T_E \ll L_E$) $S_E = (T_E/\tau_E) + S_{FI}$
- FOR A AM1 20% CELL with S_E=0.
  $J_1 < 10^{-13}$ A/cm^2 $S_B < 60$ cm/s

Performance and Requirement of 20% Silicon BSF $p^+/n/n^+$ Solar Cells

P_{IN} = 89 mW/cm^2; J_L = 32 mA/cm^2; 24.0C

•••Base Recombination Only•••

VOC mV	FF	EFF %	J_1 mA/cm^2	S_B cm/s	τ_B us	N_{TT} Ti/cm^3
660	.8375	19.88	2.0E-13	128	39	1.7E12
680	.8410	20.56	9.4E-14	58	83	6.5E11
700	.8445	21.26	4.3E-14	27	186	3.6E11
720	.8460	21.90	2.0E-14	12	407	1.6E11
LIMITS		none	none	(a)	(b)	(c)

(a) S_E=0 and P_B=$10^{20}/10^{16}$ (~1 ohm-cm)

(a) S_B increases by 10X if N_B increases by 10X to 10^{17} cm^{-3}.

(b) S_{BI}=0; T_B=50 um

(c) c_p=1.5x10^{-8} cm^3/s; τ_{AUGER}=3.6 ms.

Emitter Recombination Limitations

- $J_1 = qN_E S_E + qP_B S_B < 10^{-13}$ A/cm^2

For a Thin Emitter ($T_E \ll L_E$)

- $S_E = (S_{EI} + V_{RO})/\{1 + (S_{EI}/V_{DI})\}$
  - $V_{DI} = D_E/T_E = 1/(0.25\times10^{-4}) = 4\times10^4$

    $\therefore S_{EI} \ll 4\times10^4$ cm/s

    $\therefore S_E = S_{EI} + V_{RO} \equiv S_{EI} + (T_E/\tau_E) + V_{AUGER}$
- $J_{1AUGER} = qN_E V_{AUGER}$

  $= qc^P n_i^2 P_{TOTAL} < 10^{-13}$ A/cm^2

where

- $c^P = 9.9\times10^{-32}$ cm^6/s
- $n_i = 1.0\times10^{10}$ cm^{-3} at 24.00C
- $P_{TOTAL} = \int_0^{T_E} P(x)dx$ hole/cm^2

  $< 6.3\times10^{17}$ hole/cm^2 $\sim$ 10 S/□
- For $\Delta E_G = -4.6\,kT = -120$ mV,

  $n_i = 10^{11}$ cm^{-3} and

  $P_{TOTAL} < 6.3\times10^{15}$ hole/cm^2

  $\sim$ 0.1 S/□

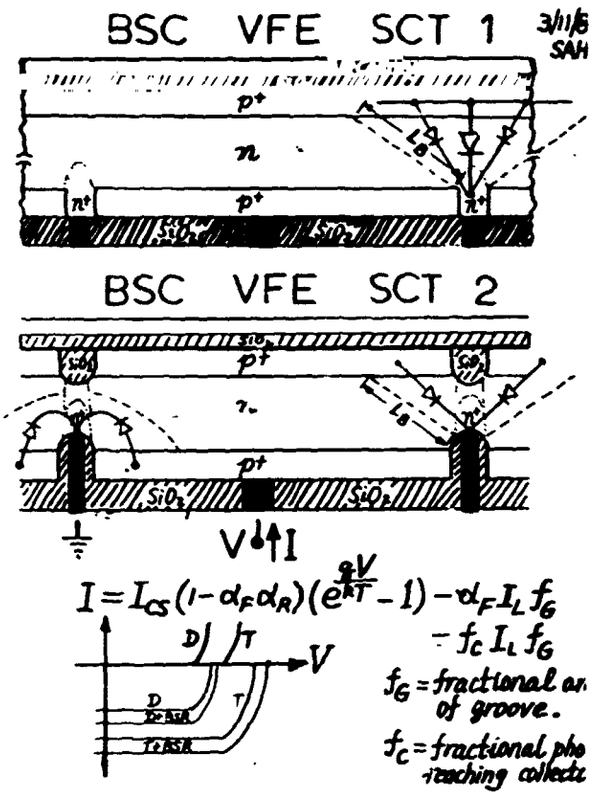

Back Surface Contact BSC
Vertical Floating Emitter VFE
Solar Cell Transistor SCT

Variations

BSC → FSC Front

VFE → LFE Lateral

$$I = I_{CS}(1-\alpha_F\alpha_R)(e^{\frac{qV}{kT}}-1) - \alpha_F I_L f_G - f_C I_L f_G$$

$$\Delta V_{OC} = \frac{kT}{q}\ln\left(\frac{\alpha_F+f_C}{1-\alpha_F\alpha_R}\right) \simeq 4.6\frac{kT}{q} \simeq 120\text{mV}$$

$$\Delta I_{SC} = I_L[\alpha_F+f_C-(1+R_{base})] \simeq 0.2 I_L$$

$$\Delta FF \cong \Delta(V_{OC}\cdot\beta)\frac{\ln\beta V_{OC}-1}{(\beta V_{OC})^2} \quad \beta=\frac{q}{kT}$$

~ 0.015

$$\therefore \frac{\Delta EFF}{EFF} \sim \frac{\Delta V_{OC}}{V_{OC}} + \frac{\Delta I_{SC}}{I_{SC}} \simeq 0.2+0.2 = 0.4$$

2nd New Cell Design for Very High Efficiency

- RESULT OF ESTIMATE
  - $\Delta V_{OC} \simeq +4.6kT/q \rightarrow 120\text{mV}$
  - $\Delta J_{SC} \simeq +0.2\bar{J}_{SC} \rightarrow 6\text{mA}$
  - $\Delta FF \simeq +0.015$
  - $\Delta EFF \simeq +0.4\,EFF \rightarrow$
- START WITH 16% cell, old design,
- New cell design $\sim 16\% \times 1.4 \simeq 22\%$
  - $V_{OC} \simeq 625+120 = 745\text{mV}$
  - $J_{SC} \simeq 32+6.4 \simeq 38\text{mA}$
  - FF ≈ little change

*SCT CELL STRUCTURE : TBA

Obstacles

1. Material Physics
   C_n^*, C_p^*, E_T^*; ΔE_G; μ, D surface/top bulk/base
   Material Chemistry
   $N_{TT}(x,t)$ *reliability, yield*

2. Device Physics
   How it works.
   Device (Modeling) Analysis
   Analytical Approximations.
   Computer-Numerical-Exact.
   Device Design
   ★★ *Innovative - new structures.* ★★

3. Fabrication Technology
   Costs. Modeling

4. Reliability
   Yield. Modeling

N85 15265

MBE GROWTH FOR HIGH-EFFICIENCY SILICON SOLAR CELLS

UNIVERSITY OF CALIFORNIA AT LOS ANGELES

F. Allen

PURPOSE: 1. TO UTILIZE THE EXTREME DOPANT PROFILE CONTROL POSSIBLE WITH MBE TO GROW SILICON SOLAR CELLS OF HIGH EFFICIENCY

2. TO MODEL BY COMPUTER A CASCADE SILICON CELL WITH TWO JUNCTIONS IN SERIES AS A MEANS OF GETTING LARGE D.C. VOLTAGE AND HIGH EFFICIENCY

UCLA Silicon MBE System as of 12/13/82

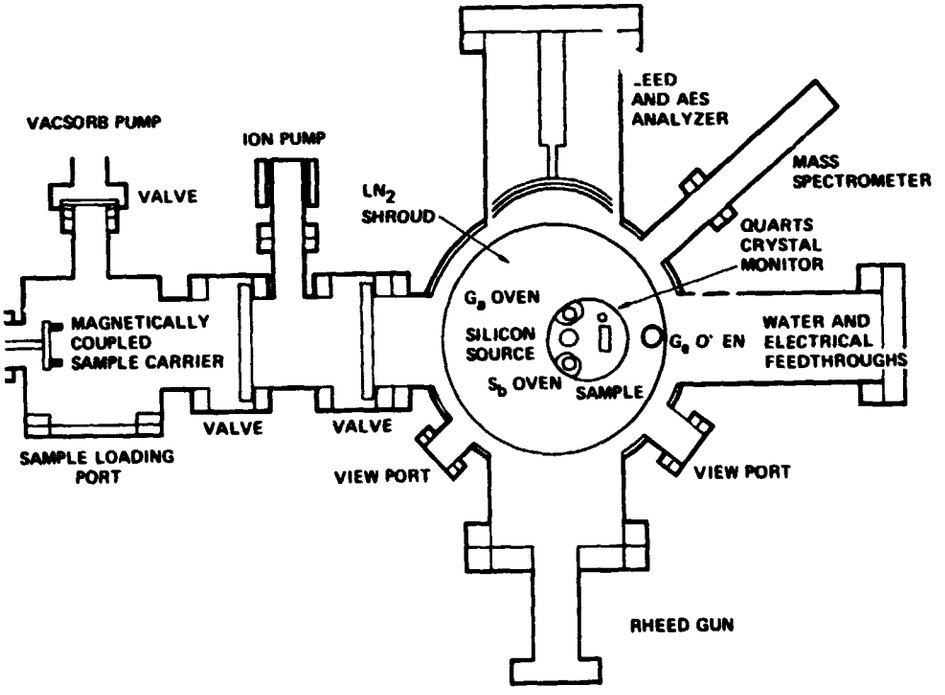

Silicon MBE for Solar-Cell Growth

ADVANTAGES:

- COMPLETE DOPANT CONTROL TO ~ 10Å
- ARBITRARY PROFILES
- ABRUPT CHANGES
- FROM 10E13 TO > 10E19cm^{-3} n-TYPE (Sb) AND p-TYPE (Ga)
- CAN PROVIDE VERY SHALLOW FRONT SURFACE FIELD AND VERY DEEP BACK SURFACE FIELD
- CAN GROW TANDEM CELLS CONNECTED BY TUNNELJUNCTIONS

CURRENT LIMITATIONS :

- HIGH REVERSE LEAKAGE AT JUNCTIONS (UCLA)
- LOW GROWTH RATE (3Å/sec UCLA)
- TOTAL DEPTH OF EPI-LAYER: < 5 MICRONS
- FINE TUNING NEEDED TO GET HIGH LIFETIME
- HIGH COST PROCESS-STILL BEING DEVELOPED

UCLA Program Results in Past Year

1. MBE CELL GROWTH

- 12 WAFERS GROWN FOR JPL
- ONLY 2 OF THESE SURVIVED TO MAKE FINISHED CELLS WHICH COULD BE TESTED

- RESULTS:
  - SIMPLE PROFILE
  - GROWN BY SOLID PHASE EPITAXY
  - PROCESSED AT JPL

SAMPLE

	#109	#110●
Voc(v)	0.46	0.49
Jsc(mA/cm²)	14.6	13.8
FF	0.71	0.71
η %	4.7	4.8

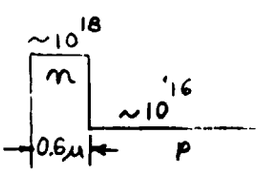

● ANNEALED IN H_2 AT 750°C FOR 1 HOUR

Problems in MBE Growth Thus Far

1. **HIGH REVERSE CURRENT AT JUNCTIONS**

PROBABLE CAUSES:

- **IMPURITIES: SIMS SHOWS C, Mo, Cu**
- **DISLOCATIONS: DEPEND UPON ATOMICALLY CLEAN SUBSTRATE BEFORE GROWTH**

REMEDIES

1. **IDENTIFY IMPURITIES AND ELIMINATE THEM**

BELL LABS RESULTS ,(J.C. BEAN) SHOW $\tau_e \sim 30$ uSEC AT JUNCTIONS ARE POSSIBLE
(IN 5×10^{15} p-MATERIAL)

Higher η Possible With Cascade Cell

MODEL: ONE SHALLOW JUNCTION NEAR SURFACE

SECOND DEEP JUNCTION BENEATH FIRST

FIRST JUNCTION p-DOPING HIGH

SECOND JUNCTION p-DOPING LOWER

FRONT AND BACK SURFACE FIELDS

(NOT PENETRATING YET)

IDEA: HIGH ENERGY PHOTONS PRODUCE HALF OF ALL

PAIRS IN 1st 2.5 MICRONS

THESE ARE MOST EFFICIENTLY COLLECTED

IN SHALLOW (2 MICRON) JUNCTION

REST OF LOWER ENERGY PHOTONS PRODUCE

PAIRS DEEP IN SAMPLE, COLLECTED BY

DEEP JUNCTION

Fraction Generated versus Depth

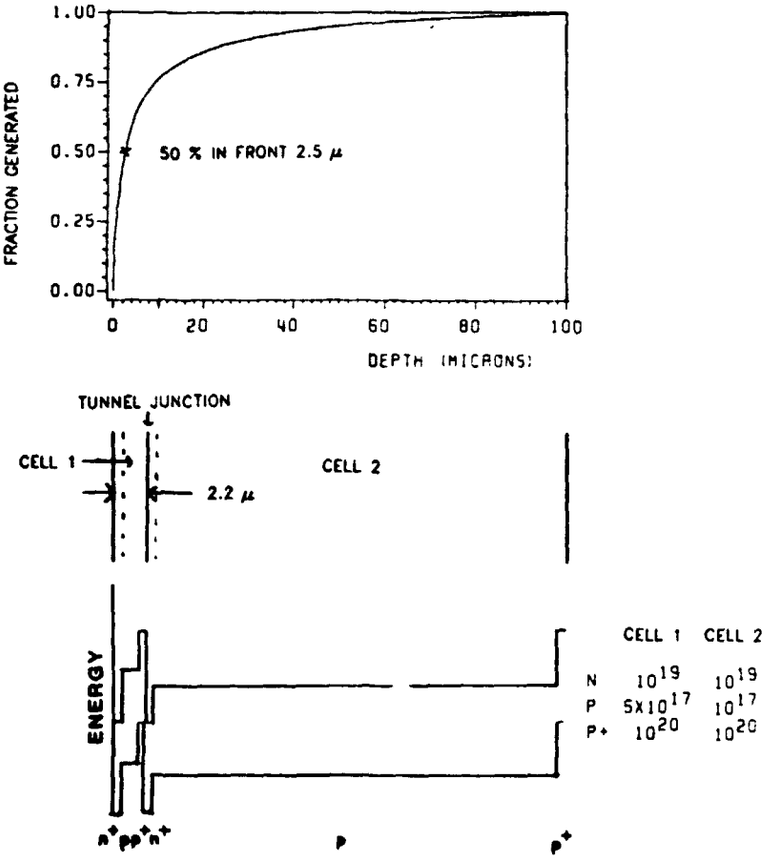

Parameters for Calculations

ρ	N_A (cm^{-3})	D_n (cm^2/s)	L_n (μ)	τ_n (μs)	W_n (μ)
0.1	5X10E17	10.9	52.2	2.5	0.05
0.3	9X10E16	19	105	6	0.12
1	1.5X10E16	27	164	10	0.28
3	4.5X10E15	31	193	12	0.47
10	1.25X10E15	36	232	15	0.93

$N_D = 10E19cm^{-3}$ $N_A = 10E20cm^{-3}$

$L_p = 7.2\mu$

$D_p = 1.295cm^2/s$

$\tau_p = 0.4\mu s$

S's ON OUTER SURFACES = 10E4 cm/s

S's AT TUNNEL JUNCTION = 0

WIDTH OF n^+ LAYERS = 0.2 μ

UCLA Program Results in Past Year

2. COMPUTER MODELLING OF CASCADE CELL IN SILICON

(P. SPARKS)

- REASONS FOR INVESTIGATING
  - UP TO TWICE Voc POSSIBLE
  - SLIGHTLY HIGHER η POSSIBLE
  - COULD GROW BY MBE–USE TUNNEL JUNCTION TO CONNECT CELLS IN SERIES

Efficiency of 100 μm Si Solar Cells

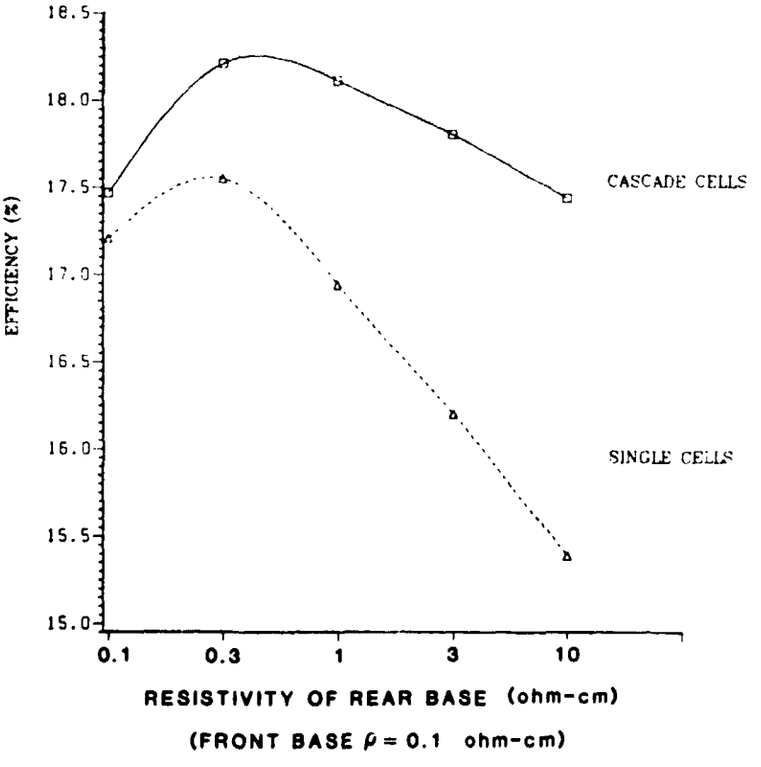

Other Progress With UCLA MBE Process

1. **DEMONSTRATED POWER OF SOLID PHASE EPITAXY**
   - **DEPOSIT AMORPHOUS SILICON ON CLEAN SUBSTRATE AT ROOM TEMP. WITH DOPANTS AS DESIRED**
   - **REGROW IN SITU AT 570°C**
   - **RESULTS:**
     - **GOOD (BULK) MOBILITY**
     - **GOOD CRYSTAL QUALITY**
     - **N_D AND N_A LEVELS UP TO $>10E19\ cm^{-3}$ FOR FIRST TIME : TUNNEL DIODES NOW POSSIBLE**
     - **NO DOPANT SMEARING**
   - **GREW FIRST TRIANGULAR BARRIER DIODES IN SILICON WHICH WORKED**

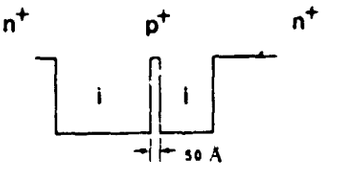

Future Effort of UCLA Group

- **DEMONSTRATE AND EVALUATE TUNNEL JUNCTION NEEDED FOR TANDEM CELL.**
  (APPEARS TO HAVE NO PROBLEMS-DOESN'T DEPEND ON HIGH QUALITY CRYSTAL AT JUNCTION-NEEDS ONLY ABRUPT n^{++}-p^{++} TRANSITION)
- **DEMONSTRATE A CASCADE CELL USING SUCH A TUNNEL JUNCTION WITH Voc HIGHER THAN POSSIBLE WITH A SINGLE CELL.**
- **CONTINUE TO WORK TO ELIMINATE IMPURITY CAUSING LEAKAGE PROBLEM.**

N85 15266

INVESTIGATION OF SILICON SURFACE PASSIVATION BY SILICON NITRIDE DEPOSITION

UNIVERSITY OF WASHINGTON

L.C. Olsen

Other Contributors

DR. BILL ADDIS
DR. WES MILLER
GLEN DUNHAM
ERIC EICHELBERGER
DAN DOYLE

Objectives and Approach

OBJECTIVES

TO EVALUATE THE USE OF SILICON NITRIDE DEPOSITED BY PLASMA-ENHANCED CVD FOR PASSIVATION OF SILICON SURFACES.

APPROACH

TASK 1 — SiN FILM GROWTH BY PECVD

- ESTABLISH PECVD SYSTEM
- DEVELOP PROCEDURES FOR SiN FILM GROWTH

TASK 2 — FILM CHARACTERIZATION

- OPTICAL CONSTANTS
- PHOTON TRANSMISSION AND PHOTOCURRENT ANALYSIS

TASK 3 — CHARACTERIZATION OF SiN/Si INTERFACE AND IMPACT ON SOLAR CELL PERFORMANCE

- INTERFACE STATE DENSITY AND FIXED CHARGE
- SURFACE RECOMBINATION VELOCITY FROM ROSIER METHOD AND PHOTORESPONSE ON SILICON CELLS
- THEORETICAL STUDIES CONCERNING SOLAR CELL PERFORMANCE

Schematic of PECVD System

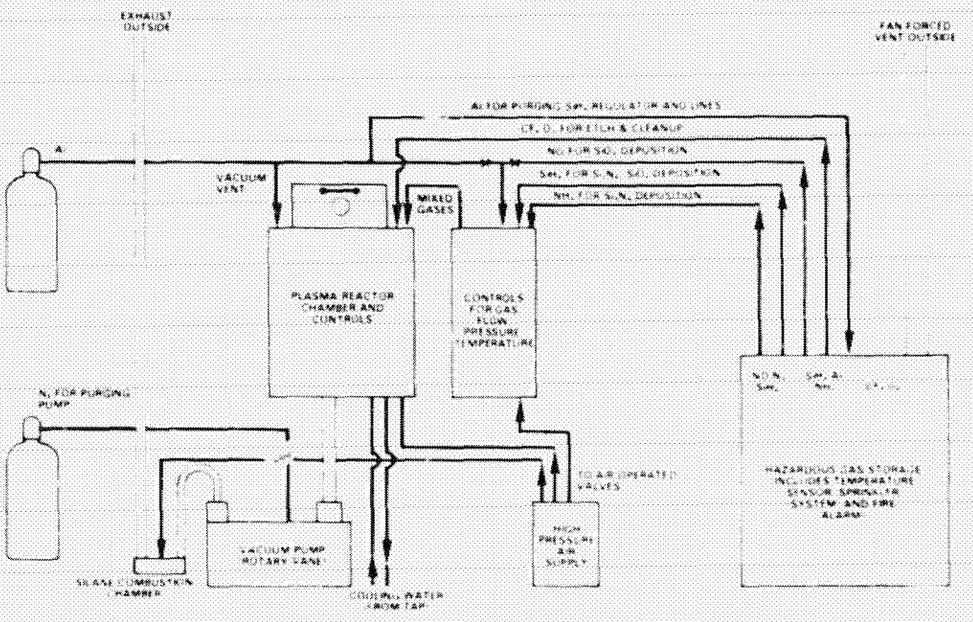

Plasma-Enhanced CVD System

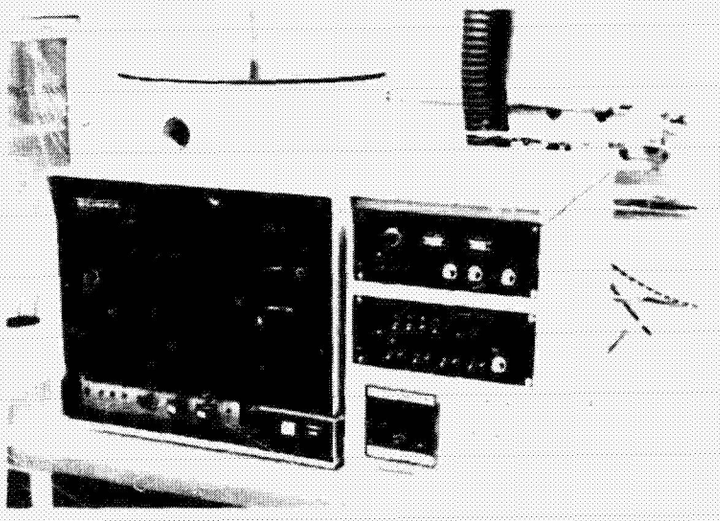

Platen of PECVD System

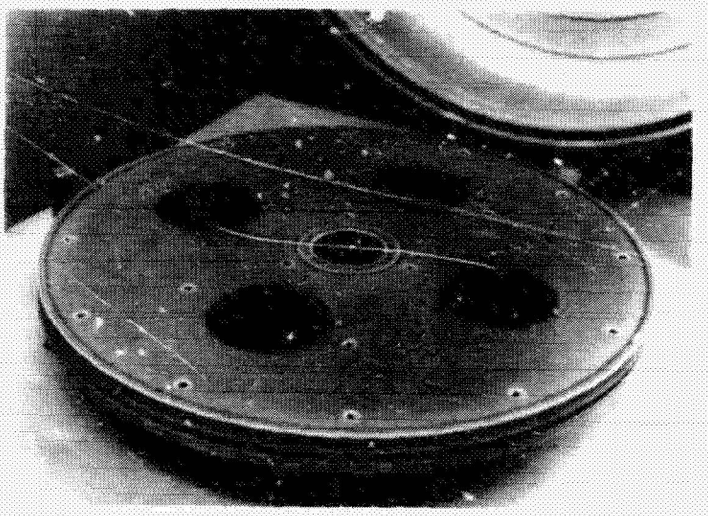

View Through Port: Plasma Between Planar Electrodes

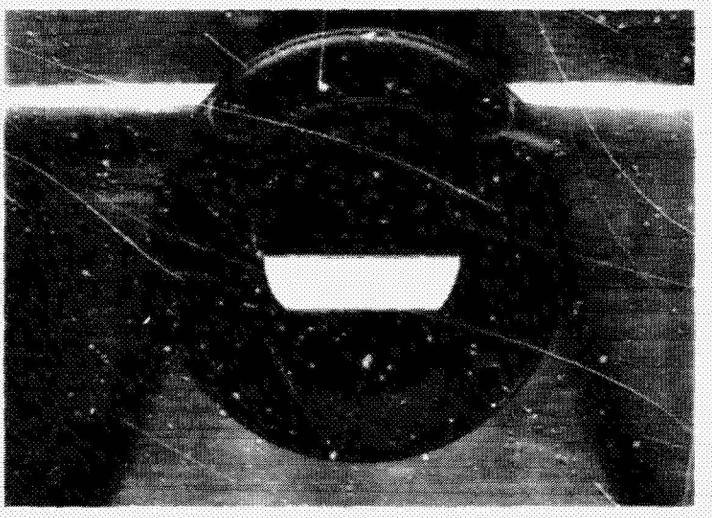

SiN Deposition Variables

- **GAS FLOW RATES**
- **NH_3/SiH_4 GAS FLOW RATIO**
- **PLATEN TEMPERATURE**
- **RF POWER**
- **CHAMBER PRESSURE**

Measurement of Indes of Refraction Of SiN Films on Silicon

- MEASURE R VS. λ
- VALUES OF N_2 VS λ AND K_2 VS. λ ARE KNOWN
- ASSUME $K_1 \sim 0$ (PARTICULARLY GOOD APPROXIMATION FOR λ >500 nm)
- DETERMINE d AND N_1 VS. λ
  - ASSUME N_1 IS CONSTANT OVER 30 nm RANGE FOR $\lambda \sim$600 nm AND DETERMINE d FROM R VS λ DATA
  - THEN DETERMINE N_1 VS λ

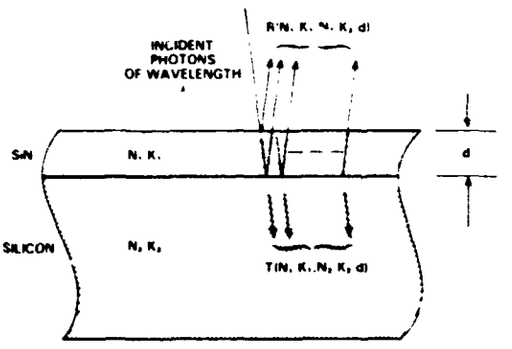

Measurements of Optical Constants of SiN Films on Quartz

- MEASURE T VS λ AND R VS λ
- DETERMINE d USING LONG WAVELENGTH R AND T DATA
- USE COMPUTER ANALYSIS TO DETERMINE N_1 AND K_1 VS λ BASED ON KNOWN VALUES OF N_2 VS λ, d AND EXPERIMENTAL DATA FOR R AND T VS λ

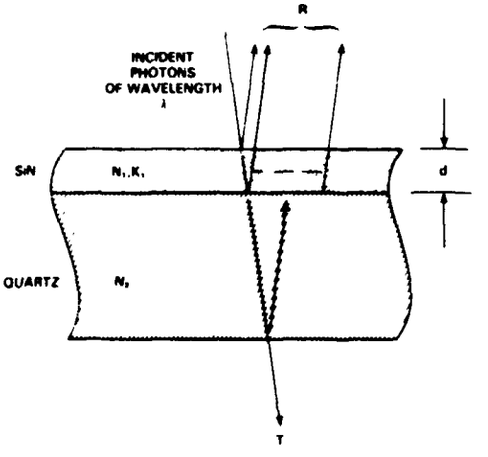

Silicon Nitride as an Antireflection Coating

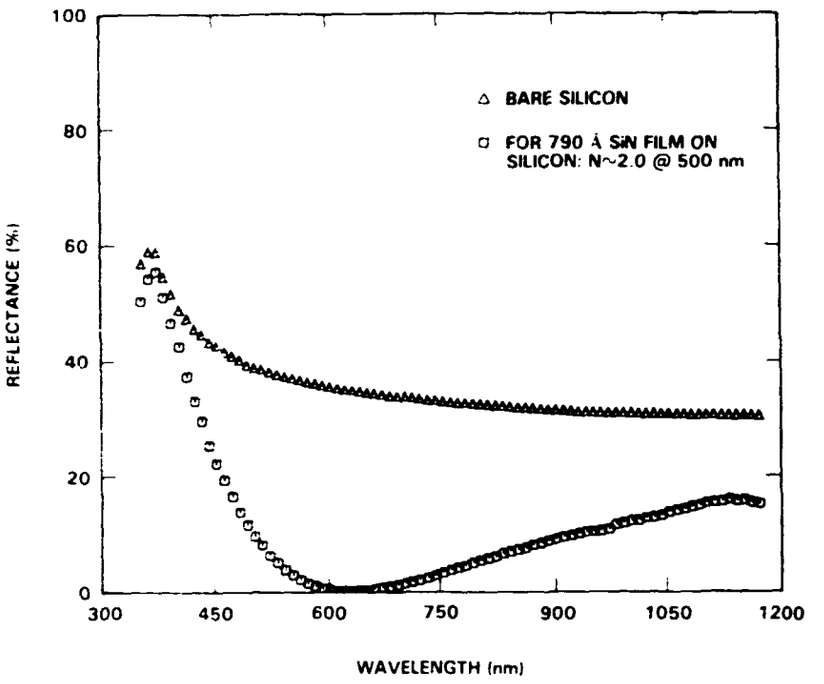

Index of Refraction vs Wavelength

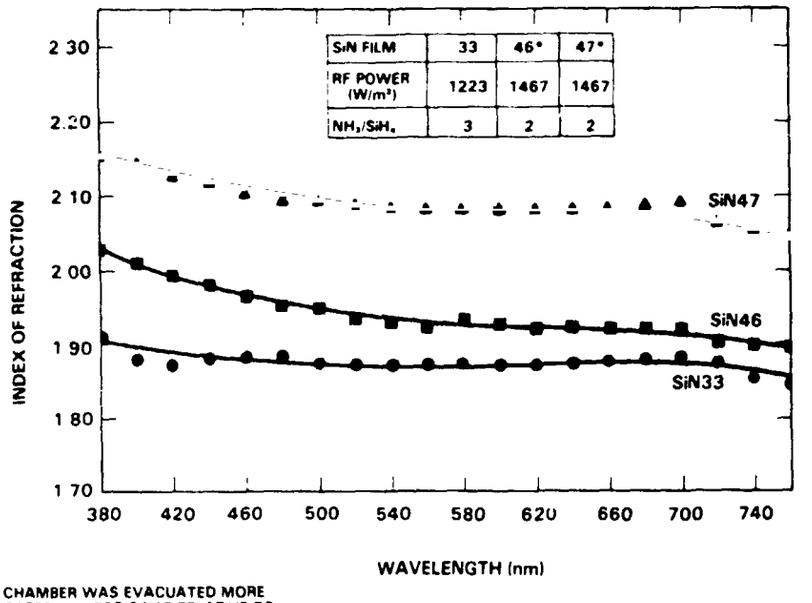

* CHAMBER WAS EVACUATED MORE CAREFULLY FOR SiN47 RELATIVE TO SiN46

SiN Film Index of Refraction vs Growth Parameters

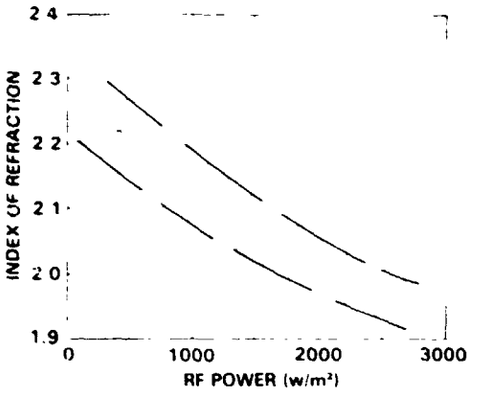

- SUBSTRATE TEMPERATURE = 270 °C
- GAS FLOWS (sccm)

Ar	NH_3	SiH_4
30	10	10

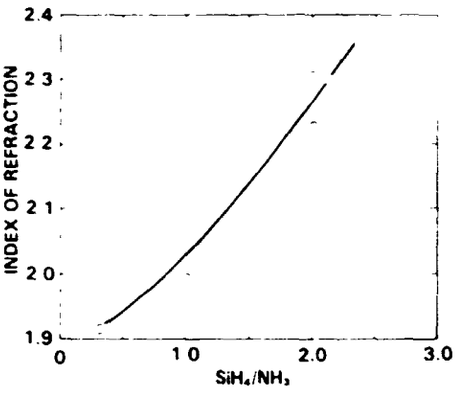

- SUBSTRATE TEMPERATURE = 270 °C
- GAS FLOWS (sccm): SiH_4 = 10, Ar = 30 AND NH_3 VARIED.
- RF POWER = 1225 w/m²

Calculated AM1 Photocurrent

AR LAYER STRUCTURE	INDEX OF REFRACTION	LAYER THICKNESS (Å)	AM1 PHOTOCURRENT (mA/cm²)	
			ACTIVE AREA	TOTAL AREA WITH 4% SHADOWING
IDEAL	—	—	38.5	37.0
SINGLE LAYER	1.8	838	35.29	33.89
	1.9	789	35.49	34.07
	2.0	746	35.52	34.10
	2.1	706	35.41	33.99
	2.2	669	35.18	33.77
DOUBLE LAYER	1.3, 2.4	1155, 593	37.49	36.00
	1.4, 2.4	1065, 587	37.63	36.12
	1.4, 2.5	1075, 562	37.71	36.20
	1.5, 2.6	1007, 535	37.77	36.26
	1.5, 2.8	1019, 493	37.73	36.22
	1.6, 2.8	955, 491	37.73	36.22
	1.6, 2.9	961, 472	37.70	36.19

COMPUTATIONAL APPROACH:

(1) EXPERIMENTAL RESULTS FOR INTERNAL PHOTORESPONSE OF SHALLOW JCT SILICON N/P CELL

(2) PHOENIX AM1 IRRADIANCE SPECTRUM

(3) PHOTON TRANSMITTANCE CALCULATED WITH COMPUTER CODE FOR MULTIPLE LAYERED STRUCTURE

Density of States Measurement

VOLTAGE DISTRIBUTION

$$V = \Psi_S - \phi_{SM} - \frac{(Q_{POS} + Q_{SC}(\Psi_S))}{C_o}$$

WHERE

$$C_o = \frac{\epsilon_{INS}}{d_{INS}} \quad Q_{POS} = Q_{FC} + Q_{SS}$$

HIGH FREQUENCY CAPACITANCE

$$dV = dV_{INS} + d\Psi_S$$

$$= \frac{dQ_{SC}}{C_o} + \frac{dQ_{SC}}{C_D}$$

$$= \frac{dQ_{SC}}{C}$$

$$C^{-1} = C_o^{-1} + C_D^{-1}$$

$$C_D = C_D(\Psi_S)$$

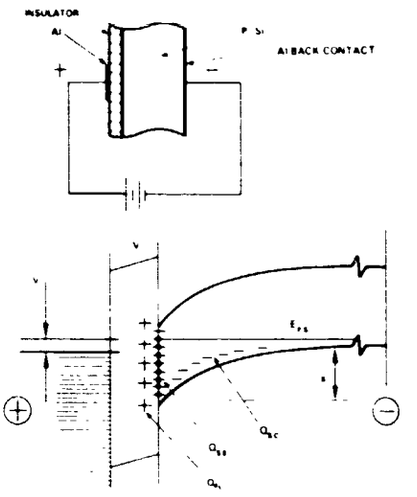

DATA ANALYSIS

- DETERMINE C_o FROM C VS V AT $V < 0$
- CHOOSE Ψ_S AND CALCULATE V
- CALCULATE C VS V FOR $Q_{POS} = 0$
- DETERMINE $Q_{POS} = Q_{INS} + Q_{SS}$ AS FUNCTION OF Ψ_S BY COMPARING EXPERIMENTAL RESULTS FOR C VS V TO THEORETICAL RESULTS FOR C VS V WITH $Q_{POS} = 0$

$$Q_{POS} = C_O \times V$$

- D_{SS} GIVEN BY

$$D_{SS} = \frac{dQ_{SS}}{d\Psi_S} \quad \frac{dQ_{POS}}{d\Psi_S}$$

C versus V for SiN Film on p-Type Silicon

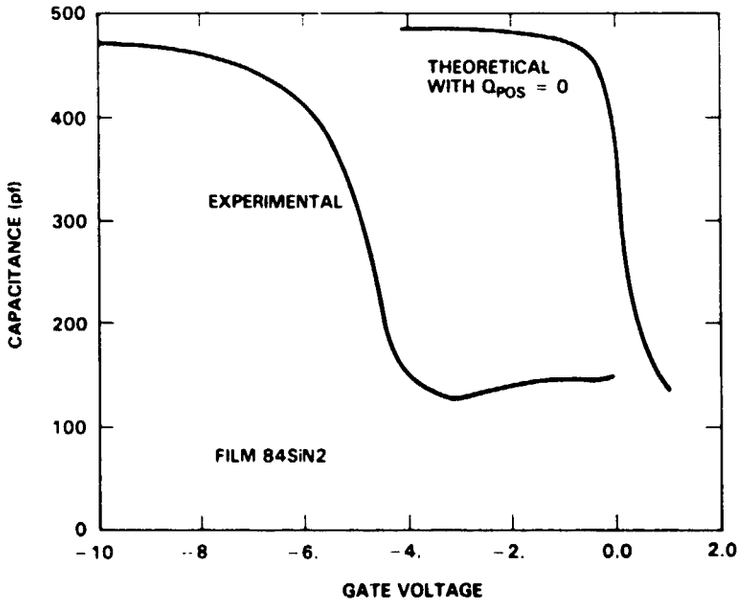

Midgap Interface State Density for SiN/pSi Substrates

SiN FILM	GROWTH PARAMETERS		D_{SS} @ MIDGAP (cm $^{-2}$eV^{-1})		ESTIMATED[3] S $\frac{(cm)}{SEC}$
	GAS FLOW (sccm) (Ar, NH_3, SiH_4)	RF POWER (w/m^2)	AS DEPOSITED	AFTER HEAT TREATMENT[2]	
SiN-2	80, 7.0, 2.8	163	1.0×10^{12}	1.0×10^{11}	500
SiN-29[1]	54, 54, 18	1468	$< 5 \times 10^{9}$	–	25
SiN-40	30, 70, 10	1223	9.2×10^{11}	8.1×10^{11}	4000
SiN-42	30, 10, 10	816	1.7×10^{12}	1.3×10^{12}	6500
SiN-47	72, 48, 24	1223	9.1×10^{11}	9.0×10^{11}	4500

(1) FILM SiN-29 HAS A 50 Å THERMAL OXIDE.

(2) 500 °C FOR 30 MINUTES IN ARGON

(3) S IS ESTIMATED FROM

$$S = \sigma v_{TH} D_{SS} \cdot 2kT$$

Surface Recombination Velocity: Rosier Method

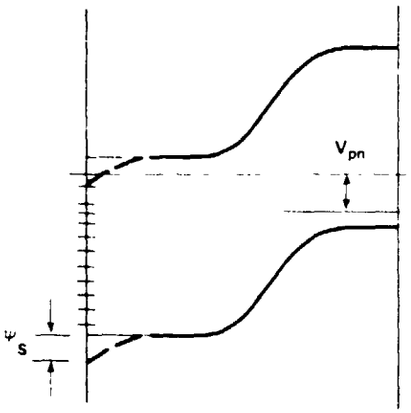

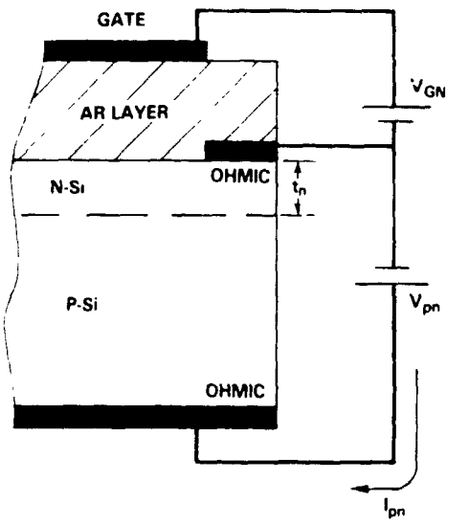

- BASED ON SOLAR CELL STRUCTURE
- ASSUMING $L_p >> t_n$, THE INJECTION CURRENT

$$I_{pn} = \left(\frac{eA_G n_i^2}{N_D}\right)\left(\frac{S}{1 + \frac{St_n}{D_p}}\right) \exp\left(\frac{V_{pn}}{kT}\right)$$

- IF CURRENT SENSITIVE TO V_{GN}, THEN:
  - –INJECTION CURRENT DOMINANT AND SENSITIVE TO S
  - –IF KNOW N_D AND n_i^2, CAN DETERMINE S

HIGH-EFFICIENCY CRYSTALLINE SILICON SOLAR CELLS RESEARCH FORUM

JET PROPULSION LABORATORY

A.H. Kachare

Pre-PIM Modeling Meeting

- DEVICE PHYSICS IS UNDERSTOOD
- RESEARCH IN MATERIAL SCIENCE IS NEEDED
  - --- HEAVY DOPING EFFECTS
  - --- INTERFACES
- MEASUREMENTS NEEDED FOR
  - --- SURFACE - INTERFACE PARAMETERS
  - --- MINORITY CARRIER LIFETIME IN THIN LAYERS
- INNOVATIVE DEVICE DESIGNS NEED FURTHER RESEARCH

High-Efficiency Silicon Solar Cell Research

- A "FLOAT EMITTER" CELL STRUCTURE HAVING $\geq$ 20% EFFICIENCY WAS PROPOSED
- BARRIERS TO ACHIEVE HIGH EFFICIENCY CELLS WERE DISCUSSED AND PERFORMANCE LIMIT WAS BROUGHT OUT
- SERI'S HIGH EFFICIENCY CELL ACTIVITIES WERE REPORTED
  - . . . ASEC 16.8%
  - . . . WESTINGHOUSE 17.2%
  - . . . SPIRE 18.1%
- LBIC AND SCCD TECHNIQUES TO MEASURE s AND γ IN EMITTER AND BASE LAYERS SHOW PROMISE

HIGH-EFFICIENCY SILICON SOLAR CELL RESEARCH

- GROWTH AND CHARACTERIZATION OF Si_3N_4 AS A SURFACE PASSIVANT IS IN PROGRESS
- LOW TEMPERATURE EBIC PROVIDES BETTER UNDERSTANDING OF AS-GROWN AND PROCESS-INDUCED DEFECTS IN LOW-COST SILICON SHEETS
- ETCH PIT STUDY HAS IDENTIFIED TWO STRESS REGIONS ACROSS AS-GROWN WEB
- INTERACTIONS OF DISLOCATIONS WITH TWIN AND CARBON WITH GB IN ANNEALED EFG WERE EXPLAINED

FSA Project Research Forum

TITLE: High-Efficiency Crystalline Silicon Solar Cells

DATE: July 9-11, 1984

LOCATION: The Pointe, Phoenix, Arizona

SESSION	SESSION TITLE	SESSION CHAIRMAN
I	Overview	M. Prince (DOE)
II	High-Efficiency Concepts	M. Wolf (U. of Penn)
III	Surface-Interface Effects	L. Kazmerski (SERI)
IV	Bulk Effects	E. Sirtl (Wacker-Heliotronic)
V	Modeling	R. Schwartz (Purdue Uni)
VI	High-Efficiency Device Processing	P. Rai-Choudhury (Westinghouse)

For additional information contact M. Phillips 818/577-9096

High Efficiency Solar Cell Program: Some Recent Results

J.B. Milstein and C.R. Osterwald
Solar Energy Research Institute
1617 Cole Boulevard
Golden, Colorado 80401

ABSTRACT

All of the I-V measurements discussed in this talk were performed in the PV Devices and Measurements Branch at SERI, and were carried out at 28°C and AM1.5 using the SERI X-25 simulator.

Roughly one year ago, SERI measured cells, fabricated by Rosa Young and co-workers at Oak Ridge National Laboratory under SERI auspices, which demonstrated 16.5% conversion efficiency. At that time, these cells were the most efficient silicon cells that we had seen. Others have claimed higher efficiencies prior to that time, which we do not dispute; however, such cells were not made available for our measurement. An account of the results of Young, et al is reported in Applied Physics Letters 43(7), 666-668 (1983).

In May, 1983, K.S. Ling of Applied Solar Energy Corporation provided us with six cells, each approximately 4cm^2 in area, to be tested at SERI. Results of these tests were reported at the Photovoltaics Advanced Research and Development 5th Annual Review Meeting, May 19-21, 1983, in Denver. Three of the six cells demonstrated in excess of 17% efficiency; the group ranged from 16.7% to 17.1%. The detailed results are presented in Table I below. SERI did not financially support the work performed by ASEC in fabricating these cells.

In August, 1983, a group of 1 cm^2 solar cells fabricated by A. Rohatgi at Westinghouse Electric Corporation R&D Center, under SERI Subcontract No. XB-3-02090-4, were measured. Three cells demonstrated 17.1% efficiency, two 17.0%, and one 16.3%. The details of our observations are presented in Table II below.

In September, 1983, a group of 4cm^2 solar cells fabricated by M.B. Spitzer at Spire Corporation, under SERI Subcontract No. ZB-3-02090-3, were measured. One cell demonstrated 18.0% efficiency, two 17.6%, and one 17.5%. These cells were remeasured at JPL on three additional simulators, with the cooperation of Bob Weiss, Bob Meuller and Gerry Crotty (all of JPL). It was found that the 18.0% cell had degraded (fill factor was reduced from 80.0 to 78.0%), but the other measurements were confirmed. Subsequently, the loss in fill factor was reconfirmed by measurement at SERI. The reason for this loss is unknown. In November, 1983, two additional Spire cells from the same batch were measured at SERI, and exhibited 18.0% and 17.9% efficiency. These results are summarized in Table III below.

In December, 1983, a series of MINP silicon solar cells fabricated by M. Green and co-workers at the Solar Photovoltaic Laboratory, University of New South Wales, Kensington, Australia, were tested at SERI. Seven cells, each approximately 4 cm^2 in area, were provided for these tests. One cell exhibited 19.1% conversion efficiency, two 19.0%, one 18.8%, two 18.7%, and one 18.1%. These results have been corroborated by tests performed at Sandia National Laboratory. The efforts at UNSW have been supported by the Australian Government and by NASA-Lewis. Details of the test results are presented in Table IV below.

HIGH-EFFICIENCY SILICON SOLAR CELL RESEARCH

On March 6, we measured several $4cm^2$ MINP solar cells fabricated by Larry Olsen and coworkers at the Joint Center for Graduate Study - University of Washington under SERI subcontract XB-2-02090-5. The best cell measured exhibited V_{oc}=636 mV, J_{sc}=31.1 mA/cm^2, FF=.787, efficiency=15.6%. Visual comparison of this device with those of Green indicates that the single antireflection coating used by JCGS is less effective than the double coating used by UNSW.

Measurements of reflectance exhibited by double layer antireflection coatings have been performed at Westinghouse by Rohatgi and at SERI on the UNSW cells by us. The observed reflectances are very similar, with integrated reflectivity from 4000 Å to 11000 Å of 5% or less. Theoretical models have been developed at Westinghouse which give predictions that conform closely to the observed data. These results are presented below.

We feel that a number of significant observations should be made. First, excellent results are being attained by a number of different research groups, using a variety of approaches, not all of whom are financially supported by SERI. Second, the Request for Proposals No. RB-2-02090, "Research on Basic Understanding of High Efficiency in Silicon Solar Cells," which SERI issued in March, 1982, was motivated by the conception that an "existence proof" (i.e. a demonstratable cell which exhibits efficiency exceeding 17% by the largest amount practicable) would provide strong impetus for research by non-SERI supported groups based on knowledge that research on high efficiency cells can be fruitful. Hopefully, such activity will be fostered by the attainment and dissemination of results such as those described here. Third, SERI has expressed an interest in testing highly efficient cells whether or not they have been fabricated with SERI support. We are pleased to assist the PV community by providing this service, and hope that this offer will be acted on by additional successful groups.

Further information on the details of fabrication of the cells we have discussed can be obtained from the groups who have performed the research, and will undoubtedly be discussed in the near future in the professional literature.

HIGH-EFFICIENCY SOLAR CELL PROGRAM: SOME RECENT RESULTS

SOLAR ENERGY RESEARCH INSTITUTE

J B. Milstein
C.R. Osterwald

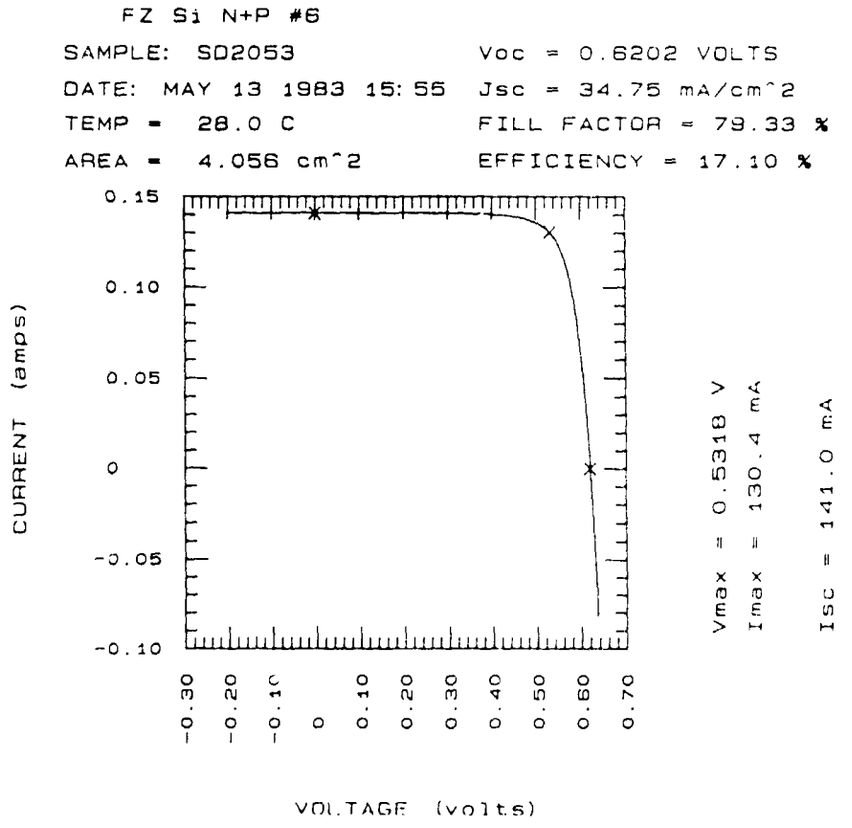

Table I. Results of Measurements on ASEC Cells, May 1983

Sample #	Area (cm^2)	J_{sc} (mA/cm^2)	V_{oc} (mV)	FF (%)	n (%)
1	4.070	34.75	620.7	78.05	16.84
2	4.062	34.58	618.6	79.88	17.09
3	4.068	34.72	619.6	79.24	17.05
4	4.062	34.02	621.8	79.92	16.90
5	4.070	33.86	622.8	79.11	16.68
6	4.056	34.75	620.2	79.13	17.10

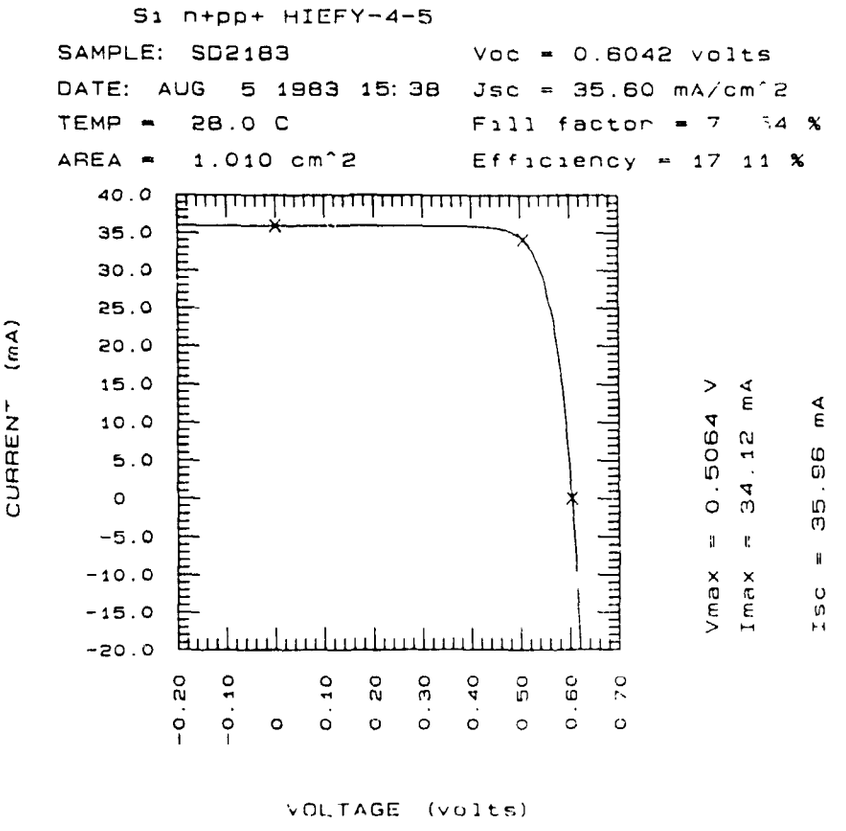

Table II. Results of Measurements on Westinghouse Cells, August 1983

Sample #	Area (cm^2)	J_{sc} (mA/cm^2)	V_{oc} (mV)	FF (%)	n (%)
HIEFY -4-4	1.01	35.5	604	79.6	17.1
-5	1.01	35.6	604	79.5	17.1
-6	1.01	35.9	605	78.6	17.1
-7	1.01	35.4	604	79.7	17.0
-8	1.01	35.3	603	79.8	17.0
-11	1.01	35.5	604	76.1	16.3

Table III. Results of Measurements on Spire Cells, September 1983

Sample #	Area (cm^2)	J_{sc} mA/cm^2	V_{oc} (mV)	FF (%)	n (%)
SD2219	4.01	35.7	618	80.0	17.6
SD2220	4.00	36.1	622	80.1	18.0
SD2221	4.01	36.3	616	78.0	17.5
SD2222	4.01	36.0	619	79.1	17.6

November, 1983

Sample #	Area (cm^2)	J_{sc} mA/cm^2	V_{oc} (mV)	FF (%)	n (%)
SD2220	4.00	36.0	620	78.0	17.4
SD2252	4.00	36.0	621	80.1	17.9
SD2253	4.00	36.2	622	80.1	18.0

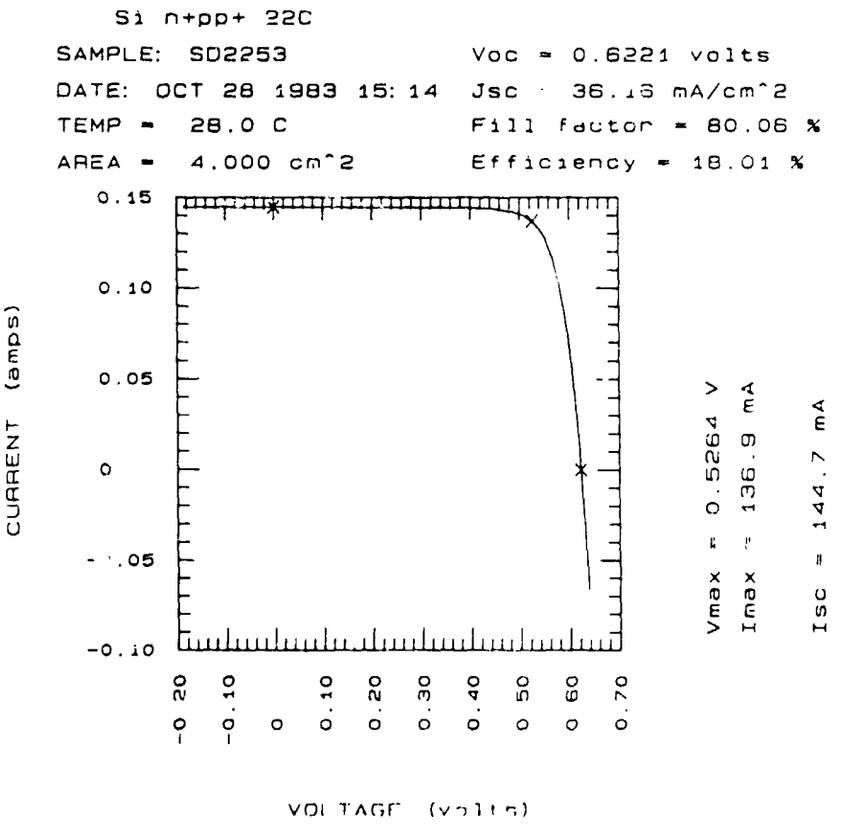

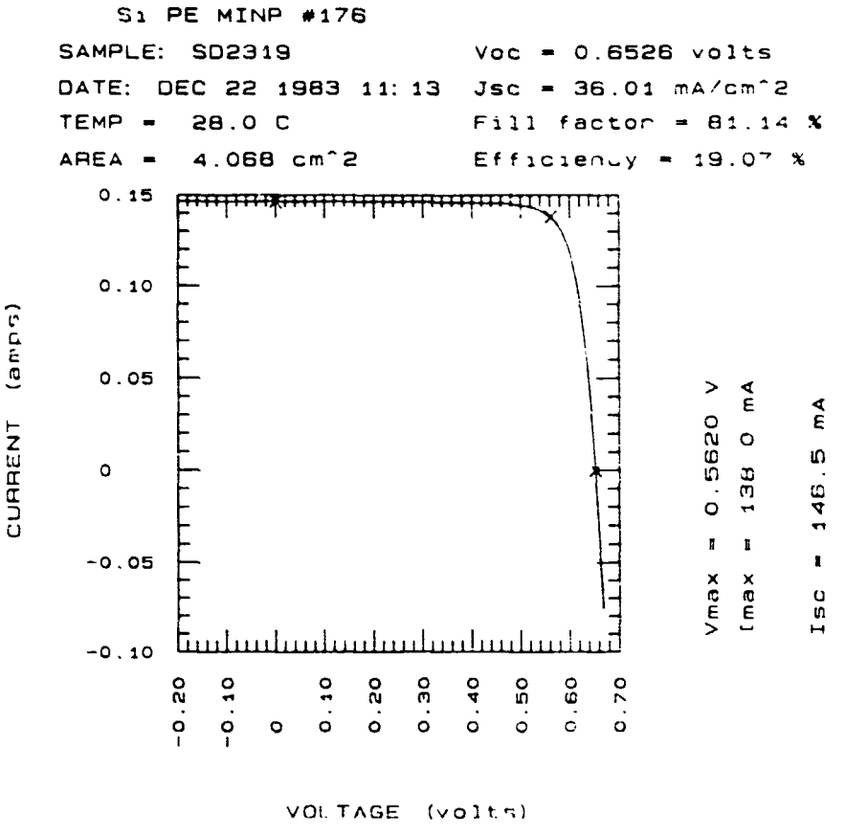

Table IV. Results of Measurements on UNSW Cells, December 1983

Device	Area (cm^2)	V_{oc} (mV)	J_{sc} (mA/cm^2)	FF (%)	Efficiency (%)
129	4.09	660	34.5	79.8	18.1
120	4.07	640	36.1	81.0	18.7
78	4.01	643	36.0	80.8	18.7
1399	4.08	650	36.2	80.0	18.8
1366	4.08	652	36.3	80.2	19.0
177	4.08	653	36.0	80.8	19.0
176	4.07	653	36.0	81.1	19.1

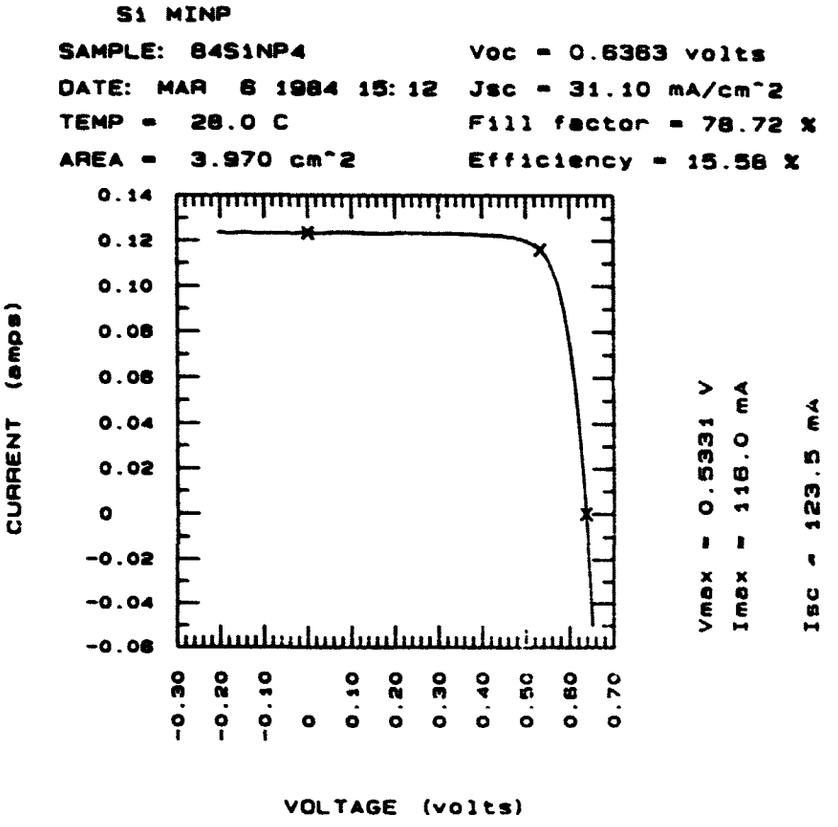
Si MINP
SAMPLE: 84SiNP4
DATE: MAR 6 1984 15:12
TEMP = 28.0 C
AREA = 3.970 cm^2
Voc = 0.6383 volts
Jsc = 31.10 mA/cm^2
Fill factor = 78.72 %
Efficiency = 15.58 %
CURRENT (amps)
0.14
0.12
0.10
0.08
0.06
0.04
0.02
0
-0.02
-0.04
-0.06
-0.30
-0.20
-0.10
0
0.10
0.20
0.30
0.40
0.50
0.60
0.70
VOLTAGE (volts)
Vmax = 0.5331 V
Imax = 116.0 mA
Isc = 123.5 mA

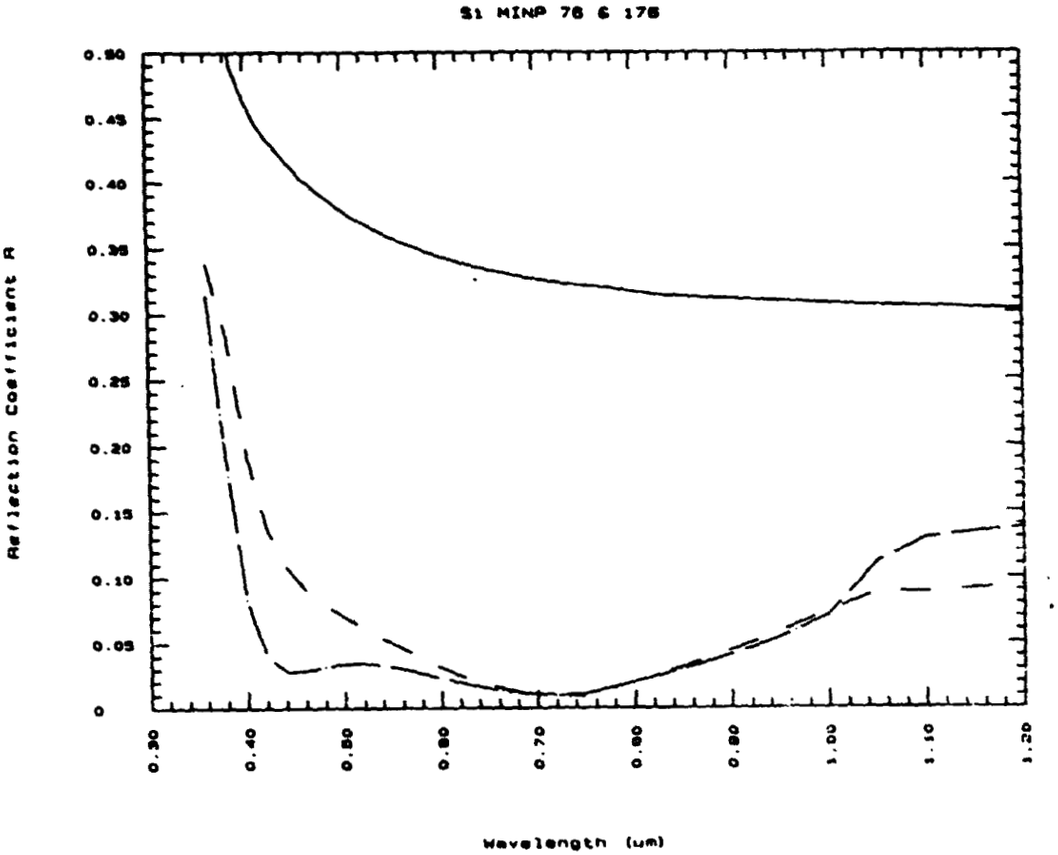
Si MINP 78 6 178
Reflection Coefficient R
0.50
0.45
0.40
0.35
0.30
0.25
0.20
0.15
0.10
0.05
0
0.30
0.40
0.50
0.60
0.70
0.80
0.90
1.00
1.10
1.20
Wavelength (um)

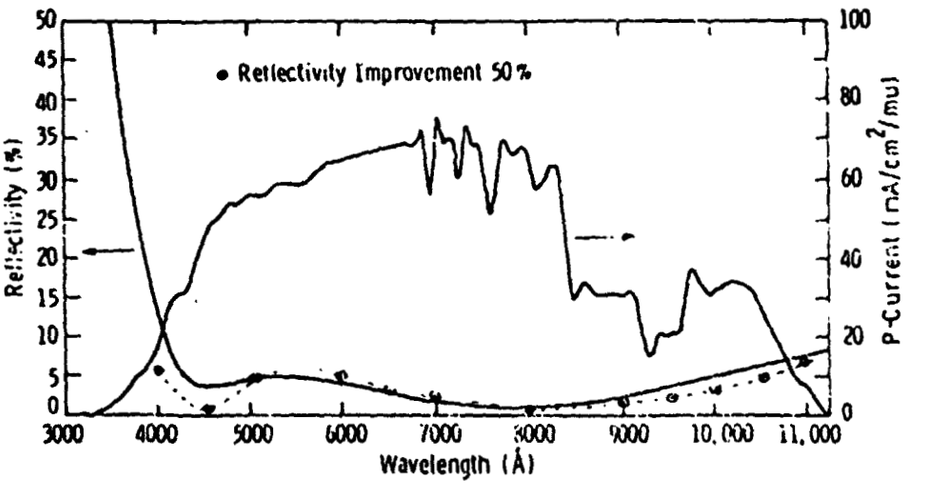
• Reflectivity Improvement 50%
Reflectivity (%)
P-Current (mA/cm²/mu)
50
45
40
35
30
25
20
15
10
5
0
100
80
60
40
20
0
3000
4000
5000
6000
7000
8000
9000
10,000
11,000
Wavelength (Å)

Isoreflectivity Curves

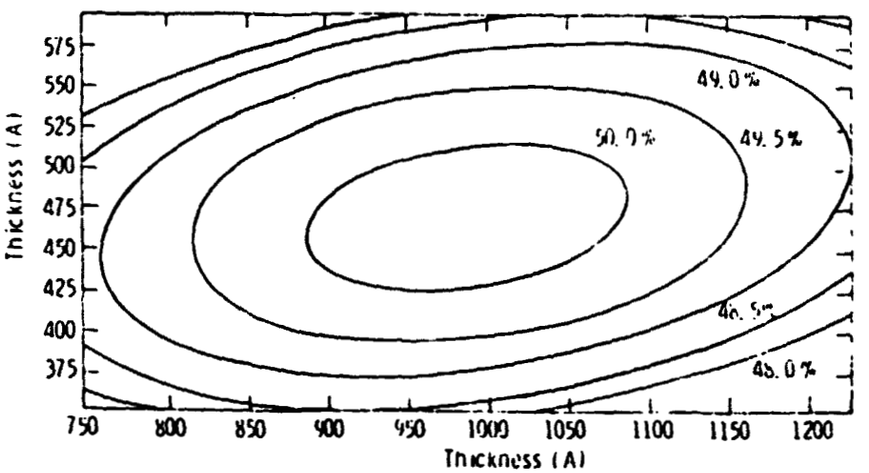

DEVELOPMENT AND ANAYLSIS OF SILICON SOLAR CELLS NEAR 20% EFFICIENCY

UNIVERSITY OF PENNSYLVANIA

M. Wolf
M. Newhouse

Calibrated Spectral LBIC

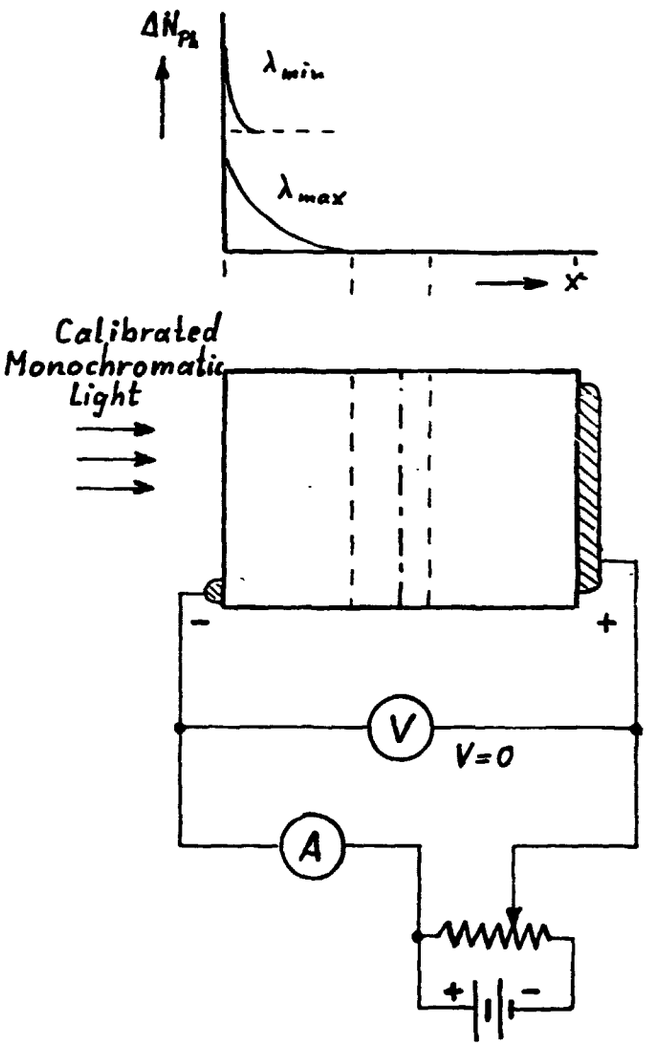

1. The calibrated spectral LBIC method when applied to an individual region uses exclusively wavelengths which do not penetrate beyond the layer under investigation.

2. The method operates only in the short circuit condition to eliminate influences of the other regions of the device, including the junction space charge region, from affecting the measured data.

3. As far as possible under the constraints of point 1., a wavelength range with widely varying absorption coefficients is used to gain sensitivity for differentiation between surface recombination and bulk recombination, or, when a layered region is involved, between the properties of the individual layers.

Front-Layer Parameters of Spire Cell 4400-20B

Surface Recombination Velocity s $cm\ s^{-1}$	Minority Carrier Lifetime τ ns			rms Error %
	Layer 1	Layer 2	Layer 3	
As received with oxide passivation				
100	0.06	10	10	1.74
	0.06	1	1	2.18
	0.06	0.4	0.4	3.79
$1.7 \cdot 10^4$	0.07	1	10	2.09
$1.6 \cdot 10^5$	0.7	0.7	0.7	0.95
$4 \cdot 10^5$	Single Layer 5			2.0
After 10s HF etch				
$1.2 \cdot 10^7$	0.04	0.3	0.3	3.96
$3 \cdot 10^7$	0.06	1	1	7.54 (slope does not match well)

In "thin" regions of high performance, only a "maximum surface recombination velocity" and a "minimum bulk lifetime" can be determined, which lie at the threshold to the "saturation" of the collection efficiency. Actual values could be more favorable, but do not improve the spectral collection efficiency.

Good cells with the usual, under 0.3 μm thick front layer, fall into this category (Spire cell with oxide layer.) After removal of the oxide layer, a 2-order of magnitude increase of the surface recombination velocity from the prior "maximum" was clearly observable, i.e., the collection efficiency is no longer saturated.

Spreading Resistance Analysis: Alloy-Regrowth BSF Structure, 2 Models

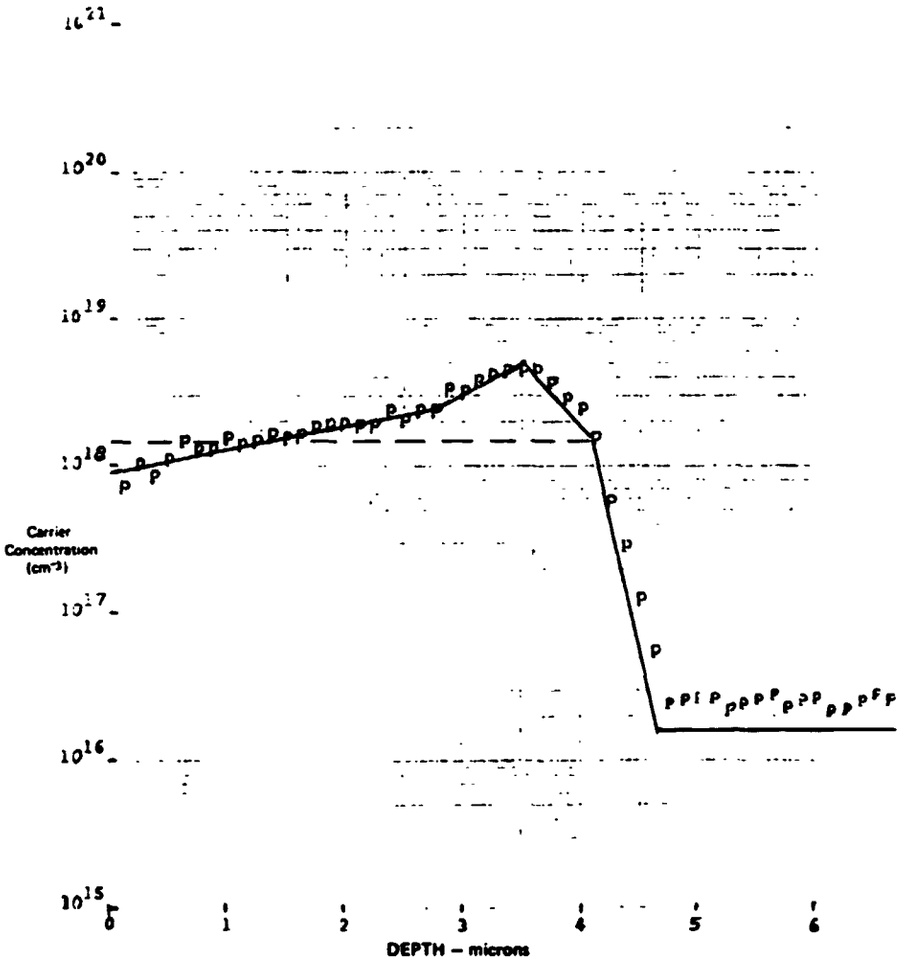

As a first, it has been possible to determine the minority carrier lifetime in the alloy-regrowth layer between the high/low junction and the back surface. For this purpose, windows have been etched into the back metallization, and the calibrated spectral LBIC method applied to the back of cells. Modeling this layer by 3 sublayers according to the spreading resistance profiles or as one layer with constant impurity concentration (dashed line) yielded the same results.

CELL W2-002 MEASUREMENTS	FRONT LAYER S	τ_1	τ_2	BASE LAYER τ_1	τ_2	τ_3	FIT % RUNS	Voc COMP'D MV	MEAS'D MV
FRONT REGION	5E5	10ns	10µs	-	-	-	2.2	-	-
BASE REGION	-	-	-	6ns	6ns	2.5µs	13.4	-	-
	5E5	10ns	100ns	6ns	6ns	1.3µs	5.5	580	-
WHOLE CELL	5E5	10ns	6µs	6ns	6ns	1.5µs	6.8	593	598
CELL 37-3 MEASUREMENTS									
FRONT REGION	1E5	-	2ns	-	-	-	-	-	-
BASE REGION	-	-	-	2.6ns	2.6ns	20µs	24.0	-	-
WHOLE CELL	1E4	-	2ns	2.6ns	2.6ns	20µs	8.9	558	563

Beyond the alloy - regrowth layer properties, the minority carrier life-time in the less heavily doped layer of the base can be determined in this measuremant. (Data labelled "base region"). All the data can then be corroborated by measurement from the front surface. (Labelled "whole cell").

Where the spectral collection efficienty saturates, a comparison of the calculated open circuit voltage (or saturation current with the measured one can indicate the need for an increase of the minority carrier lifetime value (or decrease of the surface recombination velocity, if the layer is very thin so that surface recombination dominates over bulk recombination) so as to match the measured open circuit voltage (see cell W2-002 measurements)

Measured Minority Carrier Lifetimes at Various Stages of Processing

PROCESS STAGE	ATTRIBUTE	CELL TYPE 37	W2
	SUBSTRATE DOPING (cm^{-3})	1.6 E 16	4 E 16
	EPI-LAYER DOPING (cm^{-3})	2 E 17	2 E 17
ORIGINAL WAFER	τ IN WAFER (μs)	450	120
AFTER EPI-LAYER DEPOSITION	τ IN WAFER (μs)	3-8	1-2
	τ IN 2μm THICK EPI-LAYER (μs)	~20	10-20
AFTER SOLAR CELL COMPLETION	τ IN WAFER (μs)	20	1.5
	τ IN 2μm THICK EPI-LAYER (μs)	0.002	6
	τ IN ALLOY-REGROWTH LAYER OF BASE (ns)	2.6	6

The method has enabled the determination of the minority carrier lifetimes in all regions of solar cells at various stages of the process. It has permitted the observation of lifetime degradation occuring in various process stages.

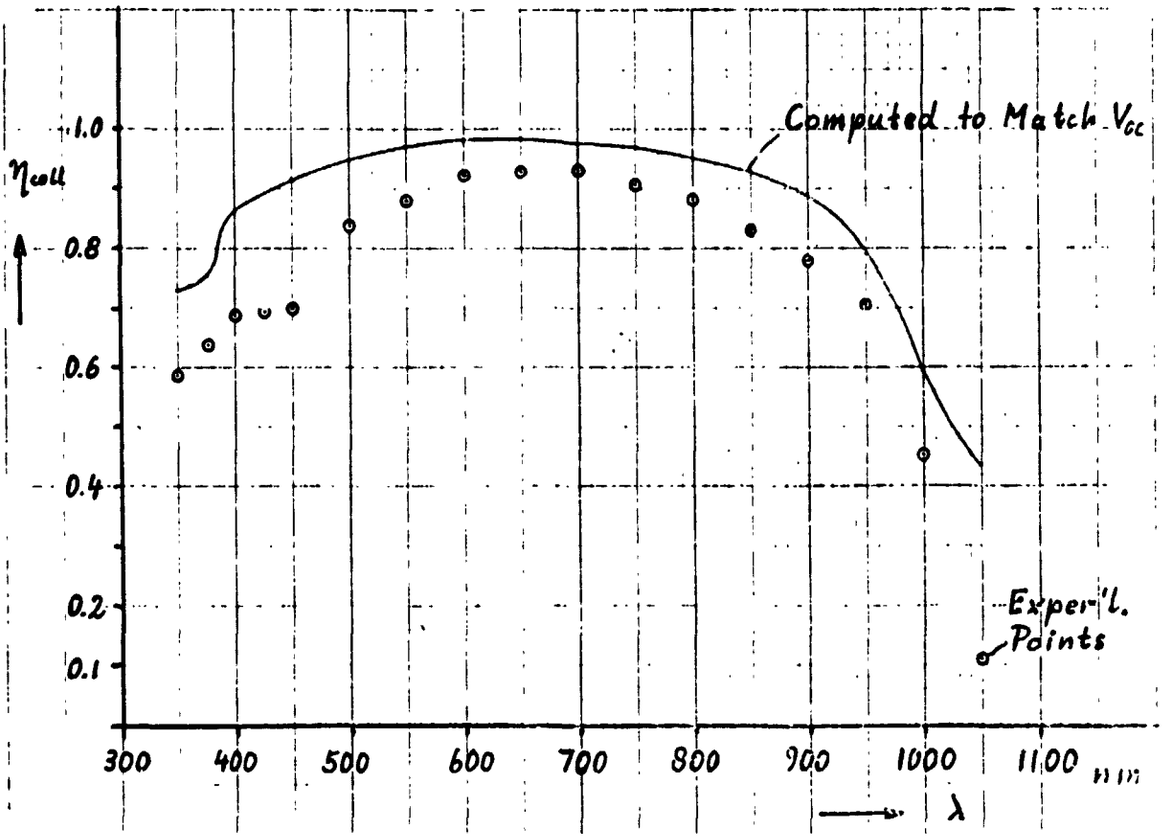

Experimental calibrated spectral LBIC data can give improper results if, e.g., an absorbing layer (AR, passivation oxide) overlays the active area of the cell. In this example, the lifetime adjusted to match the open circuit voltage yields significantly larger collection efficiency values than measured. The particular cell has a thick, absorbing oxide layer.

Limits of Calibrated Spectral LBIC

1. IF $L \geq 3 \cdot d$ AND $\frac{L}{\tau} \ll s$

   THEN: $\tau_{actual} \geq \tau_{meas'd.}$

   ($U_{tot} = U_{bulk} + U_{surface}$

   $\approx U_{surface}$ if $U_{bulk} \ll U_{surface}$.)

2. IF $\eta_{coll}(\lambda) \approx 1$:

   $\tau_{actual} \geq \tau_{meas'd.}$

   $s_{actual} \geq s_{meas'd.}$

RELIEF: (FOR FRONT LAYERS):
IF $j_{o,front} \geq 1/3\ j_{o,base}$:
HIGHER VALUES FOR τ, LOWER FOR s
CAN DETERMINED.

1. If the layers are thin and surface recombination dominates, only the surface recombination velocity can be reliably determined.

2. The collection efficiency can saturate, leading to "cutoff" values for τ and s by the LBIC method. The actual values may be more favorable and can, in some cases, be determined from the saturation current.

OMIT TO P.201

SURFACE AND ALLIED STUDIES IN SILICON SOLAR CELLS

UNIVERSITY OF FLORIDA

F.A. Lindholm
T.W. Jung
J. J. Liou

- MEASUREMENT METHODOLOGY
  - TWO-PORT MODEL--LINEARITY
    - 3 EXAMPLES
  - SHORT-CIRCUIT CURRENT DECAY
    - LIFETIME AND RECOMBINATION VELOCITY
    - SENSITIVITY--3D PLOTS
    - HOLES AND ELECTRONS IN SCR--NONLINEAR
    - MANUFACTURING--OCVD
    - NEW SCR C VS. V_R NEW OCVD
  - PROGRAMMATIC & FUTURE

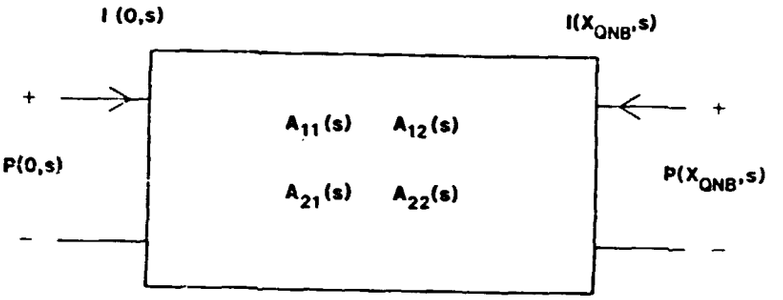

Fig. 1 Two-port network representation for hole density and hole current (density) at the two edges of the n-type quasi-neutral base region.

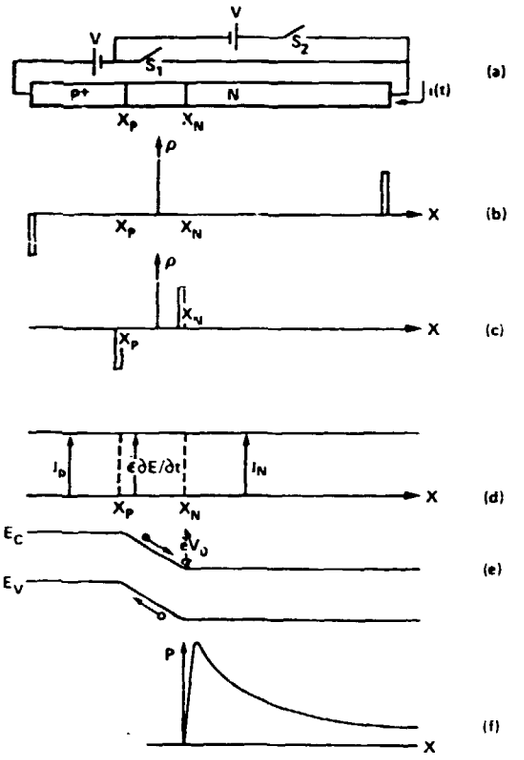

Figure A-1
(a) For $t < 0$, switch S_1 is closed, S_2 is open, conversely for $t > 0$; the junction space-charge region is defined by $x_p < x < x_n$. (b) charge density at $t = 0^+$. (c) charge density for t of the order of a dielectric relaxation time. (d) the total current is x-independent but is essentially majority-carrier convectio current in the two quasi-neutral regions and is displacement current in the space-charge region fo t of the order of a dielectric relaxation time. (e) electrons and holes drift out of the space-charge region in a transi time. (f) the resulting excess hole density in the space-charge region after a transit time has lapsed.

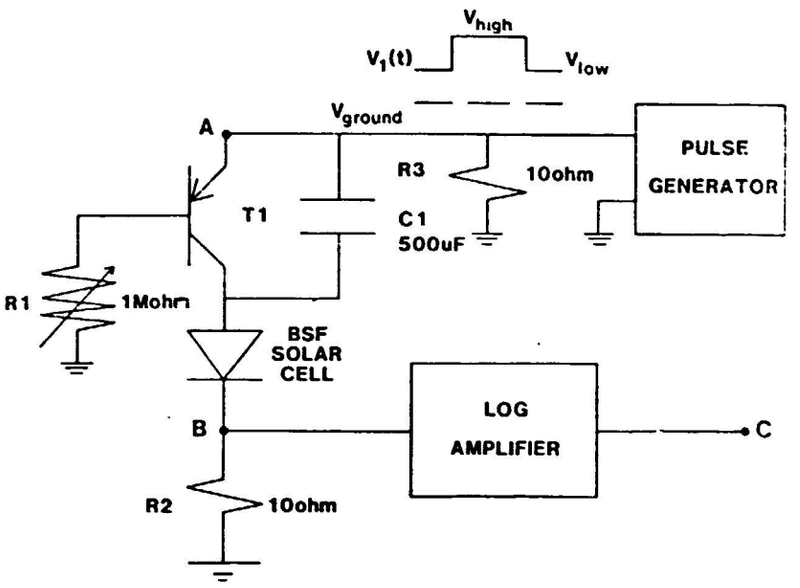

Fig. 2 The electronic switching circuit used in the SCCD method. The circuit elements are: switching transistor is 2N3906, the pulse generator is HP 8004, and the logarithmic amplifier consists of the usual configuration of an operational amplifier (Burr-Brown 3500C) connected to node B through a 100 ohm resistor and across which (between nodes B and C) two oppositely directed switching diodes (IN914) constitute the feedback loop.

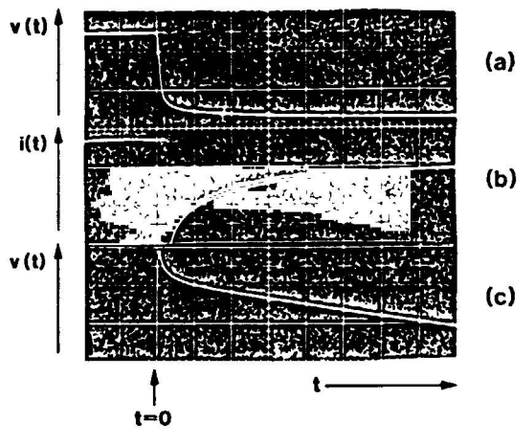

Fig. 3 (a) Voltage across BSF #1 solar cell (vertical:.2V/div).
(b) Current through BSF #1 solar cell (vertical:1mA/div).
(c) Log scale representation of (b) (vertical:.1V/div), where
$v(t) = (mkT/e)\log_e[i(t)/I_o + 1]$.
In (a)-(c), horizontal axis is 10 μs/div.

Estimated Lifetime of the Minority Carriers, T_p

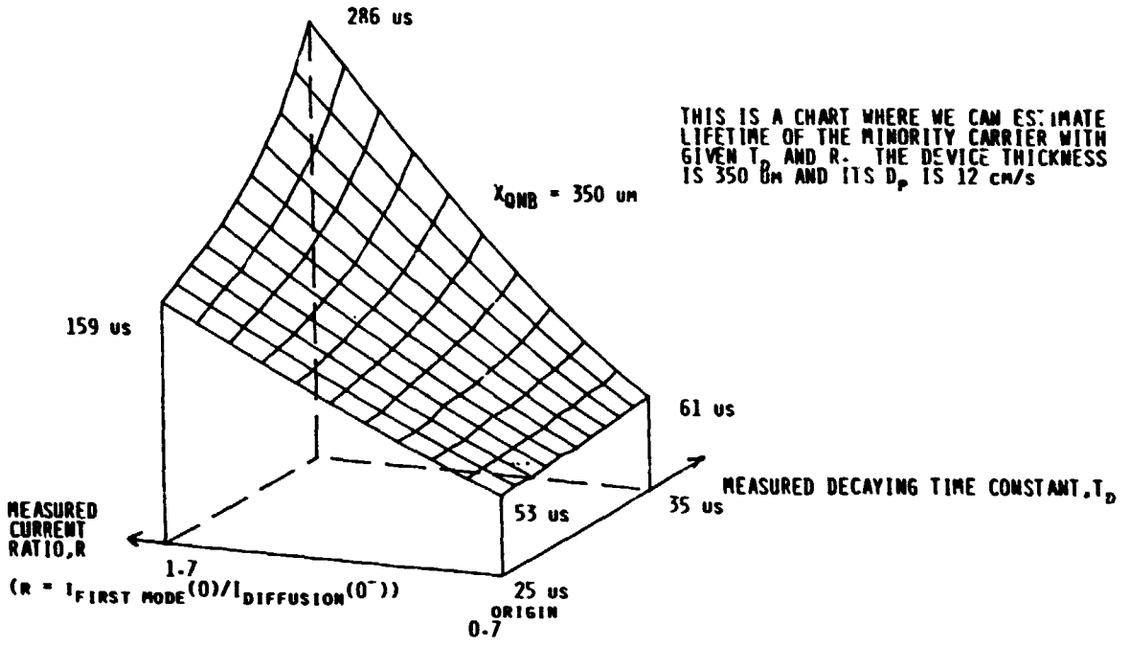

THIS IS A CHART WHERE WE CAN ESTIMATE LIFETIME OF THE MINORITY CARRIER WITH GIVEN T_D AND R. THE DEVICE THICKNESS IS 350 um AND ITS D_p IS 12 cm/s

PROGRAMMATIC & FUTURE

EXTEND 2-PORT METHOD:
IRRADIATION

EXTEND SENSITIVITY & ACCURACY

COMPARISON AMONG EXPERIMENTAL METHODS

EXTENDED OCVD: EXPERIMENTAL & P.D.E.

PROGRAMMATIC: THEORY (REPT 1)

MEASUREMENT TECHNIQUE (REPT 2)

THEREFORE AHEAD OF SCHEDULE

LOW-TEMPERATURE EBIC STUDIES ON SILICON SHEET MATERIALS

JET PROPULSION LABORATORY

Li-Jen Cheng

Contributors

JACK COLLIER
KATHY DUMAS
MARTY LEIPOLD
ANDY MORRISON
BRYAN SU
THIEN NGUYEN

Contents

* LOW TEMPERATURE EBIC IN SILICON SHEET MATERIALS

* ETCH PIT PATTERNS ON WEB SURFACES

EBIC-SEM: Electron-Beam-Induced Current

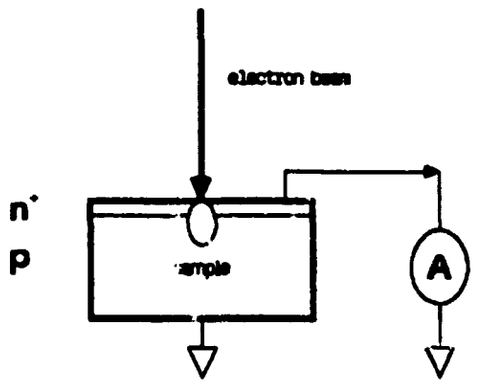

EBIC Images of EFG Solar Cell

25 °C

-160 °C

EBIC Images of Processed Wacker Sample

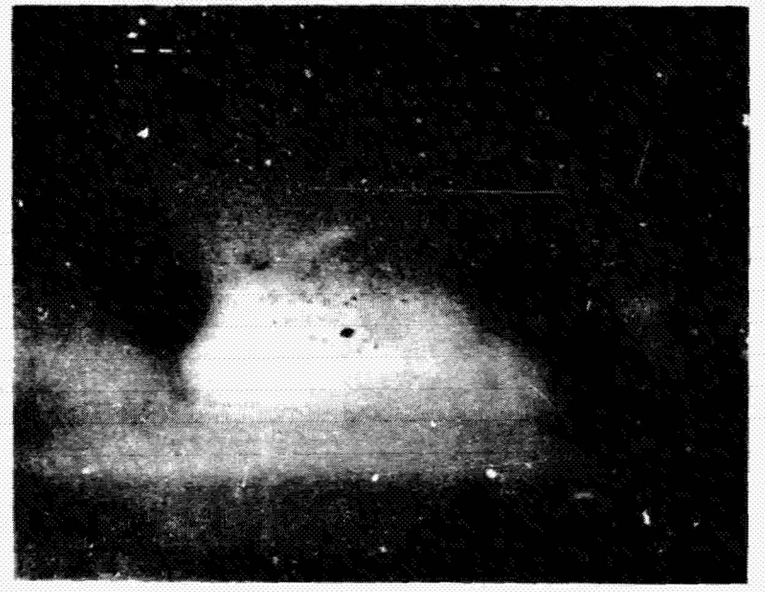

25 °C

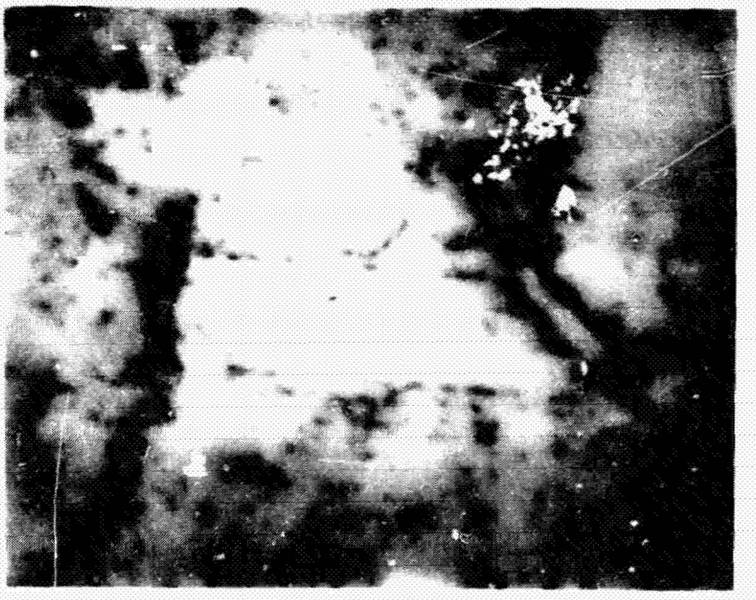

-160 °C

Advantages of Low-Temperature EBIC

- BETTER SPATIAL RESOLUTION
  - $\sqrt{R^2 + L^2}$
    - R = radius of approximate excited volume of electron-hole pairs.
    - L = minority carrier diffusion length.
  - Reduction of thermal emission
- CAPABLE OF OBSERVING MORE DEFECTS
  - Fermi level change
  - Reduction of thermal emission

Temperature Effects on Recombination

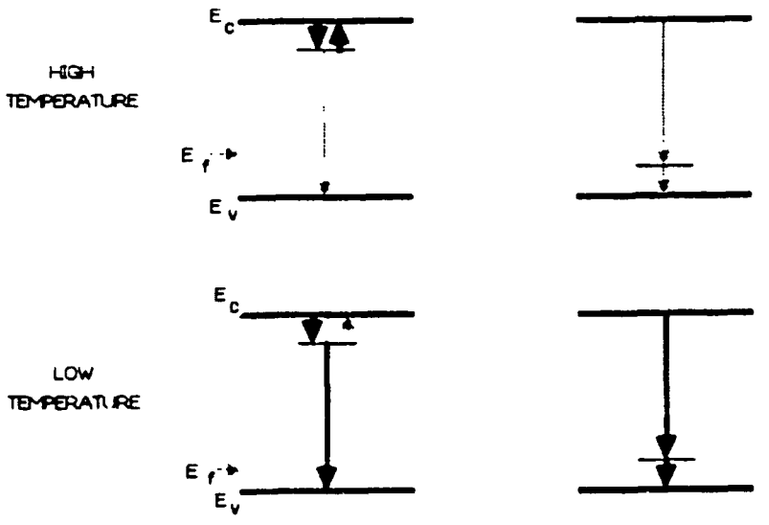

EBIC Images of As-Grown Wacker Sample

25 °C

-160 °C

EBIC Images of Processed Wacker Sample

25°C

-160°C

EBIC Image of Processed Web Sample

25°C

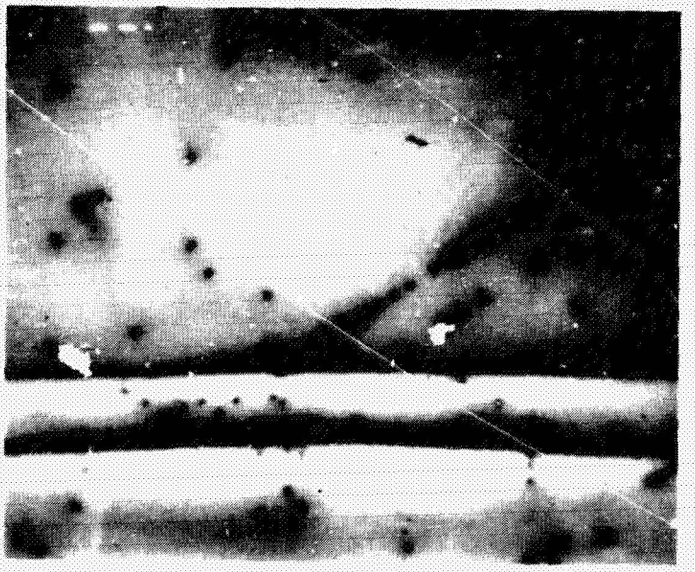

-160°C

EBIC Images of As-Grown Web Samples After Sirtl Etching

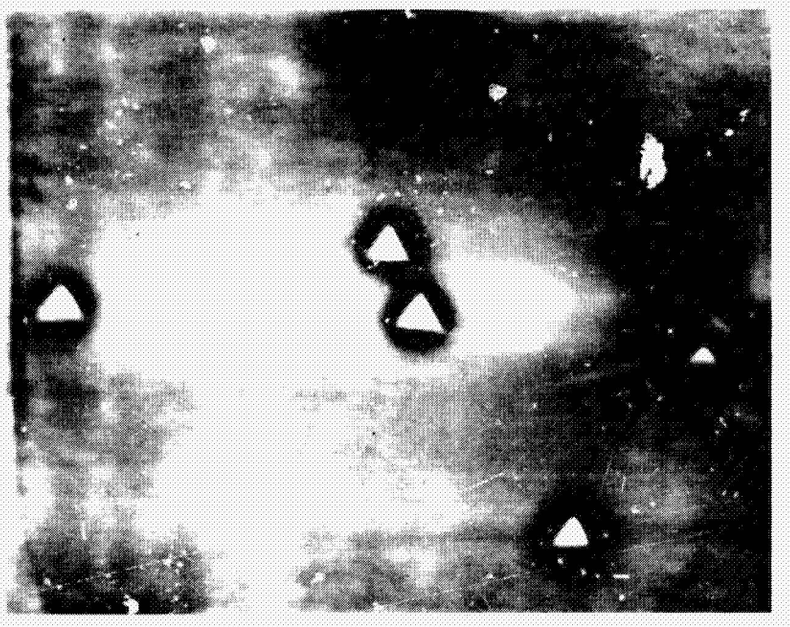

25 °C

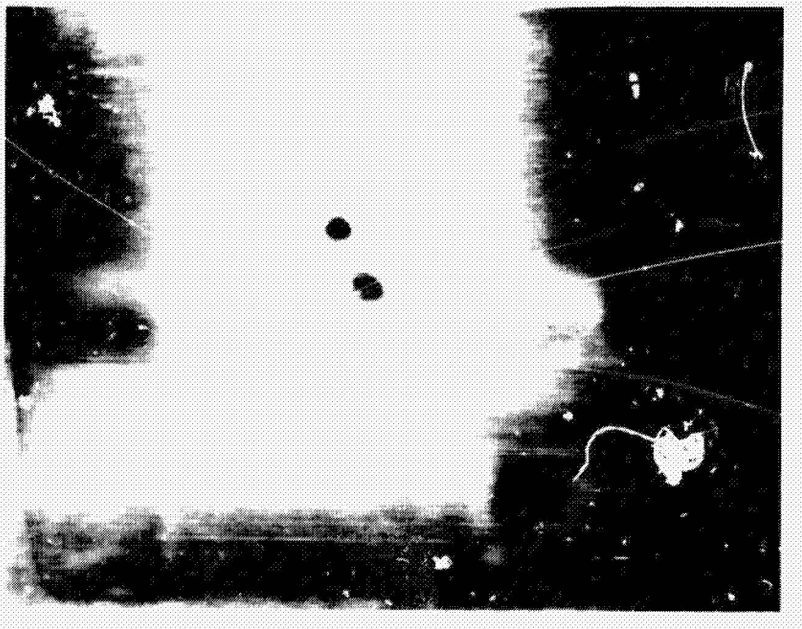

-165 °C

EBIC Scan

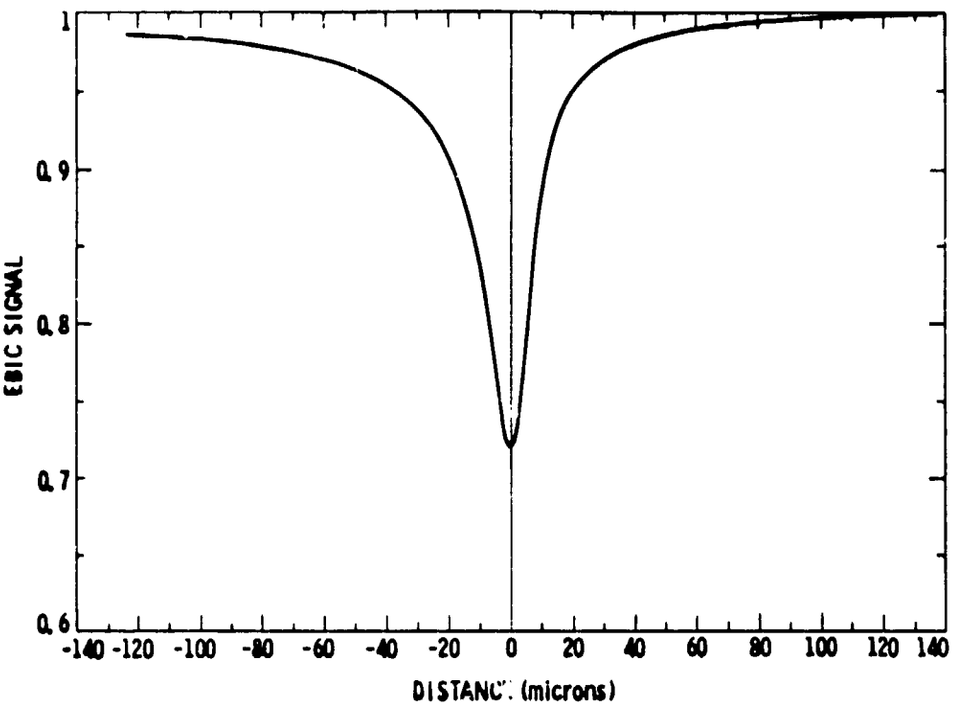

Temperature Dependence of EBIC Contrast
of Dislocations in Web Ribbons

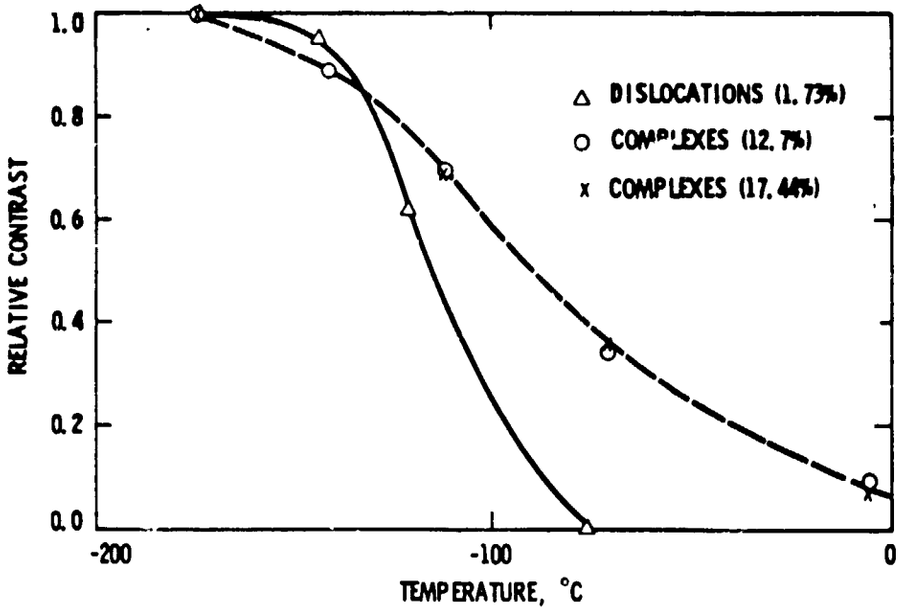

Patterns of Etch Pits on Web Ribbon Surface Due to Dislocations

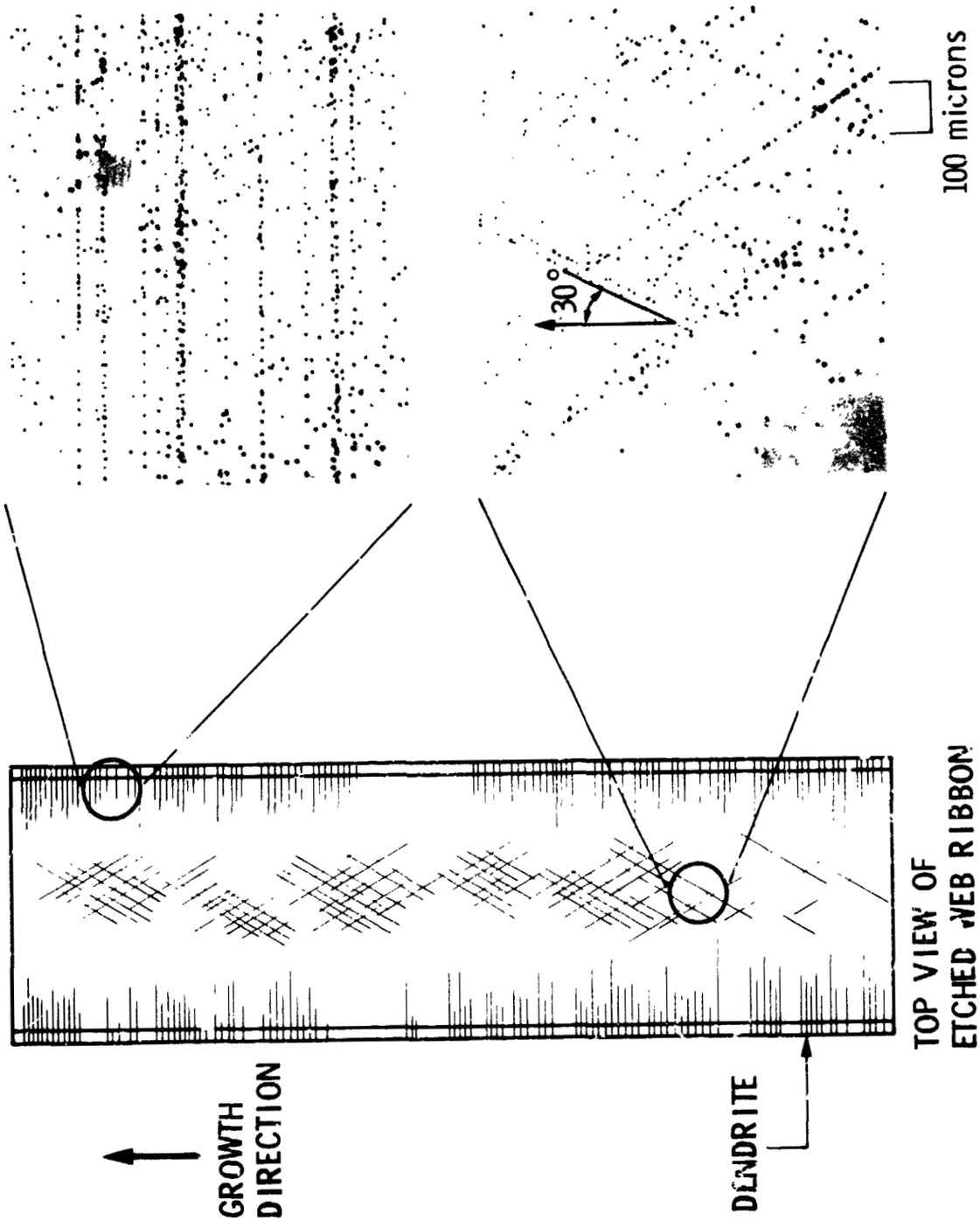

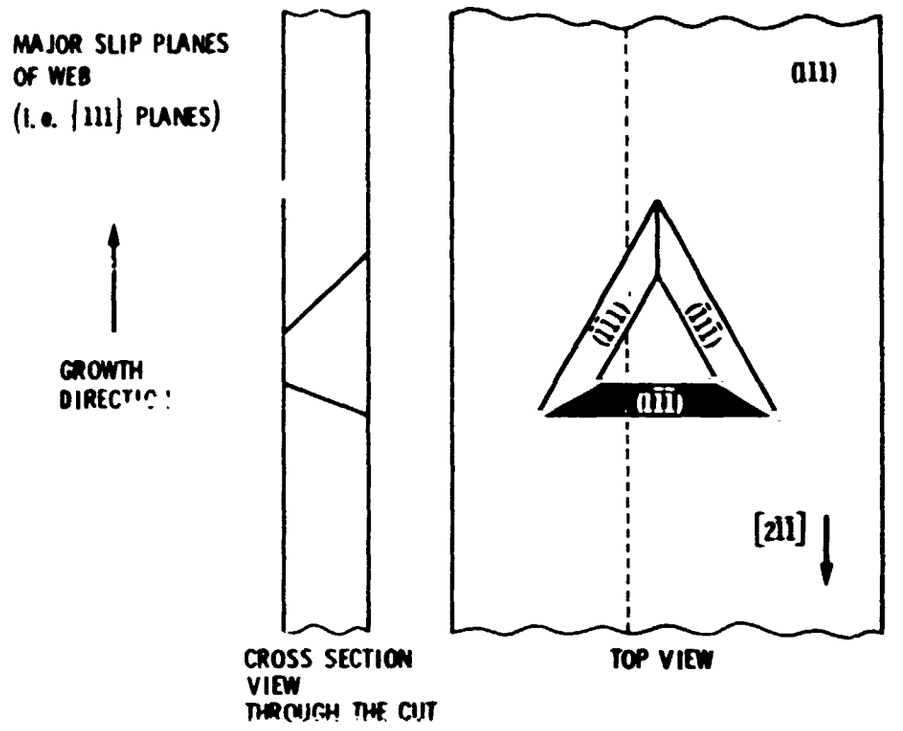

Possible Movement of Three Major Slip Planes Under Stress

NATURE OF STRESS	DIRECTION WITH RESPECT TO GROWTH AXIS	INTERCEPTS ON WEB SURFACE
TENSILE	PARALLEL	✳
	PERPENDICULAR	X
SHEAR	PARALLEL	X
	PERPENDICULAR	—

Explanation

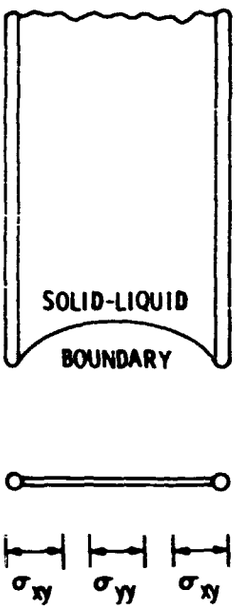

	POSSIBLE SOURCE
σ_{xy}	FLUCTUATION IN TEMPERATURE GRADIENT ALONG GROWTH AXIS
σ_{yy}	FLUCTUATION IN THERMAL CONTRACTION DUE TO STIFFNESS OF THE DENDRITE AND THE CONCAVE-DOWN SOLID-LIQUID BOUNDARY

Conclusions

- Demonstrated potentials of EBIC measurements at cryogenic temperatures for characterization of electrically active defects in silicon sheet materials.

- Showed that two distinguishable stress regions across silicon dendritic web ribbons may exist during the cooling process of the growth.

MICROSTRUCTURAL CHARACTERIZATION OF ANNEALED SILICON RIBBONS

CORNELL UNIVERSITY

D.G. Ast

Agenda

- Electrical Activity of grain boundaries
  ---------- Role of carbon.

- Basic studies of grain boundaries
  ---------- Strainfield, expansion/contraction

- Interaction of dislocations with twins
  ---------- Twins as obstacles to plastic relief.

Basic Idea

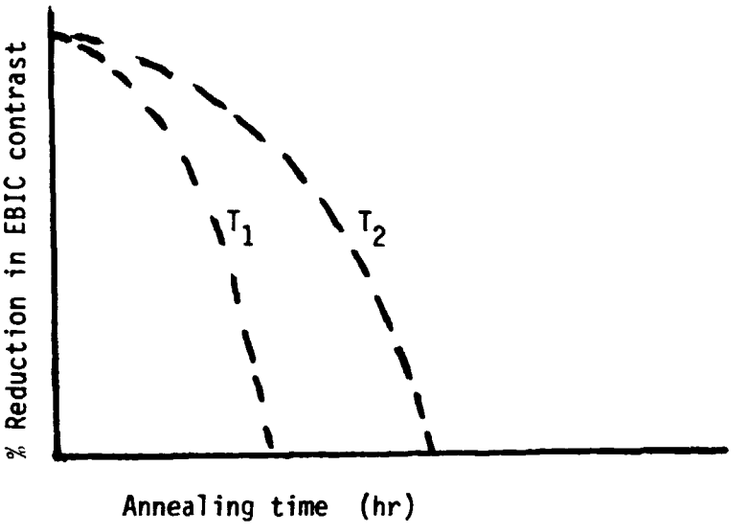

0) Assemble data for kinetic disappearance of EBIC contrast

0) Check kinetics for compatability with C diffusion

Long range effort:

0) Use DLTS to check for formation of C related states.

Electrical Activity of Grain Boundaries

Joint study with Mobil -----effects of pre-annealing

0) Pre-annealing greatly reduces electrical activity

0) Present model

Formation of competing gettering centers by C

0) Present status
Collection of kinetic data to verify C hypothesis

o) Long range effort

Study of a C based gettering system as an alternative to (conventional) O based gettering system.

C should be especially efficient in gettering those transition metals which are known to be good carbide formers; e.g. Ti, W, Mo, Fe.

C is naturally present in solar materials grown in graphite crucibles.

Basic Studies of Grain Boundaries

o) Comparative study of the width and strainfield of grain boundaries in Ge and Si.

O) Approach is to fabricate grain boundaries by grwing bicrystals and by high T sintering

o) Width and contraction/expansion of crystal lattice at grain boundary measured by diffraction techniques.

o) Study completed---- draft written up.

o) Major results

* Strain field extends about 5 to 10 lattice spacings past boundary

* Lattice in boundary plane is slightly contracted in Si noticeable contracted in Ge.

* Contraction is specific to Ge,Si as gb in metals are generally expanded but can be explained with covalent bond model.

Strain Fields and Widths of Grain Boundaries

Basic idea:

D) Treat grain boundary as a slab of thin material with a different lattice constant from bulk.

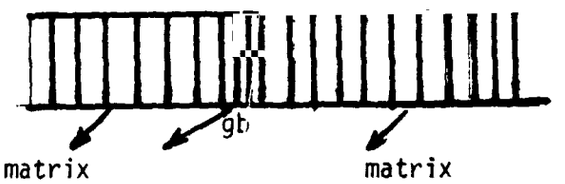

Fourier transform (i.e. diffraction pattern):

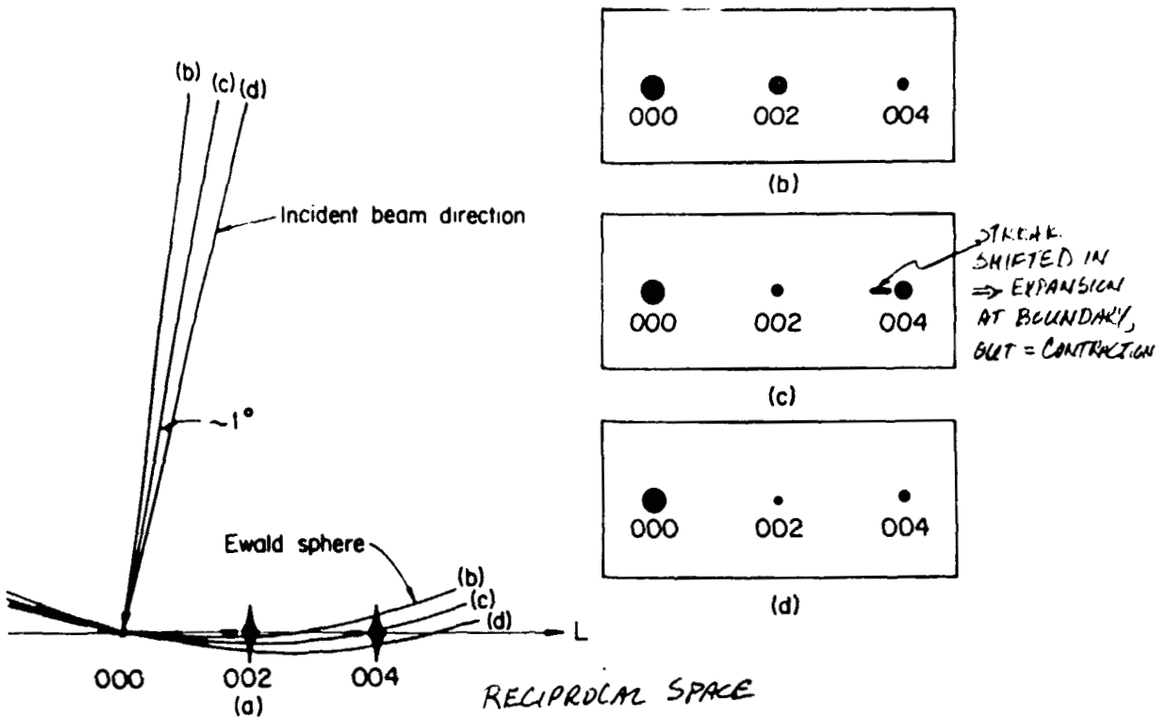
(b)
(c)
(d)
Incident beam direction
~1°
Ewald sphere
(b)
(c)
(d)
L
000
002
004
(a)
RECIPROCAL SPACE
000
002
004
(b)
000
002
004
STREAK SHIFTED IN ⇒ EXPANSION AT BOUNDARY, OUT = CONTRACTION
(c)
000
002
004
(d)

Geometry

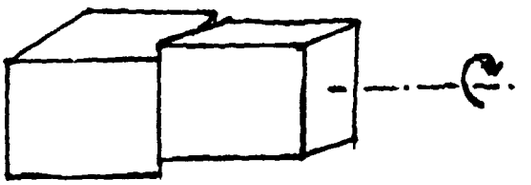

o) Real life complications:

* Unwanted presence of small tilt components

* Boundary not parallel to (004) planes.

Results to date:

Mt'l	Angle	Streak Length (Å)	Boundary Width	Streak Shift	Boundary Contr'ct'n.	CSL Σ:
Si	16	0.088	11.63A		0.4%	25
Si	22	0.10	10.0		0.37%	13 ←
Si	37	0.060	16.7		0.4%	5
Si	45	0.108	9.2		0.4%	
Ge	22	0.07	14.29		2.0%	13 ←

Twin-Dislocation Interactions

0) Coherent twins are major planar faults in solar material. They are present in high concentrations in EFG.

o) During annealing (e.g. during formation of p-n junction) or during cooldown (after heater) stress relief by dislocation motion can be limited by twins.

0) Twins accumulating many dislocations dissociate into small angle grain boundaries and coherent twins.

0) Small angle grain boundaries coalesce to form large (20 to 30 degree) angle grain boundaries.

0) Study completed--------draft written up

Dislocation-Twin Interactions

0) Very complex ---- out of scope of a 15min presentation.

0) An example will be provided to illustrate the basic proceedure used to investigate the various possible dislocation mechanisms.

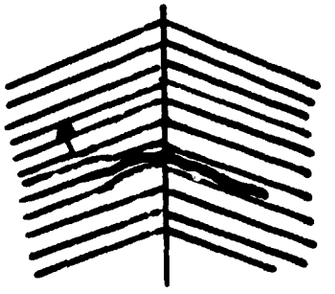

Matrix **Twin**

***) Vectors transfered from left to right must be expressed in the twinned coordinate system.**

***) The various dissociation reactions possible must then be examined.**

I have looked at the individual steps of the reaction of dislocations with out of plane Burgers vectors.

To repeat the notation:
The twin plane is (1 1 1)
Incoming dislocations move on (1 -1 -1)old plane
Outgoing (penetrating) dislocations move on the (1 -1 -1)new plane.

The relation of the new and old {111} plane is such that they have a common corner [0 1 -1].

The overall reaction was:

1/2[1 0 1] ----------> 1/6[-1 -4 -1]
(refered to old coordinate system) (same vector in twinned coordinates)

1/6[-1 -4 -1] ----------> 1/2[-1 -1 0] + 1/6[2 -1 -1]
(glissile on (1 -1 -1)new (SP glissile on (111) twin plane).

Thus it appeared that overall, a complete dislocation with an out of plane Burgersvector could cross the twin prvided there was enough strain energy relief to generate a partial dislocation.

The individual steps of this process are as follows.

The incoming dislocation is dissociated into two partials, with the leading partial pressing against the twin plane:

1/2[1 0 1] ----------> 1/6[1 -1 2] + 1/6[2 1 1]
(on (1 -1 -1) old (Both on (-1 -1) old)

The leading partial transfers across the twin plane and, in the twin coordinate system appears in new notation as:

1/6[1 -1 2] ----------> 1/18[-1 -7 2]
((1 -1 -1)old) ((1 -1 -1) new)

It dissociates during the crossing process into the following components, expressed in the twinned coordinate system:

1/18[-1 -1 2] ----------> 1/6[-1 -2 1] + 1/18 [-2 1 1]

The first term on the right side is a glissile partial on the new (1 -1 -1) plane and will glide away. The second term is an interesting product. It is one third of a glissile partial in the (111) plane. It has a very small strain field and reminds me somewhat of Marks sub DSC vectors in Sigma 5 twist boundaries. The energy of the reaction, if primitively analysed in first order as being proportional to the square of the Burgersvector is:

1/6 < 1/6 + 1/54

The reaction does require some energy, BUT VERY LITTLE. IT REQUIRES LESS ENERGY THAN CONVERTING A PARTIAL OF A IN PLANE BY DISLOCATIONS INTO A GLISSILE PARTIAL AND A STAIRROD :

1/6 < 1/6 + 1/18

Furthermore, both products of this reaction are glissile and will move away relieving the stress at the tip of the pile up against the twin plane.

The trailing partial requires more energy. Again the first step is to transform this partial from the untwinned to the twinned system:

1/6[211] ----------> 1/18[-2 -5 -5]

The dislocation on the right dissociates into:

1/18[-2 -5 -5] ----------> 1/6[-2 -1 -1] + 1/9[-2 1 1]

The energy required, treated in the square mechanism is:

1/6 < 1/6 + 1/13.5

It is somewhat higher than that of a classical stairod (which in this case can not form).

Still, the total energy for both steps is still lower than taking a dissociated dislocation with in plane Burgersvector and moving it on the twin plane by making two stairrods.

The first step of the reaction requires so little energy that it occurs likely quite often. I have not considered any further reactions of the 1/18[-2 1 1] product, which is glissile in the twin plane with dislocations which might be already in the twin plane (SP and FP). Nor have I considered the fractional steps associated with this dislocation.

Since there is a "phase shift" in the twin boundary, the leading partial of the incoming dislocation (defined in such a way that the dislocation is ssociated with an intrinsic SF) will emerge on the other side of the twin bundary as an extrinsic SF.

CRYOGENIC LASER CALORIMETRY FOR IMPURITY ANALYSIS

UNIVERSITY OF SOUTHERN CALIFORNIA

R.T. Swimm

Calorimetric Spectroscopy

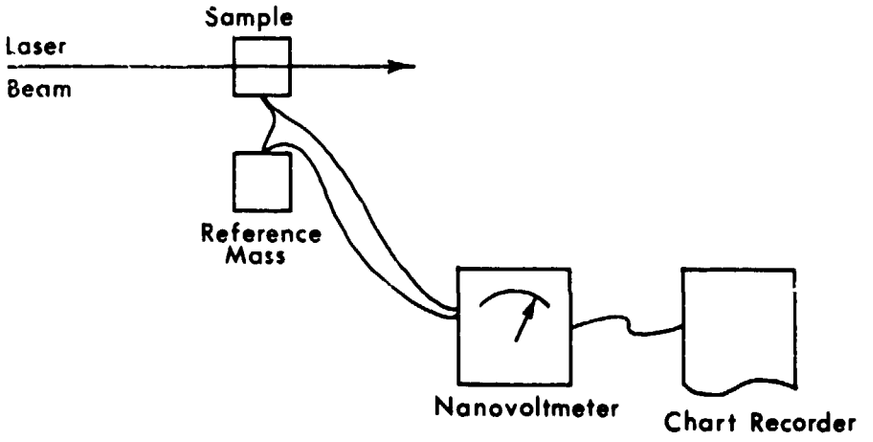

Heating and Cooling Data

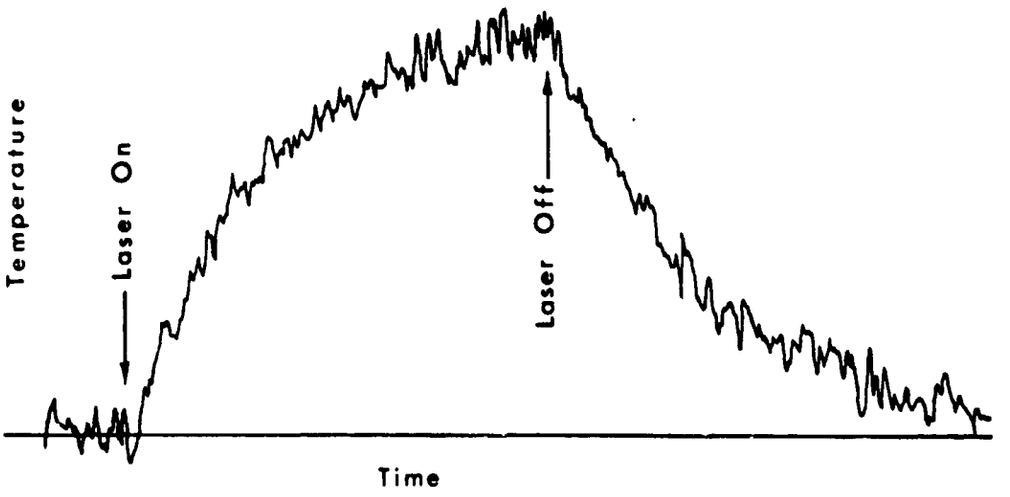

Calorimetric spectroscopy -
can not replace:
  mass spectroscopy
  deep level transient spectroscopy
but can replace:
  relative transmission spectroscopy
  (for low-absorption samples)

ENCAPSULATION

E.F. Cuddihy, Chairman

Spectrolab, Inc.

The basic FSA contract with Spectrolab, Inc., on encapsulation engineering has been completed. The presentation summarized highlights, key findings, and major technologies accomplished under this contract. These are detailed in the Spectrolab, Inc. presentation below. It was announced that a detailed final report is in preparation. Spectrolab investigated the interrelationship between encapsulation material properties and module performance features involving optical, structural, thermal, and electrical isolation behavior. The analysis also included the effects of encapsulation material interchange, and encapsulation design options on module performance.

Springborn Laboratories, Inc.

Springborn Laboratories, Inc. presented an updated summary of its work related to materials development and accelerated aging test results. Two key items: (1) copper and EVA are chemically incompatible at high temperatures, e.g., 105°C, and possibly to as low as 90°C, but there are not yet enough experimental data to define the lower temperature; (2) the protective additives (UV absorbers, antioxidants, etc.) formulated in the current A-9918 encapsulation-grade EVA are subject to physical loss at elevated temperatures, such as those that may be associated with module rooftop applications. To counter this, Springborn is exploring advanced EVA formulations containing chemically bound additives.

Jet Propulsion Laboratory

Accelerated aging almost always involves raising the exposure temperature of test specimens, to accelerate aging reactions. The question then arises as to the upper temperature limit allowable for accelerated testing. The criterion is that increases in temperature should accelerate the same mechanisms of aging operative at intended service temperatures, but should not alter mechanisms or introduce new mechanisms. JPL's sophisticated, laser-probe technique for spectroscopic identification of reaction mechanisms occurring in test samples as a function of temperature was described. This technique will be used to determine the allowable upper temperatures for accelerated aging of materials such as EVA. Some preliminary data for a model pottant compound, poly-n-butyl acrylate, were presented.

University of Toronto

J. Guillet was unable to attend. His presentation was cancelled.

ENCAPSULATION

Polytechnic Institute of New York

Otto Vogl was unable to attend, but a summary and update of his scheduled presentation was given by a colleague, A.C. Albertsson. Vogl carries out chemical synthesis of advanced polymeric and reactive stabilization additives for polymeric materials, such as EVA. These additives, such as protective UV-absorbing agents, are resistant to high-temperature physical losses.

Dow Corning

E.P. Plueddemann is the primary developer of all of the FSA adhesion promoters and primers for bonding the various material components of modules, such as EVA to glass. Plueddemann summarized his work to date, which can be found in more detail in a recent JPL publication "Chemical Bonding Technology for Terrestrial Photovoltaic Modules" (JPL Document No. 5101-232, JPL Publication 83-86). A major item was the status of his current work on self-priming EVA.

Case Western Reserve University

J. Koenig of Case Western Reserve University and J. Boerio (see below) have developed the technology to investigate a chemically bonded interface, for direct chemical information on both bonding and aging mechanisms. The technology is based on Fourier transform infrared techniques (FTIR). Koenig presented the first FTIR spectra of the bonded interface between EVA and glass, using the EVA-glass primer system developed by Pleuddemann. Eventually this technique will be used to track interfacial aging for rate data and life assessment.

University of Cincinnati

J. Boerio's efforts are identical to those of J. Koenig, except that the emphasis of his study is on polymers and metals, such as EVA and aluminum. These interfacial chemistries can be quite distinct from those between EVA and glass, for example. Boerio presented interfacial spectra of the bonded interface between EVA and aluminum, using an experimental metal primer system developed by Plueddemann. Bonding EVA to aluminum is complex, and Boerio's interfacial studies are providing clues to stable, high-strength, long-life interfacial bonds.

Jet Propulsion Laboratory

The role of polyvinyl butyral (PVB) as a direct, causative agent of module electrochemical corrosion was described by G.R. Mon of JPL. PVB contains ionic impurities that, in combination with absorbed water at high humidities, result in the PVB functioning as a solid-state battery electrolyte. The high-humidity, high-temperature (85°C, 85% RH) behavior of PVB in modules having silver metallization grids was described and compared with that of other metals, and also with other pottants such as silicones and EVA. The latter

two pottants were found not to exhibit similar electrochemical behavior. Based on theoretical considerations and experimental data, an electrochemical life-prediction model was developed and described.

Jet Propulsion Laboratory

The flammability behavior of modules fabricated with hydrocarbon pottants such as EVA and PVB was described by R.S. Sugimura and D.H. Otth of JPL. The UL790 flammability test consisted of a burning brand resting on the glass surfaces of modules. Localized surface heating caused glass fractures, internal thermal decomposition of the pottants to volatile liquid and gaseous products, and high-temperature softening or melting of conventional module back-cover materials. A buildup of internal gas pressure acting against a decreasing mechanical strength of the back cover caused rupture of the back cover, permitting an outward venting of the volatile liquid and gaseous decomposition products, which ignited upon contact with oxygen of the air and an open flame. Some preliminary flammability tests with modules fabricated with experimental high-strength, more-temperature-resistant back-cover materials showed promise.

ENCAPSULATION DESIGN ANALYSIS

SPECTROLAB, INC.

Alexander Garcia III

Acknowledgements

DESIGN, ANALYSIS, AND TEST VERIFICATION OF ADVANCED ENCAPSULATION SYSTEMS

JPL Contract #955567 (Ed Cuddihy, Technical Monitor)

Joint Effort of Spectrolab and Hughes Aircraft Company

J. F. Coakley - Thermal, Optical Analyses
L. B. Duncan - Structural Analysis
I. R. Jones - Program Management
J. M. Kallis - Electrical, Thermal Analyses
D. C. Trucker - Electrical

Objectives

- Analytical Methodology
- Verification
- Design Aids, Master Curves
- Research Direction
- TCM

Today's Topics

- Structural Analysis
  - Deflection
  - Thermal
- Optical
- Thermal
- Electrical Isolation Studies

Objective and Approach

- Develop methodology to analyze photovoltaic encapsulation system designs
- Approached using five models
  - structural deflection analysis
  - thermal structural analysis
  - thermal analysis
  - optical analysis
  - electrical analysis
- Verify model by test
- Verify model by comparison to exact solutions

ENCAPSULATION

Concept No. 1

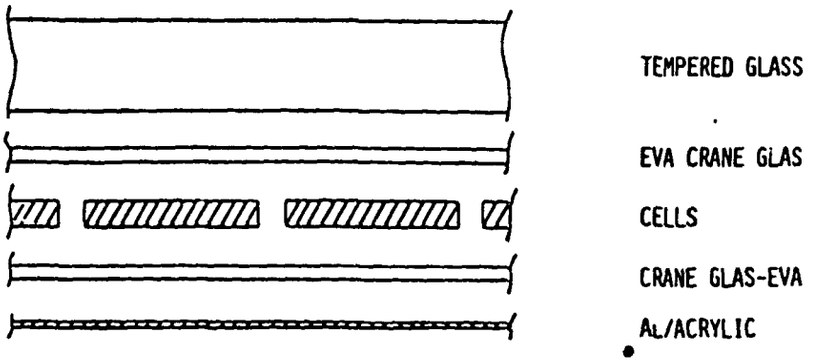

Module Concept

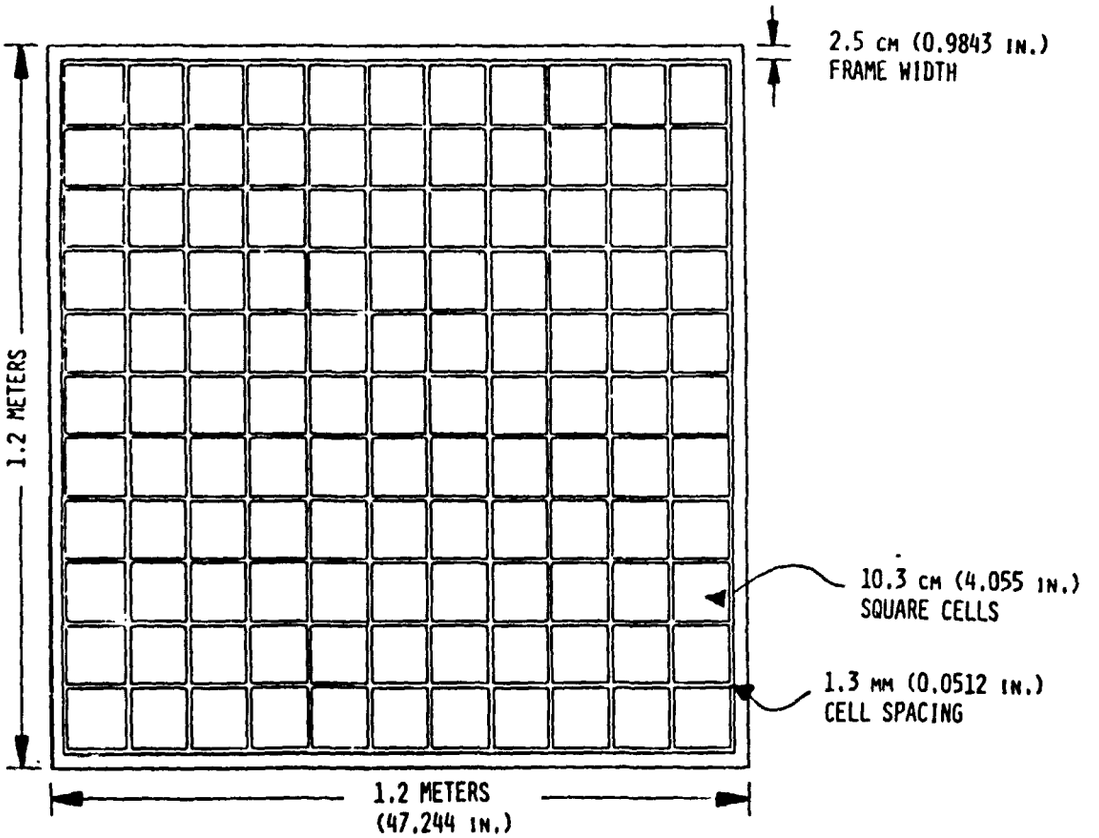

Structural Analysis Objective

DEVELOP REDUCED-VARIABLE MASTER CURVES TO ENABLE DESK-TOP CALCULATION OF SOLAR CELL STRESS

- Wind Pressure Loading
- Temperature Excursions

Assumptions

ANALYSIS:

LARGE DEFLECTION THEORY (NONLINEAR)

- Stress/Deflection Analysis of Unstiffened Flat Plates Under Pressure Loading

SMALL DEFLECTION THEORY (LINEAR-ELASTIC)

- Temperature Excursion and Deflection Encapsulation Sensitivity Studies
- Rib Design Concepts

Structural Analysis Results

- Finite Element Analyses Were Performed to Predict Solar Cell Stress
- Master Curves Were Developed to Predict Solar Cell Stress As A Function of Solar Cell, Pottant, and Structural Panel Parameters

Parameter Limits

Structural Panel	Pottant	Cell
E_{SP}: 0.75-30 MSI	E_P: 0.5 - 2.5 KSI	E_C: 5 - 30 MSI
T_{SP}: 0.04 - 0.25 IN.	T_P: 0.001 - 0.020 IN.	T_C: 0.005 - 0.015 IN.
α_{SP}: 7-24 μIN/IN/^{o}C		α_C: 1 - 12 μIN/IN/^{o}C
		L_C: 1 - 4 IN.

Thermal Stress Analysis (ΔT = 100°C); Glass Superstrate Design

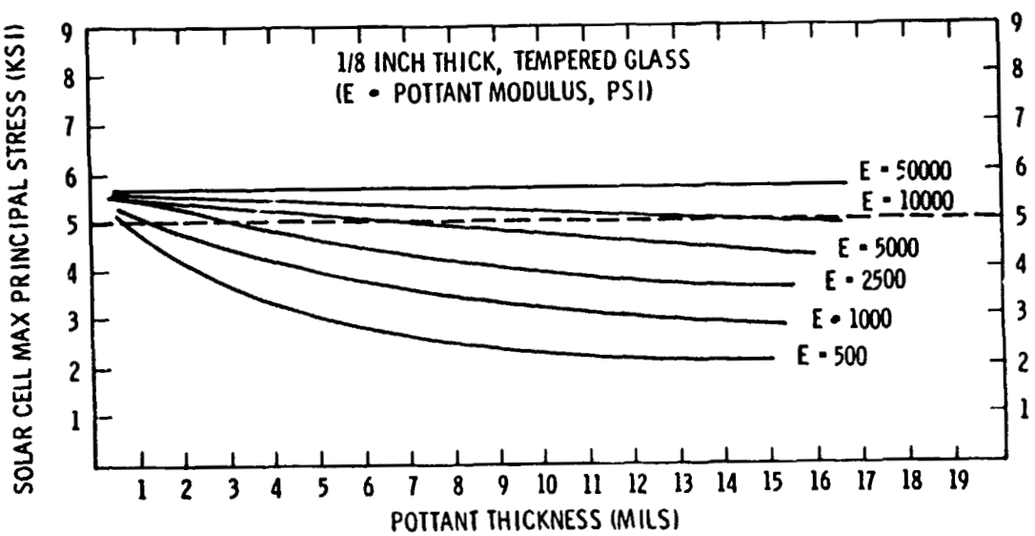

DOTTED LINE - ALLOWABLE CELL STRESS IN TENSION

Thermal Stress Master Curve

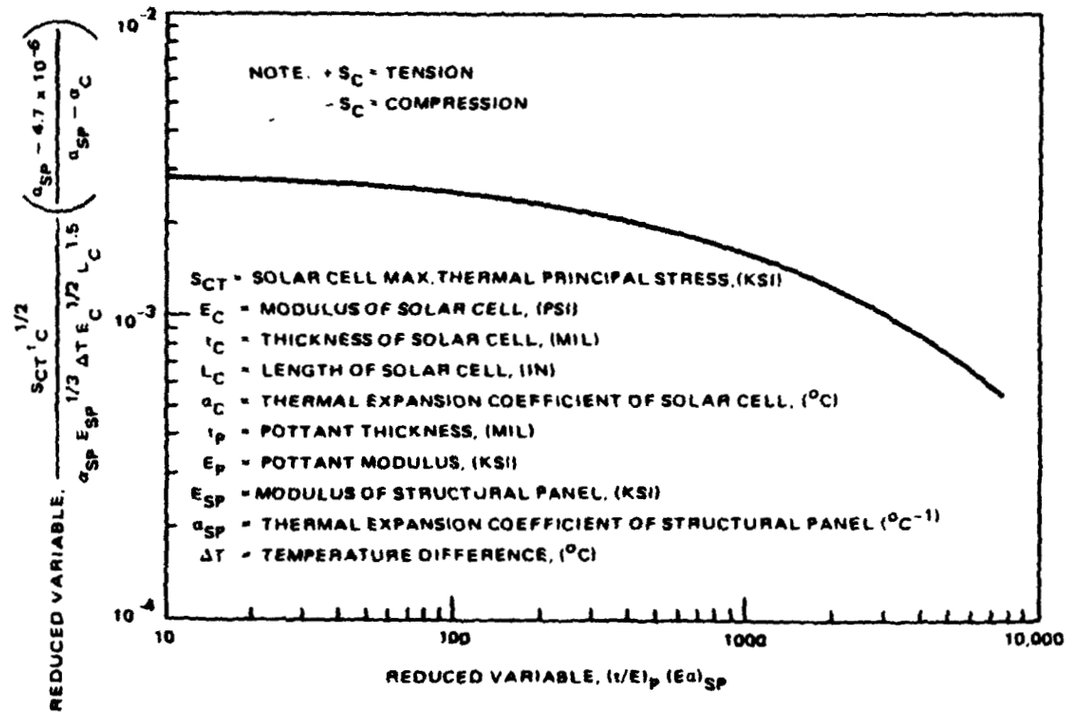

Pressure Stress Master Curve

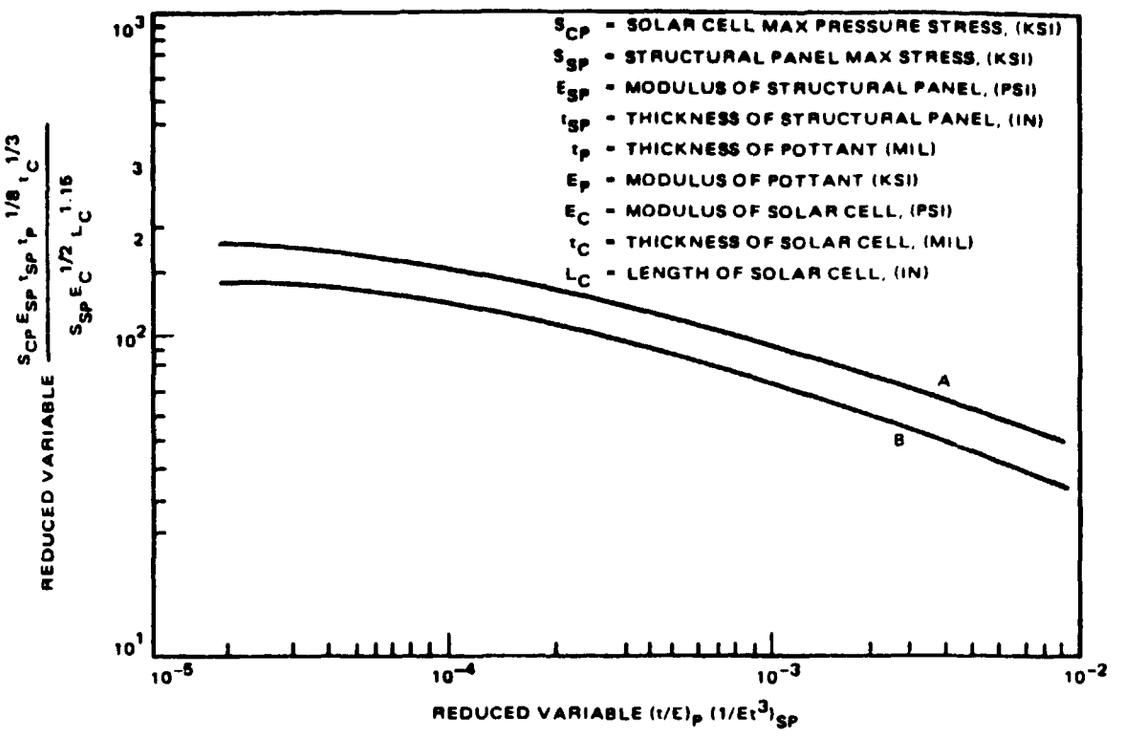

NOTE USE CURVE A FOR PRESSURE ≤ 10 PSF USE CURVE B FOR PRESSURE = 50 PSF
FOR INTERMEDIATE LOADS, INTERPOLATE LINEARLY BETWEEN A AND B

Conclusions — Structural Analyses

- Viable Master Curves
- Thermal/Hygroscopic Expansion Coefficients
- Modulus of Pottant

Optical Analysis: Objectives and Constraint

- OBJECTIVES
  - RADIANT ENERGY TRANSMISSION THROUGH ENCAPSULANT AND FRONT COVER LAYERS
  - RADIANT ENERGY ABSORBED IN CELL, ENCAPSULANT, AND FRONT COVER
  - GENERAL APPLICABILITY
    - -- CELL MATERIALS AND TYPES
    - -- ENCAPSULANT AND FRONT COVER MATERIALS
    - -- SPECTRUM OF RADIATION SOURCE
- CONSTRAINT
  - NORMAL INCIDENCE
  - AM1.5 SOLAR SPECTRUM USED IN ALL CASES STUDIED

Optical Analysis: Assumptions

- ANALYSIS STRICTLY APPLICABLE TO SPECULAR SURFACES
  - -- INCIDENT RADIANT ENERGY FLUX CONTAINS DIFFUSE COMPONENT
- CELL POWER CONVERSION EFFICIENCY DECREASES WITH TEMPERATURE (.5%/^{o}C)
- SCATTERING, IR EMISSION IGNORED
- ZERO-DEPTH CONCENTRATOR PHENOMENA
  - -- ACCOUNTED FOR IN COMPUTER PROGRAM
  - -- NEGLIGIBLE FOR CLOSELY-PACKED SQUARE CELLS
- ANTI-REFLECTION COATINGS TREATED AS IDEAL QUARTER-WAVE FILMS
- ANTI-REFLECTION COATINGS DO NOT ABSORB HEAT
- OPTICAL AND THERMAL PHENOMENA ARE UNCOUPLED

Power Conversion Efficiencies — Silicon Cells

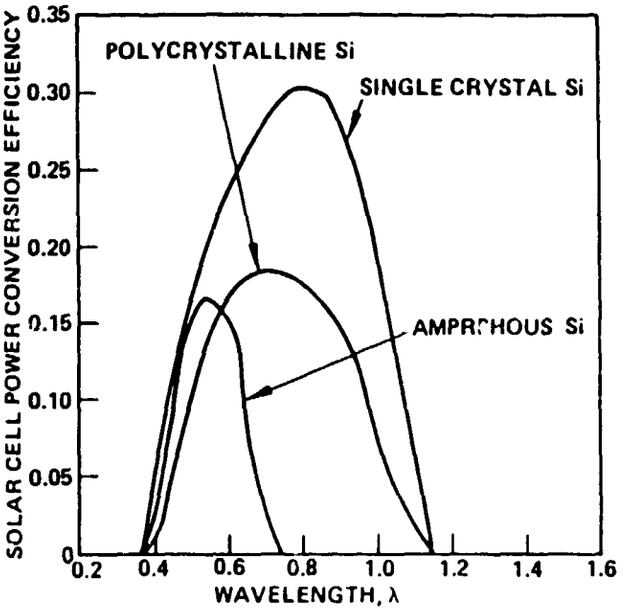

AR-Coating Reflectance vs Wavelength
(Coating Optimized for Encapsulant-Silicon Interface)

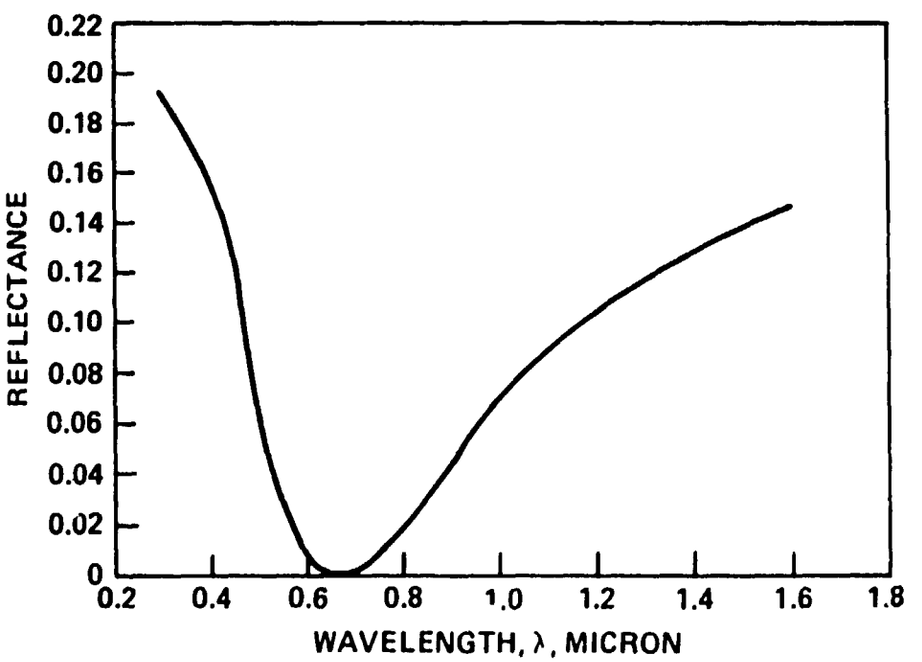

Ratio of Power Input to Power Output vs AR Coating Thickness

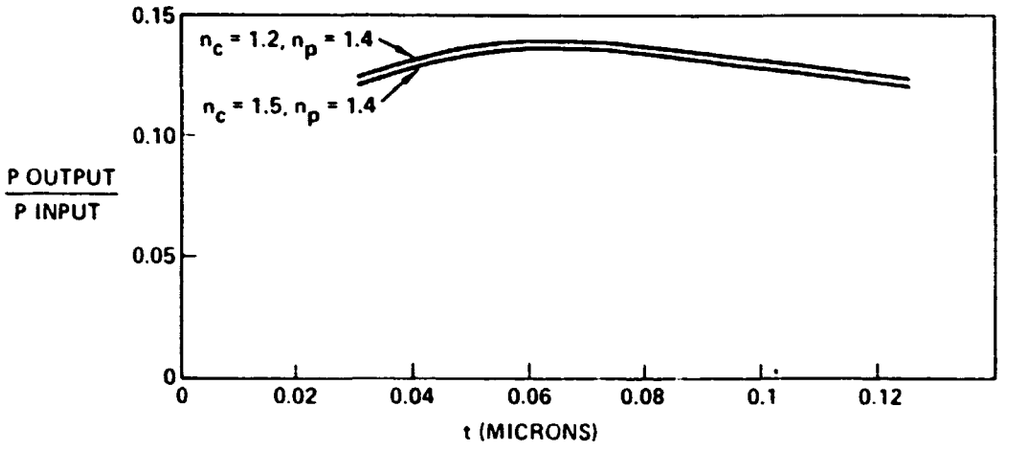

Optical Analyses Conclusions

- Transmittance > 0.45 Microns

- AR/Texturing Critical

Thermal Analysis Philosophy and Assumptions

- OBJECTIVE - PROVIDE FLEXIBLE THERMAL/OPTICAL PROGRAM FOR EVALUATION OF ENCAPSULATION DESIGNS CONSIDERING
  - -- VARIABLE NUMBER OF LAYERS
  - -- VARIABLE LAYER MATERIAL, THICKNESS
  - -- VARIABLE VOLUMETRIC OPTICAL PROPERTIES AND SURFACE PROPERTIES
- CONSTRAINTS - PROVIDE FLEXIBLE DESIGN TOOL NO EDGE EFFECTS OR INTERCONNECTION PHENOMENA ARE INCLUDED IN THE MODEL
  - -- CELL SIZE
  - -- MODULE SIZE
- ASSUMPTIONS - RADIATIVE HEAT LOSS COMPONENTS MODELLED THROUGH SPECIFICATION OF GROUND AND SKY TEMPERATURES

  CONSIDER ONE CELL CENTRALLY LOCATED IN MODULE

Module Energy Balance — Superstrate Design

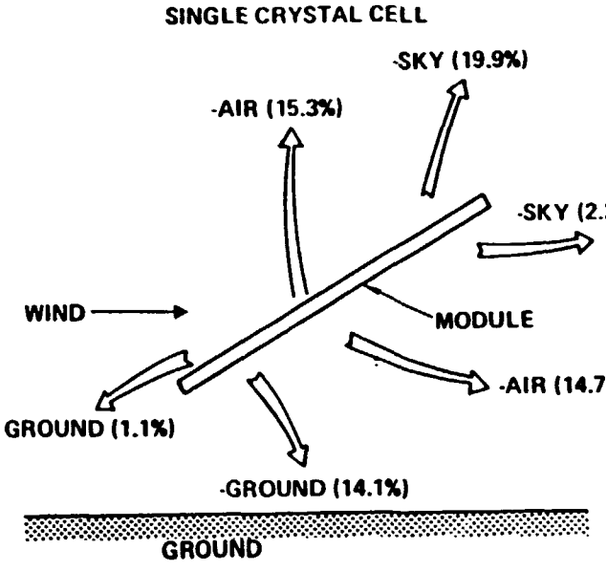

GLASS COVER LAYER
NO IRON

	POWER (ω)	%
ELECTRICAL OUTPUT	1.32	10.9
ABSORBED	8.18	67.7
REFLECTED	2.59	21.4
TOTAL	12.09	100.0

Solar-Cell Temperature vs Backside Emissivity (Glass Superstrate Design)

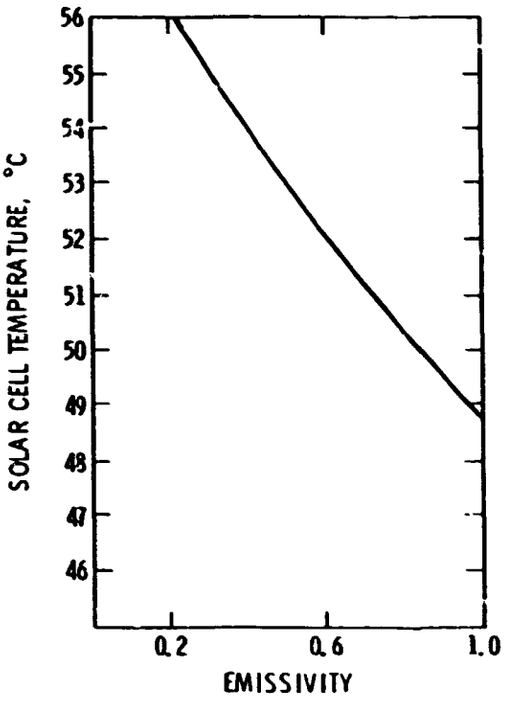

Thermal Analyses Conclusions

- Emissivity More Critical Than Thermal Resistivity

ENCAPSULATION

Electrical Analysis Objective

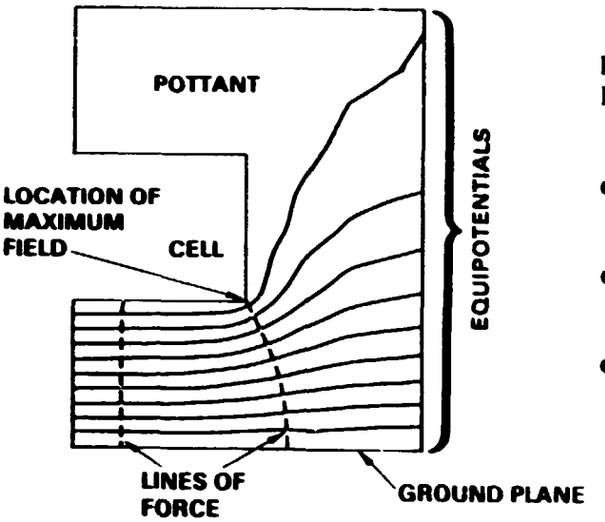

DESIGN GUIDANCE TO PREVENT BREAKDOWN

- Cell Edge/Corner Radius
- Pottant Thickness
- Cell Thickness

Electrical Isolation Studies

- Finite Element Model
- Electrical/Thermal Analogy
- NASTRAN

Thermal-Electrical Analogy

- **DIFFUSION EQUATIONS**

$\nabla \cdot \epsilon \nabla V + \rho = 0$ ELECTRICAL

$\nabla \cdot k \nabla T + \dot{q} = \rho c \left(\frac{\partial T}{\partial t}\right)$ THERMAL

THERMAL PARAMETER		ELECTRICAL PARAMETER	
TEMPERATURE	T	POTENTIAL	V
THERMAL CONDUCTIVITY	k	PERMITTIVITY	ϵ
TEMPERATURE GRADIENT	∇T	ELECTRIC FIELD	$\vec{E} = -\nabla V$
HEAT FLUX	$-k \nabla T$	ELECTRIC DISPLACEMENT	$\vec{D} = \epsilon \vec{E}$
INTERNAL HEAT GENERATION	$\dot{q}$	CHARGE DENSITY	$\rho = \nabla \cdot \vec{D}$

Formula for Family of Solar-Cell-Like Shapes

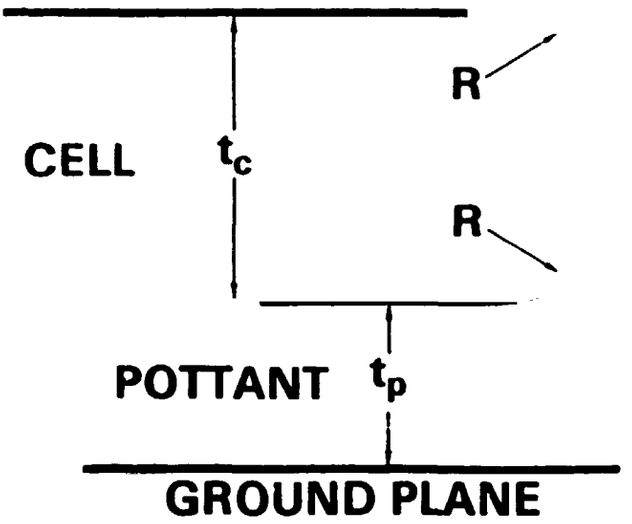

$$E_m = \frac{V}{t_p}\left(1 + \frac{t_p}{t_c}\right)^{1/2}\left(\frac{t_c}{R} - 1\right)^{1/4}$$

FOR $t_p/t_c > 2$

Electrical Analysis Results

- Finite Element Method Developed and Verified
- Electrical Stress Intensification Severe Only For
  - -- Very Sharp Corners
  - -- Very Thin Cells
- For Extreme Geometries,
  - -- Finite Element Method Inaccurate
  - -- Simple Formula Developed

Electrical Analyses Conclusions

- Visible Electrical Model
- Real World Value of R Necessary

Conclusions

- Viable Structural Master Curves
- Thermal Guidelines
- Electrical Modeling Technique
- Electrical Breakdown Most Promising for Future Fruitful Research

ENCAPSULATION MATERIALS AND PROCESSING

SPRINGBORN LABORATORIES, INC.

P.B. Willis

PHASE I

- POTTANTS
- OUTER COVER FILM
- SUBSTRATES
- ANTI-SOILING TREATMENTS
- ULTRAVIOLET STABILIZERS
- FABRICATION CONCEPTS
- ADHESIVES/PRIMERS

PHASE II

(TECHNOLOGY READINESS)

- OPTIMIZED MATERIALS FORMULATION
- MATERIALS LIFETIME AND AGING STUDIES
- FIELD EXPOSURES

Module Components (Essential)

- PLUS ADHESIVES WHERE NEEDED

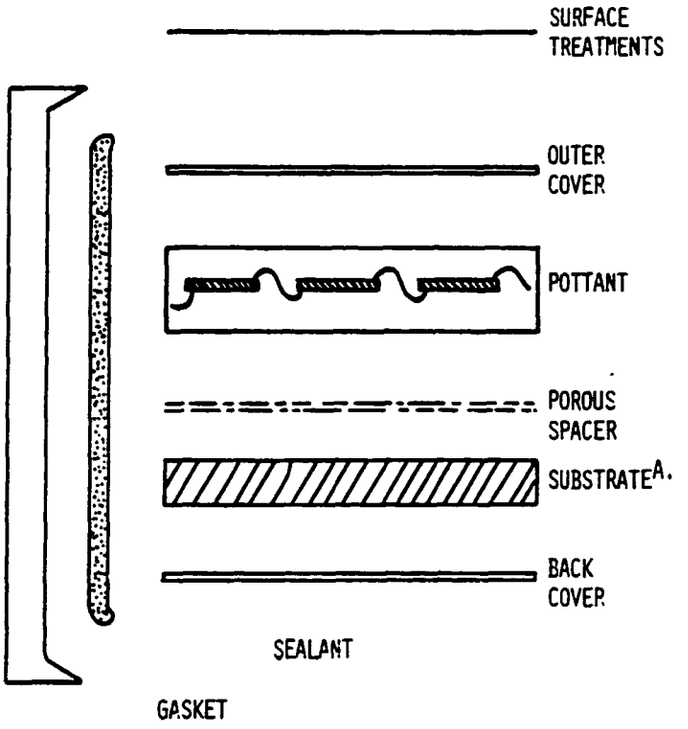

A. ELIMINATED IN SUPERSTRATE DESIGN

Candidate Polymer Encapsulation Materials

(OVERVIEW)

SUPERSTRATE: LOAD BEARING TOP COVER
SODA - LIME GLASS (LOW IRON)

POTTANTS: MECHANICAL STRESS RELIEF, ELECTRICAL ISOLATION, CELL POSITIONING, ENVIRONMENTAL ISOLATION, CORROSION BARRIER

- ETHYLENE/VINYL ACETATE (EVA)
- ETHYLENE/METHYL ACRYLATE (EMA)

} LAMINATION TYPES

- ALIPHATIC POLYURETHANE (PU)
- POLY(BUTYL ACRYLATE) (BA)

} CASTING TYPES

OUTER COVERS: PROVIDES HARD SOIL RESISTANT SURFACE, UV SCREENING, MECHANICAL BARRIER

TEDLAR 100BG30UT, TEDLAR 4462

ACRYLAR 22417

NON-SCREENING TYPES? KYNAR, FEP

POROUS SPACER: PROVIDES FIXED SPACING FOR MECHANICAL, DIELECTRIC ISOLATION: EVACUATION PATH DURING LAMINATION

CRANEGLASS (NON-WOVEN GLASS CLOTH)

BACK COVER: MECHANICAL BARRIER, ELECTRICAL ISOLATION EMISSIVITY FOR COOLING MODULE

KORAD 63000, TEDLAR 150BS30WH

SCOTCHPAR 20CP - WHITE (POLYESTER)

OTHER WHITE FILMS?

GASKETS: EPDM RUBBER

(PAWLING RUBBER CO.)

Sealants

FUNCTION AND PROPERTIES:

- PREVENTS INTRUSION OF RAINWATER
- SELF HEALING
- INEXPENSIVE
- WEATHERABLE
- NON-STAINING (NO SOLVENTS)
- APPLICABLE!

SELECTIONS: POLYSULFIDES, BUTYLS, URETHANES, OLEFIN/ACRYLIC COPOLYMERS

- BUTYLS MEET ALL CRITERIA EXCEPT APPLICATION
- AUTOMOTIVE TWO-PART URETHANES MAY BE BEST CHOICE
- MORE WORK NEEDED

Pottants

- RECEIVED GREATEST EMPHASIS TO DATE
- CONSIDERED TO BE MOST CRITICAL COMPONENT DUE TO REQUIREMENTS OF:
  - OPTICAL TRANSPARENCY
  - LOW MODULUS (STRESS RELIEF)
  - LOW SOFTENING (MELT) POINT
    BELOW SOLDER FLOW POINT
  - LOW (MELT) VISCOSITY
    LOW STRESS ON CELLS
  - LONG LIFE
    RESISTANT TO LIGHT AND HEAT
  - NO SUDDEN CHANGE IN MECHANICAL PROPERTIES
    (GLASS TRANSITION TEMPERATURE)
  - DIELECTRIC STRENGTH
  - SUITABLE FOR VOLUME PRODUCTION
  - NO CREEP AT OPERATING TEMPERATURES
    (CURABLE)
  - LOW COST

WORK HAS RESULTED IN COMMERCIAL EVALUATION PRODUCT
(SPRINGBORN EVA A 9918)

WHERE ARE WE NOW?
WHERE ARE WE GOING?

History of EVA (Springborn A-9918)

TRANSPARENT ELASTOMER	CONSIDERATIONS
Ethylene/Ethyl Acrylate	High Melt Viscosity
Plasticized PVC	Thermoplastic
Ethylene/Propylene/Diene	Not Weatherable
Ethylene/Propylene	Not Weatherable
Styrene/Butadiene	Not Weatherable
Ionomer	Process Temperature High
Polyvinyl Alcohol	Water Soluble
Thermoplastic Urethane	High Cost
"Viton" Polymers	Very High Cost
Ethylene/Methyl Acrylate	Few Grades, High Viscosity

ETHYLENE/VINYL ACETATE:

ADVANTAGES	DEFICIENCIES
Many Grades Availabale	Thermoplastic (No Creep Resistance)
Wide Range of Melt Flows	Ultraviolet Sensitive
Easy to Process	Oxidation Sensitive
Low Cost	Handling/Processing (?)
Good Adhesive Properties	

- NEED TO FORMULATE A PV MODULE GRADE

ENCAPSULATION

BASE RESIN SELECTION:

- MUST BE OVER ~30% VINYL ACETATE FOR ACCEPTABLE TRANSPARENCY
- VERY HIGH (~45% VINYL ACETATE) APPEAR TO BE LESS STABLE (HEAT LIGHT)

FINAL GRADE SELECTION:

EVA RESIN	MANUFACTURER	% VA	MELT INDEX
EY 901-25	USI	40	7.5
EY 902-30	USI	40	70.0
UE 645-35	USI	33	48.0
UE 638-35	USI	31	24.0
ELVAX 250	DUPONT	33	43.0
ELVAX 170	DUPONT	36	0.7
ELVAX 240	DUPONT	28	43.0

CHOICE: ELVAX 150

RATIONALE

- MINIMUM 7 VA FOR GOOD OPTICAL
- HIGHEST MELT FLOW THAT MAY STILL BE EXTRUDED EASILY (HANDABLE)
- LOWEST VISCOSITY AND LOWEST STRESS ON CELL STRING DURING LAMINATION

CURE CONSIDERATIONS:

- MUST BE CURED TO PREVENT CREEP AT MODULE OPERATING TEMPERATURES (50° - 85°C)
- MOST DIRECT ROUTE: PEROXIDES
- PEROXIDES MUST BE <u>ALIPHATIC</u> TO PREVENT POSSIBLE PHOTOSENSITIZATION
- MUST <u>NOT</u> ACTIVATE DURING EXTRUSION OF POTTANT INTO SHEET (70° - 115°C)
- <u>MUST</u> ACTIVATE AT TEMPERATURES BELOW THE SOLDER MELT TEMPERATURE (180°C) DURING LAMINATION

GENERAL MECHANISM:

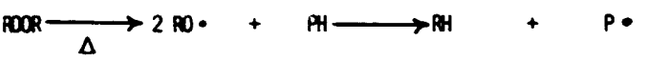

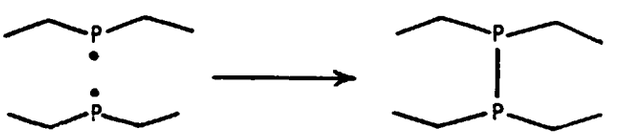

POLYMER RADICAL RECOMBINATION

CROSSLINK (CURE)

ENCAPSULATION

ELVAX 150 STRUCTURE: "BLOCK" TYPE

E-E-E-E-E-E-E-E- VA-E-VA-VA-E-VA-VA-E-E-VA

ETHYLENE SECTION ETHYLENE/VINYL ACETATE SECTION

(PARTLY CRYSTALLINE) (AMORPHOUS)

FIRST PEROXIDE CHOICE: LUPERSOL - 101 (LUCIDOL CORP.)
CURES THROUGH VINYL ACETATE GROUPS ONLY!

CONDITIONS FOR 80% GEL[A].

TEMPERATURE, °C	130°	140°	150°	160°
TIME, MIN.	NA	30	12	10

ADVANCED PEROXIDE STUDY: LUPERSOL TBEC (LUCIDOL CORP.)
CURES THROUGH BOTH ETHYLENE AND VINYL ACETATE

CONDITIONS FOR 80% GEL[A].

TEMPERATURE, °C	130°	140°	150°	160°
TIME, MIN.	10	3	2	1

A. LABORATORY CURES IN PLATEN PRESS

PHOTO-OXIDATIVE . · LIZATION

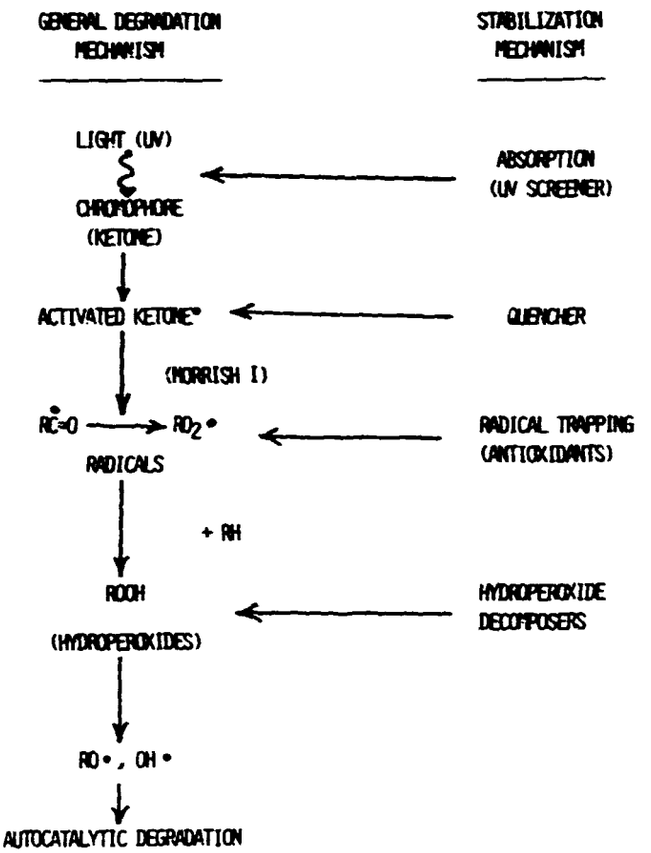

ENCAPSULATION

FORMULATION A 9918

COMPOUND	LEVEL	FUNCTION
ELVAX 150	100	POLYMER
LUPERSOL 101	1.5	CURING AGENT
CYASORB UV-531[A]	0.3	UV SCREENER
NAUGARD-P	0.2	ANTIOXIDANT
TINUVIN 770[A]	0.1	HINDERED AMINE LIGHT STAB. (FREE RADICAL TRAP AND HYDROPEROXIDE DECOPOSER)

FORMULATION 15295

LUPERSOL TBEC	1.5	(REPLACES LUPERSOL 101)

PERFORMANCE CHARACTERISTICS

EXTRUSION: (EASY)	SCREW - LDPE BARREL - 110°C DIE - 75°C L/D - 24:1
STORAGE:	ROOM TEMPERATURE - ROLLS MUST BE IN PLASTIC BAGS!
MODULE PERFORMANCE AT 50°C:	EXCELLENT
COST (SPRINGBORN):	$0.35 PER SQUARE FOOT

A. THIS COMBINATION PARTICULARLY EFFECTIVE; HALS PROTECTS UV-531 FROM OXIDATION.
(ALLEN, JAPS, V27, 2761 (1982))

ENCAPSULATION

EVA 9918 - STANDARD EVALUATION GRADE
EVA 15295 - "FAST CURE" GRADE

GOAL: THIRTY YEARS SERVICE LIFE

- HOW DO YOU KNOW?

ACCELERATED AGING PERFORMANCE

CONDITION	TIME	PROPERTY	RESULT
RS/4 50°C	40,000 HRS.	SURFACE	CRACKING
		OTHERS	NO CHANGE
THERMAL, 90°C	8,000 HRS.	OPTICAL	SLIGHT YELLOW
		MECHANICAL	NO CHANGE
THERMAL, 130°C	8,000 HRS.	MECHANICAL	10% REMAIN
		OPTICAL	74% REMAIN
RS/4 WATER	10,000 HRS.	ANY	NO CHANGE
RS/4 85°C	8,000 HRS.	ANY	NO CHANGE

- DEGRADATION NOTICED ONLY IN EXTREME CONDITIONS
- ALL CONDITIONS TAKE A LONG TIME
- NEED FOR MEANINGFUL SHORT TERM TEST

Accelerated Aging Test Program

OUTDOOR PHOTOTHERMAL AGING

- USE NATURAL SUNLIGHT, AVOIDS SPECTRAL DISTRIBUTION PROBLEMS WITH ARTIFICIAL LIGHT SOURCES
- USED TEMPERATURE TO ACCELERATE THE PHOTOTHERMAL REACTION
- INCLUDES DARK CYCLE REACTIONS
- INCLUDES DEW/RAIN EXTRACTION
- INTENDED PRIMARILY FOR MODULE EXPOSURE

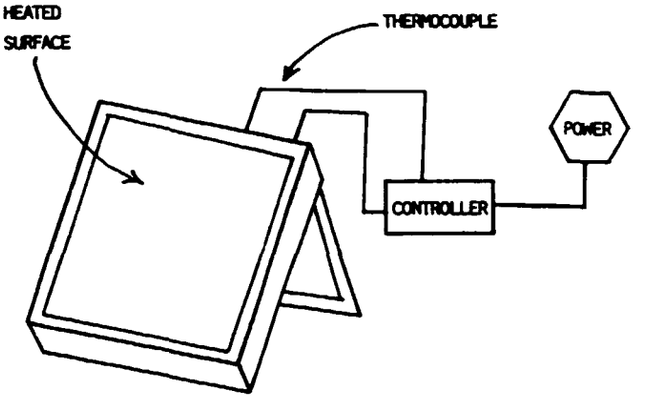

Outdoor Photothermal Reactors

(OPT)

70°C	NO CHANGE 2000 HOURS	
90°C AND 105°C		TERMINATED[A] AT:
	EVA A9918	2000 HOURS
	EMA 15257	2000 HOURS
	PU Z-2591	2000 HOURS
	EVA 16718 A (UV2098, TBEC)	1000 HOURS
	EVA 16718 B (NO TINUVIN 770)	500 HOURS

A. LOSS OF MECHANICAL PROPERTIES, SEVERE COLORATION AT 105°C

- RAINFALL DURING EXPOSURE, 9.7 INCHES
- NO DECREASE IN UV CUTOFF WAVELENGTH (UV SCREENER LOSS - SPECIMEN)
- EVA 1618B INDICATES NEED FOR TINUVIN
- FIRST SHORT TERM TEST RESULTING IN DEGRADATION OF EVA FORMULATIONS

EVA Aging

LOSS OF UV SCREENING STABILIZER

(CYASORB UV-531, 0.3%)

FORMULATION	CONDITION	RETAINED
EVA 9918	CONTROL-EXTRUDED	95%
EVA 9918	CONTROL-CURED	93%
EVA 9918	RS/4 40,000 HRS (50°C)	35%
EVA 9918	130°C 4,500 HOURS	0%
EVA 9918	OPT-105°C 1,000 HOURS	32%
EVA 9918	OPT-90°C 2,000 HOURS	50%

- HPLC TECHNIQUE DEVELOPED FOR ANALYSIS
- UV-531 SCREENER IS VOLATILE - MOST READILY LOST AT HIGH TEMPERATURE CONDITIONS

LOSS OF HALS STABILIZER
(TINUVIN 770, 0.1%)

FORMULATION	CONDITION	RETAINED
EVA 9918	CONTROL-EXTRUDED	100%
EVA 9918	CONTROL-CURED	100%
EVA 9918	RS/4 40,000 HOURS	5%
EVA 9918	130°C 4,500 HOURS	5%
ELVAX/L-101	OPT 90° 1,500 HOURS	~
ELVAX/TBEC	OPT 90° 1,500 HOURS	~
EVA 9918	OPT 105° 1,000 HOURS	~

- GC/MS ANALYTICAL TECHNIQUE DEVELOPED
- LOW MOLECULAR WEIGHT TINUVIN-770 APPEARS TO BE READILY LOST DURING ACCELERATED AGING
- LOSS OF HALS LEAVES UV-531 SCREENER WITHOUT OXIDATIVE PROTECTION
- GENERAL CONCLUSION: POLYMER FAILS DUE TO LOSS OF STABILIZER

Outdoor Photothermal Reactors: Module Results

(EVA 9918)

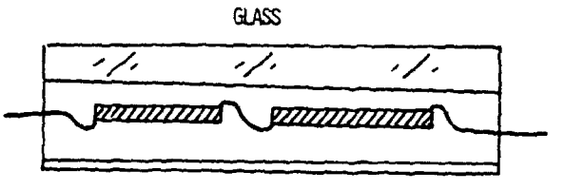

TEDLAR 150 BS 30 WH

TEMPERATURE	TIME	RESULTS
70°C	3,000 HRS	NO CHANGE
90°C	3,000 HRS	NOTICEABLE DISCOLORATION AROUND COPPER WITH SOME FLOW. OTHER PARTS OF MODULE OK.
105°C	3,000 HRS	SEVERE COLOR AND FLOW NEAR COPPER. OTHER AREAS: FLOW, DELAMINATION

- OPT REACTORS: FIRST ACCELERATED TEST TO GIVE RESULTS IN SHORT TIME. SIMULATES ACTUAL MODULE CONDITIONS.
- COPPER IS POTENT ACCELERATOR OF POLYMER DEGRADATION.

Outdoor Photothermal Reactors

USEFUL FOR:

- COMPARATIVE STUDIES OF STABILIZERS
- PERFORMANCE OF POTTANTS AND OTHER COMPONENTS UNDER "MODULE CONDITIONS"
- MAY FINALLY ANSWER QUESTION OF THERMAL ENDURANCE — HOW HOT? HOW LONG?
- IMPOSES THERMAL STRESS IN THE PRESENCE OF SUNLIGHT

THERMAL ENDURANCE [A]

—— SPECULATION ——

(1) SAFE UPPER LEVEL TEMPERATURE

(2) LOCALIZED OVERHEATING - SOME DEGRADATION BUT NO EFFECT ON MODULE

(3) LOCALIZED OVERHEATING WITH GRADUAL EFFECT ON WHOLE MODULE

(4) OVERHEATING WITH IMMEDIATE DESTRUCTIVE EFFECT ON MODULE PERFORMANCE

A. DTA AND DSC TOO SHORT TERM TO ASSESS THIS PROPERTY

Pottants

ADVANCED FORMULATIONS CANDIDATE ADDITIVES:

ADDITIVE	MANUFACTURER	FUNCTION	TYPE
UV-2098	AMERICAN CYANAMIDE	UV SCREEN	REACTIVE
UV-2908	AMERICAN CYANAMIDE	UV SCREEN	POLYMERIC
MON 79-4005	NATIONAL STARCH	UV SCREEN	REACTIVE
78-6121	NATIONAL STARCH	UV SCREEN	POLYMERIC
UV-3346	AMERICAN CYANAMIDE	HALS	POLYMERIC
HOSTAVIN N-20	AMERICAN HOECHST	HALS	REACTIVE
CHIMASSORB 944	CIBA GEIGY	HALS	POLYMERIC
A-2590-EF	GEORGIA PACIFIC	HALS	POLYMERIC

TO BE USED WITH:

LUPERSOL TBEC	LUCIDICL	PEROXIDE	CURING AGENT

- NO ADDITIONAL ANTIOXIDANT ADDED - HALS COMPOUNDS APPEAR TO BE SUFFICIENT
- FUTURE FORMULATIONS WILL USE THREE COMPONENTS: TBEC, UV SCREEN, HALS

Advanced Formulations

STATUS TO DATE

EVA 14747: CONTAINS UV-2098 COREACTED

- RESISTANT TO HYDROLYSIS
  (WATER - 1,500 HOURS - 70°C)
- RS/4 - 85°C 4,000 HRS NO CHANGE
- RS/4 - 50°C 15,000 HRS NO CHANGE
- OPT - 90°C 2,000 HRS FAILURE

EVA 17451C: CONTAINS CYASORB UV-3346 (POLYMERIC)
(NO UV SCREEN)

- OPT 90°C OVER 2,000 HRS (CONTINUING)

  BETTER RETENTION OF PROPERTIES THAN OTHER FORMULATIONS

COMBINATIONS OF ADVANCED HALS AND UV SCREEN FORMULATIONS COMING ONTO TEST.

REMAINING CONCERNS:

- MOBILITY VS. STABILIZATION: DO THE STABILIZERS HAVE TO MIGRATE THROUG THE POLYMER TO RETAIN EFFECTIVENESS?

OUTDOOR PHOTOTHERMAL REACTORS/MODULES

TIME AND TEMPERATURE	MODULE GLASS/RESIN/TEDLAR[A]	CONDITION
70°C 3,000 HRS.	EVA 9918	NO CHANGE
	EVA 16718 A	
	EMA 16717	
	EVA 14747	
90°C 3,000 HRS.	EVA 9918	SOME COLOR FLOW NEAR COPPER
	EVA 16718 A	NO CHANGE
	EMA 16717	
	EVA 14747	
105°C 3,000 HRS.	EVA 9918	SEVERE COPPER RXN DEPOLYMERIZATION DELAMINATION
	EVA 16718 A	SLIGHT COLOR (COPPER
	EMA 16717	SLIGHT COLOR (COPPER
	EVA 14747	SLIGHT COLOR (COPPER

EVA 16718 A: TBEC, UV 2098, TINUVIN 770
EMA 16717: TBEC, UV 2098, TINUVIN 770
EVA 14747: LUPERSOL 101, UV 2098, TINUVIN 770

A. TEDLAR 150 BS 30 WH/68040 ADHESIVE

Adhesion Experiments

SELF - PRIMING FORMULATIONS

(TO SUNADEX GLASS)

POTTANT/ PRIMER	LEVEL (PHR)	BOND STRENGTH, LBS/IN CONTROL*	EIGHT MONTHS* STORAGE
EVA A9918	0.25	42	44
Z-6030	0.05	29	24
EVA 15295/	0.25	31	32
Z-6030	0.05	10.9	9.5
EVA 15257/	0.25	57.4	58
Z-6030	0.05	49.0	39.3

*BONDS ALSO STABLE TO WATER IMMERSION AND BOILING WATER

- STABLE TO STORAGE CONDITIONS (8 MO. TO DATE)
- NOW COMMERCIALLY AVAILABLE (SPRINGBORN)

  EVA A9918-P (LUPERSOL 101 CURE)

  EVA 15295-P (TBEC CURE)

- WORKING ON INTERNAL PRIMING FOR CELL STRING AND METALLIZATION (MORE DIFFICULT TO PRIME)

Antisoiling Experiments

SURFACE CHEMISTRY

- HARD
- SMOOTH
- HYDROPHOBIC
- OLEOPHOBIC
- ION FREE
- LOW SURFACE ENERGY

SURFACE INVESTIGATED

- SUNADEX GLASS
- TEDLAR (100 BG 30 UT)
- ACRYLAR (ACRYLIC FILM)

TREATMENTS REMAINING

- L-1668 FLUOROSILANE (3M)
- E-3820 PERFLOUPODECANOIC ACID/ SILANE (DOW CORNING)

EXPOSURE CONDITIONS

ENFIELD, CONNECTICUT

32 MONTHS TO DATE

Soiling Experiments

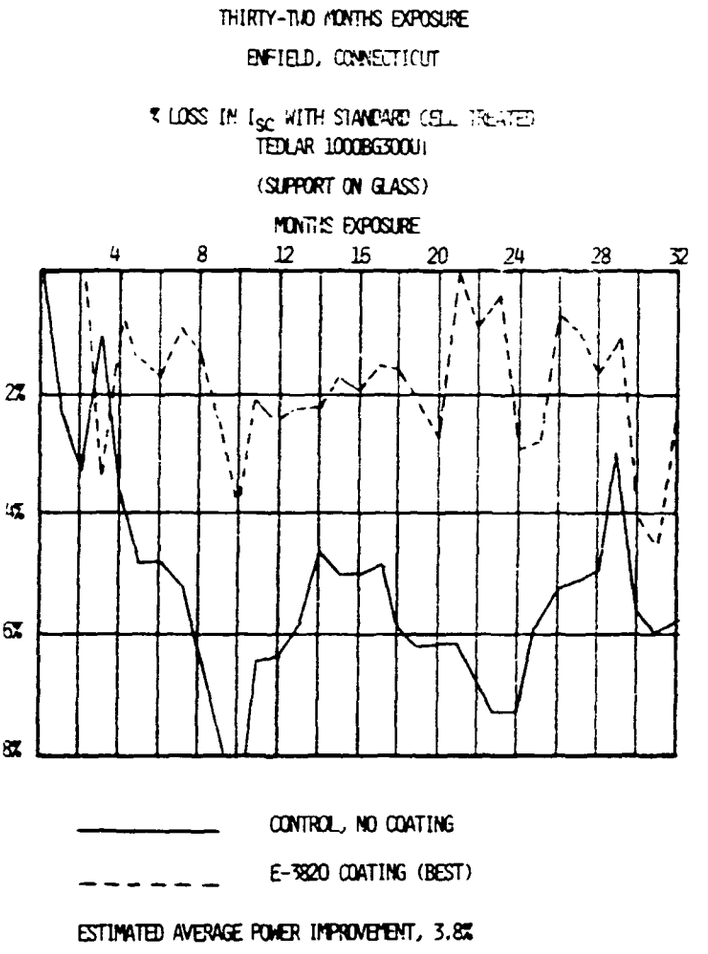

THIRTY-TWO MONTHS EXPOSURE

ENFIELD, CONNECTICUT

% LOSS IN I_{SC} WITH STANDARD CELL TREATED ACRYLAR

(SUPPORTED ON GLASS)

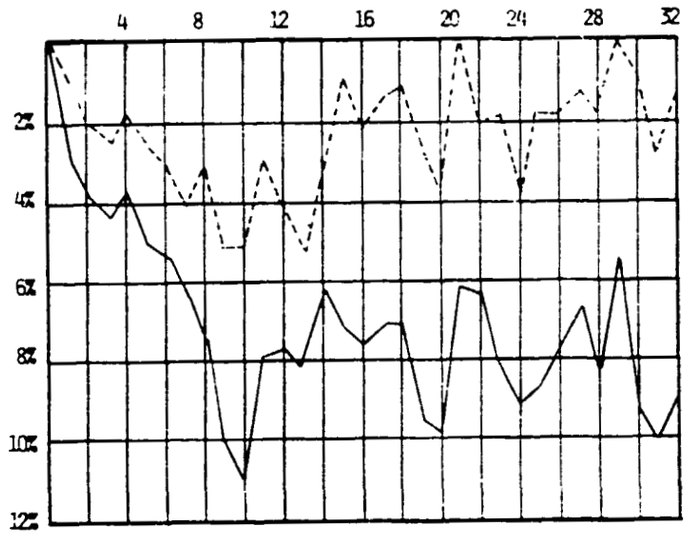

CONTROL, NO TREATMENT

OZONE WITH E-3820 (BEST)

ESTIMATED AVERAGE POWER IMPROVEMENT, 3.9%

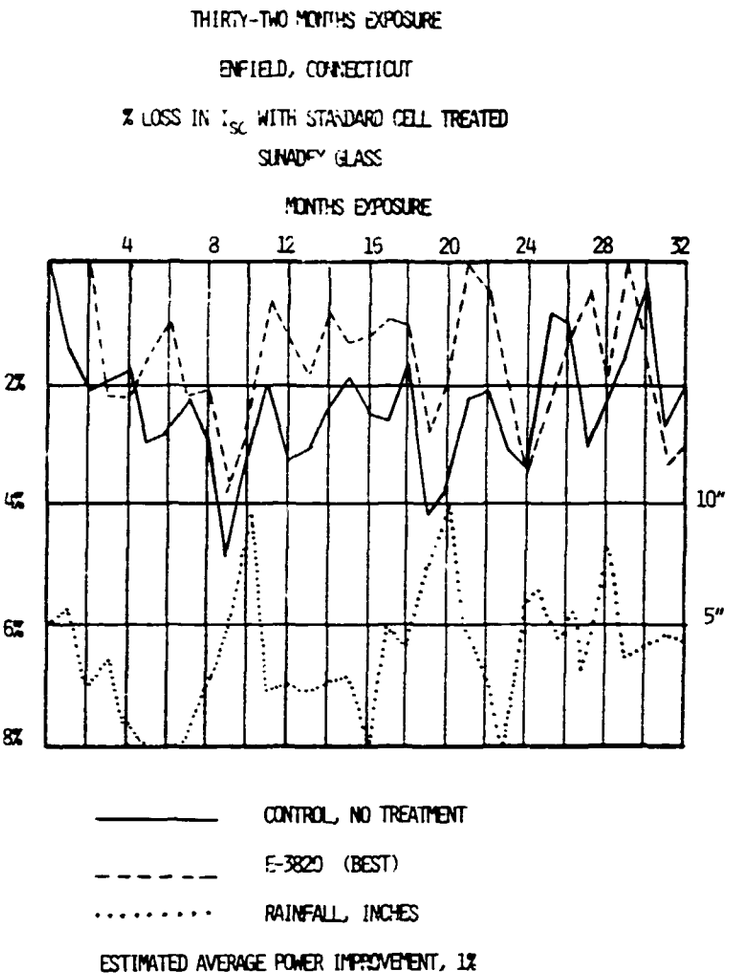
THIRTY-TWO MONTHS EXPOSURE
ENFIELD, CONNECTICUT
% LOSS IN I_{SC} WITH STANDARD CELL TREATED
SUNADEX GLASS
MONTHS EXPOSURE
4
8
12
16
20
24
28
32
2%
4%
6%
8%
10"
5"
CONTROL, NO TREATMENT
E-3820 (BEST)
RAINFALL, INCHES
ESTIMATED AVERAGE POWER IMPROVEMENT, 1%

Additional Activities

SUPPORT SERVICES

DOW CORNING: DR. ED PLUEDDEMANN

- ADVANCED PRIMER FORMULATIONS
- ADHESIVES
- SOIL RESISTANT TREATMENTS

CASE WESTERN RESERVE UNIVERSITY: DR. JACK KOENIG

- "DRIFT" ANALYSIS OF PRIMER/GLASS INTERFACE ADHESION AND LIFE

UNIVERSITY OF CINCINNATI: DR. BOERIO

- POLYMER - METAL INTERFACES ADHESION AND LIFE

TRANSPARENT CONDUCTIVE MATERIALS

- SURVEY OF POLYMER DEPOSITION METHODS
- ENVIRONMENTAL STABILITY CONSIDERATIONS
- SOLAR CELL ADHESION
- ENCAPSULATION PROCESS MATERIAL COMPATABILITY

Conclusions

- OUTDOOR PHOTOTHERMAL REACTORS (OPT)
  - APPEARS TO BE GOOD SHORT TERM TEST FOR MATERIALS UNDER MODULE CONDITIONS
  - MAY BE USEFUL FOR DETERMINING THERMAL ENDURANCE LIMITS
- METALLIC COPPER SHOULD BE AVOIDED!
- CURRENT STABILIZER SYSTEM (IN 9918) IS FUGITIVE UNDER HARSH CONDITIONS
- FORMULATIONS WITH TBEC PEROXIDE AND UV 2098 STABILIZER APPEAR TO OUTPERFORM EVA 9918
- SELF-PRIMING FORMULATIONS FUNCTION WELL AND HAVE GOOD STORAGE LIFE
- SOIL RESISTANT TREATMENTS SUCCESSFUL

Future Work

- CONTINUED SELECTION OF CANDIDATE MATERIALS WHERE NEEDED
- ADVANCED STABILIZERS: NON-FUGITIVE HALS AND UV SCREENING ADDITIVES PUT UNDER TEST
- CONTINUATION OF ANALYTICAL METHODS TO FOLLOW THE CONCENTRATION AND CHEMICAL "HEALTH" OF STABILIZERS
- STUDIES IN PROCESS VARIABLES: FACTORS AFFECTING SUCCESS OF MODULE FABRICATION AND INTEGRITY OF COMPONENTS
- INTERNAL PRIMERS FOR CELLS AND METALIZATION
- EVALUATION OF NEW SOIL-RESISTANT TREATMENTS
- STUDIES OF DIELECTRIC STRENGTH VS. AGING FOR ENCAPSULATION COMPONENTS

PHOTOTHERMAL DEGRADATION OF ENCAPSULANTS

JET PROPULSION LABORATORY

R.H. Liang

Objectives

- DEVELOP MECHANISTIC MODEL TO PREDICT LIFETIME OF ENCAPSULANTS WITH RESPECT TO PHOTOTHERMAL DEGRADATION

- DEVELOP VALID ACCELERATED PHOTOTHERMAL TESTING PROCEDURES FOR EVALUATION OF ENCAPSULANTS

Mechanistic Model

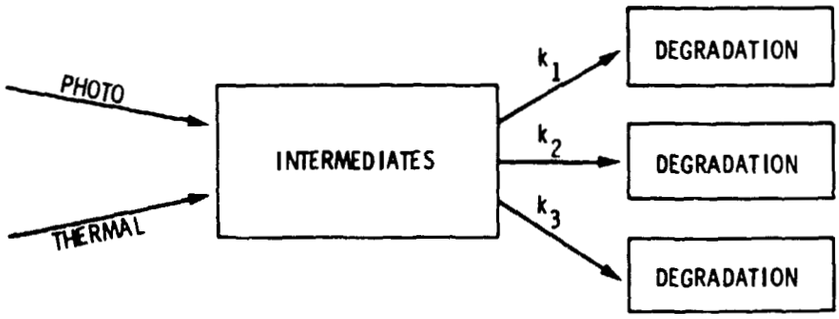

Approach

- STUDY MECHANISMS OF PHOTOTHERMAL DEGRADATION

- PHOTOTHERMAL AGING OF MATERIAL SPECIMENS

- PHOTOTHERMAL AGING OF TWO-CELL MODULES

ENCAPSULATION

Mechanistic Studies

STATUS

- LASER-FLASH ESR (ELECTRON SPIN RESONANCE) APPARATUS IN OPERATION
- KEY DEGRADATION INTERMEDIATES IDENTIFIED
- TIME, TEMPERATURE AND LIGHT FLUX CORRELATION INITIATED

Flash ESR Apparatus

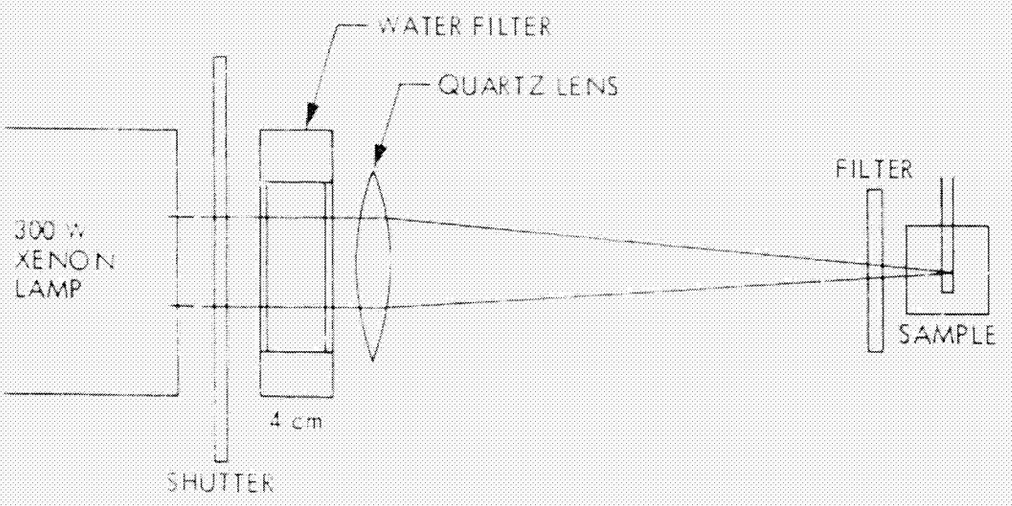

Time Profiles and Intensity of Peroxy Radical as a Function of Light Intensity

a). 100% b). 46% c). 26% d). 12%

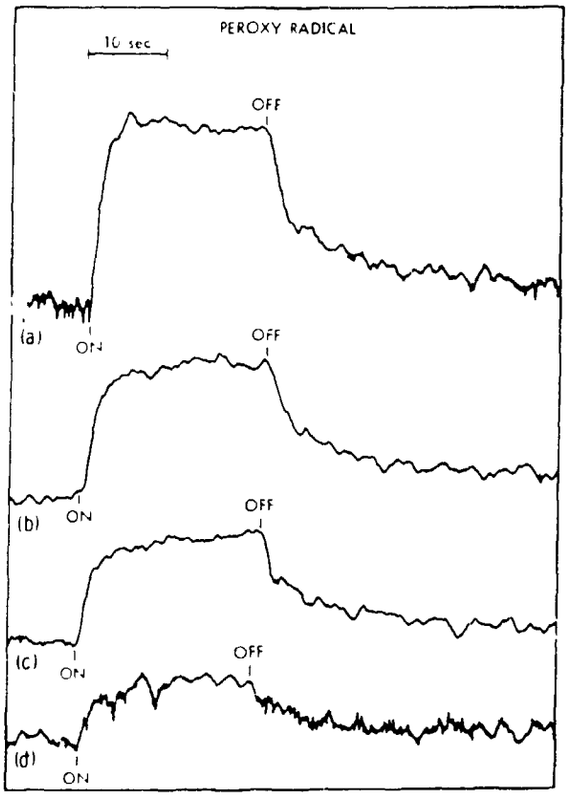

In-Situ Steady-State ESR Spectrum of Photoirradiated PnBA at Room Temperature in Air

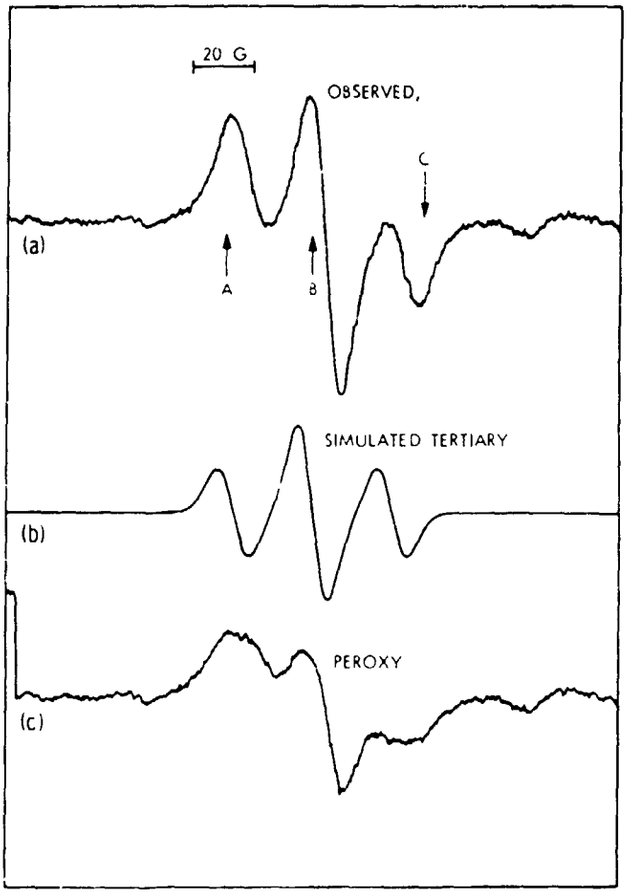

In-Situ Steady-State ESR Spectrum of
Photoirradiated PnBA at 23°C in Vacuo

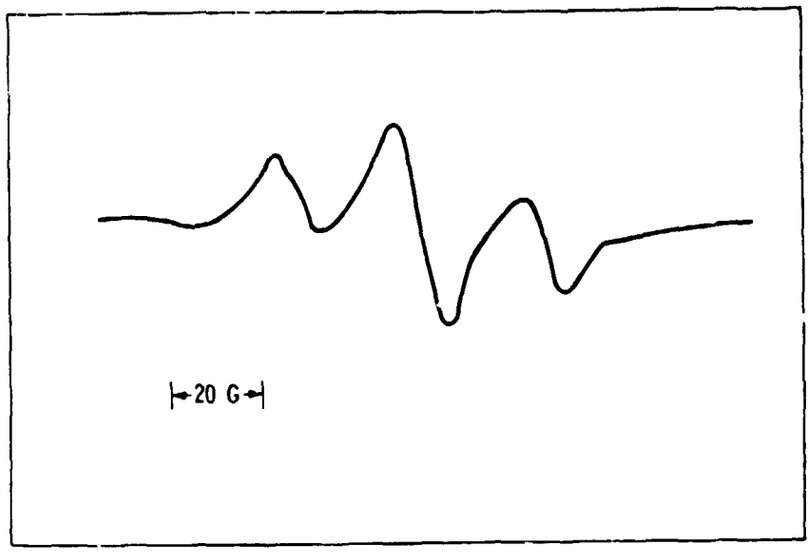

Time Profile of Tertiary Radical at 23°C in Vacuo

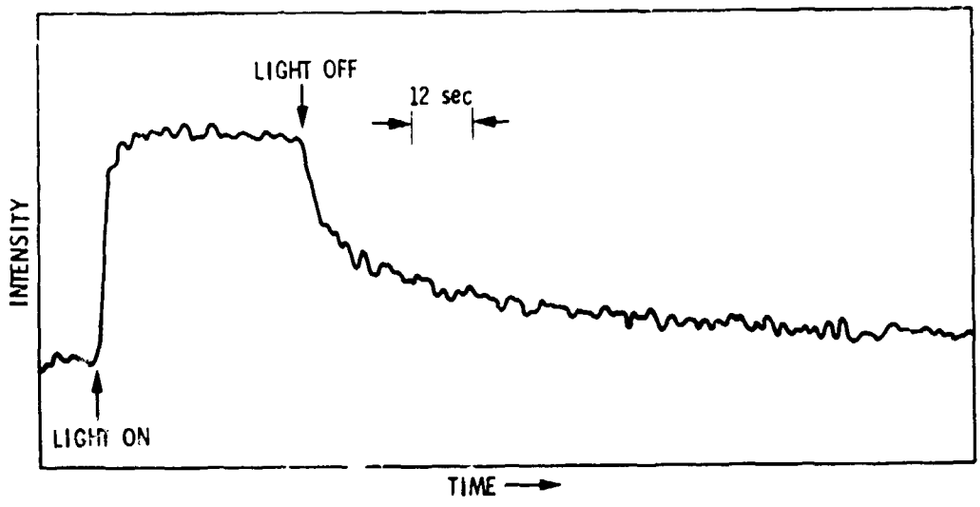

Half Life of Radical Decay as a Function of Temperature

TEMPERATURE	HALF LIFE (sec)
23 C	8.9 ± 0.4
55 C	4.6 ± 0.6
75 C	2.9 ± 0.6

Temperature Dependence of Rate Constants for Photoinduced Crosslinking of PnBA in Vacuo

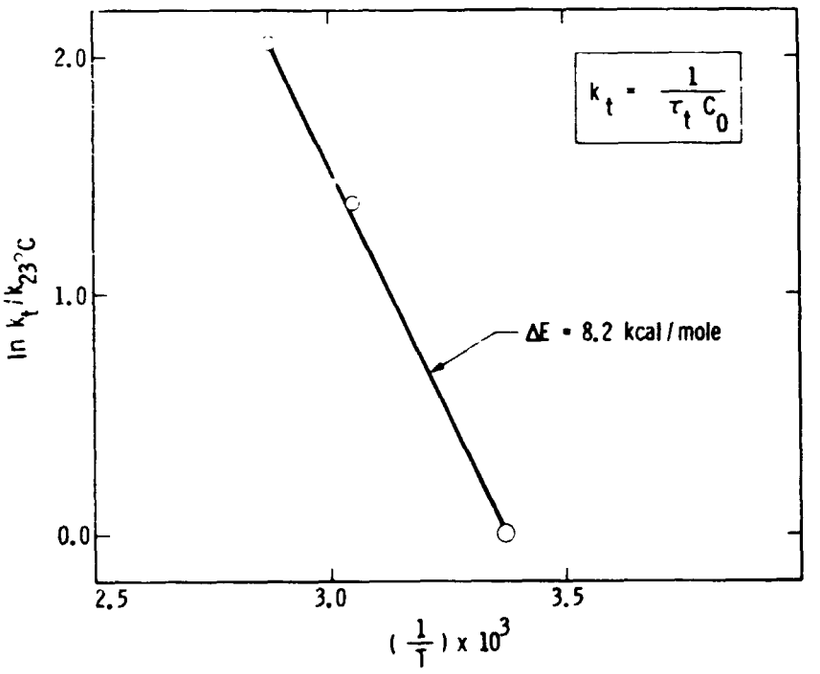

Photothermal Aging of Material Specimens

- AGING PARAMETERS
  - UV - 0 SUNS, 2 SUNS, 6 SUNS
  - TEMP. - 75°C, 85°C, 105°C, 120°C, 135°C

- SAMPLE CONFIGURATIONS
  - EVA - SUNADEX/EVA/PYREX
    TEDLAR/EVA/PYREX
  - PnBA - SUNADEX/PnBA/PYREX

STATUS

- SUNADEX/EVA/PYREX
  - 6 SUNS AT 85°C, 105°C, 120°C, 135°C COMPLETED
  - 0 SUNS AT 85°C, 105°C, 120°C, 135°C COMPLETED
  - 2 SUNS AT 85°C, 120°C IN PROGRESS

- SUNADEX/PnBA/PYREX
  - 6 SUNS AT 85°C, 105°C, 120°C, 135°C COMPLETED

Transmittance Spectra of Sunadex/EVA/Pyrex at 6 Suns and 120°C

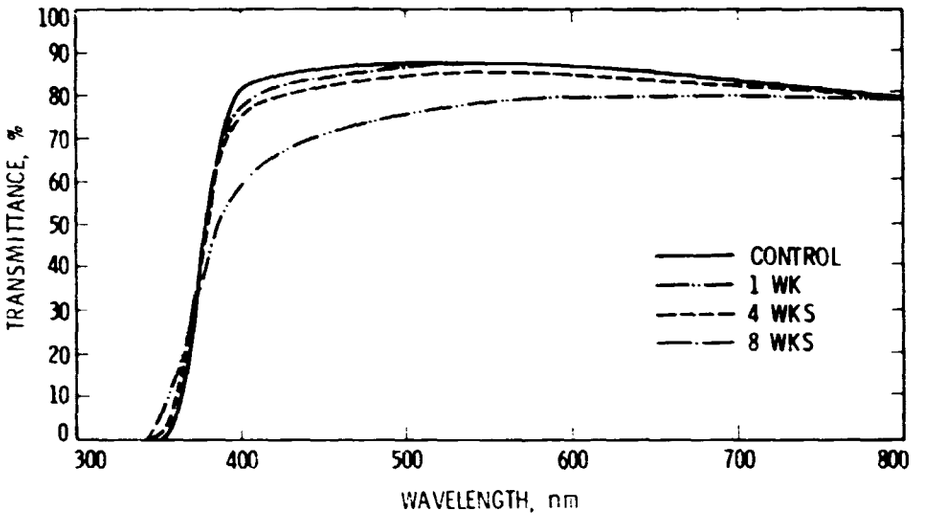

Transmittance Spectra of Sunadex/EVA/Pyrex

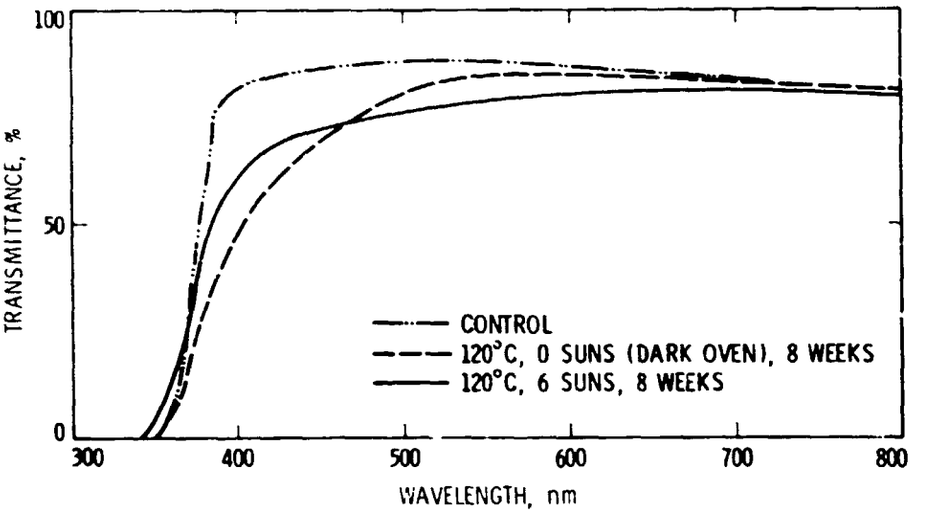

Transmittance Spectra of Sunadex/EVA/Pyrex at 2 Suns and 120°C

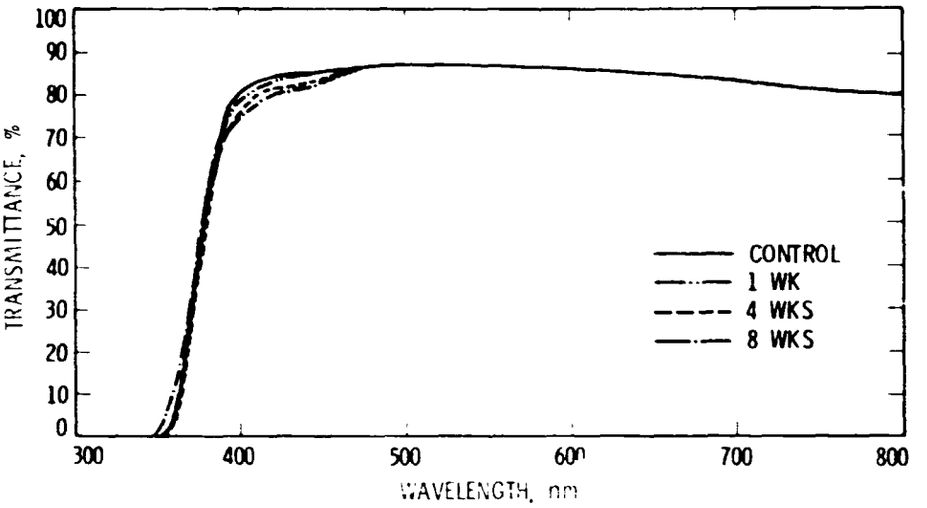

Loss Of Transmittance of Sunadex/EVA/Pyrex as a Function of Time at 120°C

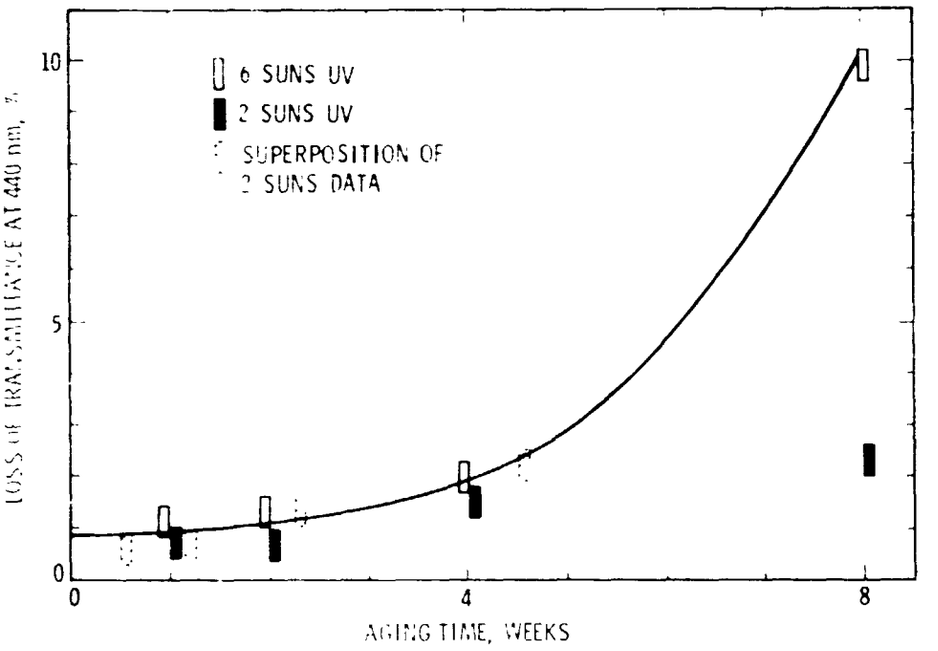

Photothermal Aging of 2-Cell Modules

STATUS

- CHARACTERIZATION OF CER-G COMPLETED

TEMPERATURE RANGE	55°C TO 120°C
UV FLUX	6 SUNS TO 15 SUNS

- TESTING AT 60°C, 85°C, 120°C AND AT 6 SUNS INITIATED

ENCAPSULATION

POLYMER-POLYMER INTERFACE BOND STABILITY

CASE WESTERN RESERVE UNIVERSITY

J.L. Koenig

Infrared Surface Spectroscopies

- DRIFT
- RAIR
- TRANSMISSION

Reflectance

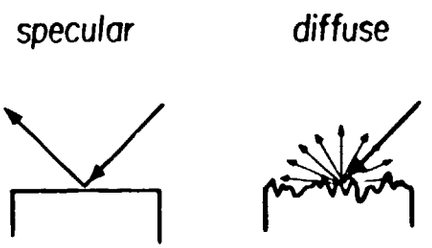

Diffuse Reflectance Optics

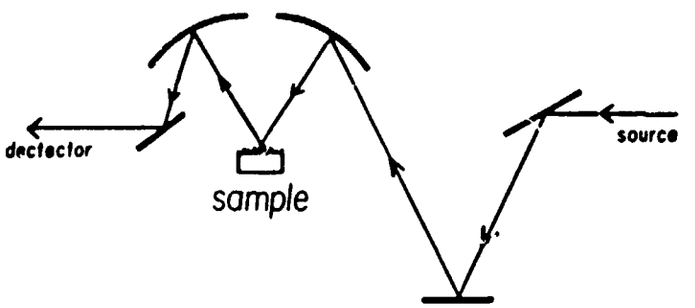

Silane Coupling Agent

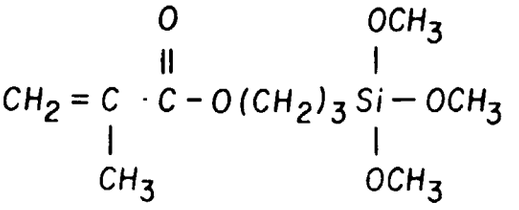

γ - M P S

Approximate Surface Coverage

% w/w	layers
0.001	0.05
0.01	0.53
0.10	5.3
1.0	53
2.0	106

* 0.269 m^2/g glass

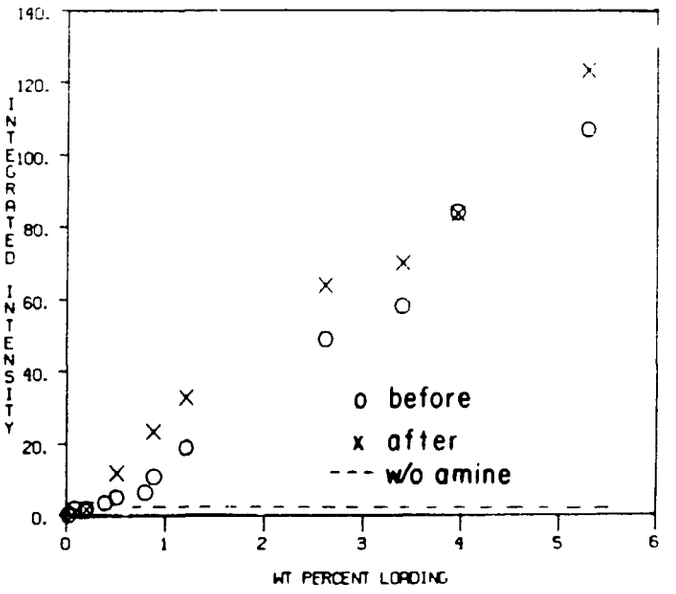

ENCAPSULATION

MPS/Amine Modified Glass

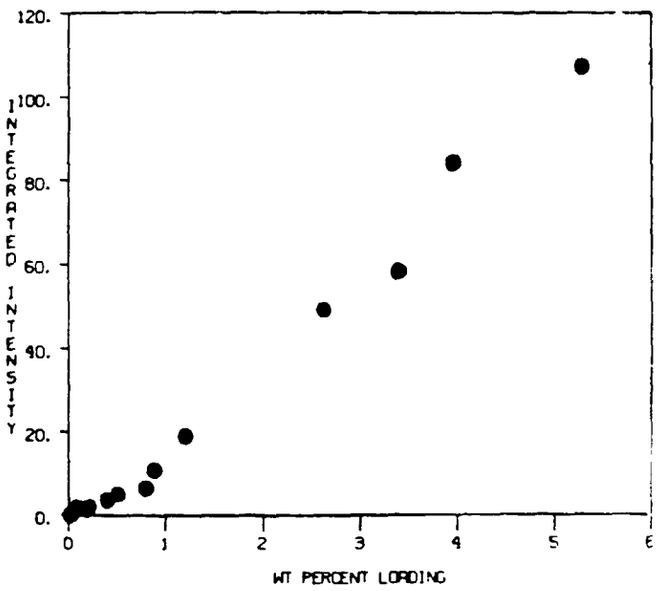

MPS/Amine Modified Particulate Glass

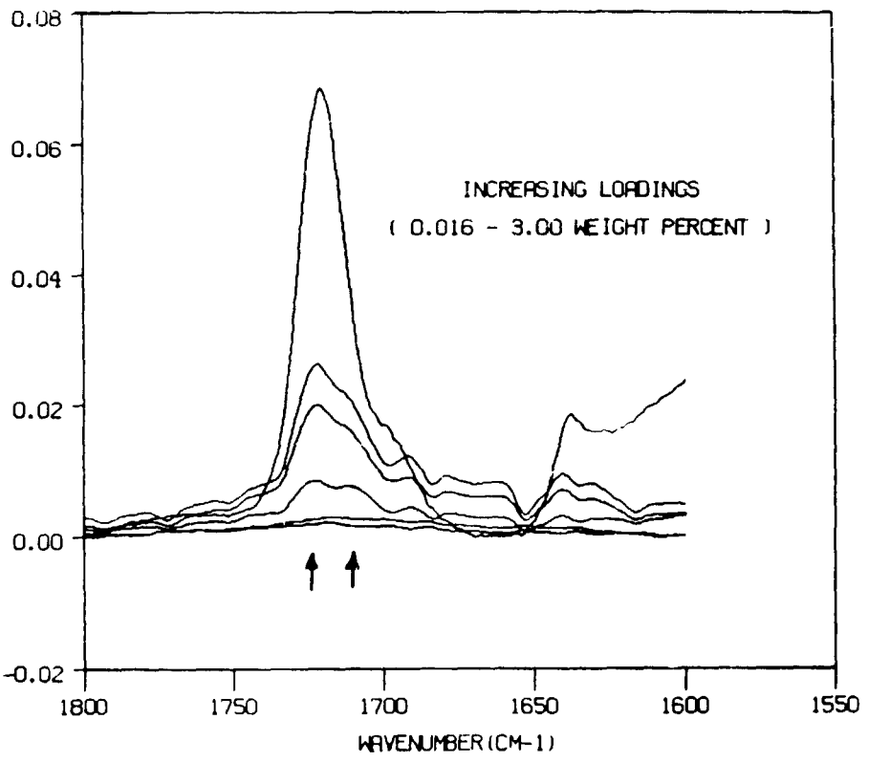

ENCAPSULATION

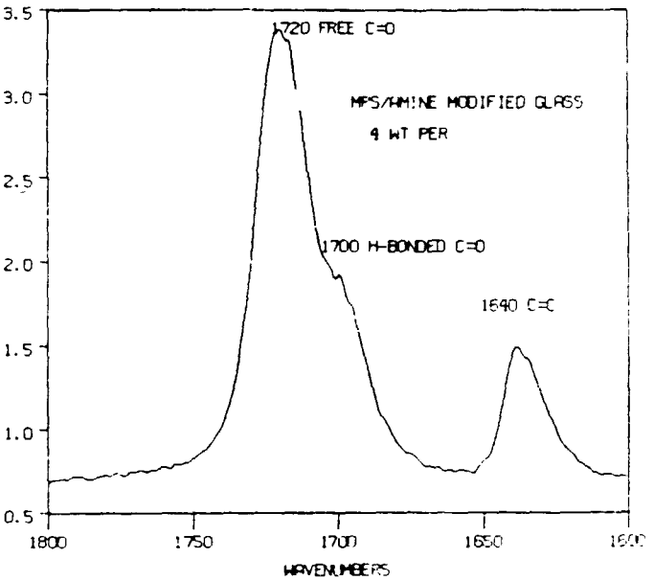

Acid Wash

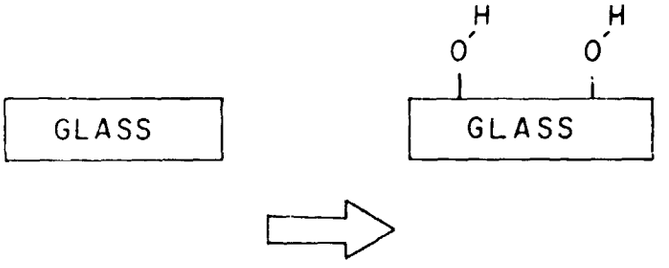

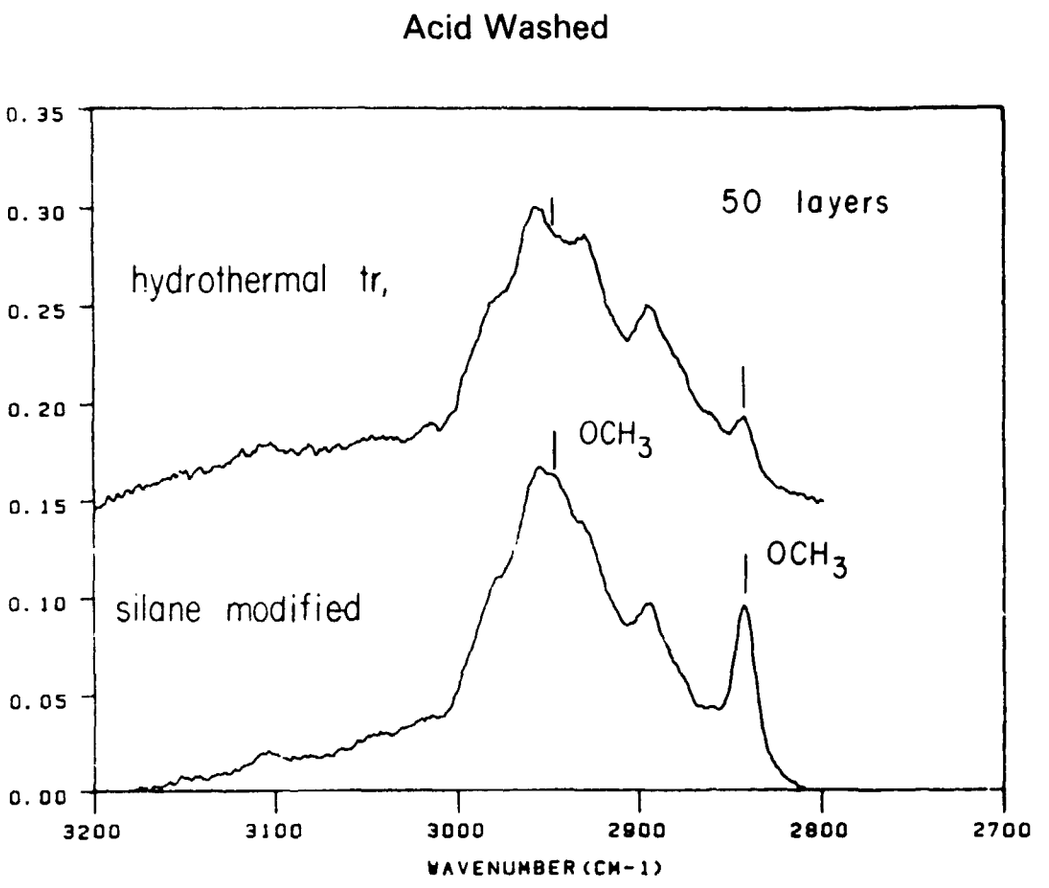
Acid Washed
0.35
0.30
0.25
0.20
0.15
0.10
0.05
0.00
50 layers
hydrothermal tr,
OCH3
OCH3
silane modified
3200
3100
3000
2900
2800
2700
WAVENUMBER (CM-1)

Base Washed

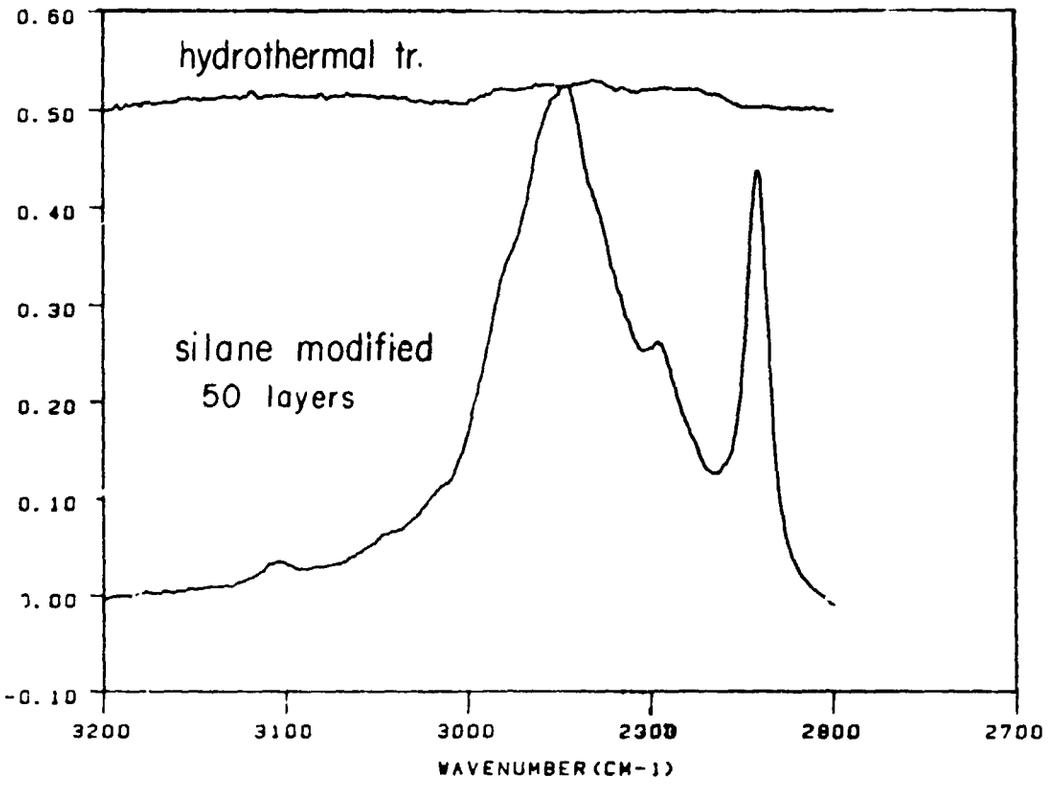
hydrothermal tr.
silane modified
50 layers
0.60
0.50
0.40
0.30
0.20
0.10
0.00
-0.10
3200
3100
3000
2900
2800
2700
WAVENUMBER (CM-1)

ENCAPSULATION

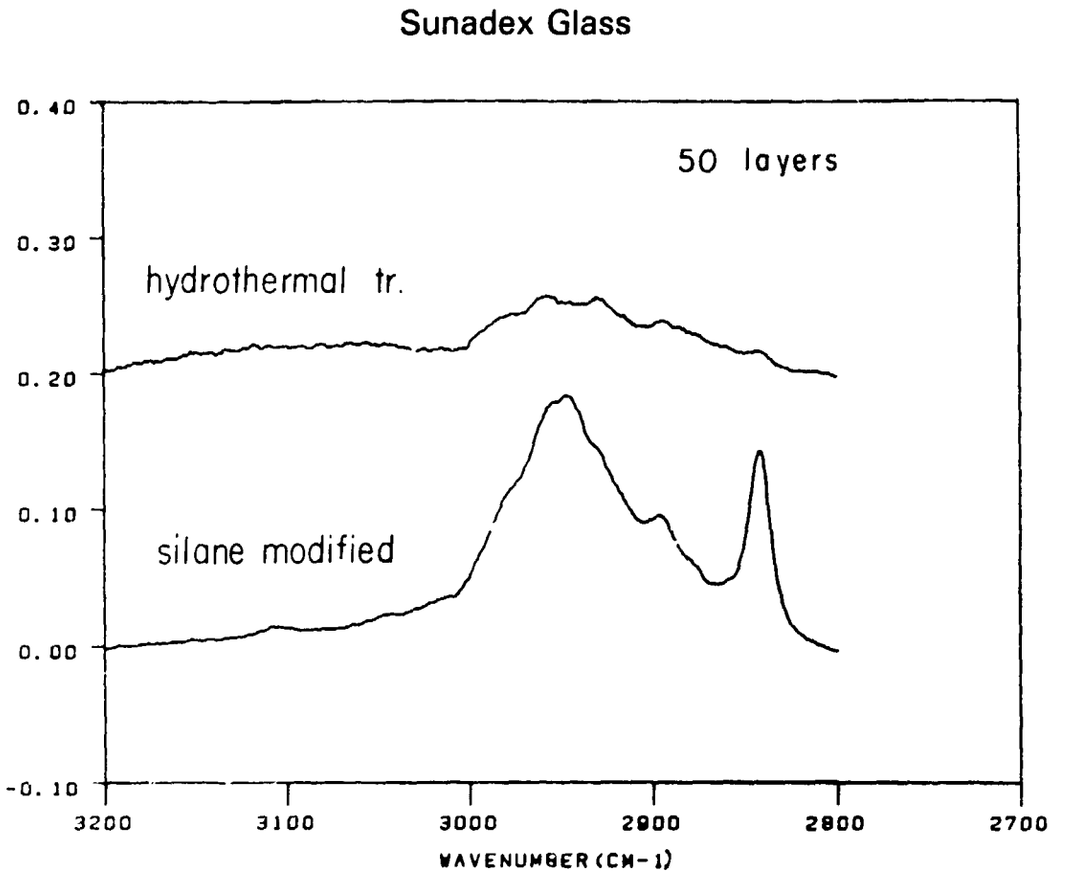

Pristine Glass (DRIFT)

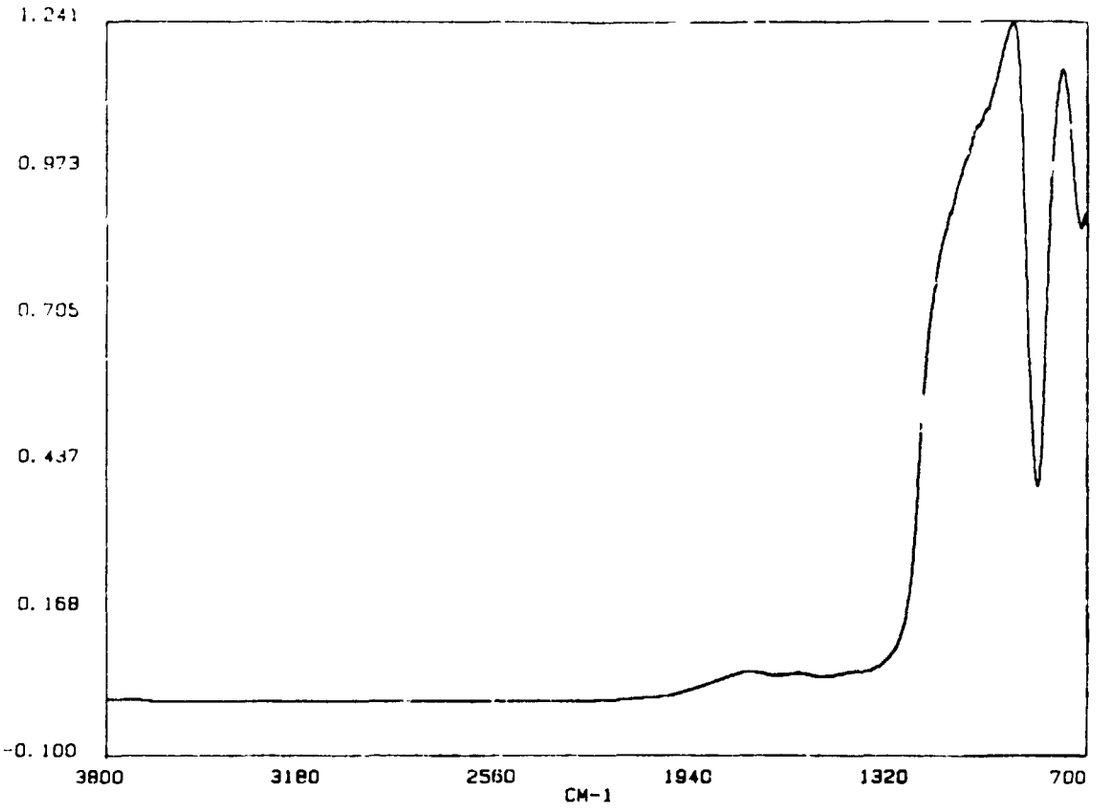

ENCAPSULATION

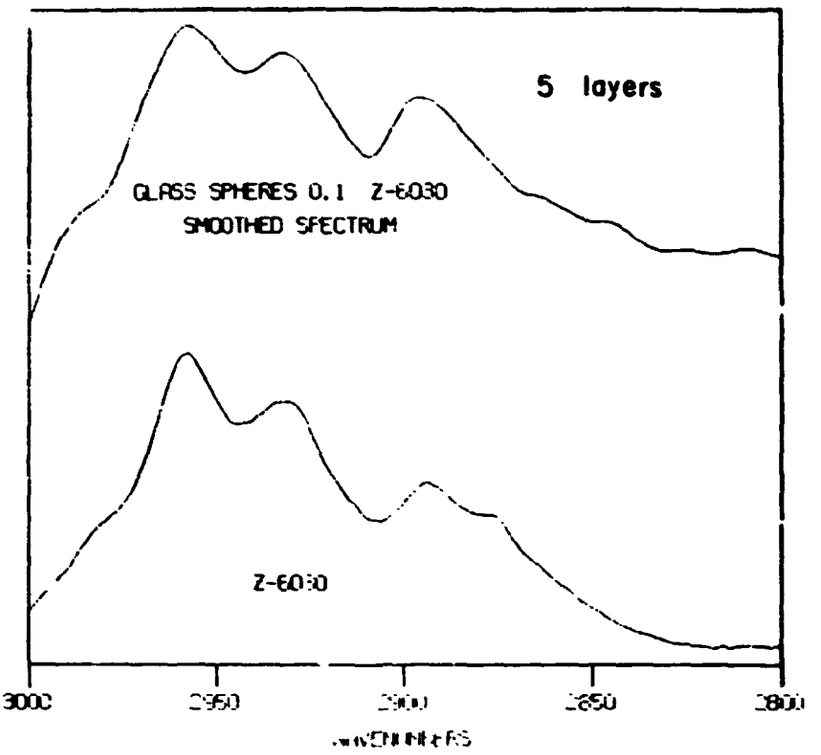

Silane Modified Glass (DRIFT)

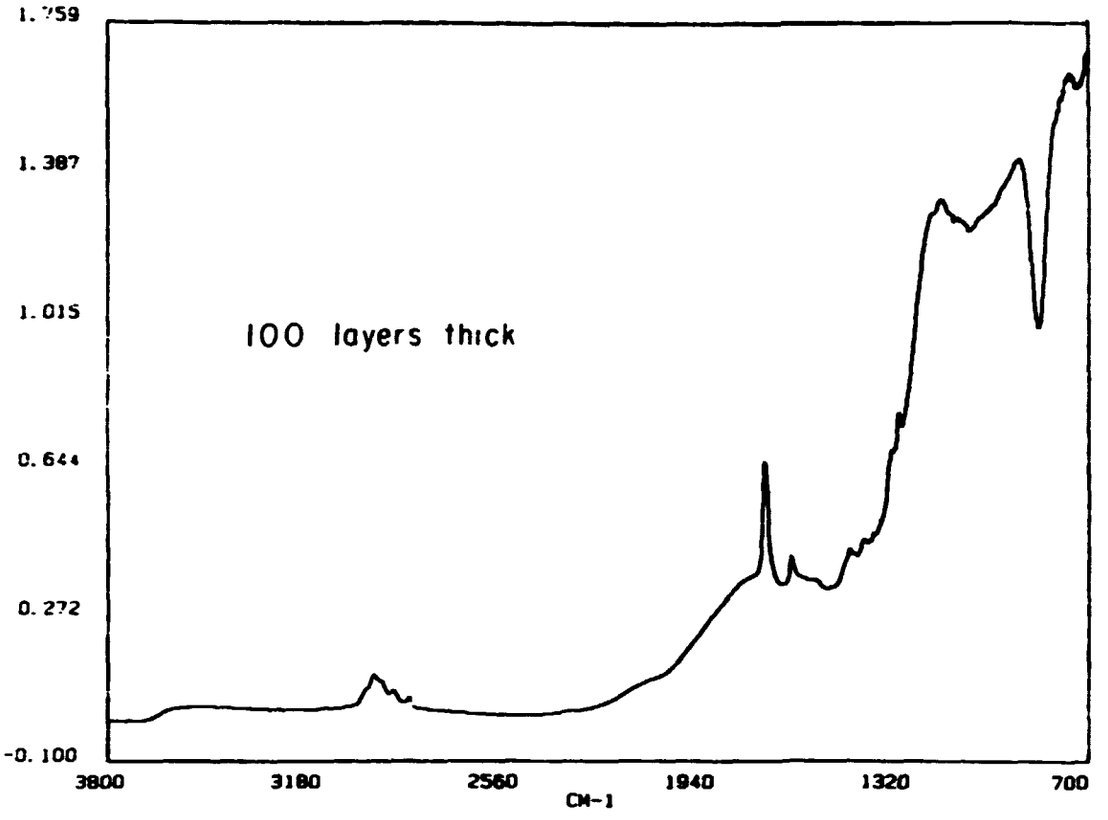

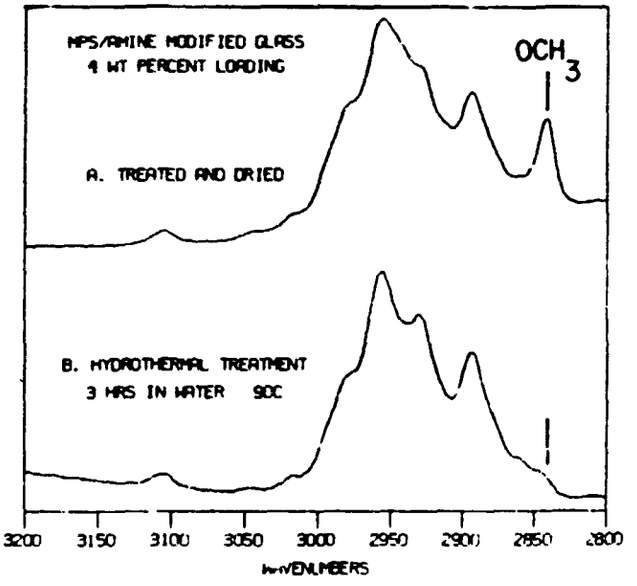

Composite Interface

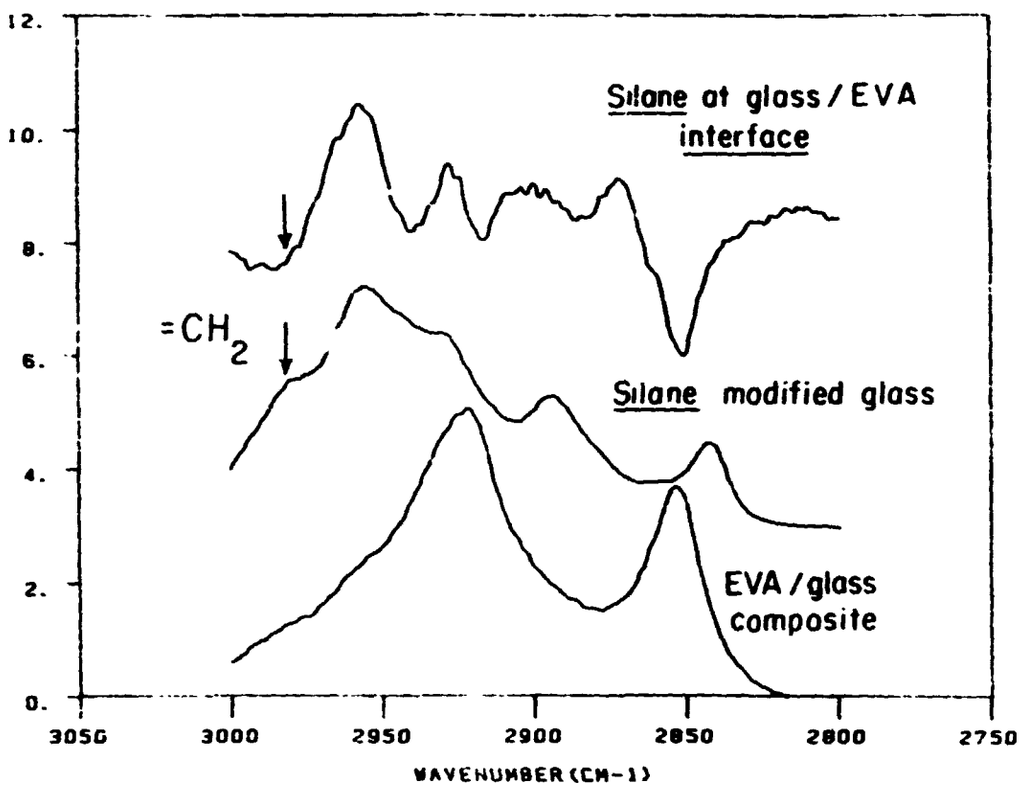

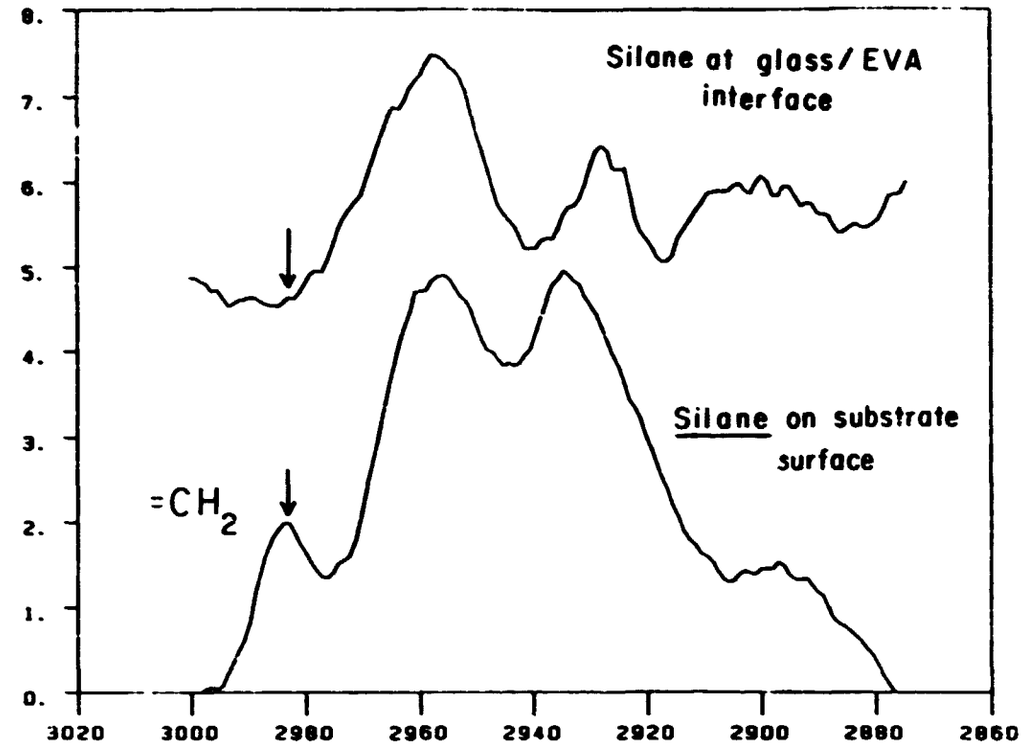
Silane at glass/EVA interface
Silane on substrate surface
=CH2
8.
7.
6.
5.
4.
3.
2.
1.
0.
3020
3000
2980
2960
2940
2920
2900
2880
2860

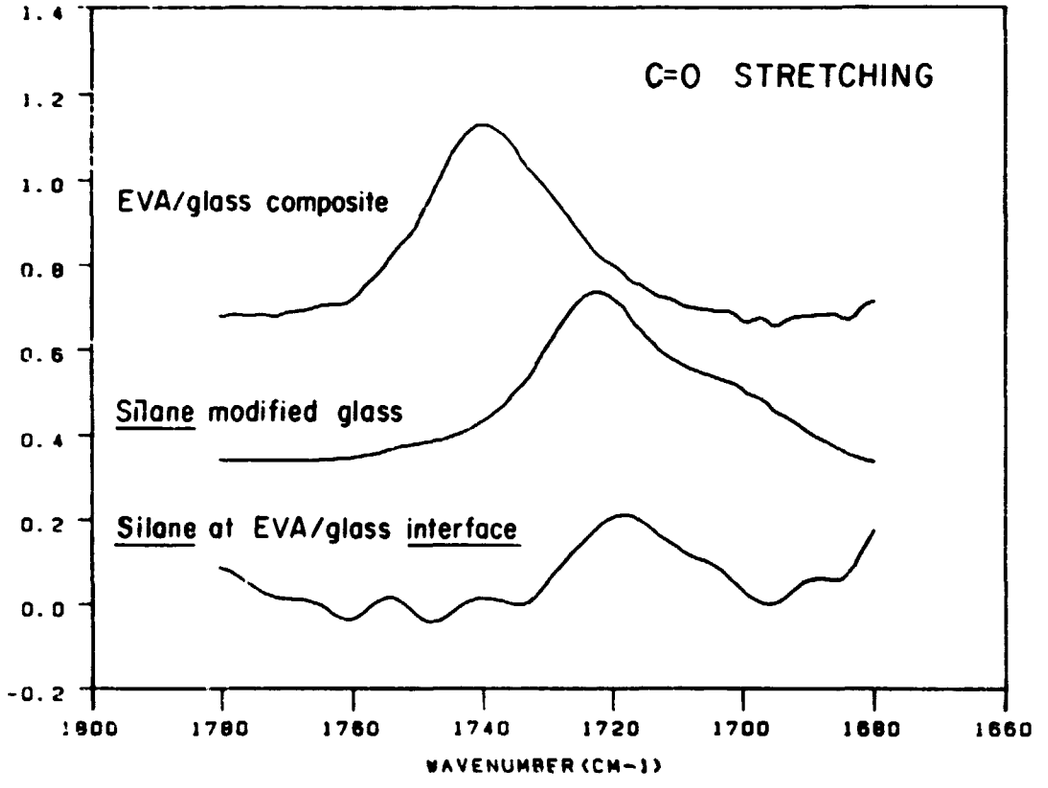
C=O STRETCHING
EVA/glass composite
Silane modified glass
Silane at EVA/glass interface
1.4
1.2
1.0
0.8
0.6
0.4
0.2
0.0
-0.2
1800
1780
1760
1740
1720
1700
1680
1660
WAVENUMBER (CM-1)

ENCAPSULATION

In-Situ Composite

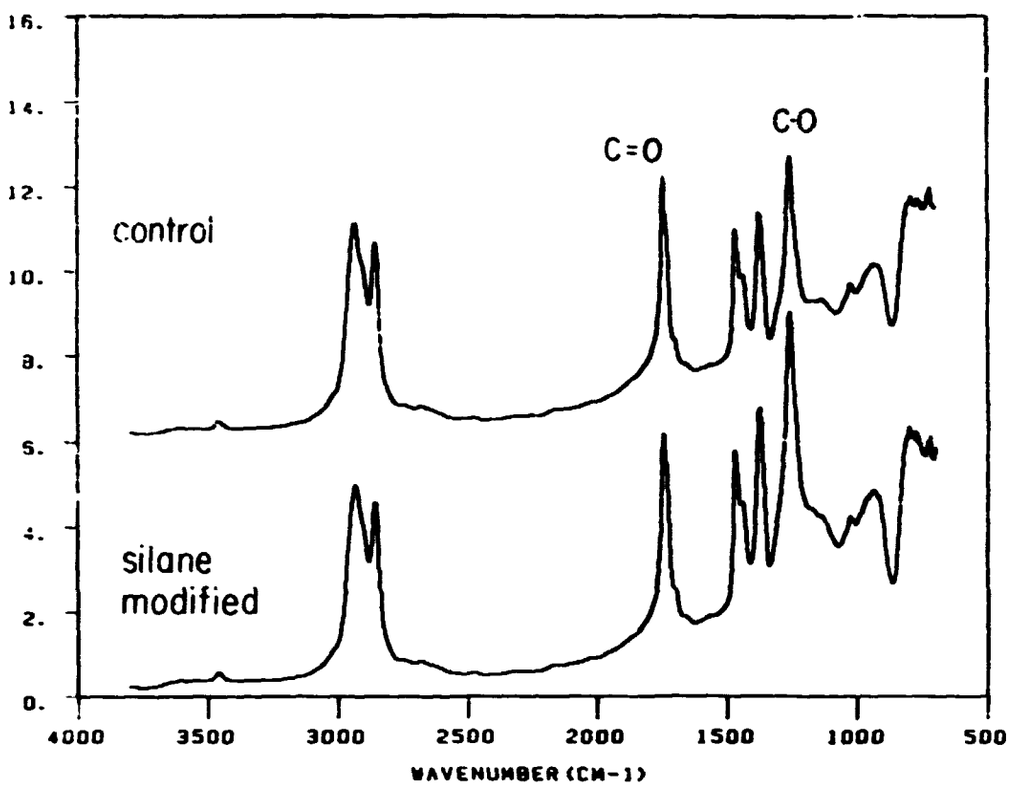

EVA-Glass Composite

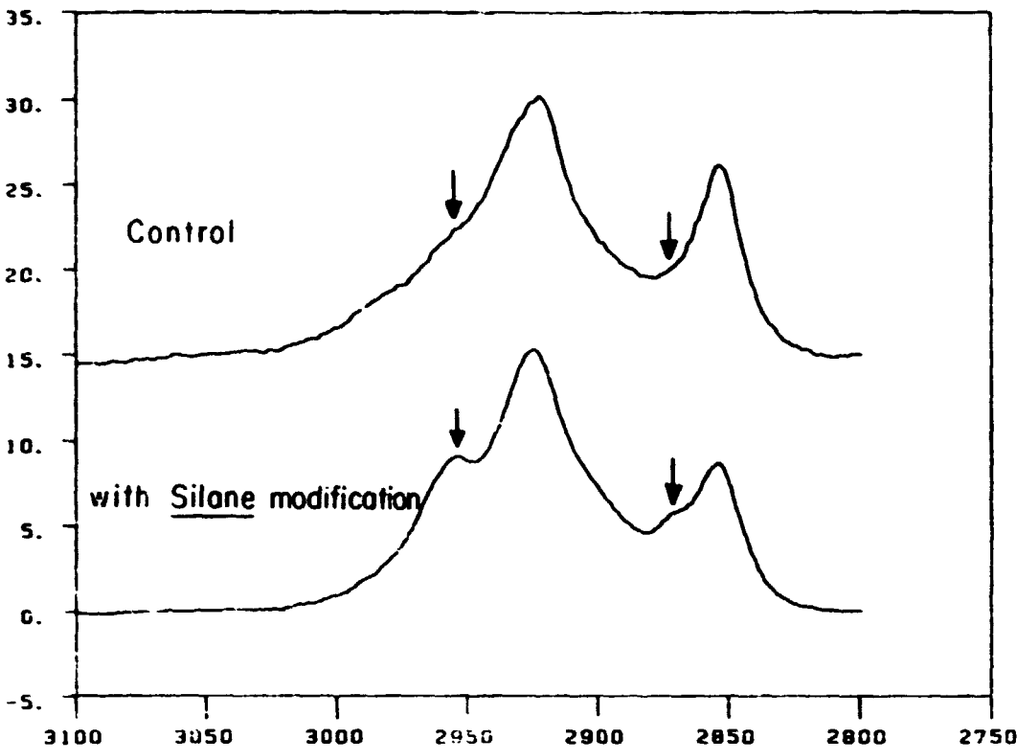

POLYMER-METAL INTERFACE BOND STABILITY

J. Boerio

Strategies

1. **Develop in-situ, non-destructive technique for determining stability of polymer/metal (oxide) interface.**

2. **Determine nature of degradation reactions occurring at polymer/metal (oxide) interface and develop methods for inhibiting those reactions.**

Ellipsometry for Determining Stability of Polymer-Metal Interfaces

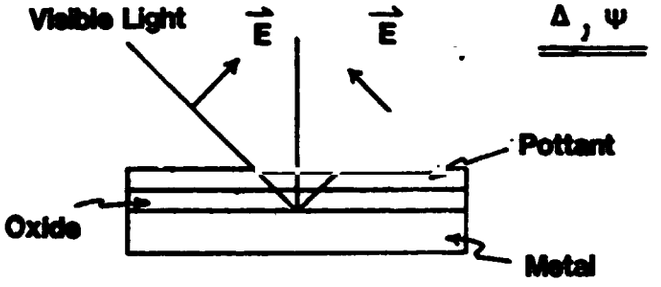

Advantages

- **non-destructive**
- **extreme sensitivity**
- **in-situ analysis**

Sample Cell for In-Situ Ellipsometry of Metals Exposed to Water

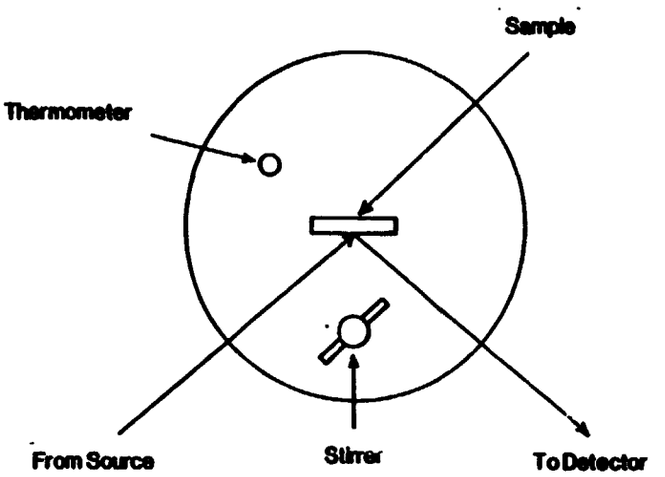

In-Situ Ellipsometry for Aluminum Undergoing Hydration in Water at 40°C

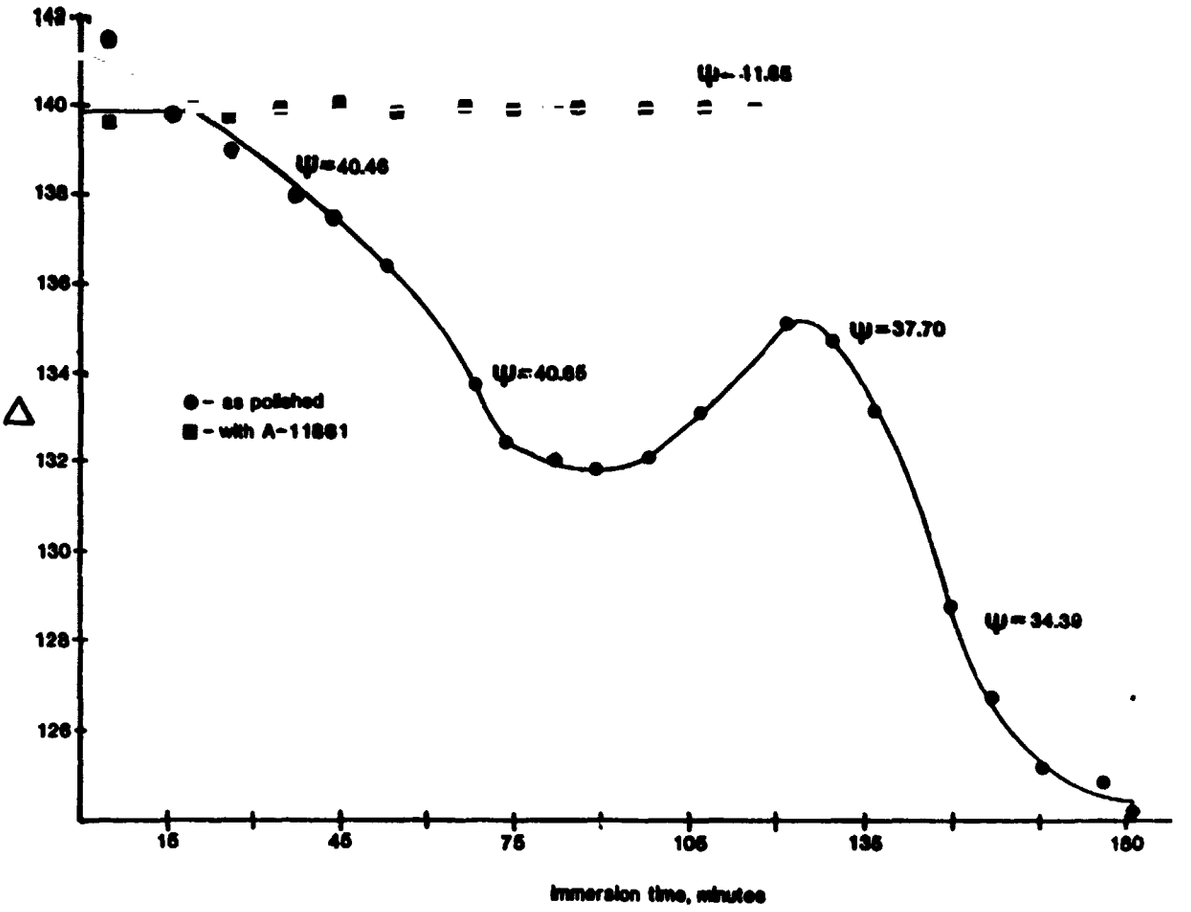

Infrared Spectroscopy for Determining Chemistry of Polymer-Metal Interfaces

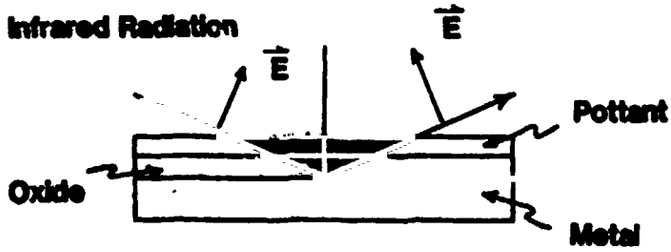

Advantages

- non-destructive
- high sensitivity
- chemical information
  - oxides
  - organics

Active Component in A-11861 Primer

γ-Methacryloxypropyltrimethoxysilane (γ-MPS)

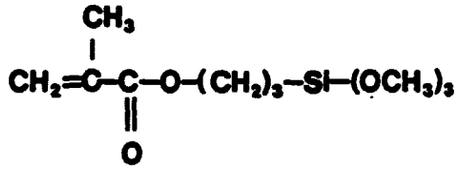

Transmittance IR Spectrum of γ-MPS Monomer

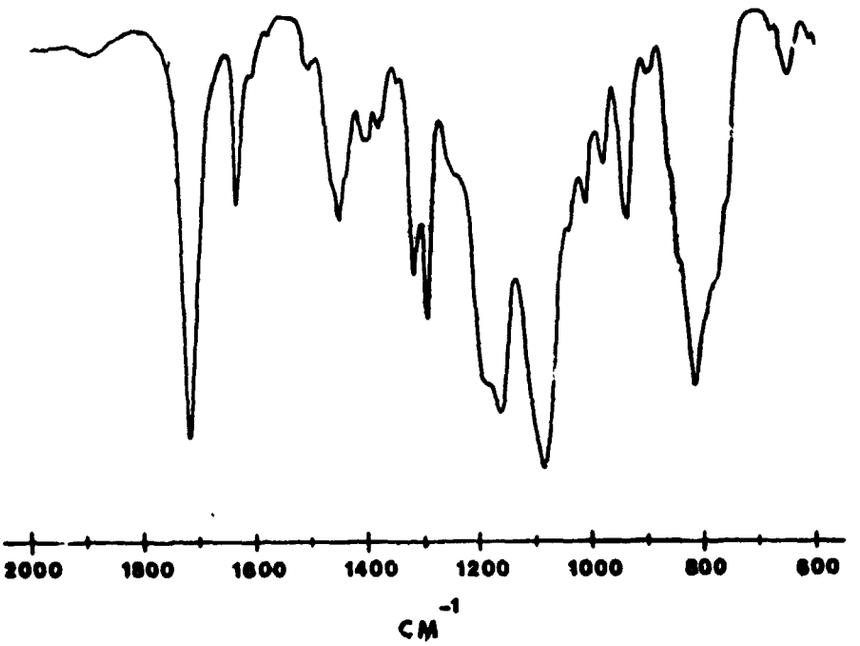

IR Spectra of γ-MPS Films With Three Different Thicknesses Deposited on Aluminum Mirrors

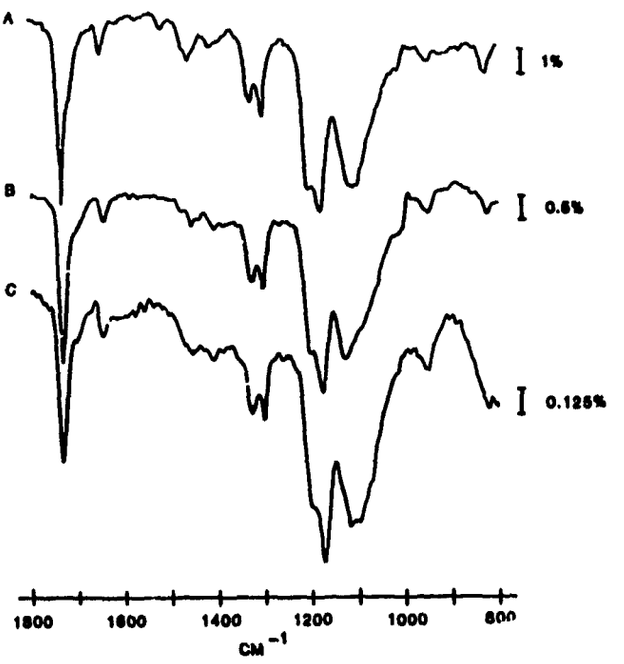

IR Spectra of (A) Thick and (B) Thin (Monolayer) Films of γ-MPS on Aluminum Mirrors

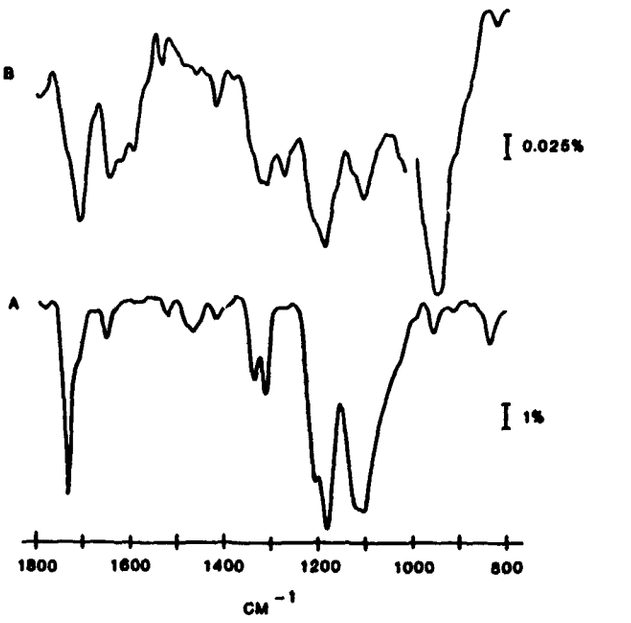

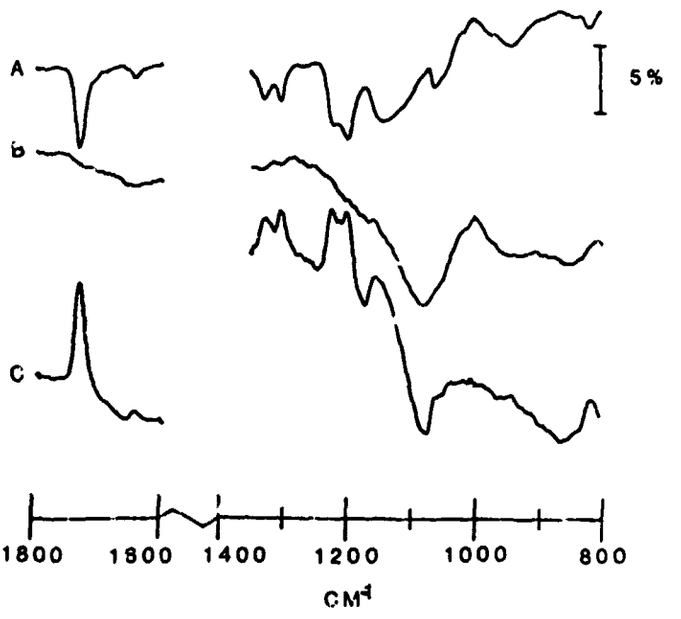

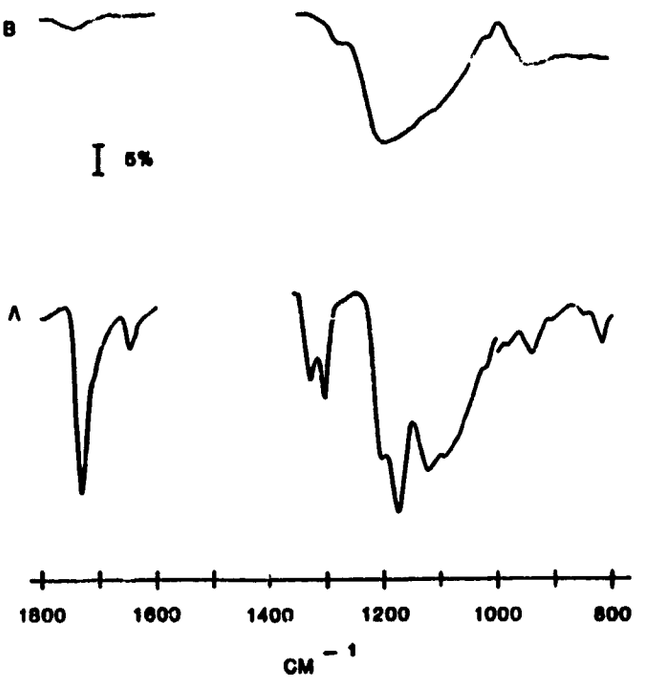

Conclusions

1. ELLIPSOMETRY IS EFFECTIVE FOR NDE OF POLYMER/METAL INTERFACES.
2. IR IS EFFECTIVE FOR CHEMISTRY OF INTERFACES.

Future Work

1. APPLY THESE TECHNIQUES TO INTERFACES BETWEEN EVA AND OTHER METALS SUCH AS Ni AND Cu.
2. MAKE RECOMMENDATIONS FOR PROPER FORMULATION AND APPLICATION OF PRIMERS FOR BONDING EVA TO METALS.

PREDICTING ELECTROCHEMICAL BREAKDOWN IN TERRESTRIAL PHOTOVOLTAIC MODULES

JET PROPULSION LABORATORY

G.R. Mon

The Problem

- **Electrochemical corrosion of PV cells can cause a cell-to-frame short circuit with two undesirable results:**
  - **Catastrophic loss of source-circuit power**
  - **High field maintenance (module replacement) costs**

The Mechanism

- **Metallization ionizes and dissolves in the encapsulant**
- **Metallization ions diffuse through the encapsulant from the electrified cell to the grounded frame**
- **Metallization products deposit on the frame as dendrites, which grow back towards the cell**
- **Breakdown (short circuit) results when a conductive path forms between cell and frame**

Electrochemical Corrosion Mechanism

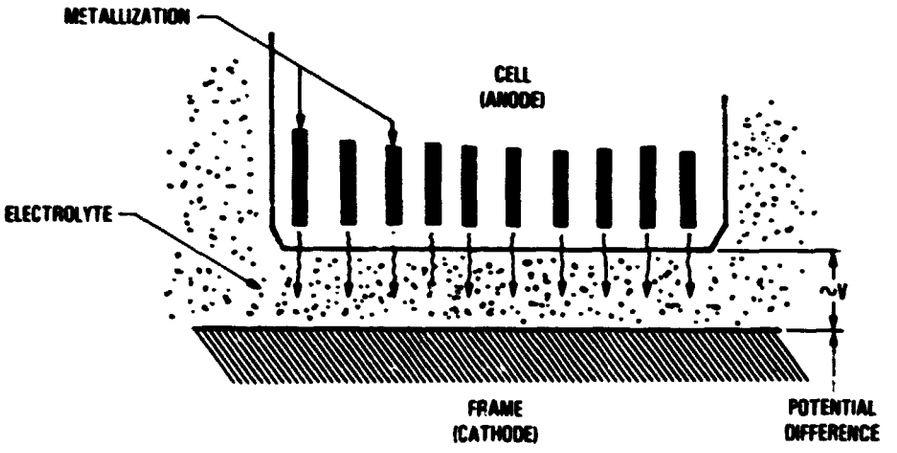

C-4

Experimental

- To determine parameter dependencies, expose encapsulated two-cell coupons to a range of voltage differences, temperatures, and relative humidities
- To assess material relative performance, test nine different metallization-encapsulation combinations

• Metallization	• Encapsulation
Silver paste	PVB
Ti-Pd-Ag	RTV
Ni-Solder	EVA

- Determine electrical conductivities of above encapsulations for a large number of temperature-humidity combinations

Test Specimen Geometry

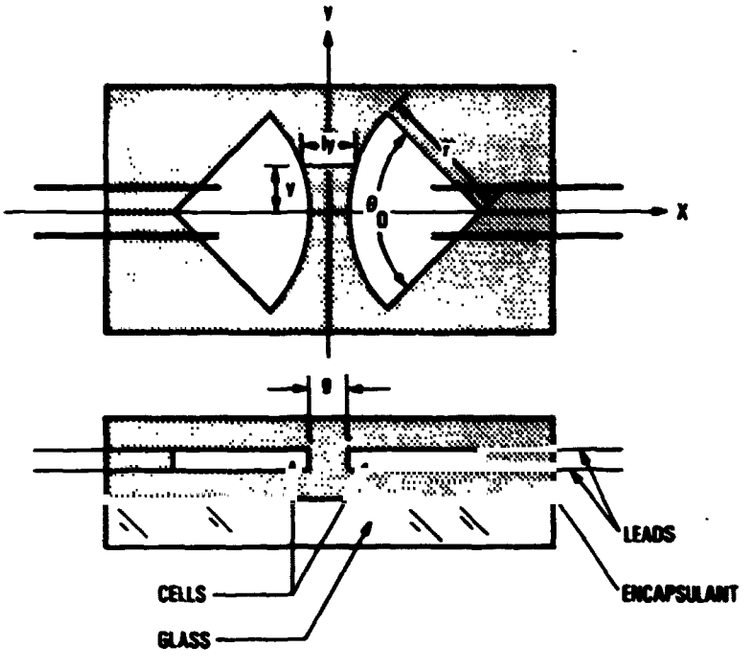

Parameter Dependencies

- **A measure of electrochemical cell corrosion is the quantity of charge transferred between cell and frame:**

$$Q = V(\sigma \cdot \tau)K \text{ (Ohm's law)}$$

K includes geometric dependencies such as cell-frame distance, size of round or square cells, etc.

- **The electrical conductivities of PVB and EVA increase with temperature and relative humidity in a known manner:**

$$\sigma = \sigma(T, RH)$$

Electrical Conductivity, PVB

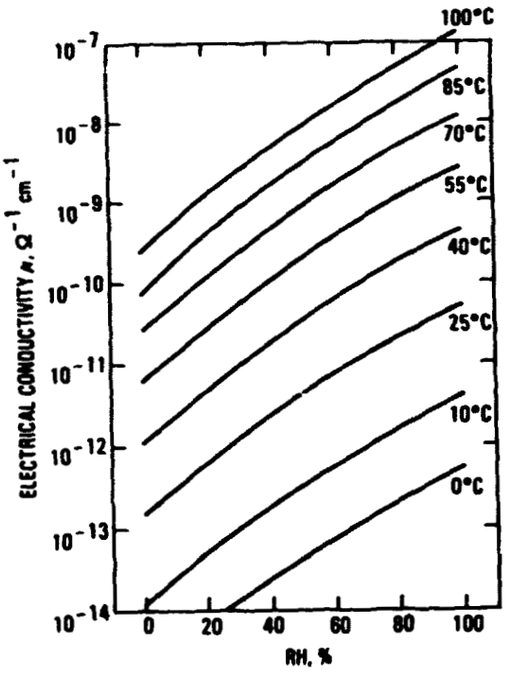

Electrical Conductivity, EVA

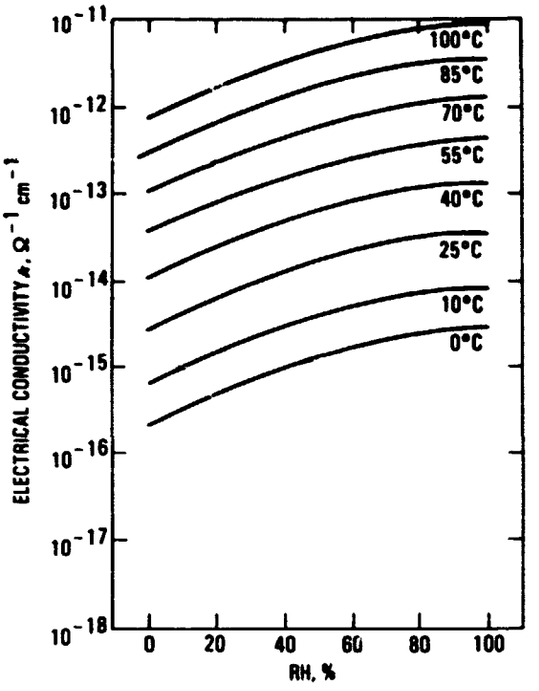

Normalized Cell Power Output vs Interfacial Charge Transferred in 1944 h of Test Exposure

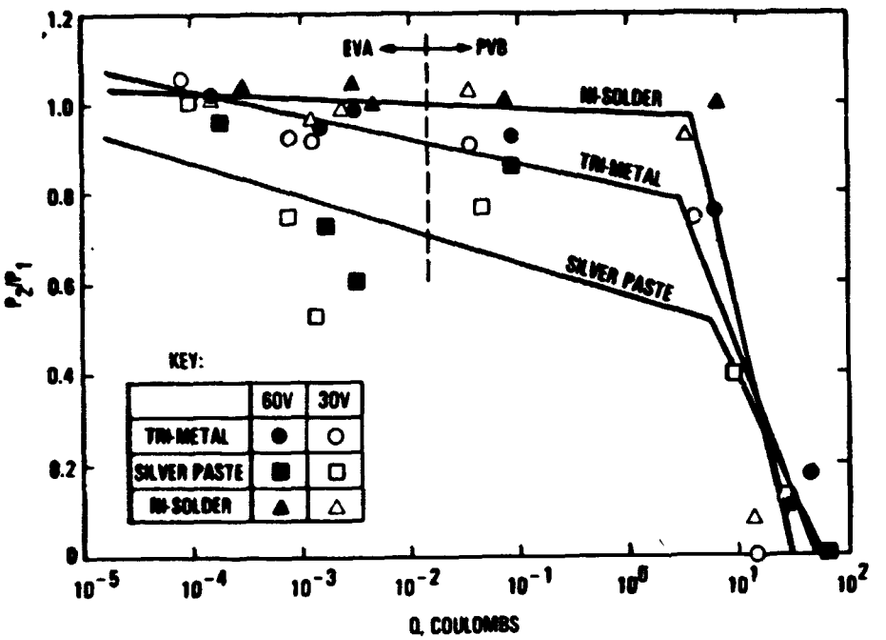

Conclusions From Experiment

- **Under conditions of the experiment, median time to cell failure occurs after the passage (between cell and frame) of about Q_T = 4 coulombs of charge per 10 cm of interface**
- **Ni-solder metallization appears to be the most stable, and silver paste seems to be the least; EVA affords the greatest protection against cell corrosion, unprotected PVB the least**
- **The electrical conductivities of PVB and EVA are known in the T-RH ranges experienced by deployed modules**

Design Algorithm

- **Life prediction**
  - **Determine median cell life for each series cell**
  - **Determine failure rates for each cell**
  - **Determine failure rates for each module**
  - **Determine the number of modules that fail each year**
- **Least life-cycle costing**
  - **Determine the break-even cost of delivered energy**
  - **Establish decision-making criteria for selecting among various cost-performance alternatives**

Life Prediction: Median Cell Life

- **For several sites around the country, SOLMET weather data give daylight hours per year that a module experiences at various T – RH combinations**
- **Use SOLMET data plus σ-data for the proposed encapsulation to generate $\Sigma\ \sigma_i\ \tau_i$; the yearly charge transferred, then, is**

$$Q_y = V(\Sigma\sigma_i \cdot \tau_i)K \text{ coulombs/year}$$

- **The median time to cell failure is**

$$\tau_M = \frac{Q_T\ (=\ 4\ \text{coulombs})}{Q_y}\ \text{years}$$

SOLMET Weather Data: Hours per Year at T_2/RH Combinations Listed (Insolation > 5 mW/cm^2)

	Cell Temp. °C	AMBIENT RH, %									
		4	15	25	35	45	55	65	75	85	95
Albuquerque	85	0	0	0	0	0	0	0	0	0	0
	75	2	0	0	0	0	0	0	0	0	0
	65	303	0	0	0	0	0	0	0	0	0
	55	579	34	0	0	0	0	0	0	0	0
	45	537	182	4	0	0	0	0	0	0	0
	35	522	217	123	33	3	0	0	0	0	0
	25	196	264	92	77	44	39	10	3	1	0
	15	20	152	150	79	32	15	15	3	2	0
	5	0	16	47	51	48	32	16	10	2	0
Boston	85	0	0	0	0	0	0	0	0	0	0
	75	0	0	0	0	0	0	0	0	0	0
	65	0	0	0	0	0	0	0	0	0	0
	55	97	101	0	0	0	0	0	0	0	0
	45	131	273	91	4	0	0	0	0	0	0
	35	104	211	164	104	60	10	0	0	0	0
	25	81	201	140	118	104	106	75	28	10	0
	15	39	91	112	86	79	80	78	92	42	1
	5	3	22	39	68	72	78	60	48	35	0
Miami	85	0	0	0	0	0	0	0		0	0
	75	0	0	0	0	0	0	0	0	0	0
	65	4	27	0	0	0	0	0	0	0	0
	55	66	663	124	0	0	0	0	0	0	0
	45	35	296	546	282	8	0	0	0	0	0
	35	11	43	158	292	372	224	81	2	0	0
	25	0	11	25	58	82	131	151	151	23	0
	15	0	0	2	5	16	10	8	8	6	0
	5	0	0	0	0	1	1	0	0	0	0

The Quantity $\Sigma \sigma_i \tau_i$ for PVB and EVA at Selected Sites

SITE	$\Sigma \sigma_i \tau_i$ (Ω^{-1} cm^{-1} . s/y)	
	PVB	EVA
ALBUQUERQUE	6.80×10^{-5}	3.16×10^{-7}
BOSTON	4.54×10^{-5}	1.84×10^{-7}
MIAMI	2.06×10^{-4}	5.98×10^{-7}

Median Time to Failure Exhibiting Dependency on Site, Encapsulation, Voltage and Cell-to-Frame Distance

		ROUND CELLS IN PVB			ROUND CELLS IN EVA		
r = 5 cm, $\theta_0 = \pi$	t = 0.114 cm	τ_M, YEARS			τ_M, YEARS		
CELL-TO-FRAME VOLTAGE, VOLTS	CELL-TO-FRAME DISTANCE, cm	ALBUQUERQUE	BOSTON	MIAMI	ALBUQUERQUE	BOSTON	MIAMI
250	0.0635	59.6	89.3	19.7	12,800	22,000	6,800
	0.254	135.1	202.5	44.6	29,100	50,000	15,400
	0.635	245.7	368.2	81.1	52,900	91,000	27,900
500	0.0635	29.8	44.7	9.8	6,400	11,000	3,400
	0.254	67.6	101.2	22.3	14,600	25,000	7,700
	0.635	122.9	184.1	40.6	26,500	45,400	14,000
1000	0.0635	14.9	22.3	4.9	3,200	5,500	1,700
	0.254	33.8	50.6	11.2	7,300	12,500	3,800
	0.635	61.4	92.0	20.3	13,200	23,000	7,000

		RECTANGULAR CELLS IN PVB			RECTANGULAR CELLS IN EVA		
a = 10 cm	t = 0.114 cm	τ_M, YEARS			τ_M, YEARS		
CELL-TO-FRAME VOLTAGE, VOLTS	CELL-TO-FRAME DISTANCE, cm	ALBUQUERQUE	BOSTON	MIAMI	ALBUQUERQUE	BOSTON	MIAMI
250	0.0635	12.7	19.0	4.2	2,700	4,700	1,400
	0.254	50.6	75.8	16.7	10,900	18,700	5,800
	0.635	126.5	189.6	41.8	27,300	46,700	14,400
500	0.0635	8.3	9.5	2.1	1,400	2,300	720
	0.254	25.3	37.9	8.4	5,500	9,300	2,900
	0.635	83.3	94.8	20.9	13,600	23,300	7,200
1000	0.0635	3.2	4.7	1.0	700	1,167	360
	0.254	12.7	18.8	4.2	2,700	4,700	1,400
	0.635	31.6	47.4	10.4	6,800	11,700	3,600

Life Prediction: Cell Failure Statistics

- **Assume log-normal failure statistics, i.e., the logarithms of the times are normally distributed**
- **The probability that a cell fails in the t^{th} year is**

$$P_{CELL}(t) = \frac{1}{\sqrt{2\pi}} \int_{\eta(t)}^{\eta(t-1)} \exp\left(-\frac{1}{2}x^2\right)dx$$

$$\eta(t) = -\frac{1}{\sigma} \ell n \left(\frac{t}{\tau_M}\right)$$

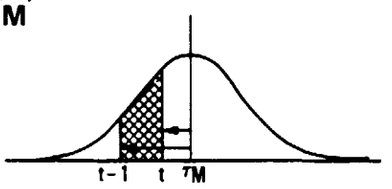

- **σ = 1.3 is assumed based upon values determined by other investigators of similar problems**

Life Prediction: Module Failure Statistics

- Assumptions
  - Only module edge cells, r in number, fail electrochemically
  - All cells of a particular module experience the same module operating voltage: the mean of the module terminal voltages
- The probability that a module fails in year t, conditional upon its not having failed before year t, is

$$q_t = 1 - [1 - P_{CELL}(t)]^r + 4$$

- The actual module failure rate — the probability that a module fails in year t — is

$$Q_t = \left[1 - \sum_{i=1}^{t-1} Q_i\right] \cdot q_t \qquad t > 1$$

$$Q_1 = q_1$$

- For an N-module series source circuit, the yearly average module failure probability is

$$\bar{Q}_t = \frac{1}{N} \sum_{K=1}^{N} Q_t^K$$

Yearly Average Module Failure Rate vs Years of Operation

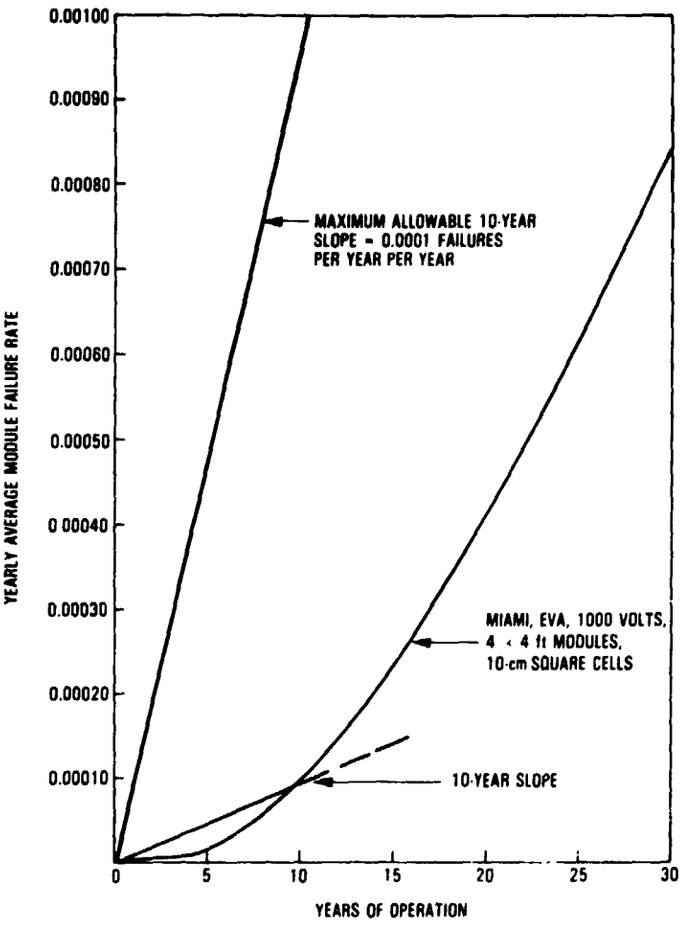

Conclusion

- **Module electrochemical breakdown rates are predictable!**

MODULE FLAMMABILITY RESEARCH

JET PROPULSION LABORATORY

R.S. Sugimura
D.H. Otth

ARCO SOLAR, INC.

J. Arnett
K. Lewis

Introduction

- **Objective:** **Develop the technology base required to construct fire-ratable modules**
- **Approach:** **Explore new materials of construction and module configurations to achieve increased fire resistance**
  - **Phase I:** **Assess fire-resistance capability of current PV module designs**
  - **Phase II:** **Perform parametric tests to characterize flammability**
  - **Phase III:** **Hypothesize and test improved construction techniques that lead to increased fire resistance**

Background

- **Tests for Fire Resistance of Roof Covering Materials, UL-790**
  - **Spread-of-flame test—distance that flame has spread. No flaming or glowing brands of roof material**
  - **Burning-brand test—until flame, glow and smoke disappear. No sustained flaming on underside, production of flaming or glowing brands of roof material**

	Spread-of-Flame		Burning Brand
	Time	Distance	Size
Class A	10 min	6 ft	12 x 12 x 2 1/4 in.
Class B	10 min	8 ft	6 x 6 x 2 1/4 in.
Class C	4 min	13 ft	1 1/2 x 1 1/2 x 25/32 in.

Chronology

Exploratory testing (June, 1980; August, 1981)

- **Glass/silicone/CRES pan** **(Blk III)**
- **Sylgard/FRP back** **(Blk III)**
- **Glass/silicone/Pan-L-Board** **(Blk IV)**
- **Glass/EVA/T** **(Blk IV)**
- **Findings**
  - **Silicone modules are inherently fire resistant**
  - **EVA modules are highly flammable, may not be fire ratable**

Manufacturers' testing (1983)

Parametric testing (January, 1984)

- **27 burning-brand tests**
- **9 different manufacturers**
- **3 different encapsulants/8 different back surfaces**

Parametric testing: findings

- Difficult to maintain module integrity
  - Glass shatters due to thermal stress
  - Penetration of back-surface material is disastrous
- Hydrocarbon encapsulants are highly flammable
- Heating from brand is highly localized

Joint ARCO/JPL test program (February, 1984)

- Fabricate and test experimental modules
  - High-temperature back-surface materials
  - Improved module construction techniques

ARCO-JPL Flame Retardant Test Program

Material Description	Cost ($/ft^2)	Configuration	Adhesive	Result
Unfilled Kapton (2 mils)	1.85	Add-on	TS	F
		↓	PS	P
	↓	Substitute	–	P
Fiberglass – fine-woven (stabilized)	0.85	Add-on	TS	P
–	↓	↓	PS	F
–	↓	Substitute	–	F
– (unstabilized)	< 0.20	Add-on	PS	F
– coarse-woven (unstabilized)	↓	↓	TS	F*
Neoprene Rubber (mineral-filled) –				
Latex (≈8 mils)	≈ 0.25		–	F
Sheet (93 mils)	≈ 1.50		TS	P
Stainless-Steel Foil (2 mils)	0.45	↓	TS	P
↓ ↓ ↓ ↓	↓		PS	AP*
Aluminum Foil (3 mils) in 4-layer laminate	0.06	Substitute	–	P
↓ ↓ ↓ ↓ ↓ ↓	↓	↓	–	AF

Summary

- Temperature measurements indicate that materials with high thermal stability are required to maintain back-surface integrity
- Available high-temperature materials are potentially effective in this application

Future Work

- Complete burning-brand effort
  - Analyze data
  - Nominate candidate materials
  - Identify cost tradeoffs
- Start spread-of-flame research

PROCESS DEVELOPMENT AND ADVANCED PROCESSES

M.H. Leipold and D.B. Bickler, Chairmen

Presentations on 11 on-going process developments were made during the technology session. Areas being investigated are metallization, junction formation, thick- and thin-film deposition and hydrogen passivation.

Westinghouse Electric Corp. Advanced Energy Systems Division reported on simultaneous junction formation using liquid dopants. A p+nn+ cell was fabricated using n-type dendritic web. Cross-doping of phosphorus into the front junction was a major problem. Earlier formation of a harder glass will be one approach to a solution. Desired diffusion profiles were obtained during simultaneous firing. Efficiencies up to 12% were found when simultaneously fired cells were measured.

The amount of LBIC (laser-beam induced-current)-imaged grain-boundary activity has little or no effect on space-charge recombination or fill factor, according to Solarex Corp. Continuing work on large-grain polycrystalline silicon (Semix and Wacker) has also shown that there is a strong correlation between quasi-neutral recombination and electrically active grain and subgrain boundaries. Additional findings were: V_{OC} of polycrystalline cells is 20 to 60 mV lower than that of single-crystal cells; large data scatter correlates with inclusions; most V_{OC} scatter is accounted for by J_{QNO} variation. Another contractual effort, hydrogen passivation of polycrystalline cells, was just starting.

Caltech diffusion barrier studies continue to produce results and have attracted interest from industry and other R&D laboratories. Certain amorphous metallic layers can be very stable at high temperatures. Areas of concern in selecting amorphous metallic layer constituents are crystallization, reaction with underlying silicon or reaction with overlying metal. Rules for selecting amorphous film constituents are: Use a transition metal plus a metalloid; use two transition metals with low solubility and that have a deep eutectic; use two transition metals of different crystallographic structure. Films are formed by ensuring a random atomic arrangement and using low-temperature deposition with high heat dissipation. Potential solutions to reactivity of amorphous metallic films are: Use an intermediate layer; use early transition metals with high reaction temperatures with silicon; nitrogen containing alloys show promise; ternary alloys show promise.

The MOD (metallo-organic decomposition) work at Purdue University continues to provide interesting results. Many organic compounds and rheology adjusters can be used to form the MOD inks. Experimental work has shown the need for fairly high-purity organic precursors so that all organics break down at essentially the same temperature. Ink requirements for screen printing are: have very low vapor pressure; have viscosity in the range of 100-500 Pa at low shear rate; be pseudoplastic and thixotropic. Available solvents are also being studied for compatibility and boiling point. Three different baseline processes with silver neodecanoate are being pursued: solution with xylene and solvent exchange, solution with toluene and solvent exchange, and

solid compound plus additive. Different furnaces and air flows are also being investigated. Important parameters are: purity of ingredients, heating rate between 70°C and 225°C, and air flow. Although the mechanism of adhesion is not fully understood, dense films with good adhesion and conductivity have been produced.

Spectrolab Division of Hughes Aircraft Co. has continued research into the non-noble front metallization system of molybdenum-tin-titanium hydride. Some interim conclusions are: molybdenum-tin combination has adequate conductivity; shunting is never a problem; solderability is a major problem; more work is needed on wetting phenomena; a cellulosic vehicle is best. A new analytical technique is being used to obtain real-time and videotaped visual SEM data that can be used to examine ink behavior during firing. More control of research findings has been gained by using fully described inks from Electrink, Inc., instead of proprietary formulations from vendors.

Electrink, Inc., has been examining viscosity measurements as a means of process control of thick-film printing. Generally, viscosity measurements are convenient to make and can be reproducible. The measurements do relate to production application and are a means of correlating composition and condition of the ink. Three different viscosity conditions can be found: Newtonian (viscosity is constant with varying shear rates); plastic (viscosity decreases with increasing shear rate); dilatent (viscosity increases with increasing shear rate). Thixotropic materials have an additional constant to define liquid structure restoration rate for disrupted states. Good reproducibility of viscosity measurements for thixotropic materials requires scheduled measurements and close temperature control. Constants relating to material rheology may be calculated from three or more measurements at different shear rates with an iterative computer program.

Ion implantation of non-Cz silicon sheet materials was studied by Spire Corp. Materials examined were: Wacker Silso; Solarex Semix; Crystal Systems, Inc. HEM; Mobil Solar EFG, and Cz controls. The ion-implantation process was held constant; annealing processes tried were one-step thermal, two-step thermal, three-step thermal and pulsed electron beam annealing (PEBA). Analysis of the one-step anneal at 850°C shows EFG improved; Semix relatively unchanged and HEM, Cz and Silso somewhat degraded. Analysis of the two-step anneal at 850°C shows EFG much improved; Semix, Cz and HEM relatively unchanged and Silso slightly degraded. Conclusions are: use of ion implantation allows tailoring of thermal annealing process to a specific material; ion implantation and rapid thermal annealing can be used successfully for junction formation.

Laser-assisted solar-cell metallization processes are being developed by the R&D Division of Westinghouse Electric Corp. Potential advantages of laser deposition techniques are high resolution, no photolithography, clean and contamination-free, in-situ sintering, and low contact resistance. Three processes are being investigated: pyrolytic deposition (thermal decomposition of liquid or gas phase), photolytic deposition (photodissociation of vapors and solutions), and laser-assisted electroplating. Results of laser pyrolysis were encouraging; lines of silver were formed by decomposition of a spun-on silver neodecanoate film provided by Purdue University. Adhesion is still a possible problem in this process. Laser-assisted gas-phase photolysis equipment is ready to use for titanium and tin depositions. Early results of

laser-enhanced electroplating of copper have been exciting. A 25-micrometer-wide line has been achieved with a 12 micrometer/second local plating rate.

Ion cluster beam (ICB) deposition research is being pursued at JPL. The intent of the research is verification of Japanese work; investigation of PV applications other than metallization (such as dielectric and semiconductor deposition), and characterization of ICB as a function of source parameters. A number of changes have been made in the ionizer chamber to achieve more reliable operation. A crucible nozzle is being considered for better collimation of the beam. Other changes being investigated are cluster detector, substrate heater, and operation of ionizer at higher temperatures.

Another JPL research effort is a program for SERI. The parameters governing large-area deposition of amorphous silicon are being established. Tests have been run on plasma stability while voltage, pressure and electrode spacing are varied. Deposition uniformity is also being studied with regard to corner effects, electrode spacing, silane feed rate and velocity, and substrate influence (aluminum, silicon or glass).

New contracts to explore the technology of advanced processes have been let for two excimer laser energy sources and one microwave source. The ability to apply energy selectively to achieve process improvements has already been seen in other research efforts. An additional benefit is the ability to get a detailed assessment of a new technology and thereby validate claims of large processing improvements or cost reductions.

N85 15275 D15

PROCESS RESEARCH OF NON-Cz SILICON MATERIAL

WESTINGHOUSE ADVANCED ENERGY SYSTEM DIVISION

C.M. Rose

R.B. Campbell

Contract Information

Objective:	Investigate High-Risk; High-Payoff Improvements to (W) Baseline Process Sequence
Time Period:	November, 1983 — March, 1984
Funding:	JPL Funds Used for Engineering Effort Only; Technician and Material Costs Borne By (W)

Contract Tasks

- Evaluate Feasibility of Simultaneously Forming Back & Front Junctions of Solar Cells Using Liquid Dopants on Dendritic Web Silicon
- Compare Simultaneous Diffusion to Sequential Diffusion
- Test of Belt Furnace for Diffusion Process
- Develop Process Control Parameters and Sensitivities
- Perform Cost Analyses

Approach

- N-Type Dendritic Web Silicon
- Liquid Phosphorous Dopant for Back N^+N Junction
- Liquid Boron Dopant for Front P^+N Junction
- Investigate Several Resistivities of Web (0.5 Ω-CM to 5.0 Ω-CM)
- Investigate Various Suppliers Dopants and Masks

Potential Benefits

- Fewer Processing Steps
- Less Opportunity for Contamination During Processing
- Less Costly Process

HOWEVER

- Process Requires N-Type Dendritic Web Due to Diffusion Constants of Dopants in Silicon

Junction Formation Process Steps

PROCESS	BASELINE PROCESS	LIQUID BORON ONLY	LIQUID BORON + LIQUID MASK	LIQUID BORON + LIQUID PHOSPHOROUS	LIQUID BORON + LIQUID PHOSPHOROUS + LIQUID MASK	SIMULTANEOUS DRIVE OF BORON AND PHOSPHOROUS
CVD SiO_2 N+ SIDE	•	•		•		
HF ETCH	•	•		•		
APPLY LIQUID BORON AND BAKE		•	•	•	•	•
APPLY LIQUID MASK AND BAKE			•		•	
PRE-DIFFUSION CLEAN	•					
DIFFUSE P+	•	•	•	•	•	
OXIDE ETCH	•	•	•	•	•	
APPLY LIQUID PHOSPHOROUS AND BAKE				•	•	•
CVD SiO_2 P+ SIDE	•	•		•		
APPLY LIQUID MASK AND BAKE			•		•	
HF ETCH	•	•				
PRE-DIFFUSION CLEAN	•	•	•			
DIFFUSE N+	•	•	•	•	•	
DRIVE BORON AND PHOSPHOROUS						•
OXIDE ETCH	•	•	•	•	•	•

Initial Results

- Diffusion Time — Temperature — Ambient Gas Determined for Desired Sheet Resistivity and Junction Depth

  Temp = 950° C ± 20° C
  Time = 20 Min ± 5 Min
  Gas Ambient = N_2 for Most Dopants

Simultaneous Diffusion

- Junction Depths of P^+N and N^+N Satisfactory
  - X_j (P^+N) — 0.2 - 0.4 μM
  - X_j (N^+N) — 0.4 - 0.6 μM
- Maximum Efficiency — 12%
- *Cross-Doping of Phosphorous into Sun Side of Cell Confirmed by:*
  - Sheet Resistivity Measurements
  - Spreading Resistivity Measurements

n^+n Back Junction by Simultaneous Diffusion
(49125-21A) X_j = 0.8μm

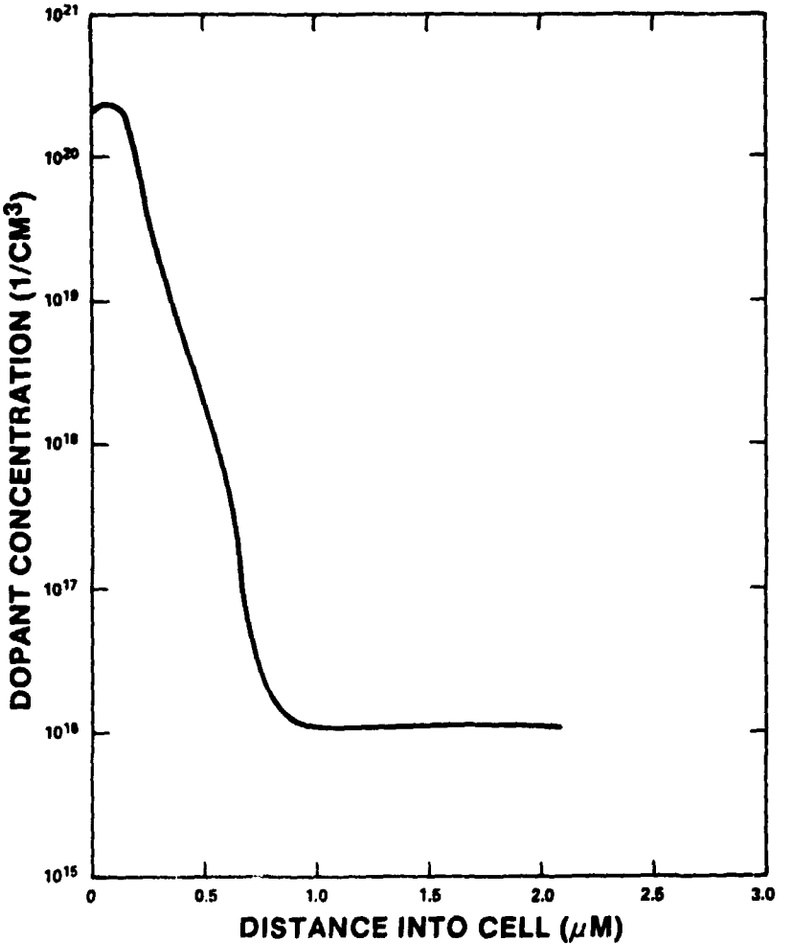

p^+n Front Junction by Simultaneous Diffusion (49125-21A) $X_j = 0.2\mu m$

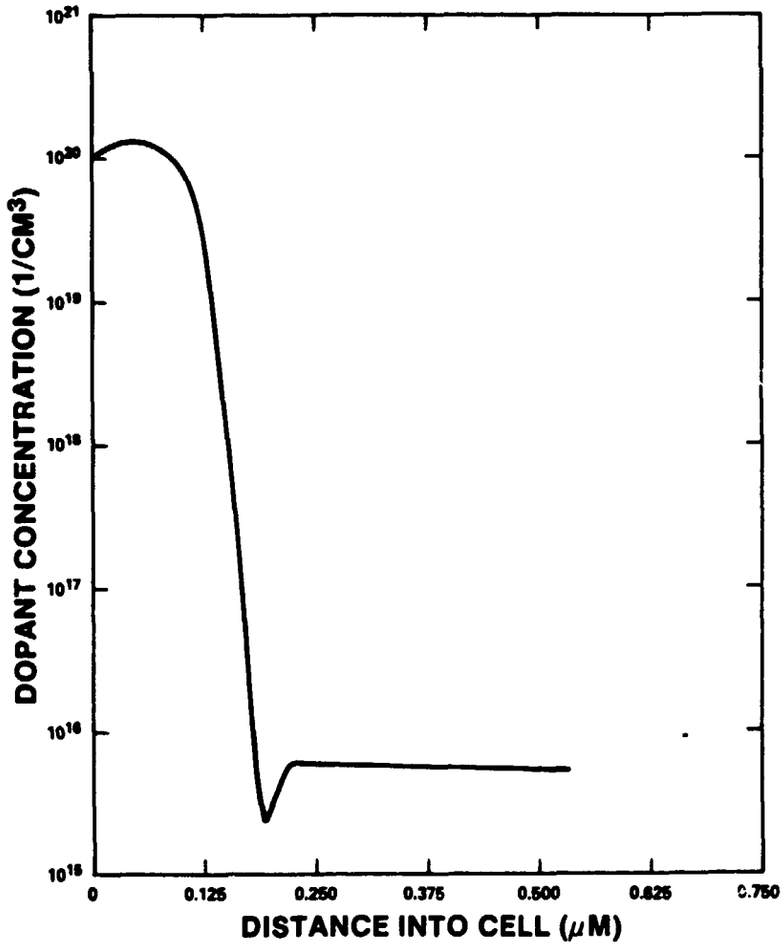

Belt Furnace Test

- Initial Test at Radiant Technology Corp.
- Proper Temperature Obtained
- Proper Junction Depths Obtained
- Cells Showed Effect of Cross Doping

Solutions to Cross Doping

- Form Impermeable – Harder Glass from Diffusant Source
- Use of SiO_2 Masks as Diffusion Barriers

Sequential Diffusion

- Process Sequence for N-Type Web Adapted from P-Type Web Sequence
- Back Phosphorous Doped Junction Diffused First
  $X_j \approx 0.4 - 0.8\ \mu M$
- Front Boron Doped Junction Diffused Second
  $X_j \approx 0.2 - 0.3\ \mu M$
- Cell Efficiency Range 12.0 - 14.5% (20 CM^2 Cell)
- Average Cell Efficiency $>$ 13%

Process Control Parameters and Sensitivities

- Three Resistivities of Silicon Web Being Tested (0.5 Ω-CM; 1.0 Ω-CM; 5 Ω-CM)
- Other Process Sensitivities will be Studied When Cross Doping Solved

Conclusions

- Sequential Diffusion of N-Type Web Yields Cells with Average Efficiency $>$ 13%
- Cells Up to 12% Obtained with Simultaneous Doping of N-Type Web
- Diffusion Masking will be Required to Prevent Cross Doping

N85 15276

PROCESS RESEARCH ON POLYCRYSTALLINE SILICON MATERIAL (PROPSM)

SOLAREX CORP.

Jerry Culik

PROPSM Programs

955902

- IDENTIFY MECHANISMS LIMITING CELL PERFORMANCE (SHORT-CIRCUIT CURRENT, OPEN-CIRCUIT VOLTAGE, FILL-FACTOR, PEAK POWER) IN LARGE-GRAIN, CAST, POLYCRYSTALLINE SILICON SHEET MATERIAL.
- DEVELOP SOLAR CELL FABRICATION PROCESSES, COMPATIBLE WITH LIMITING MECHANISMS, TO IMPROVE PERFORMANCE (GETTERING).

956698

- DEVELOP A PASSIVATION PROCESS (HYDROGENATION), INCLUDING PROCESS SENSITIVITY ANALYSIS.

Dark I-V Analysis Summary

MINI-CELL WAFERS C4-116B AND 71-01E/TOP

- QUASI-NEUTRAL (BULK) RECOMBINATION (J_{QNO}) VARIES FROM 5 X 10^{-9} mA/cm^2 .) 1 x 10^{-8} mA/cm^2. THAT IS. EFFECTIVE MINORITY-CARRIER DIFFUSION LENGTH VARIES BY FACTOR OF TWO.
- SOME CELLS HAVE J_{QNO} GREATER THAN 2 X 10^{-8} mA/cm^2.
- MAJORITY OF CELLS LOSE LESS THAN 10 mV DUE TO EXCESS SPACE-CHARGE (JUNCTION) RECOMBINATION (J_{SCO}); FEW CELLS LOSE MORE THAN 20 mV.
- MOST OF V_{OC} SCATTER IS ACCOUNTED FOR BY J_{QNO} VARIATION.
- DETERMINE CAUSE OF J_{QNO} VARIATION
  - LIGHT-BEAM INDUCED CURRENT (LBIC) - 800 NM
  - DEFECT (SECCO) ETCH
  - CORRELATE STRUCTURE WITH ELECTRICAL CHARACTERISTICS

Minicell Evaluation

1. FABRICATE 400 PHOTODIODES (ON 5 MM CENTERS, 0.19 CM^2 AREA) ACROSS 10CM X 10CM POLYCRYSTALLINE SILICON WAFERS USING MESA STRUCTURE FOR ISOLATION.

2. MEASURE ILLUMINATED I-V CHARACTERISTICS ACROSS WAFER.

3. LOCATE AREAS WHICH SUFFER FROM REDUCED V_{OC} AND/OR FILL-FACTOR.

4. DETERMINE CAUSE:

   - SHUNT CONDUCTANCE.
   - DARK I-V ANALYSIS FOR J_{QNO}, J_{SCO}, AND N-FACTOR.
   - DEFECT ETCH OF SERIAL WAFER FOR DISLOCATION CONTENT.
   - LIGHT-SPOT SCANNING TO LOCATE ELECTRICALLY ACTIVE GRAIN AND SUB-GRAIN BOUNDARIES.

Illuminated I-V Characteristics

WAFER	N (CELLS)	J_{SC} (MA/CM^2)	V_{OC} (MV)	FF (%)
SC11-1 (SINGLE-CRYSTAL)	241	30.3 (0.4)	580 (15)	61.7 (4.2)
71-01E, TOP	294	27.9 (0.6)	562 (16)	66.3 (5.7)
71-01E, MIDDLE	255	27.9 (0.8)	560 (19)	63.9 (7.2)
71-01E, BOTTOM	271	26.1 (0.5)	520 (42)	55.5 (9.6)
C4-108	287	28.2 (1.9)	540 (55)	56.9 (11.0)
C4-116B	329	29.4 (1.6)	559 (14)	64.6 (3.3)
WACKER SILSO	308	27.5 (0.8)	551 (14)	63.6 (5.2)

MEAN (STANDARD DEVIATION ABOUT MEAN)
MEASURED AT 135 MW/CM^2, AMO, $25^{0}C$

- V_{OC} OF POLCRYSTALLINE CELLS IS 20 TO 60 MV LOWER THAN SINGLE-CRYSTAL.

- EXCESS SCATTER IN V_{OC} AND FF OF 71-01E/BOTTOM AND C4-108 CORRELATED WITH INCLUSIONS (RESISTIVE SHUNTS).

LBIC Scans, Wafer C4-116B

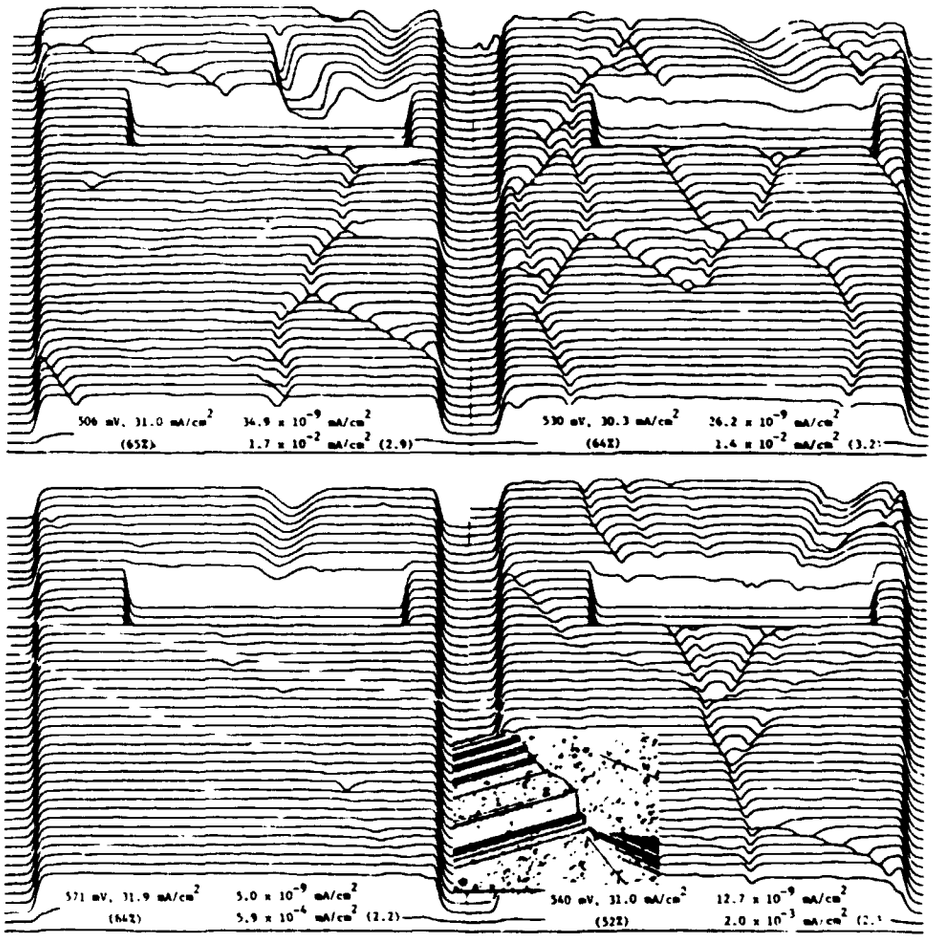

LBIC Scans, Wafer C4-116B

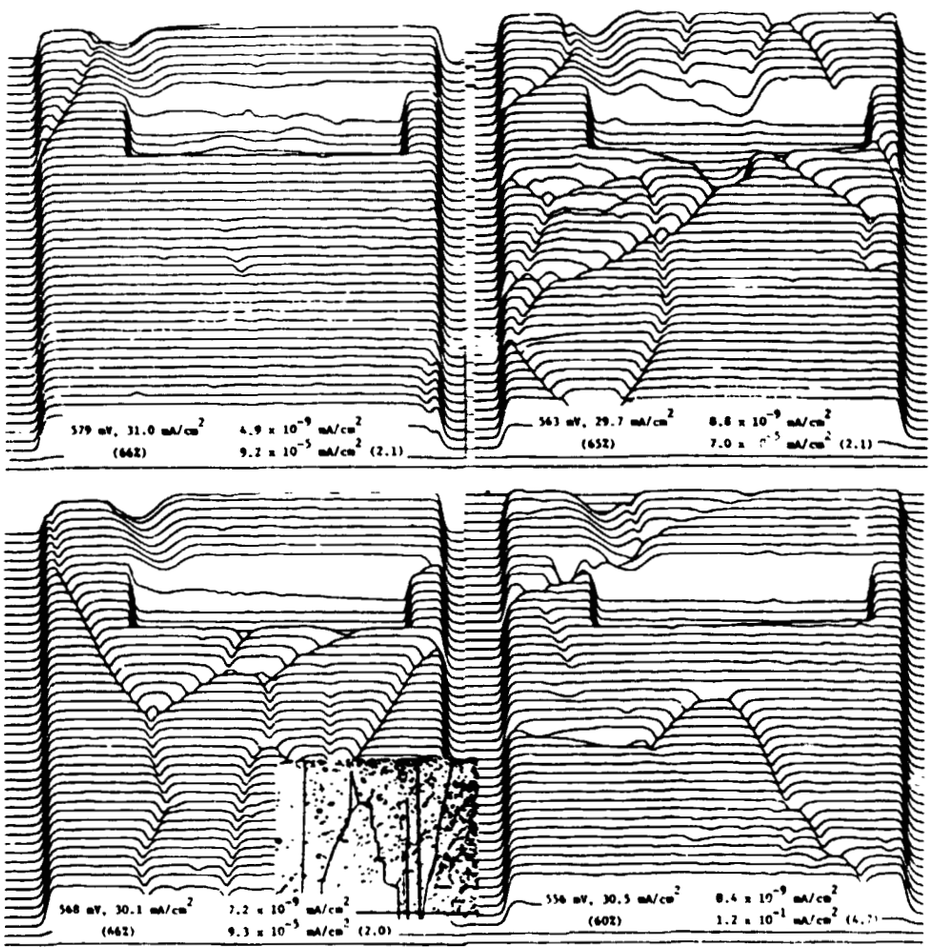

LBIC Scans, Wafer 71-01E/TOP

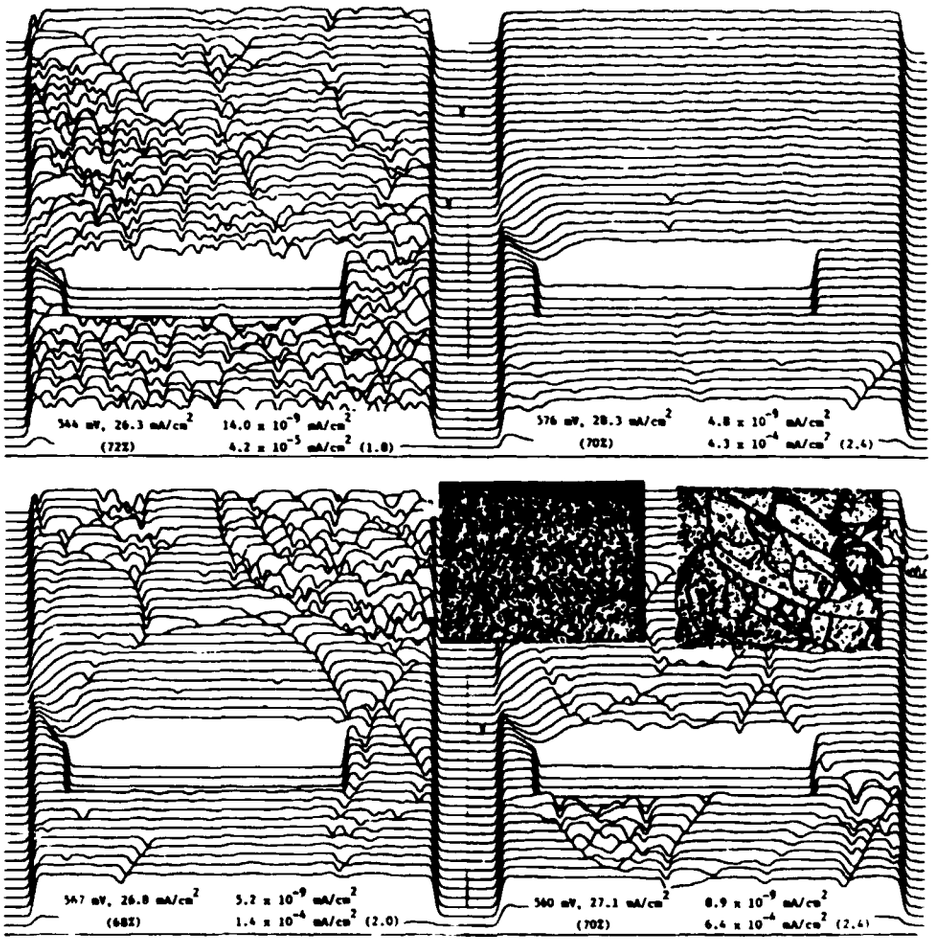

LBIC Scans, Wafer 71-01E/TOP

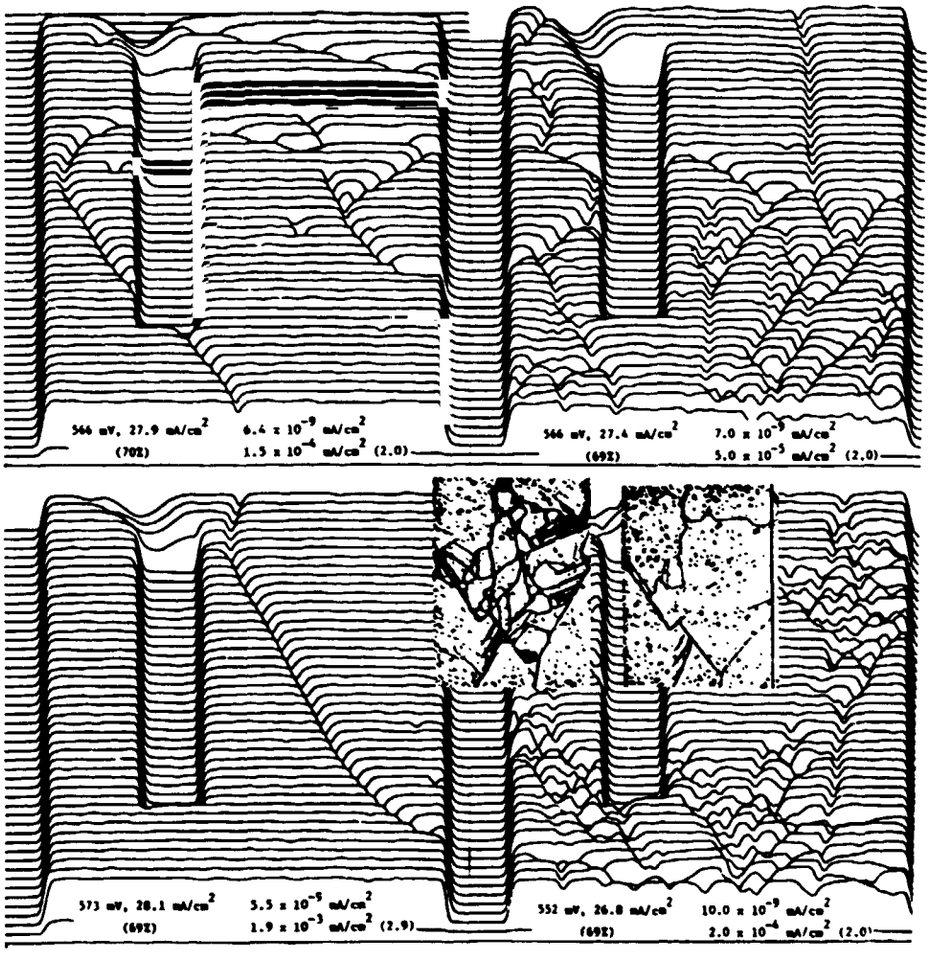

Summary of LBIC results

- STRONG CORRELATION BETWEEN QUASI-NEUTRAL RECOMBINATION AND ELECTRICALLY-ACTIVE GRAIN AND SUB-GRAIN BOUNDARIES.

- AMOUNT OF LBIC-IMAGED G.B. ACTIVITY HAS LITTLE OR NO EFFECT ON SPACE-CHARGE RECOMBINATION OR FILL-FACTOR.

- ISOLATED CELLS HAVE EXCESS J_{SCO} FROM "DEFECT" THAT IS NOT RESOLVED BY LBIC.

Limiting Mechanisms

- FOR SOME WAFERS, V_{OC} AND FF SCATTER ARE DUE TO INCLUSIONS, WHICH ACT AS RESISTIVE SHUNTS.

- FOR OTHER WAFERS, CRYSTAL STRUCTURE CONTROLS QUASI-NEUTRAL RECOMBINATION AND THEREFORE V_{OC}, FF, AND J_{SC}.

- THERE DOES NOT APPEAR TO BE A STRONG CORRELATION BETWEEN STRUCTURE AND SPACE-CHARGE RECOMBINATION.

- LOWEST J_{QNO} IS 5 X 10^{-9} mA/cm^2, WILL LIMIT V_{OC} TO ABOUT 585 mV (IDEAL DIODE, FOR $J_{SC} = J_L = 30$ mA/cm^2).

Hydrogenation

- FABRICATE SAMPLE SET.
- LOCATE AREAS THAT CONTAIN CELLS WITH LOW V_{OC}. HIGH J_{QNO}. ELECTRICALLY-ACTIVE G.B. (LBIC).
- HYDROGENATE - DC PLASMA
- EVALUATE ANY CHANGE IN GRAIN BOUNDARY ACTIVITY AND J_{QNO} BY DARK I-V CHARACTERISTICS AND LBIC.

AMORPHOUS METALLIC LAYERS IN Si METALLIZATION SYSTEMS

CALIFORNIA INSTITUTE OF TECHNOLOGY

Marc-A. Nicolet

- WHY AMORPHOUS METALLIC LAYERS?
- FORMATION OF SUCH LAYERS
- PROPERTIES OF SUCH LAYERS:
  - CRYSTALLIZATION
  - REACTION WITH Si
  - REACTION WITH METAL OVERLAYER
- CONTACT WITH SUCH LAYER AS DIFFUSION BARRIER
- PROBLEMS, OUTLOOK

Amorphous Layers as Diffusion Barriers in Metallization Systems

ADVANTAGES

- NO GRAIN BOUNDARIES
  - NO RAPID DIFFUSION PATHS
  - LOW ATOMIC DIFFUSIVITIES
- REDUCED REACTIVITY
- MANY CHOICES
  - FLEXIBILITY, OPTIMIZATION

DISADVANTAGES

- METASTABLE
- AT LEAST TWO ELEMENTS
  - MANY CHOICES
- PROPERTIES = F (DEPOSITION PROCESS AND PROCEDURE)

COMPLEX, NEW IN DEVICE TECHNOLOGY

- R&D, TOLERANCES, TESTING

Formation of Amorphous Metallic Layers

- RULES FOR SELECTION OF ELEMENTS AND COMPOSITION

  TRANSITION METAL + METALLOID } OF { $\Delta R/R \geq 10\%$, LOW SOLUBILITY, DEEP EUTECTIC
  TWO TRANSITION METALS }

  TWO TRANSITION METALS OF DIFFERENT STRUCTURE

- RULES FOR FORMATION PROCESS

  RANDOM ATOMIC ARRANGEMENT

  LOW ATOMIC MOBILITY: LOW T
  LOW HEAT
  FAST HEAT DISSIPATION

OUR PROCESS

RF DIODE SPUTTERING (13.56 MHZ)

MAGNETRON TARGET (3")

(BULK PLATE OF A) + (PARTIAL COVER SHEET OF B)

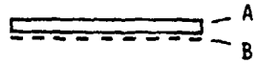

GAS: AR OR $AR_{0.9} + N_{0.1}$

Sheet Resistance of Amorphous Ni-W Layer on SiO_2 and Si Substrate

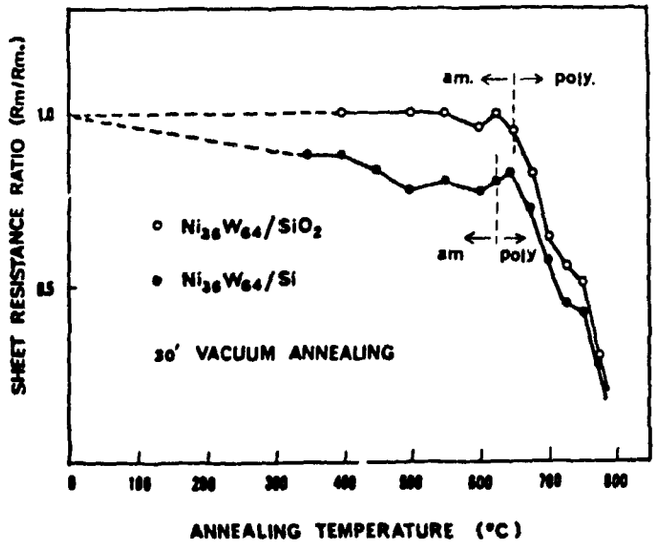

Sheet Resistance of Amorphous Ni-N-W Layer on SiO_2 and Si Substrate

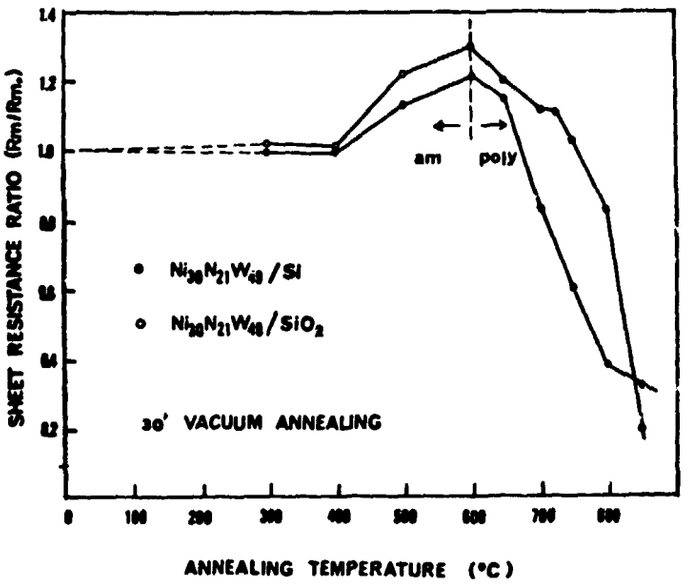

Crystallization and Reaction With < Si >

AMORPHOUS FILM	TEMPERATURE (°C, 30 MIN) T_R REACTION WITH <SI>	T_C CRYSTALLIZATION ON SiO_2
$Mo_{62}Ni_{38}$	550-600	600
$Fe_{37}W_{63}$	550-700	700
$Ni_{36}W_{64}$	625-650	650
$Ni_{30}N_{21}W_{49}$	725-750	600
$Zr_{40}W_{60}$	725-750	900

POLYCRYSTALLINE FILM	TEMPERATURE T_{REF} OF REACTION WITH <SI> (°C)
Ni	~ 200
Fe	~ 450
Mo	~ 525
W	~ 650
Zr	~ 700

CONCLUSIONS

$T_{REF} \lesssim T_C$ (EXCEPT FOR W IN Ni-N-W)
CRYSTALLIZATION SLOWER THAN REACTION

WHEN $T_{REF} < T_C$ THAN $T_{REF} < T_R$
(A) ALLOY RETARDS REACTION WITH <SI>

$T_R \leq T_C$ (EXCEPT FOR Ni-N-W)
CRYSTALLIZATION INDUCES REACTION

Metallurgical Stability of Amorphous Ni-W Layer on Si (100): Penetration of Ni Into Si (Monitored by BS)

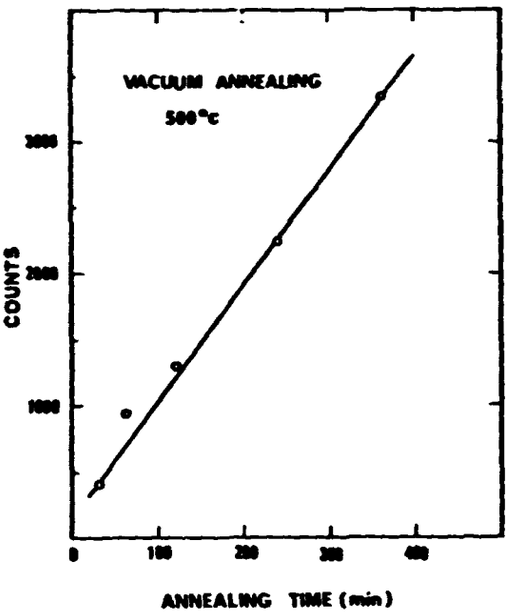

Metallurgical Stability of Amorphous Ni-N-W Layer With Al Overlayer: R. B. Analysis

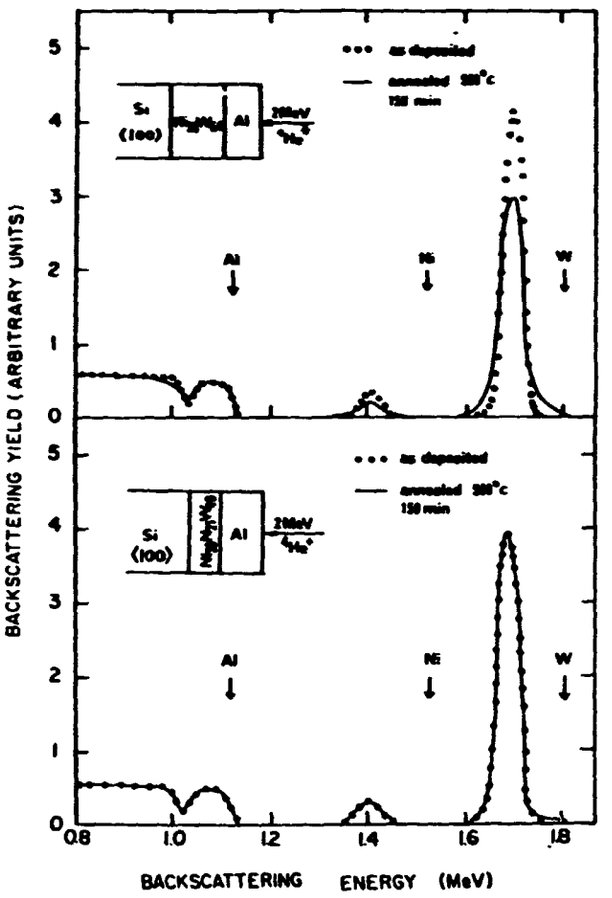

Contact Resistivities of Amorphous RF-Sputtered Metallic Thin Films

ρ_c ($\mu\Omega CM^2$)	T,°C (1/2 H)	N^+Si	P^+Si
		(AS-DEPOSITED → T, 1/2 H)	
$Fe_{45}W_{55}$	400	0.1 → 0.2	3 → 1
$Mo_{1-x}Ni_x$ $30<x<60$	500	1 → 2	1 → 2
$Ni_{36}W_{64}$	500	1 → 2	1 → 0.4

Schottky Barrier Heights of Amorphous RF-Sputtered Metallic Thin Films

ϕ_B (eV)	T (°C,1/2 H)	nSi	pSi	n
$Fe_{45}W_{55}$	AS-DEPOSITED	0.61	-	1.08
	400	0.65		
$Mo_{1-x}Ni_x$	AS-DEPOSITED	0.68	0.42	1.01
$30 < x < 60$	500	0.63	0.42	1.05
$Ni_{36}W_{64}$	AS-DEPOSITED	0.65	0.45	1.04
	400	0.65	0.43	1.08
	450	0.64	0.43	1.15

Problems, Solutions and Outlook

PROBLEMS

- Minimize Reactions of Amorphous Layers
  - With Substrate
  - With Overlayer

SOLUTIONS

- Intermediate Silicide Layer
- Early Transition Metal Alloys
  - ZrW - high T_{REF}'s
- N-containing Amorphous Alloys
- Ternary Amorphous Alloys

OUTLOOK

- Some Problems
- Many Possibilities
- Promising Results

METALLO-ORGANIC DECOMPOSITION (MOD) SILVER METALLIZATION FOR PHOTOVOLTAICS

PURDUE UNIVERSITY

G.M. Vest
R.W. Vest

MOD Film Processing

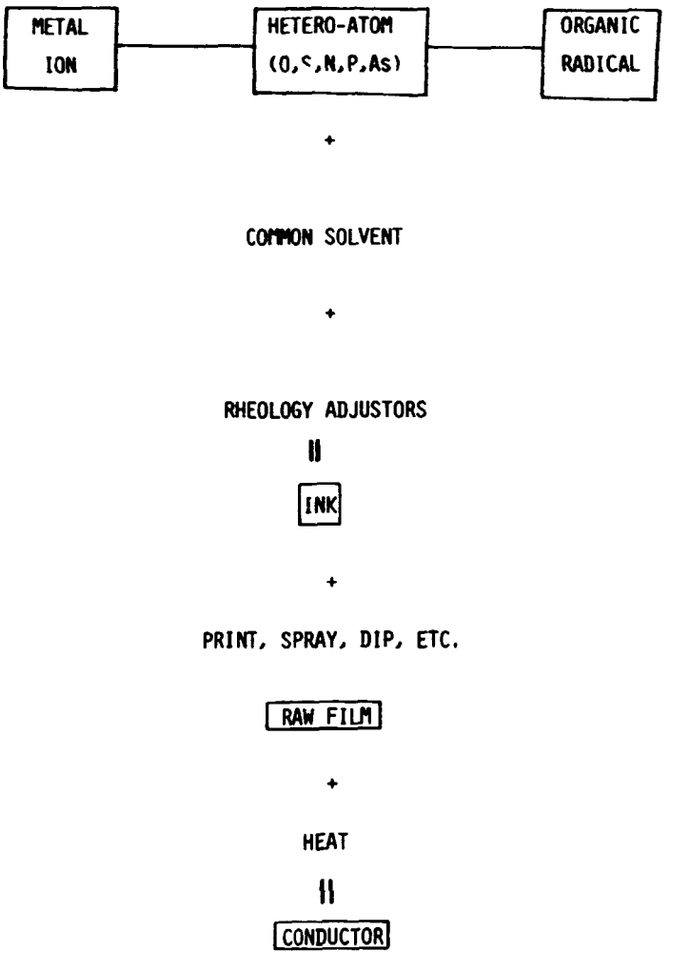

Silver Neodecanoate

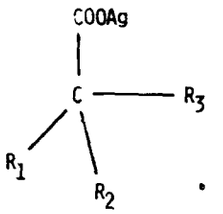

$R_1 + R_2 + R_3 = C_8H_{19}$

Substituents	% Abundance
$R_1 = CH_3$ $R_2 = CH_3$ $R_3 = C_6H_{13}$	31
$R_1 = CH_3$ $R_2 > CH_3$ $R_3 < CH_6H_{13}$	67
$R_1 > CH_3$ $R_2 > CH_3$ $R_3 < C_5H_{11}$	2

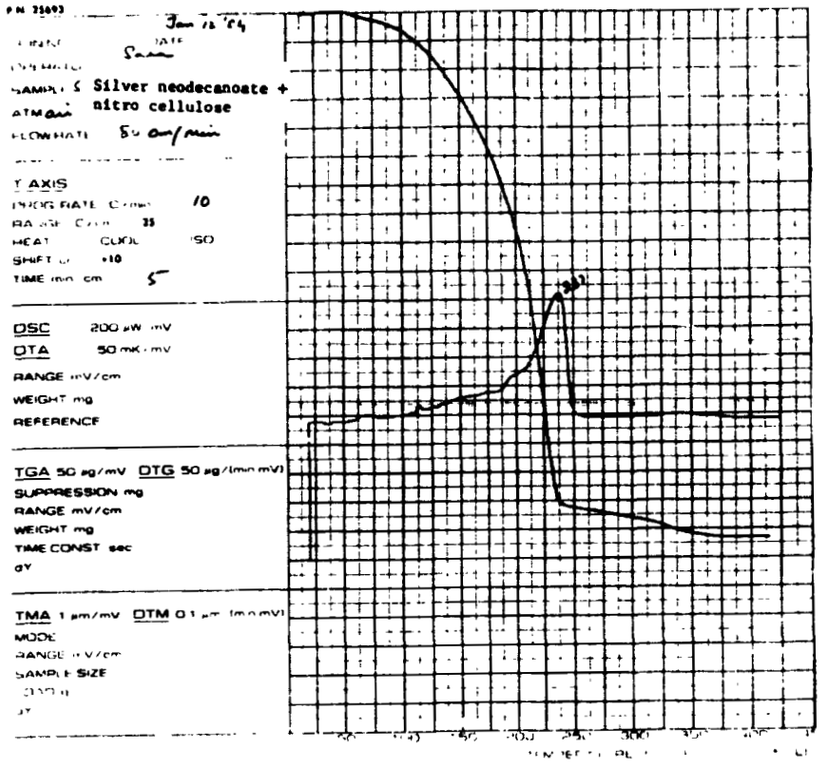

Molecular Design Criterion

1. As the Chain Length of the Organic Radical Increases:
   a) the solubility of the compound in organic solvents increases;
   b) the metal content of the compound decreases.

2. The Solubility of the Compound Increases if the Organic Radical is Branched.

Silver Compound	Formula	w/o Ag (theo)	T_d (°C)
Mono-Methyl Succinate	$CH_3OOC \cdot C_2H_4 \cdot COOAg$	45	230
2-Ethyl butyrate	$C_2H_5 - \underset{H}{\overset{C_2H_5}{C}} - COOAg$	48	235
2-Ethyl hexanoate	$C_4H_9 - \underset{C_2H_5}{\overset{H}{C}} - COOAg$	43	235
Neopentanoate	$CH_3 - \underset{CH_3}{\overset{CH_3}{C}} - COOAg$	52	230
Neodecanoate	$R_3 - \underset{R_2}{\overset{R_1}{C}} - COOAg$ $[R_1 + R_2 + R_3 = C_8H_{19}]$	38.6	230

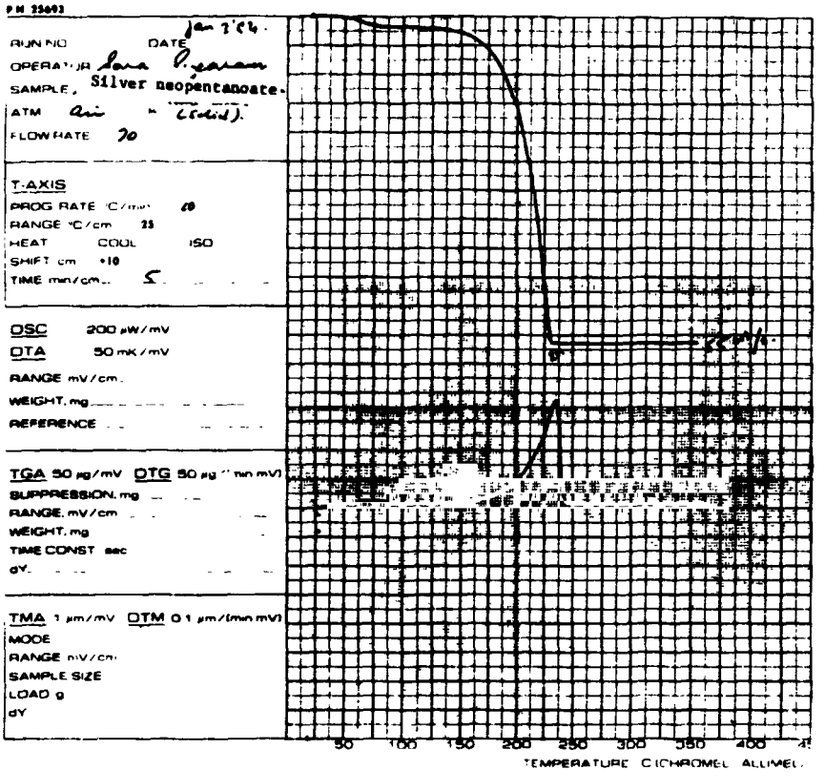

Ink Requirements for Screen Printing

1. Very Low Vapor Pressure
2. Viscosity 100-500 Pa·s at Low Shear Rate
3. Pseudoplastic
4. Thixotropic

Solvents

Commercial Name	Chemical Name	Formula	Boiling Point
Butyl carbitol acetate	2-(2-butoxy-ethoxy) ethyl acetate	$CH_3(CH_2)_3 \cdot O \cdot CH_2-CH_2 \cdot O-CH_2-CH_2COOCH_3$	$236\text{-}249^0$
α-Terpineol	α-Terpineol	$CH_3(C_6H_8)C(CH_3)_2OH$	$217\text{-}218^0$
Phenyl ether	Diphenyl ether	$(C_6H_5)_2O$	259^0
Dodecane	Dodecane	$CH_3(CH_2)_{10}CH_3$	$215\text{-}17^0$
Diglyme	2-methoxy ethyl ether	$(CH_3OCH_2CH_2)_2O$	162^0
Triglyme	Tri ethylene glycol dimethyl ether	$CH_3OCH_2CH_2OCH_2CH_2O-CH_2CH_2OCH_3$	216^0
Neodecanoic Acid	Neodecanoic Acid	$R_2-\overset{R_1}{\underset{R_3}{C}}-COOH$ $R_1+R_2+R_3 = C_8H_{19}$	$250\text{-}257^0$

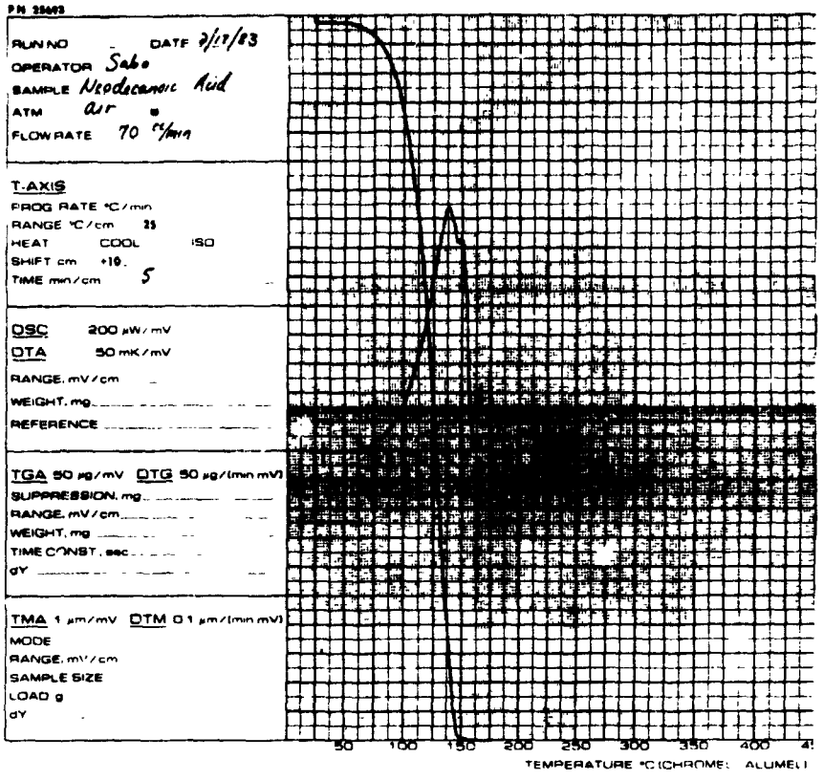

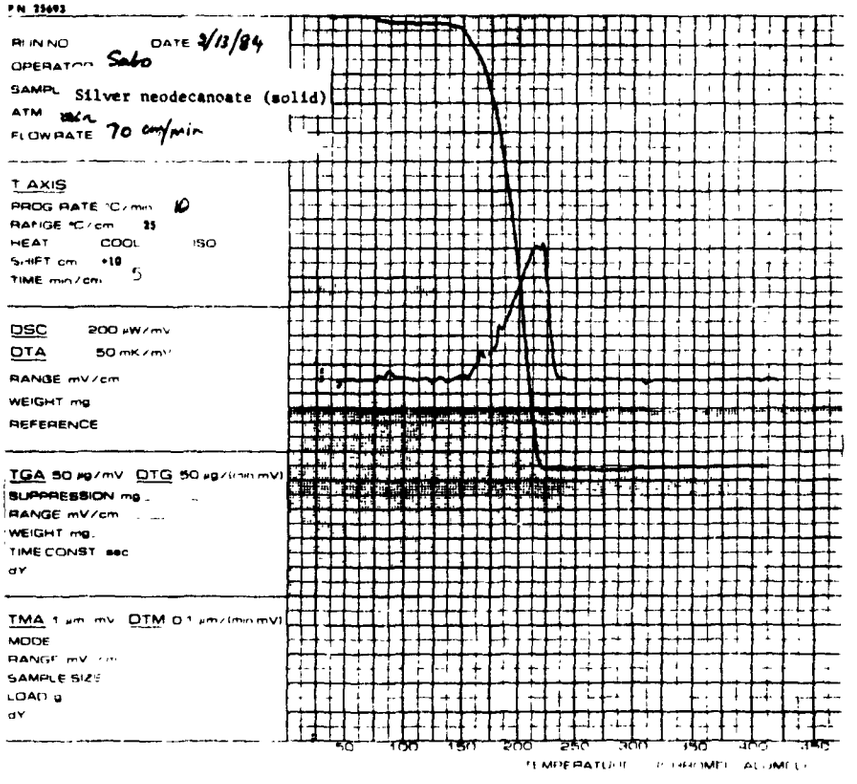

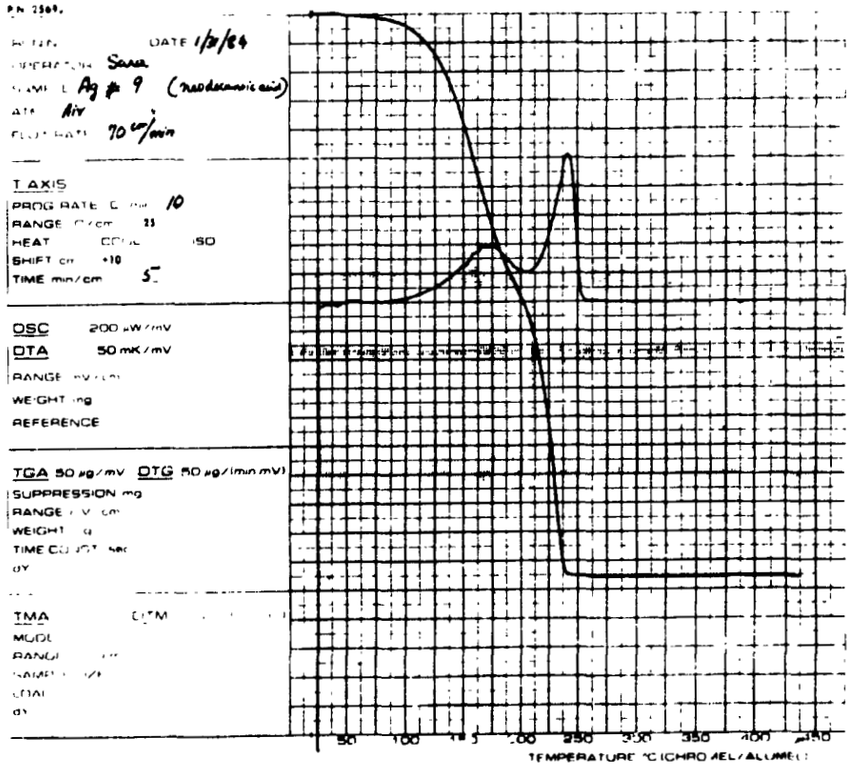
DATE 1/12/84
Sara
Ag # 9 (nanodecanoic acid)
Air
70 cc/min
T AXIS
PROG RATE
10
RANGE
HEAT
SHIFT
+10
TIME min/cm
5
OSC
200 µW/mV
DTA
50 mK/mV
RANGE
WEIGHT mg
REFERENCE
TGA 50 µg/mV DTG 50 µg/(min mV)
SUPPRESSION mg
RANGE
WEIGHT
TIME CONST sec
dY
TMA
DTM
MODE
RANGE
LOAD
dY
50
100
150
200
250
300
350
400
450
TEMPERATURE °C (CHROMEL/ALUMEL)

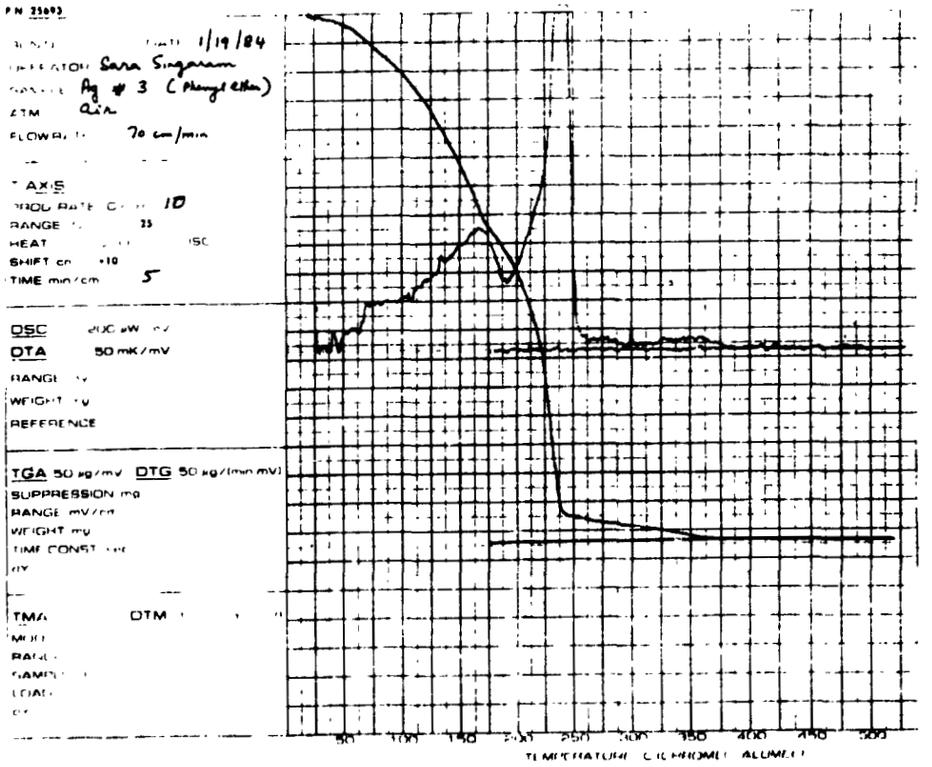
1/19/84
Sara Singaram
Ag # 3 (Phenyl ether)
Air
70 cm/min
T AXIS
PROG RATE
10
RANGE
25
HEAT
ISO
SHIFT
+10
TIME min/cm
5
OSC
DTA
50 mK/mV
RANGE
WEIGHT
REFERENCE
TGA 50 µg/mV DTG 50 µg/(min mV)
SUPPRESSION mg
RANGE mV/cm
WEIGHT mg
TIME CONST sec
dY
TMA
DTM
MODE
RANGE
LOAD
dY
50
100
150
200
250
300
350
400
450
500
TEMPERATURE °C (CHROMEL/ALUMEL)

Ink Formulating

METHOD A

Xylene Solution of Silver Neodecanoate Plus Additive

Solvent Exchange in Rotovapor at 40-60°C

METHOD B

Toluene Solution of Silver Neodecanoate Plus Additive

Solvent Exchange in Rotovapor at 25°C

METHOD C

Solid Silver Neodecanoate Plus Additive

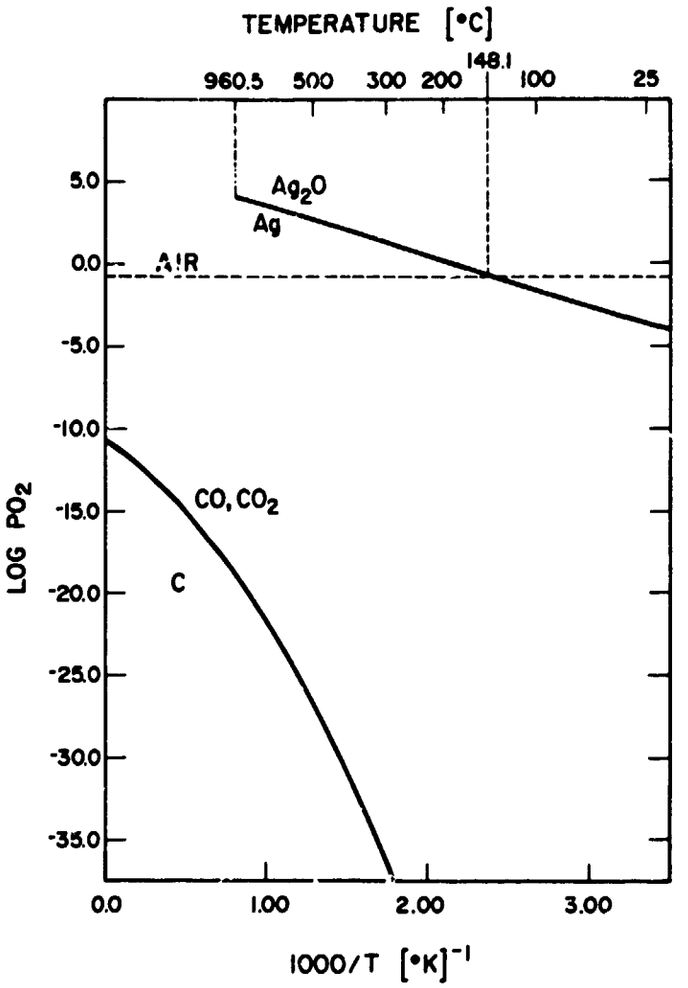

Firing

1. Muffle Furnace at Constant Temperature and Still Air

2. Muffle Furnace with Time-Temperature Programming and Controlled Air Flow

3. Belt Furnace with Variable Time-Temperature Profiles and Natural Convection

4. Combinations of No. 1 and No. 3

Results on Al_2O_3 Substrates (2)

Ink #	Firing Sequence: Temp. °C	Firing Sequence: Time (min)	Type of Furnace	Surface Appearance	Adhesion	Line Defin.	Sheet Resist. (Ω/□)	Resist. (μΩ-cm)
9	200-350 350	10°/min 20	1	silvery surface with yellow tint	poor	poor	0.113-0.112	-
11	200 350	10°/min 30	1	brownish black with oily texture	poor to fair	excellent if not smudged	-	-
12	100 200-350 350	15 10°/min 45	1	brownish grey	poor[a]	poor[a]	not measured	-
20	70 200 200-250 250 350	15 10 10°/min 10 30	1	brownish grey	good to excellent	good 0.008"-0.012"	0.460-5.36	-
21	60 200 225 350	30 20 20 30	1	dull yellowish silver	good	fair 0.020"	0.189	22.72
21	60 200 225 350 350-500 500	30 20 20 30 30°/min 12	1	whitish silver	poor to fair	fair	0.062	7.46
21[b]	60 200 350	40 20 30	1	brownish grey yellow	good	fair	0.280-0.626	-

a) good to excellent on glass
b) printed and fired on Si

Summary: Appearance

1. Pyrolysis Products Can Produce a Dark Surface Film
2. Purity of All Ink Ingredients is Very Important
3. Heating Rate in the Range 70-225^{o}C is Important
4. Air Flow Rate is Important
5. Surface Film Can Be Removed By Light Burnishing or Heating 10 Minutes at 500^{o}C.

Summary: Adhesion

1. Low Temperature Solvent Removal is of Prime Importance (15-30 minutes at 60-70^{o}C required for present inks)
2. Heating Rate in the Range 100-250^{o}C is Important
3. Air Flow Rate is Important
4. Maximum Temperature is Important
5. Possible Long Term Adhesion Problem
6. Mechanism of Adhesion is Not Understood

Summary: General

1. Generic Compounds are Essential
2. High Purity Raw Materials are Very Important
3. Proper Time-Temperature Processing is Critical
4. MOD Silver Shows Great Promise for Low Temperature Metallization

N85 15279

A NONNOBLE FRONT METALLIZATION PROCESS

SPECTROLAB, INC.

Alexander Garcia III

Objectives

- Optimization, Evaluation and Demonstration of A Novel Metallization System

- Mo/Sn/TiH System

- ITO Conductive AR Systems

Approach

- Screen Printing
- Air Firing
- Reducing Atmosphere
- Conductive AR Coating (ITO)

New Pastes Investigated

- MoO_3 Paste
- Borane-Pyridine
- Ag Neodecanate
- Ag Resinate
- In Resinate

Front Metallization Pattern

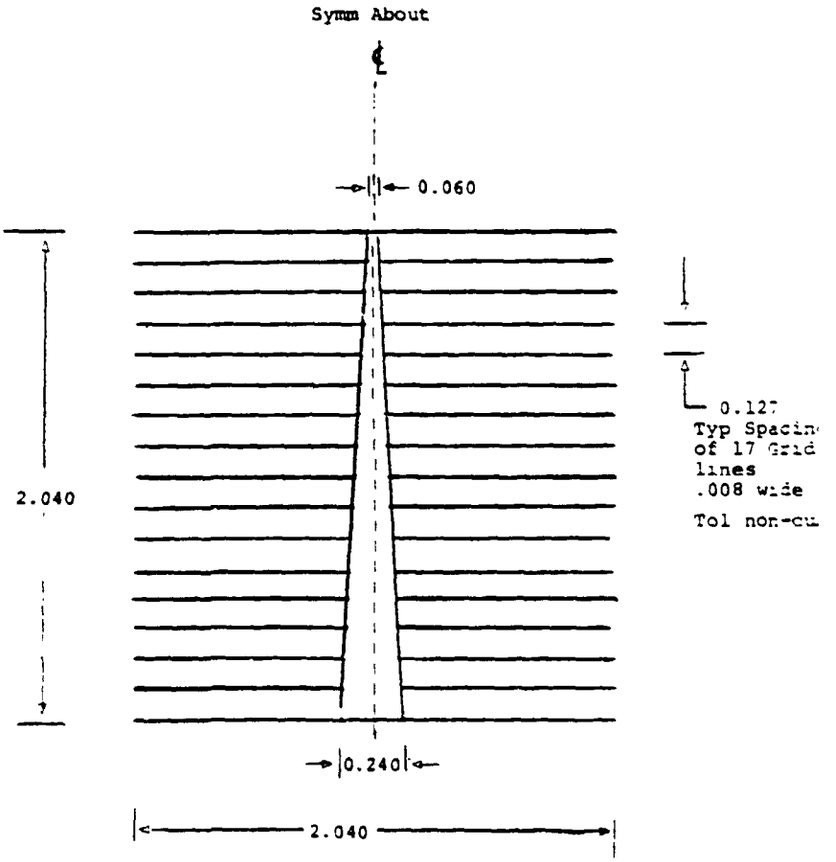

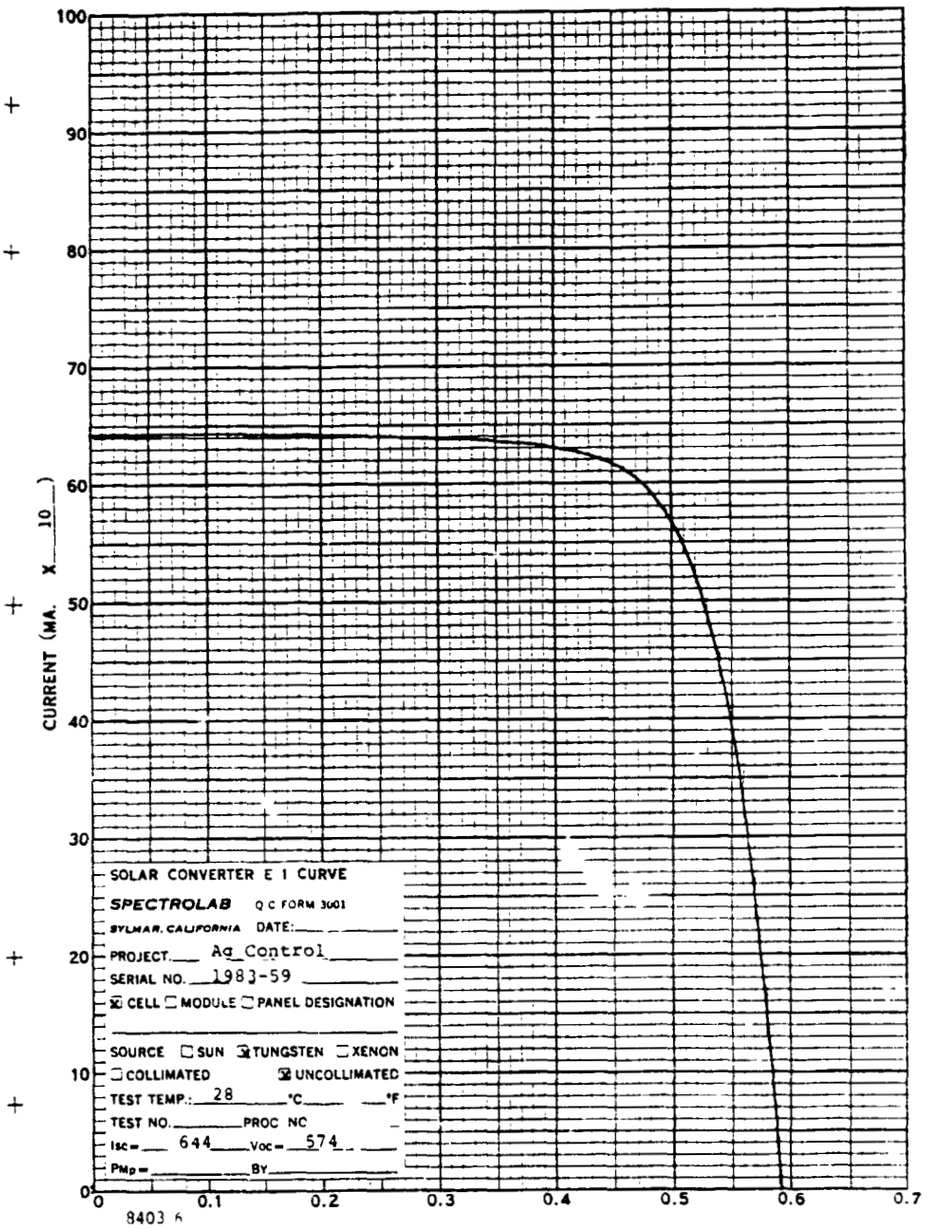

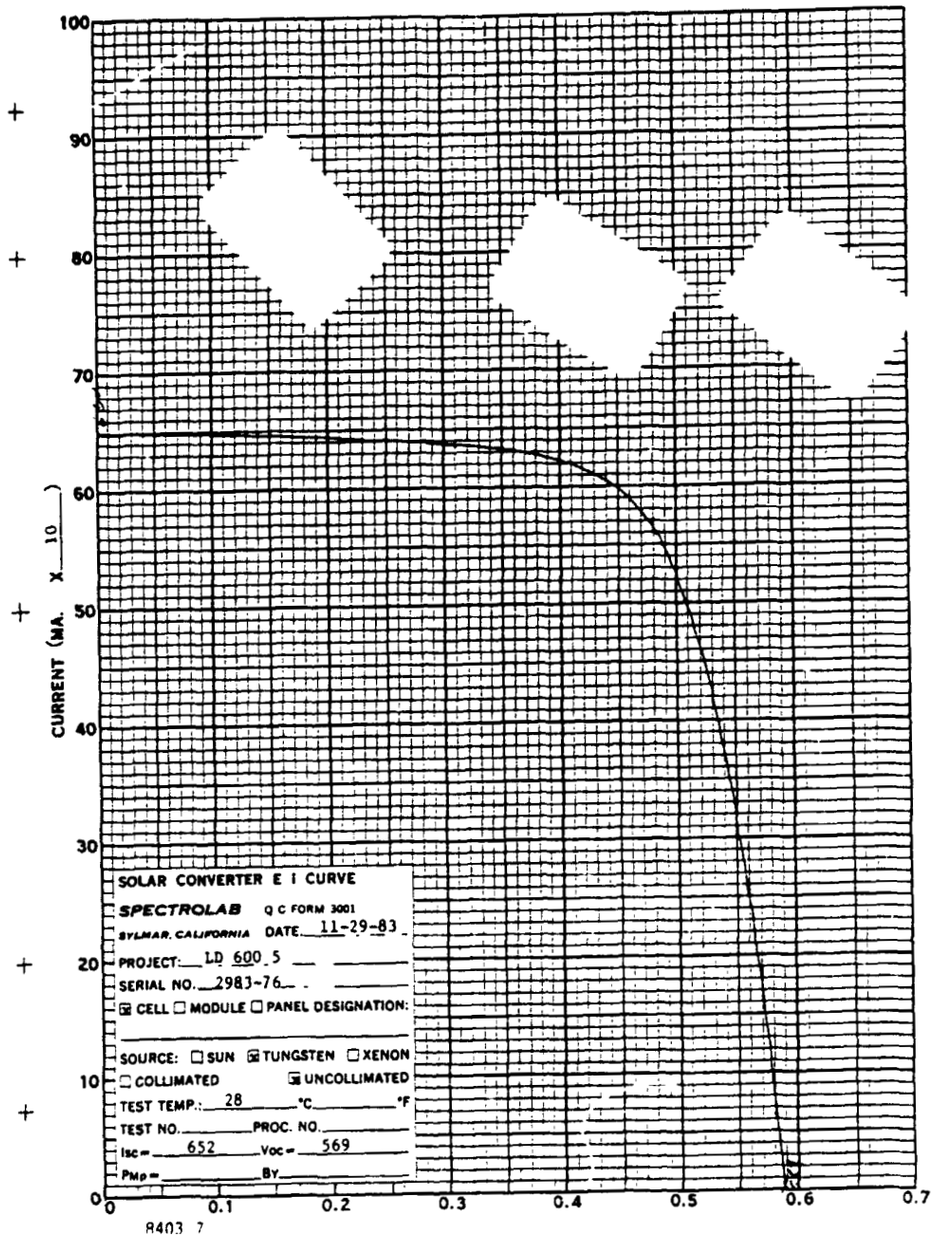

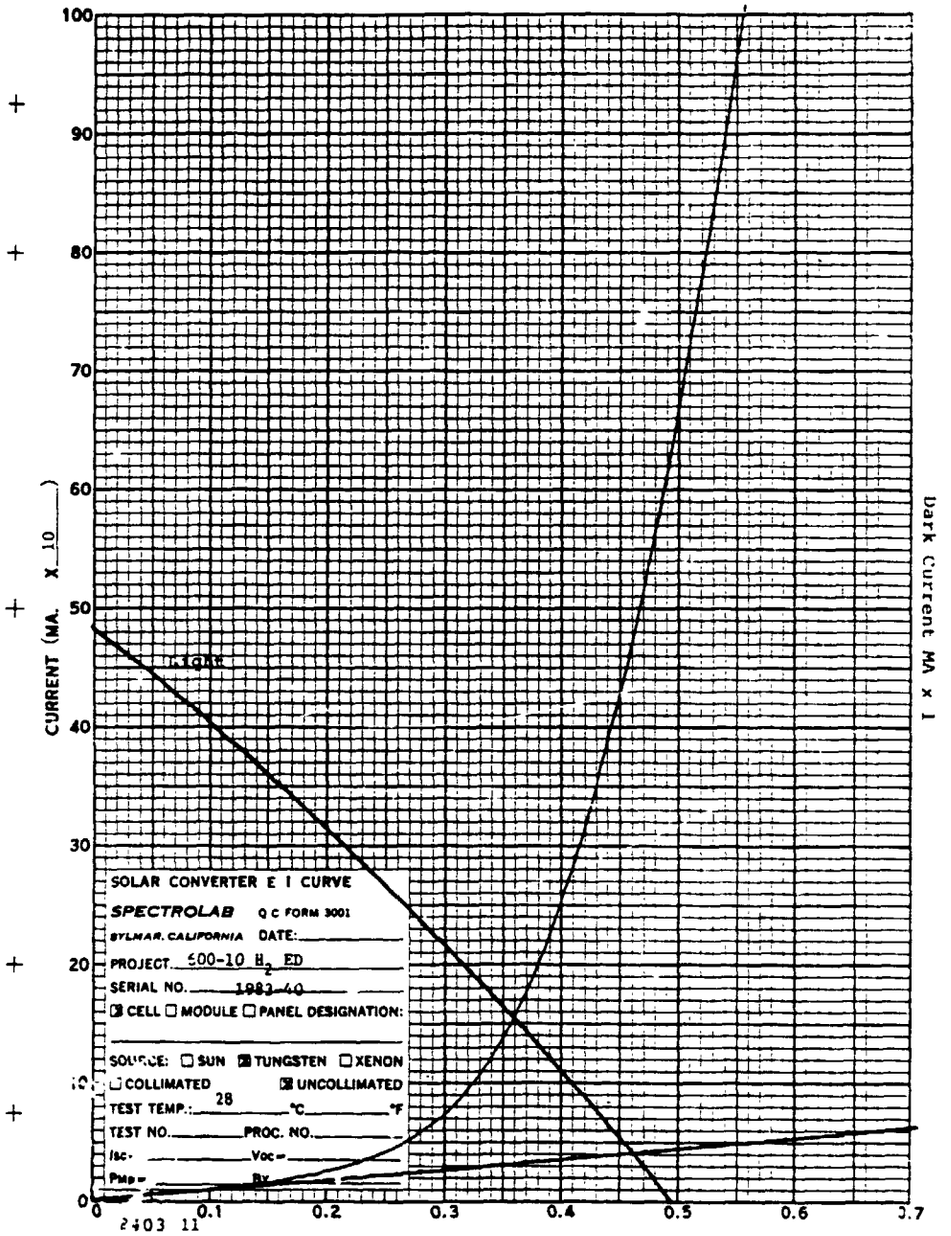

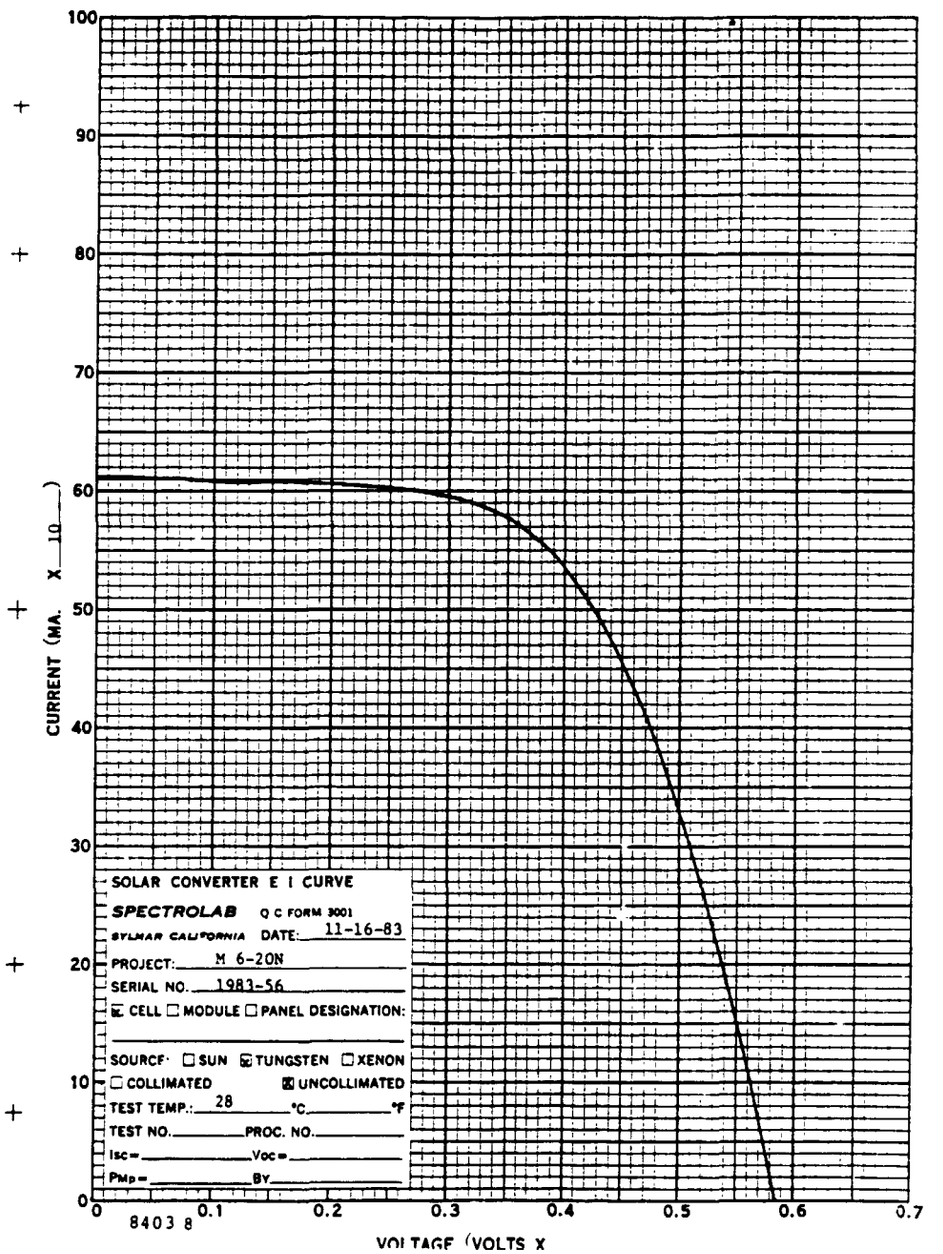

Paste N, Electrink No. F-80

FORMULATION

Item	% by Weight
Titanium Hydride (TiH_2)	.45
Molybdenum Metal Powder	16.06
Tin Metal Powder	64.24
Borane Pyridine	5.00
Vehicle V-38	14.25

VEHICLE V-38

α-Terpineol	43.62
Butyl Carbitol Acetate	43.62
Ethyl Cellulose N-14	9.76
Thixatrol ST	3.00

Paste M, Electrink No. F-82

FORMULATION

Item	% by Weight
Molybdenum Oxide (MoO_3)	17.572
Tin Metal Powder	64.907
Titanium Resinate	.002
Vehicle V-44	17.519

VEHICLE V-44

α-Terpineol	70.54
Carbitol Acetate	4.17
Trichloroethylene	19.20
Ethyl Cellulose	6.09

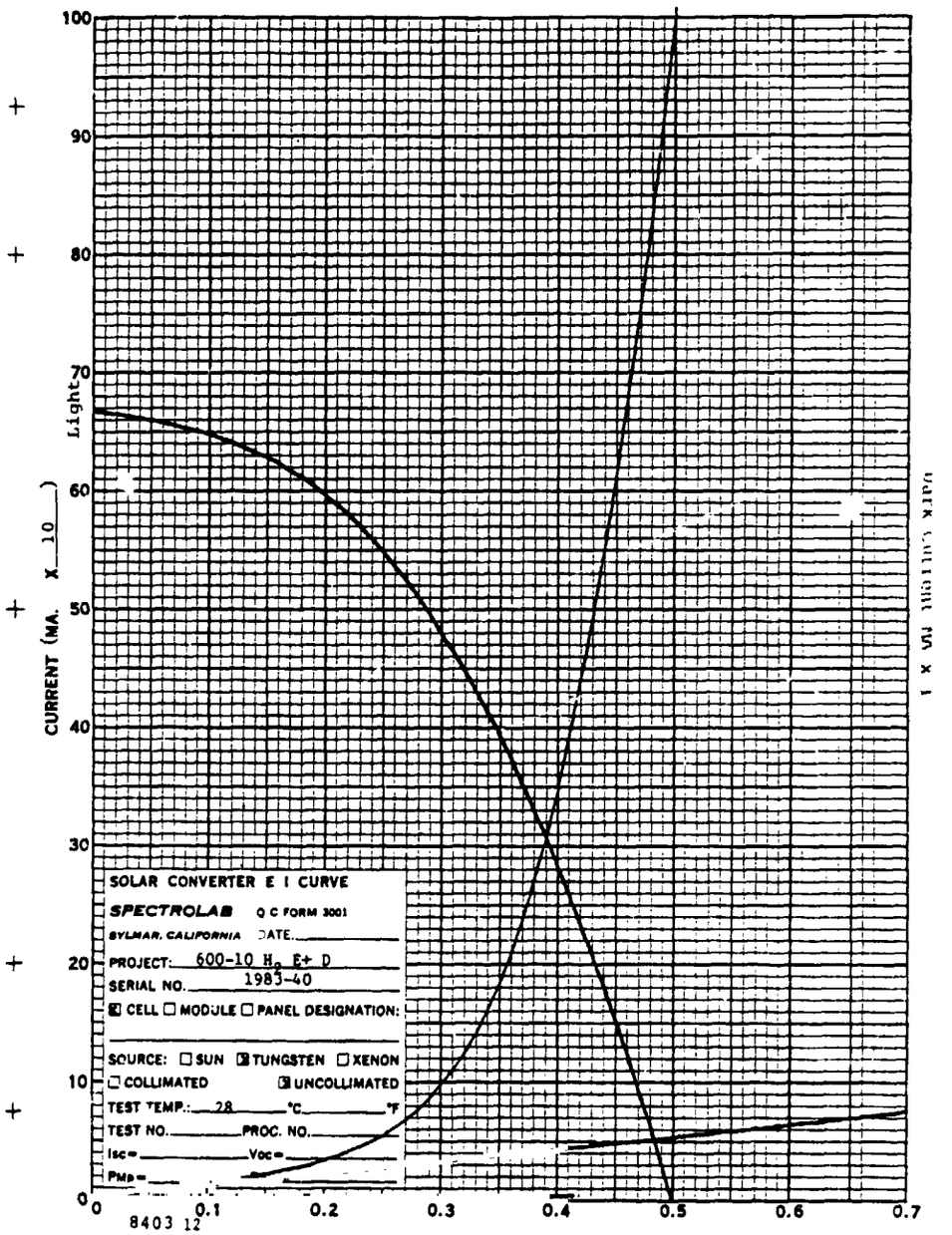

New Analytical Technique

- Controlled Atmosphere SEM
- Video Tape Picture As Sample Is Being Heated
- Various Gases Available @ 5 Torr

Controlled-Atmosphere SEM

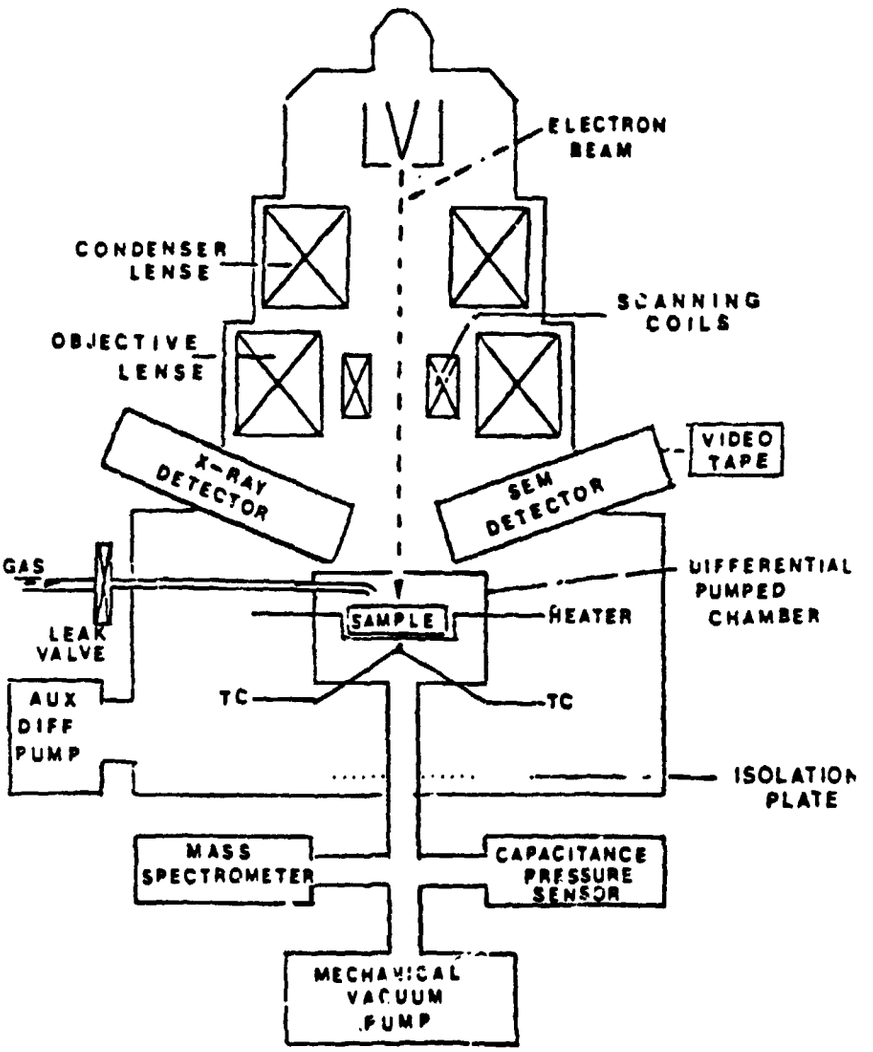

Conclusions

- Mo/Sn Has Adequate Conductivity for Screen Printing
- Shunting Is Never A Problem
- Solderability A Major Problem
- More Work Needed on Wetting Phenomena
- Cellulosic Vehicle Best

Results

- Various Additives Unsuccessful on Improving Adhesive
- SEM Results Show Tin Does Not Wet System at Low Temperature

N85 15280

VISCOSITY MEASUREMENTS FOR THICK-FILM PASTES

ELECTRINK, INC.

J. Parker

1. Are convenient + make
2. Can be made reproducible
3. Relate to production applications
4. Correlate to composition and condition of the material

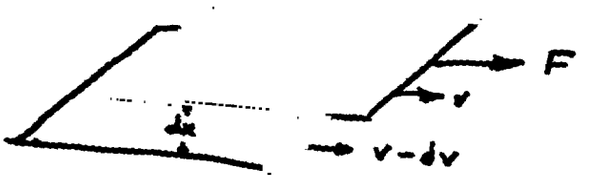

$$\eta = \frac{F}{\frac{dv}{dx}} = \frac{\text{shear stress}}{\text{rate of shear}}$$

VISCOSITY DEFINITION

The force producing a velocity gradient in a fluid is proportional to the gradient. Viscosity is the proportionality constant.

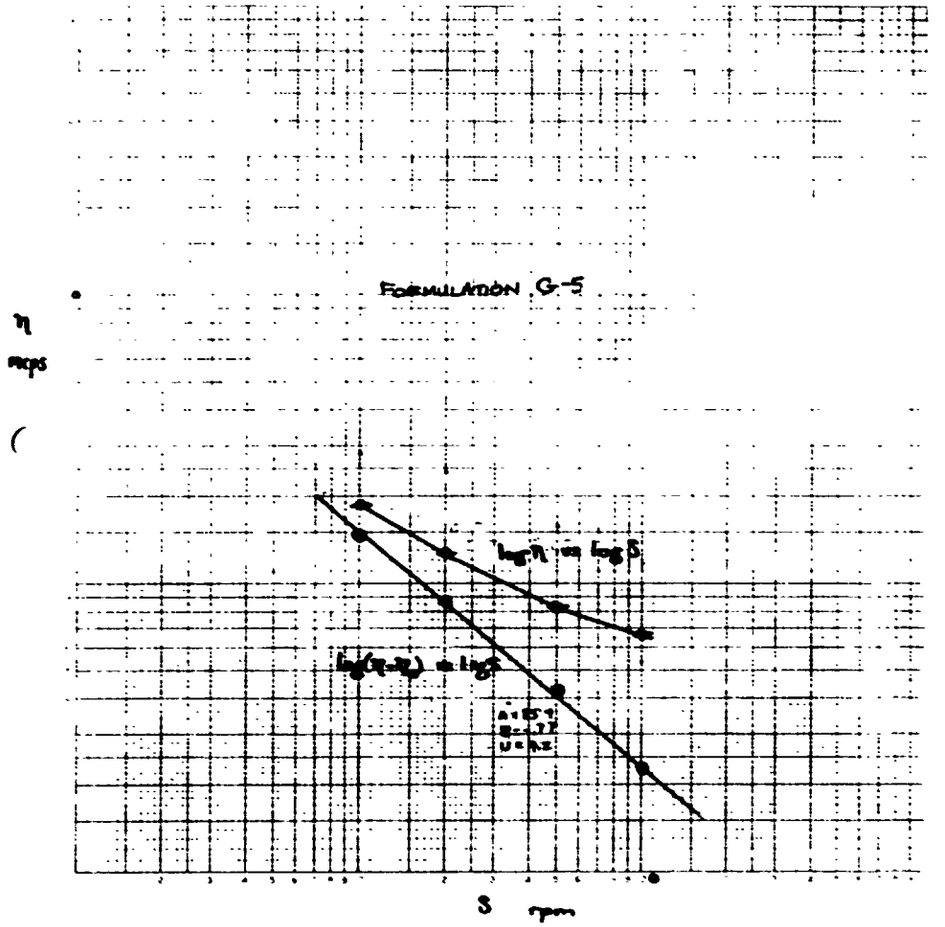

Non-Newtonians

$$\eta = cS^b$$

$b = 0$ Newtonian. (Viscosity is constant with varying shear rates)

b negative Plastic (Viscosity decreases with increasing shear rate)

b positive Dilatant (Viscosity increases with increasing shear rate)

Log Viscosity vs Log Speed

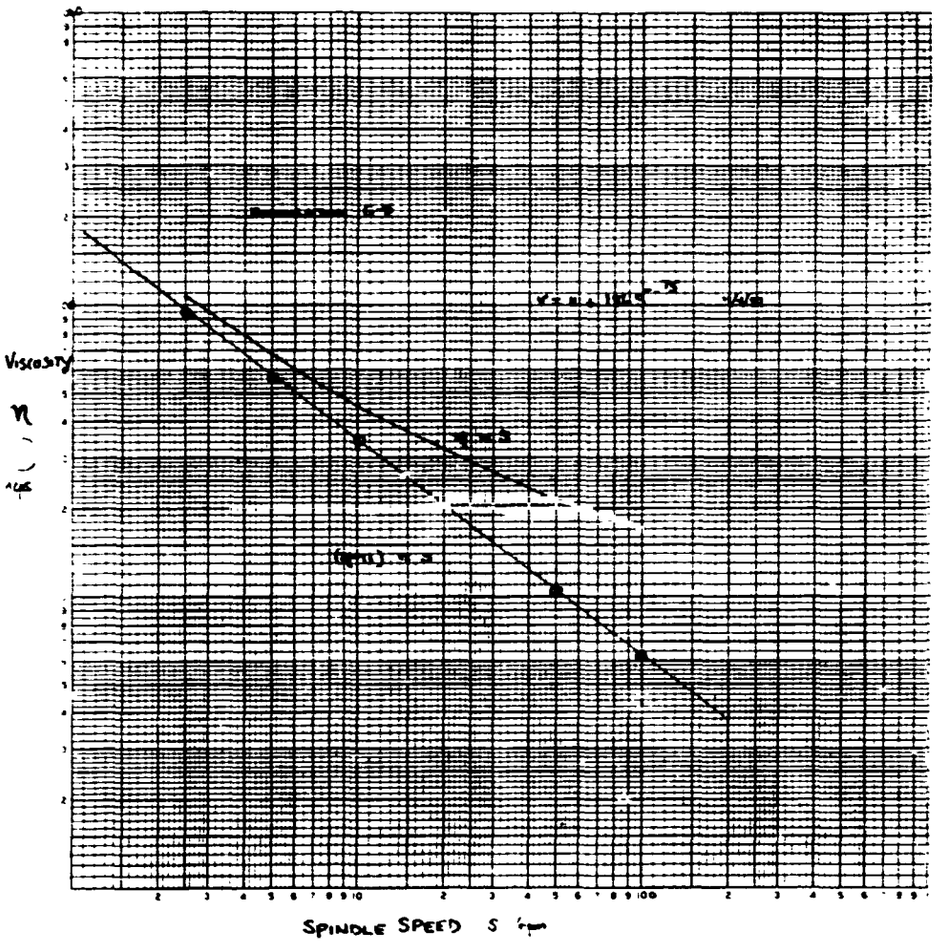

OF POOR

Thixotropic Materials

$$\eta = \eta_0 + cS^b$$

- b measures the plastic character of the liquid (change of viscosity with shear rate)
- c is the newtonian residue of viscosity
- η_0 indicates liquid structure restoration rate for disrupted states (thixotropic character)

Viscosity Procedure

The ink samples should be a minimum of 3 inches deep and a minimum of one inch in diameter. After 24 hours or more of standing the sample should be brought to and maintained at 25° C ± .3° C.

Using a leveled Brookfield RTV viscometer with a no. 7 spindle and starting with a spindle speed of 2.5 rpm, viscosity measurements are to be made after the indicated times in the following sequence of spindle speeds:

order no.	speed rpm	equilibrium time, minutes (approx. min.)	note
1	2.5	10	
2	5.0	10	after standing
3	10	10	
4	20	10	no measurement
5	10	6	
6	5.0	6	after stirring
7	2.5	6	

The ten minute period at 20 rpm serves to stir the ink in the vicinity of the spindle. No measurement at 20 rpm is required.

Acceptable viscosity value ranges are tabulated below.

speed rpm	after standing centipoise	after stirring centipoise
2.5	175,000 ± 20,000	110,000 ± 20,000
5.0	105,000 ± 15,000	75,000 ± 15,000
10	70,000 ± 10,000	55,000 ± 10,000

Viscosity measurements should be made for two different samples from a batch of ink. The average values for the two samples should fall within the above viscosity ranges.

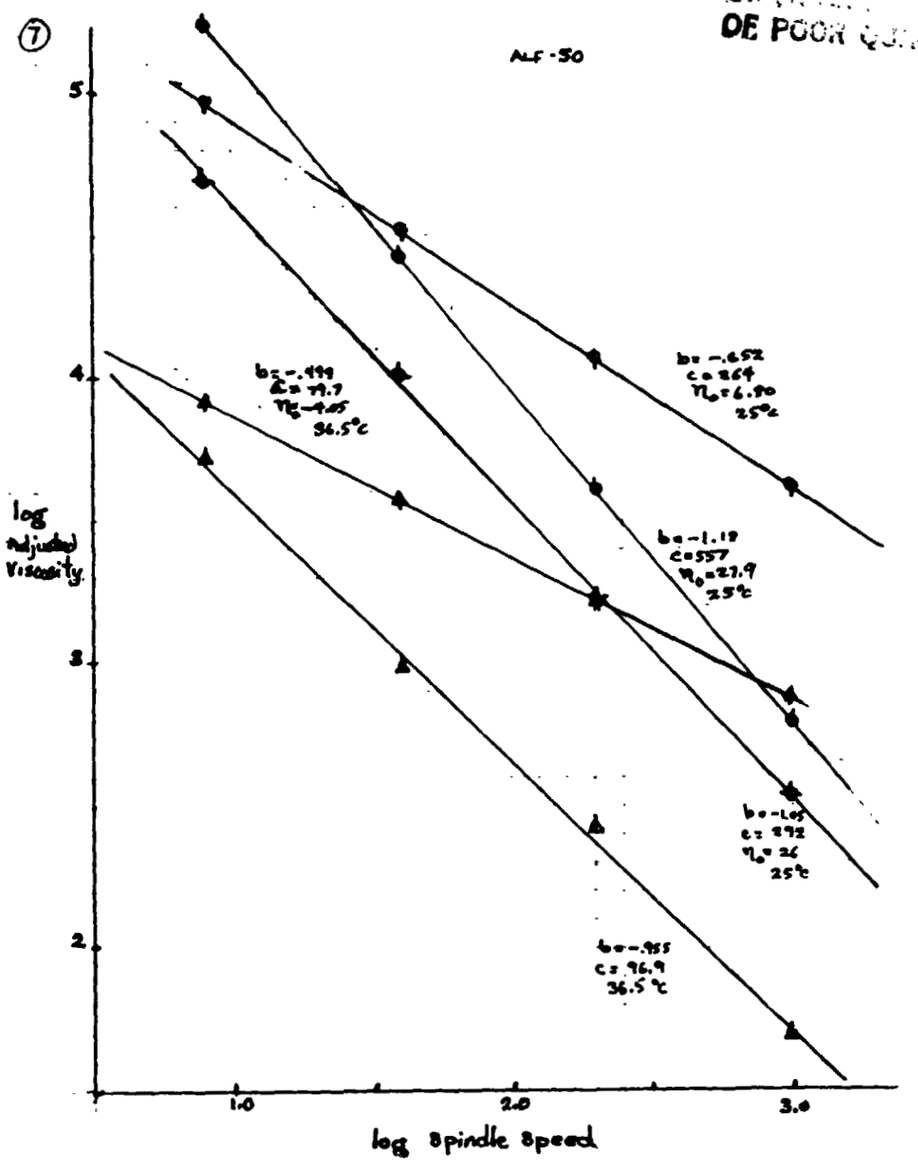

Log Viscosity vs Log Speed

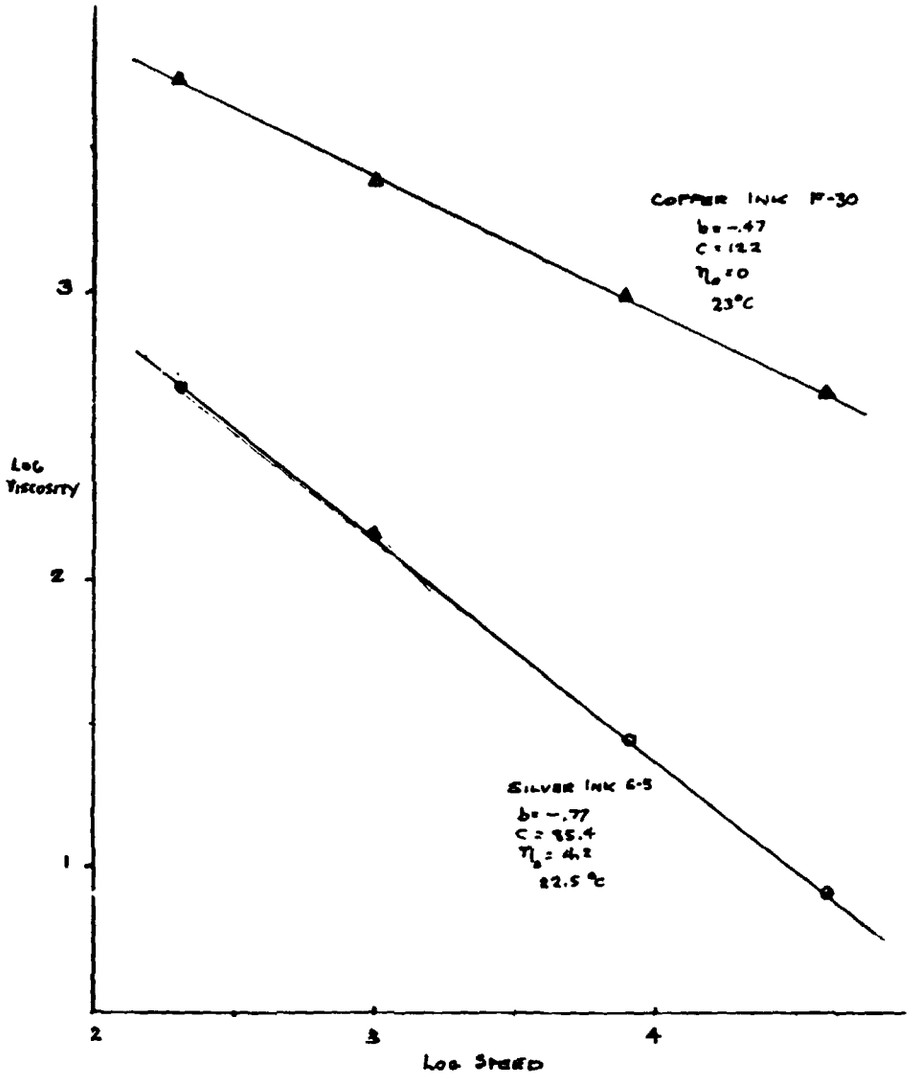

Conclusions

1. Good reproducibility of viscosity measurements for thixotropic materials requires scheduled measurements and close temperature control

2. Constants relating to material rheology may be calculated from 3 or more measurements at different shear rates and an iterative computer program.

3. Further work relating to the interpretation of viscosity constants is desirable

EVALUATION OF THE ION IMPLANTATION PROCESS FOR PRODUCTION OF SOLAR CELLS FROM SILICON SHEET MATERIALS

SPIRE CORP.

M.B. Spitzer

Objectives

- APPLY THE ION IMPLANTATION PROCESS TO PRESENT-DAY MATERIALS AND FABRICATE CELLS
- INVESTIGATE TEMPERATURE EFFECTS
- COMPARE THERMAL ANNEALING TO PULSED ELECTRON BEAM ANNEALING

Status of Program

- TECHNICAL WORK COMPLETE
- CELL DELIVERIES COMPLETE
- FIRST DRAFT OF FINAL REPORT APPROVED BY JPL
- PREPARATION OF FINAL COPY IN PROGRESS

Anneals Investigated

- ONE-STEP
  - 2 HOURS AT EITHER 550, 650, 750, OR 850°C
- TWO-STEP
  - 15 MIN AT EITHER 550, 650, 750 OR 850°C
  - FOLLOWED BY 1 HOUR AT 550°C
- THREE-STEP
  - 550°C-2 HRS.
  - 850°C-15 MIN.
  - 550°C-2 HRS.
- PULSED ELECTRON BEAM ANNEAL
  - SPI-PULSE 7000
  - ~1 J/cm^2
  - ~50 μsec PULSE WIDTH

Cell Process Sequence

NOTE: NO AR COATING, NO BSF

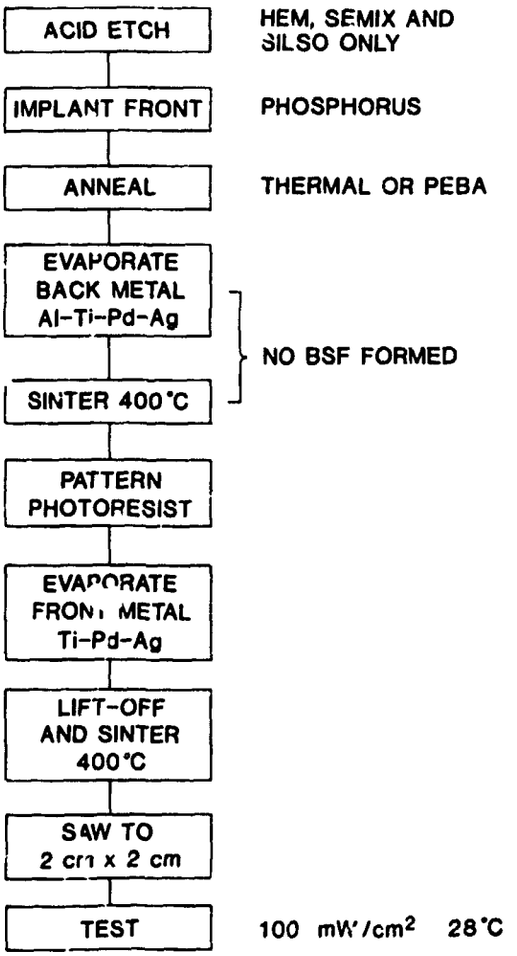

J_{SC} Analysis of One-Step Anneal

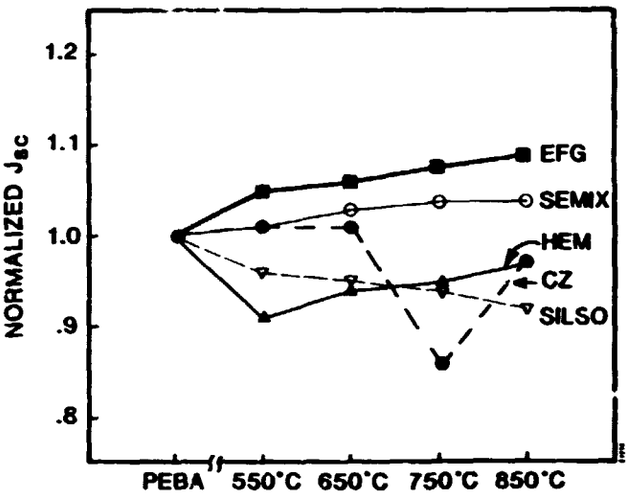

Spectral Response for Cz Controls Processed With a Single-Step 2-Hour Anneal

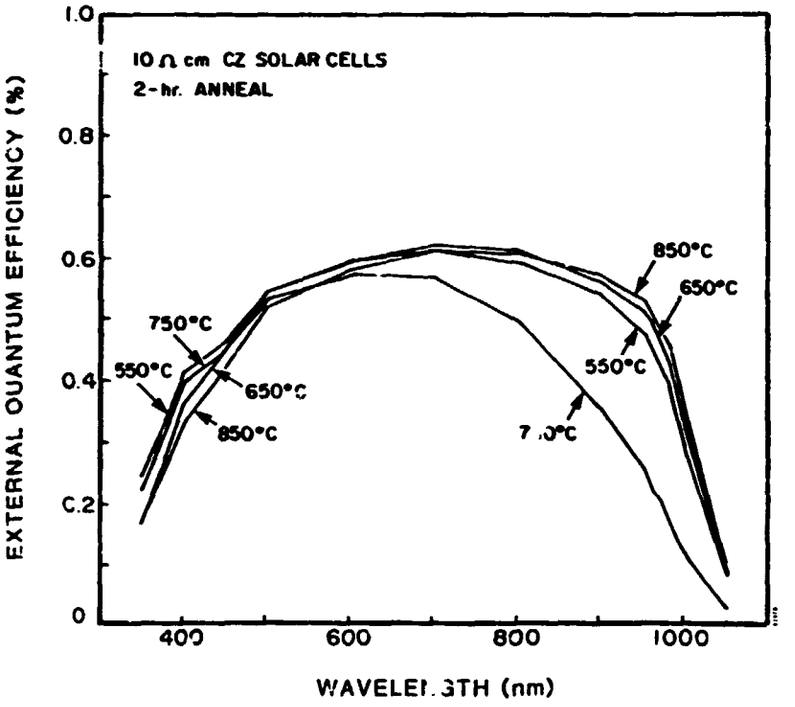

External Quantum Efficiency of EFG Cells Annealed With a Single-Step Process and With PEBA

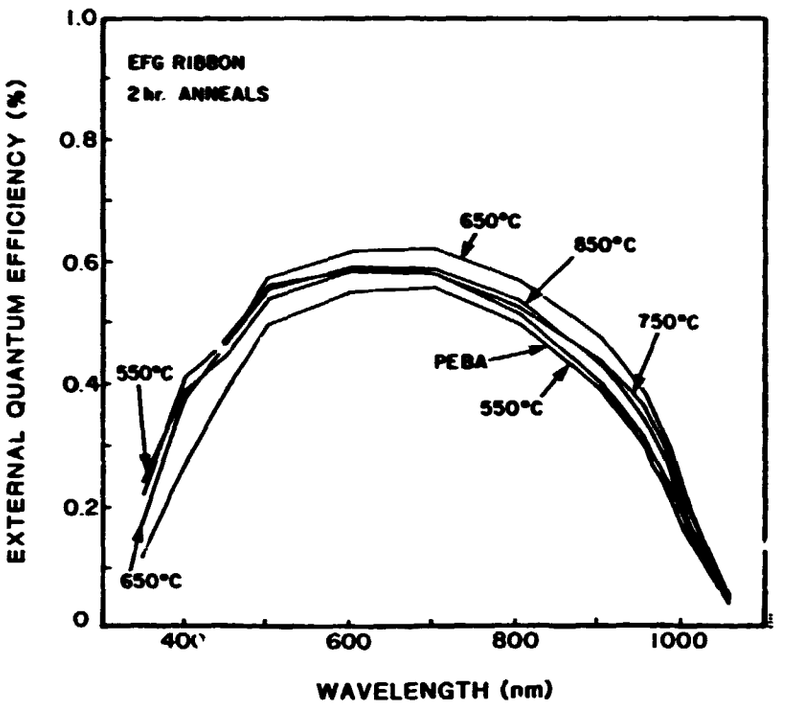

Spectral Response of Silso Cells Processed With One-Step Annealing

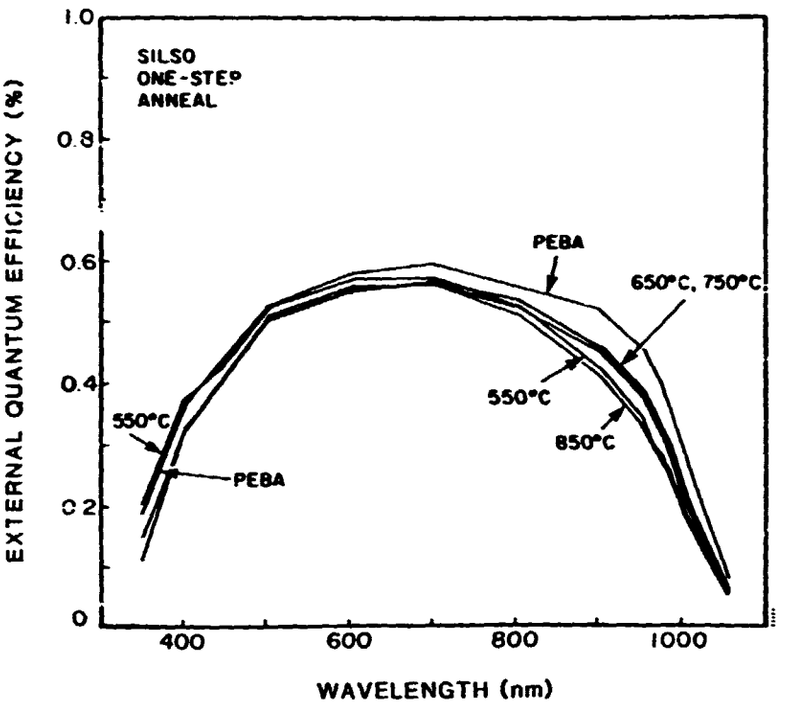

J_{SC} Analysis of Two-Step Anneal

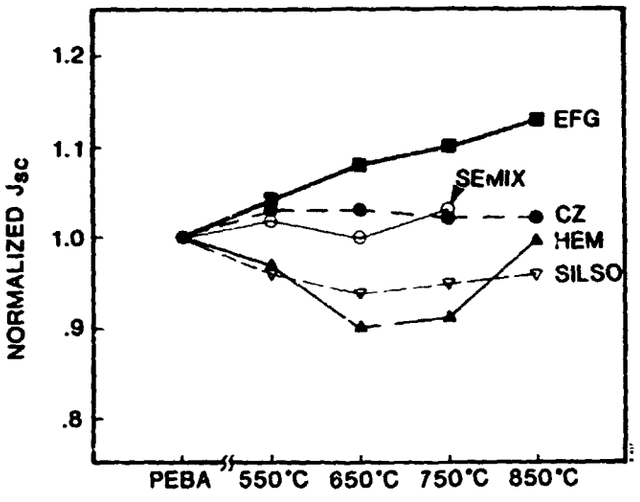

External Quantum Efficiency of Cz Control Cells Annealed With a Two-Step Process

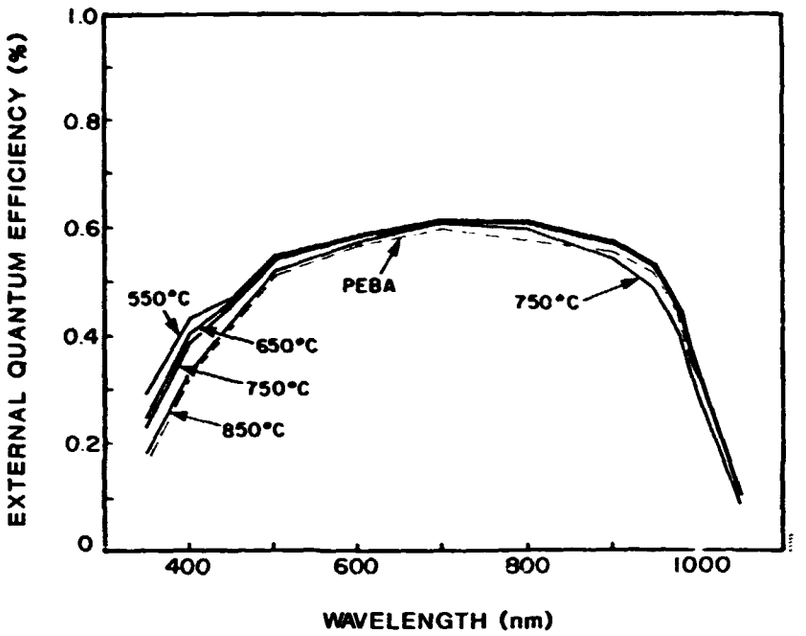

External Quantum Efficiency of EFG Cells Annealed With a Two-Step Process and With PEBA

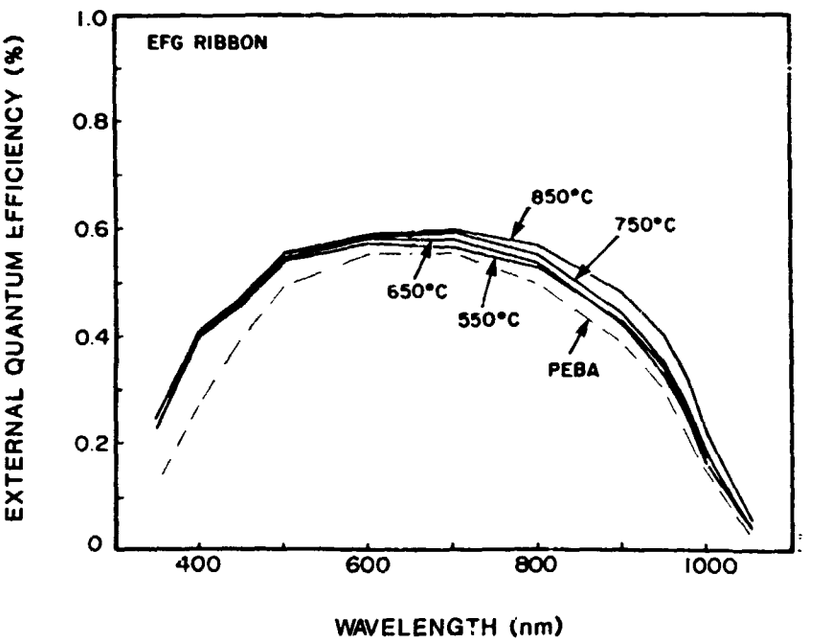

External Quantum Efficiency of HEM Cells Annealed With the Two-Step Process

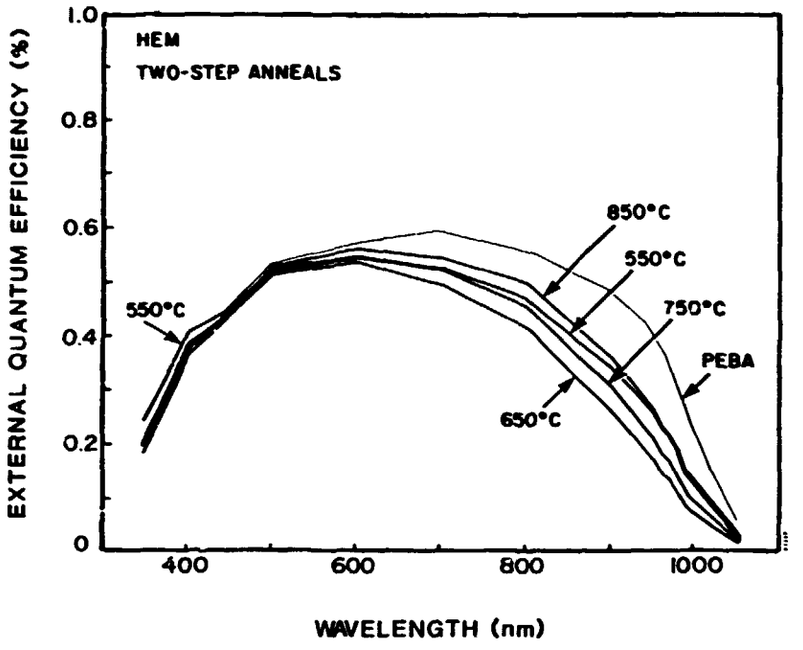

Spectral Response of Silso Cells Processed With a Two-Step Tnermal Anneal

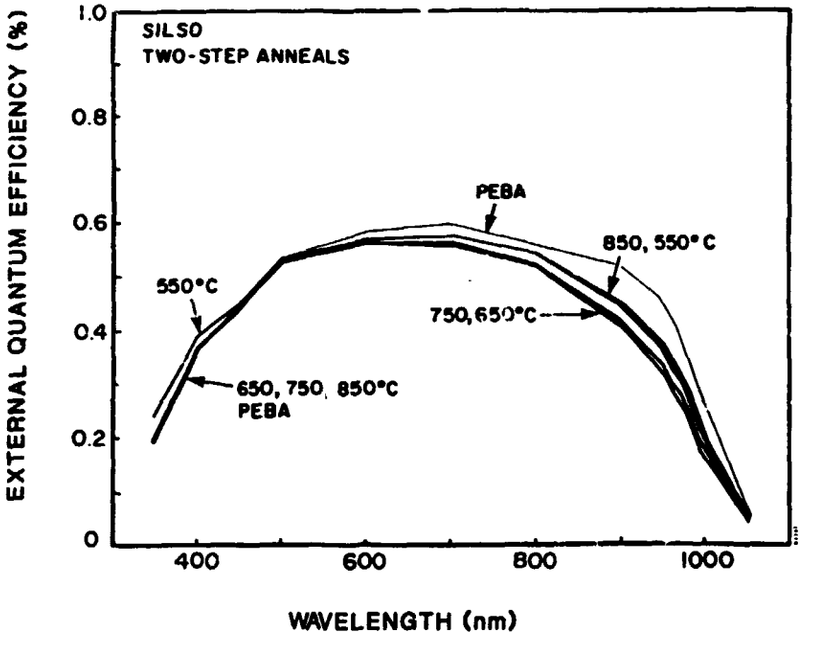

Average AM1 Performance of the PEBA-Processed Cz Control Group

IMPLANT ENERGY	V_{oc} (mV)	J_{sc} (mA/cm^2)	FF (%)	Eff (%)	Eff x 1.41 (%)
5 keV	508	23.0	65.9	7.71	10.9
(20 CELLS)	(25)	(0.3)	(2.5)	(0.67)	(0.9)
4436-1f	531	23.0	71.3	8.71	12.3
10 keV	521	23.3	68.9	8.39	11.8
(15 CELLS)	(13)	(0.5)	(4.9)	(0.88)	(1.2)
4387-17f	534	23.4	75.9	9.48	13.4
15 keV	520	23.5	69.2	8.47	11.9
(20 CELLS)	(18)	(0.2)	(3.8)	(0.77)	(1.1)
4335-2b	536	23.5	73.1	9.23	13.0

NOTES: INSOLATION WAS AM1, 100 mW/cm^2. T=28°C. STANDARD DEVIATION SHOWN IN PARENTHESIS. THE BEST CELL IN EACH GROUP IS ALSO INDICATED.

Pulsed Electron Beam Annealing of Silicon Sheet Materials

MATERIAL (No. OF CELLS)	V_{oc} (mV)	J_{sc} (m\/cm^2)	FF (%)	Eff (%)	Eff x 1.4 (%)
CZ (15)	521	23.3	68.9	8.93	11.7
BEST CZ	534	23.4	75.9	9.48	13.3
HEM (15)	525	22.3	70.9	8.29	11.6
BEST HEM	531	22.8	73.1	8.87	12.4
SILSO (15)	519	21.0	69.5	7.60	10.6
BEST SILSO	542	21.5	73.3	8.53	11.9

Conclusions

- USE OF ION IMPLANTATION ALLOWS TAILORING OF THERMAL PROCESS TO A PARTICULAR SHEET MATERIAL
- EFG IS IMPROVED AFTER HIGH TEMP
- SILSO IS DEGRADED AFTER HIGH TEMP
- HEM AFFECTED MOST AT 550–750 C
- SEMIX APPEARS INDEPENDENT OF PROCESS TEMP
- CZ IS DEGRADED BY PROCESSING AT 750 C
- ION IMPLANTATION AND RAPID THERMAL ANNEALING CAN BE SUCCESSFULLY EMPLOYED FOR JUNCTION FORMATION

SPECTRAL RESPONSE OF HEM SOLAR CELLS ANNEALED WITH A ONE-STEP PROCESS

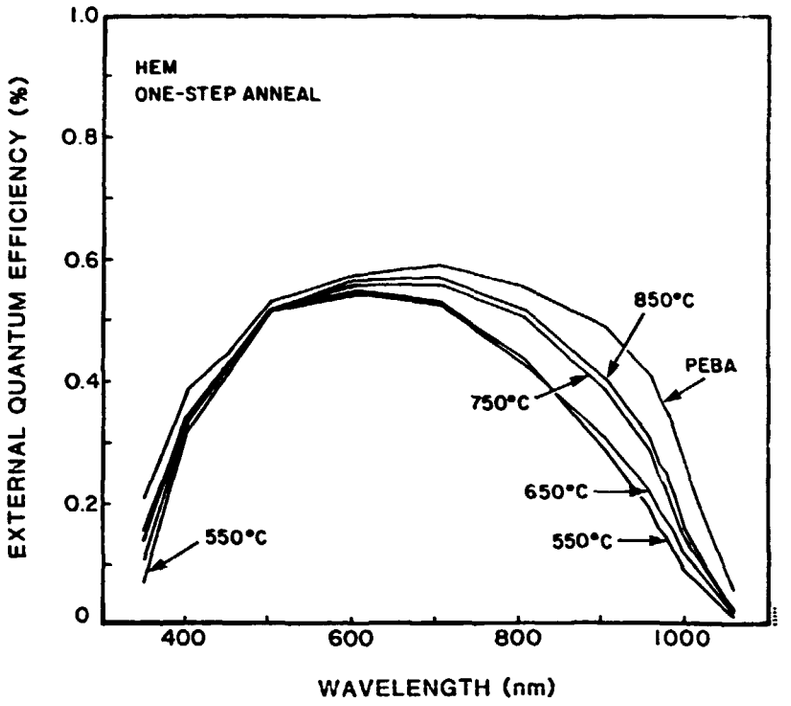

SPECTRAL RESPONSE OF SEMIX CELLS PROCESSED WITH A ONE-STEP ANNEAL

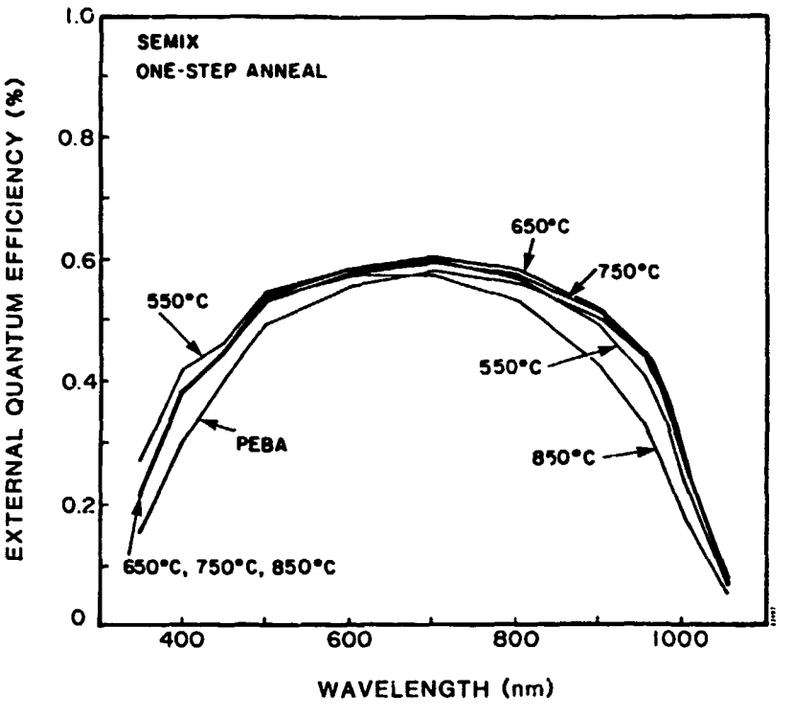

LASER-ASSISTED SOLAR-CELL METALLIZATION PROCESSING

WESTINGHOUSE ELECTRIC CORP.

S. Dutta
P.G. McMullin

Milestone Chart

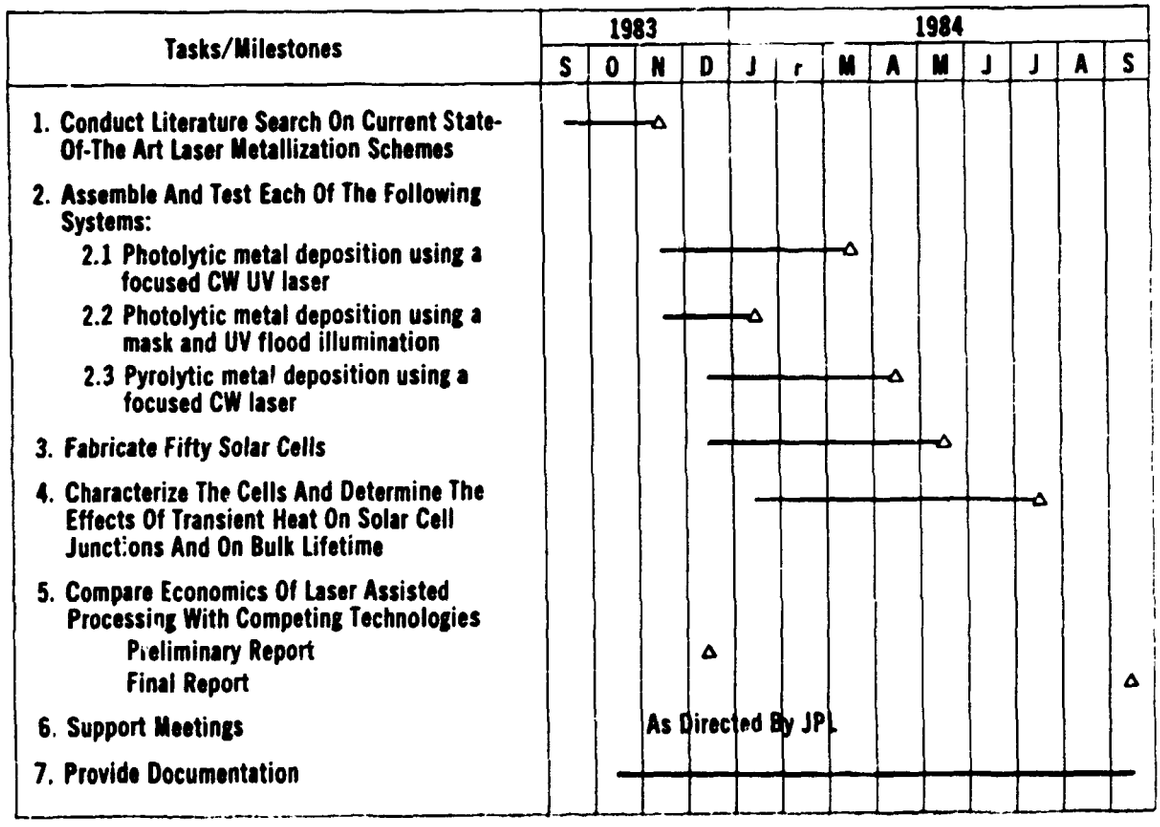

A Conventional Metallization System Employs A Sequential Multistep Process:

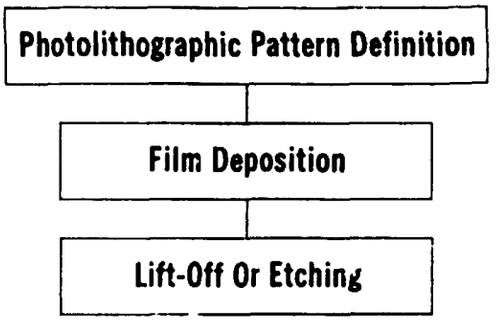

Laser-Assisted Metallization Techniques Are Essentially One-Step Processes:

Potential Advantages of Laser Disposition Techniques for Photovoltaic Systems

- High Resolution
- No Photolithography
- Clean And Contamination - Free
- In-Situ Sintering
- Low Contact Resistance

Laser-Assisted Deposition Techniques

Pyrolytic Deposition (Thermal)

- Laser Chemical Vapor Deposition (LCVD)
- Laser Deposition From Solutions

Photolytic Deposition (Non-Thermal)

- Laser Photodissociation Of Vapors
- Laser Photodissociation Of Solutions

Laser Assisted Electroplating

Experimental Setup for Laser-Assisted Electroplating

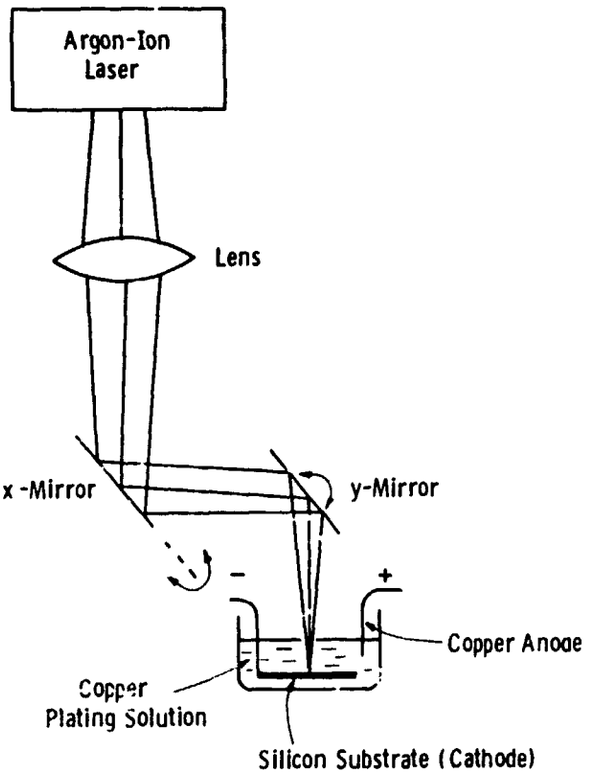

Photolytic Deposition

Laser-Induced Photodecomposition of Gas-Phase Organometallic Compounds:

This Technique is Fundamentally Different from Thermally Based Laser Processes

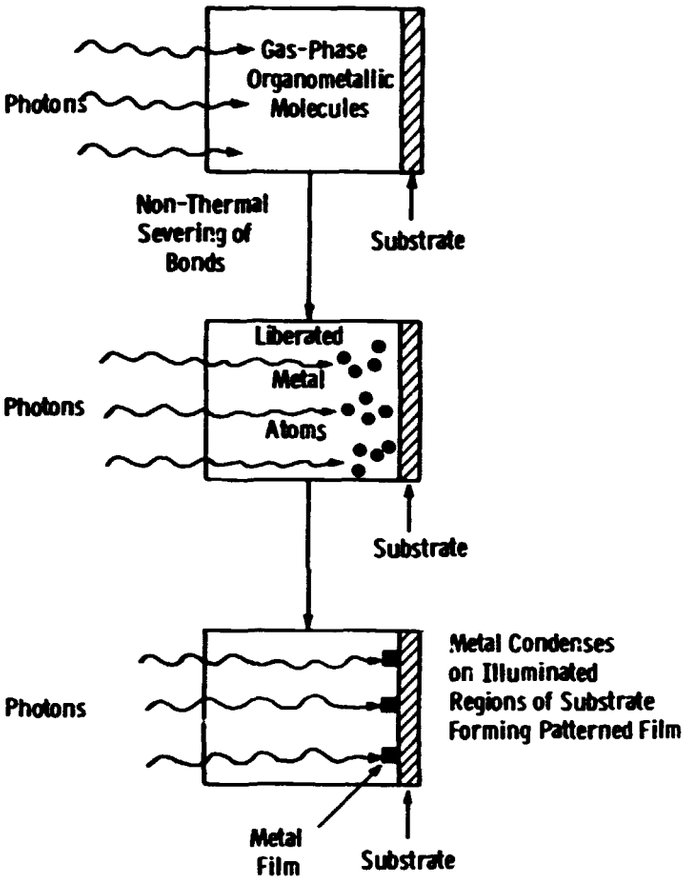

Experimental Setup for Laser-Assisted Photolysis

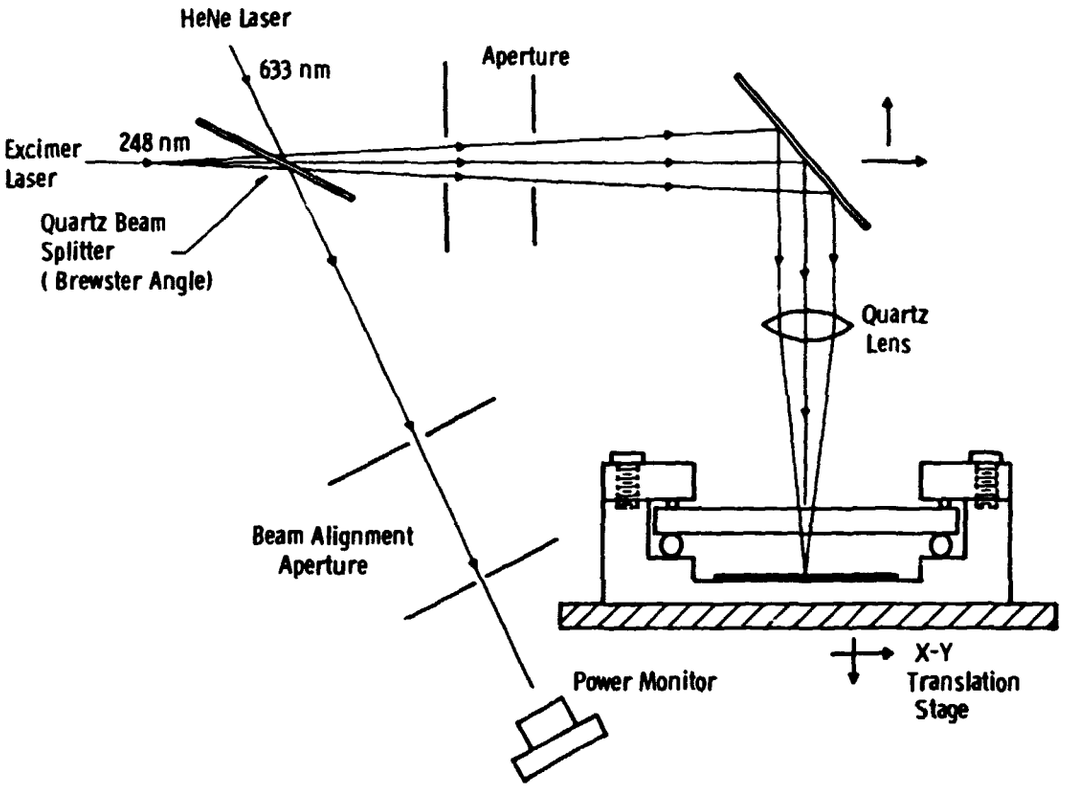

Experimental Setup for Laser-Assisted Electroplating

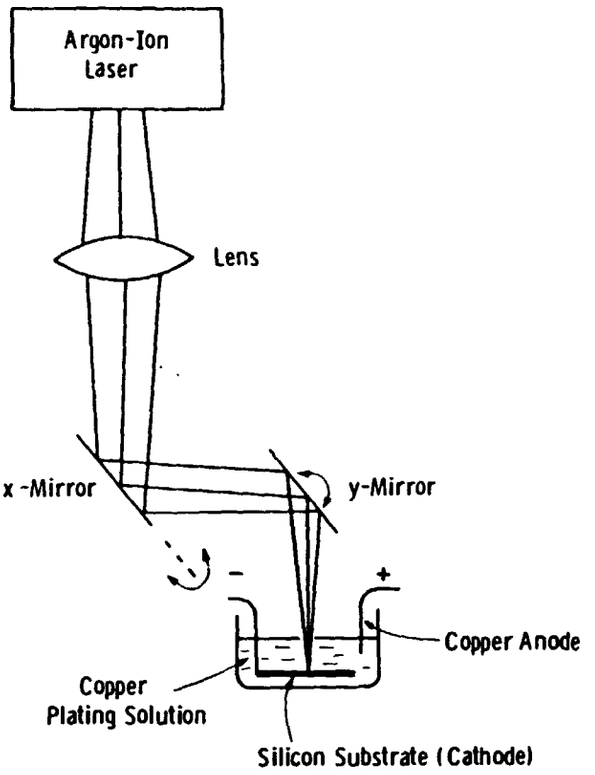

Laser Power Dependence of Electroplated Spot Size

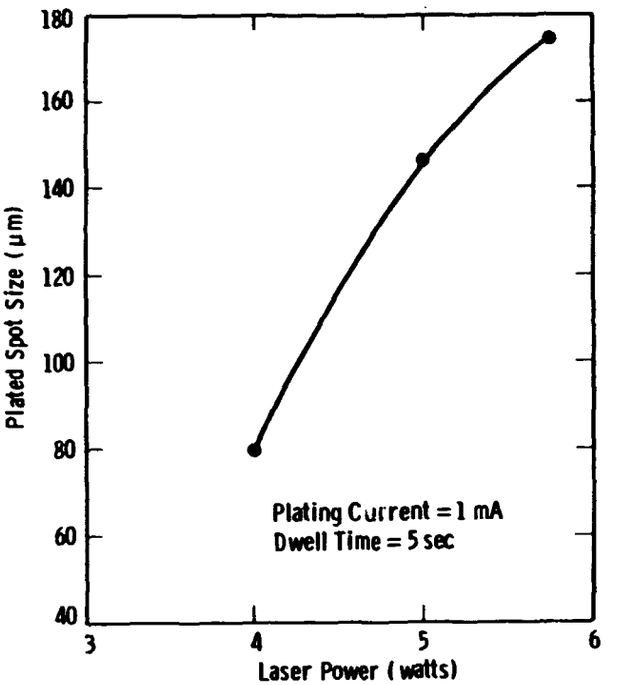

Summary of Laser-Assisted Electroplating Results

- **Novel Technique For Greatly Enhancing Local Plating Rates – Yield Fine-Line, Directly-Written Patterns With Excellent Adhesion**
- **Multiple Rapid Laser Scans Yield Finer, More Even Line And Higher Local Plating Rate Than Single Slow Scan (Same Total Exposure Time)**
- **Plated Linewidth Depends On Laser Power, Plating Current, And Electrolyte Level**
- **25 μm Linewidth And 12 μm/sec Local Plating Rate Obtained**

Laser Pyrolysis of Spun-on Metallo-Organic Film

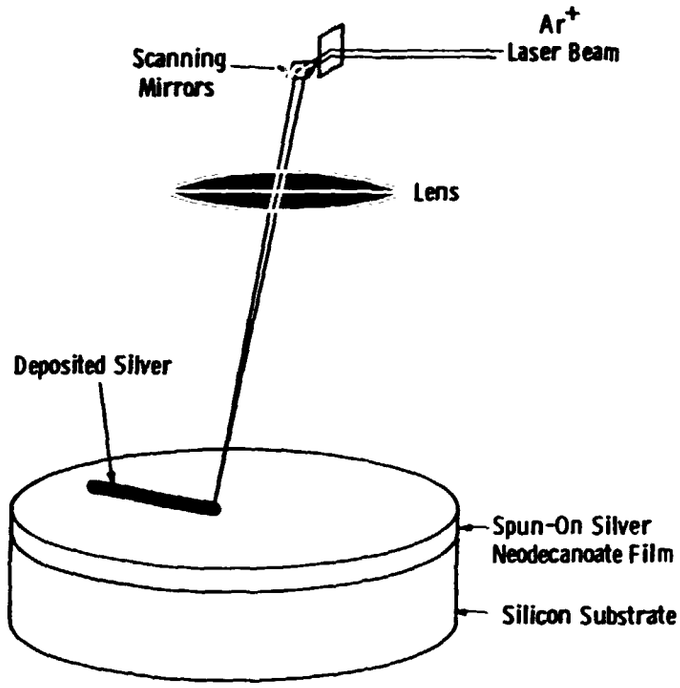

Sample Base Temperature 100°C

Focussed Laser Spot Decomposes Spun-On Film

Silver Metallization Patterns are Formed by Direct-Writing

Laser-Deposited Line Width vs Laser Power

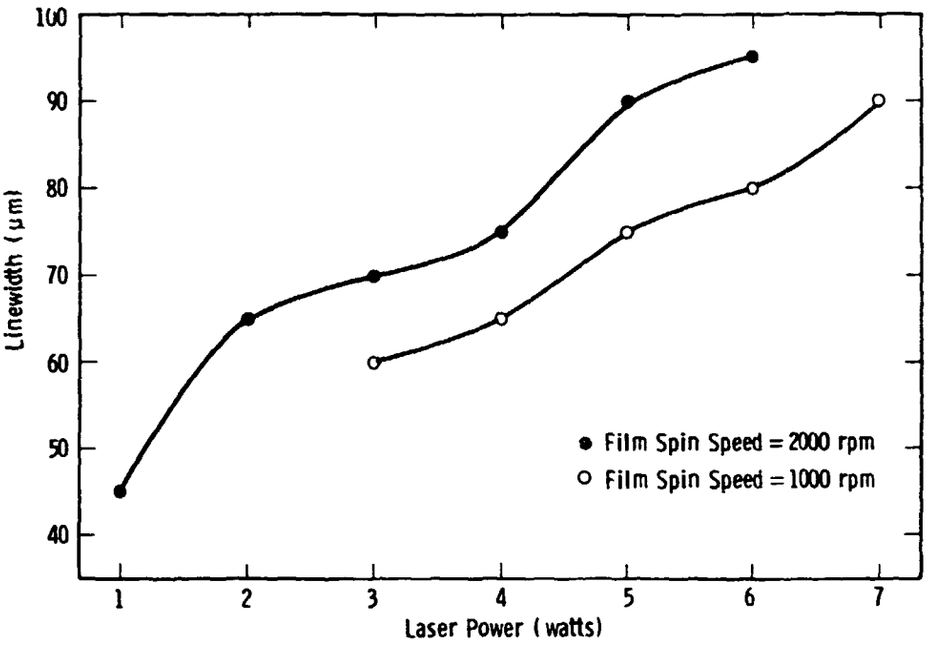

Status

Laser-Assisted Gas-Phase Photolysis

- Sample Chamber And Gas-Fill/Pumping Station Designed And Constructed
- Initial Deposition Of Titanium And Tin Planned

Laser-Enhanced Electroplating

- Exciting Early Results Using Copper Plating Solution
- 25 μm Linewidth And 12 μm/sec Local Plating Rate Achieved

Laser Decomposition Of Spun-On Metallo-Organic Films

- Ability To Rapidly Laser-Write Solar Cell Metallization Pattern Demonstrated
- Adhesion Being Studied

ION CLUSTER BEAM DEPOSITION RESEARCH

JET PROPULSION LABORATORY

Dennis Fitzgerald

Objectives and Present Plan

OBJECTIVES

- TO VERIFY CLAIMED RESULTS OF JAPANESE WORKERS WITH RESPECT TO METAL DEPOSITION ON SILICON.
- TO INVESTIGATE OTHER PV APPLICATIONS OF ICB SUCH AS DIELECTRIC AND SEMICONDUCTOR DEPOSITION.
- TO CHARACTERIZE ICB BEAM AS A FUNCTION SOURCE PARAMETERS.

PLAN

- FABRICATE/TEST ICB SOURCE FOR SILVER DEPOSITION.
- DEPOSIT SILVER CLUSTERS ON SILICON AND GLASS SUBSTRATES FOR EVALUATION AND DETERMINATION OF PROPER DEPOSITION PARAMETERS. (PULL TESTS, CONTACT RESISTANCE, UNIFORMITY, DEPOSITION RATE).
- DEPOSIT SILVER CLUSTERS THROUGH MASK TO METALLIZE FRONT OF SOLAR CELL AND MEASURE I-V (PERFORMANCE, FILL FACTOR, ENVIRONMENTAL DEGRADATION, ETC.)

Ion Cluster Beam Assembly

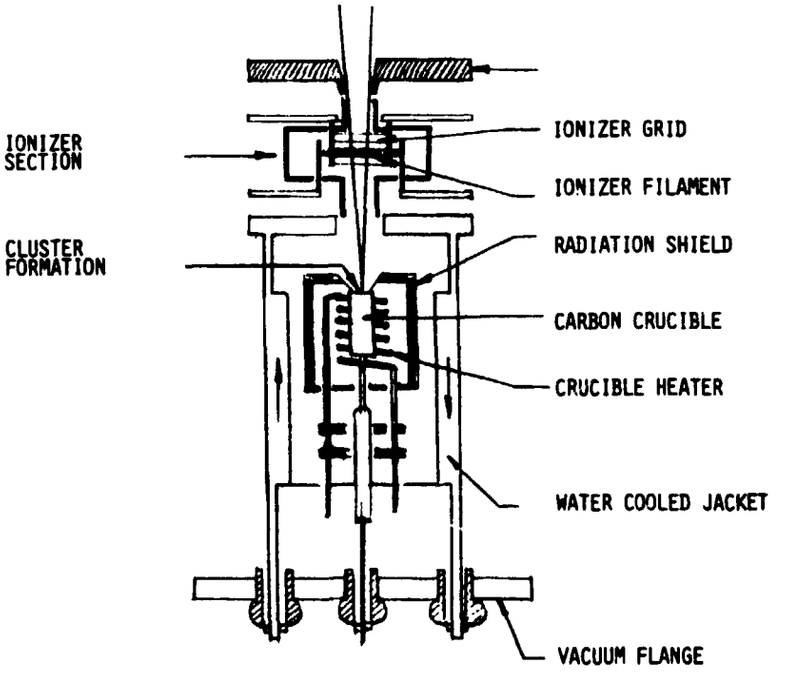

Problems and Solutions

- IONIZER FILAMENT WIRE SIZE INCREASED AND SPRING WOUND TO PROTECT AGAINST THERMAL AND MECHANICAL STRESS.
- CRUCIBLE HEATER DESIGN CHANGED TO PROVIDE BETTER SUPPORT FOR FILAMENTS AT OPERATING TEMPERATURE (2400°C).
- TOP CRUCIBLE SUPPORT ELIMINATED TO REDUCE HEAT LOSS AND VAPOR CONDENSATION ON SUPPORT STRUCTURE.
- ELECTRON BEAM SUPPLY MODIFIED TO PROVIDE BETTER MATCH TO LOAD REQUIREMENTS.
- LOWER CRUCIBLE SUPPORT BEING MODIFIED TO PREVENT ARCS DURING E-BEAM OPERATION.
- VAPOR CONDENSATION ON STRUCTURE SURROUNDING CRUCIBLE IS A WASTE OF MATERIAL, CONTAMINATES RADIATION SHIELDING AND INSULATORS, AND THE VAPOR CAUSES ARCS IN E-BEAM REGION - CRUCIBLE NOZZLE BEING CONSIDERED FOR BETTER COLLIMATION OF MATERIAL.

ICB Experimental Setup

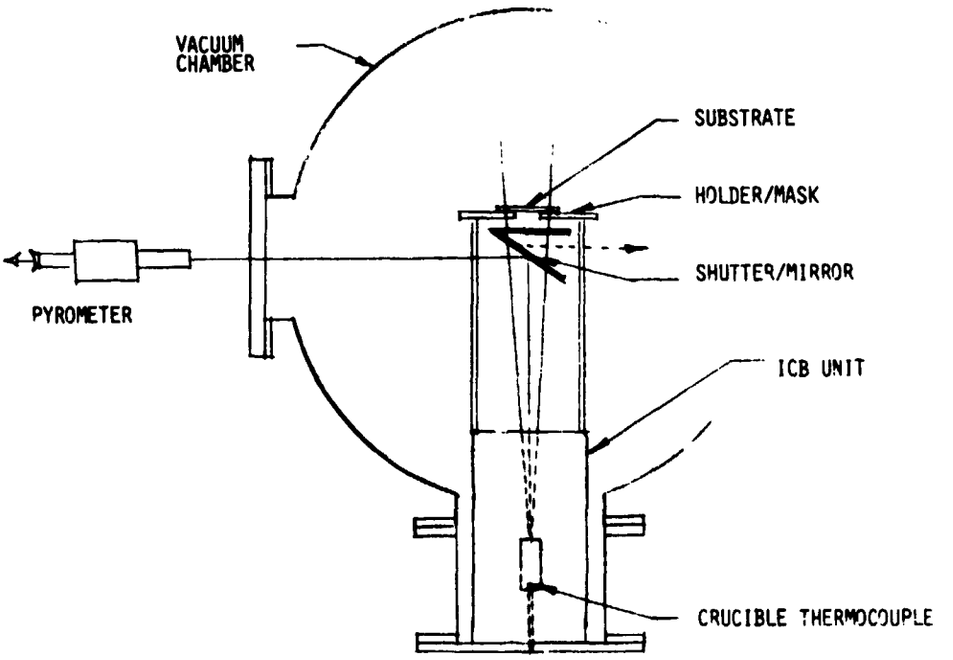

Results and Discussion

- CLUSTER FORMATION REQUIRES CRUCIBLE PRESSURE IN RANGE OF 1 TO 10 TORR (1350°C TO 1550°C FOR SILVER).
- PROBLEMS PRECLUDED OPERATION ABOVE 1400°C.
- SILVER DEPOSITION AT 1400°C LOOKED UNIFORM BUT FAILED TAPE PULL TEST (IONIZER 500V/200mA, 3kV ACCELERATION, SUBSTRATE AT 50°C).
- CURRENT ICB MODIFICATIONS SHOULD PERMIT OPERATION AT MUCH HIGHER TEMPERATURES.
- EARLY EXPERIMENTS INDICATE NEED FOR CLUSTER DETECTOR TO IDENTIFY PRESENCE AND SIZE OF CLUSTERS.
- MAY ALSO REQUIRE SUBSTRATE HEATER TO MAKE PROPER BOND OF METAL TO SUBSTRATE.

LARGE-AREA a-Si DEPOSITION CHAMBER(S)

JET PROPULSION LABORATORY

D.B. Bickler

Objective

Determine key parameters to be used in large-area deposition-chamber designs

Approach

Explore the multidimensional "parameter space" of a-Si deposition using a highly flexible learning apparatus to approximate optimal combinations

Milestone Chart

JET PROPULSION LABORATORY	FLAT-PLATE SOLAR ARRAY PROJECT	ORIGINAL SCHEDULE APPROVED: 10/01/83
APPROVAL RESPONSIBILITY M. T. Callaghan	Amorphous-Silicon Deposition Task	LAST SCHEDULE CHANGE: 12/25/83
ACHIEVEMENT RESPONSIBILITY D. B. Bickler		STATUS AS OF: 12/25/83

MILESTONES	CY	1983	1984										1985										
	FY	1984											1985										
		O	N	D	J	F	M	A	M	J	J	A	S	O	N	D	J	F	M	A	M	J	J	A	S
Large a-Si chamber operational						△																			
Three-chamber design req. identified							△																		
Three-chamber design review													△												
Demonstrate intrinsic a-Si deposition										▽															
Three-chamber construction complete											△														
Start gas reclaim study											▽														
Three-chamber system operational													△												
100 cm^2 ±2% thickness													▽												
Gas utilization report													▽												
Three-layer a-Si 1 ft^2 sample deposition																	△								
Dark & photoconductivity meas.									▽																

NOTES: 1. Key Project Milestones Underlined

△ = ACP Milestones

▽ = Non-ACP Milestones

Electrode Tests

- **STABILITY**
  - **Voltage range** 20% to 100%
  - **Pressure** 0.1 torr to 2 torr
  - **Spacing** 1/2 in to 2 in

- **UNIFORMITY**
  - **Corner effects (sharp points)**
  - **Sensitivity to spacing**
  - **Substrate influence ; Al , Si , glass**

Plasma Stability

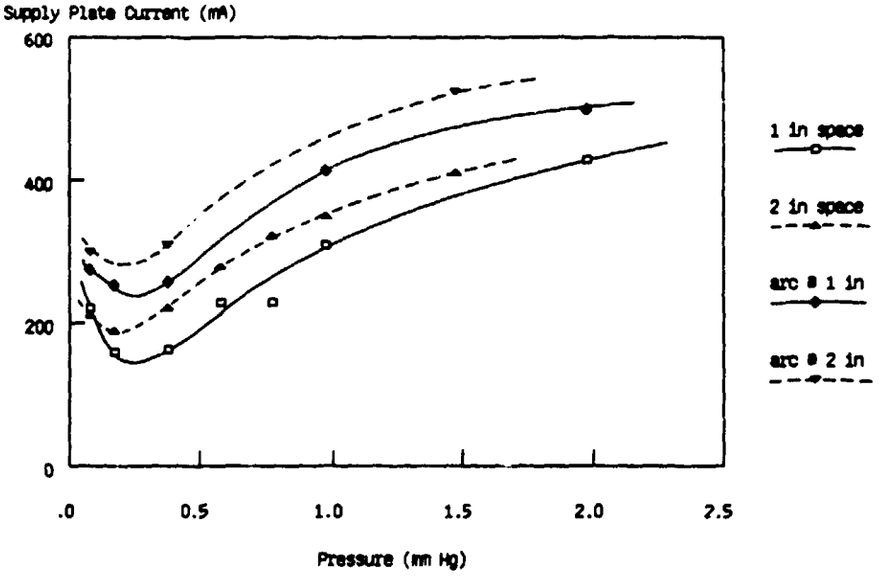

Silane Utilization Cost Influence

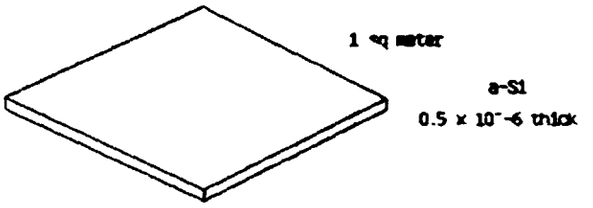

- 80 Watts output @ 8% eff.
- At 100% Silane utilization ,
  $10^4 cm^2 \times 0.5 \times 10^{-4} cm \times 2.33 g/cm^3 \times 32/28 = 1.33 g\ SiH_4$
- Silane cost 0.17 to 1.00 $/g
  @ 100% : (.17 to 1)$/g x 1.33g / 80 W = (.0028 to .0166)$/W
  @ 4% : ( ) x 25 = (.071 to .416)$/W

Deposition Dilemma

#1
EFFECTIVE SILANE UTILIZATION MEANS GAS DEPLETION WHICH YIELDS NON-UNIFORM GROWTH COMPOSITION.

#2
(TBD)

ADVANCED PROCESS TECHNOLOGIES

JET PROPULSION LABORATORY

D.B. Bickler

Material Application Methods

Energy Sources

Processing Techniques

New Contracts

Material Application Methods

- **Metallo-Organic Decomposition (M O D) metal films**
- **Ion Beams (implants, clusters, ion writing, etc.)**
- **Plasma**

Energy Sources

- **Lasers**
- **Electron Beams**
- **Microwaves**
- **R F**
- **Other Radiation (incoherent light etc)**

PROCESS DEVELOPMENT AND ADVANCED PROCESSES

Processing Techniques

- **Reduction of "cosumables"**
- **Yields**
- **Reliability (interlayer diffusion barriers,etc.)**

New Contracts

- **Excimer Laser (2)**
- **Microwave (Superwave)**

SILICON MATERIAL AND SHEET

A. Briglio, Jr., Chairman

Eleven presentations were made covering research on processes for refining silicon (Si) and on Si shaped-sheet technology.

A report was presented by JPL on the FSA-sponsored miniworkshop on the effects of stress and strain in high-speed-grown Si ribbons, held January 10 and 11 at the Westinghouse R&D Center, Pittsburgh, Pennsylvania.

Mobil Solar Energy Corp. reported on its work to develop an understanding of stress generation in Si sheet growth and to define configurations for growing low-stress ribbon at high speeds by the edge-defined film-fed growth (EFG) process. One finding was that significant creep occurs at temperatures as low as 1050°C.

Westinghouse Electric Corp. described its program to investigate the dendritic-web Si ribbon-growth process. Emphasis is currently being placed on the modeling and experimental evaluation of hardware configurations that use dynamic positioning of the critical elements during growth to obtain the best conditions for producing low-stress ribbon at high speeds.

The University of Illinois at Chicago presented results of its study to determine nondestructively the residual stresses in Si sheet, using laser interferometry for polished surfaces and Moire interferometry for rough surfaces. Using these techniques, residual stresses were measured in a Czochralski wafer and in EFG ribbon.

The Solar Energy Research Institute (SERI) described results obtained from a study of low-angle Si sheet, using a combination of secondary electron imaging, electron channeling, and EBIC techniques in a scanning electron microscope. Correlations of the structural and electrical properties of defects in the sheet material were obtained.

Semix Inc. reported on defect analysis of semicrystalline Si and thermal analysis of the ubiquitous crystallization process (UCP), which produces this material. The studies showed that a degraded structure can form in the solid behind the crystallization front due to thermal stresses, and as a result the local photovoltaic properties can be adversely affected.

Energy Materials Corp. reported on two efforts. One is for a scaled-up demonstration of a fused-salt electrochemical cell for refining metallurgical-grade Si. The system was operated in its first test, and examination of the product revealed that water was present, indicating incomplete drying of the system before the test. The other program, which had just started at the time of the PIM, is for continuation of development of the low-angle silicon sheet (LASS) process that had been previously supported by SERI. The technology involved, status, and plans were described.

SILICON MATERIAL AND SHEET

Union Carbide Corp. (UCC), presented information on its research on pyrolysis of silane in fluidized-bed reactors (FBRs) to make Si. Long-duration tests (one of nearly 45 hours) were made to demonstrate operability and determine product purity. The results showed metallic contamination from the reactor wall; modifications are being made to improve purity.

JPL described results of its research on deposition of Si from silane in FBRs. As with the UCC tests, JPL results showed contamination of the product by the wall material, and appropriate changes are being made to prevent this. Scavenging of fine particles produced in the FBR was shown to be feasible by secondary injection of small amounts of silane above the distributor.

Caltech described progress in a study of the formation and growth of Si particles by pyrolysis of silane in free-space reactors, with the aim of controlling the process to avoid or minimize the generation of fine particles. Significant increases in particle size were obtained.

SERI reported on its investigation of a process for refining metallurgical-grade Si by a chemical-vapor transport process, in which a $Cu:Cu_3Si$ anode reacts with HCl to form chlorosilanes, which are then decomposed on hot Si filaments to produce pure Si. The Si transport rate in the process was measured, and the results support the hypothesis that the transport is limited by diffusion of Si in the anode.

SILICON MATERIAL AND SHEET

A. Briglio, Jr., Chairman

MINIWORKSHOP ON EFFECTS OF STRESS AND STRAIN IN HIGH-SPEED-GROWN SILICON RIBBONS

JET PROPULSION LABORATORY

A. Briglio, Jr.

- HELD JANUARY 10, 11, 1984 AT WESTINGHOUSE R & D CENTER, PITTSBURGH, PA.
- SECOND STRESS/STRAIN MINI-WORKSHOP TO BE HELD
- 1ST WAS IN NOVEMBER 1982 AT MOBIL SOLAR ENERGY CORP., WALTHAM, MA
- THIRD MINI-WORKSHOP EXPECTED TO BE HELD IN LATTER HALF OF 1984

- GOAL OF STRESS/STRAIN PROGRAM: UNDERSTAND AND OVERCOME PROBLEM OF STRESS AND STRAIN THAT IS LIMITING RATE AT WHICH SI RIBBONS OF SUITABLE QUALITY FOR MAKING SOLAR CELLS CAN BE GROWN.
- PURPOSE OF WORKSHOP
  - ACQUAINT PARTICIPANTS WITH WORK THAT IS GOING ON
  - OPEN DIRECT COMMUNICATIONS BETWEEN PARTICIPANTS
  - IDENTIFY ASSUMPTIONS BEING USED IN WORK, TO ASSURE A COMMON BASE
  - IDENTIFY WORK NEEDED TO UNDERSTAND STRESS/STRAIN PROBLEM

STRESS/STRAIN MINIWORKSHOP

Agenda

JANUARY 10, 1984

OPENING REMARKS	A. MORRISON
WELCOME	DR. JOHN HULM (ACTING MANAGER, WESTINGHOUSE R & D CENTER)
STRESS BUCKLING MODEL	PROF. OSCAR DILLON (UNIV. OF KENTUCKY)
STRAIN-RELATED DEFECTS	PROF. OSCAR DILLON (UNIV. OF KENTUCKY)
JPL STRESS/STRAIN MEASUREMENTS ON SILICON RIBBON	T. O'DONNELL (JPL)
MOBIL SOLAR'S STRESS/STRAIN PROGRAM	DR. J. KALEJS (MOBIL SOLAR ENERGY CORP.)
NON-DESTRUCTIVE DETERMINATION OF RESIDUAL STRESSES IN SHEET SILICON	PROF. S. DANYLUK/DR. A. ANDONIAN (UNIV. OF ILLINOIS AT CHICAGO)
STRESS/STRAIN MODEL	PROF. J. HUTCHINSON (HARVARD UNIV.)

JANUARY 11, 1984

WESTINGHOUSE STRESS/STRAIN APPROACH	DR. R. SEIDENSTICKER/DR. S.-Y. LIEN (WESTINGHOUSE ELECTRIC CORP.)
GENERAL DISCUSSION	OPEN
FUTURE RESEARCH ACTIVITIES DISCUSSION	OPEN
SUMMARY REVIEW OF MEETING	DOE/SERI/JPL PERSONNEL

SILICON MATERIAL AND SHEET

- STRESS BUCKLING MODEL (DILLON)
  - UNIV. OF KY DEVELOPING BUCKLING MODEL FOR SI RIBBONS
  - CALCULATED THICKNESS AT WHICH BUCKLING OCCURS, ASSUMING, FOR EXAMPLE:
    - TEMPERATURE IS FUNCTION ONLY OF DISTANCE ALONG RIBBON LENGTH
    - MATERIAL IS ELASTIC WITH CONSTANT MATERIAL PROPERTIES
  - OBTAINED RELATIONSHIP OF CRITICAL THICKNESS (THICKNESS BELOW WHICH RIBBON BUCKLES) VS WIDTH. RESULTS ARE REASONABLY CONSISTENT WITH WESTINGHOUSE EXPERIMENTAL RESULTS
  - NEW BUCKLING ANALYSIS DESCRIBED WITH EQUATIONS INVOLVING VARIOUS BUCKLING MODES, EXTENDING INTO NON-LINEAR MATERIAL BEHAVIOR
- STRAIN-RELATED DEFECTS (DE ANGELIS)
  - CALCULATION OF DISLOCATION DENSITY
  - CALCULATION OF STRESS/STRAIN RELATIONSHIPS AS FUNCTIONS OF SUCH VARIABLES AS TEMPERATURE, DISLOCATION DENSITY, OXYGEN CONTENT, AND STRAIN RATE
- JPL STRESS/STRAIN MEASUREMENTS ON SILICON RIBBON (O'DONNELL)
  - DENDRITIC WEB RIBBON
    - RESIDUAL STRESS MEASURED BY USE OF STRAIN GAGES ON DEFORMED RIBBON
    - WITH ONE SAMPLE OF DEFORMED RIBBON, MEASURED RESIDUAL STRESSES RANGING FROM 200 PSI IN COMPRESSION TO 1000 PSI IN TENSION
  - EFG RIBBON
    - MADE VARIOUS MEASUREMENTS INCLUDING SURFACE PROFILES LENGTHWISE AND ACROSS RIBBON
    - DETERMINED DISLOCATION DENSITY BY IMAGE ANALYSIS
  - RESOLUTION OF WHETHER OBSERVED RIBBON DEFORMATIONS ARE ELASTIC OR PLASTIC AND CORRELATION WITH GROWTH CONDITIONS ARE NEEDED
- MOBIL SOLAR'S STRESS/STRAIN PROGRAM (KALEJS)
  - GOALS: DEVELOP UNDERSTANDING OF STRESS-GENERATION MECHANISM IN SI SHEET GROWTH AND DEFINE MINIMUM - STRESS GROWTH CONFIGURATIONS FOR 200-μM-THICK, 10-cm-WIDE EFG RIBBON GROWING AT 4 CM/MIN
  - CREEP STUDIES, TEMPERATURE FIELD MODELING AND MEASUREMENT, RESIDUAL STRESS MEASUREMENT
  - CREEP STUDIES (FOUR-POINT BENDING TESTS): SIGNIFICANT PLASTIC FLOW EVEN AS LOW AS 1050°C.
  - TEMPERATURE - MEASURING SYSTEM USING FIBER OPTICS BEING DEVELOPED

NON-DESTRUCTIVE DETERMINATION OF RESIDUAL STRESSES IN SHEET SILICON (DANYLUK, ANDONIAN)

- METHOD OF DETERMINING RESIDUAL STRESS BEING DEVELOPED, INVOLVING:
  - APPLY EXTERNAL LOAD TO SILICON SAMPLE
  - EXPERIMENTALLY MEASURE DISPLACEMENT USING LASER INTERFEROMETRY
  - ANALYTICALLY COMPUTE DEFLECTION
  - RELATE DIFFERENCE BETWEEN MEASURED AND COMPUTED DEFLECTIONS TO RESIDUAL STRESS
  - SCHEME FOR USING LASER INTERFEROMETRY BEING DEVELOPED FOR EXPERIMENTAL MEASUREMENT OF DEFLECTIONS, USING MOIRE PATTERNS

- STRESS/STRAIN MODEL (HUTCHINSON)
  - SIMPLIFIED MODEL DEVELOPED FOR BEHAVIOR OF STRESSES VERY NEAR MELT INTERFACE
  - MODEL SOLVED FOR DIFFERENT VALUES OF STRESS AT THE GROWTH INTERFACE
  - BEYOND ABOUT 0.1 CM FROM GROWTH INTERFACE, LATERAL STRESS AT RIBBON CENTERLINE IS INDEPENDENT OF INITIAL STRESS. INITIAL STRESS GETS RELAXED VERY QUICKLY. IN EFFECT, SI AT INTERFACE BEHAVES AS FLUID.
- WESTINGHOUSE STRESS/STRAIN APPROACH (SEIDENSTICKER/LIEN)
  - APPLICATION OF COMPUTER MODELS TO GROWTH SYSTEM DESIGN (SEIDENSTICKER)
    - TEMPERATURE MODEL - COMPUTES TEMPERATURE ALONG WEB RIBBON
    - STRESS MODEL - CALCULATES THERMALLY GENERATED STRESS IN WEB RIBBON
    - BUCKLING MODEL - STRESSES FROM STRESS MODEL SERVE AS INPUT DATA TO BUCKLING MODEL, WHICH CALCULATES THE CRITICAL BUCKLING CONDITIONS FOR A GROWING WEB CRYSTAL. INELASTIC PROCESSES ARE NOT INCLUDED IN THIS MODEL AT THIS TIME
    - BUCKLING PREDICTIONS ARE IN GOOD AGREEMENT WITH OBSERVED GROWTH BEHAVIOR.
    - BY USE OF MODELS, NEW GROWTH CONFIGURATIONS HAVE BEEN DESIGNED. THESE HAVE INCREASED WIDTH OF UNBUCKLED RIBBON FROM 2.8 CM (WIDTH PRODUCED BY MOST SUCCESSFUL EMPIRICALLY DESIGNED CONFIGURATION) TO 5.8 CM.
  - IDENTIFICATION OF WORK NEEDED TO UNDERSTAND RIBBON STRESS/STRAIN PROBLEM
    - NEED TO UNDERSTAND BETTER THE REGION ADJACENT TO LIQUID - SOLID INTERFACE
    - NEED TO HAVE ACCURATE HIGH-TEMPERATURE CREEP DATA OF SILICON
    - SYSTEMATIC EXPERIMENTAL EVALUATION OF MODELS IS REQUIRED
    - ACTUAL TEMPERATURE DESTRIBUTION IN GROWING RIBBONS AND IN GROWTH ENVIRONMENT AROUND CRYSTAL NEEDED, FOR DEVELOPMENT OF ACCURATE MODELS OF GROWTH PROCESS. REQUIRES DEVELOPMENT OF TEMPERATURE-MEASURING TECHNIQUES

STRESS STUDIES IN EFG

MOBIL SOLAR ENERGY CORP.

J.P. Kalejs

TECHNOLOGY

ADVANCED MATERIALS RESEARCH TASK

APPROACH

STRESS STUDIES IN EFG

CONTRACTOR

MOBIL SOLAR ENERGY CORPORATION, CONTRACT NUMBER 956312

GOALS

- DEVELOP UNDERSTANDING OF MECHANISM OF STRESS GENERATION IN SILICON SHEET GROWTH AND DEFINE MINIMUM STRESS GROWTH CONFIGURATIONS FOR 200 μM THICK 10 CM WIDE EFG RIBBON GROWING AT 4 CM/MIN.

REPORT DATA

MARCH 15, 1984

STATUS

VERIFICATION OF STRESS MODEL IS UNDERWAY IN AREAS OF:

- CREEP LAW STUDIES.
- TEMPERATURE FIELD MODELING AND MEASUREMENT.
- RESIDUAL STRESS MEASUREMENT.

TEMPERATURE-STRESS FIELD MODELING IS IN PROGRESS.

Projects

- STRESS ANALYSIS FOR VERTICAL SILICON SHEET GROWTH (HARVARD UNIVERSITY).
- RESIDUAL STRESS MEASUREMENTS (UNIVERSITY OF ILLINOIS).
- TEMPERATURE FIELD MODELING USING I-V DATA AND INTERFACE SHAPES (MIT).
- CREEP LAW STUDIES FOR $T \geq 1000^{\circ}C$.
- FIBER OPTICS TEMPERATURE SENSOR DEVELOPMENT.

Stress Analysis Program

- IMPACT OF INTERFACE STRESS BOUNDARY CONDITION ON STRESS DISTRIBUTIONS HAS BEEN EVALUATED.
- SENSITIVITY ANALYSIS IS IN PROGRESS TO EXAMINE STRESS DEPENDENCE ON:
  - WIDTH, GROWTH SPEED.
  - CREEP LAW.
  - POST-GROWTH TEMPERATURE FIELD.
- GROWTH CONFIGURATION IS UNDER DEVELOPMENT TO EVALUAT
  - TEMPERATURE FIELD MODEL.
  - FIBER OPTICS THERMOMETRY.
  - STRESS MODEL.

Simplified Model Predictions

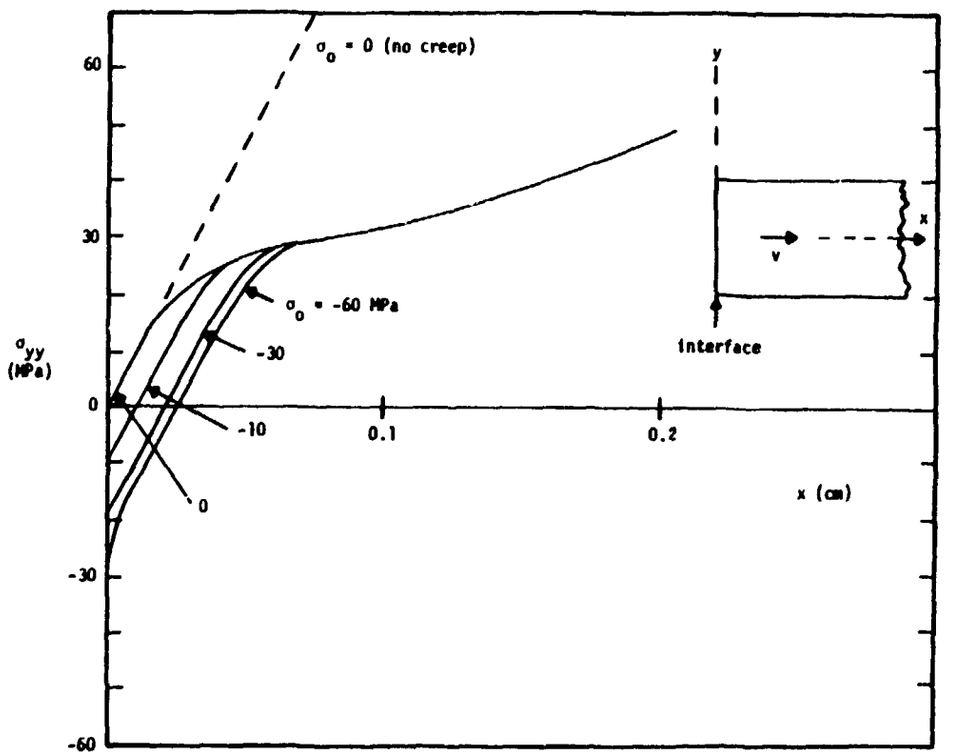

Simplified model predictions for stress near the growth interface (x = 0) at ribbon centerline for V = 0.1 cm/sec.

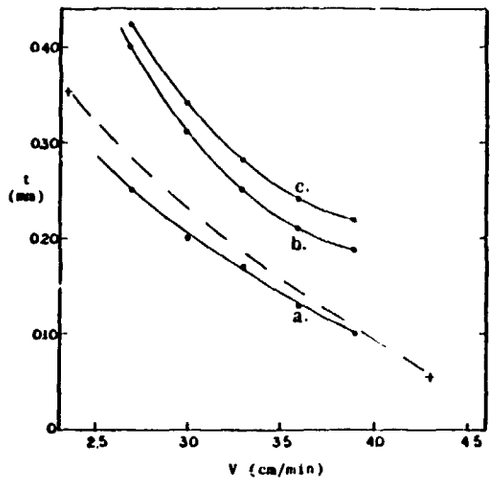

(a)

Thickness-velocity curves for 10 cm cartridge system with cold shoes at a face heater temperature setting of 1431°C. The dashed line is for a continuously imposed velocity change that terminated in a ribbon pull-out or meniscus break at the highest speed.

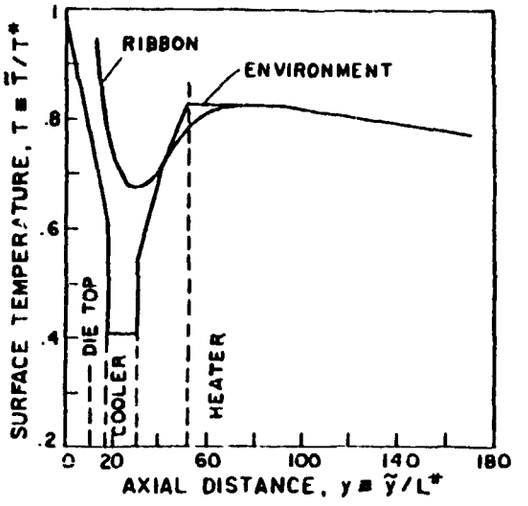

(b)

Experimental (environment) vertical temperature profile in 10 cm EFG cartridge and calculated ribbon distribution.

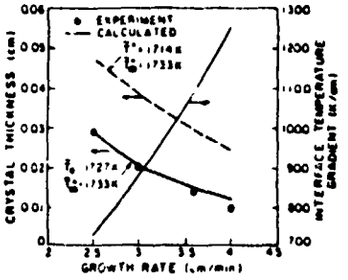

Comparison of experimental measurements and the finite element calculations of ribbon thickness versus pull speed.

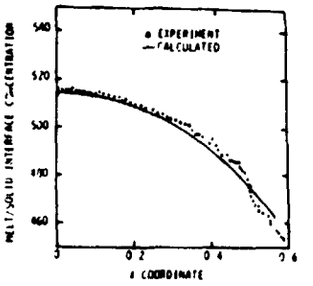

Calculated and measured aluminum profiles along the melt/solid interface at a pull rate of 2.5 cm/min.

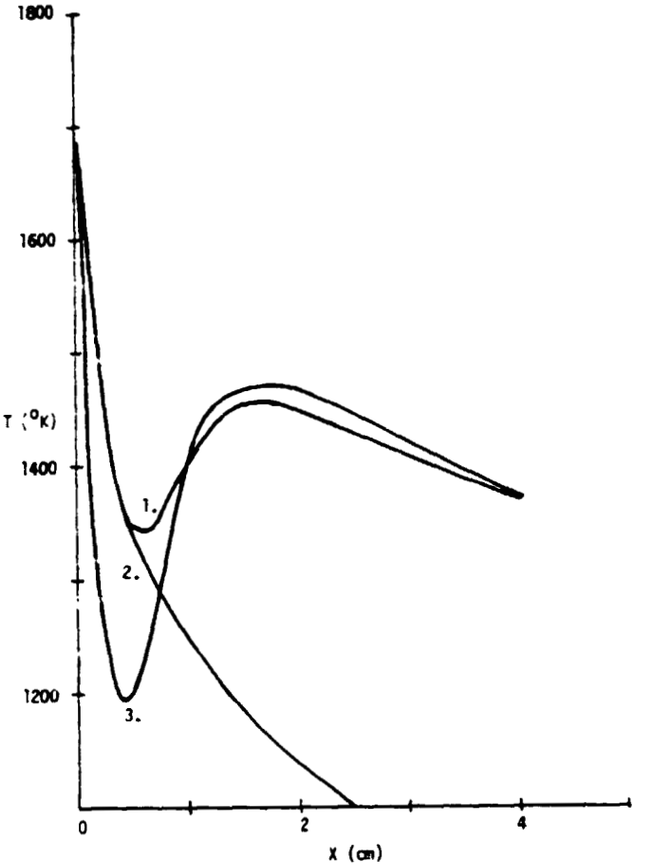

Temperature profiles used in stress analysis:
1. EFG system, 2. idealized system, 3. finite element mode' black body radiation.

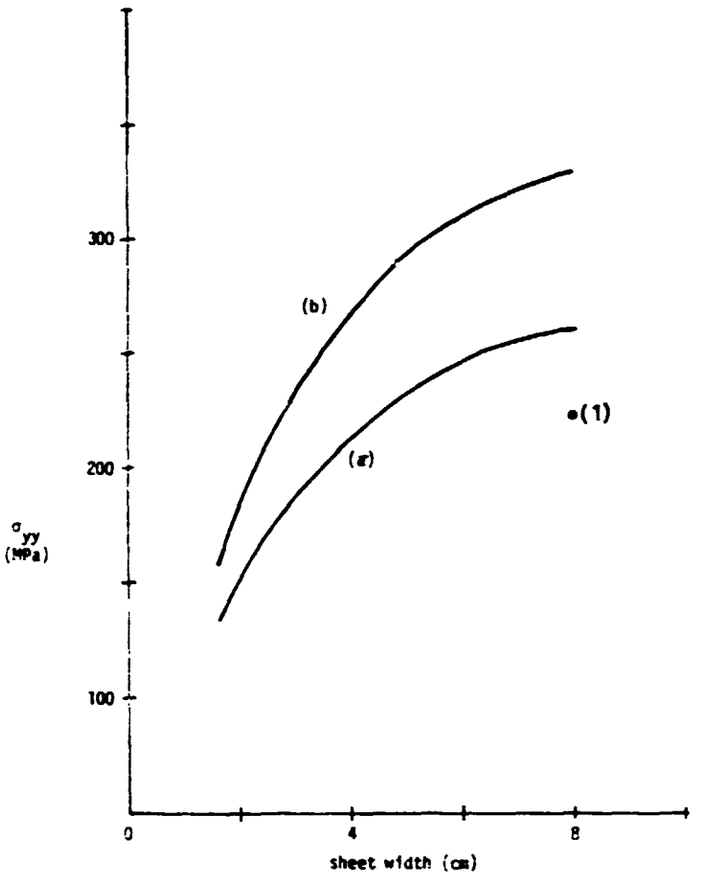

Variation of peak σ_{yy} with width of sheet at growth speeds of (a) 3 cm/min, and (b) 4 cm/min for finite element black body radiation model, and low creep intensity representation. Point (1) is previous calculations for EFG system at 6 cm/min and low creep intensity.

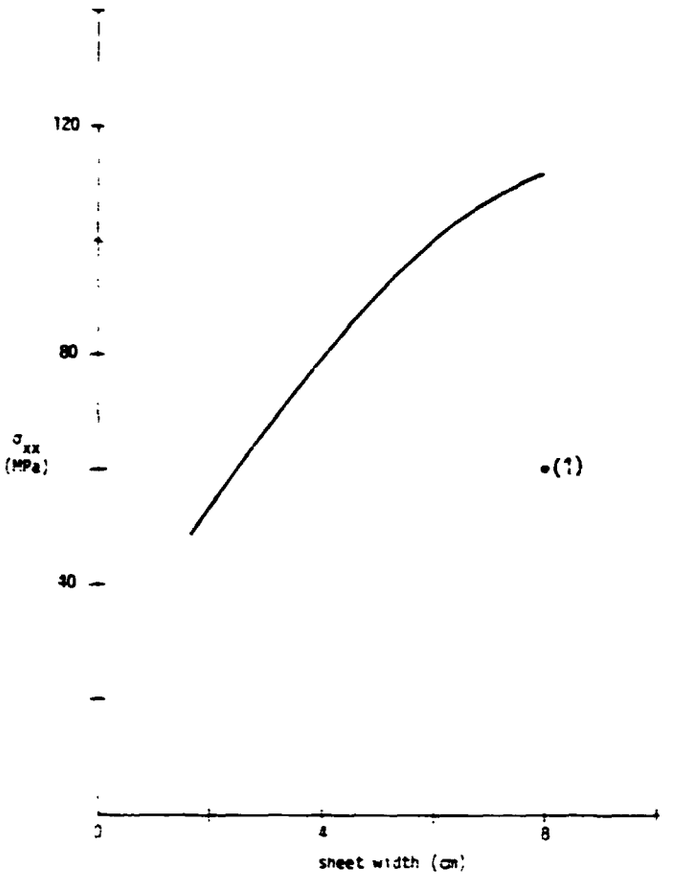

Variation of residual stress σ_{xx} at sheet edge with width of sheet at growth speed of 4 cm/min for finite element black body radiation model and low creep intensity. Point (1) is previous calculation for EFG system at 6 cm/min and low creep intensity.

Creep Law Studies (Four-Point Bending)

- MULTIPLE LOADING - DEFECT STUDIES.
- SINGLE LOAD TRANSIENT CREEP STUDIES.
- ORIENTATION AND IMPURITY DEPENDENCES.

Schematic of Stress Distribution

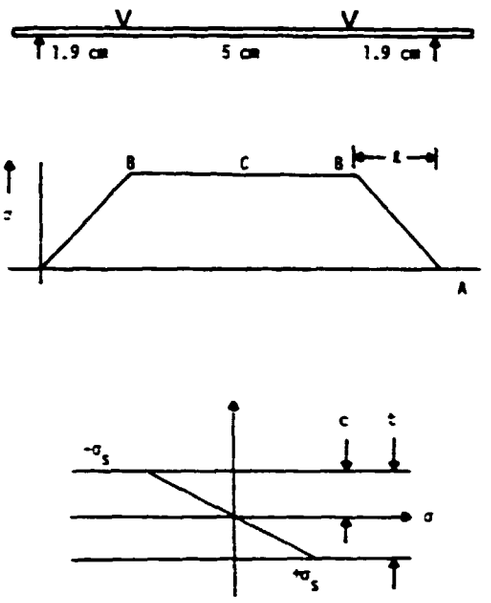

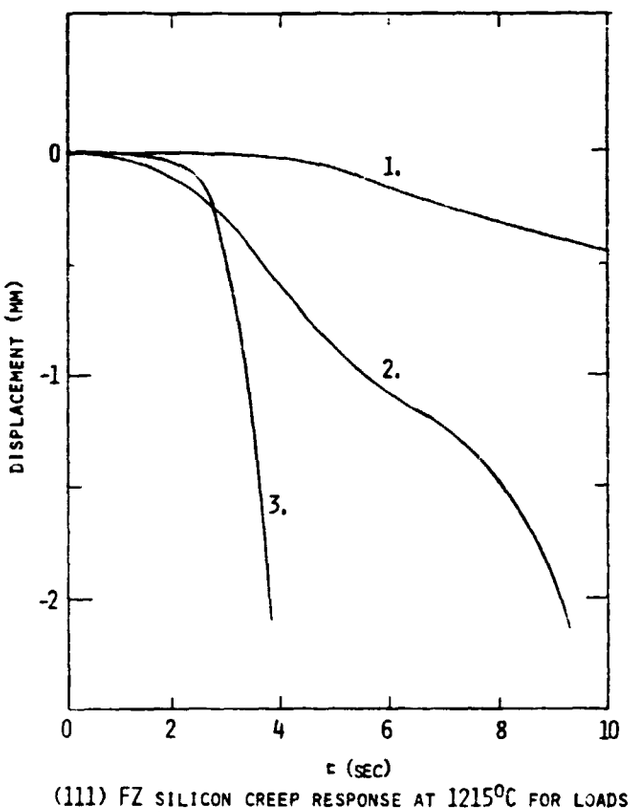

(111) FZ SILICON CREEP RESPONSE AT 1215°C FOR LOADS OF: 1. 8.6 MPA, 2. 12.7 MPA, AND 3. 15.6 MPA WITH <110> BENDING AXIS

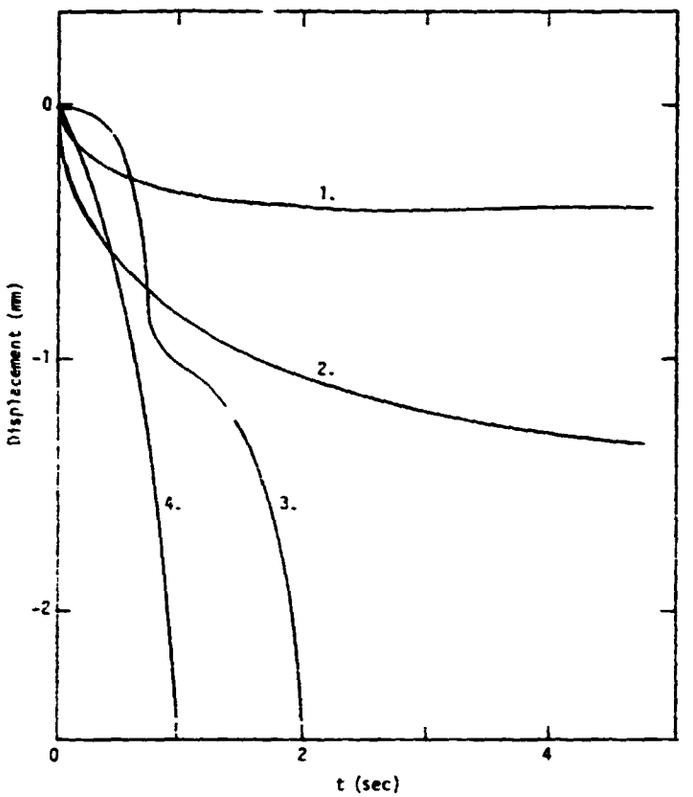

(111) FZ silicon creep response at 1360°C for loads of 1. 8.0 MPa, 2. 12.0 MPa, 3. 14.0 MPa, and 4. 15.5 MPa, with <110> bending axis.

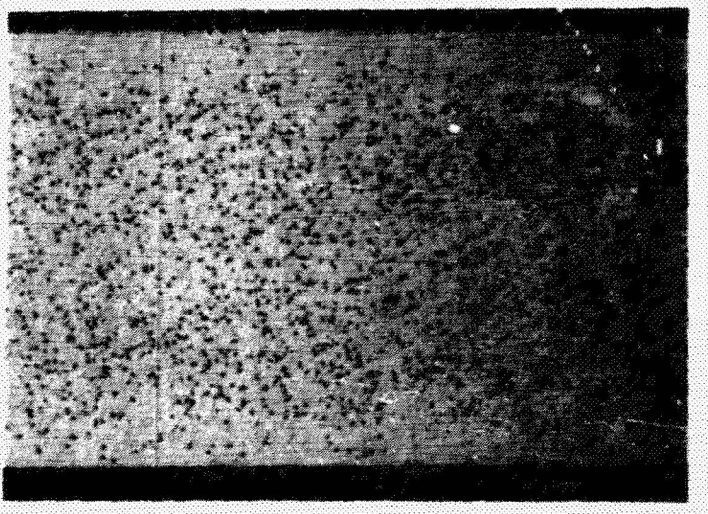

(a)

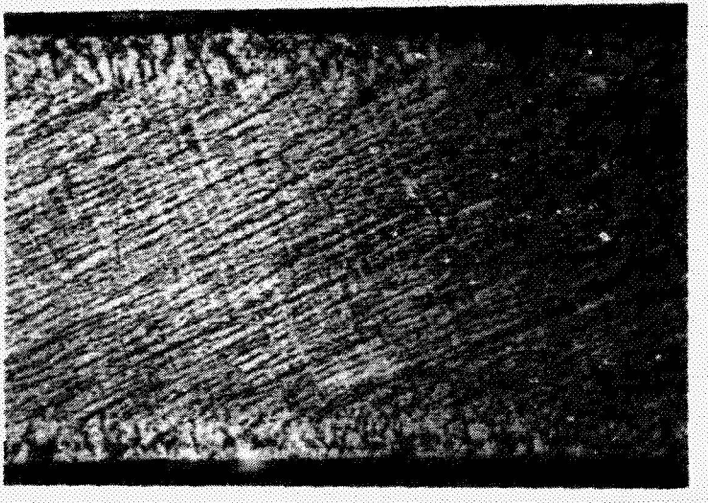

(b)

(111) FZ silicon dislocation configuration at 1360°C for loads of (a) 8.0 MPa, and (b) 14.0 MPa, tension surface at top (X164).

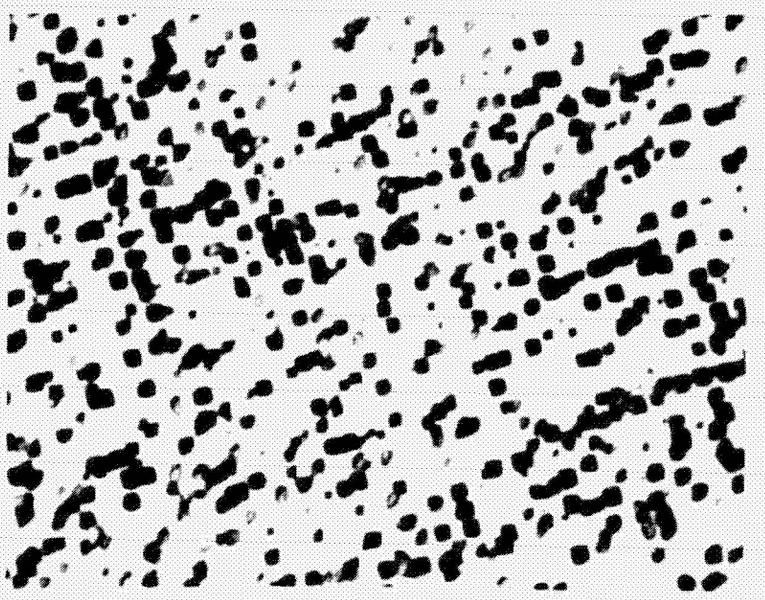

(a)

(b)

(111) FZ silicon dislocation configuration at 1360°C for loads of (a) 8.0 MPa, N_D = 6.0 x $10^6/cm^2$, and (b) 14.0 MPa, N_D = 9.4 x $10^6/cm^2$ (X652).

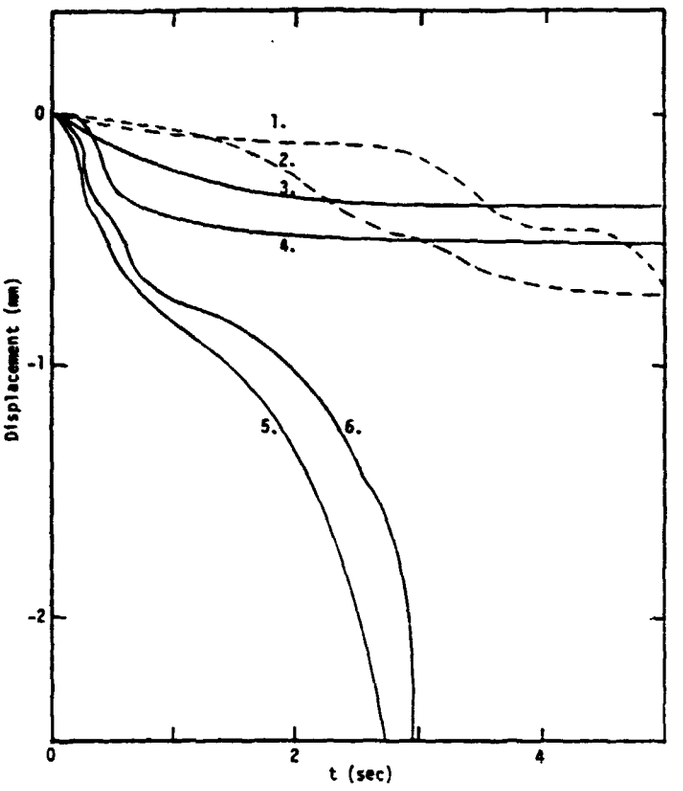

(111) CZ silicon creep response at two temperatures with <110> bending axis:

1. 1215°C, 11.0 MPa.
2. 1215°C, 13.5 MPa.
3. 1360°C, 7.0 MPa.
4. 1360°C, 12.0 MPa.
5. 1360°C, 15.5 MPa.
6. 1360°C, 15.5 MPa, $C_s = 1 \times 10^{18}$ at/cc.

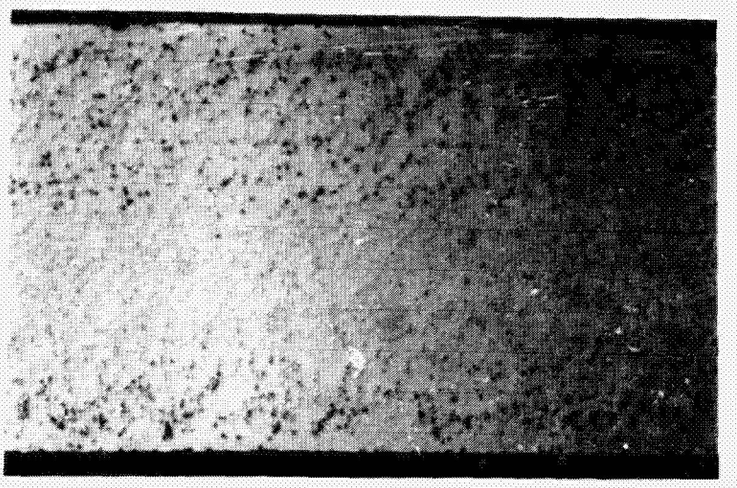

(a)

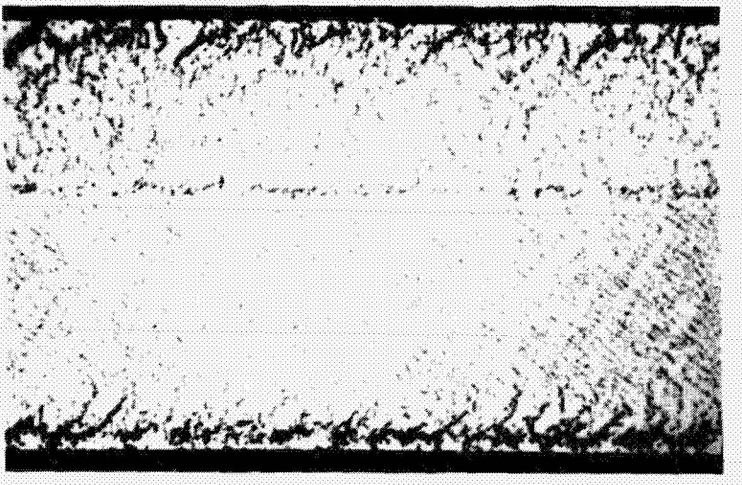

(b)

(111) CZ silicon dislocation configuration at 1360°C for loads of (a) 7.0 MPa, and (b) 15.5 MPa, tension surface at top (X164).

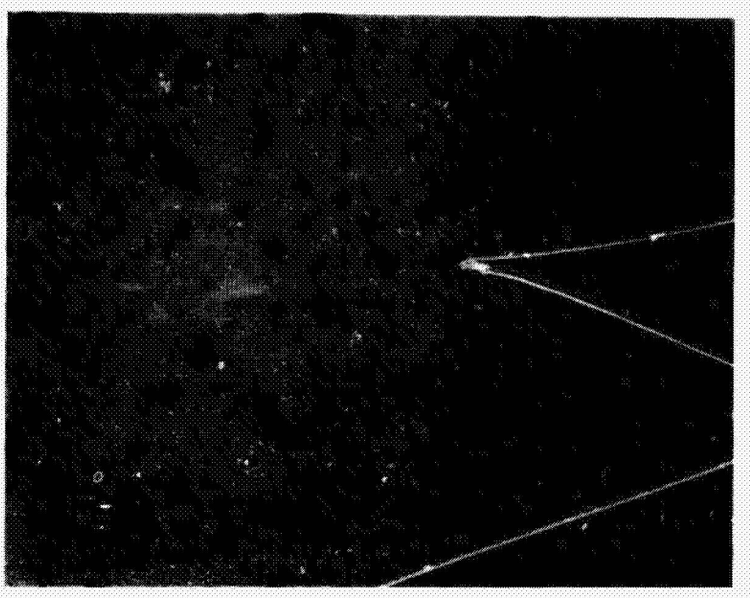

(a)

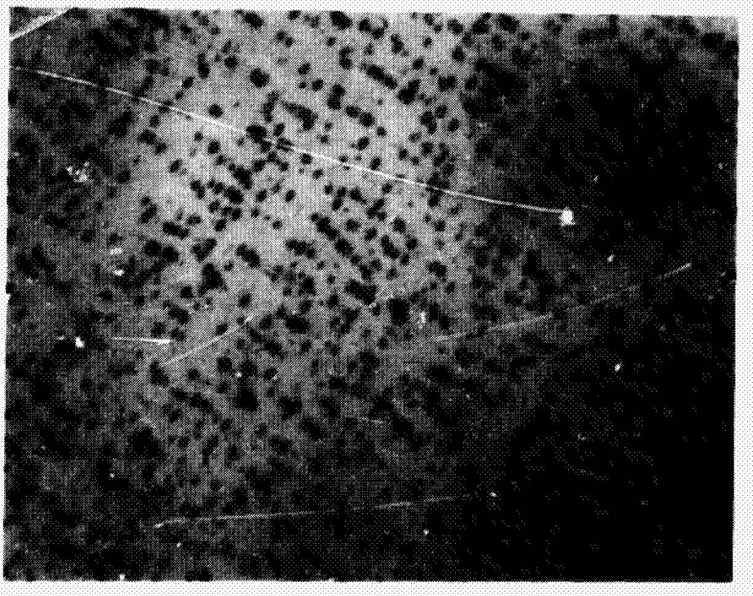

(b)

(111) CZ silicon dislocation configuration at 1360°C for loads of (a) 7.0 MPa, N_D = 9.3 x $10^5/cm^2$, and (b) 15.5 MPa, N_D = 5.5 x $10^6/cm^2$ (X652).

Creep Law Studies

- Significant creep at 1050°C.
- Primary creep likely to dominate above 1200°C.
- Stress likely to selectively act on orientations with highest resolved stresses on glide planes to:
  - Rapidly generate 10^6-$10^7/cm^2$ dislocations by multiplication.
  - Final slip band configuration and residual stress is function of structure (e.g., orientation and parallel boundaries), impurity content, and slip bands activated.

Schematic of Optical Thermometer

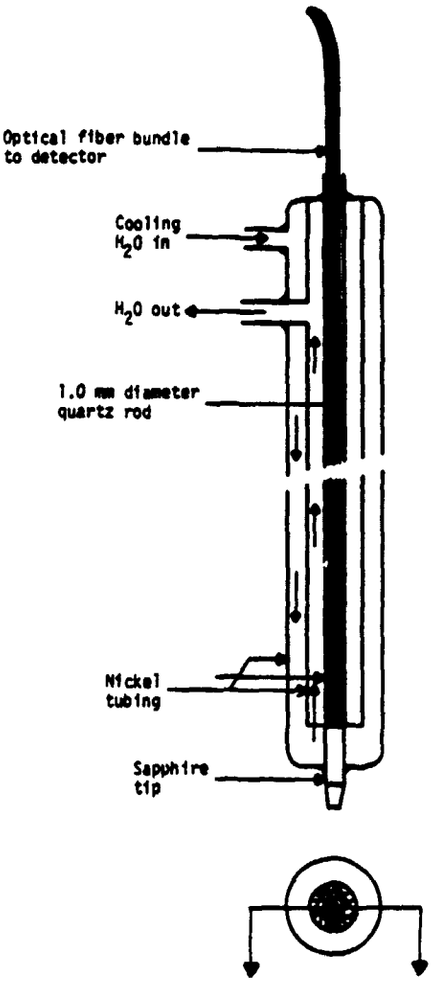

Sensor Development Status

- WATER-COOLED PROBE HAS BEEN CONSTRUCTED AND TESTED IN FURNACE ENVIRONMENT.
- SOME NON-REPRODUCIBILITY ($\pm$ 3-5°C) MAY HAVE MECHANICAL ORIGINS.
- EXPERIMENTS ON TIP CONFIGURATION AND COATINGS ARE PLANNED.
- SIGNAL STRENGTH SHOULD BE ADEQUATE WITH 0,25 MM TIP.

Low Stress Growth Configuration

- 10 CM CARTRIDGE WITH COLD SHOES FOUND NOT TO HAVE REQUIRED FLEXIBILITY FOR
  - OPERATING VARIABLE/DESIGN CHANGES.
  - TESTING OF FIBER OPTICS SENSOR.
- DESIGN AND FABRICATION OF GROWTH CONFIGURATION UNDERWAY:
  - LOWER H_{EFF} TO INCREASE FLEXIBILITY.
  - SIMPLIFY POST-GROWTH COOLING PROFILE TO FACILITATE ANALYSIS AND TEMPERATURE MEASUREMENT.

Future Work

- CONTINUE TEMPERATURE-STRESS FIELD RELATIONSHIP STUDIES.
- DEVELOP GROWTH SYSTEM FOR STRESS MODEL EVALUATION.
- CONTINUE YIELD STRESS STUDIES.

ADVANCED DENDRITIC WEB GROWTH DEVELOPMENT

WESTINGHOUSE ELECTRIC CORP.

C.S. Duncan

Long-Range Goals of Program

Long Range Goals Of Program:

- Continuously-Melt-Replenished Growth Period Of 65 Hours With An Area Rate Of Growth > 25 cm^2/Minute
- Length Of Web Crystal Greater Than 10 Meters
- Dislocation Density Less Than $10^4/cm^2$
- Resistivity Of Web In Range Of 1 To 3 Ohm-cm P-Type
- Terrestrial Solar Cell Efficiency > 15%

Principal Tasks of Current Phase of Program

- Develop Computer Specifications For Low-Stress Web Growth Configurations Having Thermal Elements In Fixed Position. Correlate With Experimental Web Growth.
- Develop Computer Specifications For Web Growth Configurations Incorporating Dynamic Positioning Of Thermal Elements. Correlate With Experimental Web Growth

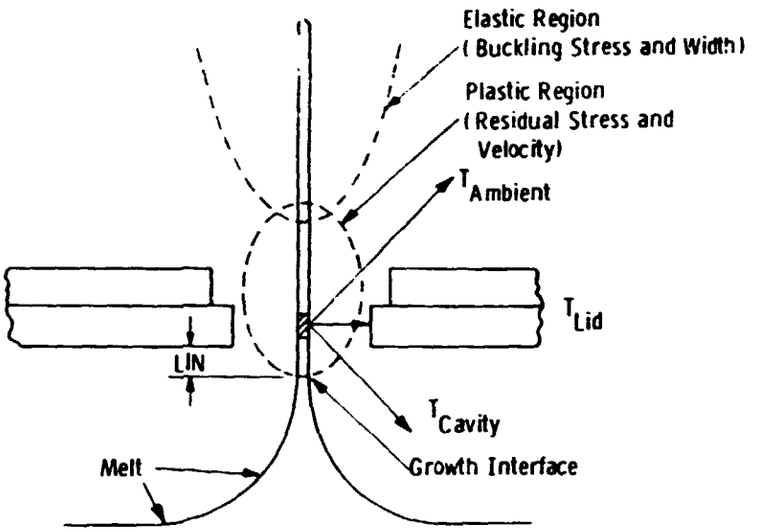

Silicon Web Area Growth Rate and Quality are Determined by the Temperature Profile in the Growing Web

Buckling and Web Width (Elastic Region)

Goal

Attain Low Buckling Stress And Increased Width Of Unbuckled Growth

Status

- **Major Reduction Of Buckling Stress Has Been Achieved**
- **Computer Models Have Been Developed And Applied To Define Growth Configurations**
- **Model Predictions Have Been Verified By Experimental Web Growth**
- **Width Has Been Increased 80% Since Application Of Models**

Current Activity

- Model Application And Experimental Verification Are Continuing With Goal Of Further Increases In Width
- Experimentally Developed Techniques Are Applied To Obtain Improved Growth
- Residual Stress Is Monitored For All New Growth Configurations

Velocity and Residual Stress (Plastic Region)

Goal

Attain Increased Growth Velocity While Maintaining Low Residual Stress

Status

- Important Increase In Growth Velocity Has Been Achieved
- Computer Models Have Been Applied To Define Growth Configurations
- Model Predictions Of Velocity Have Been Verified In Experimental Web Growth
- Gas Conduction Effect Found To Be Of Negligible Significance Near Growth Interface
- Split Width Measurement And Calculation Verified
- Velocity Has Been Increased 55% Since Application Of Models

Current Activity

- Dynamic Positioning Of Lid Relative To Growth Interface (LIN) For Velocity Improvement
- Dynamic Positioning Of Portion Of Lid And Shield Assembly For Control Of Heat Loss Above Growth Interface And Velocity Improvement
- Design Of Lids As A Control Of Temperature Profile For Reduction Of Residual Stress And Enhancement Of Growth Velocity
- Residual Stress Monitored For All New Growth Configurations

Variation of Web Velocity With LIN

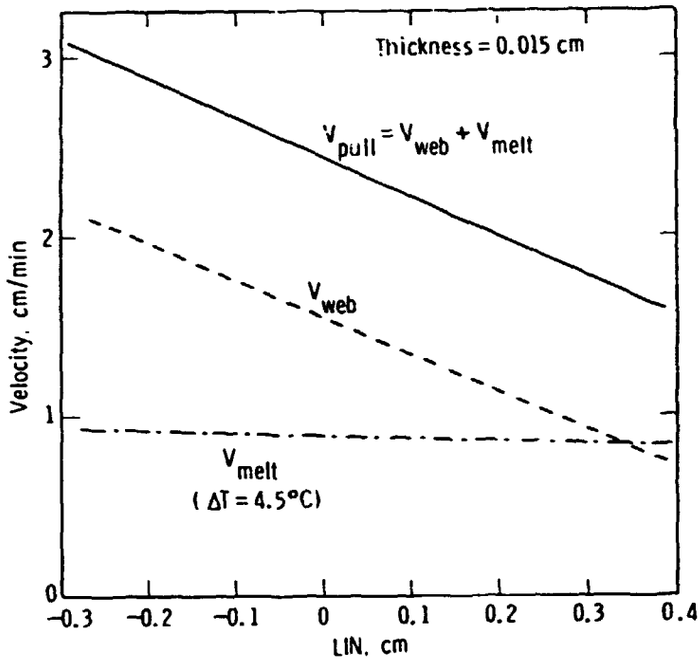

Lid Design for Increased Velocity

Factors Which Can Affect Velocity:

- Lid Thickness
- Lid Temperature
- Width Of Growth Slot
- Profile Of Growth Slot (Beveled, Etc)
- Placement With Respect To Adjacent Shields And Melt

Residual Stress Measurements

- Residual Stress Is A Critical Factor In The Development Of Higher Velocity Growth Configurations
- Split-Width Measurement Was Shown To Give Good Estimate Of Maximum Residual Stress In Silicon Web Crystals Based on Detailed Measurements
- Split-Width Method Is Routinely Used To Evaluate Residual Stress In New Configurations Of Web Growth

New Configurations for Web Growth Defined by Computer Modes and Verified Since Last PIM

- Two Static Growth Configurations (J503, J517)
- Three Dynamic Growth Configurations (RE435, RE443, RE453)

Summary

- Model-Defined Advanced Concepts For Web Growth Configurations Have Been Defined And Verified In Experimental Web Growth
- Major Increases In Achieved Width And Velocity Have Resulted From These Concepts

SILICON-SHEET SURFACE STUDIES

UNIVERSITY OF ILLINOIS AT CHICAGO

S. Danyluk

Objective

Non-destructive determination of residual stresses in short sections of sheet silicon

- Developed a Laser Interferometry Technique (for polished surfaces) and
- Applied a shadow Moiré technique (for rough surfaces) to determine deflections in sheet silicon.
- Developed an analysis of extracting residual stresses from measured deflections of circular wafers and short rectangular ribbons.

Residual Stress

Definition of Residual Stress - Stress that exists in the silicon sheet after "processing."

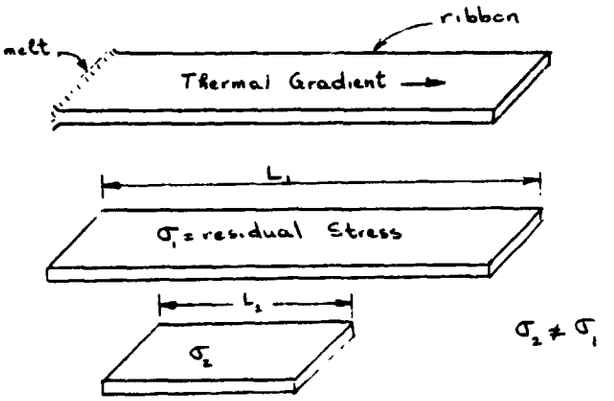

1. Residual stresses redistribute after cutting, polishing, etc.
2. Out-of-plane residual stresses are immediately evident since they produce buckling (potato chip); in-plane residual stresses are not evident and so must be measured.
3. The normal residual stresses are zero at the surfaces since these are "free."
4. Normal residual stresses decrease to zero near the ends of a ribbon. The decrease occurs in a length that is about equal to the width.

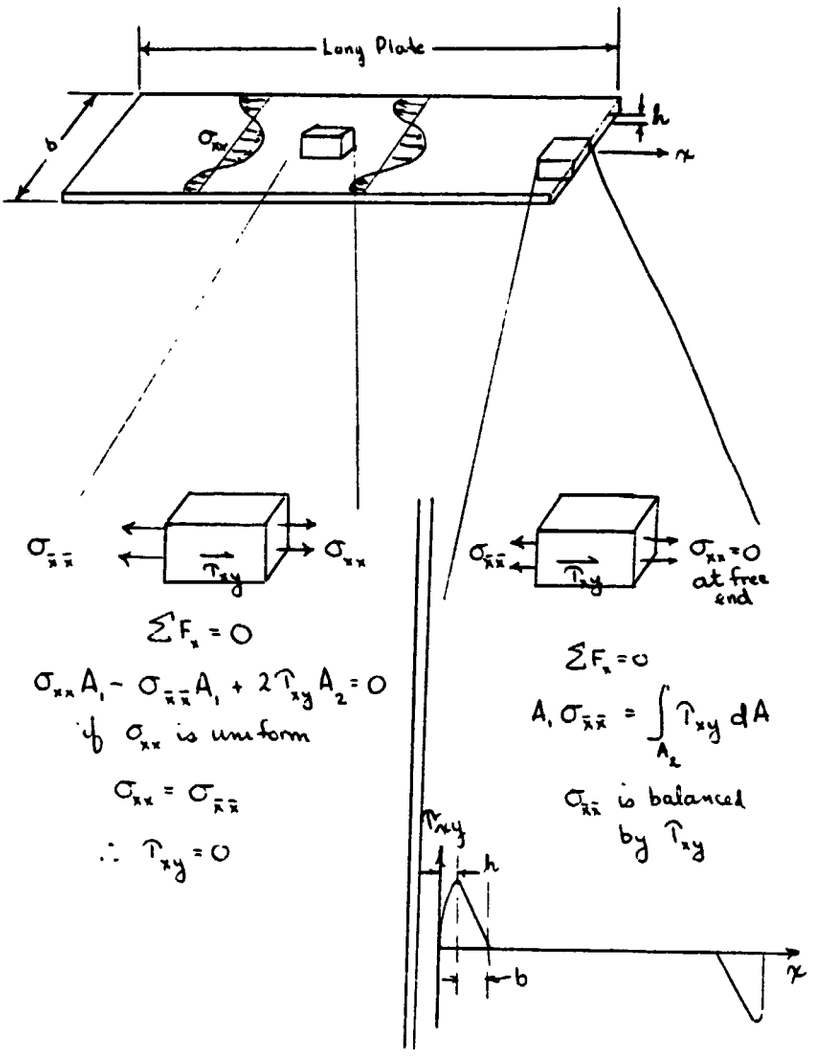
Long Plate
b
h
x
σ_{xx}
$\sigma_{\bar{x}\bar{x}}$
τ_{xy}
σ_{xx}
$\Sigma F_x = 0$
$\sigma_{xx} A_1 - \sigma_{\bar{x}\bar{x}} A_1 + 2\tau_{xy} A_2 = 0$
if σ_{xx} is uniform
$\sigma_{xx} = \sigma_{\bar{x}\bar{x}}$
$\therefore \tau_{xy} = 0$
$\sigma_{\bar{x}\bar{x}}$
τ_{xy}
$\sigma_{xx} = 0$ at free end
$\Sigma F_x = 0$
$A_1 \sigma_{\bar{x}\bar{x}} = \int_{A_2} \tau_{xy}\, dA$
$\sigma_{\bar{x}\bar{x}}$ is balanced by τ_{xy}
τ_{xy}
h
b
x

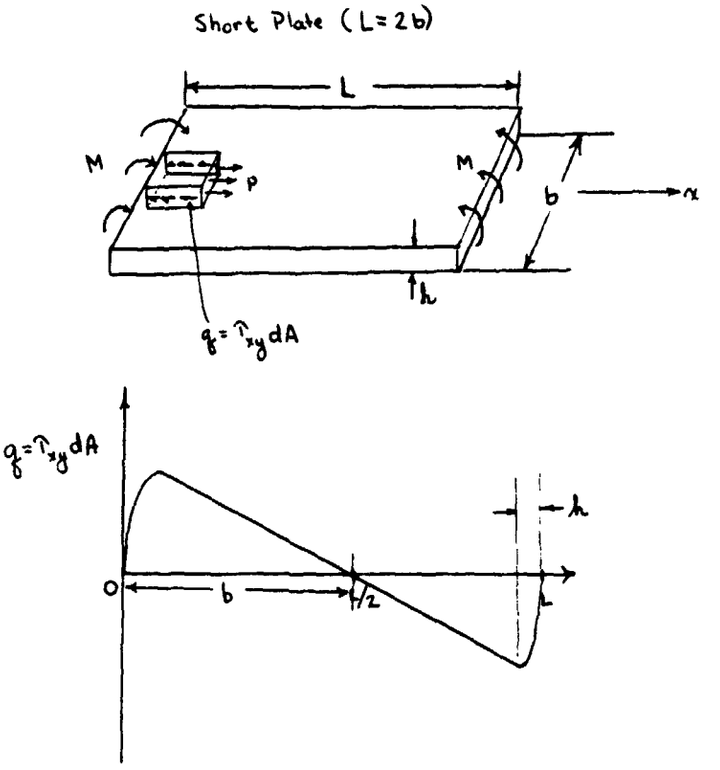

Plate Analysis:

$$\frac{d^2w}{dx^2} = \frac{M}{D} - \frac{P}{D} w + \frac{AP}{2D} (x_o^2 - Lx_o)$$

$$P = 2 \int_0^{x_o} \tau_{xy} \, dx$$

$\frac{d^2w}{dx^2}$ = 2A (curvature at x_o--to be determined experimentally)

M = applied moment

$$D = \frac{Eh^3b}{12(1-\nu^2)}$$

w = deflection at x_o

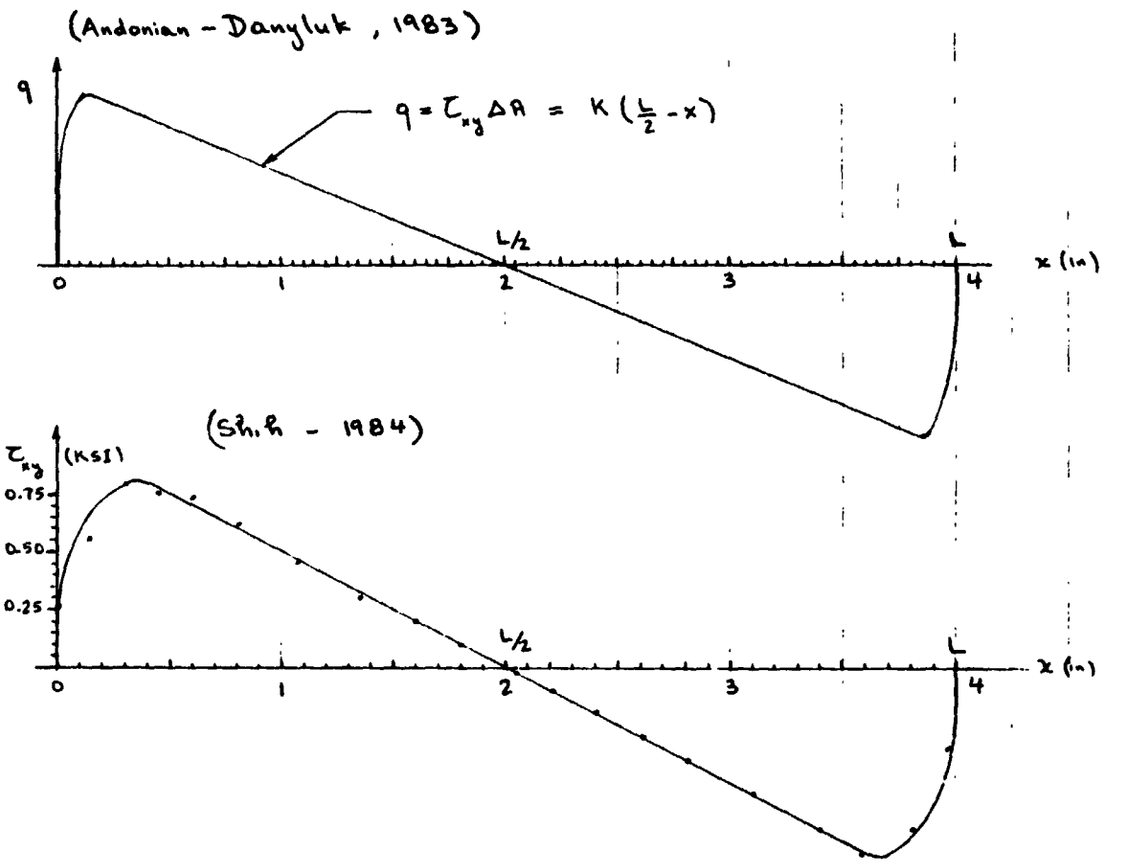

E. .erimental Nondestructive Technique for Measuring Residual Stresses

1. Short section of ribbon (2b = L)
2. Heterogeneous in-plane residual stresses are present--are zero at surfaces.
3. External normal stresses are zero.
4. Thickness is uniform.

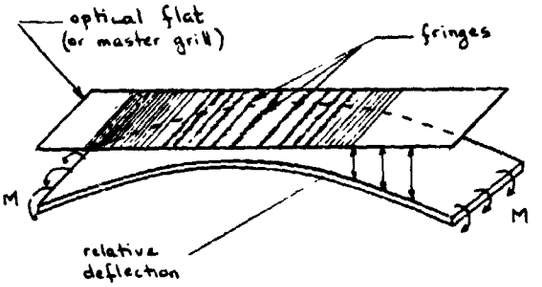

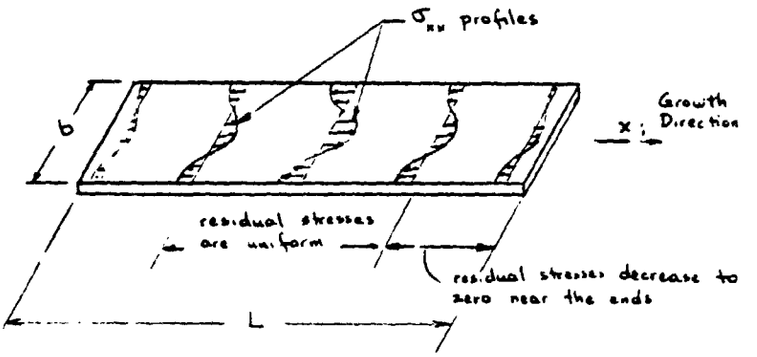

Experimental Results

Mobil Solar:

Specimen No.	Growth Speed (cm/min)
47R1-3	1.75
47R1-1	2.00
47R1-2	2.00
47R1-4	2.25

Spec 47R1-1
2.00 cm/min.

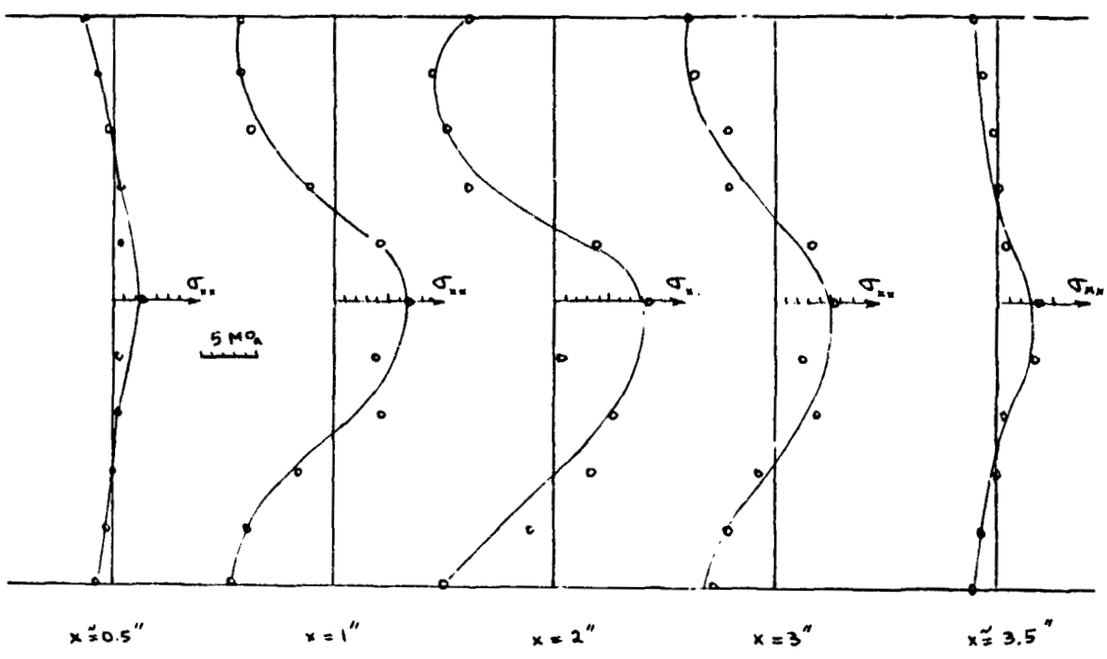

Spec 47R1-2
2.00 cm/min

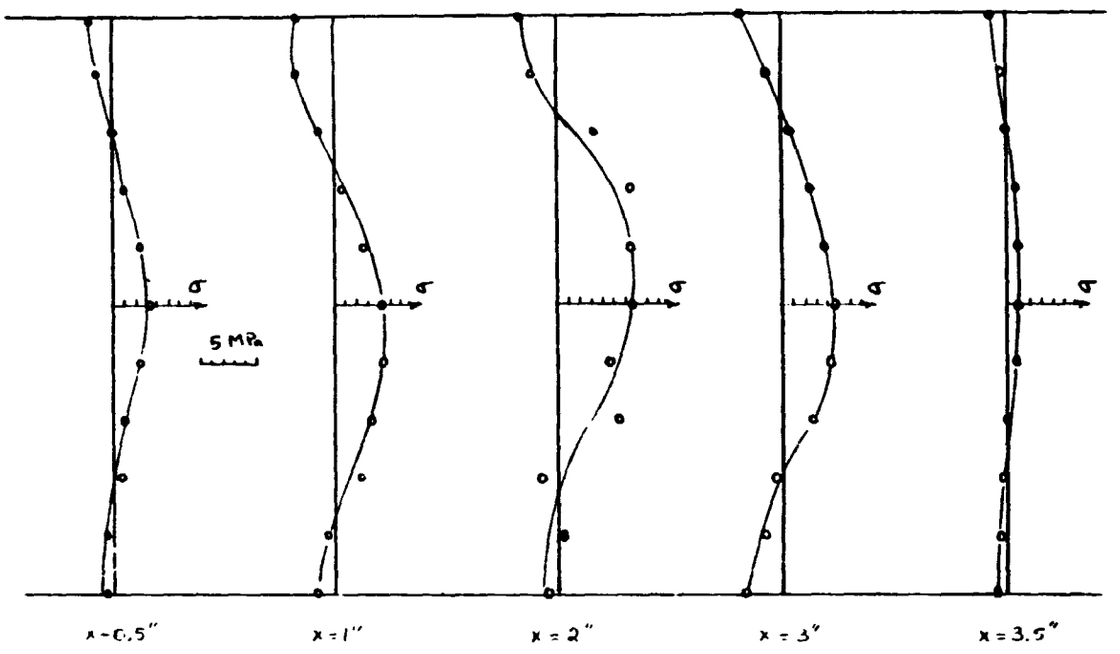

Specimen 47R1-4
2.25cm/min

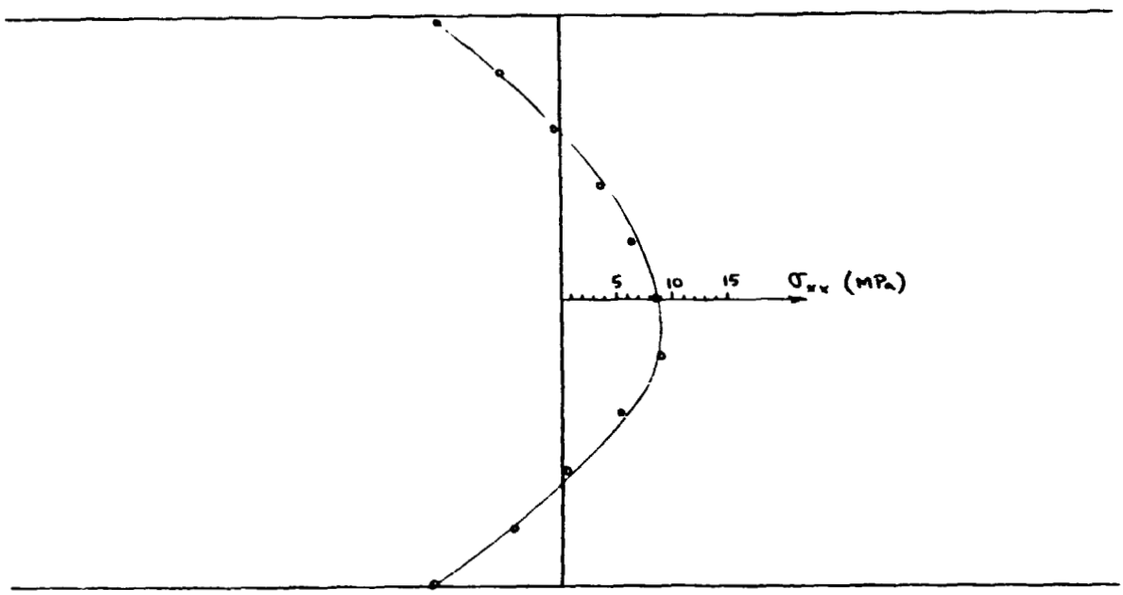

x = 2"

INVESTIGATION OF STRUCTURAL AND ELECTRICAL PROPERTIES OF LOW-ANGLE SILICON SHEET

SOLAR ENERGY RESEARCH INSTITUTE

Y.S. Tsuo
R.J. Matson
J.B. Milstein

Considerable research is being conducted in low-cost polycrystalline semiconductors in the photovoltaic solar cell industry. We have found that the combination of secondary electron imaging (SEI), electron channeling, and electron-beam-induced current (EBIC, also known as charge collection scanning electron microscopy) techniques in a scanning electron microscope (SEM) is quite useful for correlating morphology, crystallographic orientations, and electronic quality of individual grains in polycrystalline semiconductor samples. It is also possible to obtain quantitative information about the minority carrier diffusion length of individual grains and the minority carrier recombination velocity at grain boundaries using the EBIC line scan method. The high spatial resolution obtainable with electron channeling and EBIC techniques and the ability to select between the SEI, EBIC, and electron channeling modes in the SEM make them far superior to conventional structural and electrical characterization techniques in studying small-grained semiconductors.

These techniques have been applied to the studies of low angle silicon sheets. Low-angle silicon sheets (LASS) that are pulled almost horizontally from the melt at very high speeds, up to about 400 cm^2/min, were assessed. Large areas of single-crystal silicon are occasionally grown by the LASS method. However, single-crystal LASS sheets contain many defects which may result from the unusually high growth speeds, and from apparently unusual modes of crystallization.

Experimental Method

A JEOL JSM 35C SEM with a selected area diffraction component attachment was used in the experiment. An IC specimen holder was modified to operate at the 9-mm working distance required for optimal electron channeling in this microscope. A GW Electronics Model 103B specimen current amplifier was used for EBIC imaging and a Keithley Model 427 current amplifier was used for digital quantitative EBIC images and linescans. The GW Electronics Model 130 backscattered electron imaging (BEI) detector and electronics were found to be optimal for acquiring clear electron channeling patterns (ECP). Restrained by a short working distance, the BEI unit, rather than the SEI unit, was used in a topographical mode to image topographical features.

Different approaches can be taken to perform both electron channeling and EBIC analysis on the same area, depending on the requirements of the experiment. If the individual grains are relatively large and easy to locate, then the ECP work is done to establish the orientation of the grains; then, after a Schottky barrier device is made out of the material, the EBIC study is performed. Since the electron beam of the SEM is a constant current source, the EBIC line scan traces and images reveal spatial variations in the charge collection efficiency of the Schottky barrier device. To measure the effective surface recombination velocity of minority carriers at a grain boundary, an EBIC line scan normal to the boundary is obtained. To be quantitatively useful, a digital line sca

using a calibrated current amplifier, a computer, and a plotter are used to record the natural log of the EBIC signal as a function of distance. The minority carrier diffusion length within each grain can also be measured by scanning the beam perpendicular to the edge of the front contact pad and recording the EBIC current as a function of distance from the contact pad.

By switching between ECP, BEI and EBIC while moving across the material, the location, topography, electrical quality, crystalline orientation and even the crystalline quality can be correlated for polycrystalline materials. Evaluating the crystalline quality requires measuring the relative peak heights (ECP contrast) and the shape of the peaks (ECP linewidths) shown by ECP line scans (intensity vs. scan angle) normal to the crystalline bands.

Applications

Complementary electron channeling and EBIC were first used in the study of ESP silicon sheets grown at SERI.

This EBIC/ECP technique was applied to LASS samples grown at the Energy Materials Corporation. Probably because of the unusually high growth speed—the single-crystal LASS samples studied were grown at the speed of 210 cm^2/min—the defect structures we observed in these samples were rather unusual for single-crystal silicon. In addition to a relatively high density of electrically active dislocation networks, they also contain what appear to be inclusions. The sample has been chemically etched to reveal the defects. The electron channeling patterns indicate that some of these inclusions are actually silicon crystals with orientations identical or very similar to the rest of the crystal. The superposition of the ECP taken at the center of a defect and the SEI of the location of the ECP at a high magnification is shown. The dark lines of the SEI show that the stacking faults occur along 220 planes. An EBIC micrograph of the same area is shown. The sample was mechanically and chemically polished to remove etch pits before being fabricated into Schottky barrier devices for EBIC studies. The EBIC images clearly illustrate the electrical activity of the various defects. They also show electrically active dislocations that were not revealed by chemical etching. In addition, our study showed that large, electrically active dislocation networks exist under the dendrites that appear on the top surface of LASS sheet during growth. Such information is not only useful from the device point of view; it also provides insight into the mechanisms of growth in the LASS process.

Discussion

The LASS ribbon studied contains both polycrystalline regions and a large single crystal region. In this ribbon (about 6cm x 24 cm in size) which represents perhaps 40 seconds of growth, one sees the spontaneous nucleation of the single crystal region, "stable" growth of single crystal material to dimensions of several centimeters width by over ten centimeters in length, and termination of single crystal growth. We belive that much information regarding these processes may be abstracted from the ribbon by careful study.

By comparing regions of LASS material which are clearly polycrystalline with the single crystal region, we have discovered a number of remarkable features which we have not seen reported in standard texts which treat defects in semiconductors. In the polycrystalline regions, we find defects which extend throughout the thickness of the ribbon. In the single crystal region, we observe surface features on the upper surface of

as grown ribbon which are reminescent of structures commonly observed in flux-grown crystals which float on the surface of the molten flux. These features, which are readily seen in an optical microscope, appear to be crystallographically oriented hillocks bounded by crystallographic facets, with depressed central regions. Photos will be shown. To the naked eye, however, these features appear to be finely spaced oriented dendrites, which grew at an angle to the pull direction.

By the use of EBIC, ECP and SEI, we have examined defects in the single crystal region which also extend through the entire thickness of the ribbon. Some of these defects enclose crystalline regions which are oriented identically or nearly identically with the crystal, while others are definitely polycrystalline. In both instances, we observe that no apparent degradation of the crystal structure in the direction of the macroscopic growth direction has occurred. It is well known that, for example in Czochralski growth, such growth accidents rapidly lead to loss of structure. Our observation leads us to suspect that in LASS growth, the conception of an interface which simply proceeds in the growth direction is incapable of explaining all of the features seen. Accordingly, we postulate that the defects observed are generated by a more complex process, in which growth occurs behind the macroscopic interface (or leading edge). In the hypothesized process, there are liquid regions behind the growth front which close by lateral growth from adjacent solid regions. These "lakes" of molten material are first confined from below by a thin layer of solid silicon, which traps a pool of liquid silicon. When the pool freezes, the surface growth artifacts are formed, by virtue of the fact that silicon expands on freezing. As the layer which isolates the pool from the remainder of the melt is closed, defects such as dislocations and stacking faults are produced, which are observed by the methods indicated above. We observe the defect structures on the bottom surface of the ribbon as well. By comparison of optical micrographs taken at the same magnification on both surfaces, we can see that these unique structures maintain their character, but are somewhat larger on the bottom surface as compared to the top surface. This behavior is consistent with the hypothesis that the ribbon continues to grow in the thickness direction after the growth front has moved away, taken with the conception of local loss of structure as growth proceeds downward into the melt similar to Czochralski growth.

This picture is also consistent with the "popcorn effect" previously reported by Energy Materials Corporation.

Conclusion

By using a combination of secondary electron imaging, electron channeling, and EBIC techniques in a SEM, we have correlated the structural and electrical properties of defects in low-angle silicon sheet material. This technique has proven quite useful in correlating the structural and electrical properties of highly defected or polycrystalline semiconductor materials.

N85 15289

SEMICRYSTALLINE CASTING PROCESS DEVELOPMENT AND VERIFICATION

SEMIX INC.

W.F. Regnault

Principal Areas of Research

- DEFECT ANALYSIS OF SEMICRYSTALLINE SILICON
- THERMAL MODELING OF THE UCP

Investigation of Structural Defects Within Grain Volumes That Affect Efficiency of Semicrystalline Silicon Solar-Cell Materials

PURPOSE:

TO DETERMINE THE NUCLEATING MECHANISMS OF A DISLOCATION SUBGRAIN STRUCTURE OCCASIONALLY FOUND IN SEMICRYSTALLINE SILICON

APPROACH:

TO PERFORM X-RAY TOPOGRAPHIC, OPTICAL, AND EBIC STUDIES ON SEVERAL SAMPLES OF UCP MATERIAL

X-Ray and EBIC Measurements

OBJECTIVES:

TO DETERMINE THE RELATIVE CRYSTALLOGRAPHIC ORIENTATIONS OF NEIGHBORING GRAINS

TO DETERMINE THE INTERNAL DISLOCATION STRUCTURE OF THE CRYSTALLITES

TO CORRELATE THE OBSERVED DISLOCATION STRUCTURE WITH THE ELECTRICAL RESPONSE OF THE MATERIAL

Optical Observations

OBJECTIVE:

TO DETERMINE THE ORIGIN OF IRREGULARITIES ALONG THE HIGH ANGLE GRAIN BOUNDARY OF NEIGHBORING GRAINS

Conclusions

- THE DISLOCATION STRUCTURE WILL ADVERSELY AFFECT THE LOCAL PHOTOVOLTAIC PROPERTIES OF SEMICRYSTALLINE MATERIAL
- THE SUBGRAIN STRUCTURE ARISES FROM IRREGULARITIES IN THE HIGH ANGLE GRAIN BOUNDARIES OF NEIGHBORING GRAINS
- GRAIN BOUNDARY KINKS ARE FORMED BY GRAIN IMPINGEMENT AND BY A RELAXATION OF A CURVED BOUNDARY INTO A LOWER ENERGY STATE COMPRISED OF STRAIGHT LINE SEGMENTS
- WHEN TWO GRAINS ARE IN A SECOND ORDER TWIN RELATIONSHIP, THEY SHARE A COMMON SLIP DIRECTION. UNDER APPLICATION OF A SUITABLE STRESS, BOTH GRAINS CAN SIMULTANEOUSLY RESPOND BY SLIPPING ALONG THIS COMMON DIRECTION
- THE DRIVING FORCES ARE LIKELY TO ARISE FROM HIGH TEMPERATURE THERMAL STRESSES

Thermal Analysis of UCP

PURPOSE:

TO DEVELOP A COMPUTER SIMULATION OF THE UBIQUITOUS CRYSTALLIZATION PROCESS IN ORDER TO MODEL THE TIME DEPENDENCE OF THE SOLIDIFICATION FRONT AND TO AID IN THE STUDY OF THE TEMPERATURE DISTRIBUTION WITH AN INGOT

APPROACH:

TO WRITE A TWO DIMENSIONAL FINITE-DIFFERENCE MODEL USING THE IMPLICIT ALTERNATING DIRECTION SOLUTION TO THE TRANSIENT HEAT CONDUCTION EQUATION

Mathematical Symmetry Elements for Finite Element Analysis of UCP Ingot

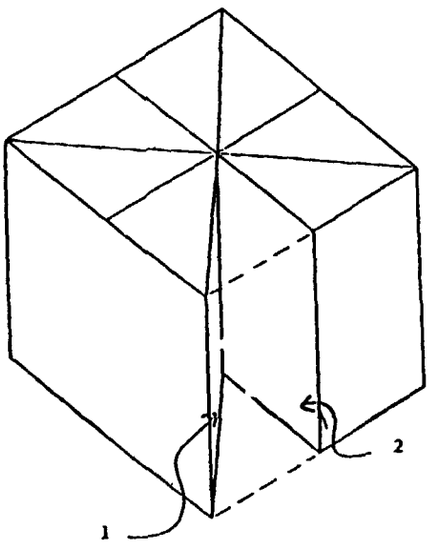

Features of the Model

- o TAKES INTO ACCOUNT VOLUME EXPANSION UPON FREEZING
- o INCLUDES EFFECTS FROM THE RELEASE OF LATENT HEAT OF FUSION

Differential Equation

$$K\left(\frac{\partial^2 T}{\partial X^2} + \frac{\partial^2 T}{\partial Y^2}\right) + F = P(c_p)\frac{\partial T}{\partial \tau}$$

X = HORIZONTAL COORDINATE, CM
Y = VERTICAL COORDINATE, CM
τ = TIME, SEC
T = TEMPERATURE, ^{o}C
K = THERMAL CONDUCTIVITY, J/SEC CM ^{o}C
F = RATE IF HEAT GENERATION DUE TO LATENT HEAT RELEASE, J/SEC CM^3
P = DENSITY, GM/CM^3
c_p = SPECIFIC HEAT, J/GM ^{o}C

Boundary Condition

$$K \frac{\partial T}{\partial N} + \alpha T = \beta$$

ALLOWS THREE IMPORTANT CASES:

1. INSULATED SURFACE AT PLANE OF SYMMETRY

   $\alpha = \beta = 0$

2. SPECIFIED FLUX β (J/SEC CM^2)

INTO THE MEDIUM:

   $\alpha = 0$

3. SURFACE INTERACTS WITH SURROUNDING FLUID AT TEMPERATURE Ts WITH HEAT - TRANSFER COEFFICIENT H (J/SEC CM^2 ^{0}C)

   $\alpha = H$

   $\beta = H\ Ts$

E.G. FOR $\alpha = 0.00568$, $\beta = 8.07$,

$$Ts = \frac{8.07}{0.00568} = 1421^0\ C$$

Physical Properties, etc.

K	=	0.67 J/CM SEC ^{0}C
P	=	2.5 GM/CM^3
C_P	=	0.917 J/GM ^{0}C
To	=	1420^0 C (POURING TEMPERATURE)
HF	=	1103 J/GM (LATENT HEAT) (264 CAL/GM)
E	=	0.1 (FRACTIONAL EXPANSION ON FREEZING)
W	=	10.8 CM (HALF INGOT WIDTH)
H	=	16.5 CM (INGOT HEIGHT)

One Cross Section of the Ingot

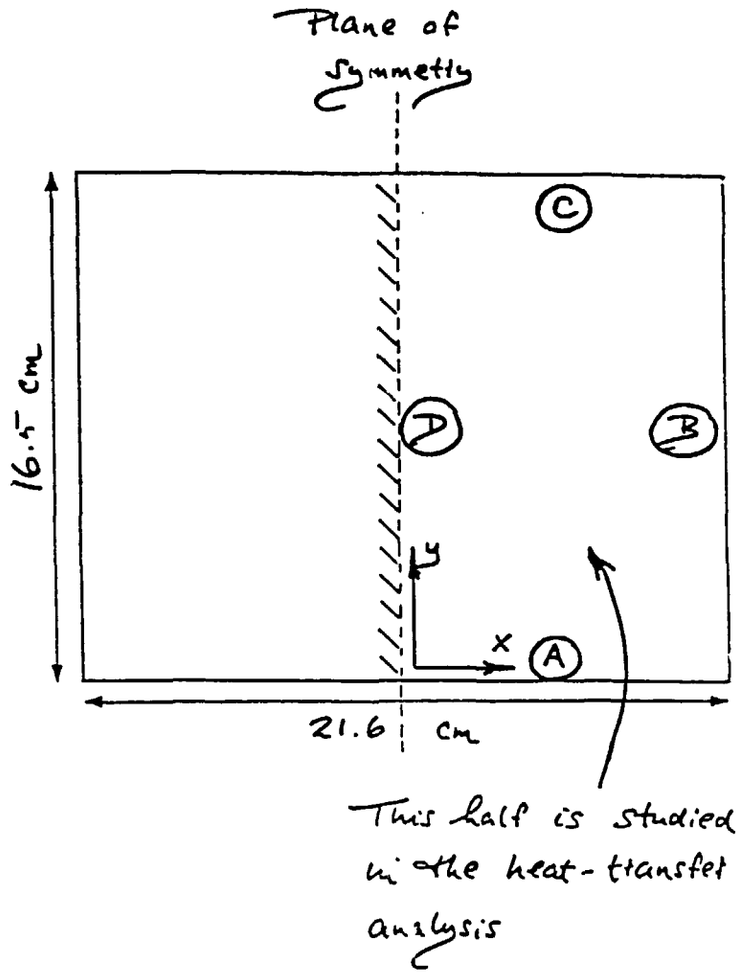

Test Conditions

CASE I. LOSS OF HEAT OUT OF THE BOTTOM

CASE II. EQUAL LOSS OF HEAT FROM BOTTOM AND SIDES

SILICON MATERIAL AND SHEET

Run 1

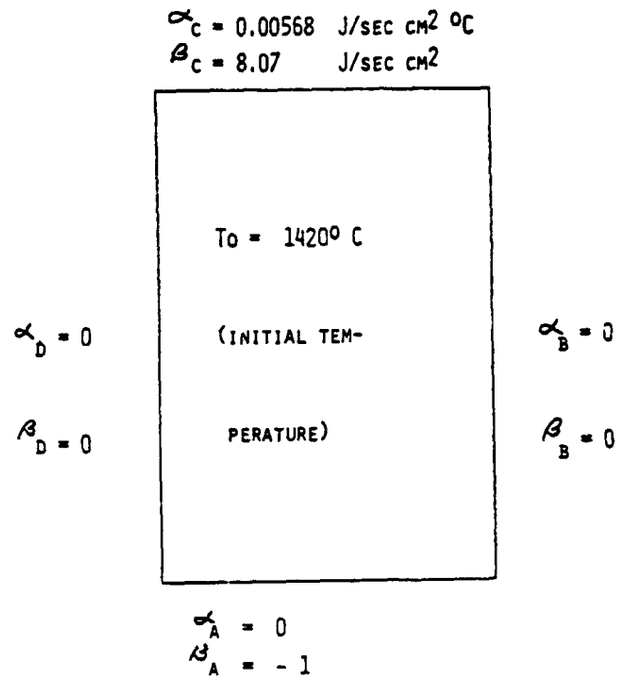

ΔT = 100 SEC

TMAX = 50400 SEC (14 HOURS)

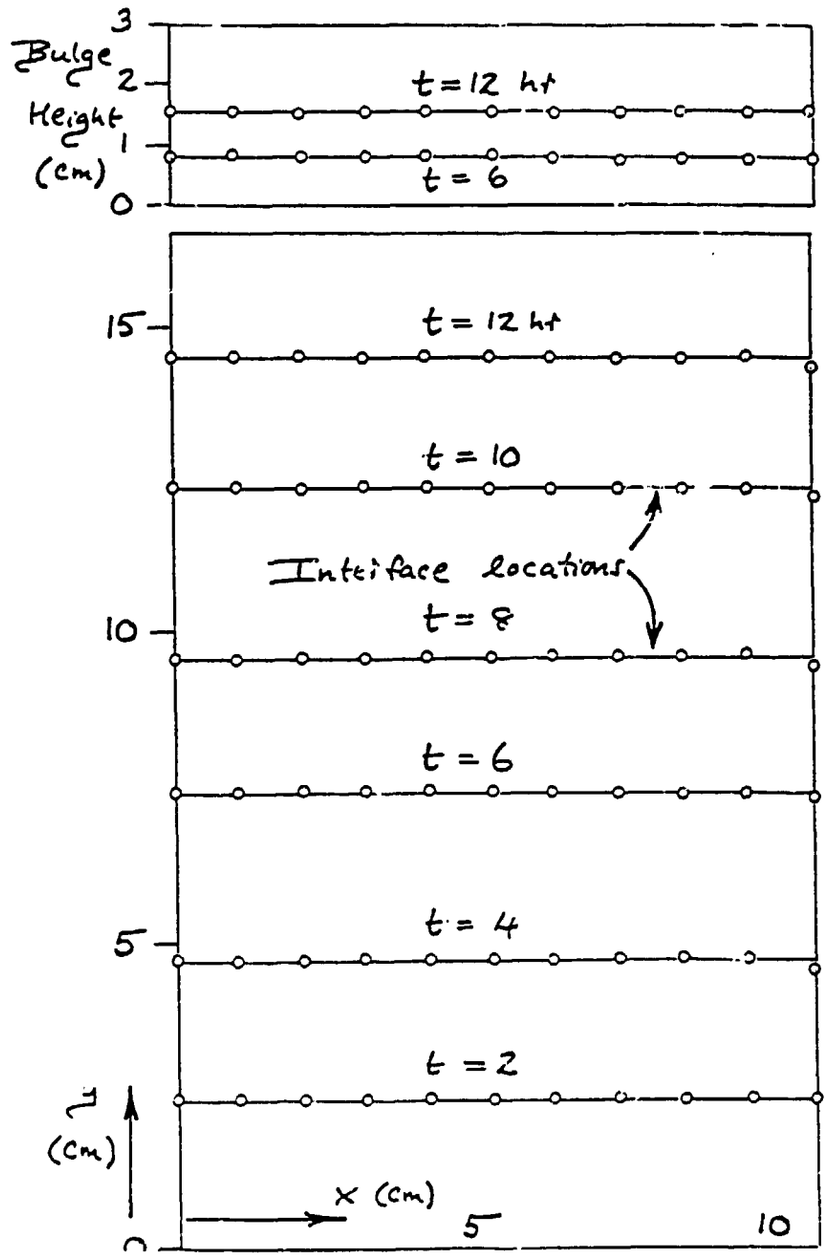
3
Bulge
2
Height
1
(cm)
0
t = 12 ht
t = 6
15
t = 12 ht
t = 10
Interface locations
10
t = 8
t = 6
5
t = 4
t = 2
(cm)
x (cm)
5
10

Run 2

$\alpha_C = 0.00568$ J/SEC CM^2 ^oC

$\beta_C = 8.07$ J/SEC CM^2

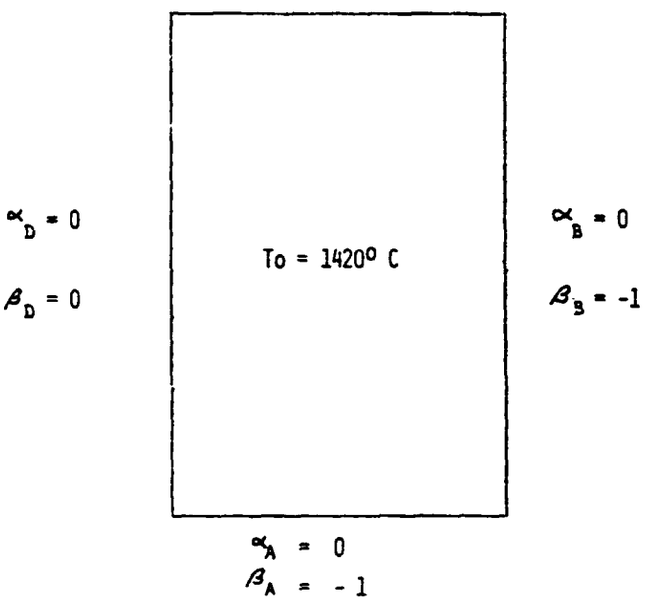

ΔT = 100 SEC

T_{MAX} = 21600 SEC (6 HOURS)

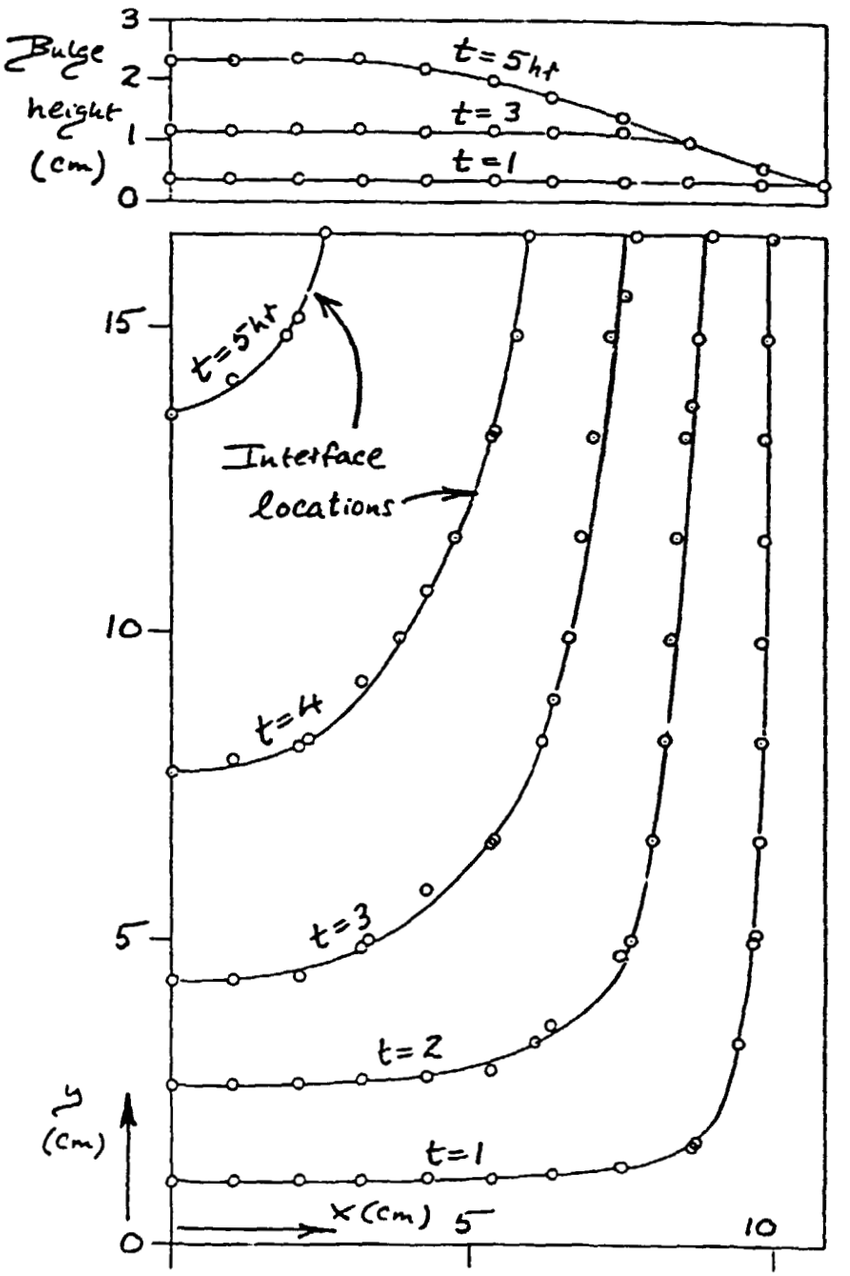
Bulge height (cm)
3
2
1
0
t=5ht
t=3
t=1
15
10
5
0
t=5ht
Interface locations
t=4
t=3
t=2
t=1
y (cm)
x (cm)
5
10

Status

A TWO DIMENSIONAL COMPUTER MODEL HAS BEEN DEVELOPED

NEED TO ESTABLISH THE TRUE BOUNDARY CONDITIONS WITHIN A UCP FURNACE

ELECTROCHEMICAL PRODUCTION OF SILICON

ENERGY MATERIALS CORP.

H.E. Bates

Program Objectives

- Design and build cell to produce 50 gm/hr
- Determine operating conditions and run cell ca. 40 hours to produce 2kg of Si
- Theoretical analysis and model of anode impurity and Si depletion behavior, correlate with experimental observations
- Analyze economic potential of large scale production

Background

- Process invented and demonstrated by Jerry Olson of S.E.R.I.
- Key element is Cu_3Si - Si anode
- Low temperature (~1000°C) fabrication of Mg - Si anode
- $D_{Si} \gg D_{METALS}$ in Cu_3Si

Electrorefining Process Schematic

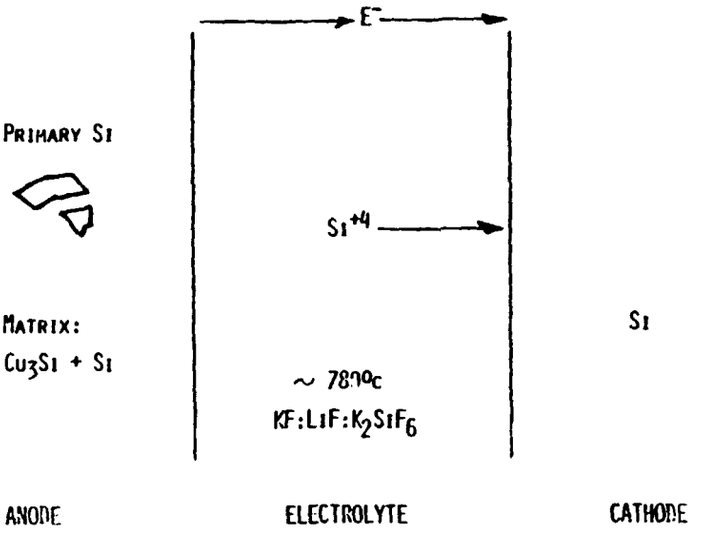

Experimental Procedure

- DRY SALT MIXTURE: $350^{0}C + 10^{-3}$ TORR
- MELT SALTS AND PRE-ELECTROLYSIS REMOVAL OF IMPURITIES
- SILICON ELECTROLYSIS: 100 MA/CM^2
- ANALYZE ANODE (STRUCTURE, IMPURITY DISTRIBUTION), ELECTROLYTE PURITY, DEPOSITED SILICON

Progress

- SYSTEM COMPLETED.
- ANODES (20x25x1CM) SUCCESSFULLY FABRICATED BY CASTING.
- SIGNIFICANT PURIFICATION OBTAINED BY SLAG FORMATION DURING ALLOYING.
- INITIAL MODEL OF ANODE BEHAVIOR DEVELOPED.
- SYSTEM SUCCESSFULLY OPERATED FOR FIRST EXPERIMENT - RESULTS BEING ANALYZED.

Copper-Silicon Anode Impurity Content

Impurity (ppmw)	Cu	Mg-Si	Cu-Si Alloys	
			Expected	Actual
B	.005	(35)	(10)	6
Al	.04	2100	~650	5
P	.005	(40)	(10)	0.6
Ca	.07	160	~ 50	0.4
Ti	NR	(400)	(120)	2
V	.01	(150)	(50)	5
Cr	2	(300)	(100)	2
Mn	.02	200)	(60)	3
Fe	9	3400	~1000	100
Ni	2	(80)	2 (25)	1
Zn	255		~ 180	1
Sn	30		~ 20	0.4
Pb	15		~ 10	0.8

( ) Indicates typical values, after Hunt and Dosaj

Structure of As-Cast 70:30 w% Cu:Si (50X)

Eutectic Phase (Cu_3Si + Si) of 70:30 Cu:Si (200X)

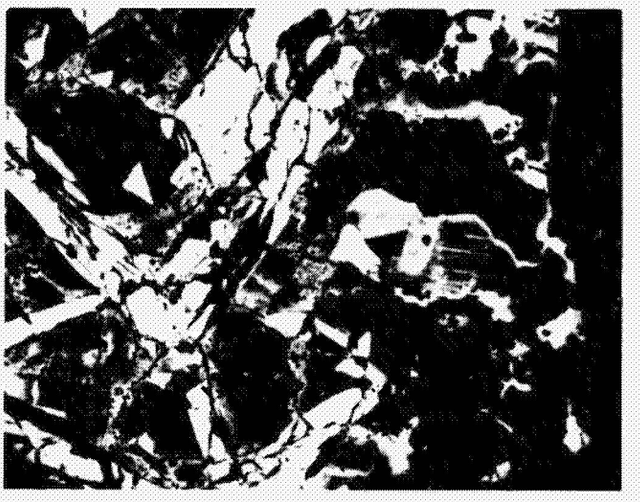

STRUCTURE OF Cu:Si ANODE AFTER 8 HOURS OF OPERATION. Si DEPLETION CAN BE SEEN IN RIGHT HALF OF PHOTO. 50x

Plans

- CONTINUE EXPERIMENTAL OPERATION OF SYSTEM.
- ANALYZE ANODE BEHAVIOR AND DEPOSIT PURITY.
- CORRELATE OBSERVATIONS WITH MODEL.

SILANE DECOMPOSITION IN AN FBR

UNION CARBIDE CORP.

S.K. Iya

TECHNOLOGY	REPORT DATE
POLYCRYSTALLINE SILICON R&D	MARCH 15, 1984
APPROACH SILANE DECOMPOSITION IN A FLUIDIZED BED REACTOR **CONTRACTOR** UNION CARBIDE CORPORATION	**STATUS** • LONG DURATION TESTS WERE CONDUCTED TO DEMONSTRATE OPERABILITY AND DETERMINE PURITY. • PRELIMINARY PRODUCT PURITY FROM METAL WALL REACTOR WAS ESTABLISHED. • FBR PRODUCT WAS MELTED AND SINGLE CRYSTALLIZED. • PDU MODIFICATIONS TO IMPROVE PRODUCT PURITY ARE CURRENTLY IN PROGRESS.
GOALS • DEMONSTRATE PROCESS FEASIBILITY. • DETERMINE OPERATING WINDOW. • CONDUCT LONG-DURATION TESTS. • DEMONSTRATE SILICON PURITY.	

Run Summary: Long-Duration Tests

- 3 LONG DURATION RUNS WERE CONDUCTED WITH TOTAL RUN TIME OVER 80 HOURS.

- LONGEST SINGLE RUN WAS FOR 45 HOURS WITH VOLUNTARY SHUTDOWN.
  - 300 μM SEED GROWN TO 500 μM PRODUCT
  - AVERAGE SILANE FEED RATE 2 KG/HR
  - MAXIMUM SILANE FEED CONCENTRATION 22%
  - BED TEMPERATURE 600°C - 700°C
  - U/U_{MF} 3.5 - 5.0
  - COMPLETE SILANE CONVERSION WITHIN THE BED
  - ON LINE PRODUCT WITHDRAWAL WAS DEMONSTRATED
  - FINE POWDER 5 - 6% OF SILANE FEED
  - POWER CONSUMPTION 15 KWH/KG

Long-Duration Run: Mass Balance

INITIAL BED WEIGHT	33.5 KG
SILICON IN	79.3 KG
TOTAL	112.8 KG

FINAL BED WEIGHT	57.6 KG
PRODUCT OUT	56.9 KG
POWDER FROM FILTERS	3.7 KG
TOTAL	118.2 KG

ERROR IN MASS BALANCE = 4.6%

Preliminary Product Characterization

PARTICLE PROPERTIES

- 500 μM MEAN PARTICLE DIAMETER
- 100 LB/CFT. BULK DENSITY
- SMOOTH, ROUNDED SURFACE
- FREE FLOWING

PARTICLE MORPHOLOGY

- DENSE DEPOSITION LAYER
- LAYERED RING-LIKE GROWTH STRUCTURE
- GROWTH LAYER THICKNESS OVER 100 μM

PARTICLE PURITY

- EMISSION SPEC AND NAA DATA SHOWED METALLIC CONTAMINANTS (FE, CR, NI) FROM REACTOR WALL.
- PARTICLES WERE MELTED AND SINGLE CRYSTALLIZED.

Product Purity Improvement Plan: PDU Modifications

- SEVERAL REACTOR LINER AND SPRAY COATING OPTIONS WERE EVALUATED.
- HIGH PURITY POLYSILICON LINER WAS CHOSEN AS FIRST CHOICE, WITH QUARTZ LINER AS A BACKUP.
- LINER WAS DESIGNED AND ORDERED.
- PRODUCT WITHDRAWAL SYSTEM WAS REDESIGNED TO ENABLE COOLING, SCREENING, AND BAGGING WITHOUT MANUAL HANDLING OR EXPOSURE TO ATMOSPHERE.

Future Plans

- PDU MODIFICATIONS COMPLETED - I Q, 1984
- HIGH PURITY EXPERIMENTS CONDUCTED - II & III Q, 1984
- SEED GENERATION METHOD TESTED - II & III Q, 1984
- TECHNICAL AND ECONOMIC ASSESSMENT - IV Q, 1984

N85 15291

JPL IN-HOUSE FLUIDIZED-BED REACTOR RESEARCH

JET PROPULSION LABORATORY

G.C. Hsu

Metallic Impurities (ppmw): Neutron Activation Analysis/LLL (11/83)

JPL RUN NO.	Cr	Fe	Ni	Co	Mo	W	Na	TOTAL IDENTIFIED
109 (SEED)	1.5				0.15	0.08	1.4	
111 (SEED)	4		1		0.05	0.04	1.3	
111-4P	16(15%)	77(72%)	11(11%)	0.16	0.76(0.7%)	0.1	2	107
111-8P	45(17%)	185(70%)	31(12%)	0.36	3.8 (1.4%)	0.15	1.3	266
115P-1	31(17%)	132(70%)	26(14%)	0.18	0.55(0.3%)	0.1	1.1	190
115P-2	46(17%)	197(71%)	30(11%)	0.4	1 (0.4%)	0.1	1.1	275
115 INGOT #1	0.7						1.3	
115 INGOT	0.2						4.2	
115 INGOT #2	0.3						1.2	

*REACTOR WALL MATERIAL S.S. 316: Cr 17% Fe 70% Ni 12% Mo 2.5% Mn 2% Si 1%

Various Wall Materials for FBR

FBR Wall Materials	Description	Advantages	Disadvantages	Decision
Quartz Liner in Stainless Steel Reactor	Placed a mechanically sealed quartz tube inside the SS reactor.	-Avoids metal contamination -Inexpensive construction	-Poor heat transfer -Quartz may crack inside the reactor	Liner System in Fabrication
Silicon Carbide Liner in Stainless Steel Reactor	Same (with SiC tube)	-Avoids metal contamination	-Poor heat transfer -Possible carbon contamination -Expensive construction	
Silicon Liner in Stainless Steel Reactor	Same (with Si tube)	-Avoids metal contamination	-Poor heat transfer -Relatively expensive construction	
Silicon Carbide Coated Graphite Reactor	Inside Surface of graphite tube is coated with Silicon Carbide.	-Good heat transfer	-Non-uniform coating -Possible carbon contamination -Expensive construction	
Zirconium Oxide Coating on SS Reactor	Inside Surface of the SS reactor is coated with Zirconium Oxide.	-Good heat transfer	-Possible zirconium contamination -Cracking of coating due to different thermal expansion	
Liquid Nitriding of SS	The hardness of SS surface is increased by treating it in a liquid cyanide bath.	-Inexpensive process	-Possible migration of metallic impurities from hot SS surface	Gas distributor, expanded head, and withdrawal assembly will be treated by this process

Quartz Liner System for 6-in. FBR

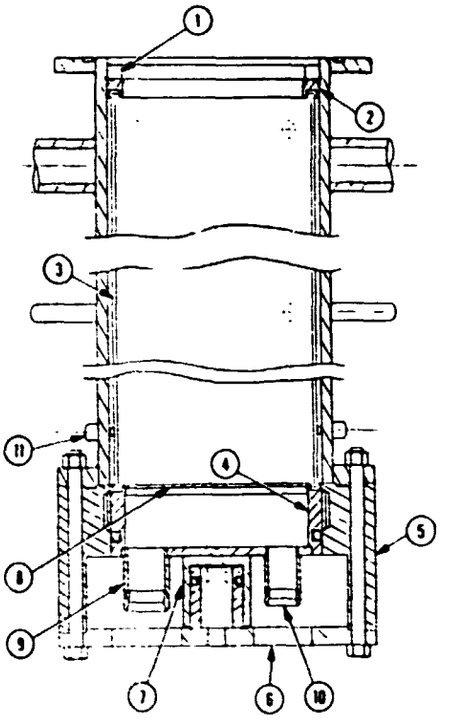

COMPONENTS:

1. STOP RING
2. SEALING RING
3. QUARTZ LINER
4. DISTRIBUTOR HOLDER
5. DISTRIBUTOR HOLDER SUPPORT
6. PNEUMATIC CYLINDER SUPPORT
7. PNEUMATIC CYLINDER
8. GAS DISTRIBUTOR
9. SILICON WITHDRAWL
10. KINETIC SAMPLER
11. HYDROGEN PURGE

Reaction Paths for Silane Pyrolysis in FBR

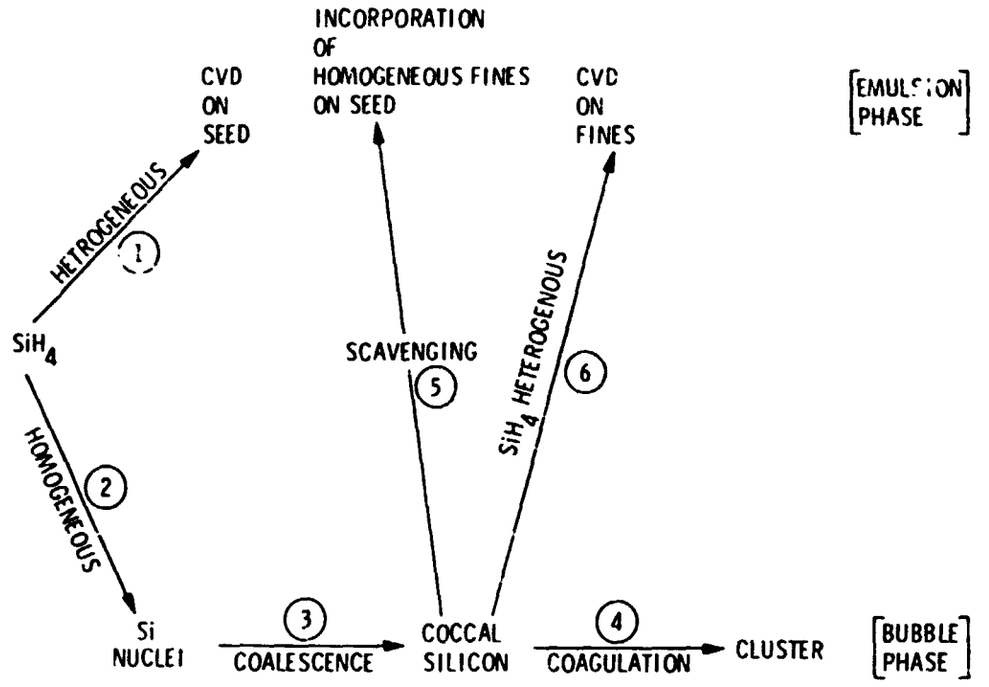

Conditions for Incorporation of Homogenous Fines Onto Seed Particle

- TEMPERATURE > TAMMANN TEMPERATURE (610°C FOR SI)
  - TAMMANN TEMPERATURE = 0.52 X (BULK MELTING POINT IN °K)
  - DEFINED AS INDEX FOR SURFACE MOBILITY OR "WETTABILITY"
- IN THE PRESENCE OF SILANE REACTION
  - CVD REACTION IS NEEDED TO SEAL FINES AFTER ADSORPTION
- SIZE OF FINE PARTICLE IS SMALL ENOUGH FOR SUCCESSFUL ADSORPTION

Fines Incorporation and CVD

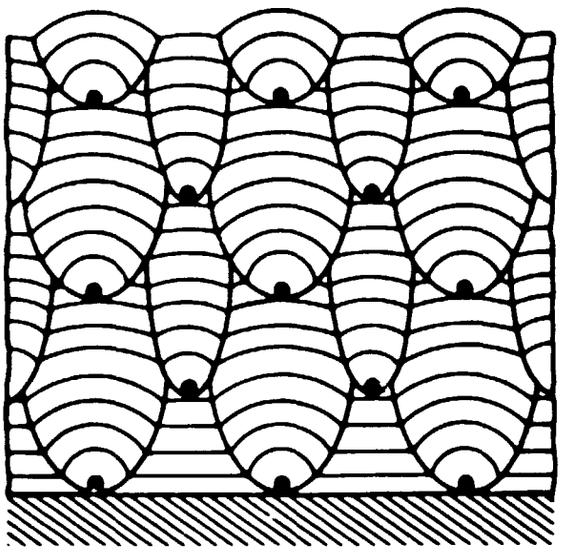

SCHEMATIC REPRESENTATION OF THE CONTINUOUS NUCLEATION OF GROWTH CONES IN "EGENERATIVE DEPOSITS"

"PYROLYTIC CARBON DEPOSITION-
L.F. COFFIN, JI. Am. CERAM-SOC. 47, 473 (1964)

Locations of Secondary Silane Injection for Enhancing Scavenging

- TEMPERATURE > TAMMANN TEMPERA.URE
- PRIMARY SILANE INTRODUCED FROM THE DISTRIBUTOR WILL DEPLETE AFTER 12 INCHES
- AT THE 13-IN. LOCATION, THE MAXIMUM SIZE OF FINE PARTICLE IN GAS PHASE IS LESS THAN 1 μm

$\Longrightarrow$ 13-INCH ABOVE THE DISTRIBUTOR

Scavenging Experiment (JPL 6-in. FBR)

- CONDITIONS :

  T = 650°C

  $\overline{U}/U_{mf}$ = 4

  #325 MESH SCREEN DISTRIBUTOR

  INITIAL BED HEIGHT 25 INCHES

  INITIAL BED WEIGHT ~13 KG

  INITIAL SEED SIZE ~225 μM

  DURATION 3 HOURS

  1) PRIMARY SILANE FEED FROM THE DISTRIBUTOR

     SILANE 20 ℓ/MIN, HYDROGEN 20 ℓ/MIN (50% SILANE FEED)

  2) SECONDARY SILANE INJECTION FROM 2 SIDE PORTS AT THE 13-IN LOCATION ABOVE THE DISTRIBUTOR

  A) SCAVENGING RUN - NO. 204
     SILANE 2 ℓ/MIN, HYDROGEN 8ℓ/MIN (20% SILANE)

  B) CONTROL RUN - NO. 206
     HYDROGEN 12 ℓ/MIN (0% SILANE)

Scavenging Experiments

- RESULTS -

	RUN 206 (CONTROL)	RUN 204 (SCAVENGING)
% OF FINES VS FEED Si (ELUTRIATED IN THE FILTER AND THE EXPANDED HEAD)	10%	6%
FINE PARTICLES IN THE BED (-75 μM)		
% IN THE SEED	5%	2.6%
% DIFFERENCE IN PRODUCT VS SEED	+ 0.1%	-1%
% PRODUCT IN BED	92%	95.5%
PRODUCTION RATE (KG/HR)	1.3	1.5

Jet-Mill Grinding of Silicon Particles (Si Fed Into 2 Opposing Jets, Single Pass)

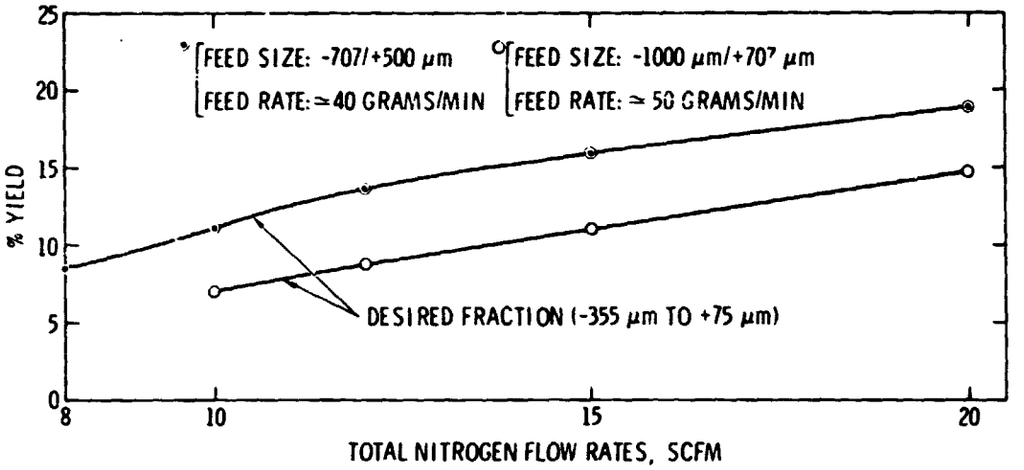

Jet-Mill Grinding of Silicon Particles

SIZE FRACTIONS	1ST PASS YIELD (%)	2ND PASS YIELD* (OVERALL) (%)
OVERSIZE (+ 355 μm)	81.7	67.7
DESIRED FRACTION (-355 μm TO + 75μm)	15.8	28.3
UNDERSIZE (-75 μm)	2.6	4.3

* +355 μm FRACTION WAS RECYCLED

FEED SIZE: -707/+500 μm
N_2 FEED RATE: 12 SCFM
SILICON FEED RATE: 40 GRAMS/MIN.

N85 15292

AEROSOL REACTOR FOR SILICON PROCESSING

CALIFORNIA INSTITUTE OF TECHNOLOGY

R.C. Flagan
M.K. Alam
B.E. Johnson
J.J. Wu

A Free-Space Reactor System for Production of Silicon

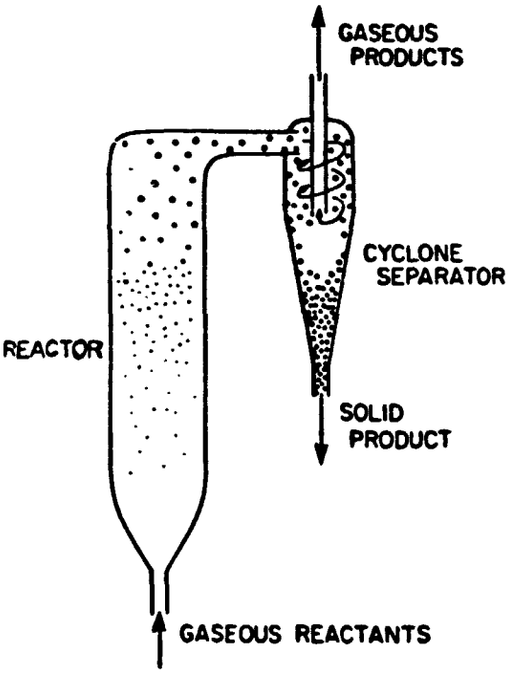

Processes in Silane Pyrolysis Reactor

- HOMOGENEOUS GAS PHASE REACTION
- HOMOGENEOUS NUCLEATION
- HETEROGENEOUS CONDENSATION
- HETEROGENEOUS REACTIONS
- COAGULATION

Silane Pyrolysis (Ring & O'Neal, 1982)

$$SiH_4 + M \xrightarrow{k_1} SiH_2 + H_2 + M$$

$$SiH_2 + SiH_2 \underset{k_{-2}}{\overset{k_2}{\rightleftharpoons}} Si_2H_4 \xrightarrow{k_3} Si_2H_2 + H_2$$

$$SiH_2 + SiH_4 \underset{k_{-4}}{\overset{k_4}{\rightleftharpoons}} Si_2H_6 \xrightarrow{k_5} Si_2H_4 + H_2$$

$$SiH_2 + Si_2H_6 \underset{k_{-6}}{\overset{k_6}{\rightleftharpoons}} Si_3H_8 \underset{k_{-7}}{\overset{k_7}{\rightleftharpoons}} SiH_3SiH + SiH_4$$

$$SiH_3SiH \underset{k_{-8}}{\overset{k_8}{\rightleftharpoons}} Si_2H_4$$

$$SiH_2 \xrightarrow{k_9} surface - SiH_2$$

$$SiH_4 \xrightarrow{k_{10}} surface - SiH_4$$

$$SiH_2 - surface \xrightarrow{k_{11}} surface - SiH_2\bullet$$

$$surface - SiH_2 \bullet SiH_4 \xrightarrow{k_{12}} surface - SiH_3 + SiH_3\bullet$$

$$SiH_3\bullet \bullet SiH_4 \xrightarrow{k_{13}} Si_2H_6 \bullet H\bullet$$

$$H\bullet \bullet SiH_4 \xrightarrow{k_{14}} H_2 \bullet SiH_3\bullet$$

.....

$k_1 = 10^{15.5} exp[-59600/RT]\ sec^{-1}$

Homogeneous Nucleation

$$A_{g-1} + A_1 \rightleftharpoons A_g$$

CRITICAL NUCLEUS

$$d_p^* = \frac{4\sigma V_m}{kT \ln S} \leq 8\ \text{Å} \quad \text{FOR Si}$$

NUCLEATION RATE (CLASSICAL THEORY)

$$J\left(\frac{\text{PARTICLES}}{\text{CM}^3\text{SEC}}\right) = 2P_1^2 \left(\frac{2\sigma}{2\pi m}\right)^{1/2} V_m^{2/3} \left[\frac{\sigma V_m^{2/3}}{kT}\right]^{1/2} \exp\left\{-\frac{16\pi\sigma^3 V_m^2}{3(kT)^3(\ln S)^2}\right\}$$

Particle Growth

-CONSIDER THE UNION CARBIDE SYSTEM

0.2 TO 1 MICRON PARTICLES WERE PRODUCED, ACCOUNTING FOR >80% OF THE MASS AT THE REACTOR OUTLET

THIS CORRESPONDS TO 10^{14} TO 10^{16} PARTICLES/M^3

GROWTH OF THESE PARTICLES TO 10 MICRON SIZE REQUIRES INCREASING THE MASS OF EACH PARTICLE BY A FACTOR OF 10^3 TO 10^5

IN ORDER TO SUPPLY SUFFICIENT SILICON, THE SEED AEROSOL MUST BE DILUTED WITH SILANE BY A FACTOR OF 10^3 TO 10^5

-CAN ADDITIONAL NEW PARTICLE FORMATION BE PREVENTED AT THE REDUCED PARTICLE CONCENTRATION?

Aerosol Reactor for Growth of Large Silicon Particles by Silane Pyrolysis

1. GENERATE SEED PARTICLES BY PYROLYSIS OF A SMALL AMOUNT OF SILANE.
2. MIX SEED AEROSOL WITH PRIMARY SILANE FLOW, LIMITING NUMBER CONCENTRATION SUCH THAT THE AMOUNT OF SILANE IS SUFFICIENT TO GROW THE DESIRED SIZE OF PARTICLES FROM THE SEED.
3. REACT THE SILANE AT A RATE WHICH IS CONTROLLED SUCH THAT THE SEED PARTICLES SCAVENGE THE CONDENSIBLE VAPORS RAPIDLY ENOUGH TO INHIBIT FURTHER NUCLEATION.

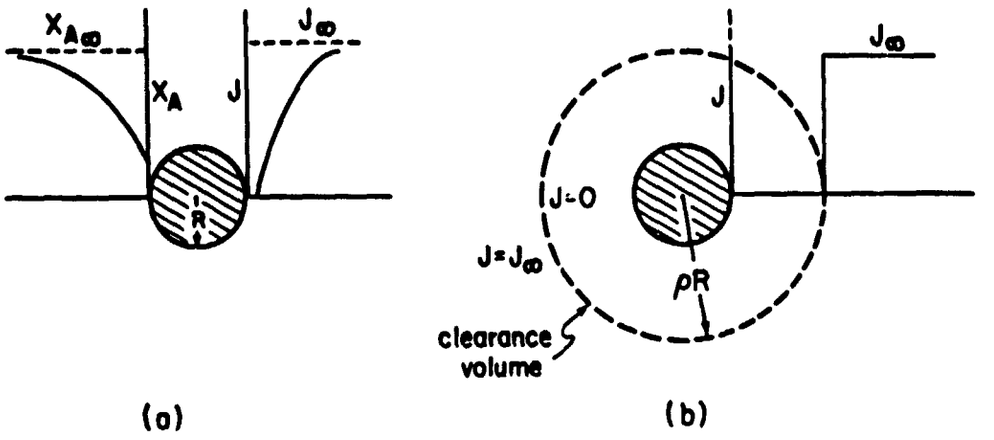

Reduction of Overall Nucleation Rate

TOTAL FRACTIONAL CLEARANCE VOLUME

$$\Omega = \int_0^\infty \frac{4}{3}\pi \rho^3 a^3 n(a,t)\, da$$

AVERAGE NUCLEATION RATE

$$J_{av} \simeq \begin{cases} J_\infty(1-\Omega) & : \quad 0 \leq \Omega < 1 \\ 0 & : \quad \Omega > 1 \end{cases}$$

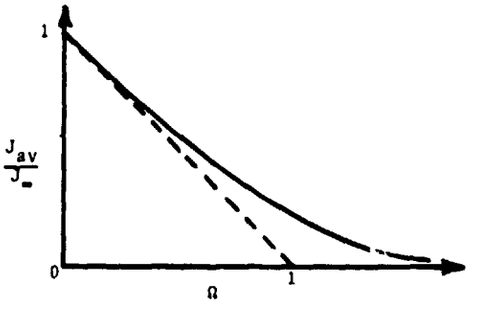

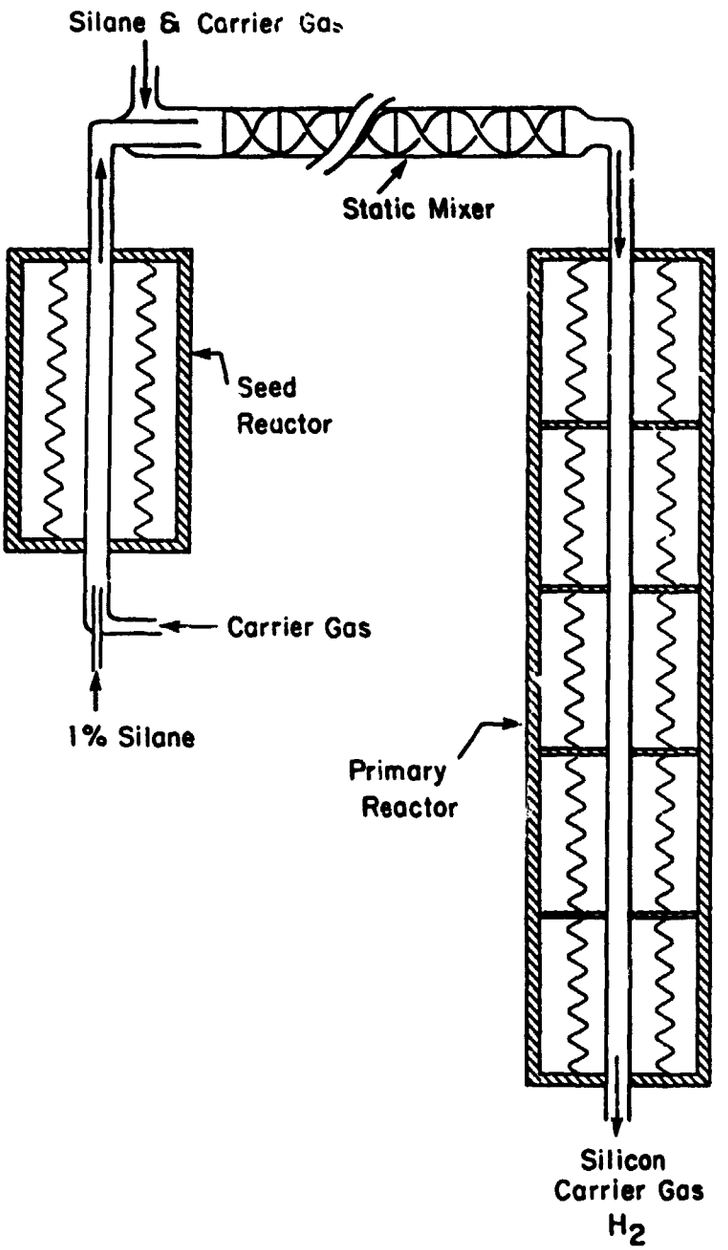
Silane & Carrier Gas
Static Mixer
Seed
Reactor
Carrier Gas
1% Silane
Primary
Reactor
Silicon
Carrier Gas
H_2

Temperature Profile and Reaction Kinetics in the Aerosol Reactor

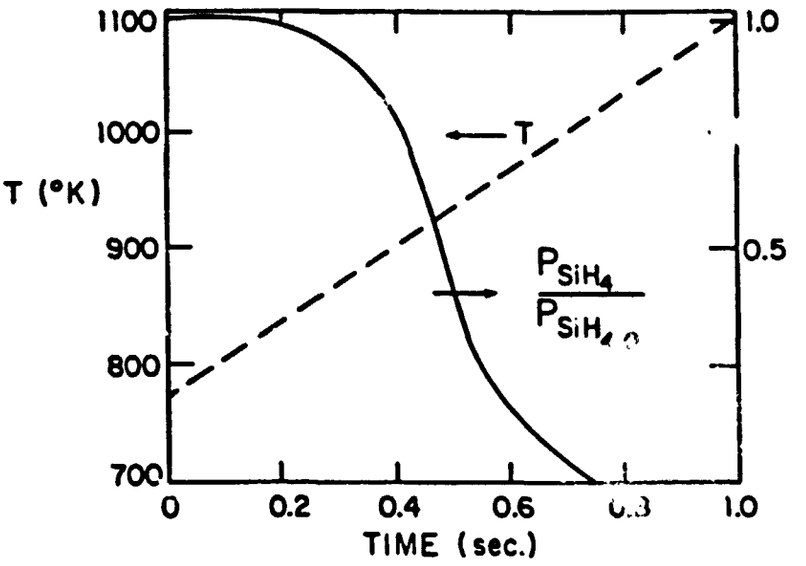

Particle Growth in the Silicon Aerosol Reactor

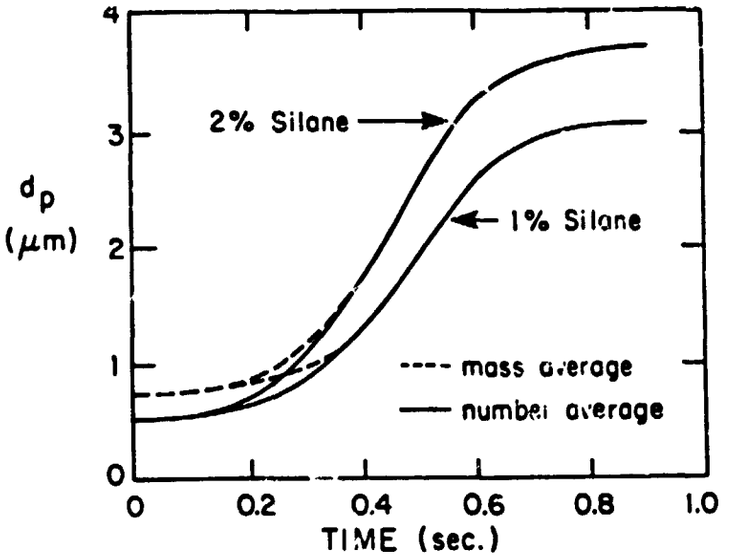

Total Clearance Volume Fraction in the Reactor

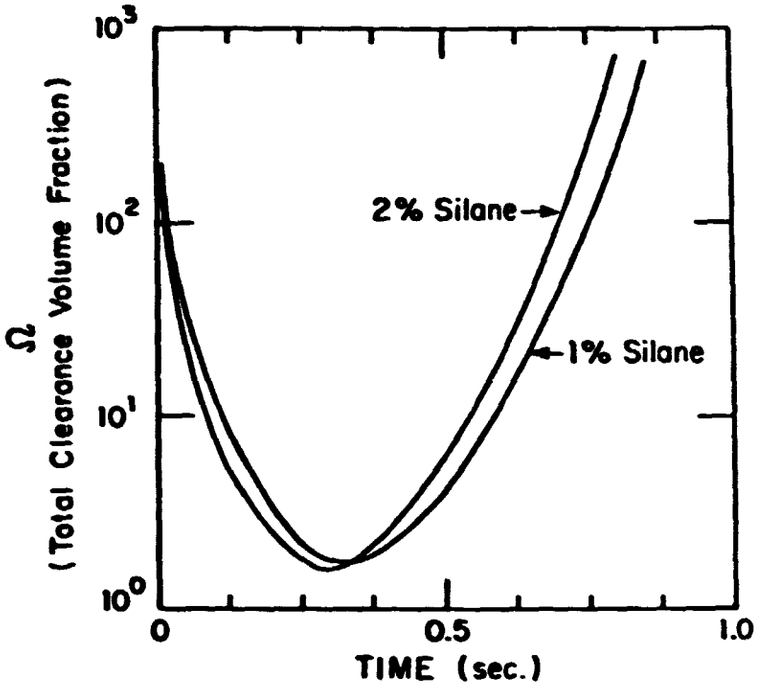

Mass Distribution of Silicon Aerosol in a High-Temperature Reactor at 900K Without Seed Aerosol (Silane Concentration 1%)

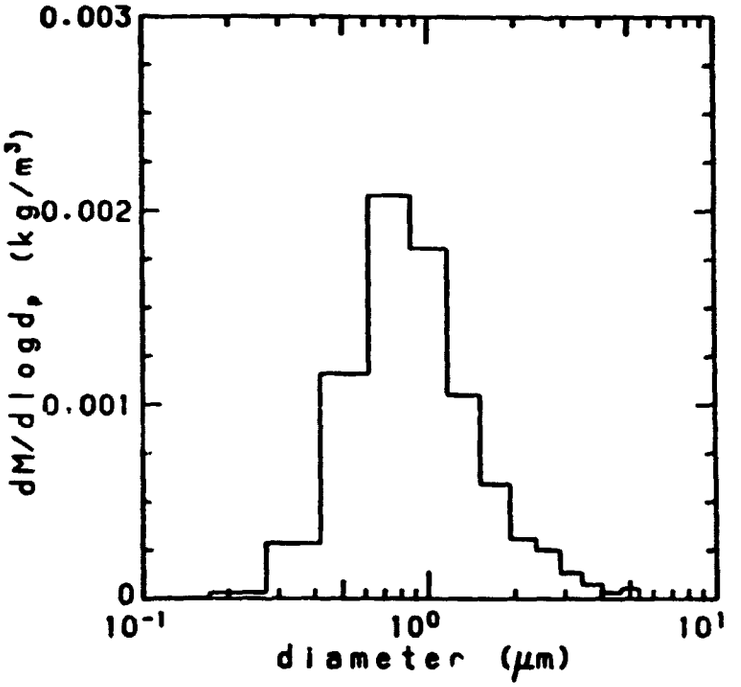

C-6

Mass Distribution of Product Aerosol After Reacting 1% Silane With Reduced Seed Concentration ($2.7 \times 10^{10}/m^3$)

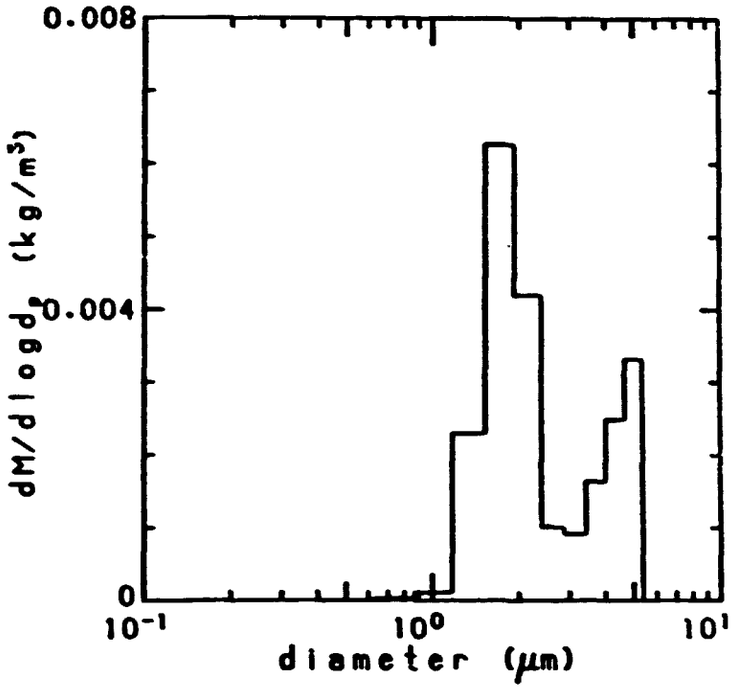

Mass Distribution of Aerosol After Reacting 2% Silane in Presence of Seed Aerosol (Total Seed Concentration $1.02 \times 10^{11}/m^3$)

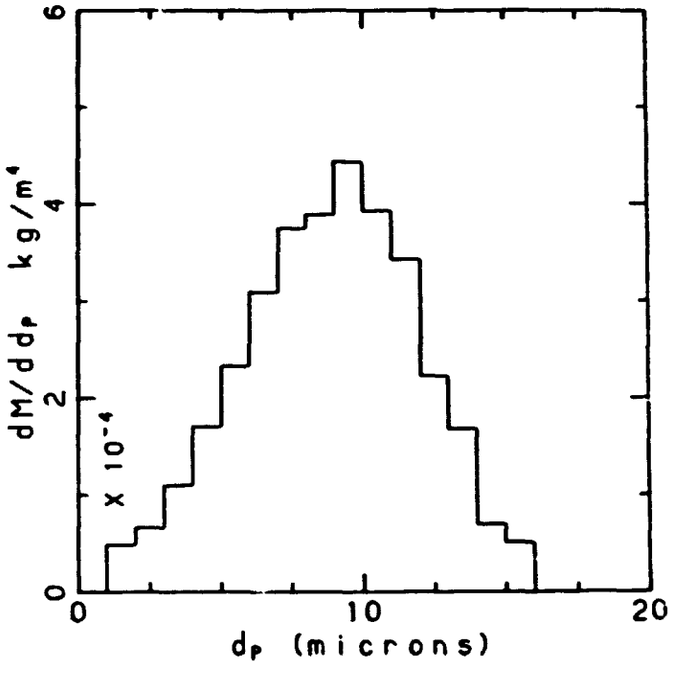

Silicon Losses in the Reactor as a Function of Input Silane Concentration

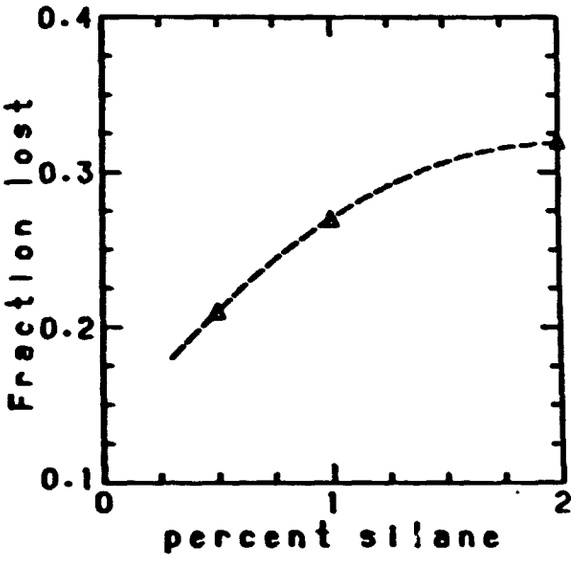

Comparison of Characteristic Times of Silane Reaction With Residence Times in Reactor

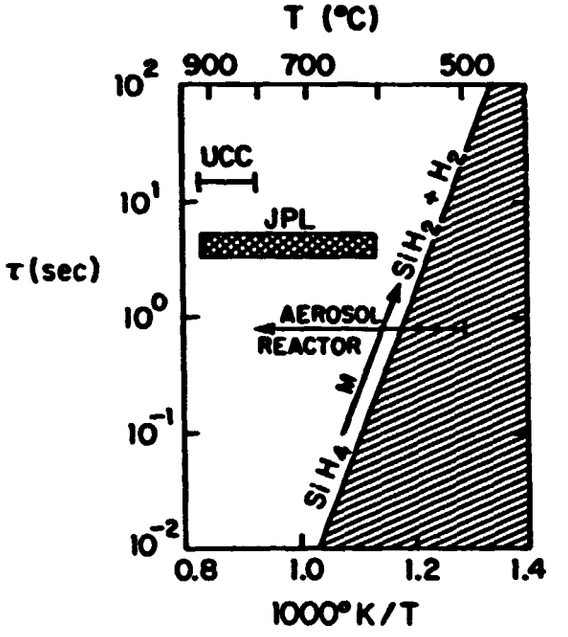

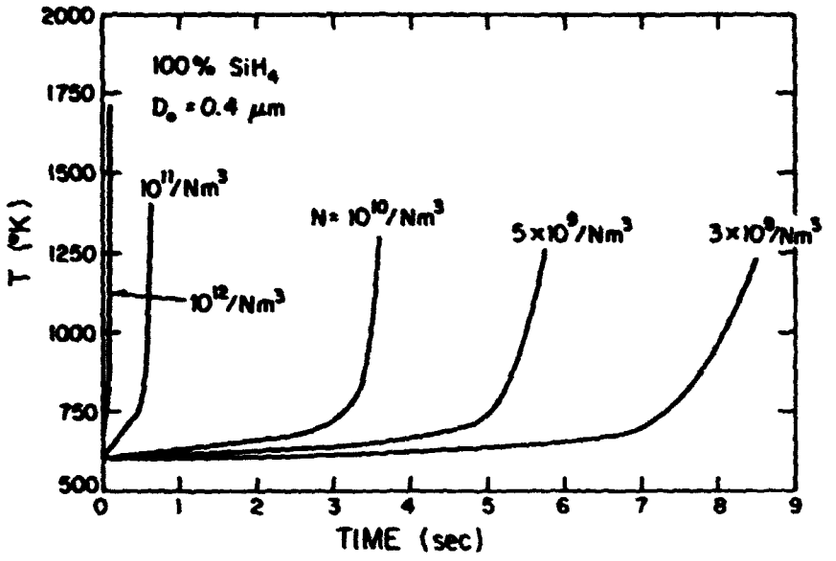
100% SiH_4
$D_o = 0.4\ \mu m$
$10^{11}/Nm^3$
$N = 10^{10}/Nm^3$
$5\times10^9/Nm^3$
$3\times10^9/Nm^3$
$10^{12}/Nm^3$
T (°K)
TIME (sec)

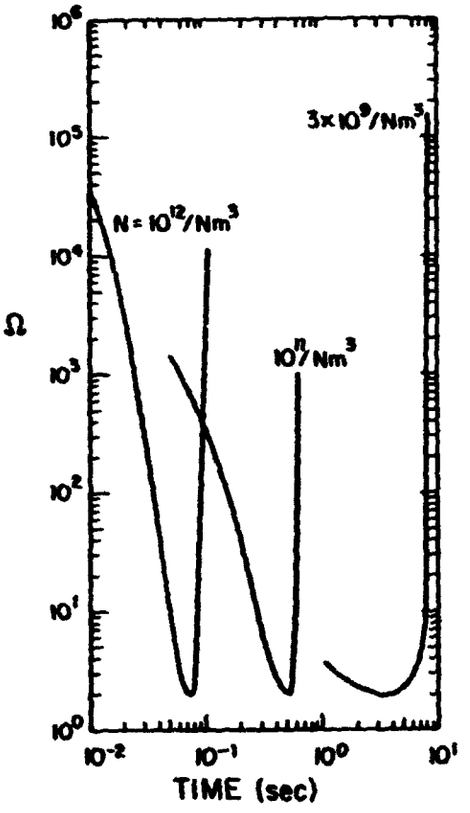
$3\times10^9/Nm^3$
$N = 10^{12}/Nm^3$
$10^n/Nm^3$
Ω
TIME (sec)

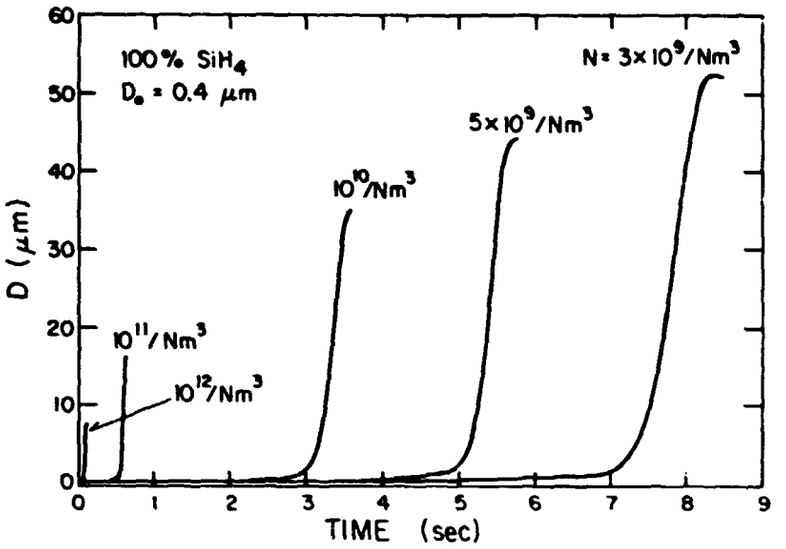
100% SiH4
D0 = 0.4 μm
N = 3x10^9/Nm^3
5x10^9/Nm^3
10^10/Nm^3
10^11/Nm^3
10^12/Nm^3
D (μm)
TIME (sec)
0
10
20
30
40
50
60
0
1
2
3
4
5
6
7
8
9

OMIT TO P479

REFINEMENT OF METALLURGICAL-GRADE SILICON BY CHEMICAL VAPOR TRANSPORT PROCESS

SOLAR ENERGY RESEARCH INSTITUTE

J. Olson

Reactor Schematic

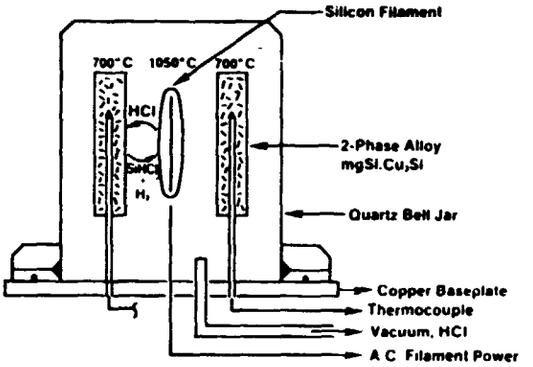

$$Si + 3\,HCl \underset{1050^\circ C}{\overset{700^\circ C}{\rightleftharpoons}} HSiCl_3 + 1/2\,H_2$$

Transport Rate Measurement

Conductance of a silicon filament with length L, width W, and thickness X is:

$$C = \frac{I}{V} = \frac{\sigma W X}{L}$$

where σ is the electrical conductivity

$$X = \frac{1}{\rho L W} \int R\,dt$$

where R is the mass transport rate and ρ the mass density of silicon

Real-time, in situ measurements of the filament conductance reveal that the transport rate varies with time as $t^{-1/2}$. This time dependence can be derived from a model of a transport process that is limited by diffusion through a depletion layer the thickness of which increases with time as $t^{1/2}$.

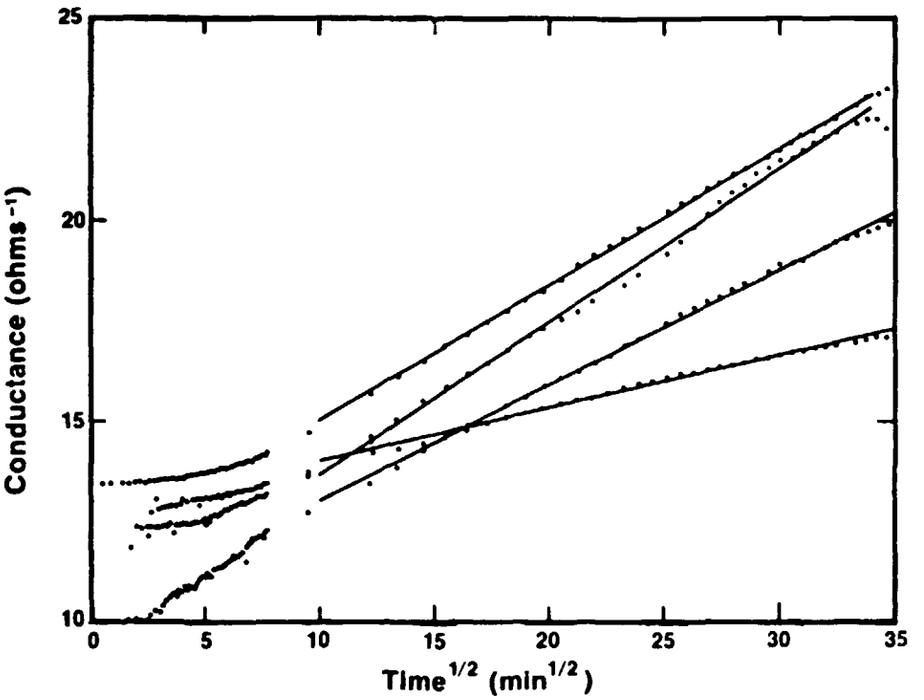
Conductance (ohms^{-1})
25
20
15
10
0
5
10
15
20
25
30
35
Time$^{1/2}$ (min$^{1/2}$)

MODULE AND ARRAY TECHNOLOGY

R.G. Ross, Jr., and L.D. Runkle, Chairmen

A status review of JPL-Clemson University cell reliability research activities was presented by J.W. Lathrop of Clemson. Included were recent results from Arrhenius-modeled combined temperature-humidity tests on encapsulated and unencapsulated cell types and failure-analysis data that further delineated the Schottky barrier formation mechanism observed earlier in p-on-n cells.

Supporting the technology objectives of refining the understanding of the physics of module thermal interaction with natural environments, L.C. Wen of JPL summarized thermal characterization studies conducted on Southwest Residential Experiment Station (SW RES) arrays. Results included correlations useful in refining NOCT determinations.

C.C. Gonzalez of JPL presented comparisons of annual array energy spectra for different tracking modes to assess the advantage of a given mode for any defined cell spectral response.

L.J. Reiter of JPL presented a summary of PV systems performance models. This study, performed for the Program Analysis and Integration Center, reviews a comprehensive set of PV systems performance models and differentiates between their wide range of purposes, approaches, and capabilities. Tables that allow a potential model user to cross-reference the models and a detailed set of characteristics are included. Recent extensions of the capabilities of this set of models and their limitations were discussed. The study assists potential users to match their requirements with an appropriate model.

The preliminary results of a study to examine what the National Photovoltaics Program could do to enhance the process of establishing voluntary consensus standards for measuring the performance of PV modules were discussed by G.A. Praver of JPL. Among the points raised, the study suggests that the prejudices regarding the selection of direct normal, global or some other spectrum as a standard for measurement must be promptly resolved, that this and other technical impediments to consensus be addressed by national laboratory task forces to facilitate resolution, and that funding be provided to support the costs of the voluntary consensus standard activity for both the international interactions and the national work.

M.G. Thomas of the Sandia National Laboratories provided highlights from the Systems PIM held recently at SNLA. He followed this by a discussion of the remaining issues for large system power conditioning subsystem and residential system development.

E.C. Kern, Jr., of the Massachusetts Institute of Technology described the cost experience of the various RES experiments between 1980 and 1983, and projected the costs for retrofit systems for the Northeast RES in 1984. These projections were made for exotic materials such as a-Si, GaAs, and GaAsSi as well as for single-crystal silicon. The single-crystal silicon costs were described in some detail and result in system costs consistent with the trends developed by actual experience.

TRANSPARENT CONDUCTING POLYMERS

JET PROPULSION LABORATORY

Amitava Gupta

Technical Approach

- MODELING AND FEASIBILITY DEMONSTRATION
- SYNTHETIC APPROACHES
- CHARACTERIZATION
- ENVIRONMENTAL STABILITY ASSESSMENT
- SWITCHING CHARACTERISTICS

Modeling and Feasibility Demonstration

- MODELING OF OPTICAL ABSORPTION PROPERTIES RECENTLY INITIATED
- MODELING OF CHARGE CONDUCTION IN PROGRESS
- TCPS ARE WITHIN A FACTOR OF TEN TO ITO IN ITS PERFORMANCE AS A TRANSPARENT CONDUCTIVE COATING
- RECENT RESULTS INDICATE THAT CONDUCTIVITY AND OPTICAL ABSORPTION MAY ARISE OUT OF DIFFERENT MOLECULAR STRUCTURAL FEATURES
- TRUE TCPs MAY BE FORMED BY LOW LEVEL DOPING OF CERTAIN OPTIMIZED POLYMERIC STRUCTURES

Synthetic Approaches

- PLASMA POLYMERIZATION
- ELECTROCHEMICAL POLYMERIZATION
- CHEMICAL POLYMERIZATION

Novel Polymerization Procedure Developed at Caltech

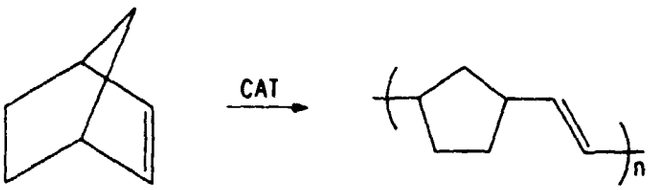

A NOVEL METALLACYCLOBUTANE CATALYST HAS BEEN DEVELOPED WHICH CAN CREATE PURE, UNCROSSLINKED POLYMERS FROM HINDERED OLEFINS

Example

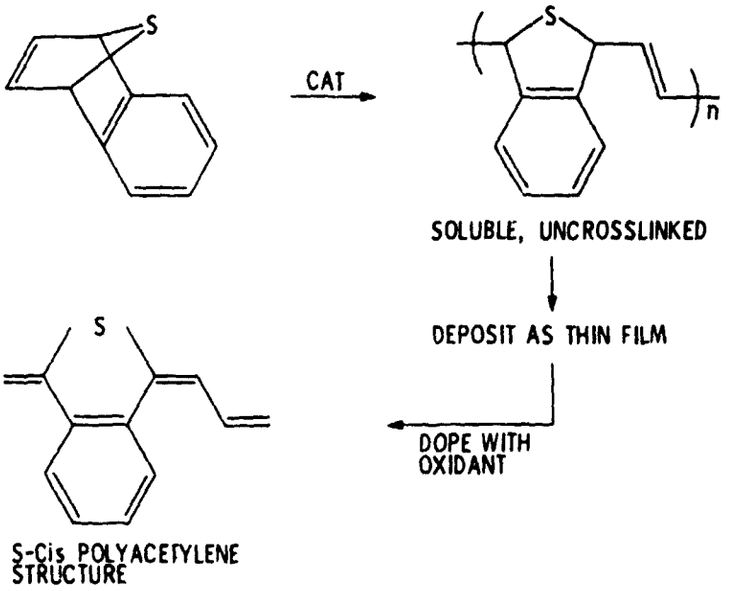

Characterization

MAIN CHARACTERIZATION TECHNIQUES WHICH WILL BE USED ARE

- ESR AND PHOTO-ESR AS A FUNCTION OF DOPING LEVEL
- CONDUCTIVITY AND ABSORBANCE MEASUREMENTS
- ELECTROCHEMICAL CHARACTERIZATION, INCLUDING PHOTOCAPACITANCE SPECTROSCOPY

Environmental Stability

- RADIATION STABILITY OF CERTAIN TCPS e.g. POLYAZULENE REPORTED TO BE EXCELLENT
- STABILITY OF NEUTRAL (NONCONDUCTING) FORM LIMITED BY RXN WITH O_2, WHILE STABILITY OF OXIDIZED FORM IS LIMITED BY RXN WITH H_2O
- STABILITY OF THESE FORMS CORRELATE WITH REDOX POTENTIALS

Polypyrrole Oxidation by I_2: Electrical and Optical Properties of 4500-Angstrom-Thick Film

[DATA FROM PFLUGER, ET. AL., J. CHEM. PHY., 78, 3213 (1983)]

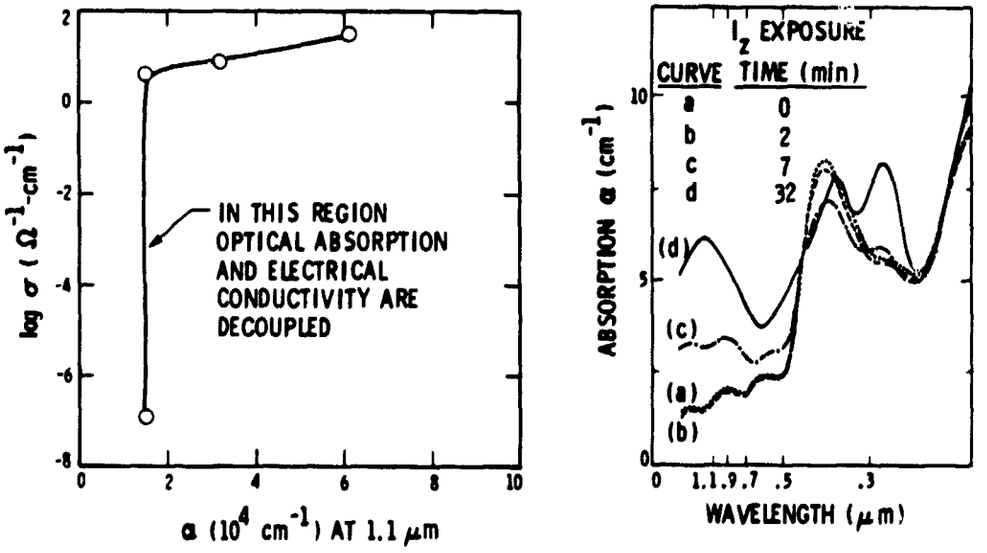

Long-Term Stability of Polaroid TCP Coatings in Ambient Laboratory Atmosphere

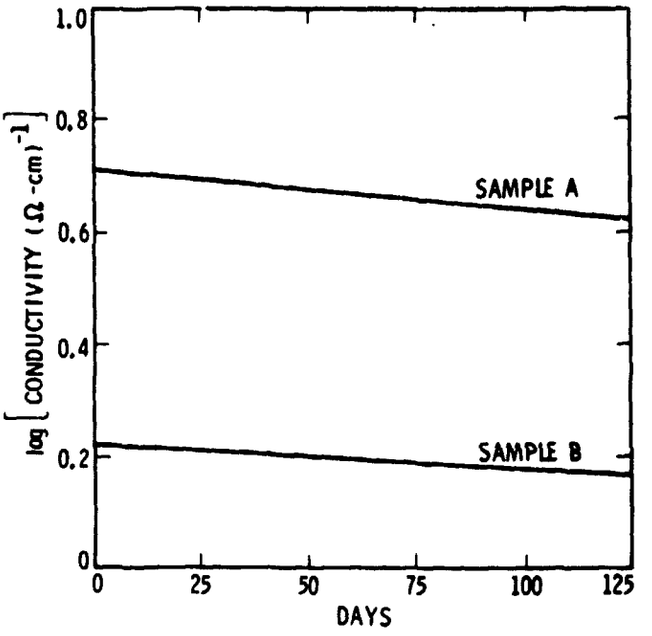

Specular Transmittance of Polaroid TCP on Glass

(UNCORRECTED FOR REFLECTION LOSSES)

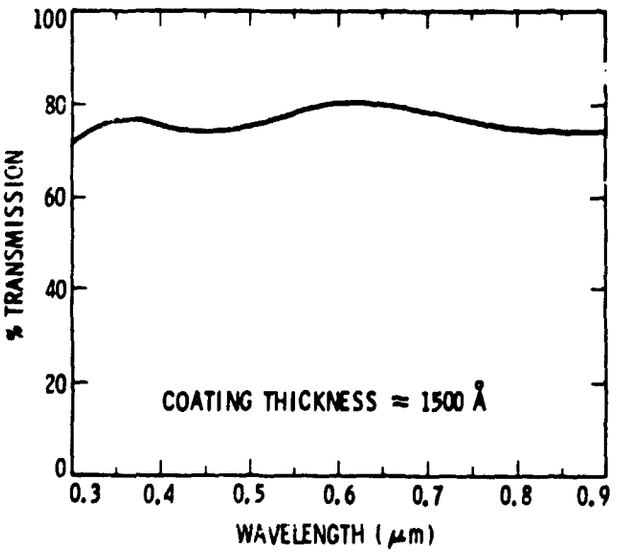

Switching Characteristics

TCPS MAY FUNCTION AS

- AN OPTICAL SWITCH i.e. A NEUTRAL TCP INCORPORATING A PHOTOACTIVATED DOPANT WILL HAVE HIGHLY NONLINEAR ABSORPTION PROPERTIES, i.e. ABSORPTION COEFFICIENT VARYING WITH LIGHT FLUX

- AN ELECTRONIC SWITCH, IN WHICH LIGHT MAY BE USED TO "TURN ON" THE CONDUCTING STATE WHICH MAY BE "TURNED OFF" BY LIGHT OF ANOTHER FREQUENCY

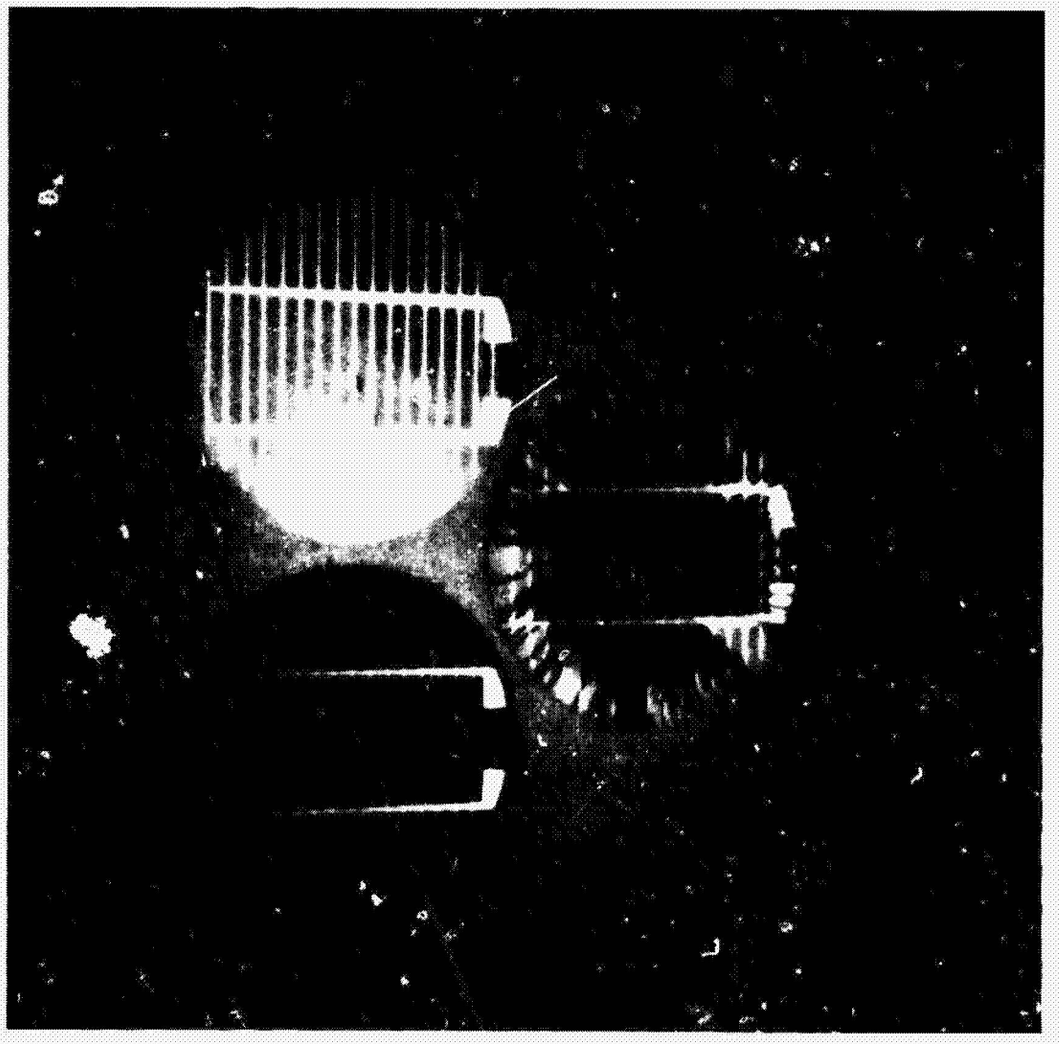

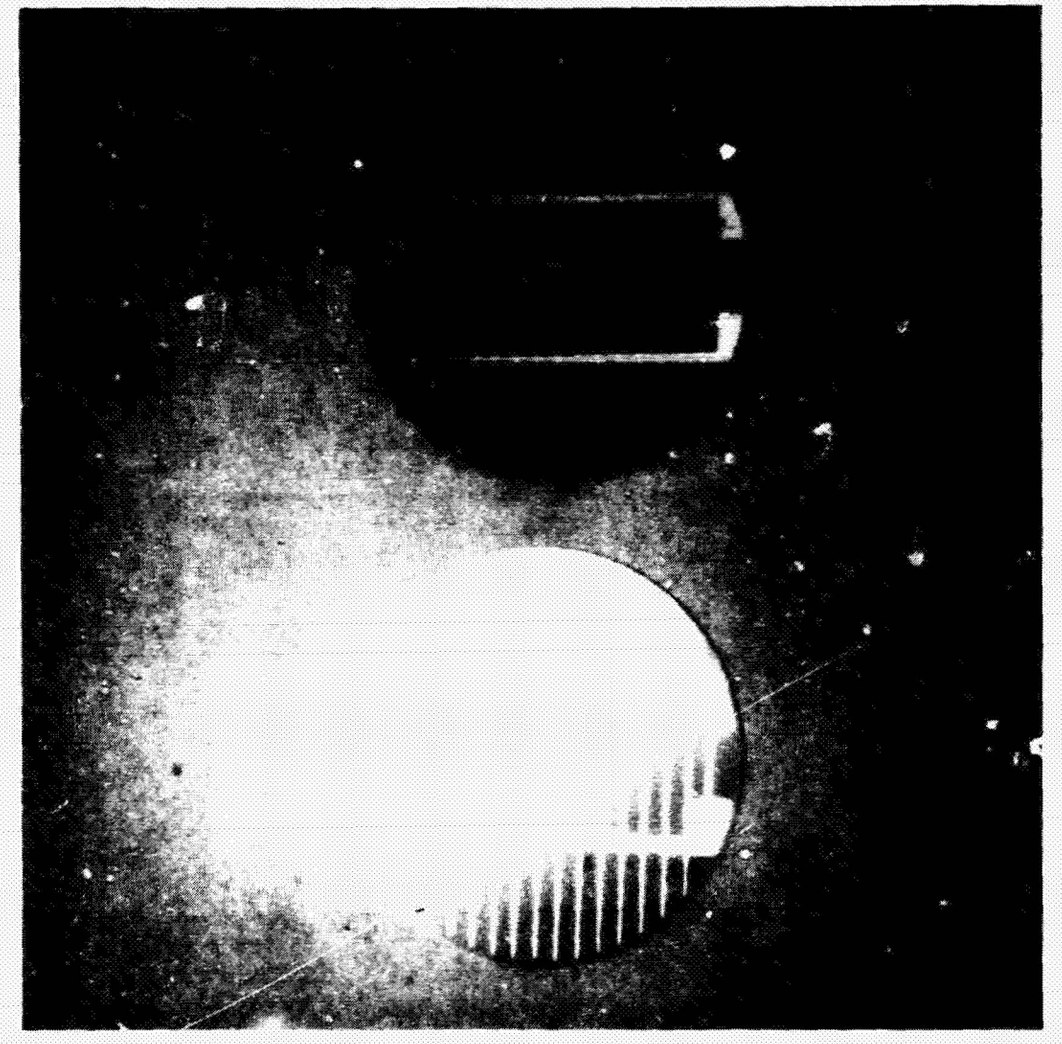

ANALYSIS OF OPTICAL AND ELECTRICAL PERFORMANCE OF A TCP-COATED SOLAR CELL

JET PROPULSION LABORATORY

R.E. Daniel

Introduction

Purpose:

To analyze the effect of the optical and electrical properties of a transparent conducting polymer (TCP) on a solar cell

Questions to be answered:

- **What affect does the transmission, reflection and absorption of the TCP have on the operating characteristics of the solar cell?**
- **What TCP film thickness and conductivity is necessary to conduct the generated photocurrent with a tolerable series resistance?**

Analytical Procedure

Optical:

Calculate the expected short-circuit current density (J_{SC}) in a solar cell with a TCP coating

- **Calculate the amount of light transmitted (TR) through the TCP to the solar cell across the spectrum**
- **Then** $J_{SC} = \Sigma QE(\lambda) \cdot S(\lambda) \cdot TR(\lambda)\, d\lambda$

where: $QE(\lambda)$ = **normalized collection efficiency**

$S(\lambda)$ = **incident light flux (AM1-5)**

$TR(\lambda)$ = **transmitted light**

- **Simple case: nonabsorbing film**

$$R = \left(\frac{N_{j-1} - N_j}{N_{j-1} + N_j}\right)^2 \qquad \text{and } TR + R = 1$$

With absorption $\bar{N} = N - iK$

where $\bar{N}$ = **complex index of refraction**

N = **real component of IR**

K = **imaginery component of IR — extinction coefficient**

Electrical:

Calculate the power lost in the TCP film due to the TCP sheet resistivity (ρ_{TCP})

- **For a TCP on a single crystal cell, consider a unit cell where the spacing between the grid lines (S) is held constant:**

$$P_l = \frac{J_{MP}^2\, S^2 \rho}{12} \qquad \text{where} \quad \rho = \frac{\rho Si \cdot \rho TLP}{\rho Si + \rho TLP}$$

- **For a TCP on an amorphous silicon solar cell, consider a series-connected cell configuration where the spacing between interconnected cells (W) is varied**

$$\rho_l = \frac{J_{MP}^2\, W^3\, l\, \rho TLP}{3} \qquad l = \text{length of the cell}$$

- **Calculated values of the power lost are then compared with those of an arbitrarily good lossless cell**

Assumed Cell Characteristics

Single-crystal:

- **Lossless cell**
  - V_{MP} (Voltage max. power) = 0.45 volts
  - J_{MP} (Current density max. power) = 35 mA/cm^2
- **Analyzed cell**
  - V_{MP} = 0.45
  - J_{MP} varies
  - ρ_{Si} = 40 $\Omega/\square$

Amorphous:

- **Lossless cell**
  - V_{MP} = 0.85
  - J_{MP} = 21
- **Analyzed cell**
  - V_{MP} = 0.7
  - J_{MP} varies
  - ρ_{Si} infinite

More Assumptions

- Only sheet resistance power loss considered
- No contact resistance problem
- Power loss through TCP film is negligible
- Film thickness is uniform
- Resistivity is linear with film thickness
- V_{MP} change with attenuated light not considered
- No environmental consideration

Short-Circuit Current Density Generated vs TCP Thickness

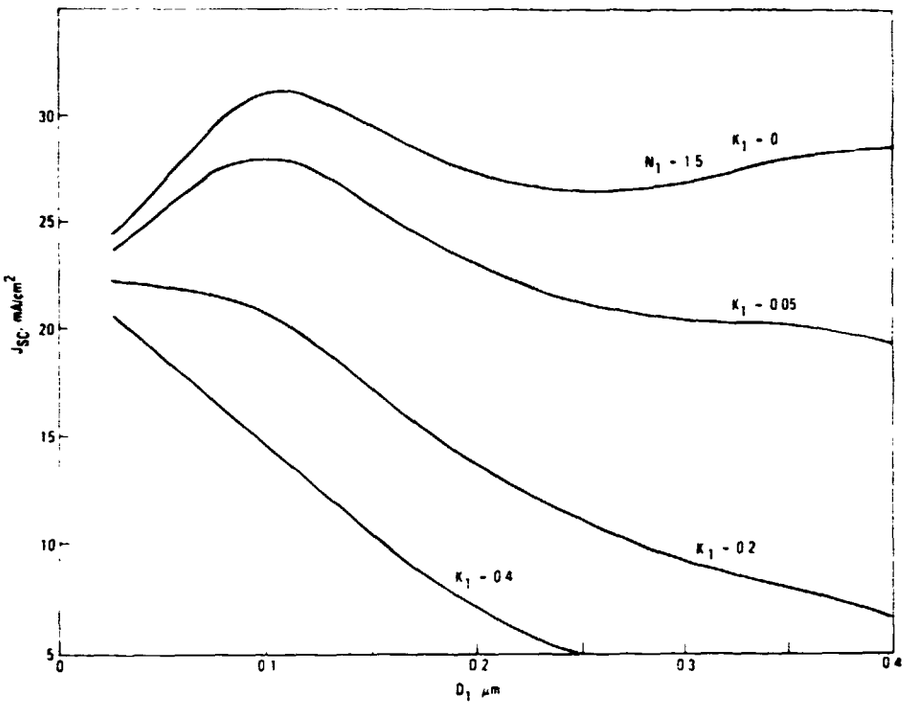

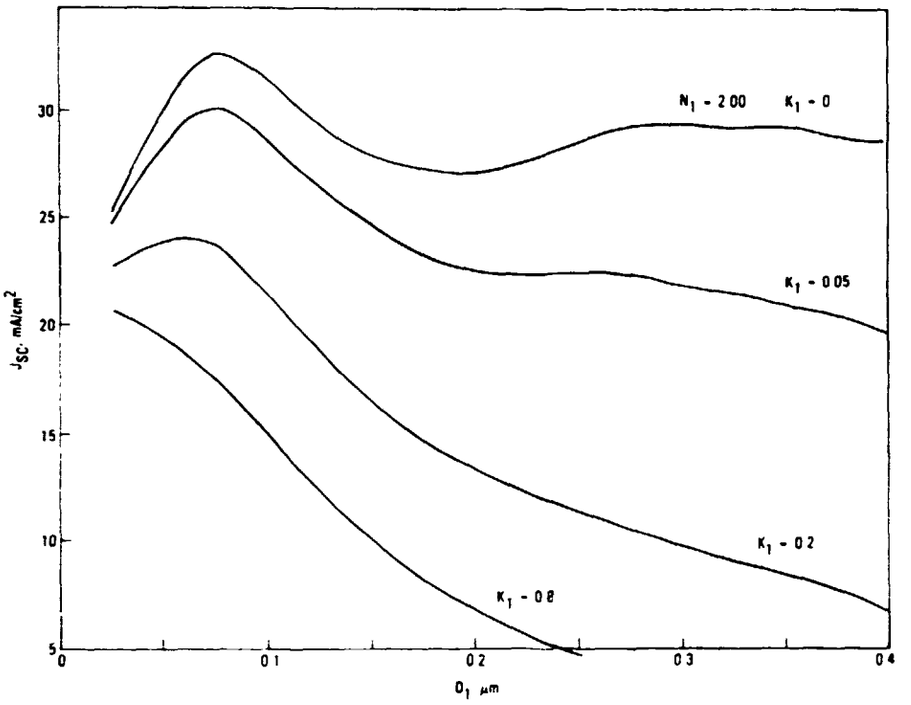
N_1 - 2 00 K_1 - 0
K_1 - 0 05
K_1 - 0 2
K_1 - 0 8
J_{SC}, mA/cm^2
D_1 μm

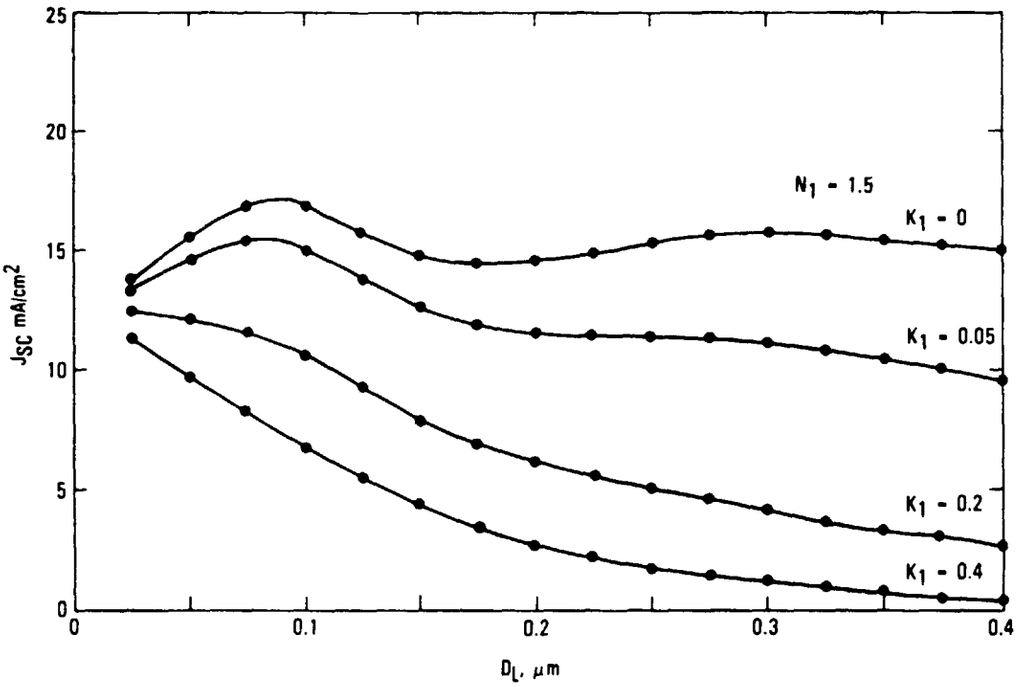
N_1 = 1.5
K_1 = 0
K_1 = 0.05
K_1 = 0.2
K_1 = 0.4
J_{SC} mA/cm^2
D_L, μm

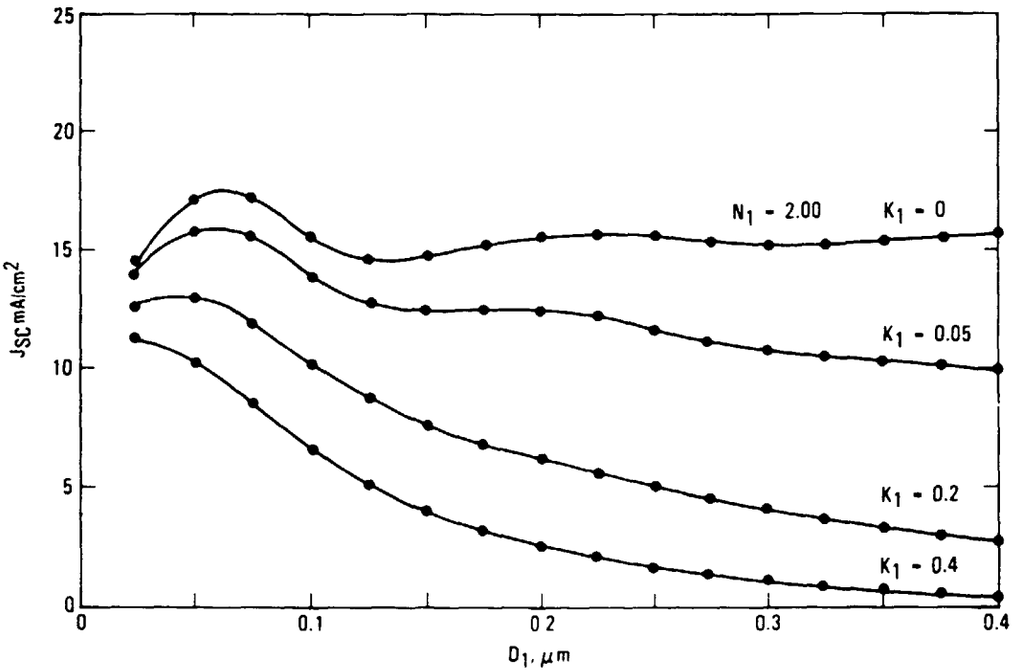
25
20
15
10
5
0
0
0.1
0.2
0.3
0.4
J_{SC} mA/cm^2
D_1, μm
N_1 = 2.00
K_1 = 0
K_1 = 0.05
K_1 = 0.2
K_1 = 0.4

TCP Sheet Resistivity vs Conductivity

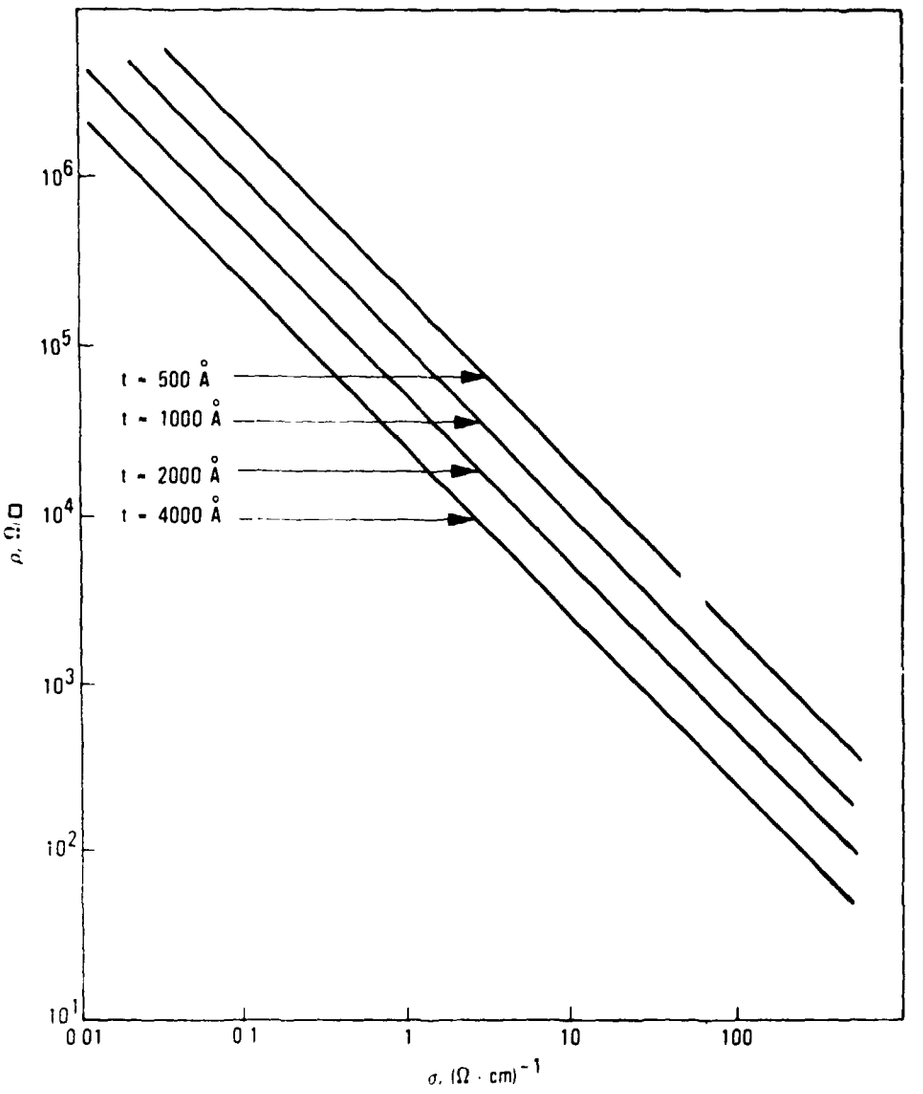

Fractional Power Lost in a TCP Due to Sheet Resistance

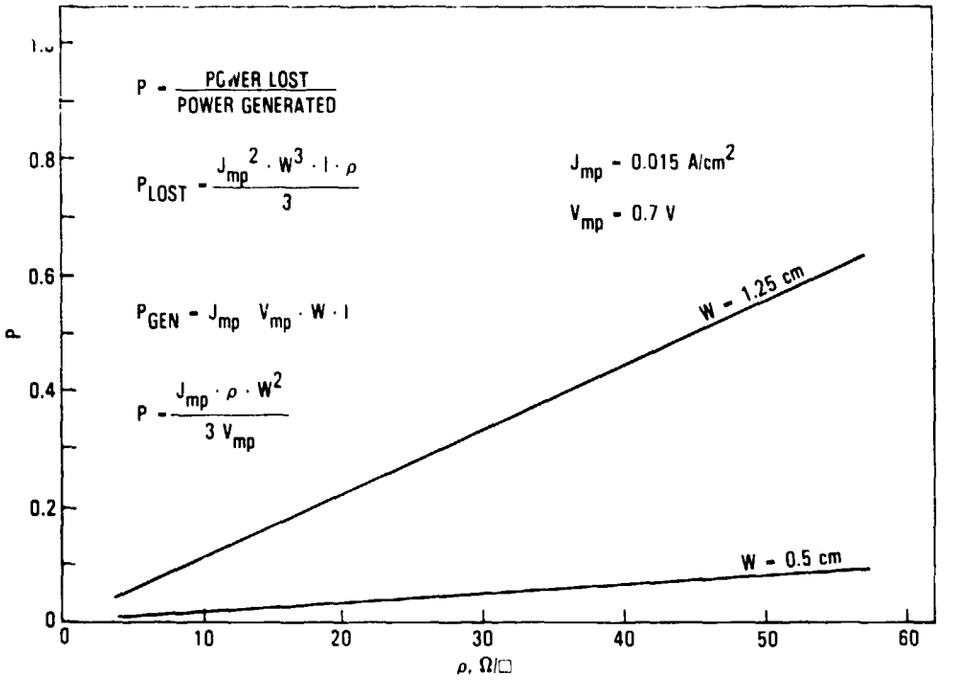

Ratio of Power Out to a Baseline Cell vs Current Density at Maximum Power

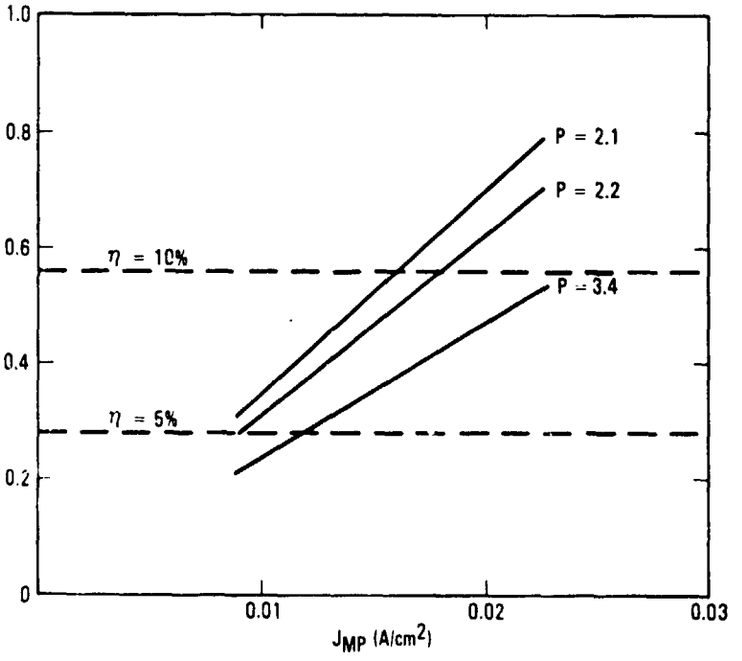

Summary

Single-crystal

- **Lateral conductivity dominated by the cell no value until $\rho_{TLP} \longrightarrow \rho_{Si}$**
- **Optical characteristics useful for modeling candidate materials**

Amorphous

- **All current must be carried by the TCP**
- **Power loss in the sheet can be controlled by the geometry of the cell**
- **Optical response complicated by the transmissibility of a – Si; however, trends are indicated**

PERFORMANCE LOSS WITH SHORTED CELLS

JET PROPULSION LABORATORY

C.C. Gonzalez

Objectives, Current Task

- Determine the power loss due to shorted cells for a given source-circuit series-parallel configuration after n years with a constant yearly failure rate
- Determine the optimum series-parallel configuration(s) minimizing power loss
- Determine the cost-effective failure level

Long-Range Objective

Determine cost-effective circuit design

Effect of Shorted Cells on Source-Circuit Maximum Power

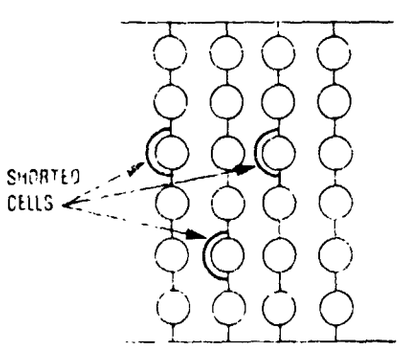

- SHORTED CELLS LEAD TO VOLTAGE MISMATCH AND MAX-POWER LOSS
- MAX-POWER LOSS INCREASES WITH INCREASE IN CROSS-TIES AND WITH INCREASE IN PARALLEL STRINGS

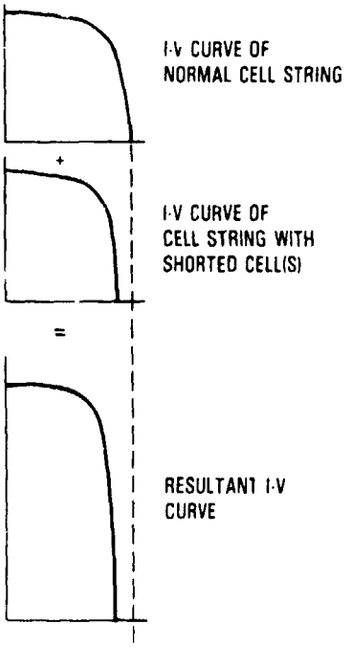

Approach

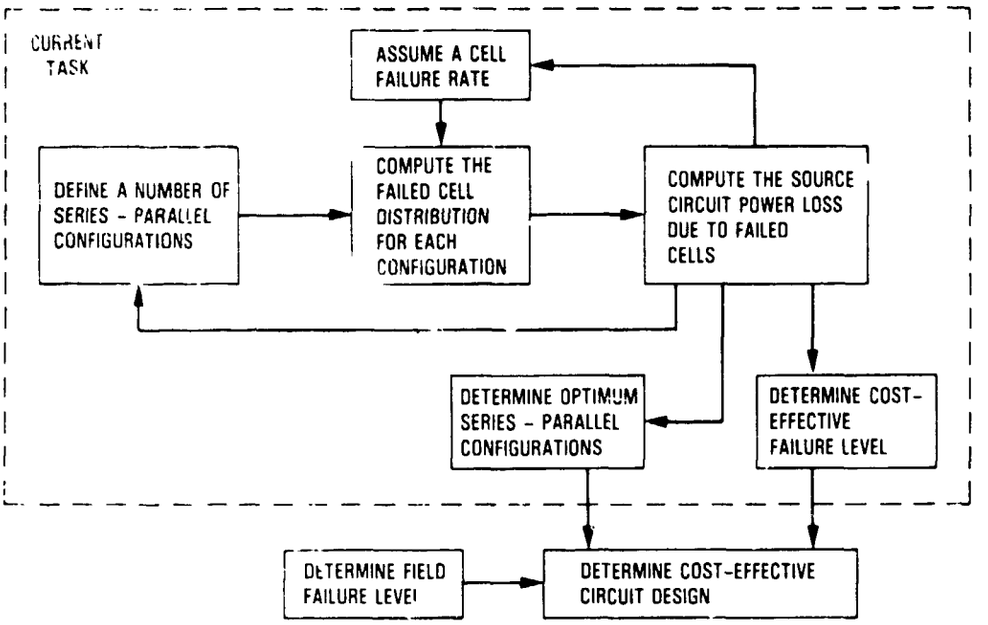

Source-Circuit Definition

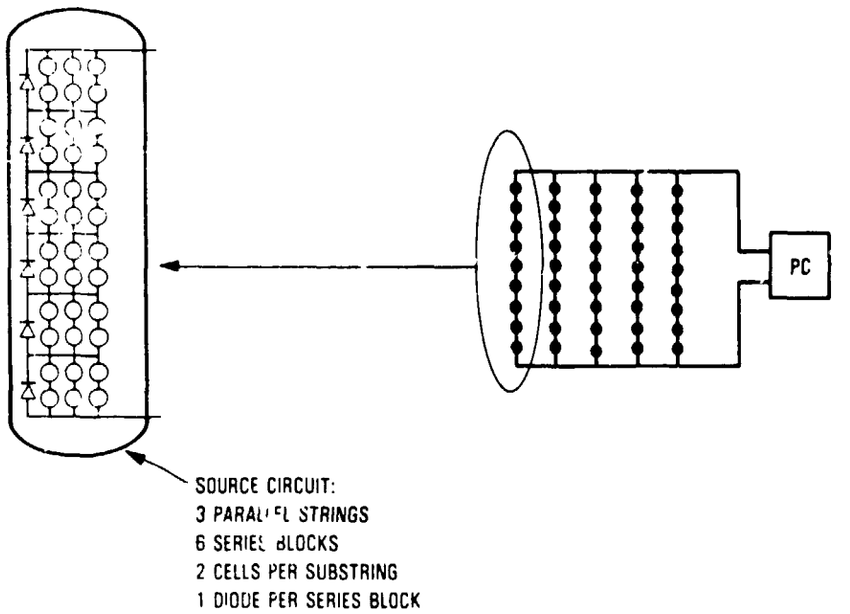

Problem

- Given a source circuit with:
  - N total series cells
  - NB series blocks
  - NS substrings per series block
  - NC cells per substring
- Determine the average number of series blocks with a given configuration of failed cells and substrings

Definition of Source Circuit With Example Parameters

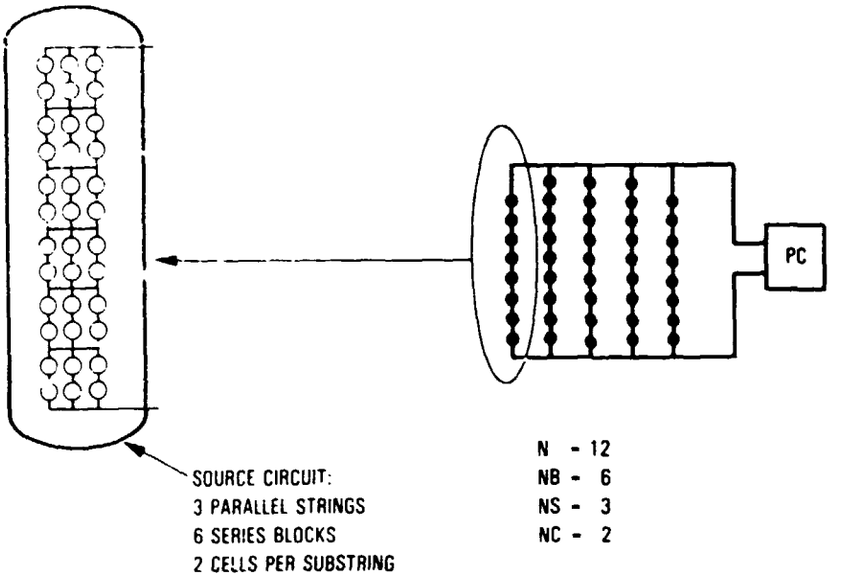

Statistical Analysis Solution Using Binomial Distribution

If p = probability of a cell failure, the probability of obtaining x failures in n cells is:

$$p(x) = \frac{N!}{x!\,(N-x)!}\,p^x\,(1-p)^{(N-x)}$$

The probability of obtaining y_1 substrings with x_1 failed cells, y_2 substrings with x_2 failed cells, y_3 substrings with x_3 failed cells, etc., out of NS total substrings is:

$$p(y_1,x_1;y_2,x_2;y_3,x_3\ldots) = \frac{(NS)!}{(y_1+y_2+y_3\ldots)![NS-(y_1+y_2+y_3\ldots)]!}\,p(x_1)^{y_1}\,p(x_2)^{y_2}\,p(x_3)^{y_3}\ldots p(0)^{(NS-(y_1+y_2+y_3\ldots)}$$

- Each value of $p(y_1, x_1;\ldots)$ is the probability of obtaining a series block with a given substring and cell failure configuration:
- $\therefore p(y_1, x_1;\ldots) \cdot NB$ is the number of series blocks with that configuration
- The following steps are performed after obtaining the above values:
  - The I-V curves of each series-block configuration (including those without failures) are added
  - The max-power is compared with that on identical source circuit with no failures

Array Power Loss: Four Parallel Strings

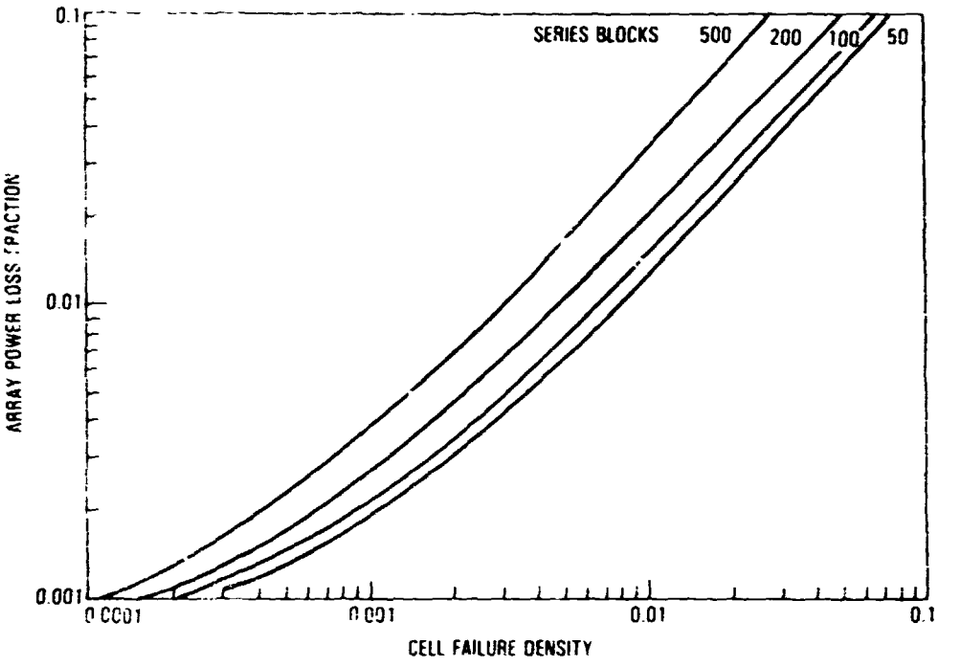

Array Power Loss: Eight Parallel Strings

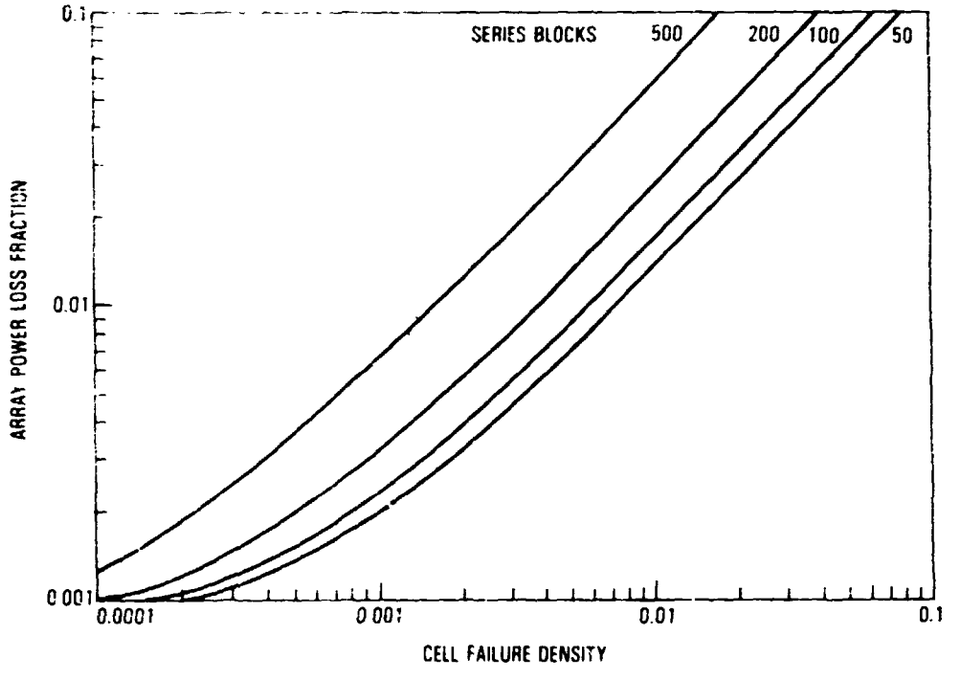

Array Power Loss: 16 Parallel Strings

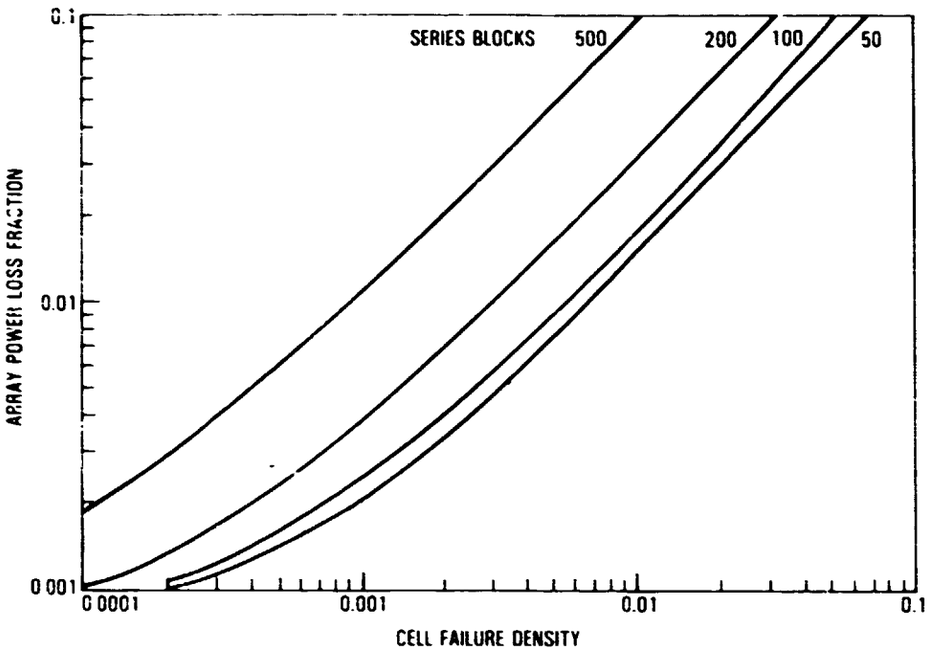

Conclusions

- **Power loss due to shorted cells increases with increased use of bypass diodes and cross-ties**
- **Yearly failure rate greater than 1/10,000 leads to power losses in excess of the allocation for cell failures**

N85 15295

INVESTIGATION OF ACCELERATED STRESS FACTORS AND FAILURE/DEGRADATION MECHANISMS

CLEMSON UNIVERSITY

J.W. Lathrop

COMMERCIAL CELL TESTING

SCHOTTKY BARRIER FORMATION

NEW TEST DEVELOPMENT

NEW ANALYTICAL FACILITY

Clemson Accelerated Test Schedule
for Unencapsulated Cells

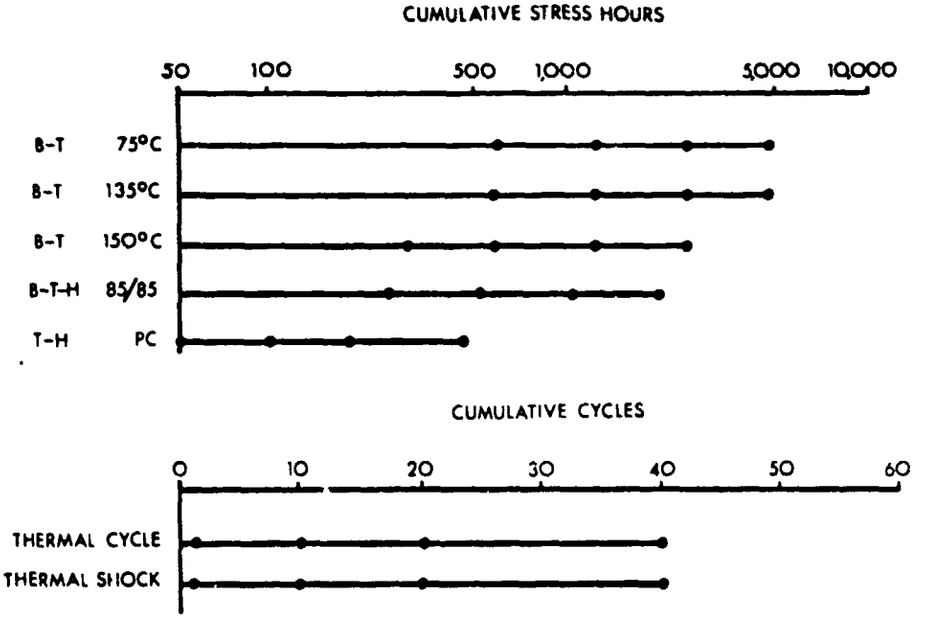

N -- Average

O -- Above average (- degradation)

P -- Well below average

Q -- Well above average (- degradation)

R -- Above average (fracture)

V -- Average

W -- Below average

X -- Above average (loss of grid metal)

Y -- Above average (+ degradation)

Z -- Above average (fracture)

N -- Below Average

O -- Above average (- degradation)

P -- Not tested

Q -- Above average (- degradation)

R -- Not tested

V -- Average

W -- Average

X -- Above average (loss of grid metal)

Y -- Above average (+ degradation)

Z -- Below average (threshold effect)

N -- Above average (back metal)

O -- Average

P -- Below average

Q -- Above average (grid metal)

R -- Not tested

V -- Above average (fracture)

W -- Above average (fracture)

X -- Well above average (grid metal)

Y -- Above average (lead loss)

Z -- Not tested

Equivalent Circuit of a Degraded Solar Cell

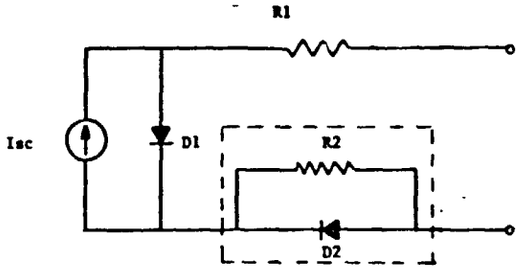

I-V Characteristics of a Degraded Solar Cell

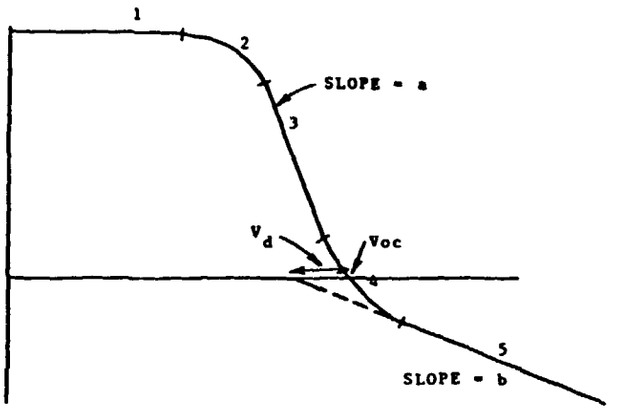

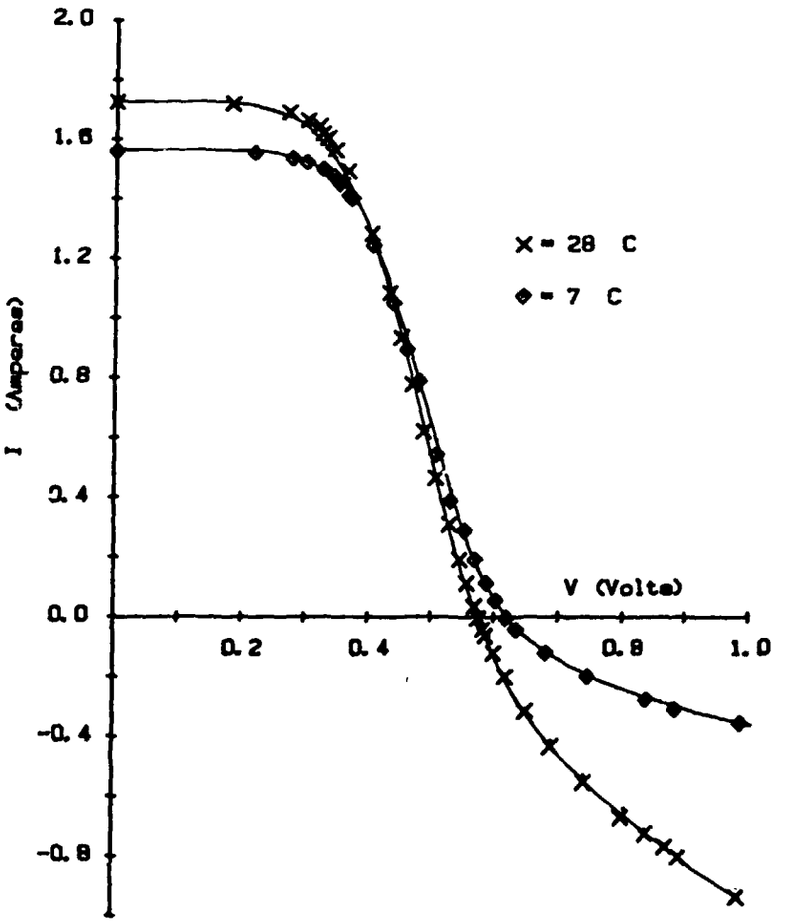

Equivalent Circuit Parameters

T (°C)	28.0	21.4	7.0
Io(Amp)	1.714E-5	0.984E-5	0.101E-5
Is(Amp)	0.465	0.332	0.162
n1	1.927	1.926	1.800
n2	2.270	2.165	2.000
R1(ohm)	0.023	0.025	0.027
R2(ohm)	0.776	0.961	1.600

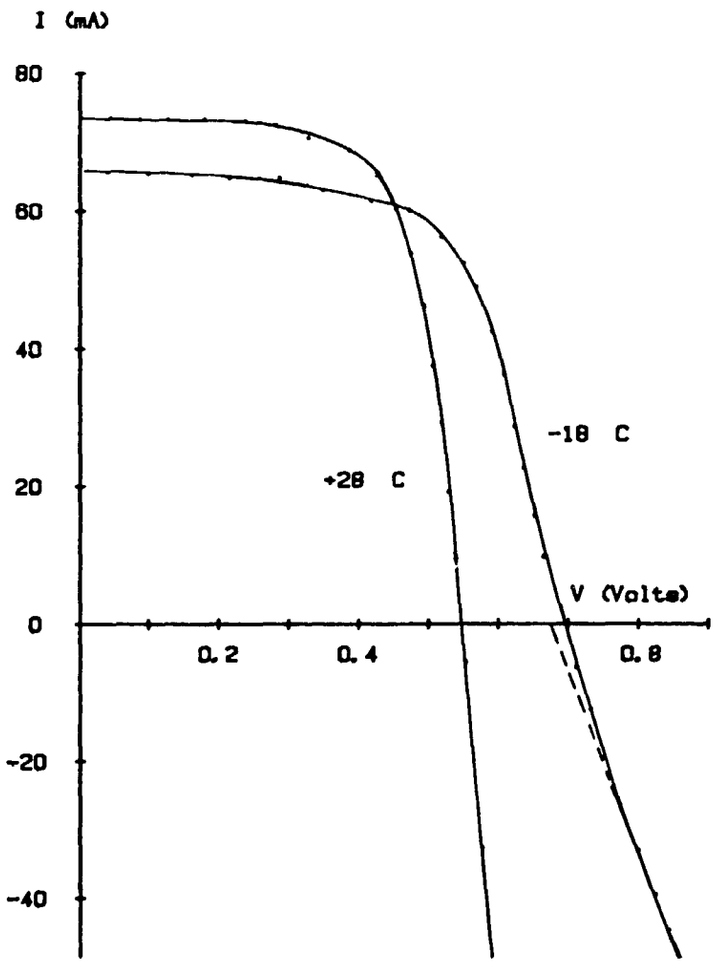

Atomic and Molecular Species at Unencapsulated Cell Surface

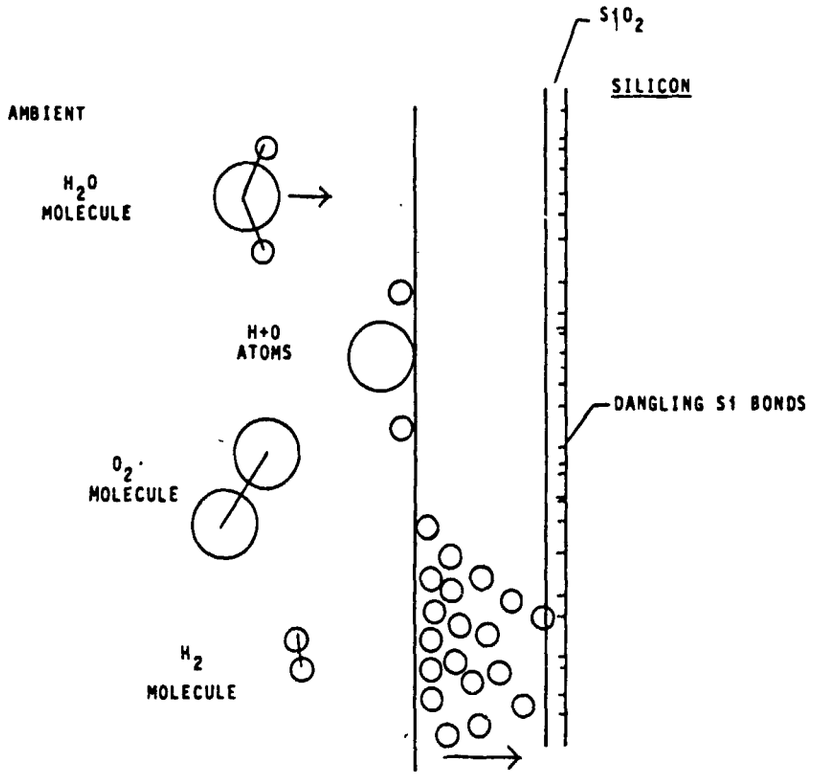

Percentage Decrease in Pm for 85/85 Test Q-Cells

	Stress Time in Hours			
	250	500	1000	2000
UNENCAP	7	8	11	16
G/EVA/F	23	41	56	53
G/EMA/T	26	38	54	53
G/EVA/T	24	36	48	50
T/EVA/S	1	0	6	6

Atomic and Molecular Species at Encapsulated Cell Surface

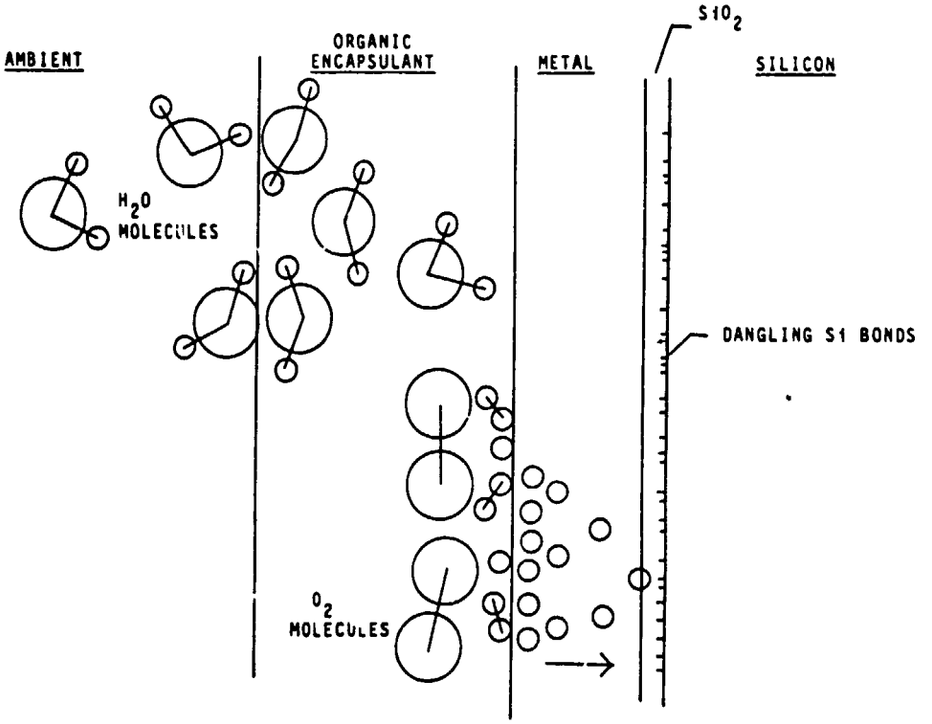

Encapsulated Cells 140 Days Outdoors

	Pm	Isc
XP (G/EVA/T)	5	4
XP (G/EMA/T)	2	5
XP (G/EVA/G)	5	5
X (G/EVA/T)	4	4
X (G/EMA/T)	3	4
X (G/EVA/G)	6	5

Unencapsulated Cells 140 Days Outdoors

	Pm	Isc	Inspection
N	18	9	Grid (severe)
O	5	2	Grid (moderate)
P	6	2	Grid (slight)
Q	4	2	
W	4	2	Grid (slight)
X	60	34	Grid (severe)
Y	14	4	Leads
Z	18	2	Leads

85/85 and 93°C/85% RH Testing

	85/85	93/85	ACCEL	Ea/(eV)
G/EVA	3.5	4.2	1.2	0.26
G/EVA/T	2.1	3.1	1.5	0.57

Measured % decrease in Pm

Calculated acceleration factor

Calculated activation energy

N85 15296

THERMAL CHARACTERIZATION OF PHOTOVOLTAIC MODULES IN NATURAL ENVIRONMENTS

Jet Propulsion Laboratory

L. Wen

Background

- **Past activities at JPL**
  - **NOCT**
  - **Wind effect**
  - **Unglazed PV/T collector study**
  - **Residential PV thermal**
- **Current concerns**
  - **Data scatter in NOCT determination**
  - **Marginal accuracy in detailed transient thermal simulation**

Representative Cell Temperature Profiles

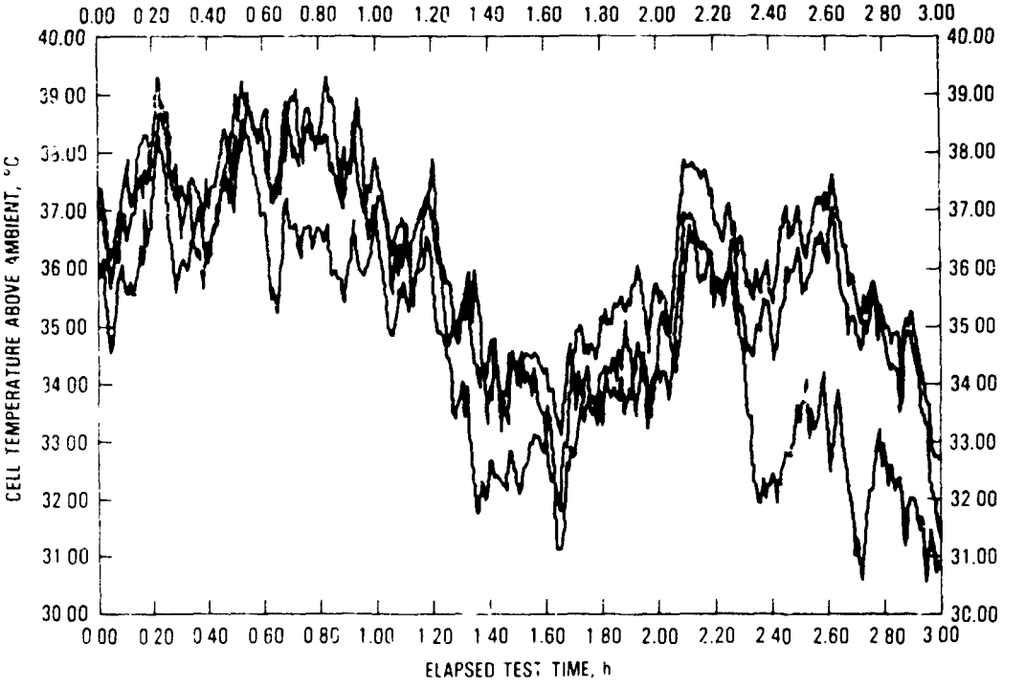

Experimental Uncertainties

- Cell temperature measurements
- Measurements of major environmental parameters
  - Solar irradiance
  - Ambient temperature
  - Wind conditions
- Estimate of secondary environmental factors
  - Ground reflection
  - Ground emission of IR radiation
  - Sky radiation

Study Objectives

- To refine understanding of the physics of module thermal interaction with natural environments
- To develop specific recommendations relative to NOCT test procedure and evaluation methodology
- To provide refined algorithms for predicting PV array operating temperatures

Study Approach

- Representative module
- NOCT type testing
- Minimize experimental error
  - Thermocouple calibration
  - Irradiance measurement calibration
  - Redundancy
- Additional instrumentation
  - Ground reflection
  - Ground IR
  - Hygrometer for sky radiation
  - Reference plates
- Validate resultant correlations by comparing transient simulation with test data

Sky Radiation, Clear Day

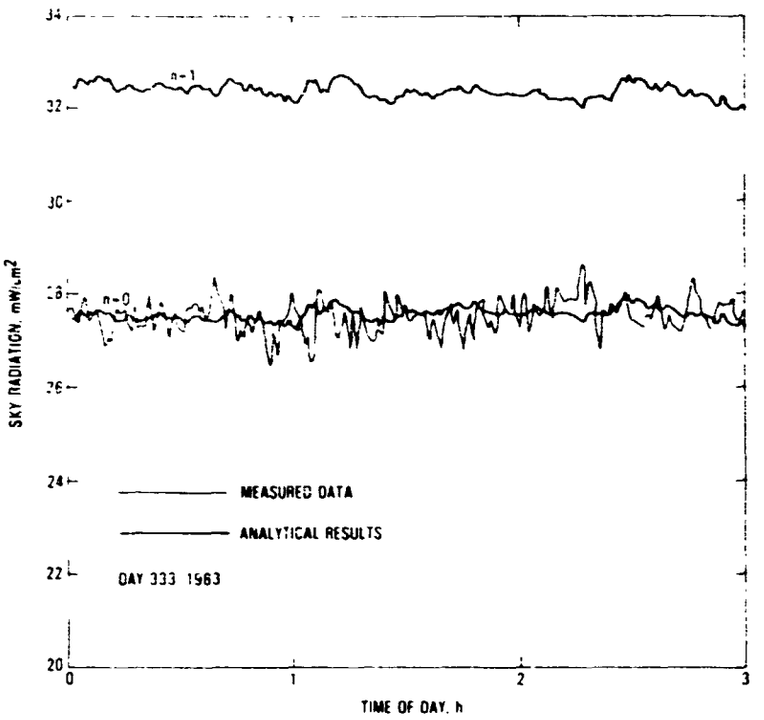

Direct (Front) and Reflected (Back Surface) Solar Irradiation

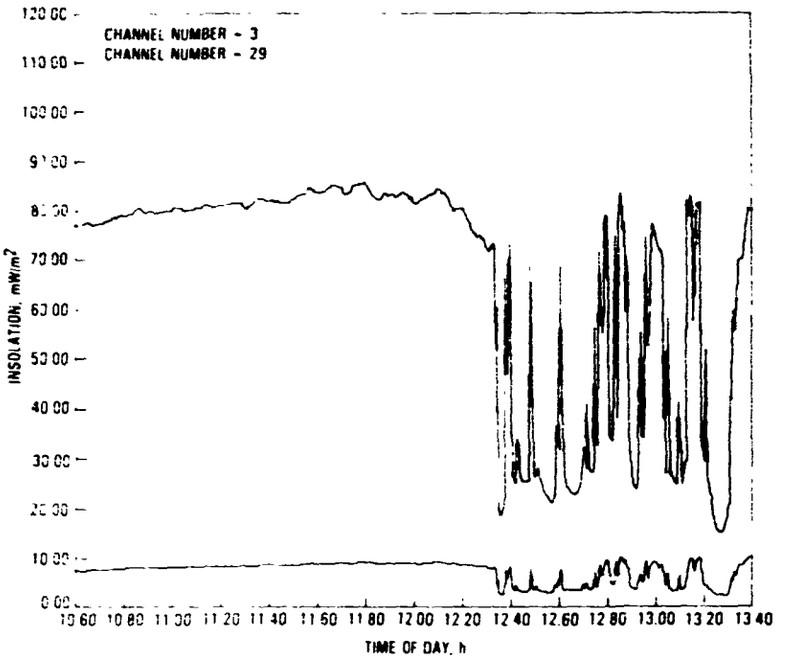

Sky Radiation, Cloudy Day

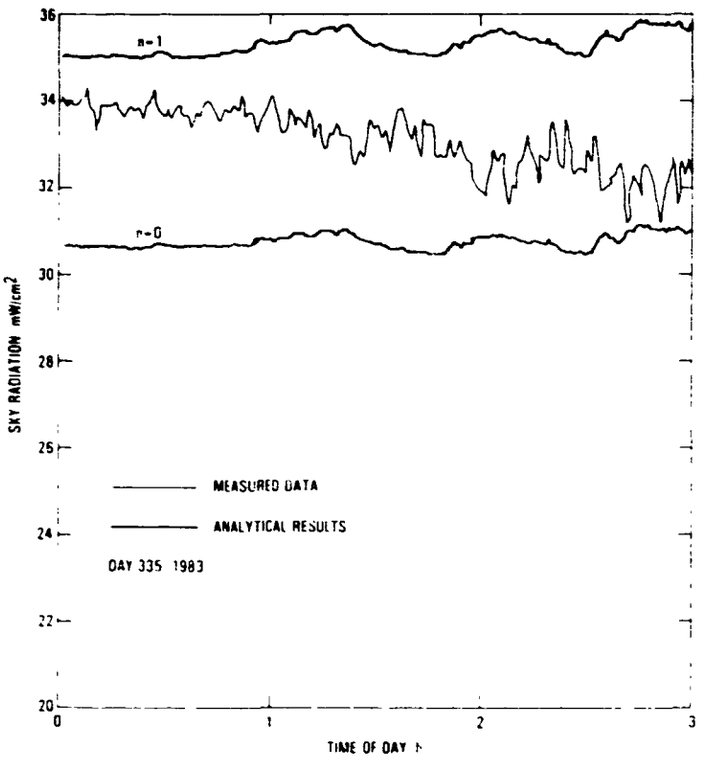

Absorbed Solar Energy

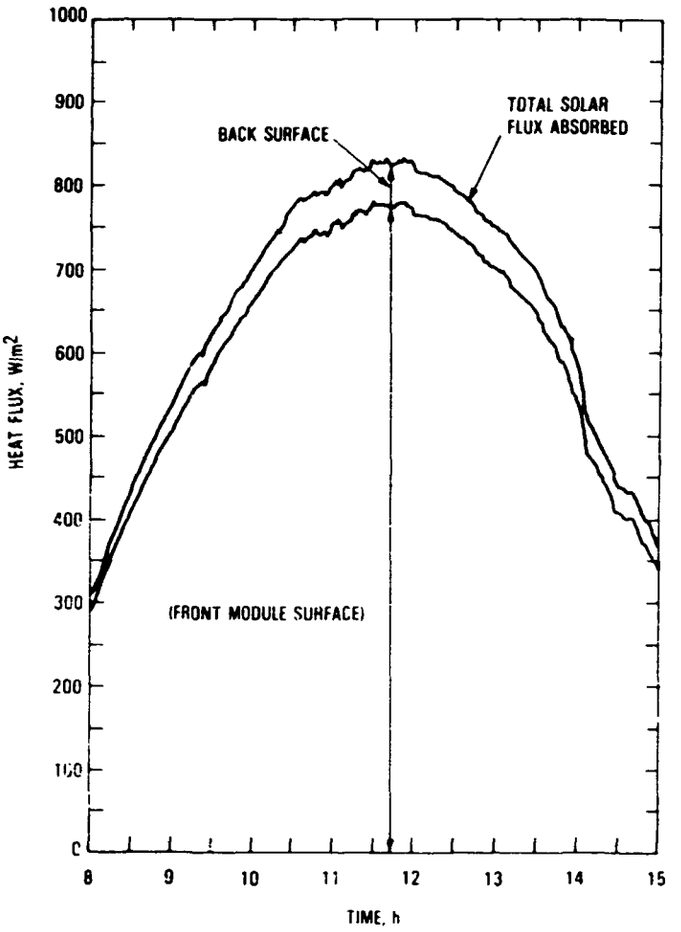

Thermal Radiaton Balance

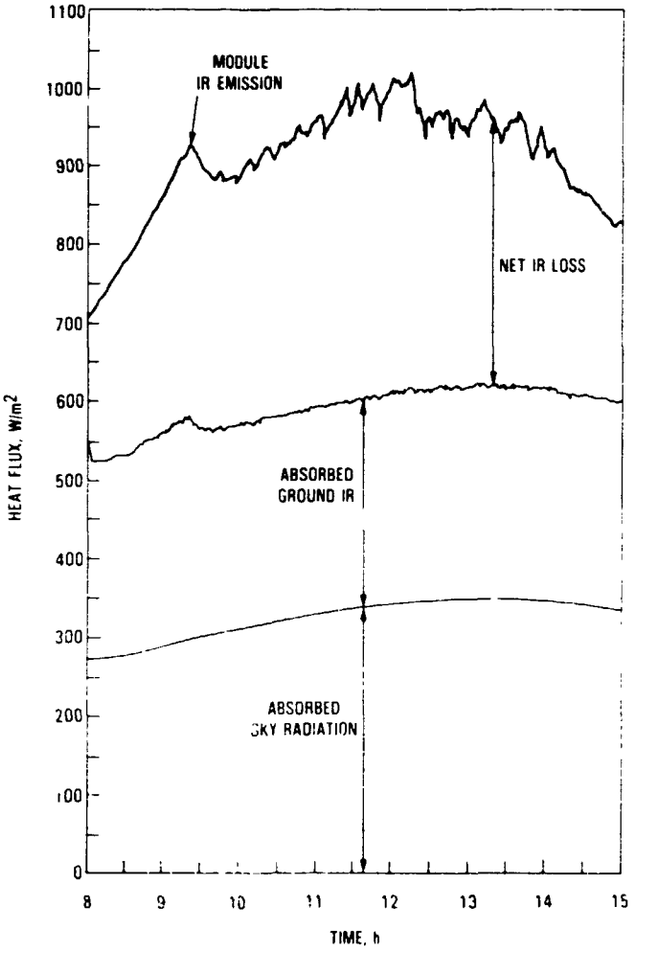

Resultant Heat Loss

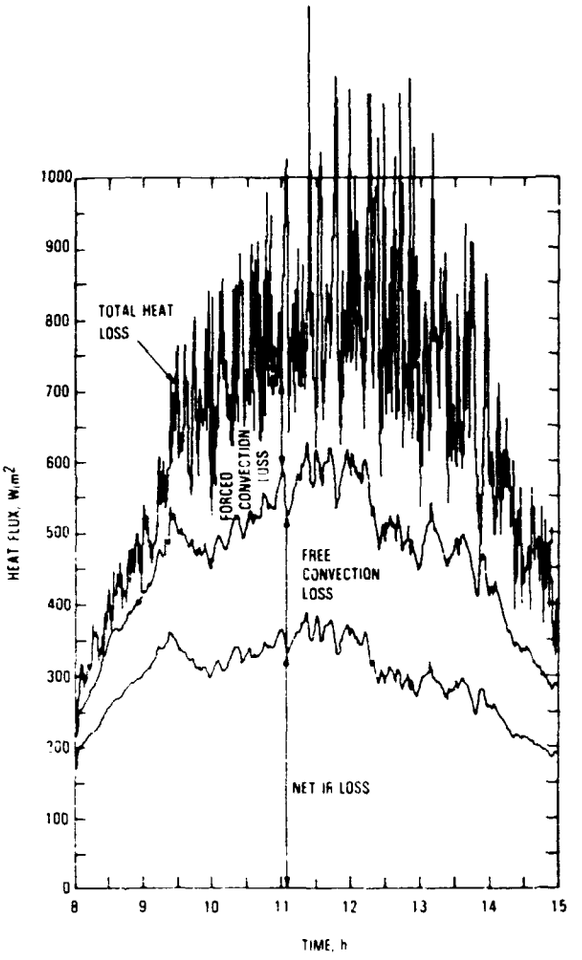

Instantaneous Heat Balance

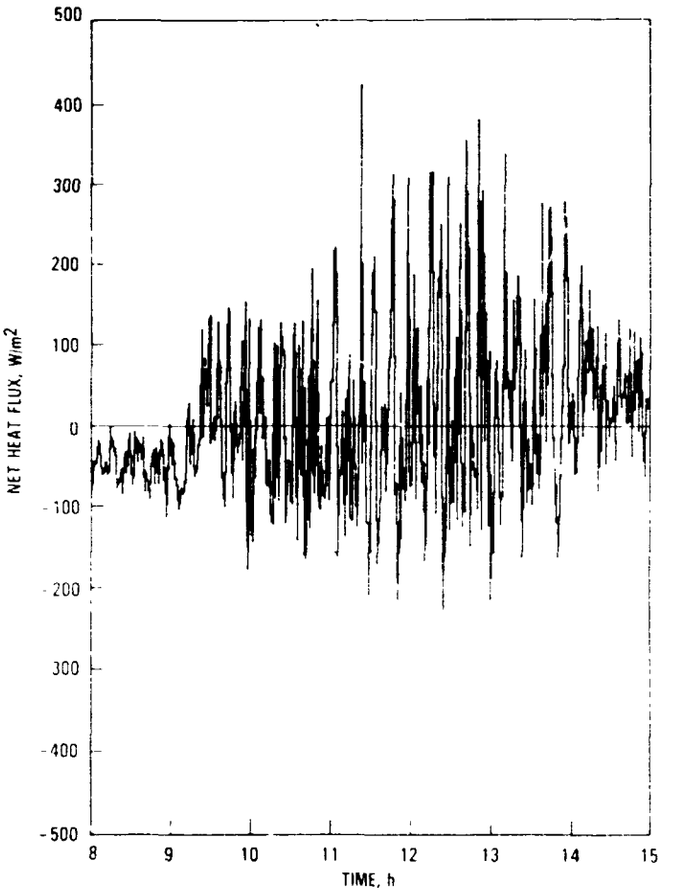

Computed NOCT Values

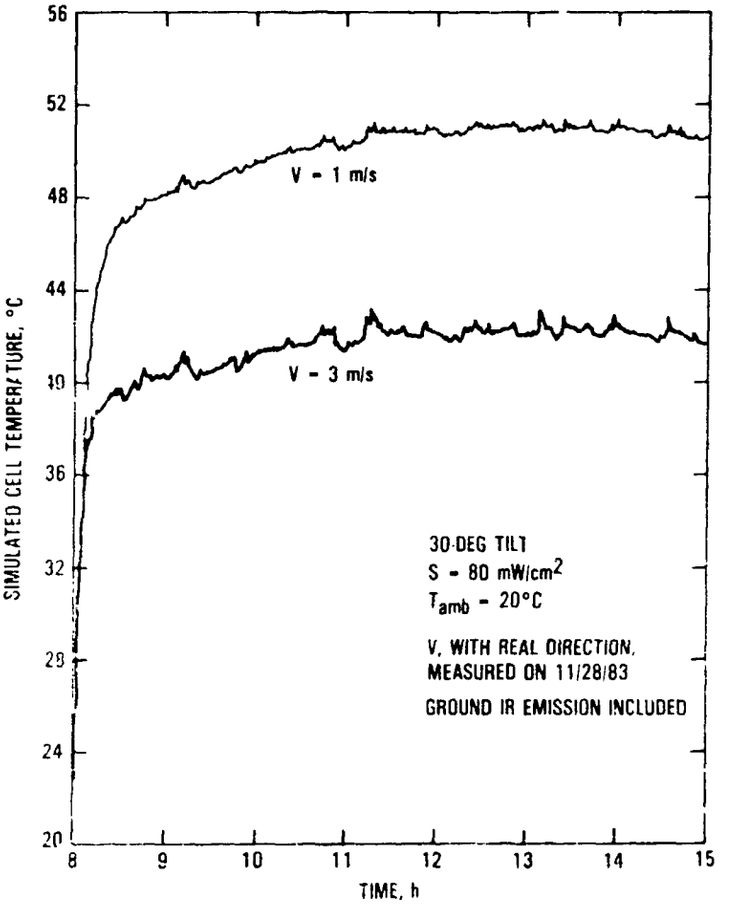

Comparison of Transient Temperature and Simulation

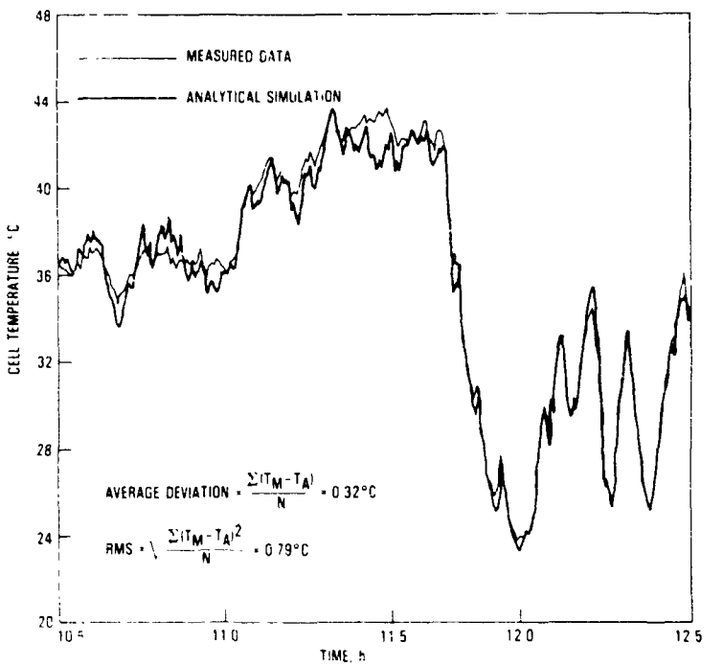

Summary

- Experimental error budget can be reduced with periodic calibrations
- Ground reflection was measured at ≈10%–12% of direct irradiance
- Ground IR reaches a plateau around 11 a.m. and is a major factor in a.m./p.m. NOCT discrepancy
- Algorithms for clear-day sky radiation can be confirmed

Conclusions

- Improved understanding of module thermal characterization
- Accurate (≈1°C uncertainty) transient prediction can be expected
- Established useful correlations to refine NOCT testing and evaluation

ANNUAL ENERGY SPECTRUM FOR TRACKING ARRAYS

JET PROPULSION LABORATORY

C.C. Gonzalez

Objective

To compare array energy spectra for different tracking modes, to assess the advantage of a given mode for any defined cell spectral response

Approach

- **Use computer code and hour-by-hour SOLMET irradiance data to obtain hourly integrated irradiance for array tracking mode**
- **Use solar radiation spectral analysis computer code to estimate amount of hourly irradiance in given wavelength intervals**
- **Do an annual and monthly integration of irradiance in each wavelength interval; result is independent of any particular cell spectral response**
- **In addition: Do an annual and monthly integration of the convolution of a given cell spectral response and the hourly solar energy spectral distribution**

Tracking Modes Considered

- **Fixed tilt at angle of latitude, facing south**
  - **Tilt angle and array direction can be varied**
- **Single-axis tracker, north-south horizontal tracking axis**
  - **Tracking-axis tilt angle can be varied**
- **Two-axis tracker**

Current Status

- **Computer code for annual and seasonal integration of irradiance is complete**
- **Computer code for convoluting cell spectral response with solar radiation spectrum is under development**

Comparison of Integrated Spectral Irradiance for Different Tracking Modes: Fresno, Summer

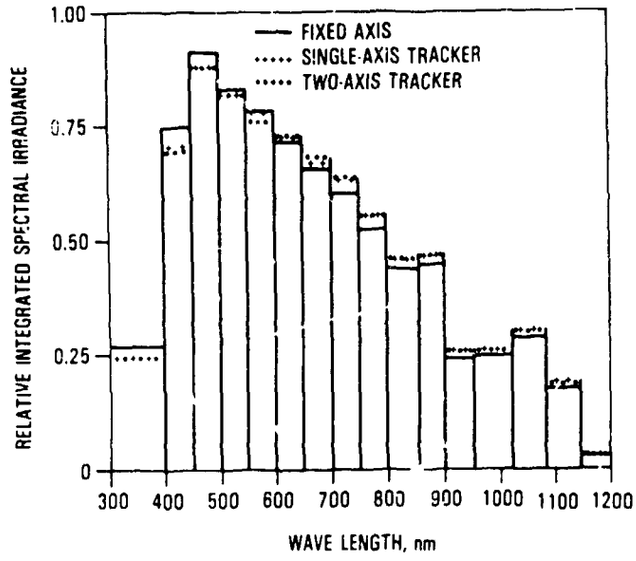

Comparison of Integrated Spectral Irradiance for Different Tracking Modes: Fresno, Annual

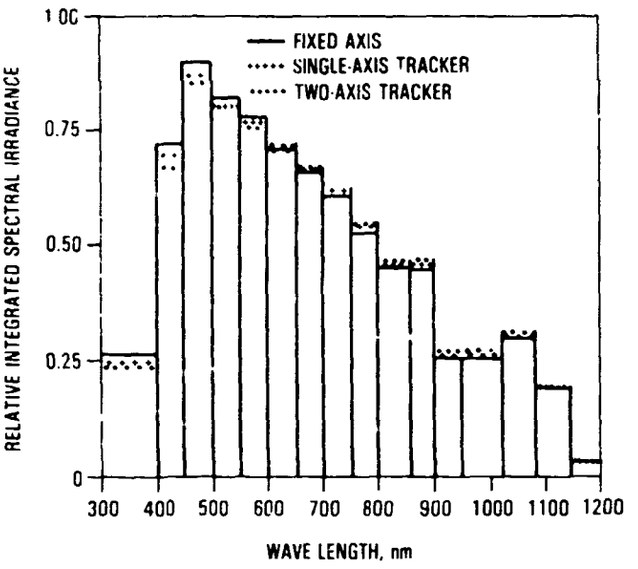

Comparison of Integrated Spectral Irradiance for Different Tracking Modes: Albuquerque, Annual

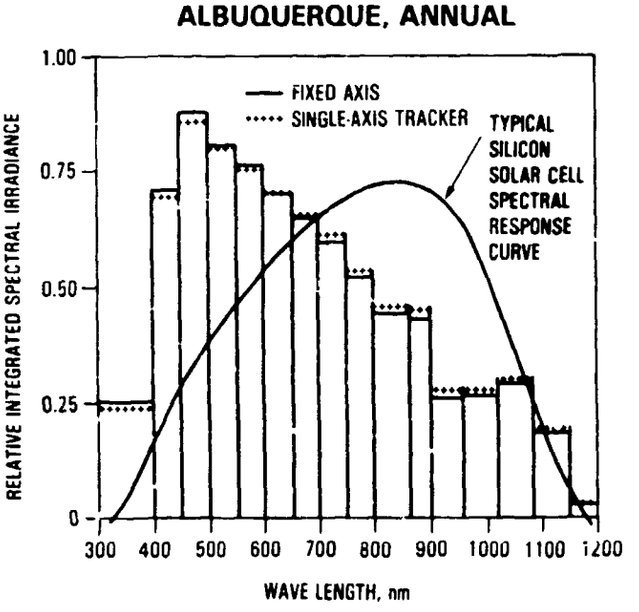

Comparison of Integrated Spectral Irradiance for Different Tracking Modes: Miami, Annual

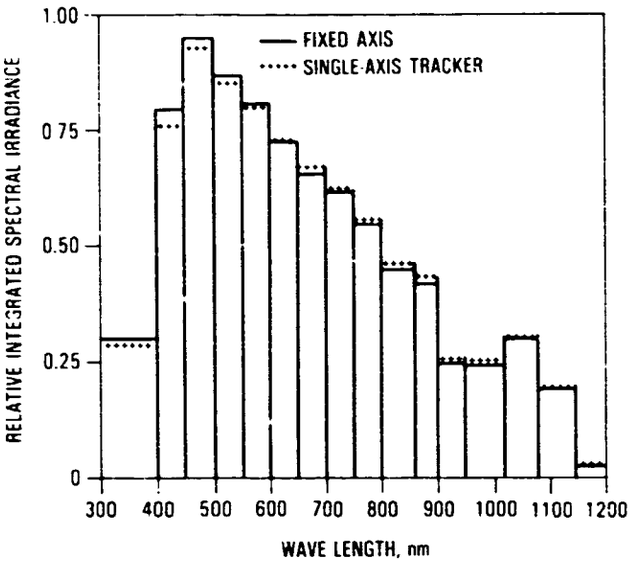

Future Work

- **Completion and checkout of computer code for convoluting cell spectral response with the solar radiation spectrum**
- **Comparison of results obtained with other than crystalline silicon solar cells**

Conclusions

- **Tracking array accumulates more integrated irradiance in the spectral region in which crystalline silicon cells are most sensitive**
  - **Effect greatest for summer in Fresno: 1.5% more for wavelengths greater than 500 nm**
  - **Effect least in Miami: 0.8% more for wavelengths greater than 500 nm**

SUMMARY OF PHOTOVOLTAIC PERFORMANCE MODELS (JPL PUBLICATION 84-8)

JET PROPULSION LABORATORY

J.H. Smith
L.J. Reiter

There are a number of computer models which are usually placed in the category of photovoltaic systems performance models. These cover a range of approaches and capabilities from aggregate, "first-order" models to far more detailed analyses of PV systems. The objective of this study was to find the complete set of models which fit our criteria; review each one in detail to determine its purpose, approach, and capabilities; and present this information in an easily referenceable format. This work was performed for the Project Analysis and Integration Center at JPL and has resulted in a report entitled, "Summary of Photovoltaic Systems Performance Models" (JPL Pub. 84-8, DOE/ET-20356-11).

Study Motivation and Scope

- **To identify, summarize and distinguish between the various PV system performance models**
- **To provide users in the PV community with an in-depth reference document for selection of appropriate PV system models**
- **Focus was on performance models of flat-plate systems; purely economic models were not included**
- **Model descriptions were reviewed by the model authors to ensure completness and accuracy**

Approach

- Identify a comprehensive set of models
- Identify a set of topics to be the basis for describing the approaches and capabilities of the models
- Perform a detailed assessment of each model's purpose, approach, and capabilities
- Tabulate information in a convenient format
- Identify recent extensions in PV performance modeling

Note: No numerical comparisons of model results were made

Model Selection

- A complete set of available photovoltaic systems performance models that:
  - Have been used by the PV community in general for PV system assessment
  - Have been used as a tool for policy analysis by the national laboratories
  - Have been used as a system design tool and in performance analysis as reported in the literature
  - Have available documentation

Models Included in the Study

Model	Name	Originator
Engineering and Reliability	E&R	Jet Propulsion Laboratory (FSA)
Lifetime Cost and Performance	LCP	Jet Propulsion Laboratory (FSA, PV PA&I Center)
Photovoltaic F-CHART	PV F-CHART	Univ. of Wisconsin Solar Energy Lab
Photovoltaic Performance Model	PVPM	Electric Power Research Institute
Photovoltaic Transient Analysis Program	PV-TAP	BDM Corp., Sandia Labs
Solar Cell Model, Version 2	SOLCEL-II	Sandia Labs
Solar Reliability	SOLREL	Battelle Columbus Labs, Sandia Labs
Solar Energy System Analysis Program	SOLSYS	Sandia Labs
Transient Simulation Program/ASU version	TRNSYS/ASU	Univ. of Wisconsin Solar Energy Lab, Arizona State Univ., Sandia Labs
Transient Simulation Program/MIT version	TRNSYS/MIT	Univ. of Wisconsin Solar Energy Lab, MIT Lincoln Lab

The following topics served as a general framework against which each model was compared. Under each topic were a number of more detailed characteristics. The models were examined to determine which characteristics they either addressed analytically (i.e., contain an analytical model of it), treated externally (e.g., the element is input by the user), or do not address.

Performance Modeling Characteristics

- Cell level
- Module level
- Array orientation and geometry
- Array level
- PCU subsystem
- Plant level
- Operations and maintenance
- Site-specific

The following is one of the nine tables of this type in the study report. It is included here to illustrate the format which was used. The manner in which each of the ten models addresses the characteristic is displayed and is easy to cross-reference. Thus, the reader can approach these tables to determine the capabilities of a certain model or to find a model which most appropriately addresses the particular characteristics of interest.

Site-Specific Characteristics

MODEL	Total Global Solar Radiation	Direct Normal Solar Radiation	Diffuse Solar Radiation: Atmospheric Type	Diffuse Solar Radiation: Method of Calculation	Diffuse Solar Radiation: Ground Reflecitivity
E&R	input file of hourly global insolation for a year	analytic model of direct (modified Liu-Jordan, 1960) or user input file of hourly global insolation	analytic model for either isotropic or anisotropic diffuse component	isotropic--modified Liu-Jordan (1960) anisotropic--Klucher, 1979	user input single value
LCP	user input file of hourly global insolation for a year	analytic model of direct insolation (Boes, et al., 1976) or user input file of hourly data	analytic model for either isotropic or anisotropic diffuse component	isotropic--Boes et al., 1976 anisotropic--Klucher, 1979	user input: 12 values (1 per month)
PV F-CHART	analytic model of 12 average profiles (1 per month) calibrated by site specific inputs (244 sites in program)	analytic model using modified Liu and Jordan (1960) approach	analytic model for isotropic diffuse component	isotropic--Erbs, et al., 1982	user input: 12 monthly values (1 per month)
PVFM	hourly input file for total global insolation for period of interest	input file for direct normal insolation or analytic model using modified Liu and Jordan (1960) approach	analytic model for isotropic diffuse component	isotropic--modified Liu-Jordan, 1960	N/A
PV-TAP	user input to electrical network equivalent of photocurrent alert generator for selected time scale	analytic model of direct insolation as nonlinear voltage controlled current generator	user input network required to characterize behavior of diffuse component	user input variable voltage element required to represent diffuse	N/A
SOLCEL-II	input files for total global hourly insolation for a year	input files for direct normal hourly insolation or analytic model using modified Liu and Jordan (1960) approach (Boes, et al, 1976)	analytic model for isotropic diftuse component	isotropic--Boes et al., 1976	user input single value
SOLREL	N/A	N/A	N/A	N/A	N/A
SOLSYS	input file for total global hourly insolation for a year	input file for direct normal hourly insolation or analytic model using modified Liu-Jordan (1960) method (Boes et al, 1976)	analytic model for isotropic diffuse component	isotropic--modified Liu-Jordan (1960)	a value of .5 is included in the code
TRNSYS/ASU	user inputs total insolation for selected timescale (SOLMET and TMY)	user inputs insolation for selected timescale (SOLMET and TMY)	analytic models for isotropic diffuse or user input of measured total (which includes diffuse) for selected timescale	isotropic-- 3 analytic options: - Liu & Jordan, 1960 - Boes, et al., 1976 - Bugler, 1977, or user input	user input single value
TRNSYS/MIT	user measured inputs at experimental sites for calibration (6 min.) or TMY/SOLMET hourly insolation for a year	user input measured values (e.g. TMY or SOLMET) or analytic model using modified Liu-Jordan (1960)	analytic models for isotropic diffuse or user input of measured total (which includes diffuse) for selected time-timescale	isotropic-- 3 analytic options: - Liu & Jordan, 1960 - Boes, et al., 1976 - Bugler, 1977 or user input	user input single value

Three General Categories of Models

First Order	Detailed	Specialized
	Flat-Plate Only	
PV F-CHART	E&R	PV-TAP
PVPM	LCP	SOLREL
	TRNSYS/MIT	
	Flat-Plate and Concentrator	
	SOLCELL-II	
	SOLSYS	
	TRNSYS/ASU	

Recent Extensions

• Modeling of anisotropic atmosphere for diffuse solar radiation	LCP and E&R
• Fresnel refraction of the encapsulant material	LCP and E&R
• Using variable time scales, especially as it applies to utility interaction	TRNSYS
• Effects of insolation spectral distribution on power output	E&R

Model Limitations

- Lack of high-quality data in some categories
- Shadowing assumptions
- Power quality not addressed
- Validation is limited

Conclusions

- **There are various models, with different capabilities, approaches, and purposes**
- **Neither the simplicity nor complexity of a model implies a more useful tool; the key is to find the appropriate model for a given task**
- **There are limitations to the PV program's current modeling capability**
  - **Data**
  - **Shadowing**
  - **Power quality**
  - **Validation**
- **This report serves to assist in the choice of an appropriate PV performance model for a user's requirements**

STANDARDS: AN OVERVIEW

JET PROPULSION LABORATORY

G.A. Praver

Purpose of Study

WHAT SHOULD THE NATIONAL PHOTOVOLTAICS PROGRAM DO TO ENHANCE THE PROCESS OF ESTABLISHING VOLUNTARY CONSENSUS STANDARDS FOR MEASURING AND RATING THE PERFORMANCE OF PV MODULES?

Map of Possible PV Cell and Module Standards

TYPES OF DEVICES \ TYPES OF STANDARDS	COMPANY	INDUSTRY	PROFESSIONAL	GOVERNMENT	VOLUNTARY CONSENSUS	SAFETY
RESEARCH CELLS						
DEVELOPMENT CELLS						
PRODUCTION CELLS						
REFERENCE CELLS					X	
R&D MODULES						
PRODUCTION MODULES					X	
PANELS/ARRAYS						

Study Approach

- Identify a set of key individuals representing a cross section of views about the standard process.
- Conduct a series of interviews with key individuals.
- Synthesize the interview results into a recommended plan of action for the National PV Program.

Key Entities

- Government Laboratories
  - JPL
  - SNLA
  - SERI
- PV Manufacturers
  - Solavolt
  - Photowatt
  - ARCO Solar
- PV Users
  - BDM
  - Rogers & Company
  - Acurex
- Others
  - DSET
  - ASU

Interview Topics

- Why do we need standards?
- What are the technological problems that are impeding the development and adoption of PV standards?
- Are there solutions to these problems?
- Are there economic limitations to obtaining the solutions?
- Who should solve the technical problems?
- What is an appropriate reference spectrum?
- Is ASTM attempting to write too many detailed standards?
- Are the proper people involved in preparing standards?
- What is the greatest impediment to getting standards written?
- What is a possible role of Government in furthering this effort?

Preliminary Synthesis

- The process of establishing voluntary consensus standards for measuring and rating the performance of PV modules <u>does</u> need enhancing.

- The National PV Program should fund travel to consensus standard meetings such as IEEE, ASTM, IEC.

- The National PV Program should sponsor small research tasks to resolve specific technical problems which are impeding particular standards
  - Funding should flow through national laboratories
  - Direction should come from consensus standards committees
  - Some example research tasks are. . .

Preliminary Consensus

- Compare direct normal, global and mathematical spectra under actual test conditions to establish a base of testing experience for various cell technologies.
- Seek a simple method to quantify effects of spectral mismatch on reference cell measurements. How much mismatch is significant? How accurately can spectral response be measured?
- Understand wide variations in round robin test results and promulgate experimental procedures to reduce these errors.
- Improve understanding of relationships between peak module performance and time-averaged performance.

RESIDENTIAL ARRAY DEVELOPMENT

MASSACHUSETTS INSTITUTE OF TECHNOLOGY

E.C. Kern, Jr.

Overview

- Residential System Cost Estimates in 1979
- Costs incurred at the NE RES and SW RES during 1980 - 1981
- Costs incurred at the SE RES in 1983
- Detailed costing for Retrofit Systems (20 square meter arrays) at the NE RES

System Cost Estimates in 1979 (C. H. Cox, III)

System Name	System Location	System Cost ($/Wp)	Module Cost ($/Wp)	Power Cond. Cost ($/Wp)	Instl Matls.& Labor ($/Wp)
EW-LO	Design	$1.18	$0.70	$0.19	$0.29
NEW-HI	Design	$3.04	$1.08	$1.36	$0.60
RETRO-LO	Design	$1.44	$0.70	$0.19	$0.55
RETRO-HI	Design	$3.30	$1.08	$1.36	$0.86

Northeast Residential Experiment Station - 1980

System Name	System Location	System Cost ($/Wp)	Module Cost ($/Wp)	Power Cond. Cost ($/Wp)	Instl Matls.& Labor ($/Wp)
SOLAREX	NERES	$18.69	$14.65	$2.56	$1.48
WESTHSE	NERES	$17.10	$11.32	$3.14	$2.65
GEN ELEC	NERES	$22.97	$20.65	$1.83	$0.49
TRISOLAR	NERES	$33.88	$32.43	$0.73	$0.72
MIT	NERES	$14.29	$12.35	$0.47	$1.47

Category	Subcategory	Description System A:	Quan	Units	$/unit (1)	$ Totl	$/Wp Summary
Photovoltaic Modules		ARCO M53 Modules	45	ea	$344.000	$15,480.00	$7.9814
PV Array Materials: Mechanical							
	Panel Assy	Alum Angle 1.50x1.50x3/16x63 inches	10	ea	$6.070	$109.26	$0.0563
		Alum Poprivets 1/4 inch hole	180	ea	$0.140	$25.20	$0.0130
	Mounting	Alum Angle 6x6x.625x37	1	ea	$36.000	$36.00	$0.0186
		Ring pin (no ball or hole)	24	ea	$0.840	$20.16	$0.0104
		Lag bolts 1/4", 2" long	64	ea	$0.248	$15.87	$0.0082
		Roof sealant	2	gal	$5.000	$10.00	$0.0052
		Black anodize (alum angles)	1	ea	$50.000	$50.00	$0.0258
						$266.49	$0.1374
PV Array Materials: Electrical							
	Conductor	Sgl-cond UF, sunlight res, grey	100	ft-12 ga	$0.120	$12.00	$0.0062
		Sgl-cond THHN, red	180	ft-12 ga	$0.067	$12.06	$0.0062
		Sgl-cond THHN, white	180	ft-12 ga	$0.067	$12.06	$0.0062
		Sgl-cond THHN, green	60	ft-12 ga	$0.067	$4.02	$0.0021
	Connectors	Amp Solarlok (5 pc sets)	12	ea	$4.740	$56.88	$0.0293
		Thomas and Betts (P/N 2690)	72	ea	$2.370	$170.64	$0.0880
	Combiner Box	Hoffman box 8x10x6 (A-606NFGLV)	1	ea	$22.760	$22.76	$0.0117
		Terminal Strip	2	ea	$1.000	$2.00	$0.0010
		Ground bus (neg bus)	2	ea	$2.500	$5.00	$0.0026
		DPST switches	3	ea	$9.880	$29.64	$0.0153
		Fuses	3	ea	$4.220	$12.66	$0.0065
		Fuse holders	3	ea	$4.140	$12.42	$0.0064
		Diodes (.6 amp, 400 volt)	3	ea	$0.820	$2.46	$0.0013
		Ground ref resistors, 1 Mohm, .25 W	3	ea	$0.050	$0.15	$0.0001
		Varistors, 400 volt, 40 amp	3	ea	$1.900	$5.70	$0.0029
		Miscellaneous wiring	1	ea	$2.000	$2.00	$0.0010
	Conduit	PVC conduit 1/2" diam (7 #12 wires)	60	ft	$0.130	$7.80	$0.0040
		Array Junction Box (Hoffman 6x6x4)	1	ea	$22.500	$22.50	$0.0116
		Conduit clamps, L-conn, box entry	15	ea	$1.000	$15.00	$0.0077
						$407.75	$0.2102

Power Conditioner		2 kW APPC Sunsine	1 ea	$3,745.000	$3,745.00	$1.9309
Power Conditioner Materials						
	Installation	10 gauge Romex	50 ft	$0.100	$5.00	$0.0026
		Circuit breaker (20 amp RED)	1 ea	$7.000	$7.00	$0.0036
		Lag bolts, framing	1 ea	$10.000	$10.00	$0.0052
	Disconnect	Outdoor box w/brkr	1 ea	$25.000	$25.00	$0.0129
					$47.00	$0.0242
PV Array: Labor						
	Panel Assy.	Wiring harness prep.	8 hr	$7.500	$60.00	$0.0309
		Mechanical assembly	6 hr	$7.500	$45.00	$0.0232
		Milling corner supports	1 hr	$15.000	$15.00	$0.0077
	Roof Prep	Layout array area, attach angles	4 hr	$15.000	$60.00	$0.0309
	Install	Place panels in position, wire, secu	16 hr	$15.000	$240.00	$0.1237
	DC Equip	Mount combiner box, conduit, disconn	4 hr	$15.000	$60.00	$0.0309
		Wire combiners to PCS	1 hr	$15.000	$15.00	$0.0077
					$495.00	$0.2552
PCS: Labor						
	Install	Mount PCS to wall	1 hr	$15.000	$15.00	$0.0077
	Wire	Install RED cir brkr, wire PCS to se	1 hr	$15.000	$15.00	$0.0077
					$30.00	$0.0155

Module Watt(pk)	43.1			
Labor Rate ($/hr)		System Total	$ Totl	$/Wp Summary
Factory	$7.50			
Field	$15.00		$20,471.24	$10.5549
System A:	Conv. Standoff			
System B:	MIT/ARCO Standoff	BOSprime	$1,246.24	$0.6426

Note:(1) Prices as quoted to MIT for quantities sufficient to built three systems each 2 kilowatts peak.

Category	Subcategory	Description System B:	Quan	Units	$/unit (1)	$ Totl	$/Wp Summary
Photovoltaic Modules		ARCO M53 Laminates	45	ea	$333.000	$14,985.00	$7.7262
PV Array Materials: Mechanical							
	Panel Assy	Hat Channels (10 ft)	10	ea	$8.000	$80.00	$0.0412
		Edge protectors/interconnects (9 ft	10	ea	$10.000	$100.00	$0.0516
	Mounting	Silicone adhesive (0.1 gallons)	5	ea	$3.000	$15.00	$0.0077
						$0.00	$0.0000
		Lag bolts 1/4", 2" long	40	ea	$0.248	$9.92	$0.0051
		Roof sealant	1	gal	$5.000	$5.00	$0.0026
						$0.00	$0.0000
PV Array Materials: Electrical						$209.92	$0.1082
	Conductor	Sgl-cond UF, sunlight res, grey	35	ft-8 ga	$0.260	$9.10	$0.0047
		Sgl-cond THHN, red	60	ft-8 ga	$0.105	$6.30	$0.0032
		Sgl-cond THHN, white	60	ft-8 ga	$0.105	$6.30	$0.0032
		Sgl-cond THHN, green	60	ft-8 ga	$0.105	$6.30	$0.0032
	Connectors	Amp Solarlok (5 pc sets)	6	ea	$4.740	$28.44	$0.0147
						$0.00	$0.0000
	Combiner Box	Hoffman box 8x10x6 (A-606NFGLV)	1	ea	$22.760	$22.76	$0.0117
						$0.00	$0.0000
						$0.00	$0.0000
		DPST switches	1	ea	$9.880	$9.88	$0.0051
		Fuses	1	ea	$4.220	$4.22	$0.0022
		Fuse holders	1	ea	$4.140	$4.14	$0.0021
		Diodes (.6 amp, 400 volt)	1	ea	$0.820	$0.82	$0.0004
		Ground ref resistors, 1 Mohm, .25 W	1	ea	$0.050	$0.05	$.0000
		Varistors, 400 volt, 40 amp	1	ea	$1.900	$1.90	$0.0010
		Miscellaneous wiring	1	ea	$2.000	$2.00	$0.0010
	Conduit	PVC conduit 1/2" diam (3 #8 wires)	60	ft	$0.130	$7.80	$0.0040
		Array Junction Box (Hoffman 6x6x4)	1	ea	$22.500	$22.50	$0.0116
		Conduit clamps, L-conn, box entry	15	ea	$1.000	$15.00	$0.0077
						$147.51	$0.0761

Power Conditioner		2 kW APPC Sunsine	1 ea	$3,745.000	$3,745.00	$1.9309
Power Conditioner Materials						
	Installation	10 gauge Romex	50 ft	$0.100	$5.00	$0.0026
		Circuit breaker (20 amp RED)	1 ea	$7.000	$7.00	$0.0036
		Lag bolts, framing	1 ea	$10.000	$10.00	$0.0052
	Disconnect	Outdoor box w/brkr	1 ea	$25.000	$25.00	$0.0129

PV Array: Labor					$47.00	$0.0242
	Panel Assy.				$0.00	$0.0000
					$0.00	$0.0000
					$0.00	$0.0000
	Roof Prep				$0.00	$0.0000
	Install	Place panels in position, wire, secu	8 hr	$15.000	$120.00	$0.0619
	DC Equip	Mount combiner box, conduit, disconn	4 hr	$15.000	$60.00	$0.0309
		Wire combiners to PCS	1 hr	$15.000	$15.00	$0.0077

PCS: Labor					$195.00	$0.1005
	Install	Mount PCS to wall	1 hr	$15.000	$15.00	$0.0077
	Wire	Install RED cir brkr, wire PCS to se	1 hr	$15.000	$15.00	$0.0077

					$30.00	$0.0155

Module Watt(pk)	43.10				---	
Labor Rate ($/hr)				System Total	$ Totl	$/Wp Summary
Factory	$7.50				---	
Field	$15.00				$19,359.43	$9.9817
System A:	Conv. Standoff				---	
System B:	MIT/ARCO Standoff			BOSprime	$629.43	$0.3245

Note:(1) Prices to MIT for the purchase of quantities sufficient to build three systems at two kilowatts apiece, with the exception of the prices for laminates, hat channels, edge protectors/interconnects and silicone adhesives which are estimates made by the author without consultation with the supplier.

MIT Retrofit System Designs (1984)

System Name	System Location	System Cost ($/Wp)	Module Cost ($/Wp)	Power Cond. Cost ($/Wp)	Instl Matls.& Labor ($/Wp)
5% Array	Design	$6.21	$1.00	$4.47	$0.74
ARCO/MIT	Design	$9.98	$7.72	$1.93	$0.32
30% Array	Design	$2.33	$1.01	$1.20	$0.13
MIT/ARCO	Design	$10.59	$7.98	$1.93	$0.68
20% Array	Design	$2.99	$1.01	$1.79	$0.19

Note:(1) Nominal $1 per watt module cost assumed for 5%,20%, and 30% arrays
(2) Two kilowatt PCU used for under one kilowatt array in the 5% array
(3) Each array fixed with an area of 180 square feet

Conclusions

- Lowest cost arrays to date are the direct mount GE shingles (their degradation, however, dictates against them).
- For new construction situations, integral mounts have proven to be the lowest cost.
- Building block panels appear to offer significant advantages for both retrofit and new construction situations.
- Installation materials and labor costs for X-Si are potentially 0.32 $/Wp; A-Si (5%) 0.74 $/Wp; GaAs (20%) 0.19 $/Wp; GaAsSi (30%) 0.13 $/Wp